ELECTRONIC AND OPTICAL PROPERTIES OF AMORPHOUS SEMICONDUCTORS: THEIR PRINCIPLES AND APPLICATIONS

Alan E Owen PhD FRSE

PART 1: PRINCIPLES

Thesis submitted for the degree of
Doctor of Science
University of Edinburgh
1994

CONTENTS - PART 1

PRINCIPLES

DECLARATION

(a) The publications cited herein have not been submitted, in whole or in part, for any other degree or diploma.

(b) I am the sole author of three of the cited papers. Publications with co-authors were the product of research projects originated by me and in which I was the named Principal Investigator and/or Principal Supervisor. I also had at least an equal role with colleagues in preparing joint papers for publication.

ACKNOWLEDGEMENTS

Many research students (PhD candidates) and research assistants, too numerous to mention individually, have worked with me over the years and contributed directly or indirectly to the papers selected for this thesis. I am grateful to all of them. Special thanks are due however to four who are now in senior academic positions in other institutions: Professor J M Marshall and Drs C Main, W K Choi and R E Belford. Their work, first as PhD students and then as postdoctoral researchers, helped to establish on-going research which formed the bases of succeeding projects.

I have had the privilege of collaborating actively in some long-running programmes which have received substantial funding from research councils and industry, with several excellent and experienced researchers whose work has had a profound influence on my own research. They are: Professors W E Spear (now retired) and the late P G Le Comber, founders of the superb Amorphous Semiconductor Group at the University of Dundee which is now ably led by Dr R A G Gibson; and my colleagues Professor A F Murray and Drs P J S Ewen (also a former research student), J Hajto and A J Snell in the Department of Electrical Engineering at the University of Edinburgh.

I am also indebted to Professor R W Douglas and Dr J O Isard, both now retired from the University of Sheffield. Professor Douglas was the supervisor of my own PhD programme; Dr Isard allowed me to share his laboratory and he provided perceptive encouragement. Both were constant sources of wisdom on the fascinating world of glass science during my two spells at Sheffield and they were instrumental in shaping the pattern of my research career.

Finally, the most sincere gratitude goes to my wife Barbara and our family for their tolerance and patient support during long periods when innumerable hours devoted to obscure research might have been spent more usefully on family activities.

SUMMARY

1. Introduction

The fundamental properties and technological applications of amorphous semiconductors have been the predominant theme in my research for over 30 years. A selection of 40 papers published between 1970 and 1992 is cited in this thesis; 23 deal with fundamental issues (P1-P23, pp1 to 340 in Part 1) and 17 with applications (A1-A17, pp341-576 in Part 2). The Appendix, in Part 2, contains a complete list of the 150 publications from which the selection was made.

2. Background

In the general context of solid-state science and technology, the field of vitreous (or glassy), or more generally, amorphous semiconductors, is a relative newcomer. The term "vitreous semiconductor" came into use in the 1950s and 60s through the work of Ioffe (1) and Kolomiets(2) and their colleagues on semiconducting chalcogenide glasses, at the A F Ioffe Physico-Technical Institute in Leningrad (St Petersburg). Professor Kolomiets, who died in 1988, is often regarded as the "father" of the field of amorphous semiconductors. It was not until the late 1960s and early 70s however that it became a subject of world-wide and rapidly expanding interest, generated mainly by the publicity given to the work of Ovshinsky and others on electrical (electronic?) switching devices fabricated from semiconducting chalcogenide glasses (3)(4). The promise of large-scale applications in mainstream electronics brought many solid-state physicists, materials scientists and electronics engineers in academia, and in most of the major companies of the electronics industry, into the field. For a variety of reasons that particular area of promise - in digital electronics - never really materialised. During the 1970s there was, however, an intense flurry of activity and sufficient momentum was developed in both the fundamental physics of amorphous semiconductors, and in their technological applications, to establish the field as a self-contained sub-set of solid-state physics and solid-state electronics.

The literature of the field contains references to an extraordinarily wide range of materials described as amorphous (or vitreous/glassy) semiconductors prepared by one or more of a variety of techniques. At one time or another my research has covered several of those different classes of materials. Much the more important from the point of view of both fundamental science and technological applications are, however:

- the chalcogenide glasses, and
- the tetrahedral amorphous semiconductors.

The papers selected for this thesis are concerned only with those two groups.

3. The Chalcogenide Glasses

The element Se and the compounds As_2S_3 and As_2Se_3 are prototypes of the chalcogenide glass category of amorphous semiconductors (5). They are sometimes known, alternatively, as "lone-pair" semiconductors because their valence bands are

formed from the non-bonding "lone-pair" p-electrons on the chalcogen atoms, a feature which is important in many of their properties (5). Also in this group are the elements S and Te, compounds such as As_2Te_3, Sb_2Se_3 etc., pseudo-binaries typified by the system As_2S_3 - As_2Se_3, and many multi-component systems such as Ge-As-Se, Si-Ge-As-Te etc.

Most of the chalcogenides, but not all, can be prepared by normal melt-quenching methods. **All** can be prepared equally readily in thin-film form by vapour deposition techniques such as thermal evaporation under vacuum, or sputtering (6).

4. The Tetrahedral Amorphous Semiconductors

Amorphous Si is typical of this group but it also includes Ge and compounds such as SiC, InSb and GaAs etc (7). They have the same tetrahedral nearest-neighbour configuration as their crystalline counterparts. So far as is known, amorphous Si and its relatives can be prepared **only** in the form of thin-films by deposition from the vapour phase. Vacuum evaporation (of Si for example) can be done straightforwardly but the glow discharge decomposition of silane gas, SiH_4 (or GeH_4 etc) is usually the favoured technique. In the latter case some hydrogen is retained in the deposited film and the material is more appropriately called hydrogenated amorphous Si, denoted a-Si:H.

5. Principles

Several common themes run through the development of theoretical models of the electronic energy band structure and transport mechanisms in both the chalcogenide glass group and the tetrahedral amorphous semiconductors (5)(7)(8). They are:

- localisation - delocalisation
- localised states - extended states
- intrinsic defect states of POSITIVE or NEGATIVE (Hubbard) correlation energy
- the mobility gap, and
- band or hopping conduction.

The first three are consequences of the structural (topological) disorder which is inherent in the amorphous state of matter. Together they lead to the idea of a **mobility** gap, rather than the characteristic **energy** gap of a crystalline semiconductor. Electronic conduction is normally trap (localised state) limited and may be dominated by band (extended state) transport, OR hopping (between localised states), OR may involve a combination of both.

Much of my early research in the field was concerned with experimental studies of electron transport in semiconducting chalcogenide glasses, interpreted in terms of band or hopping conduction, the mobility gap, defect states and the role of trapping. Papers P1 to P10 illustrate that period, with P11 and P16 providing

general reviews. Later, the emphasis shifted to optical properties and especially to studies of the various photo-induced effects which seem to be unique to the chalcogenide glasses. Papers P15, P17 and P18 were key contributions. In the early '80s collaboration with the Amorphous Semiconductor Group under Professors W E Spear and the late P G Le Comber at the University of Dundee led us into a study of a novel form of electrical switching in amorphous silicon (a-Si:H) devices (see paragraph 5, Applications) and from this work some fundamental research developed as a corollary. Papers P20 and P23 illustrate this aspect. The latter is especially significant. It reported the first observations of unusual quantised electronic transport phenomena in amorphous silicon structures. Over the past 15 months other groups have published independent confirmation and the topic has advanced considerably since P23 appeared.

6. Applications

I was involved in the early research on electrical switching devices based on semiconducting chalcogenide glasses which generated such widespread interest during the late '60s and early '70s. This was contemporaneously with the work of Ovshinsky and others (3)(4). There was great controversy at the time about the extent to which the switching mechanism is controlled by purely electronic process or is thermally induced. Papers A1, A2 and A4 summarise my contribution, the last (A4) setting out in detail the view that electrical switching in the chalcogenide glasses is basically an electrothermal process. By the late '70s it became clear that chalcogenide-based switching devices would not find major applications in mainstream electronics and paper A4 was my final contribution to that subject. I had also been involved, however, in work on thyristor-type switching devices based on monolithic single crystal silicon structure, as described in paper A3 for example. It was this combination of interests in various types of electrical switching devices which led to the collaboration with the Dundee group, under Professors Spear and Le Comber, on the possible application of amorphous silicon (a-Si:H) in similar devices. This has proved to be an extremely fruitful collaboration. The first results are contained in paper A5. This describes a direct analogue in a-Si:H of the *monolithic* single crystal silicon device which was the subject of paper A3. The switching characteristics are very different however and the joint Edinburgh/Dundee research on amorphous silicon switching devices has progressed through several substantial projects. Paper A17 is a comprehensive summary of that work, set in the general context of electronic switching in amorphous semiconductors.

When I ceased the research on switching in chalcogenide glasses my interest in applications of those materials switched (!) to possible utilisation of their unique photo-induced effects, mentioned in para.5. This is also proving to be a fruitful field. Potential applications include photoresists for high resolution microlithography, diffraction gratings - particularly for the infra-red, and in various non-linear electro-optic devices, also in the infra-red. Papers A8, A10 and A11 are typical original contributions; paper A16 is a general review.

7. Conclusions

The papers cited in this thesis have been selected to illustrate my contributions to fundamental and applied developments in the field of amorphous semiconductors

from the time when it was a fringe interest in solid state physics and electronics, to the point where it is now a recognised discipline within solid state science which also has considerable technological importance. The papers have been chosen to illustrate coherent themes in the progress of my research and the essential (and intentional) inter-dependence of the fundamental and applied aspects.

8. References

1. A.F. Ioffe and A.R. Regel, Progr. Semiconductors Vol. 4, 239 (1960)

2. B T Kolomiets, phys. stat. sol., Vol. 7, 359, 713 (1964)

3. S R Ovshinsky, Phys. Rev. Lett Vol. 21, 1450 (1968)

4. H Fritzsche, "Switching and Memory in Amorphous Semiconductors", Chap 6 of "Amorphous and Liquid Semiconductors", Ed. J Tauc. (Plenum Press) (1974)

5. A E Owen, "Electron Transport in Chalcogenide Glasses", Chap VI of "Coherence and Energy Transfer in Glasses", Ed: P A Fleury and B Golding. (Plenum Press) (1984)

6. For general references see:

   (a) R Zallen, 'The Physics of Amorphous Solids". Chap 1 (Wiley) (1983)

   (b) A E Owen, "Preparation of Amorphous Materials and the Glass Transformation", Chap 4 of "Electronic and Structural Properties of Amorphous Semiconductors", Ed: P G Le Comber and J Mort. (Academic Press), (1973)

7. For general references see:

   (a) N F Mott and E A Davies, "Electronic Processes in Non-crystalline Materials", 2nd Edition. (OUP) (1979).

   (b) J I Pankove (Editor), "Hydrogenated Amorphous Silicon", Parts A, B, C and D, Vol. 21 of "Semiconductors and Semimetals", Eds: R K Willardson and A C Beer (Academic Press) (1984)

8. S R Elliott, "Physics of Amorphous Materials", Chap 5, 2nd Edition (Longmans) (1990)

PRINCIPLES

(Where there are co-authors, the number in parenthesis indicates my position in the list of authors).

APPLICATIONS

(Where there are co-authors, the number in parenthesis indicates my position in the list of authors.)

JOURNAL OF NON-CRYSTALLINE SOLIDS 2 (1970) 40–51 © North-Holland Publishing Co., Amsterdam

ELECTRONIC PROPERTIES OF SOME SIMPLE CHALCOGENIDE GLASSES

A. E. OWEN and J. M. ROBERTSON
School of Engineering Science, University of Edinburgh, Edinburgh, Scotland, U.K.

The dc and ac conductivity, thermoelectric power, optical absorption and carrier mobility of As_2S_3, As_2Se_3 and some other chalcogenide glasses are described and discussed. The question of band or hopping conduction is considered and it is concluded that although the ac conductivity involves hopping, the dc properties are best viewed in terms of a band model with a "mobility gap" as introduced by Mott and Cohen. There are, however, some unresolved problems, particularly relating to the ac conductivity.

1. Introduction

Theoretical work[1]) suggests that the band structure of glassy semiconductors is not very different to that in similar crystalline materials except for the splitting-off of a tail of localised states below the conduction band and above the valence band. It does not follow, however, that electron transport necessarily occurs in the conduction or valence bands – a hopping mechanism between localised states is also possible. With this proviso there seems to be no reason why we should not expect to find amongst the many semiconducting glasses, counterparts of:

(a) ordinary broad-band semiconductors in which, although trap-limited to a greater or lesser degree, transport may in principle occur in non-localised states i.e. in a "band", and

(b) narrow-band materials in which the carriers are always strongly localised – because of a large effective mass – and transport occurs by hopping or, possibly, in a polaron band[2]).

On the face of it, the chalcogenide glasses on the one hand, and the transition-metal oxides on the other, provide examples of the two categories. Space does not permit a discussion of both types, however. The transition-metal oxide glasses are probably closely analogous to crystalline mixed-valence semiconductors[3]) and such anomalies as do exist may be due to the greater structural complexity of the glasses. These materials will not therefore be considered in the following sections.

2. Chalcogenide glasses

We shall consider in the main the simpler compounds As_2S_3 and As_2Se_3 but with some reference to more complex systems. These materials are often regarded as basically similar, except for the effect of the localised states, to ordinary intrinsic semiconductors. The evidence for this point of view comes largely from the dependence of the dc conductivity of these materials on temperature, the magnitude and temperature dependence of the thermoelectric effect and the appearance of an optical "absorption edge" which coincides roughly, in energy, with the thermal activation energy (from the dc conductivity). We shall look at these features, and other properties of the chalcogenide glasses in more detail below. With few exceptions we refer all the time to measurements on glasses produced in bulk by cooling from the melt and *not* to evaporated films.

2.1. dc Conductivity

Log σ versus $(1/T)$ plots almost invariably give a straight line with a single slope over the whole available temperature range. The simpler compounds

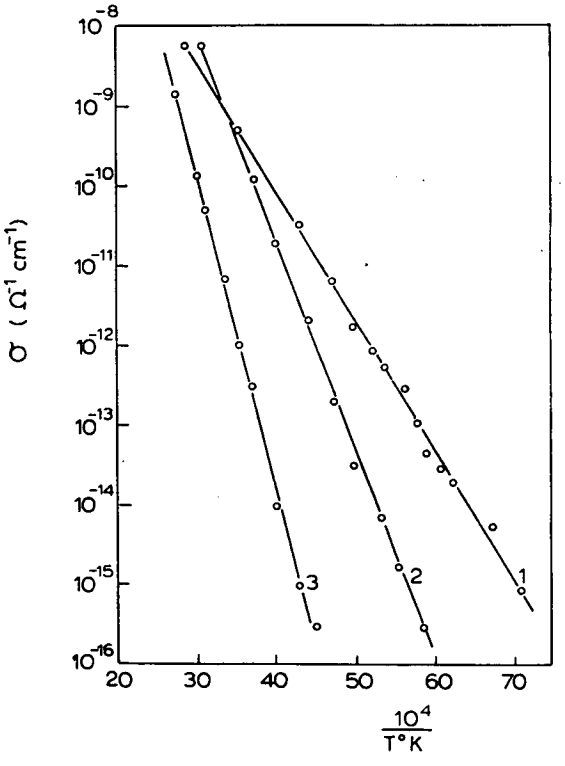

Fig. 1. dc conductivity σ versus $(1/T, °K)$ for three chalcogenide glasses. (1) 5 $As_2S_3 \cdot 2$ PbS; (2) 8 $As_2Se_3 \cdot 2$ As_2Te_3; (3) 9 $As_2Se_3 \cdot 1$ As_2Te_3.

(As_2Se_3 and As_2S_3) have high resistances and large activation energies and the temperature range over which they can be measured is limited. Fig. 1, however, shows the $\log \sigma$ versus $(1/T)$ relationship over a reasonably wide temperature range for three rather more conductive glasses. Using

$$\sigma = \sigma_0 \exp(-E_{cond}/2kT),$$

E_{cond} has been reported in the range 2.1–2.3 eV for As_2S_3, 1.8–2.0 eV for As_2Se_3 and in the 5 $As_2S_3 \cdot 2$ PbS composition shown in fig. 1, $E_{cond} \sim 0.5$ eV. In a very few cases measurements in the authors' laboratory have shown indications of a change to a lower slope at lower temperatures, suggesting "extrinsic" conduction. Similar breaks have also been observed in some of the more conductive, but complex, systems studied in the Energy Conversion Devices Laboratory (see for example Fagen and Fritzsche[4]).

2.2. Thermoelectric power

The thermoelectric power is *positive*, it has a magnitude typical of semiconductors and is approximately inversely proportional to temperature.

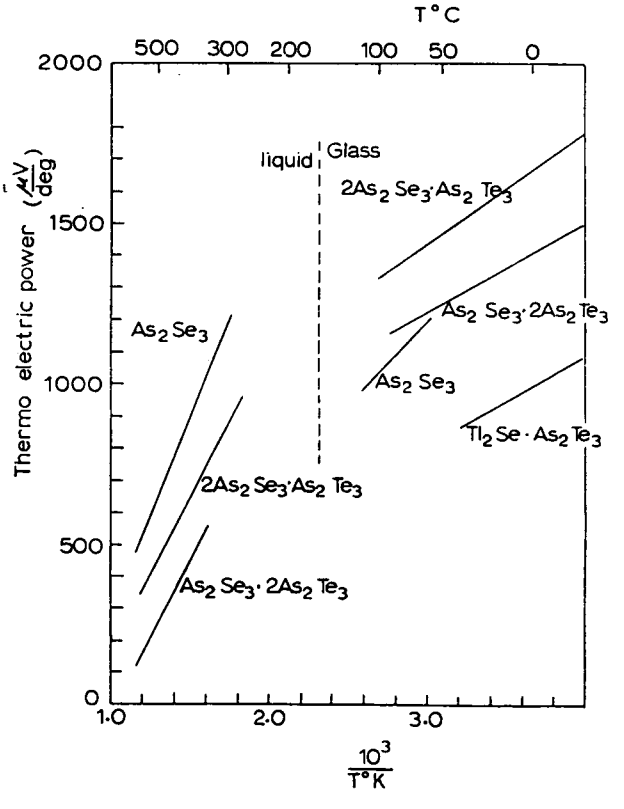

Fig. 2. Thermoelectric power as a function of temperature for As_2Se_3, 2 $As_2Se_3 \cdot As_2Te_3$ and $As_2Se_3 \cdot 2$ As_2Te_3 in the liquid[5]) and solid[6]) states. Also for vitreous $Tl_2Se \cdot As_2Te_3$[7]).

Fig. 2 contains some data on As_2Se_3 and two As_2Se_3–As_2Te_3 alloys in the liquid[5]) and solid states[6]). The data on $Tl_2SeAs_2Te_3$ are from Andriesh and Kolomiets[7]). The slopes of S versus $(1/T)$ in the solid are less than E_{cond} and using the usual formula for a two-carrier intrinsic semiconductor with a mobility ratio $(\mu_n/\mu_p)=b$ one obtains the values given in table 1.

TABLE 1

	b
As_2Se_3	0.27
$2\,As_2Se_3{\cdot}As_2Te_3$	0.31
$1\,As_2Se_3{\cdot}2\,As_2Te_3$	0.30
$Tl_2Se{\cdot}As_2Te_3$	0.13 (Andriesh and Kolomiets[7]))

2.3. Optical absorption edge

The chalcogenide glasses have a *shallow* optical absorption edge and E_{opt} corresponds *roughly* to E_{cond}. This is illustrated in fig. 3 with data taken from Edmond[5]) and Felty and Myers[8]) for As_2Se_3. The data at high absorption coefficients ($>10^3\ cm^{-1}$) were obtained with evaporated layers. Often, however, E_{opt} seems to have been measured arbitrarily at absorption coefficients much too low to be meaningful, particularly as the absorption coefficient increases exponentially over a wide range of photon energies. For example, E_{opt} in As_2Se_3 has been quoted as 1.54 eV[9]) (cf. E_{cond} 1.9 eV)

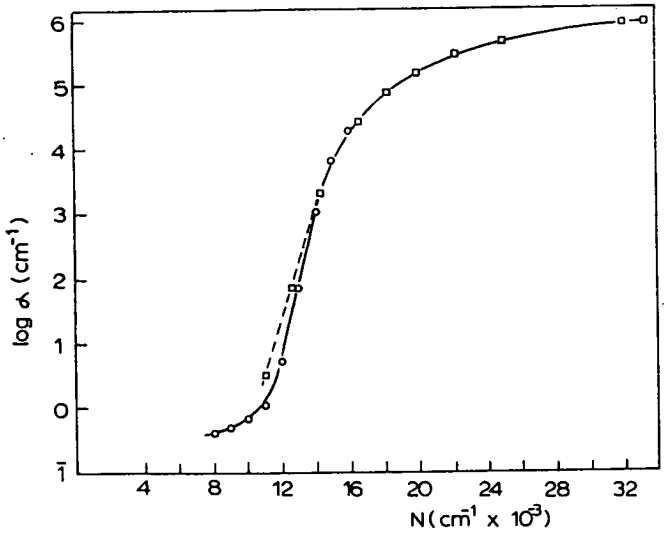

Fig. 3. Optical absorption α versus wave number N in As_2Se_3, (○) from Edmond[5]) and (□) from Felty and Myers[8]).

corresponding to $\alpha \sim 10\ \text{cm}^{-1}$. Apart from other considerations in this region of the absorption tail, α depends on the sample purity[10]).

A more justifiable procedure to estimate an "optical gap" (if by that is meant a separation between non-localised states) is to attempt to fit the absorption curve *above* the exponential edge to the standard formulae for optical transitions in semiconductors. As shown in fig. 4, except for very high energies (>3.5 eV), the indirect-allowed case fits very closely to the measured curve for As_2Se_3 right down to the shoulder of the exponential edge, with $E_{opt} \sim 1.80$ eV. Some theoretical justification for applying an equation of the form used in fig. 4 has been provided by Tauc et al.[12]) who

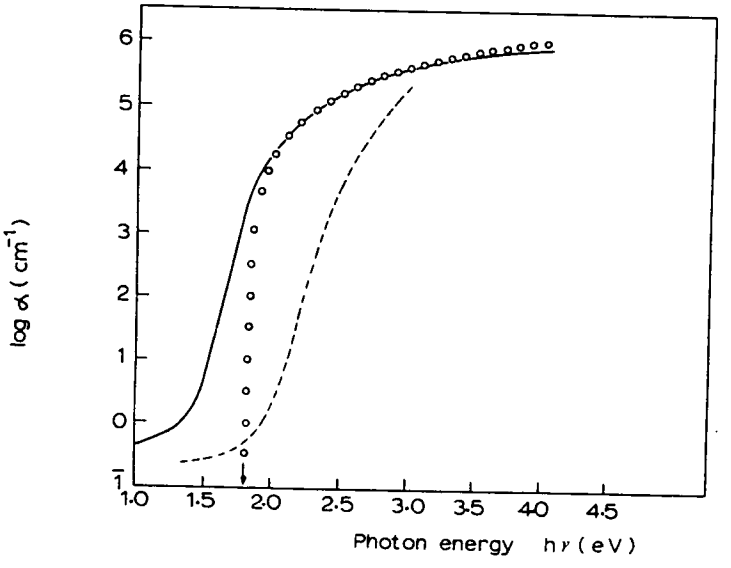

Fig. 4. Comparison of the optical absorption data for As_2Se_3 (solid line) from fig. 3, with formula for indirect-allowed transitions. Also shown are experimental data for As_2S_3 (dashed line) from refs. 15 and 16. (○) $\alpha = 8.40 \times 10^5\ (h\nu - 1.80)^2/h\nu$, indirect-allowed transitions.

points out that so long as energy is conserved and the density-of-states functions for the non-localised states are parabolic then $\alpha(\omega) \sim (h\omega - E_{opt})^2$. It is not necessary of course, that the density-of-states functions are parabolic; indeed Mott[13]) has suggested a linear form but in the absence of more exact approach the above procedure seems reasonable. It also coincides quite closely, in the example of fig. 4, with the band-gap criterion suggested by Stuke[14]) ($E_{opt} \equiv h\nu$ at $\alpha = 10^4\ \text{cm}^{-1}$).

There are not sufficient data available on other materials to make the same comparison. Some measurements on As_2S_3, taken from Doyle[15]) and Edmond[16]) are, however, also indicated in fig. 4. If the situation is the same

as in As_2Se_3, E_{opt} for As_2S_3 will be $\gtrsim 2.50$ eV. This is significantly *greater* than E_{cond}, for which the highest value quoted is 2.32 eV[17]) but which is usually in the region 2.1 to 2.2 eV.

2.4. Hall mobility

It would be extremely valuable of course, to have some conclusive data on the Hall coefficient and the Hall mobility. Unfortunately there is very little information and there is no straightforward interpretation of what data there are. So far measurements have been made only on relatively conducting, and hence more complex compounds, e.g. $Tl_2Se \cdot As_2Te_3$ (Kolomiets and Nazorova[18])) and As_2SeTe_2 (Male[19])). In contrast to the thermoelectric power, the Hall coefficient has always been found to be *negative*. The Hall mobility μ_H is low (~ 0.1 cm^2/V sec), it is virtually independent of temperature and its magnitude also seems to be practically independent of the particular material. The temperature independence of μ_H has been taken as indicative of transport in a band, but if this is so its magnitude is not consistent unless, possibly, very narrow bands are involved[20]). It is worth noting furthermore, that a temperature independent mobility is not necessarily evidence against a hopping mechanism of conduction[21]). The sign discrepancy is not understood although, of course, in an intrinsic semiconductor it is not necessary that they should agree; $(\mu_n/\mu_p)_{Hall}$ and $(\mu_n/\mu_p)_{drift}$ may be different. According to Pearson[22]) all the materials in which this discrepancy is observed are phase separated, possibly with n-type crystalline inclusions. Against this the results quoted above show that the anomaly still exists in the liquid phase, and usually there is no detectable change in μ_H on going from solid to liquid. It may be that the liquid state is still phase separated (liquid–liquid) with an n-type dispersion but it seems unlikely that the magnitude would remain unchanged.

2.5. Trap-limited drift mobility

In fig. 5 are shown some recent measurements from the authors' laboratory of the hole mobility in glassy As_2Se_3. These were obtained by generating carriers in the surface of a thin specimen with an electron beam and drifting the holes (or electrons) through with an appropriately biased field. The technique has been described and used extensively by Spear[23]) and others. Experiments on materials like As_2Se_3 with mobilities as low as those shown in fig. 5 are very difficult to make. The details of the measurements and results on other materials will be described elsewhere and it suffices to mention at the moment that the voltage pulses observed were rounded-off. That a transit time was in fact being measured was suggested however, by careful comparison with measurements on selenium; in particular the pulse

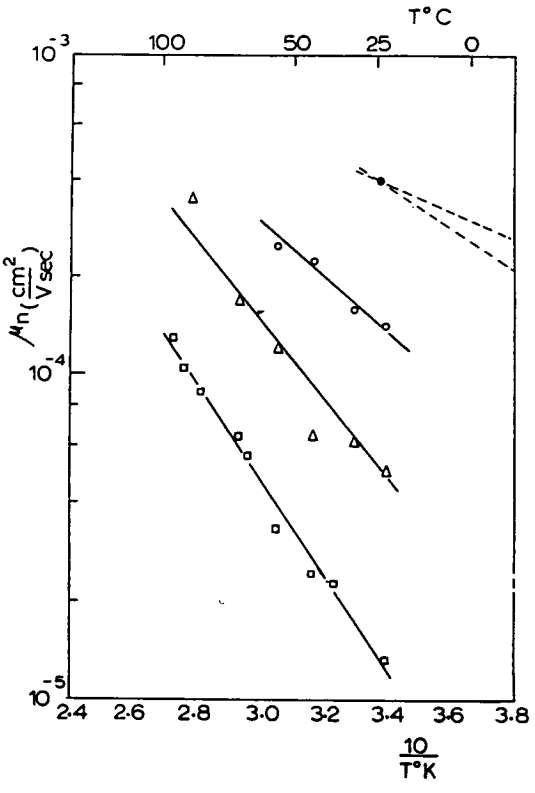

Fig. 5. The trap-limited drift mobility for holes in As_2Se_3 as a function of temperature for different fields. (□) $E = 9.4 \times 10^4$ V/cm; (Δ) $E = 18.8 \times 10^4$ V/cm; (○) $E = 28.2 \times 10^4$ V/cm. For comparison, results of Kolomiets and Lebedev[24]) are also shown: (●) $E = 55 \times 10^4$ V/cm.

height found with As_2Se_3 specimens was about the same as that observed with Se samples. As is evident in fig. 5 the hole mobility is very field-dependent. The "zero-field" hole mobility at room temperature is approximately 5×10^{-7} cm²/V sec and the mobility activation energy is 0.5 eV.

Only two other measurements of this sort on As_2Se_3 are known to the authors. Kolomiets and Lebedev[24]) report a room temperature result and an estimate of the temperature dependence; their results are illustrated in fig. 5 and are in good agreement with the present results. Kruglov, Strachov and Grisin[25]), however, report a slightly lower hole mobility (10^{-4} cm²/V sec) and a rather smaller but still significant activation energy (0.2 eV). The latter authors also report an appreciably higher electron mobility (10^{-3} cm²/V sec) but this is contrary to the present work, and to that of Kolomiets and Lebedev[24]), in which the electron pulse was barely detectable.

2.6. ac Conductivity

The conductivity of the chalcogenide glasses increases with frequency

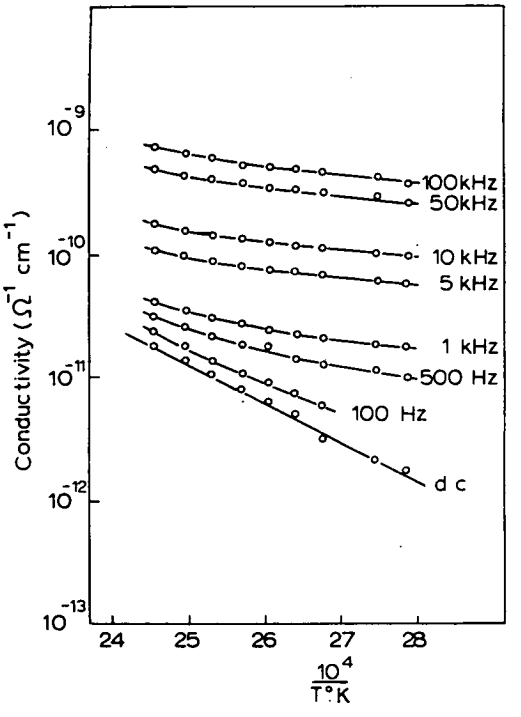

Fig. 6. Conductivity σ of As_2S_3 as a function of temperature ($1/T$, °K) for dc and frequencies up to 100 kHz.

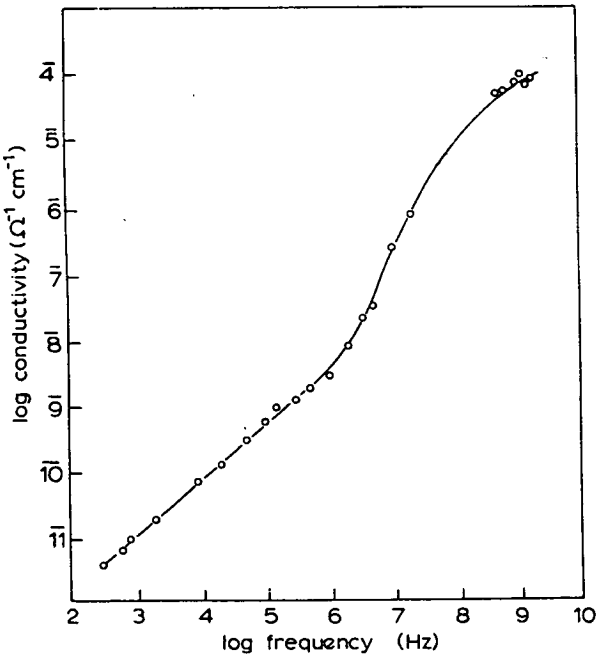

Fig. 7. Conductivity of As_2S_3 at room temperature from audio- up to ultra-high-frequencies.

sometimes, especially in the more resistive materials such as As_2S_3, at audio and sub-audio frequencies. A typical example, for an As_2S_3 glass contaminated with silver is shown in fig. 6; $\log \sigma$ is plotted versus $(1/T)$ for dc and frequencies up to 100 kHz. The conductivity in this frequency range increases slightly less than linearly with frequency; the other point to note is the tendency for the ac conductivity to become temperature-independent. At higher frequencies the conductivity increases more strongly with frequency, tending to ω^2 with, in As_2S_3, an indication of a levelling-off at frequencies greater than 10^9 Hz. This is illustrated in fig. 7 for an As_2S_3 glass at room

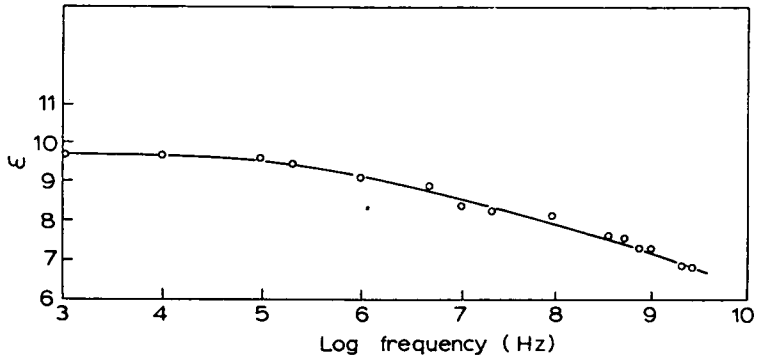

Fig. 8. The dielectric constant ε of As_2S_3 at room temperature from audio- up to ultra-high-frequencies.

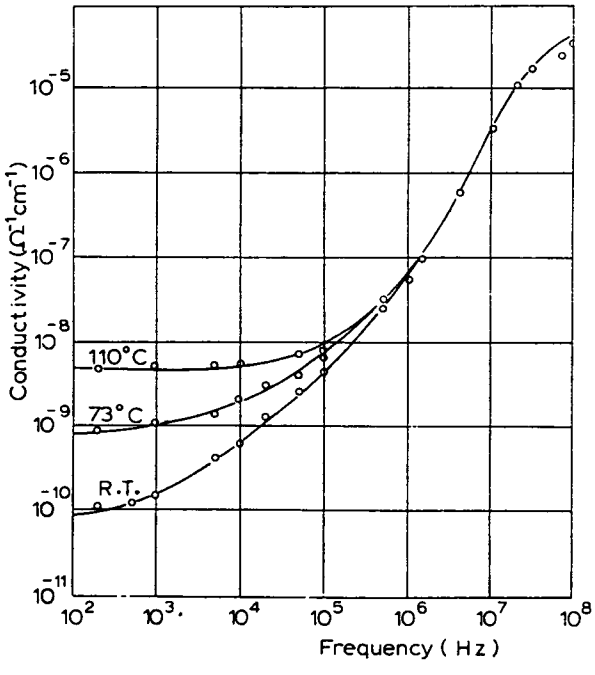

Fig. 9. Conductivity for As_2Se_3 (+0.2 at% Ag) as a function of frequency at different temperatures (R.T. = room temperature).

temperature. As expected from the form of fig. 7 the dielectric constant changes only slowly with frequency in the audio range but decreases more rapidly in the rf and uhf ranges of frequency – fig. 8. The ac conductivity at different temperatures for an As_2Se_3 glass with 0.2 at% Ag is illustrated in fig. 9. This also shows the two regions of different frequency dependence and the tendency for the ac conductivity to become temperature-independent. The flattening-off at low frequencies as the temperature increases is due to the increasing dc conductivity.

3. Discussion

3.1. General

The experimental data on the chalcogenide glasses are, in some important ways, reminiscent of intrinsic conduction (e.g. sections 2.1 and 2.2). An explanation is required however, for the low conductivity, the extremely low mobilities, the sign discrepancy between the Hall and Seebeck coefficients, and the pronounced frequency dependence of the conductivity. These features have previously been tentatively attributed, in part at least, to the presence of internal potential barriers[1,26]) but this model requires that $E_{cond} > E_{opt}$. It is suggested in section 2.3 however that in As_2Se_3, $E_{cond} \sim E_{opt}$ and in other materials possibly $E_{cond} < E_{opt}$.

3.2. Band or hopping conduction

The strongly increasing conductivity with frequency is good, *but not unambiguous*, evidence for hopping conduction. Even accepting this, however, it does not follow that in the dc limit conduction is also by hopping. The following points merit particular emphasis. If hopping does occur the trap-limited mobility would be given by

$$\mu = \frac{\gamma e a^2}{kT} \exp\left(-\frac{U}{kT}\right),$$

where γ is a phonon frequency, a the jump distance and U the mobility activation energy. Using the data mentioned in section 2.5 gives a value of approximately 100 Å for the jump distance. This is too large a value for a *direct* hop between traps but presumably this distance must represent the average separation of the traps at a depth of 0.5 eV. Carriers presumably traverse this via some intermediate state or states. Moreover, the "near-intrinsic" behaviour of the $\log \sigma$ versus $(1/T)$ plot (see section 2.1) would not be consistent with a hopping mechanism unless all the hops had the same activation energy – an unlikely event in the present context. This latter point is especially strong evidence for the model proposed by Mott, and

Cohen, Fritzsche and Ovshinsky[27]) which involves a "mobility-gap" at the boundary between the localised and non-localised states somewhere in the vicinity of the original band-edge. This model is discussed in ref. 27 and will not be described further in this paper except to say that another feature of it is an exponential tail of localised states in the forbidden-gap and probably extending right across it.

As mentioned above, a conductivity which increases with frequency is not unambiguous evidence for hopping conduction. An inhomogeneity mechanism would also lead to an increasing conductivity regardless of the conduction mechanism in the individual components. It has been pointed out before, however (e.g. ref. 26), that the approximately ω^1 dependence at low frequencies is very similar to the behaviour predicted and observed by Pollak and Geballe[28]) for hopping between a random distribution of sites in impurity conduction at low temperatures in compensated silicon. Indeed it would be difficult to account for this particular frequency dependence in any other way and it is reasonable to suppose therefore that in the present case it is also due to electron hopping between the localised sites in the forbidden gap. There are several possibilities for the approximately ω^2-dependent conductivity at higher frequencies.

1) It may be a continuation of the low-frequency process. As the frequency increases the hops will become shorter and in the limit of interatomic distances, will no longer be randomly distributed leading naturally therefore to a frequency dependence which tends to ω^2.

2) Inhomogeneities on a molecular scale. A simple "bricks and mortar" model to represent conducting and non-conducting phases may be approximated by a series combination of a resistor and a capacitor. The time constant for such a model could be made to agree with the observed relaxation time $\tau \sim 2 \times 10^{-10}$ sec.

3) Some atomic dipolar mechanism may be responsible.

The difficulty in all cases is the apparent temperature independence of the high-frequency conductivity *and* the relaxation time. An atomic dipolar mechanism would certainly be expected to show a measurable temperature dependence. The influence of temperature on the inhomogeneity model would be a function of the conductivity of the conducting "particles" and these would, therefore, have to be "metallic-like" in their temperature dependence. In electron-hopping the temperature independence of the *magnitude* of the high frequency conductivity would be understandable if states near the Fermi level were involved, but it is not obvious that the relaxation time should be unaffected by temperature. This is, therefore, an unresolved problem and it is one which is not unique to the chalcogenide glasses.

Finally, it should be mentioned that at the moment there are other features

which are unexplained by the "mobility gap" model and amongst these is the sign discrepancy between the Hall and Seebeck coefficients.

Acknowledgments

The authors wish to thank their colleagues Mr. J. M. Marshall and Mr. F. G. Mohamed for some of the experimental results discussed in this paper. One of us (J.M.R.) is grateful to the Royal Commission for the Exhibition of 1851 for the provision of a Fellowship.

References

1) N. F. Mott, Advan. Phys. **16** (1967) 49;
see also N. F. Mott and R. S. Allgaier, Phys. Status Solidi **21** (1967) 343.
2) T. Holstein, Ann. Phys. (N.Y.) **8** (1959) 325, 343.
3) R. R. Heikes, in: *Thermoelectricity*, Eds. R. R. Heikes and R. W. Ure (Interscience, New York, 1961) p. 75;
R. R. Heikes, in: *Transport Properties of Transition Metal Compounds*, Proc.Buhl Intern. Conf. on Materials (Gordon and Breach, New York, 1964).
4) E. A. Fagen and H. Fritzsche, J. Non-Crystalline Solids **2** (1970) 170, 180.
5) J. T. Edmond, Brit. J. Appl. Phys. **17** (1966) 979.
6) H. L. Uphoff and J. H. Healy, J. Appl. Phys. **32** (1961) 950; **33** (1962) 2770.
7) A. M. Andriesh and B. T. Kolomiets, in: *Soviet Research in New Semiconductor Materials*, Eds. D. N. Nasledov and N. A. Goryunova (Consultants Bureau, New York, 1965).
8) E. J. Felty and M. B. Myers, private communication of results presented at the Selenium–Tellurium Symposium, New York, 1965.
9) B. T. Kolomiets, Phys. Status Solidi **7** (1964) 359, 713.
10) A. Vasko, private communication.
11) D. L. Greenaway and G. Harbeke, *Optical Properties and Band Structure of Semiconductors* (Pergamon, Oxford, 1968).
12) J. Tauc, A. Abrahám, L. Pajasová, R. Grigorovici and A. Vancu, in: *Physics of Non-Crystalline Solids*, Ed. J. A. Prins (North-Holland, Amsterdam, 1965) p. 606.
13) N. F. Mott, private communication.
14) J. Stuke, Festkörperprobleme **9** (1969) 46. A paper presented at a meeting of the German Physical Society, Munich, 1969.
15) W. P. Doyle, Proc. Phys. Soc. (London) B **69** (1956) 865.
16) J. T. Edmond, private communication.
17) E. J. Felty, G. Lucovsky and M. B. Myers, Solid State Commun. **5** (1967) 555.
18) B. T. Kolomiets and T. F. Nazarova, Soviet Phys.-Solid State **2** (1960) 369.
19) J. C. Male, Brit. J. Appl. Phys. **18** (1967) 1543.
20) H. Fröhlich and G. L. Sewell, Proc. Phys. Soc. (London) **74** (1959) 643.
21) S. H. Glarum, J. Phys. Chem. Solids **24** (1963) 1577.
22) A. D. Pearson, J. Electrochem. Soc. **111** (1964) 753.
23) W. E. Spear, J. Non-Crystalline Solids **1** (1969) 197.
24) B. T. Kolomiets and E. A. Lebedev, Soviet Phys.-Semiconductors **1** (1967) 244.
25) V. I. Kruglov, I. P. Strachov and N. A. Grisin, Vestn. Leningr. Univ. No. 10 (1968) 63.
26) A. E. Owen, Glass Ind. **48** (1967) 637, 695.
27) M. H. Cohen, H. Fritzsche and S. R. Ovshinsky, Phys. Rev. Letters **22** (1969) 1065.
28) M. Pollak and T. H. Geballe, Phys. Rev. **122** (1961) 1742.

CONTEMP. PHYS., 1970, VOL. 11, NO. 3, 227–255

Semiconducting Glasses

A. E. OWEN

School of Engineering Science, University of Edinburgh

Part 1: Glass as an Electronic Conductor

SUMMARY. The formation and structure of glass is described and elementary wave-mechanics is used to show that, despite the disordered liquid-like configuration, electron energy-bands will nevertheless be formed in semiconducting glasses. The main effect of the disordered structure is to cause the formation of a high density of localized states in what would otherwise have been regions of forbidden energy. The localized states behave as traps for carriers and will have an important influence on the transport mechanisms in semiconducting glasses. The modes of transport are discussed and it is shown that, although a well defined energy gap does not exist, there is instead a ' mobility gap ' which has a similar effect on electrical conduction.

1. Introduction

Glass is one of the most familiar everyday materials. Common glasses, such as those used in windows, are based on the compounds soda (Na_2O), lime (CaO) and silica (SiO_2); they are made by fusing together the appropriate compounds and allowing the melt to cool sufficiently rapidly so that it becomes rigid without crystallizing. The electrical properties of glass have been of interest in science and industry for many years. Its dielectric behaviour was noticed by Benjamin Franklin in 1748, and from the earliest days of the electrical and electronics industry suitably modified silicate based glasses have been used as insulators, dielectrics, valve envelopes and seals.

On an atomic scale the conventional silicate-based glasses are made up of a relatively open but continuous ' network ' of silicon atoms each bonded tetrahedrally to four oxygen atoms, in the interstices of which are situated the cations, e.g. Na^+, Ca^{++}. As long ago as the 1880's it was shown that these glasses are basically ionic conductors—the electricity being carried by the comparatively mobile alkali ions. With some exceptions, silicate and other oxide glasses can be regarded as solid electrolytes in which only the cations (usually alkali ions) are appreciably mobile.

Specific interest in *electronic* conduction in glasses is much more recent and has developed mainly through studies of materials which have become known, inappropriately in some cases, as *semiconducting glasses* or *vitreous semiconductors*. Broadly speaking the semiconducting glasses can be divided into two chemically different groups:

(1) *The chalcogenide glasses.* One or more of the elements S, Se or Te is combined with, for example, one or more of the elements Si, Ge, P, As, Sb, Bi, Tl, Pb, etc. This list includes most of the potential glass-forming combinations outside of the oxygen-containing systems and obviously encompasses a vast number of possible compositions. Studies of the chalcogenide glasses have been pioneered by Kolomiets and his co-workers in Leningrad (for a summary of their work see Kolomiets (1964)). The

compounds arsenic sulphide (As_2S_3) and arsenic selenide (As_2Se_3) are often regarded as the typical members of the chalcogenide group of glasses, although the element selenium, which is readily prepared in an amorphous or vitreous form, is certainly the one which has been studied most quantitatively.

(2) *The transition-metal oxide glasses.* These are glasses in which the major constituent is a transition-metal oxide. Denton, Rawson and Stanworth (1954) first reported measurements on the d.c. conductivity of glasses with as much as 90 mol per cent vanadium pentoxide (V_2O_5) and vanadium-containing glasses have since been studied by many others. It is also possible to prepare many other glasses in which a major constituent is a transition-metal oxide, e.g. haematite (Fe_2O_3), titanium dioxide (TiO_2), manganese dioxide (MnO_2), molybdenum trioxide (MoO_3), tungsten trioxide (WO_3).

The above subdivision is convenient as a basis for discussion but it does not provide a completely exclusive classification. Recently, for instance, ' diamond-lattice-type ' glassy semiconductors have been reported, e.g. cadmium germanium arsenide ($CdGeAs_2$), and Russian workers have also studied mixed oxide-chalcogenide glass systems. Like the conventional silicate-based glasses all of the materials mentioned above can be prepared in bulk quantities (i.e. several cm^3 or more) by normal cooling of the melt.

In recent years, however, the term ' glass ' has come to be applied to a variety of materials produced in the form of an amorphous layer by deposition from the vapour, e.g. by evaporation, sputtering, reaction and deposition in a glow discharge (Secrist and Mackenzie 1964). Chief amongst these, in the present context, are the elements germanium and silicon produced by electron-beam evaporation or by decomposition of the hydride (GeH_4, SiH_4) in a glow discharge. Other materials, e.g. boron, and even silicon dioxide (SiO_2)—a typical glass-forming oxide—can be produced in a similar form by various vapour-deposition techniques. Such films are certainly amorphous in that they show no detectable crystallinity, but whether they are ' glassy ' or not is a question that will be considered in more detail in the next section. The feature about glass which will be of special concern to us, however, is its disordered or ' liquid-like ' structure. In this sense semiconducting glasses such as the chalcogenides and transition-metal oxide glasses are basically similar to materials like amorphous germanium. It is attractive, of course, to have a simple element like germanium, which is thoroughly understood in the crystalline state, as a ' model ' for the more complex semiconducting glasses, but as we shall see, there are differences.

Finally, it must be mentioned that several metallic alloys can be prepared in a ' glassy ' form (Duwez *et al.* 1965) by a technique known as ' splat-cooling ' in which small droplets of the alloy are subjected to extremely rapid quenching from a high temperature. These alloys are therefore more obviously glassy than the evaporated amorphous films described above.

In the right-hand column in fig. 1 the room-temperature resistivities of a variety of electronically conducting glasses are shown for comparison with the glasses which conduct ionically and with the selection of other materials on the left. Where the suffix (am) is used it means that the material in question was

produced in a thin-film form by deposition from the vapour. The iron-boroaluminate glass almost certainly contains some crystalline material, but the glassy phase is the major constituent. An enormous range of resistivity is apparent; in fact, glasses would seem to offer a range of conductivity as wide as that of materials in general. Glasses are probably not unique in this respect however; one may find almost as wide a spread in, for instance, organic polymers.

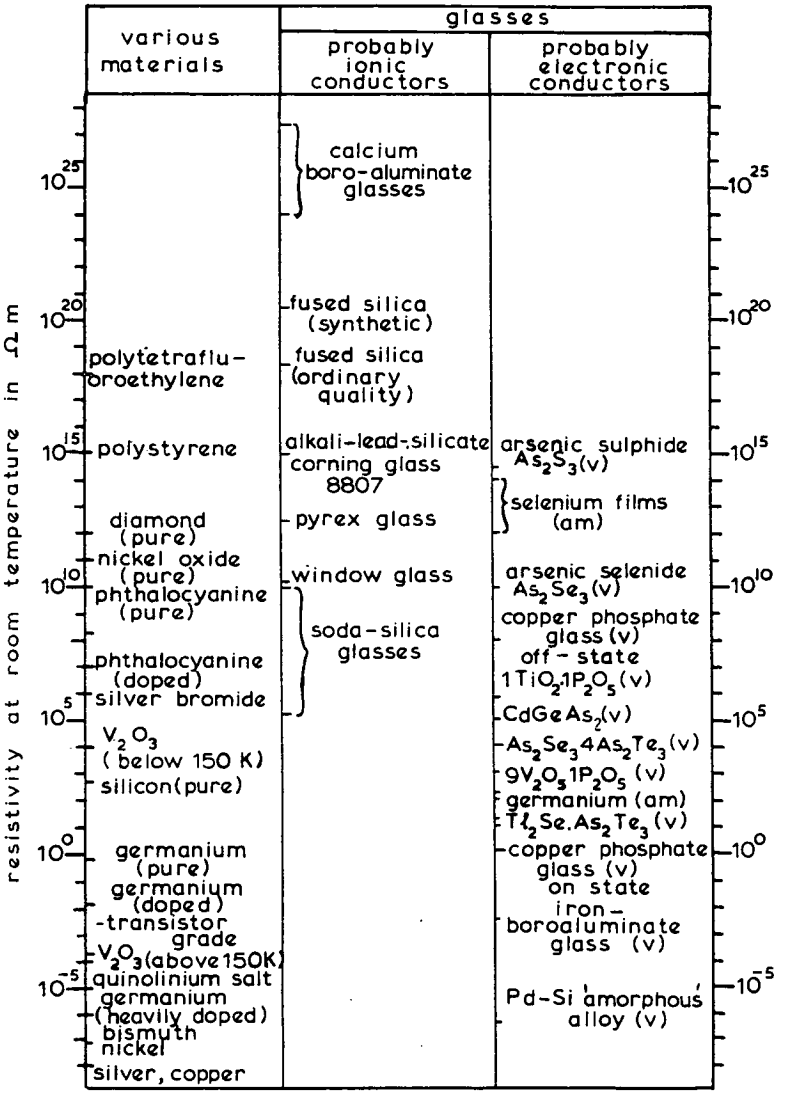

Fig. 1. A comparison of the room-temperature resistivities of a variety of materials with glasses which probably conduct ionically and electronically.

One reason for the scientific interest in electronic conduction in glass is the opportunity it affords for the study of electron transport in a disordered material as opposed to the regular periodic structure of a material like crystalline germanium. Practical interest has been aroused by the ability of many glasses to 'switch' (Mott 1969, Simmons 1969). A simple diode will, at some

critical voltage, suddenly change from a high-resistance to a low-resistance state, i.e. from an ' OFF ' to an ' ON ' state. This phenomenon seems to have been observed in most of the chalcogenide glasses, many of the transition-metal oxide glasses and in some of the amorphous evaporated films. In fig. 1 the ' ON ' and ' OFF ' resistivities of a copper phosphate glass are indicated; in switches made from chalcogenide glasses the difference in resistivity between the two states can be even larger.

2. Crystalline solids: the theoretical approach

An explanation of the electronic conductivity of *crystalline* solids is now an established part of solid-state physics and it proceeds via four well-defined steps:

(1) Geometry of the crystal structure.
(2) Energy-band structure of electrons in the crystal.
(3) Distribution of electrons among the allowed energy states.
(4) Transport of charge carriers.

In principle the same procedure could be followed—and is, in fact—to arrive at an explanation of electronic conduction in glassy solids, but steps (1), (2) and (4) involve special difficulties.

1. *Crystal structure*

This is normally obtained by x-ray diffraction studies of the crystal and the result is expressed in terms of the geometry of a ' unit-cell ' which repeats itself indefinitely through the crystal, i.e. the crystal is characterized by a periodic structure. As we shall see, a glass *does not* have a periodic structure, and the best information that we can obtain about its structure is the radial distribution function which expresses the *probability* of finding another atom at a given distance from some arbitrary reference point.

2. *Energy-band structure*

The wave-like nature of the electron is invoked to describe its interaction with the atoms of a crystal by the Schrodinger equation. The periodic structure of the crystal facilitates the solution of this equation and it is found that there are certain states (wave-functions) in which the electron can propagate unhindered through the crystal structure, i.e. these states are capable of carrying an electric current. States of specifiable energy are available to an electron, but only in certain well-defined regions or bands of energy which are separated from each other by ' forbidden gaps '. This is called the energy-band structure of solids and the particular features of the band structure depend upon the geometry of the crystal. The wave-function characteristic of a particular allowed energy describes, in effect, the way in which an electron in such a state reacts to the regular distribution of atoms in the crystal lattice. At the very least, the non-periodic structure of a glass makes the mathematics much more difficult and it is not *a priori* obvious that it is still valid to talk of an energy-band structure. Appropriate wave-functions may still exist, but they will be very complex because they now have to express the way in which an electron reacts to a highly irregular structure.

From energy-band theory we can, in principle, obtain an explicit expression for the variation of the number of states with energy, $N(E)$. The function $N(E)\,\mathrm{d}E$ is the number of states in a range of energy E to $(E+\mathrm{d}E)$ and is known as the ' density-of-states ' function; in the forbidden gap of a crystal it is zero.

3. *Distribution of electrons*

The electrons are distributed amongst the allowed energy states according to the Fermi-Dirac distribution; the probability $F(E)$ that a state of energy E is occupied by an electron is given by

$$F(E)=\frac{1}{1+\exp\left[(E-E_{\mathrm{F}})/kT\right]}$$

where E_{F} is a constant known as the Fermi level or Fermi energy, k is Boltzmann's constant and T is the absolute temperature. In some conductors the energy states of interest are often such that $E>E_{\mathrm{F}}$ and the distribution is then, to a good approximation,

$$F(E)=\exp\left[-(E-E_{\mathrm{F}})/kT\right]$$

which is equivalent to the Maxwell–Boltzmann distribution of energies. There is no reason to suppose that the electrons in a glassy solid are not subject to the same laws, although, for reasons which will become apparent later, the approximation to the Maxwell–Boltzmann law may be valid less frequently. Knowing the Fermi level and the density-of-states we can calculate the number of electrons, $n(E)$, actually occupying states of a given energy:

$$n(E)=N(E)\,F(E).$$

4. *Transport of charge carriers*

So far the crystal structure is assumed to be perfectly periodic. Even in the best obtainable real crystals, however, there will always be some structural imperfections such as impurities, vacant lattice sites, dislocations, grain boundaries, and so on. The propagation of an electron, and hence the current, is then partly limited by collisions with—or scattering by (as it is called)—these imperfections. In a collision the electron is scattered from one well-defined state or wave-function into another. In a glass the difficulty is that the states between which scattering may occur are not so readily defined. Moreover, it is not easy to define just what constitutes an ' imperfection ' in the disordered structure of a glass. Quite apart from structural imperfections, however, the perfect periodicity of the crystal lattice is also disturbed by the thermal vibrations of atoms about their normal lattice sites and an electron may also be scattered by collisions with these thermal vibrations, or phonons. The various collision processes largely determine the temperature variation of the velocity of an electron in an applied field. To take full account of the collisions with phonons requires a knowledge of the vibrational spectrum of the crystal and the calculation of this is also facilitated by the periodic structure of the crystal. In a glass the vibrational spectrum is much more difficult to analyse, just as is the energy-band structure, because of the mathematical problems caused by the non-periodic structure. An analysis of the transport

processes leads to a prediction of the mobility of electrons in different energy states, i.e. $\mu(E)$. Thus we can, in principle, calculate the conductivity,

$$\sigma(E) = qn(E)\,\mu(E)$$

$$\sigma = q\int N(E)\,F(E)\,\mu(E)\,\mathrm{d}E$$

where q is the electronic charge. In a crystal of reasonable perfection the mobility of charge carriers is limited mainly by the scattering processes mentioned above; in a glass there are, as we shall discover, other limiting processes.

In the remainder of this article we shall consider steps (1), (2) and (4) in some detail, and (3) very briefly.

3. Glass—its formation and structure

It is not appropriate in this article to discuss the phenomenon of glass formation in any detail (see Turnbull (1969) for a more comprehensive discussion), but since the term ' glass ' or ' vitreous solid ' has come to be used rather broadly in recent years to describe any solid which is amorphous (and this use is particularly widespread in the present context) it is pertinent to say something about how a glass may be defined and about its structure. The structural pecularities of glass are of special importance in discussing electronic conduction. To what extent the other main feature of glass—viz. its departure from thermodynamic equilibrium—will affect electronic transport is not clear, but this aspect should nevertheless be kept in mind. Most of the information on this subject has been obtained from a study of the more familiar silicate glasses and certain simple organic glass-forming compounds like glycerol. The principles are generally applicable however. According to Jones (1956) the term ' glass ' *can* be given a precise scientific meaning:

> A ' glass ', or a substance in the glassy or vitreous state, is a material which has been formed by cooling from the normal liquid state and which has shown no discontinuous changes in first-order thermodynamic properties such as volume (V), heat content (H) and entropy (S) but had become rigid (i.e. solid) through a progressive increase in its viscosity. Discontinuities are observed, however, in derivative or second-order thermodynamic properties such as specific heat capacity and thermal expansivity.

The range of temperature over which second-order properties like specific heat capacity change from being typically ' liquid-like ' to typically ' solid-like ' is known as the transformation range, Tg. It is important to realize that Tg is not a precisely defined, unique temperature—rather it is a *range* of temperature. Furthermore, Tg depends upon the rate at which the liquid is cooled to form a glass. Fig. 2 illustrates the volume–temperature (V–T) relationship for glassy selenium (Dzhalilov and Rzaev 1967). If liquid selenium is allowed to crystallize normally there is a discontinuous change in volume at the freezing point, Tm (approximately 220 °C), and the dashed line is followed. It is not difficult, however, to inhibit crystallization by cooling quickly enough and therefore to supercool liquid selenium below its normal freezing point. On further cooling the supercooled liquid line is followed until, in the region of Tg,

the V–T slope gradually changes to become approximately parallel to the corresponding line for the crystal, and the selenium is then said to be in the glassy or vitreous state. The lower insert of fig. 2 illustrates how the thermal expansivity varies with temperature, showing the discontinuity in this property at Tg. The dashed line indicates the behaviour of the crystalline form of the material; thus, below Tg the glass and crystal have almost identical expansivities. The specific heat capacity would show the same type of behaviour.

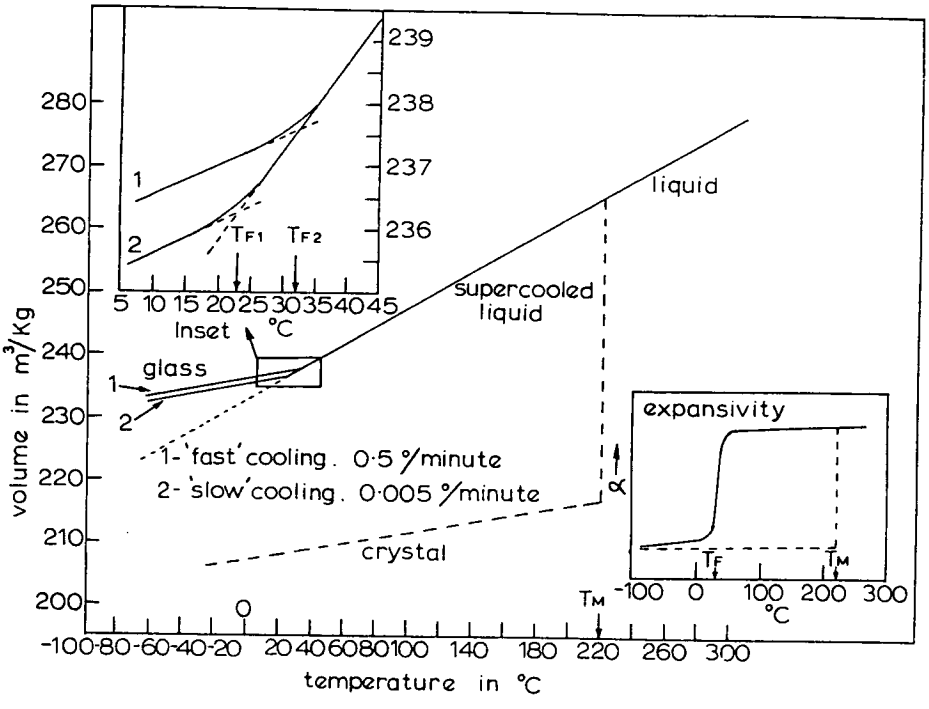

Fig. 2. The volume–temperature relationship of selenium at the liquid–crystal and liquid–glass transition. The upper insert shows in more detail the effect of different cooling rates on the glass transition and the lower one illustrates the discontinuity in the expansion coefficient (a second-order property). The data is taken from *Dzhalilov and Rzaev* (1967).

The vitreous state is therefore structurally continuous with the liquid state and glass has a structure that is essentially similar to that of a liquid.

There is a short-range order but no long-range order in a glass; i.e. the nearest-neighbour atoms of a given atom are arranged in much the same way as they would be in the corresponding crystal, but beyond the nearest-neighbour shell the arrangement becomes more and more disordered. The structure of a glass, or a liquid, is best described by the radial distribution function which gives the probability of finding another atom at a given distance from an arbitrary central atom. The radial distribution function for arsenic sulphide glass (As_2S_3) is shown in fig. 3 (*a*) (from Petz, Kruh and Amstutz 1961). Note that the first peak, representing the nearest-neighbours to the chosen central atom, is fairly well defined, but that the second, third and subsequent peaks gradually become blurred until they merge with the parabola $4\pi r^2\,dr$ which is characteristic of a random structure. A *completely* random structure would only be realized in a hypothetical perfect gas of point particles; the probability

of finding a second particle in a spherical shell of thickness dr at a radius r from a given particle is then given by the volume of the shell, viz. $4\pi r^2\,dr$. The local or nearest-neighbour order in a liquid or glass is *in part* a consequence of the finite size of real atoms as compared with the infinitesimal dimensions of the imaginary perfect gas atoms. For comparison fig. 3 (*b*) shows the radial distribution curve for liquid caesium. Note that as the

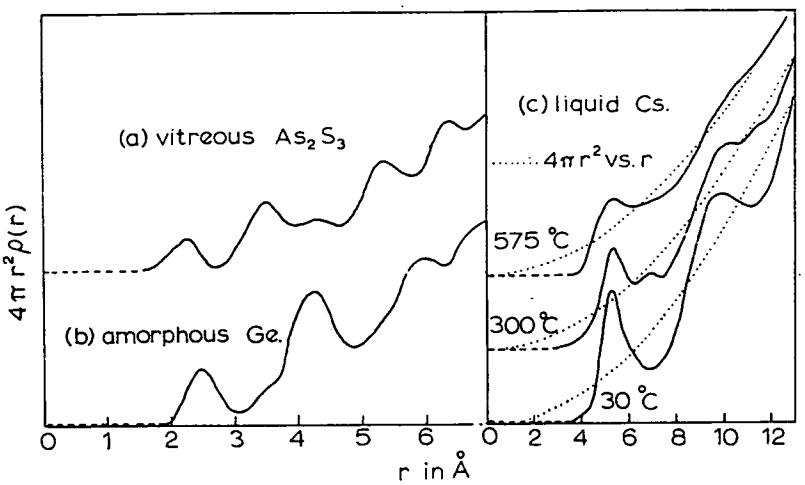

Fig. 3. Radial distribution curves for (*a*) vitreous arsenic sulphide, (*b*) amorphous germanium, and (*c*) liquid caesium at different temperatures. The dotted lines in (*c*) are parabolas for a completely random distribution.

temperature is lowered the distribution function tends to become more peaked—the configuration of the liquid changes although it is still disordered. The radial distribution function for crystalline caesium would consist of a series of vertical lines separated by distances corresponding to the interatomic spacings of the crystal. The remanent peaks in the distribution function for the liquid actually correspond closely to the expected positions of these lines showing that the local order is similar to the nearest-neighbour arrangement of the crystal (N.B.—this is not always the case, e.g. crystalline and liquid germanium have quite a different structure). The same is true of glass. Glassy arsenic sulphide, for instance, is built up of the same units—shallow triangular pyramids with an arsenic atom at the apex and three sulphur atoms at the corners of the base—as the crystalline material.

There is, however, one important difference in the significance of the radial distribution function for liquids and glasses. In a liquid the curve represents a ' time-average ' over a continuously fluctuating configuration. In a glass it represents a static distribution—a glass, it is said, has a ' frozen-in configuration '. The frozen-in configuration is characteristic of the liquid-structure at a temperature given by the intercept of the glassy and supercooled lines in, say, the volume–temperature diagram. The upper insert of fig. 2 shows the glass transformation region for selenium on an enlarged scale. For the curve labelled (1)—' fast ' cooling—the configuration frozen into the glass corresponds to the liquid structure at a temperature of 32 °C. This temperature is often called the ' fictive temperature ' T_F; at all temperatures below this the configuration

of the glass remains essentially unchanged. As also shown in fig. 2 the transformation range *Tg* and the fictive temperature depend upon the rate of cooling. For a ' slow ' cooling schedule the fictive temperature decreases and hence the volume, configuration and all other properties of the glass are sensitive to thermal history. The influence of thermal history on many properties is appreciable; the *ionic* conductivity of a silicate glass, for instance, can change by an order of magnitude. Glass is thermodynamically in an unstable state and, therefore, in or near the transformation range its properties are observably time-dependent as it strives to reach the more stable (metastable) supercooled liquid state. This as a process known in glass technology as ' stabilization '; at temperatures well below *Tg* the rate of stabilization is negligibly slow.

The fundamental reasons for these glass transformation phenomena are a matter of controversy (Gibbs 1960). It is possible to take a purely kinetic view of the process and say that, as the temperature of the supercooled liquid is lowered, so the viscosity increases until it becomes so large that *within experimental times* the configuration of the liquid can no longer readjust to its new (metastable) equilibrium state. The more slowly the liquid is cooled, the farther the supercooled liquid line can be followed, and the lower is *Tg* and the fictive temperature. Thus, below *Tg* we have a glassy solid. The only contribution to the temperature dependence of volume, for instance, comes from the thermal vibrations of the atoms. This is essentially the same as in the crystalline solid—the contribution from the changing configuration of the liquid has been ' frozen-out '—and the glassy and crystalline forms have therefore virtually the same expansion coefficients (and specific heats). (Fig. 2.)

The kinetic viewpoint does lead to some subtle difficulties, however, when we ask what would happen if the supercooled liquid could be cooled infinitely slowly. For instance, does the liquid change continuously to a crystalline state? The thermodynamic approach (Gibbs 1960) attributes the glass transition to an intrinsic second-order thermodynamic transition which is approached as the rate of cooling becomes infinitely slow.

Models of the atomic structure of glass are based upon the ideas expressed by Zachariasen (1932) in 1932. Zachariasen argued that since the strength of glass is of the same order as the strength of crystals, the atoms in glass must be linked by forces essentially the same as those in crystals. As in a crystal, therefore, the atoms in glass form an extended three-dimensional network, but as is shown by the absence of sharp x-ray diffraction spectra (Warren 1937) this network is not periodic. From the condition that the energy content should be comparable with that of the corresponding crystal it follows that the co-ordination number of an atom must be approximately the same as in the crystal. For instance, in the crystalline varieties of silica (SiO_2) and in the silicates, the silicon atom is invariably surrounded by four oxygen atoms forming SiO_4 tetrahedra; it is to be expected therefore, that fused silica and silicate glasses would also be built up of SiO_2 tetrahedra. Fig. 4 shows how a compound of stoichiometry M_2X_3 may form a crystal or a glass with a planar arrangement of MX_3 triangles in both cases, but the crystal having perfect regularity of structure and the glass a sufficient number of distorted bond angles and lengths to give a random effect which destroys the periodicity. Fig. 4 (*b*) could represent the structure of glassy arsenic sulphide (As_2S_3) and

arsenic selenide (As_2Se_3) although it is likely, in these cases, that there is a more uniform distribution of ring sizes. Zachariasen's general ideas on glass structure were amply confirmed by the detailed x-ray studies by Warren and his co-workers; the Warren–Zachariasen picture is usually referred to as the ' random-network ' theory of glasses.

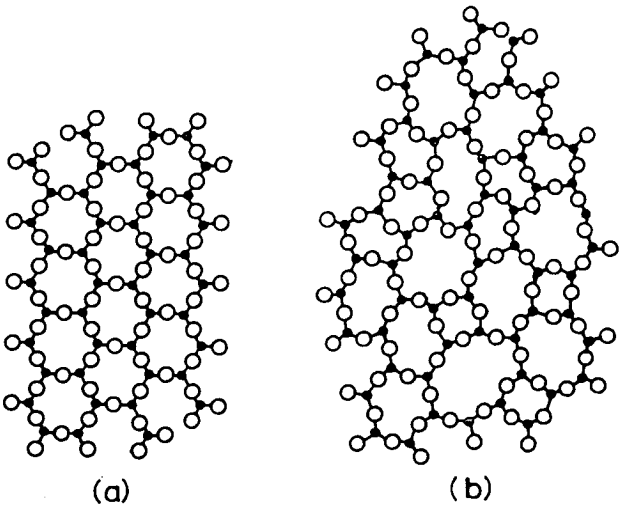

Fig. 4. A two-dimensional representation of the structure of a hypothetical compound M_2X_3 in (*a*) a crystalline form and (*b*) a glassy form.

Although the ideas originally proposed by Zachariasen still form the basis for our present views on glass structure, the random–network theory is probably best regarded nowadays as no more than a good first approximation. Various detailed aspects of the model are subject to criticism. Perhaps the first is the belief that an extended three-dimensional network must be present if a compound is to form a glass. Glasses have been found in oxide systems where no three-dimensional network is possible, e.g. silicates near the orthosilicate composition and many very stable non-oxide glasses, such as some of the chalcogenides and even selenium itself, cannot satisfy the three-dimensional network criterion.

Recent investigations have shown that certain glasses may develop a granular non-crystalline ' structure ' with dimensions in the range ten to a few hundred angstroms (1–10 nm). These regions are not separated by observable boundary surfaces and sometimes they do not alter appreciably with heat treatment. The granular structure has in some cases been interpreted as evidence of pre-crystalline nuclei which make up a major part of the glass volume, the implication being that *homogeneous* nucleation is possible on a very fine scale in some glasses. Possibly connected with this is the well-established effect in several multicomponent glasses of metastable separation into two liquids following a thermal treatment. This process is responsible for the formation of highly dispersed droplike regions, generally smaller than 1 micron, in glass. Among some glasses showing this kind of metastable phase separation it is perhaps possible to prepare samples representing any stage in a transition, from a true solution through increasing degrees of composition fluctuation to the phase-separated stage. There is indeed a school of thought which would regard

almost any glass of two or more components, even in the absence of metastable phase-separation, as inherently inhomogeneous on a submicroscopic scale because of ' spinodal ' decomposition. This is probably an extreme point of view. Nevertheless it is clear that materials in various ' precrystalline ' stages are also glasses, and the detailed structure is therefore a property which, like all others, depends on thermal history.

In the sense discussed above a glass is a well-defined substance. It is a partially ordered material in which the degree of ordering, and hence other properties, depends upon thermal history. In principle the degree of ordering could be specified by an ' ordering parameter ' such as the fictive temperature T_F. A complete specification may actually require more than one ordering parameter, but in principle this could also be done.

The status of various amorphous thin films produced by techniques such as evaporation, sputtering and deposition from a glow discharge is usually not definable in the same way although they are often referred to nowadays as ' glasses '. The use of the term is justified by, for example, the argument that some of the properties of thin films of SiO_2 deposited by sputtering are very similar to the properties of fused silica (SiO_2) prepared by cooling molten silica. But this ignores the fact that the properties of a ' glass ' are not uniquely defined unless its thermal history, particularly in the transformation range, is known. With what ' state ' of a glass, therefore, is the comparison to be made? The difficulty could be resolved if, on heating, the amorphous films showed typical transformation range phenomena on the transition to the liquid state. Unfortunately many of the amorphous materials produced as thin-films crystallize long before this can happen. Transformation range behaviour has been observed, however, in some of the amorphous alloys produced, as mentioned earlier, by ' splat-cooling ' techniques and they are clearly glasses in the generally accepted sense.

In Part II we shall be mainly interested in electronic conduction in materials which are ' glasses ' within the usual definition, but as mentioned earlier it is the *disordered* structure of glass which will be of most concern and consequently the generalizations which follow are relevant to all amorphous solids. In the present context, therefore, the question of any distinction between amorphous films and glasses is perhaps largely semantic and for convenience the terms will be used interchangeably. It is nevertheless of importance and in different circumstances it may be preferable to use the term ' amorphous ' to describe any non-crystalline solid and reserve the term ' glass ' or ' vitreous ' solid for a material which has a specifiable relationship to the liquid state.

4. Electron energy-bands in crystalline solids and glasses

The theory of electron energy-bands in crystals has reached a degree of sophistication such that fine details of the band structure arising from particular three-dimensional symmetries in a crystal can, in some cases, be calculated. For disordered solids and liquids no such precision is possible. Three-dimensional calculations have been made, but they involve difficult mathematical techniques. We shall develop therefore a simple one-dimensional model into which ' disorder ' can be introduced relatively easily. This is a simplification, of course, but just as it predicts the general features of electron bands for a

crystal (in which case it is known as the Kronig–Penney model), so for the disordered case does it lead to the essential features necessary for interpretation of most current experimental data.

The methods used here follow the theoretical treatments of Roberts and Makinson (1962) and Borland (1963). There is, however, one modification; in the present model, positive instead of negative potential barriers are used to represent atoms.

The energy-band structure of electrons in solids is derived by invoking the wave-like behaviour of electrons embodied in the Schrodinger equation. For motion in one dimension this equation reads:

$$\frac{\mathrm{d}^2\psi}{\mathrm{d}x^2} + \frac{2m}{\hbar^2}\psi(E - V) = 0. \tag{1}$$

The wave-function ψ represents the wave motion of an electron of mass m and energy E moving in a potential V; $\hbar = (h/2\pi)$ where h in Planck's constant. An analogous equation holds in three dimensions and it is this which has to be solved, subject, of course, to appropriate boundary conditions. The potential V is a function of distance x ($V = V(x)$) and would, for a crystalline solid, represent the periodic-potential due to the atoms of the crystal through which the electron moves, so that in one dimension,

$$V(x) = V(x + a) \tag{2}$$

where a is the lattice spacing. It is this periodicity of potential which makes the mathematics reasonably tractable because an important general theorem—Bloch's theorem—states that where V is represented by periodic functions of this type in the Schrodinger equation, the solutions are of the form

$$\psi(x) = u_k(x)\, \mathrm{e}^{ikx} \quad \text{with} \quad u_k(x) = u_k(x + a). \tag{3}$$

These are known as ' Bloch functions ' and the wave-function for an electron is, therefore, a travelling wave, amplitude-modulated by a function u_k which has the same periodicity as the lattice. The parameter k is a propagation wave-vector which characterizes a particular ' Bloch wave '; it is often called simply the wave-number and it is related to the momentum of the electron. For some point x', given by $x = (x' + a)$, we can write

$$\psi(x) = u_k(x' + a)\, \mathrm{e}^{ik(x'+a)} = u_k(x')\, \mathrm{e}^{ikx'}\, \mathrm{e}^{ika}$$

whence

$$\psi(x) = \psi(x')\, \mathrm{e}^{ika} = \psi(x - a)\, \mathrm{e}^{ika}. \tag{4}$$

The essential features of the band theory of solids can be deduced from these relationships and a simple one-dimensional model. For a *crystal* imagine that we have (fig. 5 (*a*)) a one-dimensional ' lattice ' of atoms with a regular spacing a, and that the potential at each atom can be represented by a rectangular potential barrier of height V and width b (fig. 5 (*b*)). For our purposes this can be simplified a stage further by making the barriers infinitely thin ($b \to 0$) and infinitely high ($V \to \infty$) but in such a way that the product Vb remains finite (fig. 5 (*c*)). Mathematically the barriers are then said to have the form of δ-functions. Schrodinger's equation for the δ-barrier model reduces to

$$\frac{\mathrm{d}^2\psi}{\mathrm{d}x^2} + \alpha^2 = 0 \quad \text{with} \quad \alpha = \left(\frac{2mE}{\hbar^2}\right)^{1/2} \tag{5}$$

since $V=0$ except in the infinitely thin barriers. For a *glass* or similar disordered material, the appropriate one-dimensional model would be as shown in fig. 6 (*a*) where the interatomic spacings fluctuate about the mean spacing a and the δ-barriers are also, therefore, irregularly spaced (fig. 6 (*b*)).

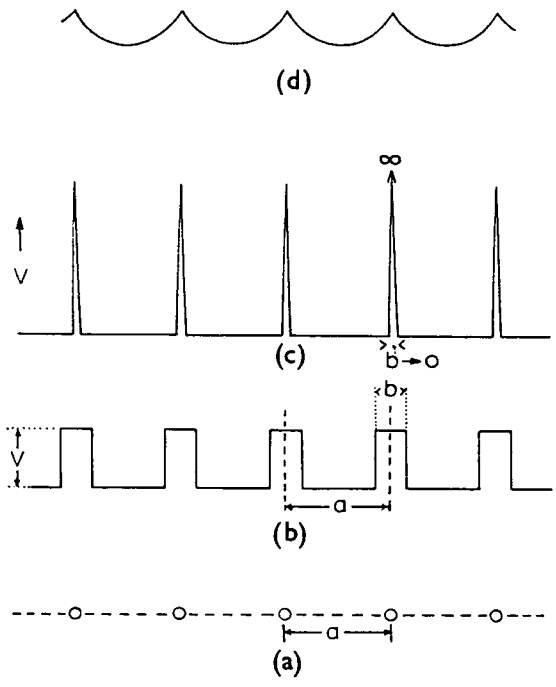

Fig. 5. (*a*) A regular (crystalline) one-dimensional array of atoms with spacing 'a'. (*b*) Potentials of atoms in (*a*) approximated by rectangular barriers of width 'b' and height V. (*c*) Rectangular potential barriers approximated further by δ-barriers, $b\to 0$ and $V\to\infty$. (*d*) Possible form of the wave-function in a one-dimensional crystal of δ-barriers.

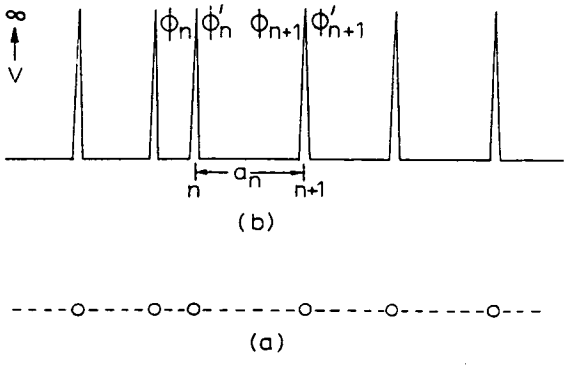

Fig. 6. (*a*) A disordered (glassy) one-dimensional array of atoms. (*b*) Corresponding δ-barrier model.

In our wave mechanical representation the problem of an electron in these one-dimensional δ-barrier models reduces to one of investigating the effects of the barriers on the wave-function. If the function ψ is to represent an electron

propagating in some way through the lattice then it is physically reasonable to suppose that ψ is continuous; in particular, at each δ-barrier

$$\psi+ = \psi- \tag{6}$$

where $\psi+$ and $\psi-$ refer to the values of ψ immediately to the right and left of a particular barrier. The barriers will, however, change the slope of ψ and this can be seen most easily by integrating eqn. (1) across a barrier of width b and taking the limit $b \to 0$, $V \to \infty$, (Vb) finite, $E \ll V$:

$$\frac{d\psi_+}{dx} - \frac{d\psi_-}{dx} = \frac{-2m(E-V)\psi b}{\hbar^2} \to 2Q\psi \quad \text{with} \quad Q = \frac{mVb}{\hbar^2}. \tag{7}$$

The constant Q may be regarded as a measure of the ' strength ' of a barrier. Mathematically the limiting form (fig. 5 (*c*)) of the potential barriers may be represented by the condition (7) and this discontinuity of slope implies that the wave-functions in a crystalline solid represented by the δ-barrier model have the scalloped form illustrated in fig. 5 (*d*). Eqns. (6) and (7) are also, in effect, boundary conditions for the Schrodinger equation, and since this is a second-order differential equation they are sufficient for its solution.

The change of slope predicted by eqn. (7) will also have other consequences; a δ-barrier will in general also cause a change in wavelength, phase and amplitude of ψ. In the absence of a δ-barrier we could represent an electron wave travelling from right to left by $\psi = A \cos(\alpha x + \xi)$ for example. If there is a barrier at $x = 0$, however, the slope will increase or decrease according to eqn. (7) and this will have the effect of making the node (zero) in ψ occur at P' instead of P, say (fig. 7). If succeeding barriers are irregularly spaced

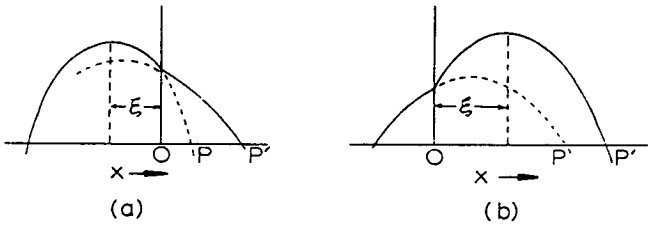

Fig. 7. The effect of a δ-barrier at $x=0$ on a cosine wave-function; (*a*) when a maximum in the wave-function is on the left of the barrier and (*b*) when it is on the right.

(as in our model of a glass) but the *minimum* separation a is greater than the half-wavelength (π/α) of the electron wave, then the δ-barriers have the effect of ' pulling ' the local or effective half-wavelength (the node separation) closer to their own spacing. If the δ-barriers are weak (Q in eqn. (7) is small) the ' pull ' ΔP obtained by applying conditions (5) and (6) is

$$\Delta P \simeq \frac{2Q}{\alpha} \cos^2 \xi. \tag{8}$$

This is greatest when the δ-function occurs at the peak of ψ (i.e. $\xi = 0$) and falls off on either side. The amplitude also changes:

$$\frac{A'^2}{A^2} = 1 - \frac{4Q}{\alpha} \cos^2 \xi \left(\tan \xi - \frac{Q}{\alpha} \right), \tag{9}$$

so that the amplitude decreases when the δ-function is on the right (ξ positive, fig. 7 (*a*)) and increases when it is on the left (ξ negative, fig. 7 (*b*)).

Crystalline solid

It is not necessary to obtain complete solutions for ψ from the Schrodinger equation but only to investigate under what conditions physically meaningful solutions can be obtained. Because of the periodicity in a crystal we can restrict our attention to two ' cells ' on either side of a barrier at $x=a$, say. The general solution of eqn. (5) in the cell $0 \leqq x \leqq a$ may be written

$$\psi - = A\, e^{i\alpha x} + B\, e^{-i\alpha x},$$

and in the cell $a < x \leqq 2a$, making use of eqn. (4),

$$\psi + = e^{ika}[A\, e^{i\alpha(x-a)} + B\, e^{-i\alpha(x-a)}].$$

Applying the two boundary conditions (6) and (7) provides two equations for the arbitrary constants A and B, and apart from the trivial case $A=B=0$ these two equations are consistent only if, on eliminating A and B,

$$\cos(\alpha a) + \left(\frac{Q}{\alpha}\right)\sin(\alpha a) = \cos(ka). \tag{10}$$

The left-hand side of this equation can be put into slightly more convenient forms:

$$\sqrt{\left[1 + \left(\frac{Q}{\alpha}\right)^2\right]} \cdot \cos(\alpha a - \eta) = \cos(ka) \tag{11 a}$$

or

$$\frac{\cos(\alpha a - \eta)}{\cos \eta} = \cos(ka) \tag{11 b}$$

where the ' phase factor ' η is defined by $\eta = \tan^{-1}(Q/\alpha)$. Eqns. (10) and (11), it should be remembered, state a condition which must be satisfied for solutions to the Schrodinger equation in the δ-barrier model; they are not themselves solutions. The right-hand side of eqn. (11) is a constant and has the limiting values ± 1, and hence *real* solutions to the δ-barrier model can occur only when the *left-hand side* also has values between ± 1. From eqns. (11 *a*) or (11 *b*) we can see that this will occur when the electron energy α is such that

$$2 \tan^{-1}\left(\frac{Q}{\alpha}\right) \leqq \alpha a \leqq \pi \quad \text{— ALLOWED BANDS.} \tag{12}$$

This condition corresponds, therefore, to allowed bands of electron energy. If the left-hand side of eqn. (11) exceeds 1 in *magnitude* then this would correspond to imaginary, and hence physically unacceptable, solutions to the Schrodinger equation. This will occur if the electron energy α satisfies the inequality.

$$\pi \leqq \alpha a \leqq \pi + 2 \tan^{-1}\left(\frac{Q}{\alpha}\right) \quad \text{— FORBIDDEN GAPS} \tag{13}$$

and this corresponds to regions of unallowed energy, or forbidden gaps, in the energy-band structure. The left-hand side of eqn. (11 *a*) is plotted as a function of electron energy (αa) in fig. 8 (*a*) and the allowed bands occur when this curve lies between ± 1, as illustrated. At low energies the bands are

narrow and the gaps wide, but as the energy increases the bandwidth increases and the forbidden gaps decrease. These trends also follow, of course, from the conditions (12) and (13). Electrons in the allowed bands can be represented by Bloch-type functions and can, therefore, propagate essentially unhindered through the one-dimensional lattice.

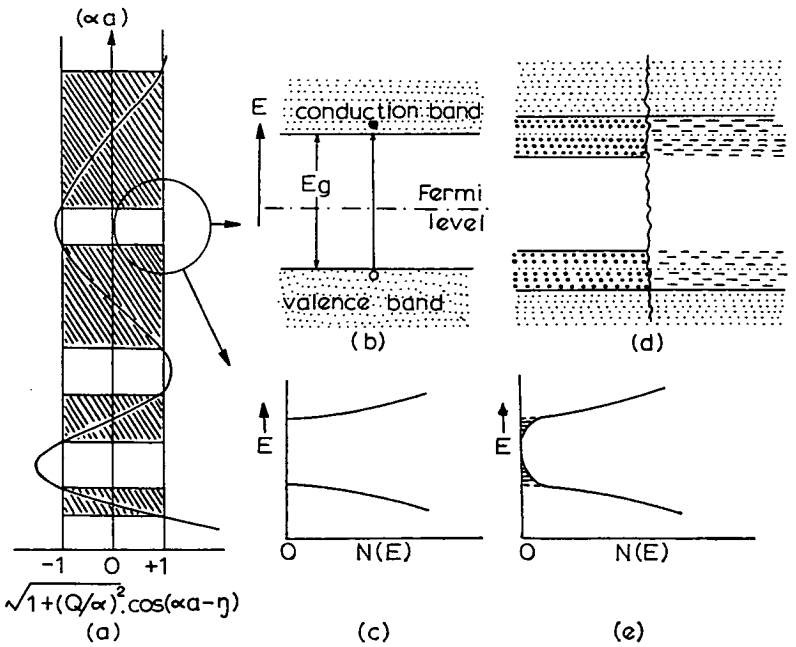

Fig. 8. (*a*) A plot of $\sqrt{[1+(Q/\alpha)^2]} \cdot \cos(\alpha a - \eta)$ as a function of electron energy (αa)— the formation of allowed (hatched) and forbidden energy-bands. (*b*) Simple band diagram for an intrinsic crystalline semiconductor. (*c*) The corresponding density-of-states function. (*d*) In a disordered (glassy) solid the band-edges of (*b*) are displaced into the forbidden gap. States on both sides of the original band-edge are localized, as illustrated schematically in the right-hand part of (*d*). (*e*) The density-of-states (schematic) corresponding to (*d*). The localized states are shown shaded.

Fig. 8 (*b*) illustrates the simplified form of the band scheme usually used in discussing semiconductors. We are only interested in the uppermost full band—the valence band (V.B.)—and the next highest empty band—the conduction band (C.B.)—separated by the forbidden gap of width E_g. At the absolute zero of temperature the Fermi level (F.L.) will normally lie roughly midway in the gap so that the V.B. is full and the C.B. is empty. Conduction depends, therefore, on electrons being ' activated ' across the energy gap E_g into the C.B., leaving positively charged holes in the V.B. Both negative electrons and positive holes may take part in the conduction of electricity. In diagrams like 8 (*b*) the horizontal axis represents a spatial coordinate in the crystal, and drawn in this way as a continuous line implies that electrons or holes in the allowed bands may, other things being equal, propagate freely through the crystal.

The bands of allowed energy do not have a uniform distribution of states, and from results which we have derived it is an easy matter to show that near

the edge of the conduction band (E_c), for example, the distribution is parabolic in energy.

For a one-dimensional crystal of length L the Bloch theorem implies that $\exp[i\alpha(x+L)] = \exp(i\alpha x)$, and this can only be true if $\alpha = (2\pi/L)n$ where n is a positive or negative integer. For a three-dimensional crystal similar conditions hold in each coordinate of α-space, α_x, α_y, α_z. Thus α-space is divided into cubes of volume $(8\pi^3/L^3)$, each contributing one allowed wave-number and hence one energy state. In a crystal of volume L^3, therefore, a sphere of radius α can contain $(L^3\alpha^3)/(6\pi^2)$ states and the density of allowed states is $(\alpha^3)/(6\pi^2)$. Substituting for α from eqn. (5) we obtain, on differentiating, the density of allowed electron states in the region of energy E to $(E + \mathrm{d}E)$, remembering that by the Pauli principle each state can hold two electrons:

$$N(E)\,\mathrm{d}E = \frac{4\pi}{\hbar^3}(2m)^{3/2}E^{1/2}\,\mathrm{d}E.$$

Or, if the zero of energy is measured from the bottom of the conduction band, E_c:

$$N(E)\,\mathrm{d}E = \frac{4\pi}{\hbar^3}(2m)^{3/2}(E - E_c)^{1/2}\,\mathrm{d}E. \tag{14}$$

This is the density-of-states function and is illustrated in fig. 8 (*c*).

Glassy solid

The δ-barriers are now irregularly spaced, as in fig. 6, and we can no longer make use of the properties of Bloch-functions. Our first concern, however, is to investigate whether or not forbidden gaps may still exist in the disordered material and it can be shown fairly easily, in this one-dimensional model, that they will.

Suppose the disorder is such that the inter-barrier spacing can have any value between the limits a and $a + \Delta a$. We have already seen that the barriers have the effect of increasing the wavelength (fig. 7), and if $a > (\pi/\alpha)$ they will tend to pull the effective wavelength closer to their own mean spacing. This would imply a synchronization of ψ to the lattice spacings, and if this persisted over a range of energies this range would correspond to a forbidden gap. That a gap exists can be shown with slightly more rigour by counting the nodes of ψ. Suppose, for example, we require the wave-functions to satisfy the boundary condition $\psi = 0$ at the ends of the chain. It is well known that the nth stationary-state wave-function for any one-dimensional problem with discrete energy levels—e.g. the harmonic oscillator, electron in a box, *or* the vibrating string or resonant cavity—has exactly $(n-1)$ nodes inside the relevant domain of x. Energies over which the number of nodes remains unchanged are ' not allowed '; the discrete allowed-levels correspond to the appearance of new nodes. Thus if we can count the number of nodes of ψ as a function of energy, a range of energy over which no new nodes occurs is a forbidden gap. To do this it is convenient to introduce a phase $\phi = \phi(\alpha, x)$—a function of energy and distance—such that

$$\tan\phi = -\left(\frac{\mathrm{d}\psi}{\mathrm{d}x}\right)\frac{1}{\alpha\psi}. \tag{15}$$

If $\psi = \cos(\alpha x + \xi)$ then ϕ defined in this way is a linear function of x and it coincides, except for an additive constant, to the phase as usually defined. For $\alpha > 0$ the value of ϕ is fixed for certain values of x; it is $(n - \frac{1}{2})\pi$ at the nth node of ψ and $n\pi$ at the next node of $(\mathrm{d}\psi/\mathrm{d}x)$. Thus, if the ' phase ' of ψ increases by $\Delta\phi$ in a given range of x the number of nodes in this range increases by $(\Delta\phi/\pi)$. The function ϕ combines, therefore, the effect of the δ-barriers and distance x, and the problem of counting the number of nodes is equivalent to calculating the total phase increase in the chain. Consider, for example, the nth and $(n+1)$th barriers (fig. 6 (a)) separated by a distance a_n, and denote the phases to the left and right of the barriers by ϕ and ϕ' respectively. In the region *between* the potentials ψ has the form $A\cos(\alpha x + \xi)$ and our definition of ϕ means that in going from the left of barrier n to the right of barrier $(n+1)$, ϕ increases by αa_n:

$$\phi_{n+1} = \phi'_n + \alpha a_n. \tag{16}$$

The phase change across the barrier is obtained from eqn. (15) using conditions (6) and (7):

$$\phi'_n = \tan^{-1}\left(\tan\phi_n - \frac{2Q}{\alpha}\right), \tag{17}$$

so that from one barrier to another the ϕ's are related by

$$\phi_{n+1} = \tan^{-1}\left(\tan\phi_n - \frac{2Q}{\alpha}\right) + \alpha a_n. \tag{18}$$

Referring to the condition (13) for forbidden gaps in a *crystal* we can now show that in the one-dimensional disordered *glass*, with interatomic spacings fluctuating between a and $(a + \Delta a)$, an energy gap exists for a range of energy x which satisfies the inequality:

$$\pi \leqq \alpha a \leqq \pi + 2\tan^{-1}(Q/\alpha) - \alpha\Delta a. \tag{19}$$

Suppose there is an integer m for which the phase ϕ_n on the left of barrier n lies in the interval

$$m\pi - \tfrac{1}{2}\pi \leqq \phi_n \leqq m\pi + \tan^{-1}(Q/\alpha). \tag{20}$$

Applying (17) to the extremes of this interval shows that on the right of the barrier ϕ'_n is in the interval

$$m\pi - \tfrac{1}{2}\pi \leqq \phi'_n \leqq m\pi - \tan^{-1}(Q/\alpha).$$

Between the barriers at n and $(n+1)$ the phase then increases by an amount less than $\alpha(a + \Delta a)$, but greater than αa, so that ϕ_{n+1} is in the interval

$$m\pi - \tfrac{1}{2}\pi + \alpha a \leqq \phi_{n+1} \leqq m\pi - \tan^{-1}(Q/\alpha) + \alpha(a + \Delta a).$$

Using the inequality (19) gives

$$(m+1)\pi - \tfrac{1}{2}\pi \leqq \phi_{n+1} < (m+1)\pi + \tan^{-1}\left(\frac{Q}{\alpha}\right).$$

Thus if for any value of n the phase ϕ_n is in the interval (20), then all subsequent phases are bound within similar intervals. The average phase increase is π per atom; there is, therefore, only one node per atom for the range of energies satisfying eqn. (19) and this range is a forbidden gap. Thus, provided $(\Delta a/a)$ is not too large, forbidden gaps will still exist in the ' one-dimensional glass '.

It is difficult to extend these arguments to three dimensions where, apart from the increased mathematical complexity there may also be orientational disorder as well as the spatial disorder which we have considered in one dimension. Experimental observations do suggest, however, that this result is qualitatively valid in real glasses, but compared with a crystal of the same *mean* spacing the gaps will become narrower, as suggested on the left of fig. 8 (*d*). The penetration into the originally forbidden gap will depend upon the magnitude of the fluctuations Δa, and since large positive fluctuations will become increasingly less likely we can expect the density of states in the disordered solid to decrease roughly exponentially into the gap producing the so-called ' tail-of-states '. This is illustrated in fig. 8 (*e*) in which the position of the original density-of-states curve is shown by the dotted line. If the fluctuations Δa are large these exponential tails may extend right across the gap and overlap.

Localization

Our arguments so far have been concerned, in effect, with the consequences of disorder on the density of states, but the lack of periodicity may also destroy the Bloch-function form of the electronic wave-functions, i.e. their property of propagating freely through the lattice. We can investigate the nature of the wave-functions conveniently by returning to the situation in a crystalline solid which has just one defect, e.g. one cell of greater width. In the perfectly periodic chain all the spacings a_n are equal to a, say, and there will be an equilibrium phase of ϕ which does not vary with n because the wave-function is synchronized or ' locked-in ' to the lattice. Denote this equilibrium phase by θ, so that according to (18) θ satisfies the equation:

$$\tan(\theta - \alpha a) = \tan\theta - \frac{2Q}{\alpha}.$$

This is a quadratic in $\tan\theta$ and has solutions

$$\tan\theta_{\pm} = \frac{Q}{\alpha} \pm \frac{\sqrt{(K^2-1)}}{\sin \alpha a} \tag{21}$$

in which

$$\frac{Q}{\alpha}\sin(\alpha a) + \cos(\alpha a) = K. \tag{22}$$

The phases are real if $|K| \geqq 1$ and the corresponding energy interval will be an energy gap. This condition and eqn. (22) is, of course, identical with eqns. (10) and (11) and the conclusions we reached from these. For the periodic chain the right-hand side of eqn. (18) depends on ϕ in the way illustrated in fig. 9, in which the vertical axis represents the net change in ϕ. When this is positive the electron wavelength is being ' pulled ' into coincidence with the lattice spacing; when it is negative the wavelength is ' drifting ' away. The two effects are represented by the arrows in fig. 9. Thus, ϕ_- is a point of stable equilibrium since the net change is directed towards θ_- from either side of it; θ_+, however, is a point of unstable equilibrium. If ϕ_1, say, is such that $\theta_- \leqq \phi_1 \leqq \theta_+$, successive ϕ's decrease monotonically to the limit θ_-; if $-\pi/2 \leqq \phi_1 < \theta_+$ they monotonically increase to θ_-. In terms of ϕ this implies one node per ' cell ' or perfect synchronization of the wave-function with the

lattice spacing and hence an energy gap. If, however, $\theta_{\mp} < \phi_1 < \pi/2$, ϕ_n first increases to $\pi/2$ until ϕ_m, say, is so close to $\pi/2$ that ϕ_{m+1} jumps into the interval $(-\pi/2, \theta_-)$ and, further, ϕ_n again tend to θ_-. Hence in the mth cell there will be no node in the wave-function; there will be a ' node-jump '. Instead of phase we can, however, discuss this node jump in terms of energies

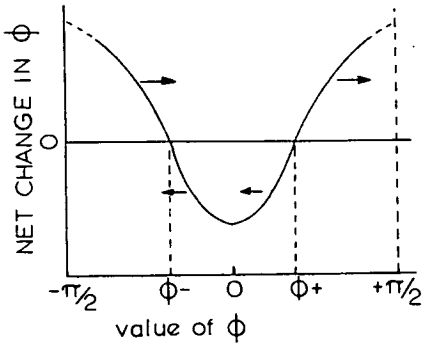

Fig. 9. The ' pull ' (positive) and ' drift ' (negative) of the phase ϕ in a regular chain of atoms, as a function of ϕ. (*Adapted from Roberts and Makinson* (1962).)

by keeping ϕ fixed at ϕ_1, say. Eqn. (22) implies that the energy gap occupies an interval $(\pi/a) < \alpha < \alpha_c$ (α_c is some critical energy) and at these points θ_+ has the values:

$$\theta_{\mp}(\alpha_c) = \tan^{-1}\left(\frac{Q}{\alpha}\right), \quad \theta_{\mp}\left(\frac{\pi}{a}\right) = \frac{\pi}{2}.$$

Thus, it is always possible to pick ϕ_1 and energies E_1, E_2 *in the forbidden gap* such that

$$\theta_{\mp}(E_1) < \phi_1 < \theta_{\mp}(E_2), \quad E_2 > E_1.$$

A node jump then occurs at E_2 but not at E_1, i.e. at E_1 there is an extra node in the wave-function and there is an allowed level in the forbidden gap. Now consider an otherwise perfect chain with one larger cell, say, $a_m = a(1+f)$, $(0 < f < 2)$. If m is sufficiently large, then according to our previous discussion $\phi_m = \theta_-$, but from (16) and (17)

$$\phi_{m+1} = \theta_- + \alpha a f.$$

If $\alpha a f > (\theta_+ - \theta_-)$, ϕ_{m+1} lies in the unstable interval $(\theta_+, \pi/2)$ and consequently a node jump will occur giving rise, as mentioned above, to an allowed level in the forbidden gap. We can estimate the form of the wave-function for this allowed state as follows. To the left of the defect the phase is in the vicinity of θ_- and $(-Q/\alpha) < \tan^{-1}\theta_- < -\infty$. From (9), therefore, the ratio of amplitudes in successive cells $(A^2_{n+1}/A^2_n) > 1$ and the wave-function is increasing roughly exponentially. On the right the phase is in the vicinity of θ_+ with $(Q/\alpha) < \tan^{-1}\theta_+ < \infty$, so that $(A^2_{n+1}/A^2_n) < 1$ and the wave-function decreases exponentially. This means that, in contrast to the Bloch-states, the probability of finding an electron in a ' defect ' state falls off roughly exponentially with distance from the defect, as illustrated schematically in Fig. 10. The single defect at a_m in fig. 10 is, in a sense, a localized disorder and in a crystal

the state at a_m would be called an ' impurity state '. In a uniformly disordered chain, points such as a_m may appear at any point with equal probability and a distribution of localized states results. The tail-of-states discussed in the previous section which are caused by the disorder have this localized character. On the right of fig. 8 (*d*) they are, therefore, indicated by short horizontal lines to emphasize their localized property as compared with the non-localization of the Bloch states. In the density-of-states diagram (fig. 8 (*e*)) the localized tail of states is shown shaded. Mott and Davis (1968) have argued that there will be a sharp boundary between the localized states and the non-localized Bloch-type states characteristic of the allowed energy-bands in ordinary semiconductors. Since these localized states have lower energies than the band states, carriers will tend to fall into them and become ' trapped '; the trapped carriers then cannot take part in conduction unless activated (thermally or optically) into the band states or unless they hop directly to neighbouring localized states.

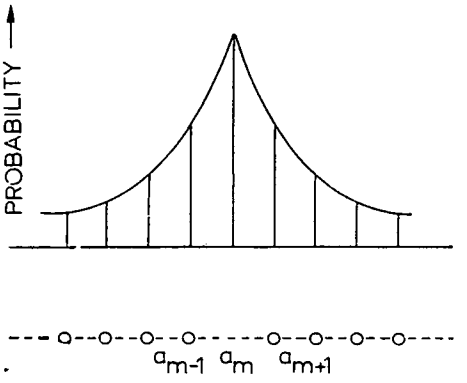

Fig. 10. Exponentially decreasing probability of an electron at a defect—an atom missing at a_m.

5. Distribution of electrons

As mentioned in the introduction there is no reason to suppose that the distribution of carriers among the allowed states of a glassy semiconductor is not governed by the Fermi–Dirac function just as in a crystalline solid. In a crystalline semiconductor, the Fermi level is often removed from any allowed states by energies several times kT and it is usually possible therefore to use the classical approximation. The presence of the tail-of-states going into the previously forbidden gap may, however, invalidate this procedure particularly as, in principle, there is no reason why the tail should not penetrate right into the middle of the gap.

6. Transport

Transport in the non-localized states (bands)

Just as in crystalline semiconductors there is the possibility that electrons (or holes) will be thermally or optically activated into the bands of non-localized levels, above some critical energy, in which they can drift in an applied electric field. In these states the carriers in a glassy semiconductor will be subject to the same collision (scattering) and trapping processes as in a crystal, but there

will be at least one important additional scattering mechanism resulting from the disappearance of strict periodicity in the lattice. This will decrease the mean-free-path and mobility of the carrier and hence increase the resistance. It is difficult to estimate by how much the mean-free-path will be reduced, but in mercury—in which the ' disorder ' scattering might be expected to contribute more effectively than in a high melting-point metal—the resistance increases on melting by four times. This compares with a value of just over two predicted on the basis of an increase in phonon (thermal) scattering only, the difference presumably being due mainly to scattering induced by the disorder.

To take account of scattering processes we introduce the mean-free-time between collision, the *relaxation time*, τ. In a field E the accelerating force on an electron is qE (q = electronic charge) and in τ seconds it will acquire a drift velocity v which balances that force:

$$\frac{vm}{\tau} = qE$$

where m is the mass of the electron. The mobility $\mu = (v/E)$, and hence the mobility of electrons in these normal band states is

$$\mu_0 = \frac{q\tau}{m} \tag{23}$$

We can estimate a *lower* limit for μ_0 as follows. The relaxation time $\tau = (L/v)$ where L is the mean-free-path and v the thermal velocity of an electron. The free electrons can be regarded as particles in a perfect gas and the mean thermal velocity at room temperature is, from the Maxwell–Boltzmann distribution, approximately 10^{-1} m s^{-1}. Since we are talking about the propagation of an electron wave, the mean-free-path L, to be meaningful, must be at least equal to the de Broglie wavelength of an electron of momentum mv, i.e. $L > (h/mv)$, which gives $L \geqq 50$ Å (note that this is at least an order of magnitude greater than interatomic distances which typically are ~ 3 Å). From eqn. (23), therefore

$$\mu_0 \geqq 10^{-2} \text{ m}^2 \text{ V}^{-1} \text{ s}^{-1}. \tag{24}$$

Trapping and trap-limited mobilities

In a disordered semiconductor the large density of localized states or traps will probably have an overriding influence and we should picture the transport of carriers proceeding via many trapping events (capture and thermal release) with, perhaps, transport in a band in between.

For simplicity, suppose that there is a discrete level of traps of density N_t at energy U below the conduction band. The effective mobility will be

$$\mu_{\text{eff}} = \mu_0 f$$

where f is the fraction of time that the carriers are free, and this is related to the densities n_0 and n_t of free and trapped electrons respectively, i.e.

$$f = n_0/(n_0 + n_t).$$

If the trapped and free electrons are in thermal equilibrium, then

$$\frac{n_t}{n_0} = \frac{N_t}{N_C} \exp\left(\frac{U}{kT}\right)$$

where N_C is the density of states in the conduction band. These equations lead to

$$\mu_{eff} = \mu_0 \left[1 + \frac{N_t}{N_C} \exp\left(\frac{U}{kT}\right) \right]^{-1}$$

and at high temperatures $\mu_{eff} \approx \mu_0$. At low temperatures, however,

$$\mu_{eff} \approx \mu_0 \frac{N_C}{N_t} \exp\left(-\frac{U}{kT}\right). \tag{25}$$

A trap density, N_t, of 10^{22} m^{-3} or higher is quite probable and N_C in a typical *crystalline* semiconductor is 10^{25} m^{-3}, so with $U = 0{\cdot}5$ eV, for example, eqn. (25) gives, at room temperature,

$$\mu_{eff} = 10^{-5} \mu_0.$$

A few traps of reasonable depth will, therefore, drastically reduce the mobility and hence the conductivity. In a semiconducting glass the traps will not be at a discrete energy but will be distributed over a range of energies, but an equation of the form of (25) still holds in certain cases.

If the mean-free-path of a carrier in between trapping events is $\geqq L$ the mobility μ_0 in eqn. (25) will be the same as that discussed in paragraph 5·1. It is possible, however, that a carrier will traverse distances of only a few atomic spacings before becoming retrapped, in which case it will not be the same. We shall return to this point later.

Transport by hopping in the localized states

The likelihood that a large fraction of carriers in a semiconducting glass will, at any instant, be trapped and the potentially high density of localized states makes it necessary to consider direct hopping of carriers between traps as a possible mechanism of transport. The carrier is imagined as spending most of its time trapped at a particular localized state and making more or less instantaneous transitions to neighbouring empty traps. The problem of estimating the mobility of carriers in this circumstance is the same as that encountered in the random-walk theory of diffusion. In the absence of an electric field a carrier trapped at some particular localized state will have an equal probability p of jumping in either direction. Consider two parallel planes separated by a distance a equal to the average distance between traps. Suppose there is a concentration gradient such that the concentration of carriers at one plane is n m^{-3} and at the other $[n + a(\mathrm{d}n/\mathrm{d}x)]$. The concentration in a section of thickness a and unit cross section is $a \,.\, n$ at the first plane and $a \,.\, [n + a(\mathrm{d}n/\mathrm{d}x)]$ at the second. The flux J in the x-direction is therefore

$$J = pa^2 \frac{\mathrm{d}n}{\mathrm{d}x}.$$

In a field E, derived from a potential $\phi[E = -(\partial\phi/\partial x)]$, there is also an electric current $nq\mu_H E$, where μ_H is the hopping mobility, and at equilibrium this is equal to the flux J, i.e.

$$nq\mu_H E = pa^2 \frac{\mathrm{d}n}{dx}.$$

Assuming the carriers in the potential $\phi(x)$ are distributed according to Maxwell–Boltzmann statistics

$$n(x) = \text{const. } \exp\left(-\frac{q\phi(x)}{kT}\right),$$

and using this with the equation above, gives

$$\mu_H = \frac{pa^2q}{kT}.$$

If two adjacent sites are separated by an energy W, the probability per unit time that the carrier jumps will be of the order

$$p = \nu_p \exp\left(-\frac{W}{kT}\right)$$

where ν_p is a phonon frequency since the energy required to bring the two levels into coincidence will come from thermal vibrations. Further, if the wave-functions do not overlap appreciably, we must include a tunnelling factor $\exp(-2\alpha a)$ in this probability, hence

$$\mu_H = \frac{\nu_p a^2 q}{kT} \exp\left(-\frac{W}{kT}\right) \exp(-2\alpha a). \tag{26}$$

The hopping mobility μ_H will have its maximum value when $W \to 0$ and the tunnelling factor tends to 1, conditions likely to be realized in the localized states just inside the originally forbidden gap, but not deep in the localised tail of states. Taking typical values of the parameters in eqn. (26), ($\nu_p \sim 10^{12} - 10^{13}$ s^{-1}, $a \sim 3$ Å, $T = 300$ K) the *maximum* hopping mobility will be

$$(\mu_H)_{max} \sim 3 \times 10^{6} — 3 \times 10^{-5} \text{ m}^2 \text{ V}^{-1} \text{ s}^{-1}.$$

The mobility gap

In paragraph 5.1 we concluded that the microscopic mobility μ_0 of an electron in non-localized states in which the mean-free-path is equal to or greater than the de Broglie wavelength will be 10^{-2} m^2 V^{-1} s^{-1}. This is only likely to be achieved in states well above the critical energy E_c which separates the localized from non-localized states. What happens, therefore, between these states and the localized states at E_c where the mobility is only 10^{-5} m^2 V^{-1} s^{-1}? In this region the electron mean-free-path is of the order of atomic spacings, and both Mott (1969 *a*) and Cohen (1970) have pointed out that the migration of an electron is then best viewed as a diffusive process rather like that described above for hopping, except that now thermal activation and tunnelling are not limiting factors and the appropriate frequency is an electronic frequency ν_e, not ν_p. Thus, in this diffusive region the mobility μ_D is given by

$$\mu_D = \frac{\nu_e a^2 q}{kT}. \tag{27}$$

The electronic frequency $\nu_e \sim 10^{15}$ s^{-1} so that μ_D is a factor of 100–1000 times greater than $(\mu_H)_{max}$. We have ignored a small integral factor in the denominator of eqn. (27) (and (26)) which should be included for three-dimensional diffusion, but this does not affect the conclusion that there is a sudden increase in mobility on crossing E_c from localized to non-localized states.

Cohen (1970) argues that the hopping and diffusive regions are continuous, and in his derivation eqn. (27) includes a ' correlation factor ' f such that $0 \leqq f \leqq 1$. The three regions—thermally-activated hopping in the localised tail of localized states below E_c, diffusive motion in the non-localized states just above E_c and free-wave propagation at higher energies—are illustrated schematically in fig. 11. For clarity only the conduction band is drawn, but the same happens in the valence band. We should probably regard μ_D, not μ_0, as the ' microscopic ' mobility for transport processes in a semiconducting glass (see the remark at the end of paragraph 5.2).

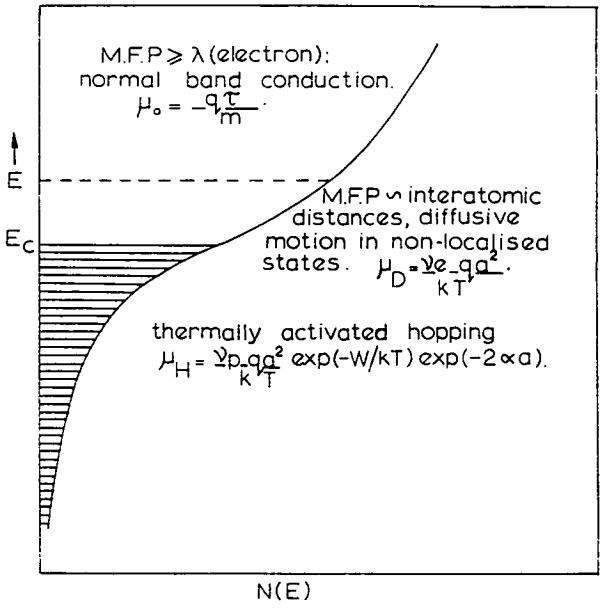

Fig. 11. The conduction-band density-of-states for a semiconducting glass showing the three different regions of transport mechanisms. The energy E_c separates localized from non-localized states.

Fig. 12 summarizes the situation. Fig. 12 (*a*) is the density-of-states diagram showing the tails of localized states below and above the critical energies E_c and E_v respectively; the Fermi level E_F is assumed to be in the middle. Fig. 12 (*b*) shows the corresponding $\mu - E$ diagram and the ' mobility gap ' at $(E_c - E_v)$. The electron distribution is given, as usual, by the normal Fermi function (fig. 12 (*c*)). Finally, the contributions to conductivity from states of different energy are depicted in fig. 12 (*d*). It should be noted, however, that the conductivity energy gap E_g will not necessarily coincide with $(E_c - E_v)$, nor will the two shaded areas in fig. 12 (*d*) normally be equal, i.e. holes could make a greater contribution to the conductivity than electrons or vice versa.

It is not intended to imply that the density-of-state diagram of fig. 12 (*a*) is necessarily typical. Amongst the wide range of semiconducting glasses there may be many variations. In some cases, for instance, there could be maxima in the densities of localized states corresponding to particular structural features. In the very complex chalcogenide glass alloys the tails from the conduction and valence bands may well overlap. They will still retain their

identity, however, and the valence band states above the Fermi level will lose their electrons to empty conduction-band states below it, becoming positively and negatively charged respectively. Such a glass will have, therefore, a fluctuating band of charged centres in the middle of the mobility gap and these centres may be important in the switching phenomena mentioned in the Introduction.

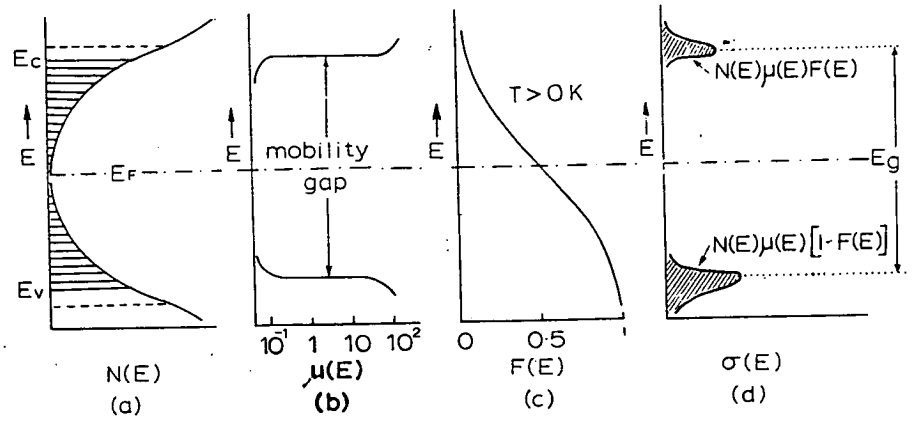

Fig. 12. (*a*) Density-of-states in conduction and valence bands. (*b*) The mobility–energy relationship and the ' mobility gap '. (*c*) The Fermi function for $T > 0$ K. (*d*) The contributions to the conductivity from states at different energies.

7. Optical absorption

Optical studies have played an important role in elucidating certain features of the electronic band-structure of crystalline semiconductors and it is relevant to consider, briefly, what effect disorder will have. In the region of the spectrum where the photon energy $h\nu \sim E_g$ (fig. 8 (*b*)) there should be a rapid increase in optical absorption as a function of frequency because electrons are excited across the energy gap of the crystal and photons of the corresponding frequency are absorbed. The spectral region where this occurs is called the optical ' absorption edge ' and the corresponding photon energy should give a measure of E_g. In a crystal the absorption process is governed by two conservation rules: conservation of momentum (or wave-number) and energy. If k_i and k_f are the initial and final wave-numbers of the electron and k the wave-number of the photon of frequency ν, then we must have

$$k_f = k_i + k; \quad E(k_f) = E(k_i) + h\nu.$$

The wavelength of a photon corresponding to the absorption edge of a semiconductor is very large compared with the lattice spacing (e.g. in germanium the absorption edge is at $h\nu \sim 0{\cdot}65$ eV for which $\lambda \sim 8 \times 10^{-6}$ m, whereas the lattice spacing is a few angstrom units). The momentum conservation rule is therefore $k_f \approx k_i$ and transitions obeying this condition are called ' direct transitions '. The absorption coefficient α in this case is given by

$$\alpha = \text{const.}\ (h\nu - E_{gd})^{1/2}$$

and this dependence comes essentially from the density of states in free space. In the region $h\nu \leqq E_{gd}$, α is expected to rise very rapidly with frequency. The

direct gap E_{g^d} will not necessarily correspond to the thermal gap E_g obtained from the temperature variation of conductivity. 'Indirect' optical transitions, involving the absorption or emission of a *phonon*, may also occur (e.g. in crystalline Si and Ge) and the absorption coefficient is then given by

$$\alpha = \text{const. } (h\nu - E_{gi})^2.$$

Since phonon participation is required in both cases, the indirect optical gap E_{gi} will normally be close to the thermal gap E_g.

For a vitreous semiconductor we have to consider the influence of both the localized and non-localized (band) states. In the latter Tauc (1969) assumes that the electronic wave-functions are only slightly perturbed compared with the crystal and this allows him to deduce

$$\alpha = \text{const. } P_{if}^2 \int N_C(E)\, N_V(E + h\nu) dE \tag{28}$$

where P_{if} expresses the probability of transitions between initial and final states (and is assumed independent of energy) and $N_C(E)$ and $N_V(E)$ are the density states in the conduction and valence bands respectively. Thus the absorption coefficient is now a function of the density of states in the two bands taken separately and if these are still parabolic this leads to

$$\alpha = \text{const. } (h\nu - E_g)^2. \tag{29}$$

This is of the same form as the equation quoted above for indirect transitions in a crystal. We should not regard this as implying the distinguishability of direct and indirect transitions in a glass since these terms are meaningful only if momentum conservation rules can be defined. Rather it implies that the absorption is determined by an integral over the product (eqn. (28)) of the densities of states in the valence and conduction bands for which *energy* is conserved.

In this case, of course, E_g corresponds to the minimum distance between non-localized states, i.e. $(E_c - E_v)$ in fig. 12 (*a*), or to some extrapolated, not real, zeros in the density of states. Moreover, we should not necessarily expect E_g determined from eqn. (29) to agree exactly with the E_g shown in fig. 12 (*d*) and obtained from the temperature dependence of conductivity.

Optical transitions between two localized states are not likely to contribute effectively to the absorption since they are spatially separated. Transitions between occupied localized states in the valence-band tail and non-localized empty states in the conduction-band could be important, however, and these would mask the *apparent* absorption edge predicted by eqn. (29). Since the tail-of-states falls off roughly exponentially with energy we might, at first sight, expect the absorption coefficient to rise exponentially with photon energy before merging with the region of eqn. (29), but this will only happen if the transition probabilities, P_{if}, are independent of energy over a very wide range.

8. The effective-mass and narrow-band semiconductors

The theories we have discussed so far are appropriate to semiconductors in which the bands are wide (several eV sometimes), and only a few states near the bottom of a band (for electrons) or near the top (for holes) are involved in transport processes. From the formalism described in Section 3 it can be shown that the E-k (or α in the notation of the δ-barrier model) relationship in the

range $-(\pi/a) < k < (\pi/a)$ is as shown in fig. 13. It also follows from our description of electron propagation as a wave-motion that the electron in a band behaves as though it has an *effective-mass* m^* of $[\hbar^2/(d^2E/dk^2)]$. Near the bottom (or top) of a band where the E–k relationship is parabolic (eqn. (5)), m^* will not be very different from that of a free electron. In the centres of bands, however, the E–k curve goes through an inflexion and $m^* \to \infty$. If the bandwidth is narrow, states of large effective mass may become important in transport processes. Narrow bandwidths are to be expected in materials in

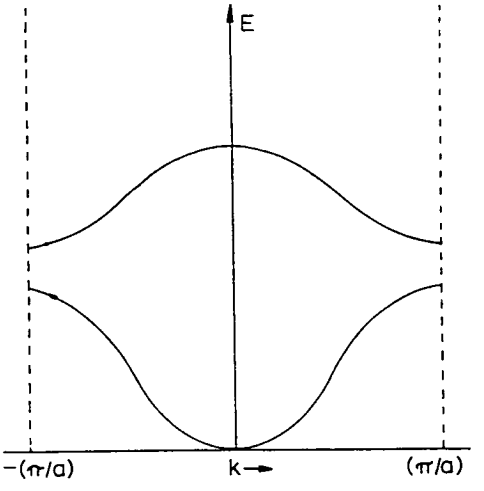

Fig. 13. The E–k curve for a crystalline semiconductor.

which the overlap of outermost atomic or molecular wave-functions are small and this is usually reflected in a large *forbidden* gap (e.g. > 2–3 eV). A large effective-mass has an important consequence on the mode of transport which is related to our discussion in Section 5 of band or hopping mechanisms. For an electron of thermal energy kT and momentum p we can write, using the de Broglie relationship,

$$kT = \frac{p^2}{2m^*} = \left(\frac{h}{\lambda}\right)^2 \frac{1}{2m^*}$$

or

$$\lambda = \frac{h}{(2m^* kT)^{1/3}}.$$

The electron wavelength is of the order of a lattice spacing (3 Å) if the effective mass, m^*, is greater than about a hundred times the free electron mass; the electron is therefore *localized* at a particular site and in this circumstance only one particle can occupy a given site at any instant. The migration of an electron (or hole) is then best regarded as a hopping from site to site and the mobility will be determined by the same sort of considerations we discussed in paragraph 5.3.

Amongst the wide variety of vitreous semiconductors we may expect to find glasses which, in the crystalline analogue, would have narrow energy bands.

If localization occurs in the glass it may not be primarily a result of the disordered structure, although potential fluctuations induced by the disorder will tend to reduce the already weak overlap of wave-functions.

9. Conclusions

Glass formation is a very widespread phenomenon and it is not surprising to find glasses with typically semiconducting properties. Glass has a structure which is like that of a liquid with some instantaneous disordered configuration ' frozen-in '; there is short-range order of nearest-neighbours but no long-range order. The main features of the electron energy-bands of a crystal are expected to be retained, however, but modified by the presence of a high density of localized states or traps which may extend deep into the forbidden gap of the analogous crystalline structure.

In the energy-band structure of a glass three regions can be delineated, each with a different mode of transport. In the region of localized states carrier migration can only occur by thermally-activated hopping between states. At energies well inside the non-localized bands, electrons will propagate freely with a mean-free-path equal to or greater than the de Broglie wavelength of the electron. In between, there is a region of non-localized states in which the mean-free-path becomes of the order of atomic spacings and the movement of carriers is best thought of as a diffusive process. Between these states and the localized states there is a sharp decrease in mobility and we can speak of a mobility gap, rather than an energy gap, separating the valence and conduction bands. In Part II these theoretical ideas are used in interpreting, so far as is possible, the properties of some typical semiconducting glasses.

References, Part I

Borland, R. E., 1963, *Proc. Roy. Soc.*, **274,** 529.

Cohen, M., 1970, Proc. 3rd Int. Conf. on Liquid and Amorphous Semiconductors, Cambridge, September 1969. To be published in *J. Non-Crystalline Solids*, Vol. 4.

Denton, E. P., Rawson, H., and Stanworth, J. E., 1954, *Nature*, **173,** 1030.

Duwez, P., Willens, R. H., and Crewdson, R. C., 1965, *J. Appl. Phys.*, **36,** 2267.

Dzhalilov, S. U., and Rzaev, K. I., 1967, *Phys. Stat. Sol.*, **20,** 261.

Gibbs, J. H., 1960, Nature of the glass transition and the vitreous state, in *Modern Aspects of the Vitreous State*, Vol. 1 (ed. J. D. Mackenzie) (London: Butterworths).

Jones, G. O., 1956, *Glass* (London: Methuen Monograph).

Kolomiets, B T., 1964, *Phys. Stat. Sol.*, **7,** 359, 713.

Mott, N. F., 1969, *Contemp. Phys.*, **10,** 125.

Mott, N. F., 1969 a, *Phil. Mag.*, **19,** 835.

Mott, N. F., and Davis, E. A., 1968, *Phil. Mag.*, **17,** 1269.

Owen, A. E., 1963, Electric conduction and dielectric relaxation in glass, in *Prog. Ceramic Science*, Vol. 3, pp. 78–198 (ed. J. E. Burke) (Oxford: Pergamon).

Petz, J. I., Kruh, R. E., and Amstutz, G. C., 1961, *J. Chem. Phys.*, **34,** 526.

Roberts, A. P., and Makinson, R. E. B., 1962, *Proc. Phys Soc.*, **79,** 630.

Secrist, D. R., and Mackenzie, J. D., 1964, Preparation of non-crystalline solids by uncommon methods, in *Modern Aspects of the Vitreous State*, Vol. 3, pp. 149–165 (ed. J. D. Mackenzie) (London: Butterworths).

Simmons, J. G., 1970, *Contemp. Phys.*, **11,** 21–41.

Tauc, J., 1969, Optical properties and electronic structure of amorphous semiconductors, in *Optical Properties of Solids*, Chap. 5, pp. 123–136 (ed. S. Nudelman and S. S. Mitra) (New York: Plenum Press).

Turnbull, D., 1969, *Contemp Phys.*, **10,** 473–488.

Warren, B. E., 1937, *J. Appl. Phys.*, **8,** 645.

Zachariasen, W. H., 1932, *J. Amer. Chem. Soc.*, **54,** 3841.

CONTEMP. PHYS., 1970, VOL. 11, NO. 3, 257–286

Semiconducting Glasses
Part II: Properties and Interpretation

A. E. OWEN

School of Engineering Science, University of Edinburgh

SUMMARY. The properties of amorphous germanium and silicon, vitreous selenium chalcogenide glasses and transition-metal oxide glasses are described and discussed. Much of the current experimental data can be interpreted within the framework of the theoretical models developed in Part I, in which the main influence of disorder is the so-called 'tail of localized states'. Typical semiconducting properties are observed and in many cases the amorphous materials behave rather like ordinary intrinsic semiconductors. It must be recognized, however, that at the moment only a qualitative interpretation is possible and many problems remain to be solved.

1. Introduction

In Part I it was argued that a glass may have an electronic band structure which is not too dissimilar from that of the corresponding crystal; the main difference is likely to be the tail of localized states in the forbidden gap. Conduction can occur in the non-localized states or by hopping amongst the localized states.† But which? Can they both occur together? Will one predominate over the other and, if so, under what conditions? Will there be, for example, a change of conduction mechanism on going from low to high temperature, or from low to high field strength, or between d.c. and a.c. fields? As for the localized states we should like to know:

(1) Their density and energy distribution.
(2) Their nature—i.e. are they traps for carriers or recombination centres or both?
(3) Their origin. For instance, density or compositional fluctuations as well as distorted bonds (fig. 4, Part I) will also lead to a breakdown of long-range order and hence cause localization. In addition, broken bonds (in a polymeric glass for example) and other atomic defects will form localized states just as they would in a crystalline semiconductor.

We should also like to know the structure of the non-localized bands of electronic states.

The following sections will discuss the main groups of semiconducting glasses which have been studied in recent years, namely, the elements silicon and germanium; the element selenium and the chalcogenide compounds; the transition-metal oxide glasses.

Bearing in mind all the time the influence of the localized states, most of the interpretation of the properties of semiconducting glasses has been in terms of the well-established theories of crystalline semiconductors.

In the early days, in fact, a very close similarity was often tacitly assumed, sometimes with good reason, for as we shall see there are some important experimental similarities. It is now recognized that there are also significant and important differences, but because of this comparative approach we should remind ourselves of the main features of crystalline semiconductors.

† It is worth noting, in passing, that hopping conduction can and does occur in crystalline semiconductors.

2. The properties of crystalline semiconductors

2.1. *Intrinsic conduction*

In a completely pure crystalline semiconductor conduction can only occur by excitation of carriers across the energy gap, E_g. Thus, the carrier concentration n varies as

$$n = (N_C N_V)^{1/2} \exp\left(-\frac{E_g}{2kT}\right) \tag{1}$$

where N_C and N_V are, respectively, the densities of available states in the conduction and valence bands. The conductivity σ is given by

$$\sigma = n\mu q \tag{2}$$

where μ is the carrier mobility and q the electronic charge. The mobility μ is a slightly *decreasing* function of temperature ($\mu \alpha T^{-3/2}$ for scattering by lattice vibrations in a non-polar material) and hence

$$\sigma = \text{const.} \exp\left(-\frac{E_g}{2kT}\right). \tag{3}$$

From the slopes of the $\log \sigma$ or $\log n$ vs. $(1/T)$ lines, the energy gap E_g may be obtained.

In this region of *intrinsic* conductivity, eqn. (2) should be expressed as the sum of two terms, one for electrons, the other for holes, which are present in equal numbers.

2.2. *Extrinsic (impurity) conduction*

An atom with an extra electron (e.g. As in Ge) forms discrete donor levels at an energy E_D below the conduction band edge. At $T = 0$ K the Fermi level lies halfway between the donor levels and the conduction band, and all the donors are occupied. As the temperature is raised electrons are excited to the conduction band, and the carrier concentration and conductivity increase, but the slopes of the $\log n$ or $\log \sigma$ vs. $(1/T)$ graphs are now $(-E_D/2k)$. The conductivity occurs by electrons and is said to be n-type. If the donor concentration is not too high the carrier concentration becomes constant or 'saturated' because all donors are ionized before the intrinsic portion is reached. In this region of saturation the $\log \sigma$ curve decreases with increasing temperature because μ, in eqn. (2), decreases. If the donor concentration is high, the *extrinsic* curves for both n and σ intercept the intrinsic lines directly. Likewise an atom with a deficiency of one electron (e.g. B in Ge) introduces an acceptor level above the valence band, and when these are ionized conduction is by holes in the valence band (p-type). It is this sensitivity of crystalline semiconductors to impurities, and our ability to 'dope' them reproducibly with n- or p-type impurities, which makes them extremely useful materials.

2.3. *Thermoelectric power*

If a temperature gradient exists across a semiconductor a voltage is developed. The thermoelectric power S (in V/K) is related to the Peltier coefficient π ($S = \pi/T$). For an n-type semiconductor, say, the Peltier coefficient is given by $[(E_C - E_F) \times AkT]$; the first term is the potential energy

gained by raising an electron to the conduction band and the term AkT is the kinetic energy transported. Hence

$$S = -\frac{k}{q}\left[\frac{(E_C - E_F)}{kT} + A\right], \tag{4}$$

and if the semiconductor is intrinsic, or near-intrinsic and one carrier is much more mobile than the other,

$$S \approx -\frac{k}{q}\left(\frac{E_g}{2kT} + A\right). \tag{5}$$

The thermoelectric power has the sign of the most mobile and/or most numerous carriers.

2.4. *The Hall effect and mobility*

When a current I is passed through a semiconductor and a magnetic field B applied at right angles to it, a voltage V is developed in the mutually perpendicular direction,

$$V = \frac{RIB}{b} \tag{6}$$

where b is the thickness in the direction of the magnetic field. The constant R is the Hall coefficient and it has its origin in the deflection of the carriers by the magnetic field. It can be shown that $R = (1/nq)$ and hence comparison with eqn. (2) gives

$$R\sigma = \mu. \tag{7}$$

The mobility obtained in this way is often specifically called the Hall mobility and designated μ_H since it differs by a small factor $(3\pi/8)$ from the true microscopic mobility defined by eqn. (2). The Hall coefficient normally has the sign of the majority carriers. In semiconductors the mobility is usually of the order of 10^{-2} m^2 V^{-1} s^{-1}, and in group IV elements (Si, etc.) and III–V compounds it can be of the order 1 m^2 V^{-1} s^{-1}.

2.5. *Optical absorption and photoconductivity*

As was discussed in Part I (Section 6) light of frequency ν such that $h\nu < E_g$ will not be strongly absorbed, but in the region $h\nu \geqq E_g$ there will be a sudden increase in absorption. We have to distinguish between processes in which energy and momentum are conserved *without* phonon participation—'direct' transitions—and *with* phonon assistance—'indirect' transitions. In the two cases the absorption coefficient α is given by

$$\alpha = \text{const.}\ (h\nu - E_1)^{1/2} \ \ldots \ \text{(direct)} \tag{8}$$

and

$$\alpha = \text{const.}\ (h\nu - E_2)^2 \ \ldots \ \text{(indirect.)} \tag{9}$$

The energy E_1 of the absorption edge for direct transitions will not necessarily be closely related to the thermal energy gap E_g (but we should have $E_1 > E_g$). On the other hand, E_2 in eqn. (9) should be close to E_g.

If the optical absorption occurs between states in which the carriers are free to carry current, i.e. non-localized Bloch states, then we should also observe an enhancement of conductivity, or photoconduction. Clearly the spectral

dependence of photoconductivity should be correlated in some way with the frequency variation of the absorption coefficient.

2.6. *Contact phenomena*

An important feature of crystalline semiconductors is the sensitivity of current flow through them to the nature of the metal contacts made to their surfaces or to 'internal' contacts such as the p–n junction between regions of different conductivity type. For example, at the contact between an n-type semiconductor and a metal with a larger work function, electrons will flow from the semiconductor to the metal until the Fermi level (E_F) in both is the same. The surface of the semiconductor is therefore depleted of electrons and there is built up a *positive* space charge in the depletion region, providing a barrier to current flow across the contact. If the metal is made positive with respect to the semiconductor this barrier is lowered and a current will flow which increases exponentially with voltage. With reverse polarity the barrier is effectively raised and the current saturates at relatively small values—i.e. the metal-semiconductor contact is a rectifier. Similar effects will occur with a p-type semiconductor. Because of the relatively low carrier density in the semiconductor the depletion region may extend as much as 10^{-6} m into it. With rectifying contacts the current flowing through a semiconductor is a function of the 'barrier' at the surface and not of the bulk material, and it is not possible, therefore, to measure the conductivity of the semiconductor. To do this an 'ohmic' contact is required which has a supply of electrons freely available to enter the semiconductor as necessary to maintain the current flow. It is often difficult to find such contacts for some semiconductors.

3. Amorphous germanium and silicon

3.1. *Preparation and structure*

There are reports of amorphous germanium and silicon having been prepared from the melt, but presumably only in minute quantities. Amorphous Ge can also be prepared by ion bombardment of the crystalline form, but all investigations of the electrical properties of the amorphous form of the two elements have been made with films deposited from the vapour. Amorphous films up to several thousand angstroms thick can readily be deposited by electron-beam evaporation of the elements on to a cold substrate (less than about 400 °C in the case of Ge, 600 °C for Si). They can also be prepared by other vapour deposition techniques, e.g. sputtering or decomposition of a volatile compound (usually a hydride) in a glow discharge. At about 450 °C and 825 °C respectively the amorphous Ge and Si films crystallize and become polycrystalline; the melting points of the two elements, it should be noted, are 937 °C (Ge) and 1420 °C (Si) so that it is not possible to observe the glass transition (see Part I) in the amorphous films.

The most extensive studies of structure have been made by Grigorovici and his colleagues (see Grigorovici and Manaila 1967/68) on amorphous Ge. A radial distribution curve is illustrated in Part I. In amorphous Ge the nearest-neighbour configuration is thought to be just the same as in the crystalline variety, each Ge atom being surrounded tetrahedrally by four others. In the crystal lattice of Ge (diamond-type) adjacent tetrahedra are

orientated to each other in a 'staggered' configuration (fig. 1 (*a*)). The 'eclipsed' configuration (fig. 1 (*b*)) is energetically less favourable. Grigorovici suggests nevertheless that the eclipsed configuration occurs in amorphous Ge and that this allows five Ge tetrahedra to be connected in a five-membered pentagonal ring with only a small distortion of the tetrahedral angle (108° instead of 109° 28′). The gain in entropy will tend to balance the increased

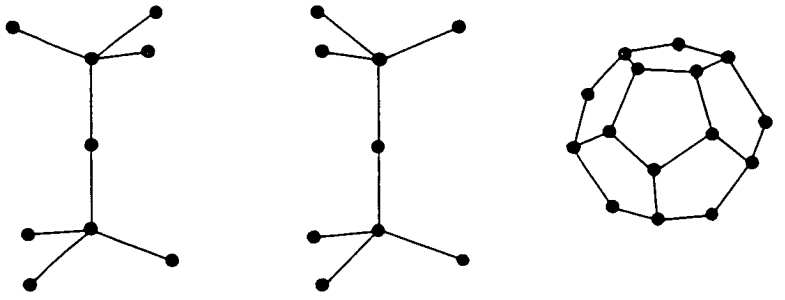

(*a*) (*b*) (*c*)

Fig. 1. The staggered (*a*) and eclipsed (*b*) configurations of adjacent Ge tetrahedra. Five-membered rings in a pentagonal-dodecahedron (*c*). (*After Grigorovici and Manaila* 1967/68.)

internal energy. Structures with fivefold symmetry cannot be joined together to fill space and at the same time provide translational symmetry—i.e. long-range order. This fact was noted many years ago by Bernal (1959) who suggested that while fivefold structures are prohibited for crystals, pentagonal arrangements may well be the rule for irregular, non-crystalline structures. Grigorovici proposes that a basic structural unit in amorphous Ge is a pentagonal dodecahedron (fig. 1 (*c*)) made up of twelve pentagonal rings with each of the 20 Ge atoms at its corners being at the centre of a tetrahedron. This he calls an 'amorphon' and because of the non-crystallographic fivefold symmetry it will give rise to an amorphous radial distribution curve. A similar structural unit—called the 'vitron'—was proposed several years ago as a basis for the structure of vitreous silica (SiO_2). The 'amorphonic' units of amorphous Ge cannot fill space completely and it is imagined that the regions between them are filled with Ge atoms in a diamond-like configuration. An important feature of this model is that all Ge atoms have their normal tetrahedral arrangement of near neighbours and that essentially all tetrahedra are connected to others, i.e. there are few, if any, broken or 'dangling' bonds.

3.2. *Electrical and optical properties*

There has been some disagreement about the resistivity of amorphous Ge and Si films and there is no doubt that, in part at least, this is because their properties are sensitive to the conditions of deposition. For films produced by electron-beam evaporation, for instance, Walley (1968) has shown that only when the residual gas pressure is less than 10^{-5} torr and the deposition rate greater than about 5 nm s^{-1} (50 Å s^{-1}) is the resistivity independent of these parameters. In addition, the resistivity increases approximately with the logarithm of time after deposition and is also dependent upon thermal history. Bearing this in mind, the general features of the resistivity of amorphous Ge as a function of temperature are shown in fig. 2 where $\log \rho$ is plotted vs.

$(1/T)$, and T is in K. Grigorovici's (1968) data includes the effect of thermal history; curve 1 is for the Ge film as deposited on a substrate at below 200° C, and curves 2, 3 and 4 show the effect of successive annealing in the range 200–350 °C. On heating above about 400 °C the amorphous layer crystallizes

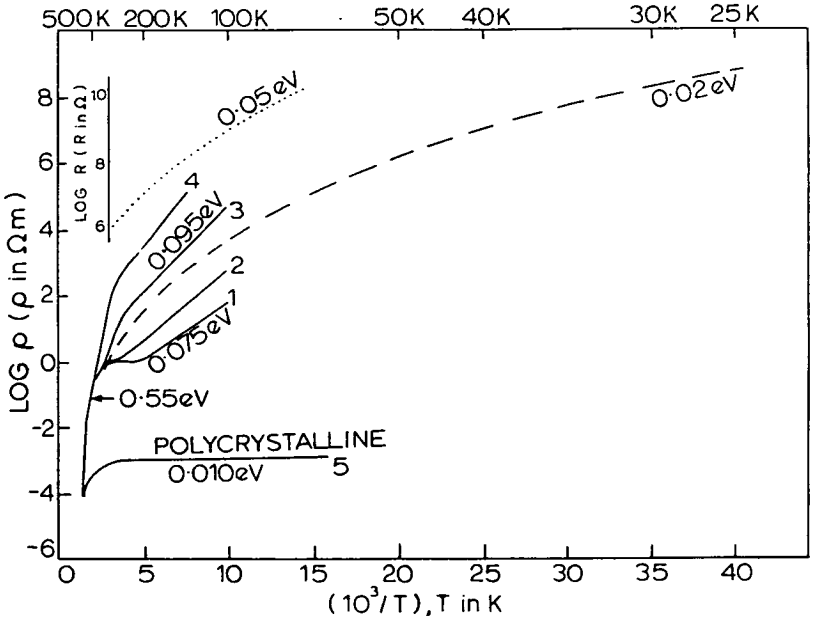

Fig. 2. Temperature dependence of the resistivity of amorphous Ge films. ----- Clark (1967). —— Grigorovici (1968). Curves 1, 2, 3 and 4 obtained after successive annealing. The upper curve ..... Walley (1968) is of *resistance*, not resistivity.

and finally curve 5 is obtained for the polycrystalline film. According to Grigorovici there are regions in which there is a straight-line relationship between $\log \rho$ and $(1/T)$, and typical activation energies calculated from the slopes are given on fig. 2. The data of Walley (1968) and Clark (1967), however, show a continual curvature down to low temperatures; approximate 'activation energies' at 'low' temperatures are also shown in fig. 2, but these are not, of course, constant. Amorphous silicon behaves in a very similar way. An important feature, implicit in fig. 2, is the insensitivity of the conductivity of amorphous Ge and Si to impurities. The polycrystalline material, from which the amorphous films were obtained and to which they reverted on heating, clearly contained an appreciable impurity concentration. Using the conductivity as a measure, the impurity concentration must have been in the region $1\text{–}5 \times 10^{22}\ \mathrm{m}^{-3}$. At room temperature intrinsic crystalline Ge has a carrier concentration of $2 \times 10^{19}\ \mathrm{m}^{-3}$ and a resistivity a little less than $1\ \Omega\,\mathrm{m}$. This lack of sensitivity to impurities seems, as we shall see, to be a general feature of vitreous semiconductors although there are some exceptions.

Measurements of the thermoelectric power of amorphous Ge, also from Grigorovici (1968), are shown in fig. 3; for comparison the resistivity curve 4 from fig. 2 is also reproduced as are some typical results for the thermopower of a p-type crystal of Ge. Over most of the temperature range the thermopower indicates p-type conductivity, but at low temperatures it becomes n-type.

An extrapolation of the high temperature part of the curve also suggests that the thermopower will become n-type again. Like the conductivity, these features are also not sensitive to impurities, and once more the behaviour of amorphous Si is qualitatively similar. The Hall effect of amorphous Ge has been measured at room temperatures (i.e. where the thermopower indicates positive carriers) by Clark (1967) and the Hall coefficient was found to be

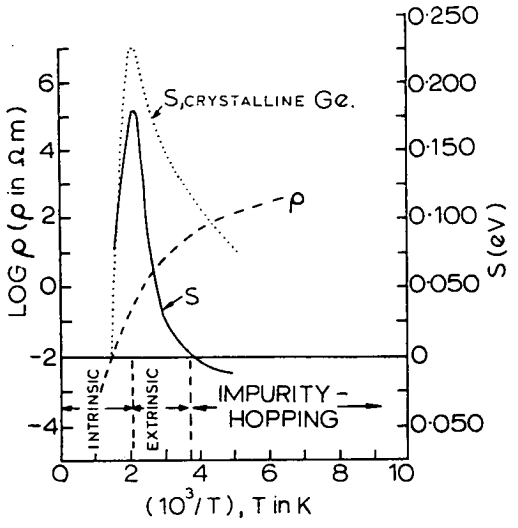

Fig. 3. Temperature dependence of the thermoelectric power of amorphous Ge with, for comparison, resistivity data, and the thermoelectric power of crystalline Ge. (*After Grigorovici* 1968.)

negative, indicative of n-type conductivity. The Hall coefficient is extremely low, however, and using the measured d.c. conductivities corresponds to a mobility of about 10^{-6} m^2 V^{-1} s^{-1} (carrier concentration approximately 10^{24} m^{-3}). Such low mobilities are extremely difficult to measure and at a recent conference (the Symposium on *Semiconductor Effects in Amorphous Solids*, New York, May 1969) the negative Hall coefficient of amorphous Ge was disputed. The anomaly between the signs of the thermoelectric power and the Hall effect is nevertheless clearly established in some other materials (see later).

It is not possible to prepare n-type amorphous Ge and Si, but the combination of p-type amorphous Ge or Si on n-type single crystals give good rectifying junctions; with p-type single crystals the rectification is poor.

The existing optical absorption data on amorphous Ge are contradictory, but some results are shown in fig. 4. Clark (1967) and Abraham (quoted by Stuke (1970)) both find rather slowly varying absorption coefficients in the region of the absorption edge, but according to Donovan, Spicer and Bennet (1969) the edge is as sharp as in crystalline Ge. These discrepancies are disturbing and Stuke (1970) suggests that they are due to different preparative techniques and structures. Donovan *et al.* do not, unfortunately, say whether the electrical properties of their amorphous Ge films are very different from data reported by others.

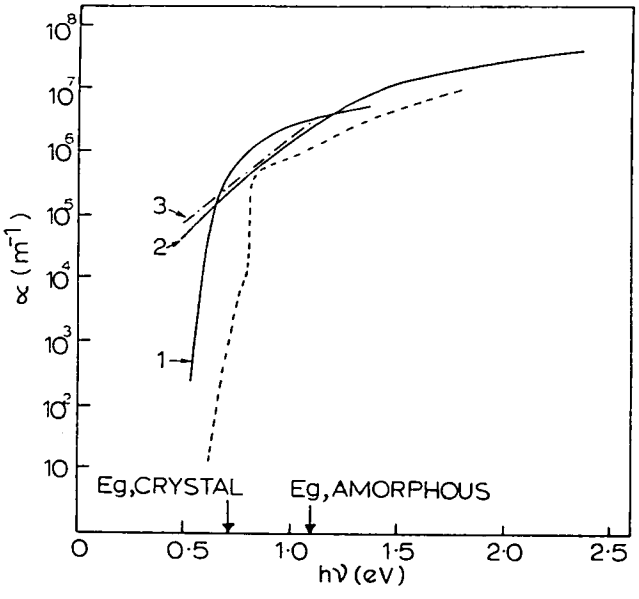

Fig. 4. Optical absorption in amorphous Ge. (1) Donovan *et al.* (1969); (2) Abraham, see Stuke (1970); (3) Clark (1965). ----- Single crystal Ge.

3.3. *Discussion*

Accepting the evidence of the thermoelectric power measurements (fig. 3) we must conclude that there is a region of extrinsic conductivity at intermediate temperatures, going over to intrinsic at higher temperatures (cf. with the change from extrinsic to intrinsic of the crystalline sample). The two regions are also evident in Grigorovici's resistivity data (fig. 2) and this implies that the high temperature slope (0·55 eV) corresponds to half the energy gap, thus $E_g = 1{\cdot}1$ eV in amorphous Ge. The corresponding value for amorphous Si is 1·70 eV. Both these values are considerably greater than the thermal energy gaps for crystalline Ge and Si which, at *room temperature* (they increase slightly with decreasing temperature), are 0·67 eV and 1·12 eV respectively. They are also greater than the *optical* energy gaps for the amorphous forms, although from the results of Clark and Abraham (fig. 4) it is difficult to know where to measure the gap. The thermal energy gaps for the crystalline and amorphous forms of Ge are indicated by the arrows in fig. 4. Using Stuke's (1969) empirical rule that the optical gap corresponds to an absorption coefficient of 10^6 m^{-1} gives values of about 0·9 eV and 0·95 eV respectively, but the results of Donovan *et al.*—curve 1 of fig. 4—clearly indicate a much lower value. At temperatures below the extrinsic region Mott (1969) suggests that the conduction occurs by the impurity-hopping mechanism. The three regions of conductivity (intrinsic, extrinsic and impurity hopping) are not obvious in the results of Clark and Walley (fig. 2); in fact, the continuous curvature of both of these sets of results could indicate hopping over the whole temperature range since, as the temperature is lowered, the more energetic phonon assisted hops will become progressively less favourable. Furthermore, as the temperature is lowered, carriers will tend to hop larger distances, i.e. beyond nearest neighbours in order to find energetically favourable sites (Mott 1969), and

taking this into consideration leads to a temperature dependence of conductivity:

$$\sigma = \text{const.} \exp\left[-\left(\frac{A}{T}\right)^{1/4}\right]. \tag{10}$$

Both Clark's and Walley's measurements fit this equation over a wide temperature range.

The evidence of the thermoelectric power is fairly conclusive, however, and this is also supported by measurements of piezoresistance in amorphous Ge—results of Grigorovici and Devengi quoted by Mott (1969). We shall accept, therefore, that the three regions exist—as delineated in fig. 3—and try to account for them by the type of model derived in Part I. We must recognize that the conductivity and mobility of amorphous Ge (and Si) is much lower than the corresponding crystal, and the conductivity is insensitive to impurities but is sensitive to heat treatment. Clark's (1967) Hall mobility data must be considered a little doubtful, because of the experimental difficulties, but from the temperature at which the thermoelectric power goes through zero in the intrinsic region an acceptor density of 10^{24} m^{-3} can be calculated, and if these are all ionized this also gives a value of 10^{-6} m^2 V^{-1} s^{-1} (Grigorovici 1968). Mott (1969) suggests the band scheme illustrated in fig. 5. With the addition of a reasonably well defined set of acceptor states near the valence band this is identical with the models of Part I. The acceptor states may be associated with unsaturated Ge bonds (note: a vacancy in crystalline Ge behaves as an acceptor) with a density in the region of 10^{24}–10^{25} m^{-3}. This concentration would not be inconsistent with the structural model described in para. 3.1. To account for the impurity-hopping conduction and the n-type thermopower at low temperatures it is also necessary to assume the presence of a *few* donors (not shown, and of unspecified origin). At low temperatures the Fermi level E_F will lie in the band of localized acceptor states, a small fraction of which will be occupied by electrons from the donors. The electrons can conduct by hopping (impurity-hopping) to vacant acceptor sites, and since these sites are less than half filled with electrons, the thermopower is negative. As the temperature is raised, the Fermi level moves through the acceptor states which are now ionized by electrons from the valence band and extrinsic p-type conduction occurs. Finally, as the Fermi level approaches the centre of the 'gap', the conductivity becomes intrinsic with $E_g = 1{\cdot}1$ eV, and since this is eventually n-type the mobility of electrons in the conduction band must be higher than that of holes in the valence band. The E_g mentioned above is, in the terminology discussed in Part I, a 'mobility gap' rather than an energy gap. The mobility, and hence the conductivity, is low because the conduction occurs in the 'diffusive' region of non-localized states in which the mean free path is of the order of an interatomic spacing (see Part I). It must be admitted, however, that the experimental value (10^{-6} m^2 V^{-1} s^{-1}) is on the lower borderline even for this mode of band transport. The insensitivity to impurities is, according to Mott (1969), a consequence of the randomized structure of the amorphous material which allows arrangements in which every valence electron can be used in a bond. Thus a donor such as phosphorus in amorphous Ge can find a site in which it is surrounded by five Ge atoms and so use all its five valence electrons instead of, as in crystalline Ge (four neighbours), having one left over which it can 'donate' to the conduction bond.

This effect will also reduce the conductivity of an amorphous semiconductor.

The transport properties, so far as they go, are reasonably consistent with the above model, but the low values for the optical energy gap, compared with E_g, are disconcerting. The results of Donovan *et al.* (1969), especially, indicate that at the band edges a large number of states over a wide range of energies are effective in optical absorption but make little contribution to the conductivity. One explanation might be that the amorphous films contain internal potential barriers between otherwise homogeneous regions. These barriers would influence the transport properties but not the optical absorption.

4. Vitreous selenium

4.1. *Preparation and structure*

The form of Se which behaves as a semiconductor is the hexagonal (or trigonal) form known as grey selenium. Its structure consists of very long spiralled chains of Se atoms with their axes arranged parallel to each other. The bonding within the chains is covalent and between them it is probably van der Waals type. Red selenium is an insulator and it has a monoclinic structure formed from eight-membered rings, Se_8.

Vitreous Se can readily be prepared by cooling from the melt or by evaporation and deposition from the vapour. The glass transformation range T_g is in the region of 30° C (fig. 2, of Part I) so we must expect vitreous Se to devitrify (crystallize) if it is heated much above room temperature. Evidence from a variety of sources (e.g. spectroscopy, viscosity, glass transformation temperatures) shows that vitreous Se, like the liquid with which it is continuous, is made up of a mixture of polymeric chains of Se and Se_8 rings. In the liquid there exists a dynamic equilibrium between rings and chains, the proportion of Se_8 rings decreasing and the average chain length also decreasing as the temperature increases. In vitreous Se, therefore, the ratio of rings to chains will depend upon the thermal history and the temperature from which the liquid is quenched. As much as 50 per cent of the Se may be in Se_8 rings and the polymeric chain length may range from hundreds to many thousands of Se atoms. At the ends of the Se chains there will be broken bonds and hence unpaired electrons, and these have been detected by electron-spin resonance.

4.2. *Electrical and optical properties*

The conductivity of amorphous Se is so low at room temperatures (see fig. 1, Part I) that it is extremely difficult to measure, and because it devitrifies so readily if heated much above room temperature, it is virtually impossible to obtain an accurate assessment of the temperature dependence of conductivity. Measurements have been made of the resistivity of liquid Se, however, and as shown in fig. 6 plots of $\log \rho$ vs. $(1/T)$ do extrapolate reasonably to the room temperature values. The activation energies of the two resistivity plots in fig. 5 are slightly different and the average is 1·13 eV. If we are to interpret this as an energy or mobility gap it gives $E_g = 2{\cdot}26$ eV. Because of the high resistivity the thermoelectric power of amorphous Se is also very difficult to measure. Again, measurements on the liquid are probably more reliable and some results are also shown in fig. 6. The thermoelectric power of liquid Se

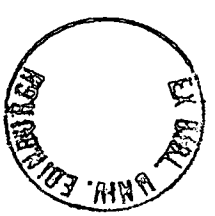

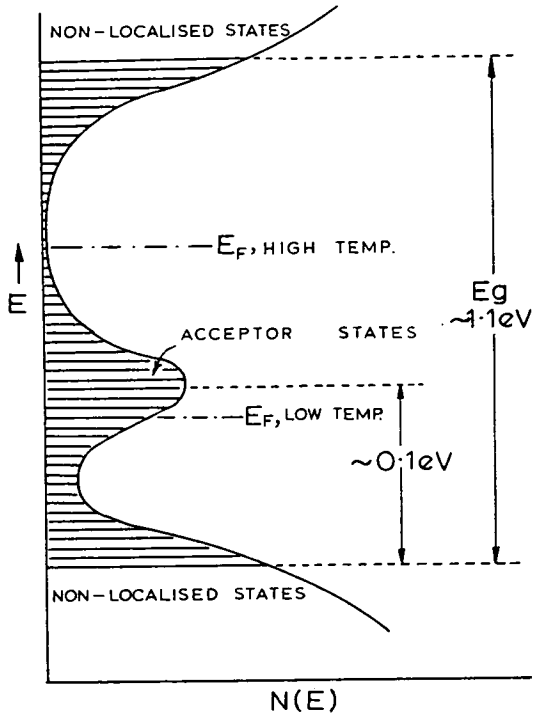

Fig. 5. Suggested density-of-states diagram (schematic) for amorphous Ge. (*After Mott*; 1969.)

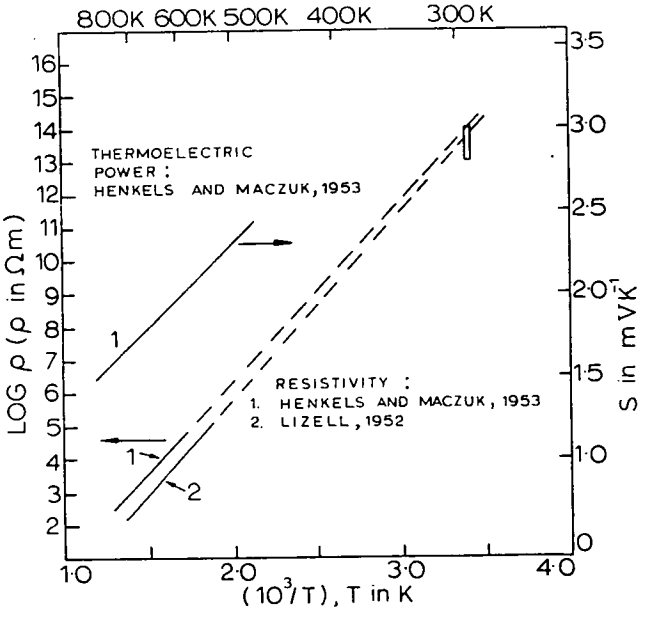

Fig. 6. Temperature dependence of the resistivity and thermoelectric power of Se. Data for the liquid taken from (1) Henkels and Maczuk (1953) and (2) Lizell (1952).

is p-type and it follows eqn. (4) quite accurately from which $(E_C - E_F) = 1{\cdot}15$ eV. Hence if the conductivity is intrinsic, the holes being much more mobile than electrons, eqn. (5) gives $E_g = 2{\cdot}30$ eV.

The high resistivity of amorphous Se and the ease with which it can be prepared in thin-film form makes it particularly suitable for the measurement of drift mobility by the techniques developed by Spear (1969) and others. A thin layer of excess carriers (electrons and holes) is generated by electron bombardment or strong light pulses just inside the surface of the specimen. A field is applied across the specimen and, depending upon its polarity, either the excess electrons or holes are drifted through. The pulse is collected at an electrode on the other side of the specimen and displayed on an oscilloscope. From the transit time the velocity of the carriers and hence their mobility can be obtained directly. Several series of measurements of this kind have now been made by various workers on evaporated amorphous Se films over a range of temperatures from about -60 °C to $+30$ °C. Results differ slightly, probably because of slight differences in the condition of preparation, but at room temperature the electron mobilities are in the range $4{\cdot}5$–$6{\cdot}0 \times 10^{-7}$ $m^2\,V^{-1}\,s^{-1}$ and the hole mobilities $1{\cdot}1$–$1{\cdot}4 \times 10^{-5}$ $m^2\,V^{-1}\,s^{-1}$. Both are temperature dependent, giving a straight-line relationship between $\log \mu$ and $(1/T)$, and the activation energies are in the range 0·25–0·33 eV for electrons and 0·14–0·25 eV for holes. These are trap-limited mobilities of the type discussed in para. 5.2 of Part I, and the activation energies are, therefore, a measure of the energy levels of the localized states, or traps, which limit the mobility.† It is of interest, therefore, to try and calculate the free or microscopic mobility μ_0 which occurs in eqn. (25) of Part I. This is not easy since

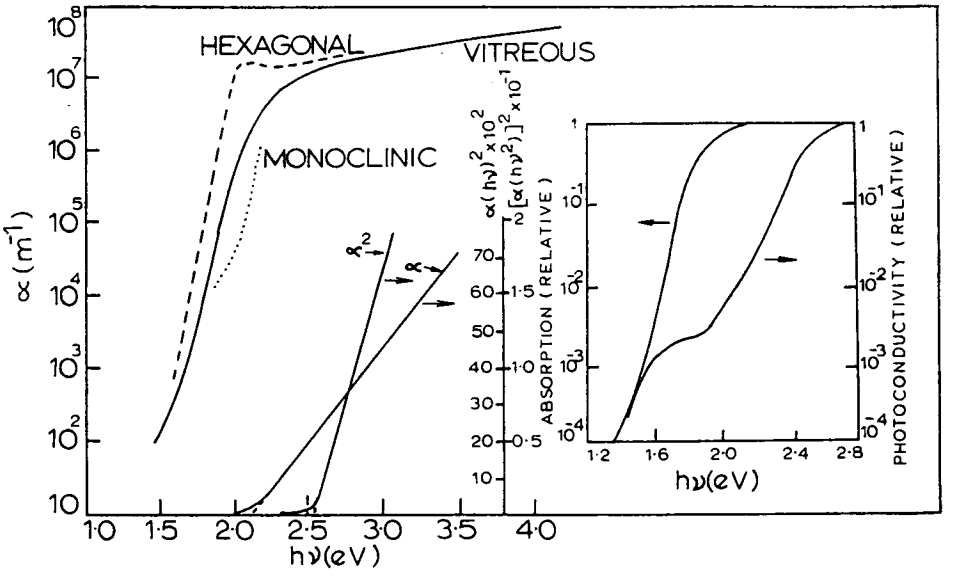

Fig. 7. Optical absorption and photoconductivity (relative) in vitreous Se with some data for the crystalline modifications for comparison.

† The exponential temperature dependence of the mobility is not in itself conclusive evidence of this. Conduction by "polaron" hopping, for example, will have the same form of temperature dependence (see para. 6.2).

it involves making an estimate of N_c and N_t, but by a slightly different procedure Grunwald and Blakeney estimate that for holes μ_0 is about $3{\cdot}5 \times 10^{-5}$ $m^2\,V^{-1}\,s^{-1}$. The microscopic mobility for electrons probably has about the same value.

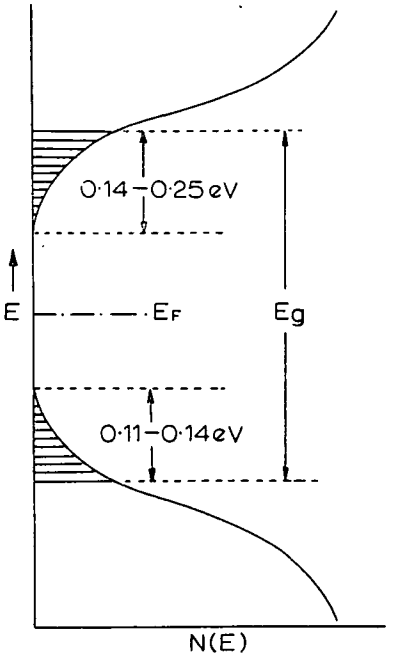

Fig. 8. Density-of-states diagram (schematic) for vitreous Se.

The optical properties of vitreous Se are summarized in fig. 7 and the absorption coefficient is compared with that for the hexagonal and monoclinic forms. A notable feature of the frequency (energy) dependence of the absorption edge is that it increases relatively slowly (compared with the absorption edge in crystalline Ge for example) and exponentially with energy over several decades of absorption coefficient. In this region, therefore,

$$\alpha = K \exp\left[\frac{ah\nu}{kT}\right] \tag{11}$$

where K and a are constants, a usually being about 1·0 or less. Eqn. (11) is known as Urbach's rule and the behaviour which it describes is well known in many materials, both crystalline and non-crystalline (it occurs in hexagonal Se, for instance, fig. 7). There is no satisfactory theory for Urbach's rule at the moment, even for crystalline solids. From the model of the disordered band structure developed in Part I it is tempting, in the present case, to attribute the Urbach rule behaviour to transitions between the exponentially distributed tail of localized states, i.e. to assume that it reflects the density of states shown schematically in fig. 11 of Part I. As mentioned there, however (Section 6), this is probably not so. In the first place transitions between two non-localized states are most unlikely since they are spatially separated. Transitions between localized states in the valence band and non-localized states in the conduction band may contribute, but the absorption coefficient

will only reflect the density of states if the transition probability (eqn. (28) of Part I) is independent of energy. This is unlikely in the present case since the localization (i.e. the rate of decay of the wave-functions) depends upon energy.

Clearly, however, it is not possible, except in an arbitrary way, to take any point on the 'absorption edge' as indicative of an 'optical energy gap'. The difficulty is underlined by the inset of fig. 7 in which the absorption coefficient, on a relative scale, is compared with the spectral response of photoconductivity. The photoconductivity does not reach its maximum until frequencies (energies) well above the absorption edge are reached. This means that over an appreciable energy range absorption processes occur between states in which carrier transport is not possible. In other words, there are absorption processes which do not result in the formation of a *free* electron and/or a free hole.

4.3. *Discussion*

Accepting the validity of the extrapolation, the experiments on liquid Se suggest that the vitreous form is an intrinsic p-type semiconductor with an energy gap, $E_g \sim 2{\cdot}3$ eV. On going from the liquid to the vitreous state there is sometimes a slight change in the slopes of $\log \sigma$ vs. $1/T$ curves, so E_g in the glassy state may be a little lower, say 2·1 eV, as suggested by Davis (1970). As before, this will represent a mobility gap, not an energy gap. The comparatively low activation energies for the drift mobility of electrons and holes suggest that the tails of localized states do not extend far into the previously forbidden gap and that the band structure is now as shown schematically in fig. 8 with the Fermi level E_F near the centre of the gap.

According to Davis (1970) this model is supported by the optical absorption data. He finds that the absorption coefficients in the region *above* the

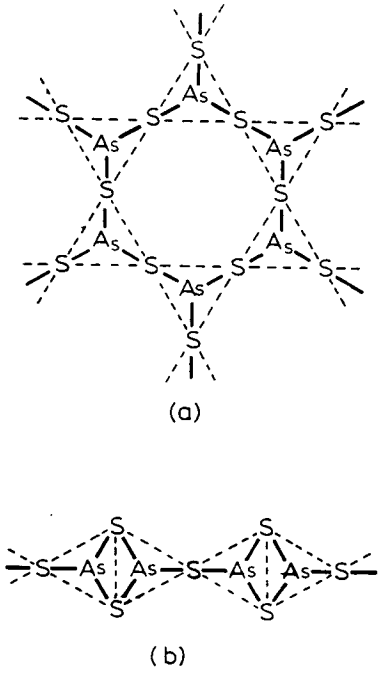

Fig. 9. Two possible structures for As_2S_3; (*a*) layers and (*b*) chains.

exponential edge are linearly dependent on energy, and when plotted in this way (fig. 7) give a straight line which cuts the axis at an energy of 2·1 eV. This is interpreted as an optical energy gap corresponding to the mobility gap, i.e. the energy separation of the non-localized states. The linear dependence can be obtained by assuming that the momentum conservation rule is relaxed and that the transition probability (see eqn. (28), Part I) is constant, hence

$$\alpha\, h\nu \sim \text{const.} \int N_V(E) N_C(E + h\nu)\, dE. \tag{12}$$

As we have seen, the range of localized states is small and for transitions beyond the mobility gap the densities of states N_V and N_C are large and taken as constant, leading to

$$\alpha\, h\nu \sim (h\nu - E_g). \tag{13}$$

According to Hartke and Regensburger (1965), however, the optical absorption at energies above the edge is best fitted by the equation

$$\alpha\, h\nu \sim (h\nu - E_g)^{1/2} \tag{14}$$

and a plot of $(\alpha\, h\nu)^2$ vs. $h\nu$ (fig. 7) then gives a straight line with $E_g = 2{\cdot}53$ eV. Eqn. (14) is the normal form for direct allowed transitions between parabolic energy bands, the $E^{1/2}$ dependence of the density of states being reflected in the $(h\nu - E)^{1/2}$ behaviour of the absorption coefficient. If E_g were as large as this the model of fig. 8 would be consistent if the Fermi level were displaced somewhat from the centre of the gap—towards the valence band for p-type conduction. In Davis's model the higher energy required for photoconduction is pictured as arising from the mutual Coulombic attraction of the hole and electron in the non-localized states just above the mobility gap where the mean-free-path is small (about an atomic spacing); an extra energy which may be as much as 1 eV is required to overcome this attraction. Hartke and Regensburger, on the other hand, suggest that the non-photoconductive absorption is due to an electronic transition to a bound (exciton) level just *below* the mobility gap.

Apart from the (qualitative) difference in the extent of the tail of localized states the only difference between the model of fig. 8 for Se and fig. 5 for Ge is the absence of the acceptor states. This is a consequence of the presumed intrinsic behaviour of Se. There is some evidence, however—not well documented at the moment—of impurities having a significant effect on electrical properties. 'Oxygen-free' liquid Se, for example, has been reported to have a much higher conductivity and a much lower activation energy (0·6 eV). Also, the thermopower has been observed to change sign at lower temperatures in the liquid state when certain impurities are present. The latter could be incorporated into the model by postulating an appropriate donor (or acceptor) level and a temperature-dependent Fermi level, but the first observation (the conductivity being higher and the activation energy lower in the 'purer' material) is contrary to ordinary semiconductor behaviour and would require an explanation on different lines. If the atomic structures we have described for amorphous Ge and Se are correct it would, in fact, be rather surprising if there were not some more radical difference in their behaviour.

5. Chalcogenide glasses

5.1. *Preparation and structure*

The chalcogenide glasses are formed from compounds of sulphur, selenium and tellurium with a wide variety of other elements, e.g. phosphorus, arsenic, antimony, bismuth, thallium, lead, germanium and silicon. As pointed out in Part I this list includes most of the potential glass-forming combinations outside of the oxygen-containing systems. The binary systems As–S and As–Se are especially well known and these include the compounds As_2S_3 and As_2Se_3, both of which readily form glasses; in fact, As_2S_3 probably forms the most 'stable' glass known. Glasses are also known in the As–Te system, but the compound As_2Te_3 can only be prepared in the glassy state by evaporation or special cooling techniques. Other binary systems in which glass formation has been studied include Si–S, Ge–S, Ge–Se, Si–Te and Se–I. Amongst

Table 1. Glass formation in ternary chalcogenide systems: A-B-C.

A	B	C: Ia Group			IIa Group			IIIa Group			IVa group		Va Group				VIa Group		VIIa Group		
		Cu	Ag	Au	Zn	Cd	Hg	B	Ga	In	Tl	Sn	Pb	P	As	Sb	Bi	Se	Te	Cl	Br	I
As	S	X	X	X	X	X	X		X	X	○	X	X	X		⊗	X	●	⊗	X	⊗	●
	Se	○	○	X	○	○	○	○	X	X	⊗	○	X	⊗		⊗	X		⊗			⊗
	Te										⊗										X	⊗
Ge	S				X				X	○		X		●	●				X			
	Se					X				X	○	X	X	⊗	●	⊗	X		X			
	Te													○	⊗							
Si	S															⊗						
	Se														⊗	⊗						
	Te													⊗	⊗							

EXTENT OF GLASS FORMING REGION :– X VERY SMALL
○ SMALL
⊗ MODERATE
● LARGE

ternary systems the choice obviously becomes even larger. Table 1 lists some of the ternaries in which glass formation is known and it indicates roughly the extent of the glass-forming region. Quaternary and other multicomponent glasses can be also formed from most of these systems and clearly the range of compositions quickly becomes embarrassingly large. We shall only be able to touch on some of the general features of these materials.

Most of the chalcogenide glasses can be prepared by normal cooling from the melt, although it is necessary to melt under vacuum or in an inert atmosphere. The glass-forming region can always be extended by special rapid cooling techniques and, in the limit, by deposition from the vapour phase. All of the chalcogenide glasses can be prepared by methods such as sputtering or evaporation, but it must be remembered that if a complex composition is evaporated the different components will probably evaporate at different rates.

Not surprisingly, very little is known about the structure of most of the chalcogenide glasses and only for the simplest compounds are there any x-ray diffraction data. Where information exists about corresponding crystalline forms we can make use of the general rule that in the glass the nearest-neighbour configuration is probably the same. As_2S_3 and As_2Se_3 crystallize in the orpiment structure. In this each As atom is linked to three S (Se) atoms with the As at the apex and the S atoms at the base of a shallow triangular pyramid. The (AsS_3) triangles are joined together to form parallel sheets or layers of puckered 12-membered rings, the layers being held together by van der Waals forces. This structure is shown schematically in a *two-dimensional* form in fig. 9 (*a*). Glass formation is sometimes pictured as the breaking up and 'crumpling' of the layers into aggregates of rings with, probably, a distribution of ring sizes (see fig. 4 of Part I). The chain structure of fig. 9 (*b*) has also been suggested for As_2S_3 and As_2Se_3. X-ray diffraction studies of the glass, however, show only that the local configuration is (AsS_3)—as in the crystal—and there are other structures that cannot be ruled out. A molecular structure is possible, for example, and there is some evidence of this from mass spectrometric studies and the viscous behaviour of simple chalcogenide compounds.

5.2. *Electrical and optical properties*

Although there are some exceptions, the d.c. conductivity almost invariably obeys the usual equation

$$\sigma = \sigma_0 \exp - \left(\frac{E}{kT}\right) \tag{15}$$

with E having the same value over the whole measured temperature range. Some typical results for three psuedo-binary glasses are illustrated in fig. 10. These three compositions were chosen because they allow measurements over a wide range of temperatures. Simple compounds like As_2S_3 and As_2Se_3 are so resistive that measurements are only possible over a limited range of higher temperatures. From our previous discussion of Ge and Se, and anticipating a little, we may interpret this as indicating intrinsic conduction. Thus, the *mobility* gap $E_g = 2E$. In many chalcogenide glasses E_g is in the range 1 to 2 eV, but values from 0·4 to 3·0 eV have been observed. Likewise the constant σ_0 is often in the region 10^5–$10^6\ \Omega^{-1}\ m^{-1}$, but values as low as 10^{-3} and as high as $10^{10}\ \Omega^{-1}\ m^{-1}$ have been recorded. One important practical point to note is the ease with which ohmic contacts of low resistance can be made to the chalcogenide glasses, especially the more complex compositions. This is in marked contrast to the situation in crystalline semiconductors (para. 2.6). We shall return to this point later. The d.c. conductivity of the chalcogenide glasses is also largely insensitive to the addition of impurities (although, again, there are exceptions to this) and this is further evidence for intrinsic conduction.

The thermoelectric power has been measured in many chalcogenide glasses and has always been found to be *positive*. It has a magnitude typical of semiconductors (mV K^{-1}) and it decreases with temperature as predicted by eqn. (5). In this case it is more appropriate to modify eqn. (5) so as to take account of the contribution of both electrons and holes, thus

$$S = \frac{k}{e}\left[\frac{(1-b)}{(1+b)}\frac{E_g}{2kT} + A^1\right] \tag{16}$$

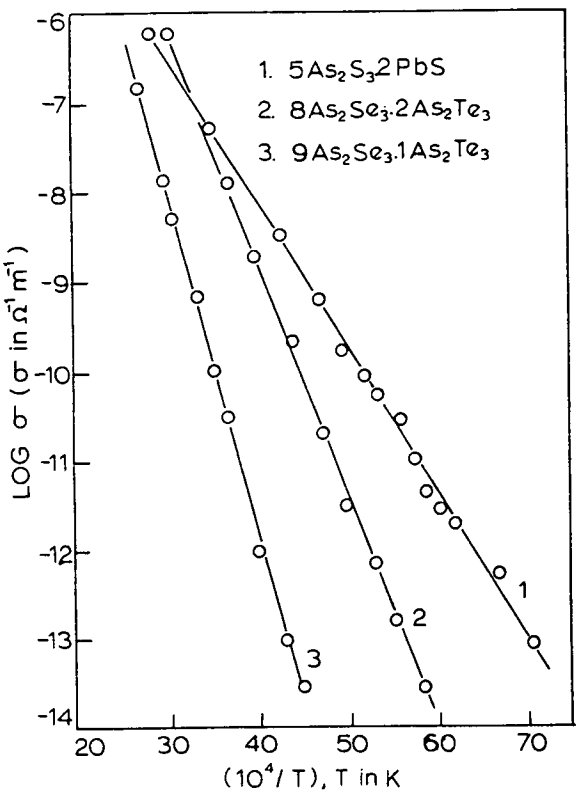

Fig. 10. Temperature dependence of the conductivity of three chalcogenide glasses. (1) 5 As_2S_3 2 PbS; (2) 8 As_2Se_3 2 As_2Te_3; (3) 9 As_2Se_3 1 As_2Te_3. (*From Owen and Robertson* 1970.)

where $b = (\mu_e/\mu_h)$, the ratio of electron (μ_e) to hole (μ_h) mobility. Using this equation and values of E_g obtained from the conductivity, reasonable values of b in the range 0·1 to 0·3 are obtained (see Owen and Robertson 1970). Once again this is consistent with intrinsic conduction and since the holes are more mobile it will be p-type.

The Hall effect has been measured in a few chalcogenide glasses and it has always been found to be *negative*. The mobilities derived from the Hall coefficient and the d.c. conductivity are about 10^{-6} m^2 V^{-1} s^{-1} for most of the compositions measured and this mobility is practically independent of temperature. It is more difficult to measure the drift mobilities in the chalcogenide glasses than in Se, but Marshall (quoted by Owen and Robertson 1970) has estimated a low-field mobility of 5×10^{-11} m^2 V^{-1} s^{-1} for *holes* at room temperature in As_2Se_3. In contrast to the Hall mobility, this decreases exponentially with temperature and an activation energy in the region 0·4 to 0·5 eV was estimated. The electronic drift mobility could not be observed.

The optical absorption in the chalcogenide glasses is very similar to that in vitreous Se. It is characterized by a relatively shallow edge which rises exponentially over a wide range of absorption coefficient (Urbach's rule) followed by a tendency to saturation only at very high absorption coefficients. As mentioned before, no part of this exponential edge can be identified with an 'optical gap', nor is it *a priori* obvious that it can be associated with the

exponential tails of localized states. Some typical data for the three compounds As_2S_3, As_2Se_3 and As_2Te_3 (obtained in the vitreous state by electron-beam evaporation (Weiser 1970)) are shown in fig. 11 and compared, where possible, with the data for the crystalline phase. As also shown in fig. 11

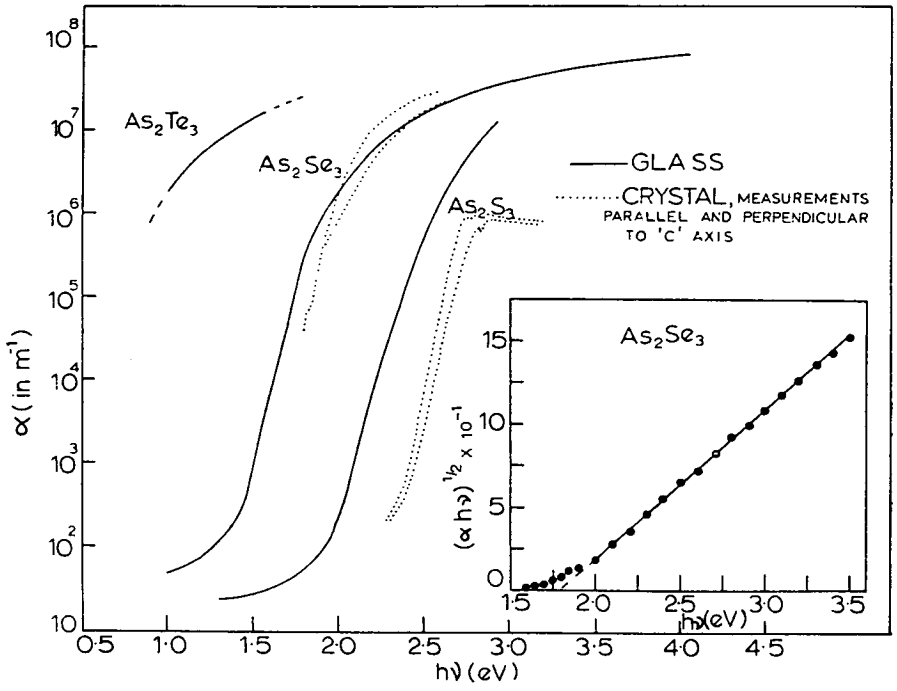

Fig. 11. Optical absorption in vitreous As_2S_3, As_2Se_3 and As_2Te_3 with data on the crystalline forms for comparison.

in the region above the exponential edge of As_2Se_3, $(\alpha h\nu)^{1/2}$ is a linear function of photon energy, i.e. it obeys an equation of the form

$$\alpha h\nu \sim (h\nu - E_g)^2. \tag{17}$$

According to Weiser (1970) his data on As_2Te_3 fits the same equation. We shall call the values of E_g derived from this $E_{g(opt)}$. Hence at *room temperature* $E_{g(opt)} = 1{\cdot}80$ and $0{\cdot}82$ eV for As_2Se_3 and As_2Te_3 (Weiser) respectively. We noted in Part I (Section 6) that an equation of this form has been derived for the absorption coefficient of an amorphous semiconductor. It also has the same form as that predicted for indirect absorption processes in a crystalline semiconductor (eqn. (9)). The implication of its validity in the present context is not that we can distinguish between direct and indirect transitions, but that the momentum conservation rule is relaxed in the amorphous material. There is not sufficient data to make the calculation for As_2S_3, but an estimate in this case gives $E_{g(opt)} \sim 2{\cdot}5$ eV. As Weiser (1970) points out, however, these energies are temperature dependent and for As_2Te_3 he estimates $E_{g(opt)}$ to be $0{\cdot}95$ eV at 0 K. This is significantly different from the mobility (energy) gap deduced from the conductivity which is $0{\cdot}80$ eV in the case of As_2Te_3. The corresponding values for As_2Se_3 and As_2S_3 are, respectively, $1{\cdot}80$ eV and $2{\cdot}1$–$2{\cdot}3$ eV. Thus, in both cases, $E_{g(opt)}$ is probably greater than E_g. There is evidence that this also happens in the more complex chalcogenide glasses.

As in vitreous Se, the photoconductivity of the chalcogenide glasses does not attain its maximum (i.e. unit quantum efficiency) until energies appreciably above the absorption edge are reached.

5.3. *Discussion*

We are once again led to the type of model drawn in fig. 8 for vitreous Se. The tails of localized states probably extend much further into the energy gap for the chalcogenide glasses, but otherwise the general features apply and in this case the 'mobility gap' E_g is less than the optical energy gap. Weiser (1970) suggests that this is because the mobility rises abruptly in a region of energy where the states are not *completely* delocalized, whereas the optical absorption occurs between delocalized bands with the parabolic density-of-states typical of ordinary broad-band semiconductors. Alternatively one could assume that the Fermi level is not in the centre of the 'gap'.

In the complex chalcogenide glasses containing several components the tails of localized states may extend right across the gap and could even overlap. In this event the highest localized valence-band states would lose their electrons, becoming positively charged, to the lower lying conduction band states which would then be negatively charged. Hence in the middle of the gap there would be a band of charged localized states and these could have a profound influence on switching (see Mott 1969 a). It has been estimated (Cohen *et al.* 1969) that the density of localized states in the centre of the 'gap' of a complex chalcogenide glass may be as high as $10^{25}\ \mathrm{m^{-3}\,(eV)^{-1}}$ (cf. with the *effective* density of states in the conduction or valence band of a semiconductor, $\sim 10^{25}\ \mathrm{m^{-3}}$, and atomic densities, $\sim 10^{28}\ \mathrm{m^{-3}}$). The high density of localized states in the gap of the chalcogenide glasses provides the clue to the ease with which ohmic contacts can be applied to them. The localized states behave as traps for carriers and the trapped charges reduce the barrier (space-charge) width at the surface. For a trap density of $10^{25}\ \mathrm{m^{-3}\,(eV)^{-1}}$ the barrier width will be reduced to a few angstroms and carriers from the metal electrode can readily pass through this by quantum-mechanical tunnelling.

It has been emphasized several times that the localized states in the previously forbidden gap provide the possibility of conduction by direct hopping. The current view is that the d.c. conduction does not occur by this mechanism, but instead by excitation of carriers to states above the mobility gap. In principle, however, hopping conduction should be observable in a.c. fields through an increasing conductivity with frequency. This has indeed been observed in the author's laboratory, and by others, in several of the chalcogenide glasses. At frequencies up to about 1 MHz the conductivity normally increases with frequency according to a power law

$$\sigma(\omega) \quad \alpha \quad \omega^n \tag{18}$$

with $n \leqq 1$. There is more than one way to interpret this behaviour, but this particular frequency dependence is consistent with the equations derived by Pollak and Geballe (1961) and others for impurity-band hopping amongst *randomly* distributed sites—a model which is also appropriate in the present circumstances. In a few cases evidence for *d.c.* hopping conduction has also been observed in the form of a decreasing slope (activation energy) for the $\log \sigma$ vs. $(1/T)$ curves at low temperatures where, since the higher delocalized

states will become depopulated, hopping would be expected to contribute more effectively.

In most essential features, therefore, the model band-structure of fig. 8 fits the present facts. As remarked in the case of Se, however, it would be surprising if the chalcogenides, which are probably complicated polymeric materials, have such simple band-structures. Indeed Kolomiets (1968) and his colleagues have evidence from a variety of sources, e.g. space-charge-limited and thermally stimulated currents, for various more or less discrete levels of traps which would be superimposed on the model of fig. 8.

To sound a cautionary note, there are several features which are not readily explicable. The discrepancy in sign between the Hall coefficient and the thermoelectric effect is not understood for example.† There are some impurities which increase the conductivity very markedly (e.g. Ag and Cu in As_2S_3 and As_2Se_3) and, as in Se, there is some evidence that quite small amounts of oxygen *decrease* the conductivity of As_2Se_3. None of these effects are incorporated in the present models, but this does not necessarily mean they are wrong, of course, merely incomplete. At a recent conference, however, measurements were shown which suggested that the $\log \sigma$ vs. $(1/T)$ plots are not straight lines, but instead show a gradually decreasing slope over the whole temperature range (Hulls and McMillan 1970). The straight-line relationship of $\log \sigma$ vs. $(1/T)$ over a wide temperature range has been one of the main pieces of evidence for intrinsic conduction and the 'mobility gap' model, but deviations from linearity could be accounted for in its framework.

6. Transition-metal oxide glasses

6.1. *Basic ideas and comparison with crystalline transition-metal oxides*

We are concerned here with glasses in which the transition-metal oxide is, or can be, a major constituent, i.e. $\geqq 50$ mol per cent. Of these the vanadium phosphates (V_2O_5–P_2O_5) are much the most thoroughly studied, although several papers have appeared on iron phosphate (FeO–P_2O_5) glasses. High-field phenomena and switching in copper phosphate glasses has been described in some detail (Drake *et al.* 1969). In the V_2O_5–P_2O_5 system, glasses with up to 95 mol per cent V_2O_5 can readily be prepared by normal cooling from the melt and it has been reported that a 'pure' V_2O_5 glass can be obtained by deposition from the vapour. Among other binary systems measurements have been reported on the V_2O_5–TeO_2 (up to ~ 55 mol per cent V_2O_5) and the V_2O_5–BaO (60–75 mol per cent V_2O_5) systems; the latter is specially notable since neither of the components alone is considered to be a glass-forming oxide. A variety of ternary and more complex systems are also known, e.g. V_2O_5–P_2O_5–R_2O (or RO) where R is any one of the alkali or alkaline-earth oxides. Several other transition-metal oxides, e.g. TiO_2, MoO_3, WO_3, CuO, are capable of glass-forming in relatively large amounts, but there is very little data on their electrical properties—at the most a measurement of d.c. conductivity. A list of the various systems which have been studied up to 1964, and references to data on them, has been tabulated by Mackenzie (1964); this is still probably a fairly complete list.

† Such a discrepancy could occur, however, in near-intrinsic crystalline semiconductors.

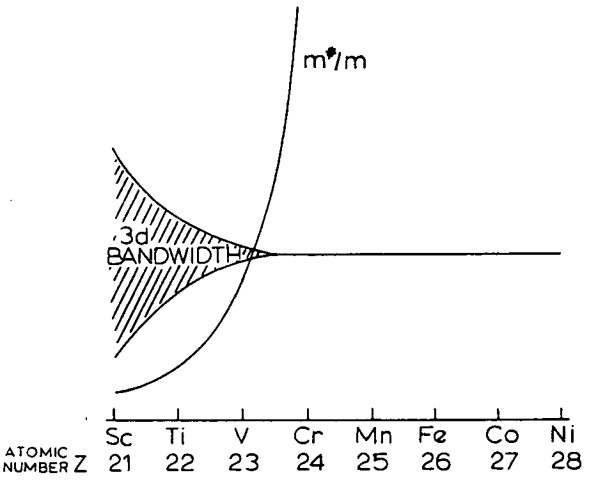

Fig. 12. Illustrating schematically the variation of bandwidth and effective mass in the 3d-transition-metal oxides. (*After Morin* 1969.)

The *crystalline* transition-metal oxides are typical examples of solids in which we may expect the formation of narrow-bands (see Part I, Section 9) and the consequent possibility of localization, whether or not the material is disordered (glassy). The characteristic feature of the electronic structure of the transition-*elements* is the filling-up by electrons of an inner d-level. In the oxides CaO, SrO and BaO which immediately precede the three series of transition-elements, the ions will have a closed-shell electronic configuration and, to a first approximation, the energy bands arise from the filled 2p levels of the O^{2-} ion (valence band) and the empty 4, 5 or 6s levels of the cations (conduction band) (more accurately, there will be some mixing—hybridization—of the s and p levels in both bands). The conduction and valence bands will be separated by a forbidden gap several eV wide in each case and these oxides are insulators. In the same way s and p (or s–p) bands are to be expected in the transition-metal oxides, but in addition there will now be d-levels in between. The d-levels may or may not overlap and broaden out to form a band, but we can say straight away that if d-bands do form they will certainly be narrower than the s–p bands. This follows because the d-states correspond to inner electronic orbitals and because they can hold up to 10 electrons per atom compared with the 2 in s-states. Furthermore, taking the 3d series as an example (inner electronic configuration of argon), as electrons are added to the core the radius of the electron cloud tends to increase because of the mutual repulsion of electrons, and on the other hand to decrease because of the increased nuclear charge. In the 3d series there is an overall *decrease* in ionic radius on going from Ca^{++} ($r = 0{\cdot}099$ nm (0·99 Å)) to Zn^{++} ($r = 0{\cdot}083$ nm (0·83 Å)) indicating that the latter effect predominates and the electron cloud contracts; therefore, if it occurs at all, 3d band formation in the oxides is to be expected at the beginning of the series. Fig. 12, taken from Morin (1959), illustrates the situation schematically. The 3d bandwidth is appreciable in scandium (Sc)—element 21—but decreases rapidly and is essentially zero in chromium (Cr)—element 24; at the same time the effective mass increases. This picture is supported by experimental data which suggests some evidence of a 3d-band

in scandium oxide (Sc_2O_3) and, at high temperatures at least, in the *lower* oxides of titanium (TiO and Ti_2O_3) and vanadium (VO, V_2O_3 and VO_2). Oxides such as Cr_2O_3, MnO, Fe_2O_3, CoO and NiO are normally insulators and the electronic wave-functions are best thought of as being localized on a particular site.

Pure stoichiometric V_2O_5 will also normally be at best a semi-insulator since the 3d-levels are unoccupied (V^{5+} has the configuration $3d^0$) and the band gap will again be 2 eV or more. Conduction will occur more readily, however, in the impure or, more typically, in the non-stoichiometric oxide V_2O_{5-x} in which some of the V^{5+} will occur in a lower valence state, V^{4+} ($3d^1$), V^{3+} ($3d^2$) or V^{2+} ($3d^3$). Some d-electrons are then available for conduction, but in contrast to the lower oxides there is no evidence for the formation of a d-band. This is probably because the V–V separation is somewhat greater in V_2O_5 than in the other oxides (i.e. it is a *minimum* of 3·09 Å in V_2O_5 compared with 2·93 Å, 2·88 Å and 2·85 Å in the conducting (metallic) forms of VO, V_2O_3 and VO_2 respectively). In a *glass* of composition 9·5 V_2O_5 0·5 P_2O_5 (the maximum concentration of V_2O_5 readily attainable) the *average* V–V separation will be approximately 3·75 Å and d-band formation is even less likely.

6.2. *Band model and d.c. conductivity*

A crude band model for a vanadate or other transition-metal oxide glass will be as shown in fig. 13. There will be localized states in the energy gap, a fraction C of which will be occupied by electrons (corresponding to V^{4+}, say) and a fraction $(1-C)$ therefore will be empty (V^{5+}). These localized states, separated from the conduction band by an average energy E, will be distributed over a range of energies W_D because of the randomly fluctuating potential field of the disordered structure. Conduction occurs by an electron hopping directly between occupied (V^{4+}) and unoccupied (V^{5+}) sites or, schematically,

$$V^{4+} + V^{5+} \rightarrow V^{5+} + V^{4+}.$$

Materials in which electronic conduction depends in this way upon the presence of ions in different valence states are often called mixed-valence-semiconductors.

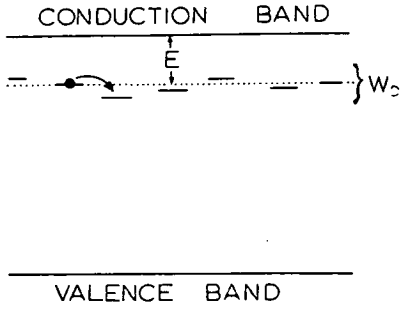

Fig. 13. Localized energy-levels of the transition-metal ions in a transition-metal oxide glass.

Now we saw in Part I (para. 5.2) that the mobility in a hopping process (see also Mott 1969) is given by

$$\mu = \frac{\nu e a^2}{kT} \tag{19}$$

where a is the jump distance and ν the jump frequency. For the present case this must be multiplied by $(1-C)$, the probability of an adjacent site being unoccupied, and for the jump frequency we can write

$$\nu = \nu_0 \exp(-2\alpha a) \exp\left(-\frac{W_D}{kT}\right) \tag{20}$$

in which ν_0 will correspond roughly to a phonon frequency ($10^{+12}-10^{+13}$ Hz) and the first exponential factor containing $\alpha = \sqrt{[(2mE)/\hbar]}$ is the tunnelling probability. Thus

$$\sigma = ne\mu = \frac{\nu_0 n e^2 a^2 (1-C)}{kT} \exp(-2\alpha a) \exp\left(-\frac{W_D}{kT}\right). \tag{21}$$

It remains to substitute for n, the carrier concentration. If N_0 is the total number of sites (occupied or unoccupied) in a solid of volume V, then $n = (N_0/V)C$ since C is the probability that one of these is occupied. Defining n_0 as the number of sites in a 'unit' volume a^3, i.e. $n_0 = N_0(a^3/V)$, then $n_0 = (n/a^3)C$, thus

$$\sigma = (constant) \times \frac{C(1-C)}{kT} \exp(-2\alpha a) \exp\left(-\frac{W_D}{kT}\right) \tag{22}$$

$$\text{with } (constant) = \nu_0 n_0 e^2/a.$$

In addition to the term W_D in eqn. (22) there is another and probably larger source of activation energy which must be taken into account. In a polar material such as a transition-metal oxide, the extra charge introduced by an electron or hole on a particular site will tend to distort or 'polarize' the surrounding ions. This is illustrated, following Austin and Mott (1969), in fig. 14. Consider two identical groups of V^{5+} plus its surrounding oxygen ions (fig. 14 (*a*)) which, as indicated by the arrows, are vibrating with simple harmonic motion about their equilibrium positions. The internuclear distances of groups (1) and (2) are q_1 and q_2 respectively. The energies of the two groups are therefore Aq_1^2 and Aq_2^2, and as illustrated in fig. 14 (*b*) this will be indeterminate for a particular site by the energy W_D. Now introduce an extra electron on site (1), i.e. V^{5+} becomes V^{4+}. This displaces the oxygen ions (fig. 14 (*c*)) which still nevertheless oscillate about their new mean positions. The extra electron has 'polarized' group 1 and has trapped itself in that group by the polarization energy. Let the energy of the extra electron of group 1 be $-Bq_2$ with respect to the same zero as in fig. 14 (*b*); the energy of group 1 and its electron is then

$$Aq_1^2 - Bq_1 \tag{23}$$

which is a minimum at $q_1 = q_0$, where

$$q_0 = \frac{B}{2A}. \tag{24}$$

This is illustrated in fig. 14 (*d*). If the electron is to jump from group (1) to (2) its energy must be the same on either group, i.e.

$$Bq_2 = Bq_1 + W_D \tag{25}$$

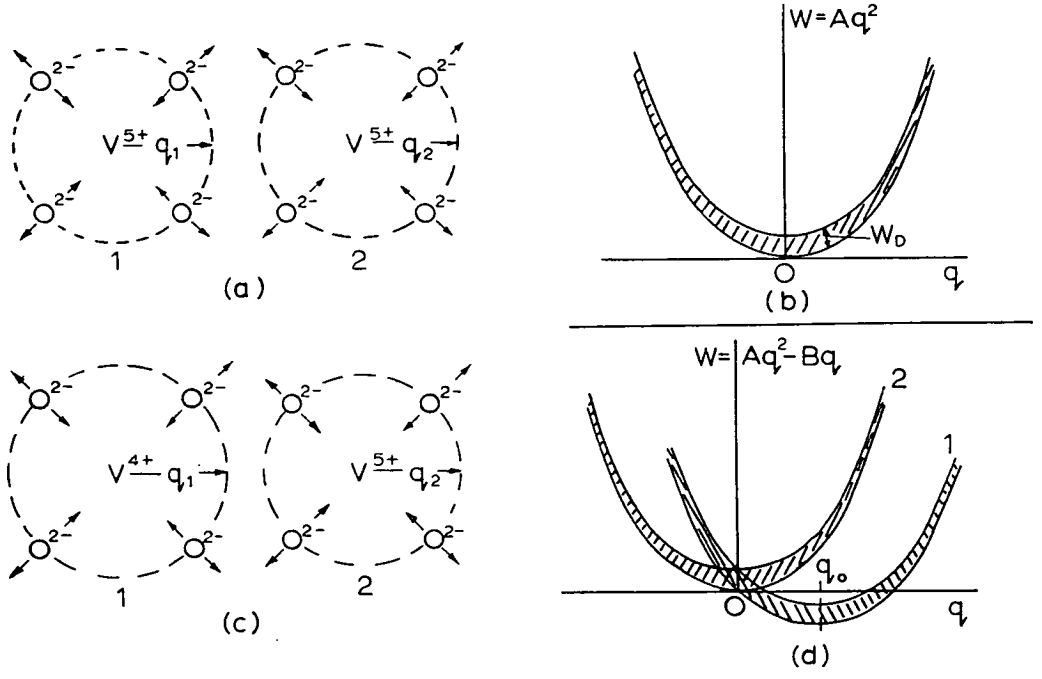

Fig. 14. (*a*) and (*c*) represent vanadium ions (V^{5+} or V^{4+}) and their surrounding oxygen ions; (*b*) and (*d*) illustrate, respectively, their energies as a function of the configurational parameter q. In (*c*) and (*d*) group 1 is 'polarized' by the extra electron (V^{4+}).

and the energy required to produce this state of affairs is

$$W = Aq_2^2 + A(q_0 - q_1)^2$$
$$= A\left(q_1 + \frac{W_D}{B}\right)^2 + A(q_0 - q_1)^2. \tag{26}$$

This is a minimum when $q_1 = (q_0/2) + (W_D/2B)$ and substituting in eqn. (25) gives

$$W \sim W_H + \tfrac{1}{2}W_D \tag{27}$$

where

$$W_H = \tfrac{1}{2}Aq_0^2 = \tfrac{1}{2}W_P. \tag{28}$$

The energy W_P is the polarization or *polaron* energy. 'Polaron' is the name given to the electron with its polarization cloud. In some circumstances it can be treated as a quasi-particle, and just as electron wave-functions overlap to form a band so also may polaron wave-functions form a *polaron band*. The polaron is a large 'particle' with a large effective mass; bandwidths will be small and polaron bands are normally significant, therefore, only at low temperatures. Furthermore, in a glass the potential fluctuations W_D will also reduce the overlap of polaron wave-functions and hence reduce still further the possibilities of polaron-band formation. Hopping is more likely to be the dominant mechanism of transport and W_H is the activation energy for polaron hopping. In place of eqn. (22), therefore, we now have

$$\sigma = (constant) \times \frac{C(1-C)}{kT} \exp(-2\alpha a) \exp\left(-\frac{W}{kT}\right) \tag{29}$$

with

$$W = W_H + \tfrac{1}{2}W_D.$$

Both terms in W will tend to decrease as the temperature decreases. The first, W_H, because as the temperature is lowered the optical (polar) vibrations of the lattice, which make the self-trapping possible, are 'frozen-out'. The second, W_D, for exactly the same reasons discussed in para. 3.3 in connection with amorphous Ge; at low temperatures the electron will make larger hops to find energetically favourable sites leading (Mott 1969) to eqn. (10) for the conductivity. Thus, in contrast to the other semiconducting glasses, we expect plots of log (σT) vs. $(1/T)$ for the transition-metal oxide glasses to show a continuous curvature over a wide temperature range. From eqn. (29) we also expect the conductivity to be zero when C (the mole fraction of V^{4+}, for example) is 0 or 1 and to go through a maximum at $C = \frac{1}{2}$, as also follows from the schematic mechanism shown above.

6.3. *Preparation and structure of transition-metal oxide glasses*

The electrical properties of a transition-metal oxide glass are obviously going to depend upon the two fundamental factors:

(A) The total concentration of the transition-metal oxide.

(B) The ratio of ions in the low and high valence states, e.g. (V^{4+}/V^{5+}), (Fe^{2+}/Fe^{3+}), etc.

Both of these are influenced by a variety of factors which in some instances may be difficult to control:

(1) The amount and nature of other (glass-forming) oxides, and this in turn could affect the situation in several ways.

(a) For the same mole percentage of V_2O_5, V_2O_5–P_2O_5 and V_2O_5–B_2O_3 glasses, for example, will have different densities and hence the average V–V separation will be different. Indeed, the structure of the glasses and distribution of the vanadium ions may be quite different. This could affect the whole question of conduction mechanisms, but at the very least the conductivity, according to eqn. (29), varies inversely as the jump distance.

(b) The oxidation-reduction potential of the melt from which the glass is prepared will be different in the presence of basic (e.g. BaO), amphoteric (e.g. B_2O_3, GeO_2) or acidic (e.g. P_2O_5) oxides, and this will alter the ratio of low to high valence transition-metal ions.

(c) If other reducible species are present (e.g. TeO_2 or other transition-metal oxides) they will affect the oxidation-reduction equilibrium. If present in large amounts they may also enter into the conduction process and possibly change the mechanism. The V_2O_5–TeO_2 system is a case in point.

(d) The nature of the other oxides will affect the polarizability of the glass network and hence the term W_H in eqns. (29) and (31).

(2) The thermal history, involving both the temperature of melting and the cooling schedule. This may also influence the situation in several ways:

(a) The oxidation-reduction potential of the melt, and hence the low/high valence ratio, will depend upon the temperature of the melt and to some extent on the rate of cooling.

(*b*) In what are probably very complex systems, possibly containing large polymeric anions and with a tendency to phase separation (see Section 2 of Part I), the structure of the glass will depend on both the temperature at which it is melted and the rate of cooling.

(*c*) As we saw in Section 2 of Part I the density of glass, in common with other physical properties, depends upon thermal history and this will alter the metal–metal separation. This effect is likely to be a minor one.

Very little is known about the structure of the transition-metal oxide glasses. Plausible assumptions could probably be made about certain features of the structure in some glasses, but only the vanadate glasses have actually been investigated. Optical absorption measurements on some V_2O_5–GeO_2–P_2O_5 glasses have been interpreted as evidence that the vanadium is in sixfold octahedral co-ordination with oxygen ions (VO_6) but, in contrast, electron–spin resonance studies have been interpreted in terms of tetrahedral co-ordination. Crystalline V_2O_5 has a complex layered structure with the V atoms in fivefold co-ordination. Ohashi (1964) has studied the V_2O_5–P_2O_5 system containing up to 50 mol per cent V_2O_5 by paper chromatography. He concludes that the glasses are composed of a mixture of various polymeric vanado-phosphate anions in which the vanadium replaces phosphorus isomorphously. When V^{4+} is present he suggests that it occurs 'interstitially' in the form of the vanadyl cation $(VO)^{2+}$ and that it acts to break down the polymers into smaller groups. Electron microscopy has revealed evidence of phase separation in vanadium-phosphate glasses with 85–90 mol per cent V_2O_5, but so far there have been very few direct structural studies on either a microscopic or macroscopic level.

6.4. *Electrical properties*

Of the transition-metal oxide glasses those in the V_2O_5–P_2O_5 system have been most thoroughly studied and the temperature dependence of conductivity behaves as expected from para. 6.2 and eqn. (29). Some typical results, taken from Linsley *et al.* (1970), are shown in fig. 15 where log (σT) is plotted against $(1/T)$. In the case of the 90 V_2O_5 10 P_2O_5 glass, for example, the activation energy decreases from about 0·33 eV at the highest temperatures to about 0·07 eV at the lowest temperatures. These values are certainly consistent with the W_H and W_D terms in eqns. (27) and (29), but without a much more detailed analysis it is not possible to say to what extent each contributes as the temperature varies except that W_H will predominate at high and W_D at low temperatures. In other transition-metal oxide glasses the results are very similar, but in some cases the activation energies are higher. In copper phosphate glasses, for example, it is approximately 1 eV and there may be a contribution other than the two already considered.

The conductivity of the V_2O_5–P_2O_5 glasses goes through a maximum as $C = (V^{4+}/V_{total})$ is varied, but at a much lower value than that predicted by eqn. (29) (i.e. $C = \frac{1}{2}$). According to Linsley *et al.* the maximum occurs at $C \approx 0{\cdot}1$ in the composition 90 V_2O_5 10 P_2O_5 and shifts to slightly higher values as the amount of V_2O_5 is reduced. The reasons for this are not known, but it suggests that a large fraction of the V^{5+} ions are not available to take part in

the conduction process due, perhaps, to their location in the structure. Hansen (1965), on the other hand, finds that in FeO—P_2O_5 glasses the conductivity *is* a maximum at $C \approx \frac{1}{2}$, but the σ vs. C curves are much broader and flatter than predicted by eqn. (29).

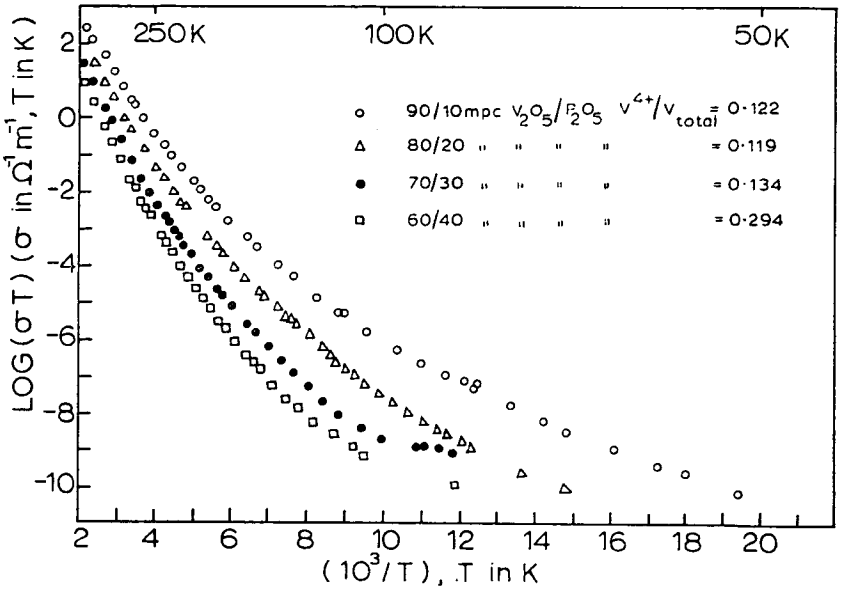

Fig. 15. Temperature dependence of the conductivity of some vanadium phosphate glasses:

○ 90/10 mol per cent V_2O_5/P_2O_5 $V^{4+}/V_{total}=0{\cdot}122$
△ 80/20 mol per cent V_2O_5/P_2O_5 $V^{4+}/V_{total}=0{\cdot}119$
● 70/30 mol per cent V_2O_5/P_2O_5 $V^{4+}/V_{total}=0{\cdot}134$
□ 60/40 mol per cent V_2O_5/P_2O_5 $V^{4+}/V_{total}=0{\cdot}294$

(*From Linsley, Owen and Hayatee* 1970.)

Since conduction occurs by a hopping mechanism we expect the conductivity to increase with frequency. This has been observed in several typical transition-metal oxide glasses, and Linsley *et al.* find that in appropriate temperature ranges the frequency dependence of conductivity in V_2O_5–P_2O_5 glasses is virtually the same as in the chalcogenides (see para. 5.3).

Thermoelectric power measurements have featured prominently in studies of the transition-metal oxides in both crystalline and glassy forms. Seebeck coefficients are usually not more than a few tenths of millivolts, compared with millivolts in the chalcogenide glasses (para. 5.2), and above room temperature there is little or no temperature dependence. In this region the thermoelectric power is given approximately by the formula

$$S = \frac{k}{e}\left[\ln\frac{C}{1-C} + A\right] \tag{30}$$

where A is a constant which is usually small (i.e. $< 0{\cdot}5$) and is often zero. The origin of his equation can be seen by noting that in an ordinary extrinsic n-type semiconductor the first term in eqn. (4) is given by (cf. eqn. (1))

$$\frac{(E_C - E_F)}{kT} = \ln\frac{N_C}{n} = \ln\frac{\text{Effective density of states in the conduction band}}{\text{Density of carriers}}.$$

In the present context the density of carriers is C and the density of states available to these carriers is $(1-C)$, leading to eqn. (30). The Seebeck coefficient is therefore negative if $C<\frac{1}{2}$, zero for $C=\frac{1}{2}$ and positive for $C>\frac{1}{2}$; this is physically reasonable even though electron transport is always involved, for if $C>\frac{1}{2}$ the effective result is the migration of a positive *vacancy*. Although the compositional dependence of eqn. (30) is often obeyed approximately S is not always zero at $C=\frac{1}{2}$ and this implies $A\neq 0$. It is implicit in eqn. (30) that $W_D \approx 0$ and that the polaron energy W_H does not contribute to the thermopower. The temperature independence of the thermopower (at room temperatures and above) means that all the available carriers are 'free' and we can, therefore, take the V^{4+} concentration in a vanadate glass, for example, as the free carrier concentration. From $\sigma=n\mu q$ this leads to very small values of the mobility, e.g. 10^{-6} to 10^{-8} cm^2/V s in V_2O_5–P_2O_5 glasses. At low temperatures (<200 K in vanadate glasses) the thermopower begins to increase rapidly as the temperature decreases, presumably because electrons are being trapped at donor centres (oxygen vacancies) and a term (E/kT), where E is the donor ionization energy, should be included in eqn. (30).

7. Conclusions

Of the questions we posed in the Introduction, we can provide partial answers to some at least. There *is* evidence for band and hopping processes, but normally one mechanism does predominate. In the elemental amorphous semiconductors and the chalcogenide glasses electronic transport is by the band mechanism in steady fields and at high temperature, whereas hopping processes occur in alternating fields and at low temperatures. In the transition-metal oxide glasses conduction is probably by hopping in all circumstances. For some materials we have information about the density of localized states and approximate ideas about their energy distribution. The localized states certainly behave as traps for carriers and probably also as recombination centres, although the evidence for this was not discussed. On their origin we can say little except that all the sources mentioned in the Introduction will contribute. So far as the non-localized bands are concerned there is some evidence (from optical data) that in the chalcogenide glasses these may have the parabolic energy distribution typical of ordinary broad-band semiconductors.

Amongst the semiconducting glasses we seem to have, in fact, examples of broad- and narrow-band semiconductors. That the transition-metal oxide glasses are similar to their crystalline counterparts is not, perhaps, surprising because the localization in this case is not primarily a consequence of the disorder. That the other glasses retain major features of the 'crystalline' band-structure is more noteworthy. As we have noted, differences do exist, but these are mostly of degree (e.g. lower conductivity and mobility) and can be explained by the band-models developed in Part I. There are more fundamental differences, however, notably the effect of impurities. It is not just that many impurities have *no* influence (in contrast to the situation in crystalline semiconductors), but where effects are observed they seem to be of a different kind. Another factor not readily accounted for is the sign discrepancy between the Hall and Seebeck coefficients in the chalcogenide glasses. There is no doubt that a serious obstacle at the moment is the lack of detailed

structural information on most of these materials, both on a microscopic and a macroscopic level.

ACKNOWLEDGMENTS

The author is grateful to Dr. A. Vasko for providing the information contained in table 1.

REFERENCES

AUSTIN, I. G., and MOTT, N. F., 1969, *Adv. in Physics*, **18,** 41.
BERNAL, J. D., 1959, *Nature*, **183,** 141. See also, 1960, *Sci. Am.*, **203,** 124.
CLARK, A. H., 1967, *Phys. Rev.*, **154,** 750.
COHEN, M. H., FRITZSCHE, H., and OVSHINSKY, S. R., 1969, *Phys. Rev. Letters*, **22,** 1065.
DAVIS, E. A., 1970, Proc. 3rd Int. Conf. on Liquid and Amorphous Semiconductors, Cambridge, September 1969. To be published in *J. Non-Cryst. Solids.*
DONOVAN, T. M., SPICER, W. E., and BENNET, J. M., 1969, *Phys. Rev. Letters*, **22,** 1058.
DRAKE, C. F., SCANLON, I. F., and ENGEL, A., 1969, *Phys. Stat. Sol.*, **32,** 193.
GRIGOROVICI, R., 1968, *Mat. Res. Bull.*, **3,** 13.
GRIGOROVICI, R., and MANAILA, R., 1967/68, *Thin Solid Films*, **1,** 343.
HANSEN, K. W., 1965, *J. Electrochem. Soc.*, **112,** 994.
HARTKE, J. L., and REGENSBURGER, P. J., 1965, *Phys. Rev.*, **139,** A970.
HENKELS, H. W., and MACZUK, J., 1953, *J. Appl. Phys.*, **24,** 1056.
HULLS, K., and MCMILLAN, P. W., 1970, Proc. 3rd Int. Conf. on Liquid and Amorphous Semiconductors, Cambridge, September 1969. To be published in *J. Non-Cryst. Solids.*
KOLOMIETS, B. T., 1968, *Proc. IX Int. Conf. on the Physics of Semiconductors, July* 1968, Vol. 2, p. 1259 (Acad. Sci. U.S.S.R.; published by 'Nauka', Leningrad).
LINSLEY, G. S., OWEN, A. E., and HAYATEE, F. G., 1970, Proc. 3rd Int. Conf. on Liquid and Amorphous Semiconductors, Cambridge, September 1969. To be published in *J. Non-Cryst. Solids.*
LIZELL, B., 1952, *J. Chem. Phys.*, **20,** 672.
MACKENZIE, J. D., 1965, *Modern Aspects of the Vitreous State*, Vol. 3, p. 126 (ed. J. D. Mackenzie) (London: Butterworths).
MORIN, F. J., 1959, *Semiconductors*, pp. 600–633 (ed. N. B. Hannay) (New York: Reinhold).
MOTT, N. F., 1969, *Phil. Mag.*, **19,** 835.
MOTT, N. F., 1969 a, *Contemp. Phys.*, **10,** 125.
OHASHI, S., 1964, *Topics in Phosphorus Chemistry*, Vol. 1, p. 189 (ed. Grayson and Griffiths) (New York: Interscience).
OWEN, A. E., and ROBERTSON, J. M., 1970, Proc. of the Symposium on Semiconductor Effects in Amorphous Solids, New York, May 1969. *J. Non-Cryst. Solids.* **2,** 40.
POLLAK, M., and GEBALLE, T. H., 1961, *Phys. Rev.*, **122,** 1742.
SPEAR, W. E., 1969, *J. Non-Cryst. Solids*, **1,** 197.
STUKE, J., 1969, *Festkorperprobleme*, **9,** 46.
STUKE, J., 1970, Proc. 3rd Int. Conf. on Liquid and Amorphous Semiconductors, Cambridge, September 1969. To be published in *J. Non-Cryst. Solids.*
WALLEY, P. A., 1968, *Thin Solid Films*, **2,** 327.
WEISER, K., 1970, Paper presented at 3rd Int. Conf. on Liquid and Amorphous Semiconductors, Cambridge, September 1969. To be published in *Phys. Rev.*

The Author:

The author is Reader in the Department of Electrical Engineering at Edinburgh University. He obtained his Ph.D. from Sheffield University for work on the electrical properties of glasses. After three years research in the U.S.A. on ordinary crystalline semiconductors he returned to this country in 1962 and for several years now his research interest has been in semiconducting glasses.

phys. stat. sol. (a) 1, 297 (1970)

Subject classification: 2 and 14.3; 22.8

University of Edinburgh, Electrical Engineering Department, School of Engineering Science, Edinburgh

Current Noise in Vitreous Semiconductors

By

C. MAIN and A. E. OWEN

Preliminary measurements of the current noise spectrum in the audio frequency range are reported for two glasses of the chalcogenide type, and for a copper phosphate glass of the type used by Drake et al. [1] in their studies of switching. In a glass of composition $As_2Te_3Tl_2Se$, the current noise can be extremely low, — less, for example, than in a single crystal germanium filament. The other materials show a greater current noise, but in each case, the spectrum obeys an equation of the form noise $\sim I^\alpha f^{-\beta}$, where I is the dc current, f the frequency, the constant $\alpha = 1.5$ to 2.0, and $\beta \approx 1$. Some tentative suggestions are made concerning the interpretation of the results.

Es werden vorläufige Messungen des Stromrauschens im Hör-Frequenzbereich an zwei Chalkogenidgläsern und an einem Kupferphosphatglas des Typs, den Drake u. a. [1] für das Studium von Schaltvorgängen benutzt haben, mitgeteilt. Bei Glas der Zusammensetzung $As_2Te_3Tl_2Se$ wurde ein extrem niedriges Stromrauschen gefunden — z. B. niedriger als an monokristallinen Germaniumschichten. Die beiden anderen Materialien weisen zwar ein höheres Stromrauschen auf, aber in allen Fällen ist das Rauschspektrum durch eine Gleichung der Form Stromrauschen $\sim I^\alpha f^{-\beta}$ gegeben, wo I der Wert des Gleichstromes und f die Frequenz bedeuten und die Konstanten $\alpha = 1{,}5$ bis 2.0 und $\beta \approx 1$ sind. Vorläufige Vorschläge für die Interpretation der Resultate werden angegeben.

1. Introduction

Considerable interest has developed in recent years in the properties of so called semiconducting glasses [2 to 4]. These materials are of interest because of the problems they pose about electron transport in disordered systems [3], and also for more practical reasons, because they all seem to have the ability to "switch" between high and low resistance states. The switching behaviour has been observed by Pearson et. al. [5] and Ovshinsky [6] in glasses of the chalcogenide type and by Pearson et al. [5] and Drake et al. [1] in glasses of the transition metal oxide type.

Although measurements have been reported by many workers on most of the basic electrical properties of semiconducting glasses, to the author's knowledge the only report of current noise measurements has been a very brief paper by Kornfeld and Sochova [7]. These authors made measurements at a single frequency and report that current noise in glasses of composition $Tl_2Te \cdot As_2Te_3$ and $Tl_2Se \cdot As_2Te_3$ was so low that it could not be detected against the background of thermal noise. Bearing in mind the disordered, non-equilibrium state of glass, this observation is, at first sight, a little surprising.

The present paper reports the results of a preliminary investigation of current noise in two glasses of the chalcogenide type ($As_2Te_3Tl_2Se$ and As_2SeTe_2) and in a copper phosphate glass switch of the kind studied extensively by Drake et al. [1]. One special reason for making measurements on the latter was to ascertain whether the considerable variations in threshold voltage observed in these

switches, which are essentially current controlled devices, could be due to unusually large current fluctuations (noise). Measurements of the noise spectrum have been made in the audio frequency range as a function of sample current.

1.1 Noise in semiconductors and semiconducting glasses

Noise in semiconductors is observed as fluctuations in the voltage across, or the current through a sample of the semiconductor. The characteristics of these fluctuations may reflect the various mechanisms of carrier generation, recombination, drift and diffusion. Noise also sets limits on the usefulness of semiconducting devices.

Semiconductor noise is generally discussed in terms of three components, each of which may contribute to the total viz. thermal, generation-recombination, and modulation noise. The origin of the first two components is implicit in their names; the origin of modulation noise is still a matter of controversy.

1.1.1. Thermal noise

Under thermal equilibrium conditions, with no applied field, the only observable noise in a semiconductor sample will be thermal noise, arising from fluctuations in diffusion rates of free carriers. The spectral density of this noise will follow the Nyquist relation and the amplitude distribution will be Gaussian. The mean square voltage spectral density $S_v(f)$ is given by

$$S_v(f) = 4\,kT\,R(f)\,,$$

where $R(f)$ is the resistive component of the sample impedance at frequency f.

In vitreous materials, however, thermal equilibrium may never by obtained. As Burgess [8] has pointed out, in glassy materials, internal readjustments may be fairly slow, and this may result in electrical noise in excess of, or of a different character than that expected e.g. discrete impulses, rather than a Gaussian noise voltage, due to abrupt changes in molecular disposition or bonding at individual locations in the solid.

1.1.2. Generation-recombination noise

Spontaneous fluctuations, in the generation rates, recombination rates, trapping rates etc., produce fluctuations in the free carrier densities, and therefore in conductivity. Although these fluctuations occur in thermal equilibrium "no field" conditions, they can be observed only when current is passing through the sample. For example, in the simple case of direct transitions, or when the density of recombination centres is much less than the density of free carriers, the spectral density of the noise voltage is of the form

$$S_v(f) \sim I^2 \frac{\tau}{1 + \omega^2 \tau^2}\,,$$

where I is the dc current through the sample, and τ is the transient electron-hole pair lifetime, or the Shockley-Read lifetime in the case of indirect transitions. Noise spectra measurements can thus give information about carrier lifetimes and transition probabilities.

1.1.3. Modulation noise

Modulation noise and contact noise have a $1/f$ spectral characteristic which may mask any structure caused by generation-recombination noise. The $1/f$

noise observed in many materials can be attributed to slow modulations of conductivity. According to some investigators e.g. McWhorter [9] this is a surface effect resulting from the slowly fluctuating occupancy of "slow" surface states. Carriers trapped in these states may influence the surface recombination velocity over a wide area, and could therefore have a much larger effect on the conductivity than would be expected from the simple trapping of a single carrier. Bulk effects due to trapping states at imperfections may also occur, especially in highly disordered materials — glasses and amorphous films. Various mechanisms essentially dependent on contact effects have also been proposed to explain modulation noise.

More recently Hooge [10] has suggested that $1/f$ noise is a general bulk effect in semiconductors, inversely proportional to the total number of mobile charge carriers in a sample. He speculates that $1/f$ noise is related to the influence of the *drift* velocity on the Brownian motion of charge carriers, and arrives at an empirical relation based on dimensional reasoning that

$$S_I(f) = \frac{4\gamma I^2}{N_{\text{tot}} f} v^2 \,(\text{A}^2\,\text{cm}^2\,\text{Hz})\,,$$

where $S_I(f)$ is the $1/f$ noise current spectral density, I the dc sample current, N_{tot} the total number of mobile carriers in the sample, and γ is a numerical constant.

Experimentally, $1/f$ noise is stable, and according to Hooge [11] is stationary in the statistical sense (although a recent paper by Brophy [12] does not agree with this) but this would imply, by application of the Wiener-Khintchine transform, that the spectrum is an *even* function of frequency, see e.g. Bell [13], and much of the theoretical work in this field has been aimed at approximating the $1/f$ form from even functions e.g. using lifetime distributions.

1.2 Noise in vitreous semiconductors

If the mechanisms of noise generation in crystalline semiconductors are assumed to operate in non-crystalline semiconductors, then it might be expected (perhaps naively) that the noise associated with trapping centres, defects etc.. would be greater in a glass, because of its higher density of defects. In the case of chalcogenide glasses, for example, where the presence of resistive barriers has been postulated to explain the dependence of conductivity on frequency (and other results) Mott [3], Owen [4], the current noise might be expected to be similar to that in polycrystalline semiconductors i.e. contact-type $1/f$ noise of high intensity. As mentioned earlier, however, a report by Kornfeld and Sochova [7] on current noise measurements on two chalcogenide glasses showed that, under their experimental conditions, this noise was four to five times lower than background thermal noise. Their measurements were made on samples of $As_2Te_3Tl_2Se$ and $Tl_2Te \cdot As_2Se_3$, at 1.4 kHz with dc currents of up to 3 mA. These two glasses have relatively low resistivities of 250 and 15 Ω cm, respectively, at room temperature. There appear to have been no measurements on current noise in transition metal oxide glasses — the other main type of semiconducting glass.

2. Experimental Method

The glass systems $As_2Te_3\,Tl_2Se$ and As_2SeTe_2 were made by melting the constituent components in sealed evacuated silica tubes at about 600 °C. The composition $As_2Te_3\,Tl_2Se$ has a fairly low resistivity ($3 \times 10^3\ \Omega$cm in this case)

and As_2SeTe_2 has a resistivity (3×10^5 Ωcm) which provides samples of the maximum impedance for noise measurement with the existing apparatus. Samples of this glass also have about the same impedance as the copper phosphate glass switches and hence noise measurements in the two different materials are comparable. Disc shaped samples of the low resistivity glass, 10 mm diameter and 2 mm thick, were made by cutting with a diamond saw, while a flat sample of the high resistivity glass was made by a pressing technique, giving dimensions 0.5 mm thick and area 1.5 mm². Painted on indium gallium amalgam (on both glasses) and evaporated silver (on the low resistivity glass) were applied as electrode materials. Resistances of about 1 kΩ and 1 MΩ, for low and high resistivity glass respectively were obtained, ensuring low noise operation of the appropriate amplifiers.

The copper phosphate switches were kindly supplied by Mr. C. F. Drake of S.T.L. Laboratories and were in the form of small beads of glass fused onto two contact copper wires. The switches were selected to have an impedance in the "off" state of ≈ 1 MΩ. Measurements on these switches were made only in the "off" state.

The current noise spectra were measured by a standard technique, described for instance, by Brophy [14], which employs wire resistors as noise sources, followed by an amplification of about 100 dB by low noise wide band and band pass circuitry, and r.m.s. or linear detection. The spectrum of the additional noise generated in a sample when direct current is passed may then be calculated using standard methods (van der Ziel [15]).

3. Experimental Results

Spectral density measurements were made on two samples of the composition $As_2Te_3Tl_2Se$. Sample 1 had gallium-indium electrodes and a dc resistance of

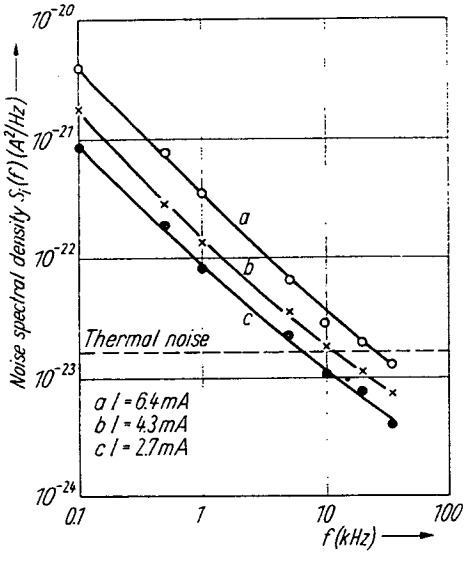

Fig. 1. Current noise spectra for sample 1, $As_2Te_3Tl_2Se$, with gallium-indium electrodes

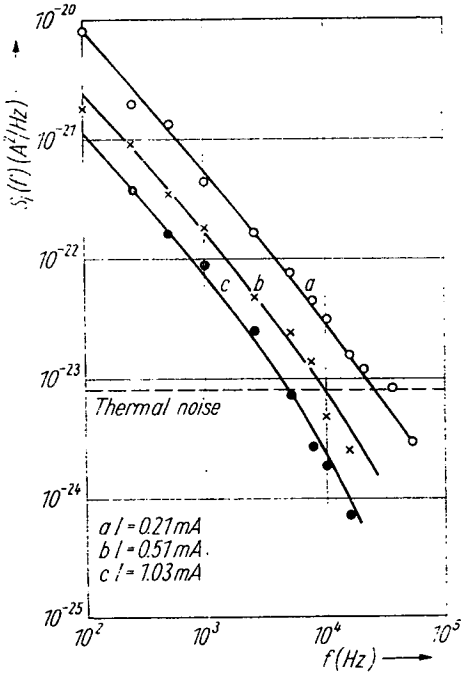

Fig. 2. Current noise spectra for sample 2, $As_2Te_3Tl_2Se$, with silver electrodes

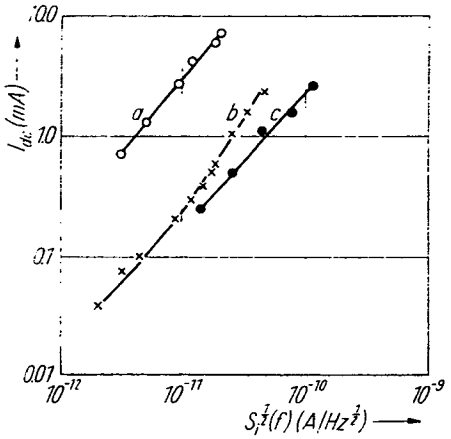

Fig. 3. The dependence of the r.m.s. noise spectral intensity on sample dc current, for (a) sample 1, (b) sample 2, and (c) 3.3 °K carbon composition resistor

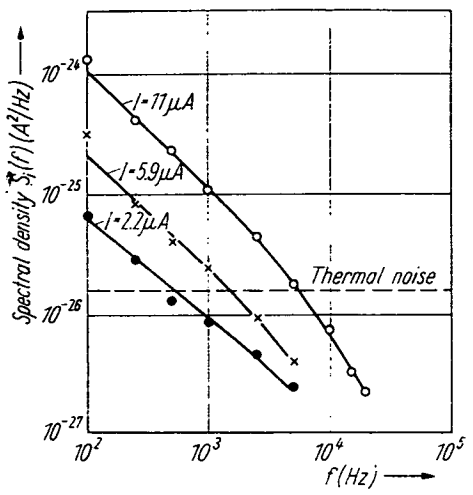

Fig. 4. Current noise spectra for a sample of As_2SeTe_2 with gallium–indium electrodes

1.03 kΩ, and sample 2, silver electrodes and a dc resistance of 2.01 kΩ. For comparison, measurements were also made on a carbon resistor (3.3 kΩ). Spectral density curves, for different sample currents are shown in Fig. 1 and 2 for samples 1 and 2, respectively. The relevant thermal noise levels are also shown. The spectral noise density at a frequency of 1 kHz is plotted as a function of sample current in Fig. 3, for samples 1, 2, and the carbon resistor. Spectral density curves for the composition As_2TeSe_2 and for the copper phosphate switch are shown in Fig. 4 and 5 respectively. In Fig. 6, the noise at 1 kHz is plotted as a function of current for these two materials, and also, for comparison, for a 1 MΩ carbon resistor.

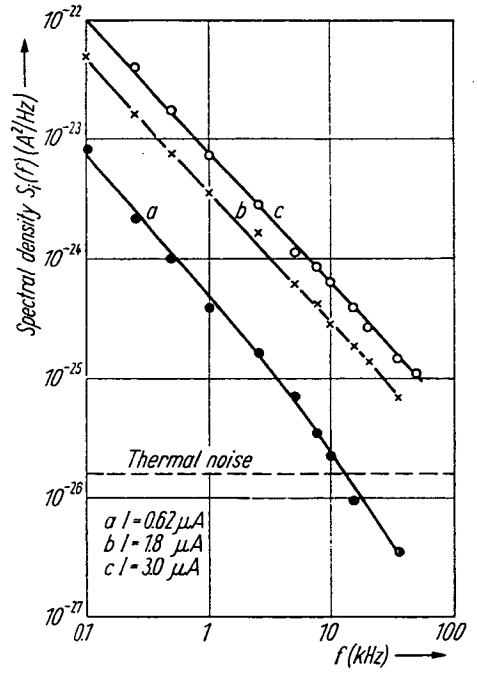

Fig. 5. Current noise spectra for a copper phosphate glass switch in the "off" state

Fig. 6. Dependence of the r.m.s. noise spectral intensity on sample dc current for (a) As_2SeTe_2 sample, (b) carbon resistor (1 MΩ), and (c) glass switch

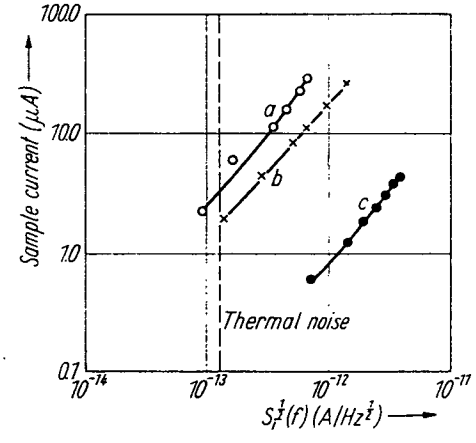

The glass switch was about 3 orders of magnitude more noisy than the other two high resistance samples, and it was noticed that the switch, immediately before switching, oscillated between off and on, or intermediate states. This phenomenon lasted for less than 1 s, and measurements (considering it to be noise) could not be made. The noise prior to "oscillation" was, however, reproducible after switching cycles had been performed.

In all cases, the spectra are of the form

$$S_i(f) = K\, I^{\alpha} f^{-\beta}, \tag{1}$$

where K is a constant depending on the sample, and α and β are constants. To obtain a more direct comparison of the relative "noisiness" of the samples, noise *power* spectra $S_w(f)$ were interpolated for a fixed sample current of 2.5 mA, and the coefficients P in the relation

$$S_w(f) = P\, I^{\alpha} f^{-\beta} \qquad (\mathrm{W/Hz})$$

were normalised with respect to that for sample 1. Results on a *single crystal* germanium filament obtained by Hyde [16] are also included for comparison (Table 1).

Table 1

Experimentally determined values of the parameters K, α, β, and the normalised noise power coefficient P'

Sample	R (kΩ)	K	α	β	P'
$As_2Te_3Tl_2Se$, In–Ga electrodes	1.03	2.04×10^{-15}	1.65	1.12	1
$As_2Te_3Tl_2Se$, Ag electrodes	2.01	1.94×10^{-13}	1.51	1.22	95
Carbon resistor	3.3	4.55×10^{-13}	1.80	1.05	2.2×10^{2}
As_2TeSe_2 In–Ga electrodes	1000	1.1×10^{-13}	1.86	1.14	5.4×10^{4}
Copper phosphate switch	1000	2.8×10^{-11}	1.70	1.06	1.4×10^{7}
Carbon resistor	1000	9.1×10^{-14}	1.80	0.94	4.4×10^{4}
Germanium filament					20

4. Discussion

The values for α and β give the current and frequency dependence of the current noise voltage spectral density. Theoretically, for conductivity fluctuations, α should be 2, but most of the values were lower than this. This can occur when the current is not uniformly spread over the cross-section of the sample, as the noise produced at points of high current density is increased out of proportion to the increase in resistance arising from the constriction of the current path (Bell [17]). In most cases, the value of β corresponds nearly to a $1/f$ dependence.

There are several difficulties in trying to relate these results to physical mechanisms. There is, first of all, the lack of data on various important parameters such as carrier densities, trap densities, mobilities and lifetimes in glassy semiconductors. Secondly, and probably the more important consideration at the moment, the conduction mechanism itself is not fully understood. Any interpretation must therefore be very tentative and qualitative but it may nevertheless be useful particularly if, in turn, it can throw more light on conduction mechanisms.

The chalcogenide glasses are often regarded as being similar in many ways to ordinary semiconductors (Owen [4], Owen and Robertson [18]). There are differences, of course, but Cohen, Fritzsche, and Ovshinsky [19] suggest that these can be explained by a band model in which a high density of localized states with a low carrier "mobility" ($< 10^{-2}$ cm^2/Vs) are separated from bands of non localized states with relatively high carrier mobilities (> 10 cm^2/Vs); i.e. the familiar energy gap of ordinary semiconductors is replaced by a "mobility gap". The dc conductivity is supposed to occur by the excitation of carriers into the bands of non localized states and the "free" carrier population will be in equilibrium with carriers trapped in the localized states.

As a first approximation we could assume normal semiconductor band transport and obtain an order of magnitude estimate of the level of generation-recombination noise in the chalcogenide glasses from Machlup [20] and van der Ziel's [21] results for a semiconductor with traps. In this picture, the chalcogenide glass would be a semiconductor with an exceptionally high density of traps so that the time a carrier spends in trap (τ_t) may be much greater than the "free" lifetime (τ_f) in the conduction or valence band. Van der Ziel's [21], [22] formula for the current spectral density treating electrons and holes *equally* assuming binominal statistics and adapting to include a distribution of lifetimes expected in the present case, is

$$S_i(f) = \frac{4\, I^2\, p}{N} \int \frac{\tau\, G(\tau)\, d\tau}{1 + \omega^2 \tau^2}, \tag{2}$$

where $p = \tau_t/(\tau_t + \tau_f)$ the probability that the carrier is trapped, $\tau = \tau_t \tau_f/(\tau_t + \tau_f)$, $G(\tau)$ expresses the distribution of τ's, and $N = N_0 + P_0$ the total average number of free carriers in the sample.

In this present case, $p \approx 1$, $\tau \approx \tau_f$, and $I = N e \mu V/L^2$, where e is the electronic charge, μ the drift mobility of free carriers, V the voltage across the sample, and L is the sample length.

Thus

$$S_i(f) = 4\, I \left(\frac{e \mu V}{L^2}\right) \int \frac{\tau_f\, G(\tau_f)}{1 + \omega^2 \tau_f^2}\, d\tau_f. \tag{3}$$

As is well known (McWhorter [9]) a distribution function such that

$$G(\tau_f)\, d\tau_f = \frac{1}{\tau_f}\, d\tau_f, \tag{4}$$

formally accounts for the $1/f$ frequency spectrum of noise, and substituting in (3) gives

$$S_i(f) = I \left(\frac{e \mu V}{L^2}\right) \frac{1}{f\, 2.3 \lg\left(\frac{\tau_{f2}}{\tau_{f1}}\right)}, \tag{5}$$

where frequency $f = 2\pi\omega$, for $\omega \tau_{f1} \ll 1 \ll \omega \tau_{f2}$ from the experimental data on specimen 1 at $f = 1$ kHz, $I = 1$ mA,

$$S_i(f) = 2 \times 10^{-20} \frac{\mu}{\lg\left(\frac{\tau_{f2}}{\tau_{f1}}\right)} = 10^{-23}\ (\mathrm{A^2/Hz}) \tag{6}$$

experimentally. Hence if $\lg(\tau_{f2}/\tau_{f1}) \geqq 4$, from observation of the range over which the spectrum is of $1/f$ form, then $\mu \geqq 20$, which is consistent (allowing for the approximation involved) with conduction in a band (non-localized states). The ratio τ_{f2}/τ_{f1} is, however, virtually a disposable parameter, and this "comparison" cannot be regarded as proof of this model.

It is perhaps of more significance to note that in many chalcogenide glasses it seems to be almost a general rule that the ac conductivity in the audio frequency range (at least up to 1 MHz) increases approximately linearly with frequency

$$\sigma(\omega) = A\,\omega^n \tag{7}$$

with $n \approx 1$ (Owen and Robertson [18], Rockstad [23]) the frequency dependence of the ac conductivity is given by

$$\sigma(\omega) \sim \int \frac{\omega^2\,\tau\,F(\tau)\,\mathrm{d}\tau}{1+\omega^2\,\tau^2}\,. \tag{8}$$

In this equation, τ is a relaxation time and does not necessarily have the same significance as the τ in equation (2) or the τ_f in equation (3). The distribution function $F(\tau)$ required to give the linear dependence on frequency of equation (7) is, however, of exactly the same form as equation (4)

$$F(\tau)\,\mathrm{d}\tau = \frac{1}{\tau}\,\mathrm{d}\tau\,.$$

It is tempting to conclude, therefore, that the time constants of equations (8) and (2) or (3) are the same and hence, that the ac conductivity and the current noise spectrum have their origins in the same mechanisms. This would not be consistent with current ideas, according to which, the ac conductivity occurs through hopping between localized states and the dc conductivity by excitation of carriers into non localized levels, (cf. Mott [24]). It must be recognized however, that there are several possible sources of $1/f$ noise (van der Ziel [25]) and the correlation between current noise and the ac conductivity would have to be established *quantitatively* before the connection could be regarded as substantiated. The point clearly warrants further investigation.

A comparison with Hooges observation on $1/f$ noise can also be made, using his empirical relation

$$\left\langle\left(\frac{\Delta\sigma}{\sigma}\right)^2\right\rangle = \left\langle\left(\frac{\Delta I}{I}\right)^2\right\rangle = C\,\frac{\Delta f}{f}$$

or

$$\frac{S_i(f)}{I} = \frac{C}{f}\,,$$

where $S_i(f)$ and I as above, and the constant C is given approximately by

$$C \approx \frac{2\times 10^{-3}}{N_f}\,,$$

where N_f is the total number of *free* charge carriers in the sample. Applying this result to sample 1 gives a value for N_f of about 10^{11}. The total number

of carriers, trapped and free (N_{tot}) is given by

$$N_{tot} = \frac{\sigma}{e\,\mu_t} \times \text{volume} .$$

Ivkin, Kolomiets and Lebeder [26] estimate an *upper limit* of 10^{-1} cm^2/Vs for the *trap limited* mobility μ_t of a glass of this kind and hence $N_{tot} = 6 \times 10^{15}$. Hence the ratio of trapped to free carriers is very large ($\approx 10^4$) as suggested above.

One further point to be made about the results for the chalcogenide glasses is that the extremely low noise of sample 1 (the $As_2Te_3Tl_2Se$ composition) is not consistent with the "potential barrier" model which was once proposed for materials of this sort (Mott [3], Owen [4]). For the same reason, a "microcrystalline" model would be inappropriate for the structure of these glasses. The more resistive glasses are *comparatively* more noisy and this may indicate that potential barriers or other internal discontinuities might play some role in these cases, but it remains to be determined to what extent the noise is a property of surface or contact effects.

As mentioned in the introduction, the measurement on the copper phosphate glass switch were primarily made in order to determine whether or not current fluctuations (noise) might be responsible for the wide variation in threshold voltage of these devices (Drake et al. [1]). The results indicate that this is probably not the case, since the wide band r.m.s. noise across the device prior to switching was about 100 μV, while the threshold voltage varied by tens of volts.

Acknowledgements

The authors thank the referee for bringing to their notice recent work by F. N. Hooge. One of us (C. Main) is grateful to the Science Research Council for the provision of a research studentship.

References

[1] C. F. Drake, I. F. Scanlan, and A. Engel, phys. stat. sol. **32**, 193 (1969).
[2] B. T. Kolomiets, phys. stat. sol. **7**, 359 (1964); **7**, 713 (1964).
[3] N. F. Mott, Adv. Phys. **16**, 49 (1967).
[4] A. E. Owen, Glass Ind. **48**, 637 (1967); **48**, 695 (1967).
[5] A. D. Pearson, W. R. Northover, J. F. Dewald, and W. F. Peck, Proc. VI. Internat. Congress on Glass, Washington, 1962 (p. 357).
[6] S. R. Ovshinsky, Phys. Rev. Letters **21**, 1450 (1968).
[7] M. I. Kornfeld and L. S. Sochova, Soviet Phys. — Solid State **1**, 1256 (1960).
[8] R. E. Burgess, J. Polymer Sci. (Part C) **17**, 51 (1967).
[9] A. L. McWhorter, M.I.T. Lincoln Lab. Report 80 (1955).
[10] F. N. Hooge, Phys. Letters (Netherlands) **A29**, 139 (1969).
[11] F. N. Hooge, Proc. Conf. Physical Aspects of Noise in Electronic Devices, Nottingham, Peregrinus, Stevenage 1968 (p. 123).
[12] J. J. Brophy, Phys. Rev. **166**, 827 (1968).
[13] D. A. Bell, Proc. Conf. Physical Aspects of Noise in Electronic Devices, Nottingham, Peregrinus, Stevenage 1968 (p. 107).
[14] J. J. Brophy, J. appl. Phys. **25**, 222 (1954).
[15] A. van der Ziel, Noise, Prentice-Hall, Englewood Cliffs, 1954.
[16] F. J. Hyde, Report of the Meeting on Semiconductors held by the Physical Society, Rugby 1956 (p. 57).

[17] D. A. BELL. Electrical Noise. Van Nostrand, London 1960 (p. 241).
[18] A. E. OWEN and J. M. ROBERTSON, J. non-cryst. Solids **2**, 87 (1969).
[19] M. H. COHEN, H. FRITZSCHE, and S. R. OVSHINSKY, Phys. Rev. Letters **22**, 1065 (1969).
[20] S. MACHLUP, J. appl. Phys. **25**, 341 (1954).
[21] A. VAN DER ZIEL, J. appl. Phys. **24**, 222 (1953).
[22] A. VAN DER ZIEL, Fluctuation Phenomena in Semiconductors. Butterworths, London 1959 (p. 56).
[23] H. ROCKSTAD, Paper presented at the Symposium on Semiconducting Effects in Amorphous Solids, New York, May 1969, to be published in J. non-cryst. Solids.
[24] N. F. MOTT, Festkörperprobleme **9**, 22 (1969).
[25] A. VAN DER ZIEL, Fluctuation Phenomena in Semiconductors, Chap. 5, Butterworths, London 1959.
[26] E. B. IVKIN, B. T. KOLOMIETS, and E. A. LEBEDER, Bull. Acad. Sci. URSS. Sér. phys. **28**, 1190 (1964).

(Received November 10, 1969)

Reprinted from
PHILOSOPHICAL MAGAZINE, Vol. 24, No. 192, p. 1281, December 1971

Drift Mobility Studies in Vitreous Arsenic Triselenide

By J. M. MARSHALL and A. E. OWEN
Department of Electrical Engineering, University of Edinburgh

[Received 7 May 1971]

ABSTRACT

The drift of charge carriers in thin vitreous films of arsenic triselenide has been examined by a transit time technique. The specimens used were prepared by cooling from the molten state, rather than by evaporation.

Electron mobility measurements were found to be impractical, the mobility being estimated as less than 10^{-10} m^2 v^{-1} sec^{-1} at room temperature. The hole mobility was measurable, however, and was found to be strongly dependent on temperature and applied electric field. The hole transit pulses were of a ' rounded ' form, indicating a spread of carrier transit times.

The field dependence was of a form attributable to the Poole–Frenkel effect (field-stimulated emission of carriers from charged trapping centres). After extrapolation of the measurements to zero applied field, the temperature dependence of the mobility indicated an activation energy of about 0·43 ev.

These results, and those of a subsidiary examination of the temperature and field dependence of the specimen conductivity, are discussed in terms of the band structure of the material. A possible cause of the transit pulse rounding is also advanced.

Finally, an account is given of the observation of bistable switching action in the specimens.

§ 1. INTRODUCTION

WITH the development of transit time methods for the measurement of carrier drift mobilities in low-mobility materials, a large volume of information has been accumulated in recent years. The practical knowledge of the transport properties of vitreous semiconductors is still, however, extremely fragmentary. As far as drift mobility measurements are concerned, all examinations to date appear to have been performed using evaporated amorphous film specimens, and the comparison of such measurements with other physical parameters obtained from studies of bulk vitreous material is not necessarily straightforward. Many measurements have been made of the carrier mobilities in amorphous selenium. Spear (1957, 1960) and Hartke (1962), for example, have reported hole drift mobilities characterized by an activation energy of about 0·14 ev and room temperature values of the order of 10^{-5} m^2 v^{-1} sec^{-1}. Grunwald and Blakney (1968) have reported that the activation energy is dependent upon the method of specimen preparation, and indicate a value of the order of 0·21 ev. A recent study by Tabak (1970) appears to confirm this higher value, and suggests that the value of 0·14 ev obtained by earlier investigators is in error because of an insufficiently large temperature range of

measurement. An examination by Marshall (1970) indicates that the characteristics of vitreous specimens, prepared directly from molten material, may exhibit significant differences from those of evaporated films.

Investigations of the mobilities of carriers in amorphous arsenic triselenide have been performed in less detail, primarily because of the low mobility values. Kolomiets and Lebedev (1967) have reported a hole drift mobility of the order of $4 \times 10^{-8}\,m^2\,v^{-1}\,sec^{-1}$ at room temperature, decreasing by a factor of 1·5 to 2 at $-10°C$. The observed transit pulses were of a 'rounded' form. Tabak (1969) has also examined arsenic triselenide during the course of a study of arsenic doping in selenium. A room-temperature hole mobility of about $10^{-9}\,m^2\,v^{-1}\,sec^{-1}$ was found, the transit pulses again being described as 'rounded'. Tabak used a comparison of results obtained in specimens of different thicknesses at identical values of applied field to identify the observed pulse with a transit, rather than with a trapping phenomenon. A more extensive examination has recently been reported by Scharfe (1970). In this study, the hole drift mobility was found to be field-dependent. Once again, the mobility at a particular field value was consistent between specimens of varying thicknesses. Scharfe has also reported that the shape of the hole transit pulse depends on the choice of electrode material. With aluminium electrodes, as used by Kolomiets and Lebedev (1967) and by Tabak (1969), the transit pulse is of a rounded form, indicating the lack of any unique transit time. However, with gold electrodes, Scharfe does observe a 'break point' in the transit pulse although appreciable rounding of the pulse is still observed. The actual magnitudes of the mobilities measured by Scharfe ($10^{-9}\,m^2\,v^{-1}\,sec^{-1}$ at a field of $4 \times 10^6\,v\,m^{-1}$ increasing to $6 \times 10^{-9}\,m^2\,v^{-1}\,sec^{-1}$ at a field of $2 \times 10^7\,v\,m^{-1}$) were of the same order as those indicated by previous investigators.

In the present paper we report measurements on vitreous films of arsenic triselenide over a range of values of temperature and electric field, and discuss the results in terms of the band structure of the material.

§ 2. Specimen Preparation

Films of vitreous arsenic triselenide, with thicknesses in the range 1 to 5 microns, were prepared by a 'bubble blowing' technique. A small silica crucible containing the material was heated to a temperature sufficiently above the melting point as to produce a viscous liquid. This operation was performed under a nitrogen atmosphere in a glove box. Excessive heating was avoided, and the crucible was normally covered to minimize evaporation. A section of fine bore glass tubing was dipped into the melt and withdrawn, forming a globule of molten arsenic triselenide on the end of the tube.

A bellows arrangement then forced nitrogen gas down the tube, producing a thin-walled bubble of vitreous material. In this manner it was possible to produce bubbles of up to 10 cm length and 5 cm diameter. The bubbles

were cut up into sections measuring approximately $1{\cdot}5 \times 0{\cdot}5$ cm and semitransparent electrodes were deposited by evaporation. Aluminium and gold were initially evaluated as electrode materials and in both cases the hole drift transit pulses were found to be of a 'rounded' form. The specimens with aluminium electrodes showed larger transit pulse heights than those with gold electrodes, probably because of a smaller injection of hole carriers from the contacts into the bulk in the former case. Aluminium was thus adopted as an electrode material for the detailed examination of the mobility properties.

The specimen films with evaporated electrodes were mounted on thin glass substrates, using 'Dag' silver dispersion to make contact to the electrodes. It was necessary to use evaporated offset contact pads, allowing no silver to approach the area of contact overlap, since it was found that silver diffused rapidly into the films and drastically modified their electrical properties. Figure 1 illustrates the specimen configuration.

Fig. 1

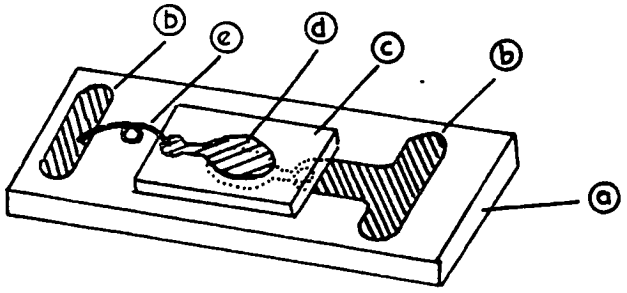

Specimen assembly : (*a*) glass substrate ; (*b*) silver 'Dag' contact pads ; (*c*) specimen film ; (*d*) evaporated metal electrodes ; (*e*) thin copper tension wire.

The above method of specimen preparation may result in the presence of nitrogen as an impurity in the material, but this is not felt to be a serious problem since impurities in general (with the exceptions of silver, copper, and possibly of oxygen) appear to have little effect on the electrical properties of arsenic triselenide. It is likely that the situation in this respect may be similar to that in amorphous selenium, in which the hole drift mobility has been found to be insensitive to the presence of a wide range of impurities (see Kolomiets and Lebedev 1966, and Schottmiller, Tabak, Lucovsky and Ward 1970). Equally, of course, specimen preparation by an evaporation technique introduces problems of non-stoichiometry which might be more serious.

§ 3. Experimental Considerations

Drift mobility measurements were performed by a transit time method, as developed by Spear (1969) and others. In the present case, carriers were produced close to one surface of the specimen by means of a short

(60 nsec) pulse of high energy electrons from an electron gun. The drift of carriers of one sign through the bulk of the specimen, under the influence of an applied electric field, was observed as indicated in fig. 2.

Fig. 2

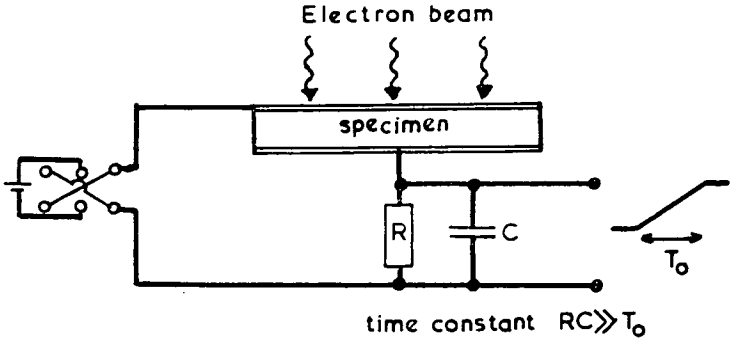

Basic measurement system.

Fig. 3

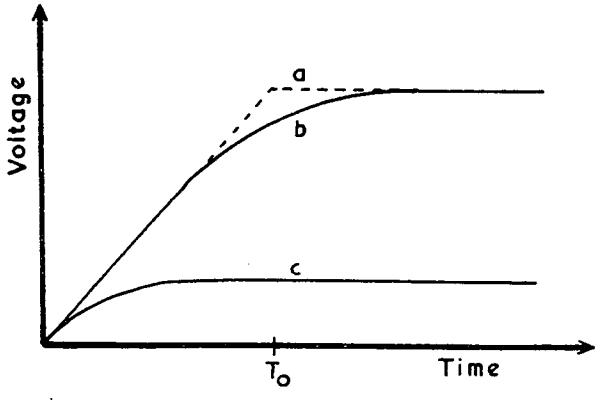

Transit pulse shape : (*a*) ' Ideal ' (no recombination or diffusion effects) : (*b*) slight diffusion of the charge sheet during transit : (*c*) exponential rise, all carriers permanently trapped before transit is complete.

It was arranged that the time constant of the sampling resistor R and capacitor C was much longer than the transit times to be examined. In this situation, and under the ideal conditions of a unique transit time, no carrier trapping or diffusion of the charge sheet, and zero charge sheet width, the observed transit pulse is of the form shown in fig. 3 (*a*). The transit time, T_0, is directly measurable as the interval between the slope discontinuities of the trace. However, if trapping and diffusion modify the form of the charge sheet during the transit, the pulse can assume the shape shown in fig. 3 (*b*) and the transit time must be extracted by extrapolation as indicated. A good analysis of trapping effects in this type of

experiment has been provided by Tefft (1967). In the limit where a large number of traps with a short trapping time (much less than T_0) and long release time (much greater than T_0) are present in the material, the probability of a carrier completing a transit without being trapped becomes very small. The observed trace then becomes exponential with a rise time equal to the trapping time, as shown in fig. 3(*c*). If, however, the trapping and release times are both short, the effect is to produce a longer carrier transit time, averaging out the time spent in traps. Here, an effective (trap limited) drift mobility can be defined as:

$$\mu_d = \mu_0 T_t/(T_t + T_r)$$
$$\approx \mu_0(T_t/T_r) \quad \text{for} \quad T_r \gg T_t, \qquad \ldots\ldots (1)$$

where μ_0 is the mobility of free (untrapped) carriers, and T_t and T_r are the trapping and release times. This is a situation frequently encountered in low-mobility materials. Of course, it is still possible for a second set of trapping levels, with a much longer release time, to be present, and these may produce rounding of the pulse and, ultimately, an exponential rise determined by the longer trapping time.

Since pulses exhibiting a pronounced degree of rounding are frequently observed in the examination of materials of low mobility, it is necessary to consider what exactly is being measured. In the present examination, where the pulses were typically of the shape shown in fig. 4, the following factors were considered to indicate that a true transit effect, rather than a 'deep' trapping phenomenon, was being observed. We concern ourselves here with the slow rounded region of the pulse, rather than with the fast initial response. The reason for the occurrence of the latter will be discussed further at a later stage.

Fig. 4

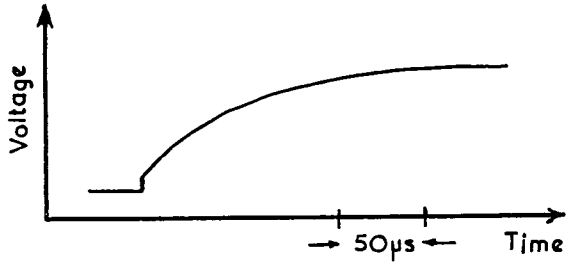

Typical hole transit pulse as observed in vitreous As_2Se_3.

3.1. *The Scaling Laws*

Measurements in specimens of different thicknesses at identical values of applied field should yield a direct dependence of the transit time on the specimen thickness. In the present examination, the results obtained for the mobility in a number of specimens were consistent (see fig. 7),

indicating that the observed pulse shape was not due to 'deep' trapping. We note that Tabak (1969) and Scharfe (1970) reached similar conclusions in their examinations.

3.2. *The Height of the Observed Pulse*

Analysis (e.g. Tefft 1967) shows that, as the 'deep' trapping or recombination time decreases with respect to the transit time, the observed pulse height also decreases. Practically, unless the transit time is less than or of the order of the 'deep' trapping time, the pulse becomes very small in amplitude. Thus, observations taken over a wide range of temperature and field, in which the transit time can vary by several orders of magnitude, should show large variations in pulse height if significant 'deep' trapping occurs. If, as in the present examination, the pulse amplitude does not show major variations, it suggests that a true transit effect is being measured. It is worth noting that in the absence of field effects, the relationship between the pulse height and the transit time can be used to determine the 'deep' trapping time by means of a 'Hecht curve' (Hecht 1932). However, field-dependent carrier generation effects are sometimes encountered, and the interpretation then becomes more difficult. For instance, Tabak and Warter (1968) have reported such effects in amorphous selenium and, by allowing for them, have calculated 'deep' trapping times substantially longer than those reported by earlier investigators. Even so, it would appear that the Hecht analysis gives a lower limit for the 'deep' trapping time, and it is this that is of interest in the present context. Figure 5 shows a 'Hecht curve' obtained in the present examination, and indicates a 'deep' trapping time of approximately 125 μsec. We think that field-dependent carrier generation effects are to be expected in vitreous As_2Se_3 and that the above figure is thus substantially less than the true recombination time in the material. The contention is supported by the data of Scharfe (1970) in which hole transit pulses of up to 10^{-2} sec duration were observed.

Fig. 5

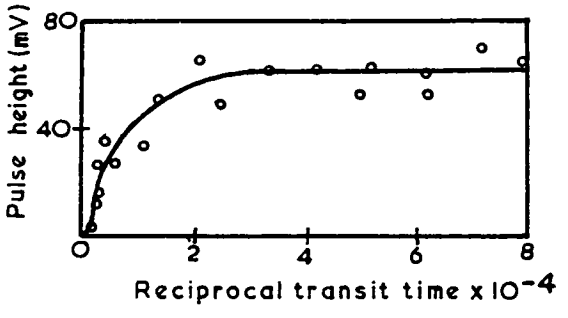

'Hecht curve' for the hole transit measurements. A 'deep trapping'/recombination time of 125 μsec is indicated.

Tefft (1967) suggests that a representative transit time is measured provided the recombination or 'deep' trapping time is not substantially less than the transit time. In the present study, no transit pulse with a response time greater than 100 μsec was included in the results, and the average response time was of the order of 30 μsec. It is therefore concluded that the data obtained were representative of a true transit phenomenon.

Having established that recombination or 'deep' trapping effects were not responsible for the observed pulse rounding, other possible causes were considered. It is to be expected that transit pulses of long duration would exhibit appreciable rounding due to diffusion and spreading of the drifting charge sheet, although the dependence of pulse shape on electrode material as observed by Scharfe is not easily explained. Scharfe himself attributes the effect to the filling of deep trapping levels by holes injected from gold contacts, thus preventing deep trapping of the charge sheet during the transit. However, such deep trapping effects would be expected to be progressively less significant as the transit time decreased, so that the transit pulses would be expected to approach the 'ideal' form, even in specimens with aluminium electrodes, as the pulse duration decreased. Scharfe's experiments do not indicate such an effect and neither do our own measurements on thin specimens with aluminium electrodes, even for transit pulse response times as short as 3 μsec. In § 7 of this paper we shall discuss the possibility that the carriers may experience only a few trapping/release events during transits at high fields and that pulse rounding under these conditions may be due to significant statistical fluctuations in the transit times of individual carriers.

The procedure for calculating mobility values for the rounded response traces was as follows:

(i) The response time, T_0, was estimated as indicated in fig. 6. The point C at which the slow region of the trace reached 50% of its final magnitude was identified. A straight line AC was then drawn through the origin of the slow region (A) and (C). This line was extrapolated to intersect a line drawn back horizontally from the top of the pulse, B. The time interval between A and the intersection point, D, was then taken as T_0. In the particular case for which the response curve is exponential in shape, This procedure gives a value of T_0 equal to approximately 1·4

Fig. 6

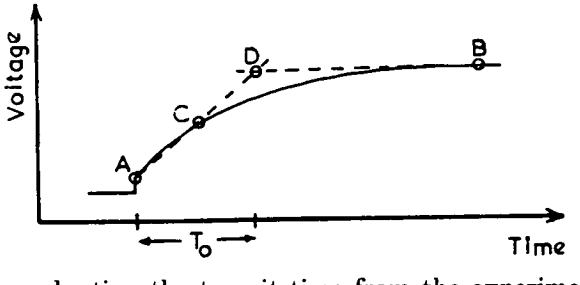

Method for evaluating the transit time from the experimental pulses.

times the exponential time constant. In the 'ideal' case of a linearly rising pulse, the method gives the correct value of T_0.

(ii) Having obtained a value of T_0, the drift mobility was estimated using the usual equation

$$\mu_d = S/(ET_0), \quad \ldots\ldots\ldots \quad (2)$$

where S is the specimen thickness and E the applied electric field.

§ 4. Measurement of Specimen Thickness

In view of the very fragile nature of the films used in this examination, it was necessary to defer thickness measurements until the measurement of electrical properties was complete. The specimen films were then broken into small pieces which were individually measured using a 'Talysurf' instrument. Most films were found to be flat to within $\pm 5\%$ of their thickness.

§ 5. Experimental Results

At room temperature, the measured values of hole drift mobility and conductivity exhibited a strong field dependence. Figure 7 shows the mobility of three specimens displayed as a function of $E^{1/2}$. The room

Fig. 7

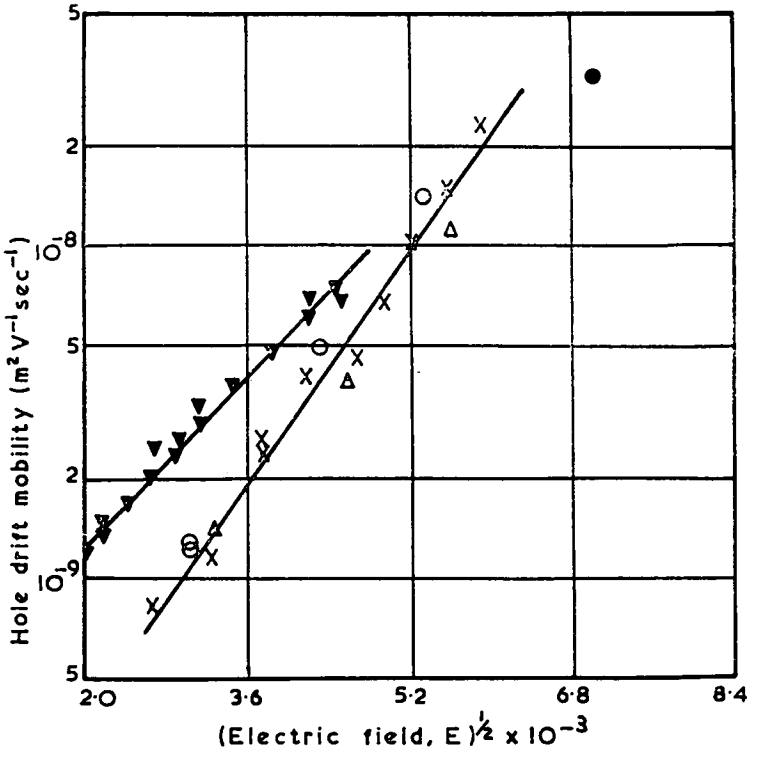

The relationship between hole drift mobility and applied electric field: ○, specimen 1, 1·28 μm; ×, specimen 2, 2·90 μm; Δ, specimen 3, 0·95 μm; ●, Kolomiets and Lebedev (1967); ▼, data from Scharfe (1970).

temperature measurement by Kolomiets and Lebedev (1967), and the data of Scharfe (1970) (presumably taken at room temperature), are included for comparison purposes. They are seen to exhibit a moderately good agreement with the present data although some differences are evident. Figure 8 shows the conductivity of one of the films displayed in the same manner.

Fig. 8

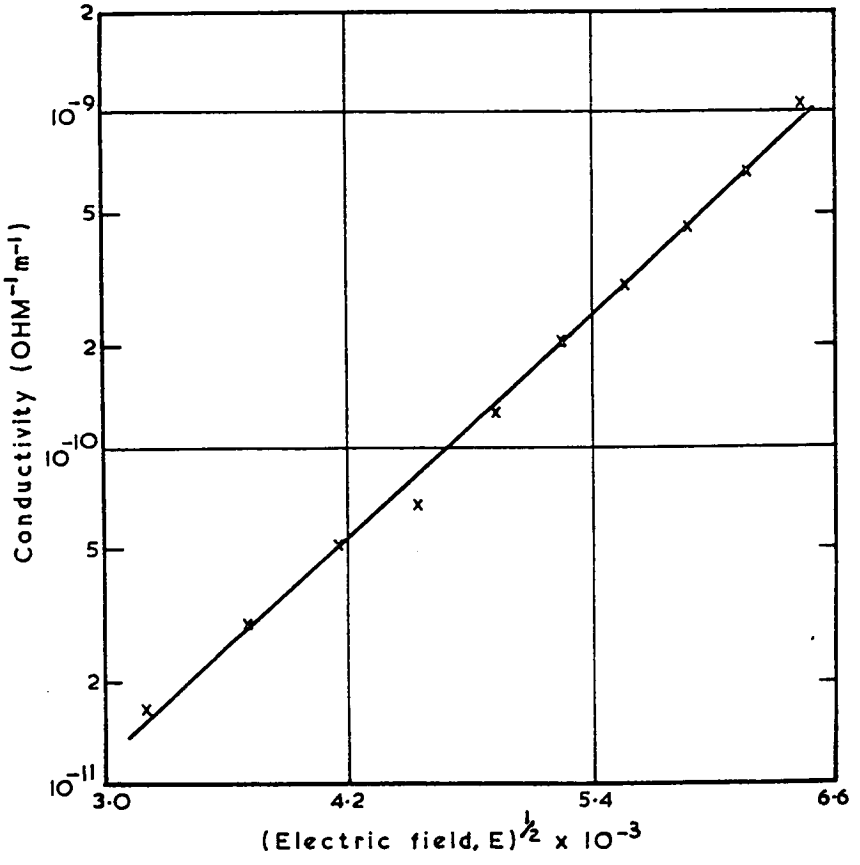

The relationship between conductivity and applied electric field ; specimen 2, 2·90 μm.

Upon varying the temperature, the applied field was found to influence the activation energy, as well as the magnitude, of the mobility, as shown in fig. 9. The measurements of Kolomiets and Lebedev are again included. Figure 10 shows measurements of the variation of specimen current with temperature in one film, of which it was unfortunately impossible to measure the thickness. The applied voltage was 65·5 v, and the thickness was *estimated* as of the order of 2 microns.

It was not possible to measure the electron drift mobility, the indications being that this was less than $10^{-10}\,m^2\,v^{-1}\,sec^{-1}$ at 370°K and with fields up to 10^7 v/m.

Fig. 9

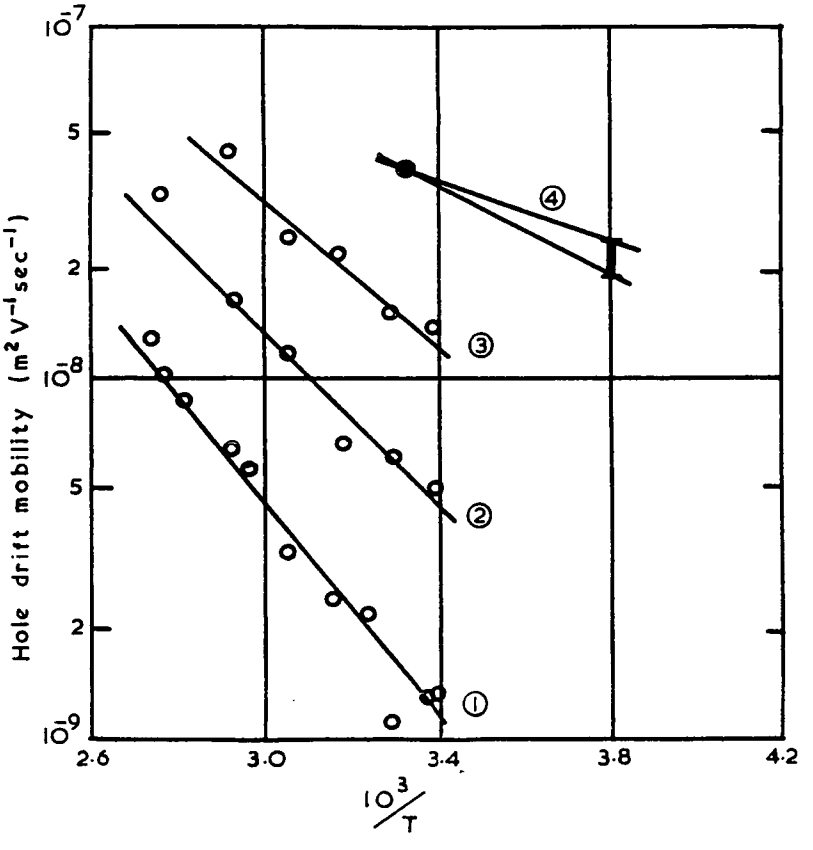

Temperature dependence of the hole drift mobility at various values of electric field, E. (1), (2), (3), specimen 1 ; $E = 0{\cdot}94$, $1{\cdot}88$ and $2{\cdot}83 \times 10^7$ v/m respectively. (4), Kolomiets and Lebedev (1967) ; $E = 5{\cdot}5 \times 10^7$ v/m.

§ 6. Discussion and Analysis

The dependence of the trap-limited drift mobility and conductivity upon applied electric field, illustrated in figs. 7 and 8, is consistent with the field-assisted release of carriers from trapping centres which are charged when empty; i.e. the Poole–Frenkel effect. A simple one-dimensional analysis of this mechanism (e.g. Lamb 1967) predicts a field dependence of the form

$$\mu_d = (N_v/N_t)\mu_0 \exp(-U_0/kT) \exp(\beta E^{1/2}/kT), \quad . \; . \; . \quad (3)$$

where μ_0 is the carrier's microscopic mobility, U_0 is the thermal activation

Fig. 10

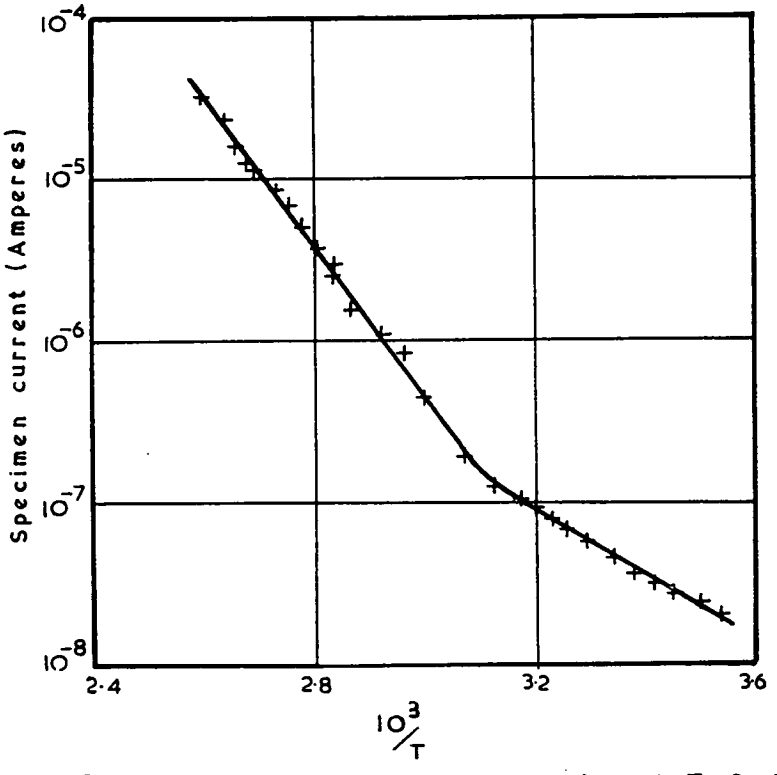

Dependence of specimen current on temperature, specimen 4, $E \sim 3 \times 10^7$ v/m.

energy at zero field, β is the Poole–Frenkel constant, N_v is the density of states in the valence band, N_t is the density of trapping centres.

In the one-dimensional analysis,

$$\beta = [e^3/\pi K K_0]^{1/2}, \quad \ldots\ldots\ldots \quad (4)$$

where e is the electronic charge, K is the relative high frequency dielectric constant, K_0 is the permittivity of free space.

The high frequency dielectric constant of As_2Se_3 is about 9·2 (Austin 1971), so that $\beta \simeq 2{\cdot}5 \times 10^{-5}$ ev/v$^{1/2}$ m$^{-1/2}$. From the mobility data of fig. 7, a value of $\beta = 2{\cdot}6 \times 10^{-5}$ ev/v$^{1/2}$ m$^{-1/2}$ is obtained, whilst the conductivity data of fig. 8 give $\beta = 3{\cdot}3 \times 10^{-5}$ ev/v$^{1/2}$ m$^{-1/2}$ (Scharfe's mobility data, interpreted in this manner, give $\beta \approx 1{\cdot}85 \times 10^{-5}$ ev/v$^{1/2}$ m$^{-1/2}$). There is therefore fairly good quantitative agreement with the theory. It should, however, be noted that there is some doubt about the true magnitude of the Poole–Frenkel coefficient since the extension of the model to three dimensions and consideration of non-Coulombic trapping centres lead to a lowering of the calculated constant (Hartke 1968). Furthermore, under conditions where the carriers have a short mean free path between trapping events, the validity of the mechanism has been questioned (Jonscher 1967). In the present case we shall show that there are indications that the mean

free path between trapping events in the charged trapping states is relatively long ($\sim 10^3$ Å) so that the latter restriction may not be relevant. On the other hand, the high calculated density of trapping centres suggests a small trap separation (20 to 50 Å) and we would expect this to result in a lower value of β than those which we obtain since the Coulombic potential of a trap would be perturbed at relatively short distances.

By applying the usual expression for the conductivity

$$\sigma = ne\mu_d \quad . \quad . \quad . \quad . \quad . \quad . \quad . \quad . \quad . \quad . \quad (5)$$

the *total* carrier density n (i.e. the sum of the free carriers and those in the Coulombic centres) is found to be of the order of 10^{17} m^{-3} at room temperature. The carrier density is relatively insensitive to the applied field since σ and μ_d have virtually the same field dependence (figs. 7 and 8).

In the Poole–Frenkel mechanism, the thermal activation energy is given by

$$U = U_0 - \beta E^{1/2}. \quad . \quad . \quad . \quad . \quad . \quad . \quad . \quad . \quad (6)$$

The data from fig. 9 may be analysed in terms of this equation, giving $U_0 = 0{\cdot}43$ ev and $\beta = 4{\cdot}3 \times 10^{-5}$ ev/v$^{1/2}$ m$^{-1/2}$. By extrapolation of the measured mobility values to zero field, as shown in fig. 11, a 'zero field' mobility is obtained. This is plotted as a function of temperature in fig. 12, from which a zero-field activation energy of 0·43 ev is again obtained and the pre-exponential factor of eqn. (3) is calculated as

$$(N_v/N_t)\mu_0 \approx 3 \times 10^{-3}\,\mathrm{m^2\,v^{-1}\,sec^{-1}}. \quad . \quad . \quad . \quad . \quad . \quad (7)$$

Fig. 11

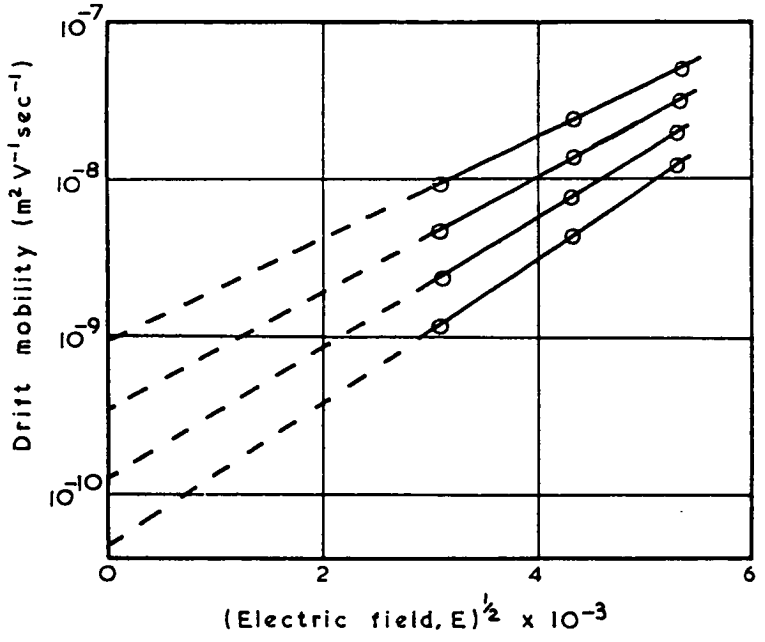

Extrapolation of hole drift mobility to zero applied field for data taken from fig. 9.

Fig. 12

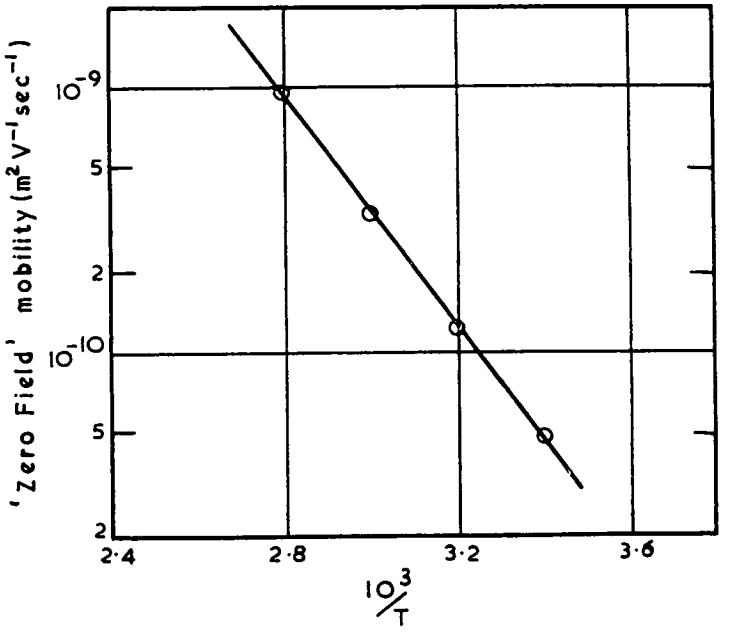

Temperature dependence of the 'zero field' hole drift mobility.

The conductivity of *bulk* specimens of vitreous As_2Se_3 is invariably found to fit the usual exponential expression

$$\sigma = \sigma_0 \exp(-\epsilon_\sigma/2kT), \quad \ldots\ldots\ldots \quad (8)$$

with ϵ_σ reported by different investigators to be in the range 1·8 to 2·0 ev and σ_0 between 10^5 and 10^7 ohm^{-1} m^{-1} (Kolomiets 1964, Edmond 1968). In the present analysis we shall take a value of 1·9 ev for ϵ_σ.

If the conduction process is dominated by one type of carrier, $\epsilon_\sigma/2$ represents the separation of the Fermi level and the appropriate band edge. Thus, for As_2Se_3 in which the conduction process is dominated by hole carriers, the Fermi level is situated 0·95 ev above the edge of the valence band.

The value of ϵ_σ is *approximately* the same as the energy of the optical absorption edge, and evidence of this sort has often been quoted in support of the view that chalcogenide glasses like As_2Se_3 are intrinsic semiconductors (Owen and Robertson 1970, Owen 1970). However, eqn. (7) indicates a high density of localized levels within the band gap, and we shall show that the assumption of 'intrinsic conduction' is not necessary to explain the data.

Using the usual expression for σ_0 in a case dominated by hole conduction,

$$\sigma_0 = N_v e \mu_0 \approx 10^5 \quad \text{to} \quad 10^7 \text{ ohm}^{-1} \text{m}^{-1}. \quad \ldots\ldots \quad (9)$$

Combining eqns. (7) and (9), we obtain

$$N_t \approx 10^{26} \quad \text{to} \quad 10^{28} \text{ m}^{-3}.$$

This figure seems high, probably because of accumulated errors in the calculation. Even so, a value of N_t of the order of N_v (10^{25} to $10^{26}\,m^{-3}$) is indicated.

Mott (1969a) and others have suggested that a mobility of about $10^{-2}\,m^2\,v^{-1}\,sec^{-1}$ is the minimum to be expected for transport in the extended band states. For carrier motion just inside the extended states the propagation has been regarded as a diffusive process (Mott 1969a) with μ_0 given by

$$\mu_0 = e\nu_{el}a^2/kT,$$

where ν_{el} is an electronic frequency of the order of $10^{15}\,sec^{-1}$. Re-analysing the present mobility measurements on this basis and allowing for the pre-exponential temperature dependence gives

$$(N_v/N_t)(e\nu_{el}a^2/k) = 1{\cdot}05\,m^2\,v^{-1}\,sec^{-1}\,^\circ K.$$

With $a \approx 3$ Å (interatomic distance), this also indicates $N_t \approx N_v$.

The present results, in conjunction with other available data, suggest a band structure of the form shown in fig. 13.

All the energy values given in this figure refer to $T = 0^\circ K$. The main features of the model are as follows:

(*a*) A 'band gap' of approximately 1·95 ev at $T = 0^\circ K$. This is obtained from optical data and is interpreted as the minimum energy between the *de-localized* states in the conduction and valence bands. Interpreted in this way, the experimental measurements of the absorption edge in vitreous As_2Se_3 indicate an 'optical gap' of 1·80 ev at room temperature (Davis and Mott 1970, Owen 1970, Kolomiets and Pavlov 1967). Grant and Yoffe (1970) report a temperature coefficient of the optical gap of

$$-0{\cdot}56 \times 10^{-3}\ ev/^\circ K$$

and this would imply an optical gap of about 1·95 ev at $T = 0^\circ K$.

(*b*) Below the de-localized states of the conduction band, and above those of the valence band, there are the usual exponential 'tails' of localized states which are to be expected in amorphous materials (Mott 1960a). The extension of these states for about 0·2 ev, as shown in fig. 13, is derived from drift mobility data on amorphous selenium (Schottmiller *et al.* 1970, Tabak 1970), since there is some evidence to suggest that these states are not radically modified by the addition of arsenic to selenium. Of particular relevance here are the results of Schottmiller *et al.*, who observed a fast 'selenium' hole transit pulse and a slow 'As_2Se_3 tail' response *simultaneously* in arsenic-doped selenium. These investigators found that the height of the 'As_2Se_3 tail' pulse tended to increase at the expense of the 'selenium' pulse as the arsenic concentration was increased, until the latter finally disappeared at high arsenic concentrations. Such an observation suggests that the arsenic sets up localized states distinctly different from those present in pure selenium rather than simply modifying the depth and density of the tail of localized states. We shall discuss this point further at a later stage.

Fig. 13

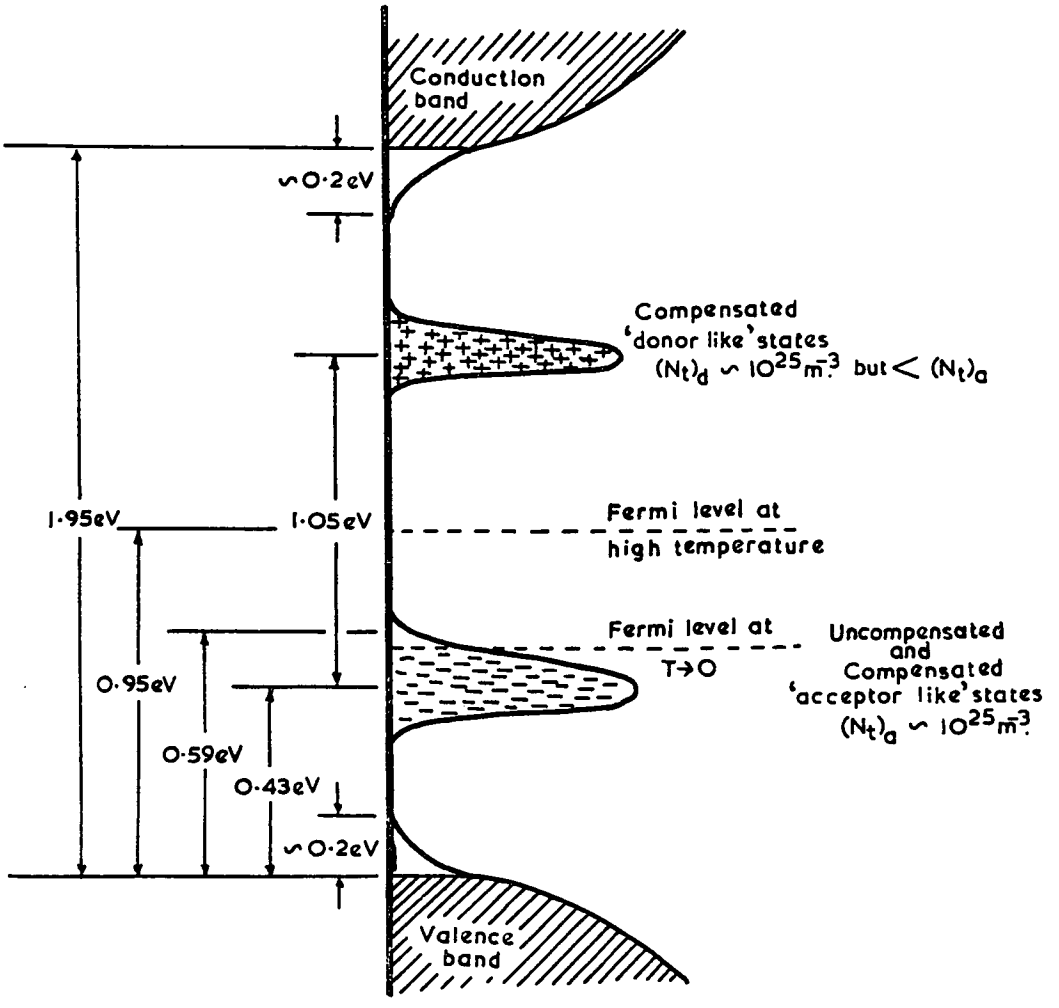

Suggested band structure of vitreous As_2Se_3.

(*c*) A large concentration of 'acceptor-like' localized states occurs at an energy $U_0 = 0{\cdot}43$ ev above the 'mobility edge' of the valence band. These are the trapping centres which limit the hole drift mobility and, as described above, their density is estimated as $(N_t)_a \approx N_v$. It is necessary to postulate that these states are acceptor-like in view of the strong Poole–Frenkel type field dependence of the drift mobility; i.e. these states must be *charged when empty* and are not on this evidence neutral traps.

(*d*) To explain the apparent intrinsic behaviour of vitreous As_2Se_3 it is also necessary to assume the existence of a compensating set of 'donor-like' states of about the same density as the acceptors $(N_t)_d \approx 10^{25}$ to $10^{26}\,m^{-3}$.

For complete compensation, the Fermi level will lie halfway between the two sets of states at all temperatures. If the compensation is not

quite perfect, the Fermi level will lie inside the 'under-compensated' set of levels at zero temperature and will move to a position approximately symmetrically between the two sets of levels at high temperatures. Measurements in As_2Se_3 above room temperature correspond to the high temperature case and calculations put the Fermi level almost exactly halfway between the two sets of levels as shown.

The change of slope of the $\log\sigma$ versus $1/T$ curve (fig. 10) is consistent with the presence of a relatively small number of excess (uncompensated) acceptor levels so that at zero temperature the Fermi level would lie just inside the acceptor states. We shall give further consideration to this situation presently.

It will be noted that fig. 13, as drawn from the above data, indicates the separation of the compensated donor states from the conduction band to be slightly larger than the separation of the compensated acceptor states from the valence band (0·48 ev as compared to 0·43 ev). Such a situation would be consistent with the low value of the electron drift mobility as compared to the hole drift mobility.

(*e*) The main features of the model have been set out above. There are, however, several points to be noted here. Firstly, it must be recognized that the localized states shown in fig. 13 are *only* those required to account for the present mobility and conductivity results. There may well be other localized states within the energy gap. Kolomiets (1968), for example, has reported measurements of the thermally stimulated conductivity, indicating a distribution of localized levels in the range 0·4 to 0·75 ev above the edge of the valence band, whilst a study of the optical quenching of the photoconductivity in *crystalline* As_2Se_3 by the same author indicates discrete levels at energies of 0·49, 0·58, and 0·72 ev above the valence band edge. Davis and Mott (1970) have interpreted low frequency a.c. conductivity measurements in terms of a high density ($\approx 10^{25}\,m^{-3}$) of localized states at the Fermi level (i.e. close to the centre of the gap), although this is not the only possible explanation of the data. Kolomiets (1968) has also proposed states near the centre of the gap from measurements of space-charged-limited currents. We note here that deep-lying states with a release time appreciably longer than the transit times observed in the present measurements would not be detectable from the experimental transit pulses.

(*f*) The relatively small number of uncompensated acceptor states shown in fig. 13 is introduced to explain the shape of the $\log\sigma$ versus $1/T$ curve (fig. 10). In the situation shown in fig. 13, the $\log\sigma$ versus $1/T$ curve should, at some point, show a decrease in slope to a value corresponding to an activation energy ϵ'. The energy ϵ' will be approximately equal to the height of the uncompensated acceptor-like states above the valence band 'mobility edge' and the conductivity at lower temperatures will be given by

$$\sigma = \sigma^1{}_0 \exp(-\epsilon^1/kT). \qquad (10)$$

In fig. 10 such a change of slope occurs at about $10^3/T = 3{\cdot}1$, and the low temperature section indicates an activation energy of 0·4 ev, giving $\epsilon^1 \approx 0{\cdot}6$ ev after applying a correction for the effect of the applied field. Thus, the acceptor-like states probably extend over a range from about 0·4 to 0·6 ev above the band edge, in rough agreement with the region of localized levels suggested by Kolomiets (1968). The only other 'low' temperature conductivity measurements known to the authors are those of Shaw (1969) on evaporated thin films of As_2Se_3, which indicate a continuous decrease of activation energy with decreasing temperature. Shaw attributes this effect to a change to a hopping form of conduction. It is possible that such a change of mechanism does occur more readily in evaporated specimens than in vitreous ones, since the 'tails' of localized levels may well be more prominent in the former case. Also, the positions of the various localized levels and the extent of the compensation may vary somewhat with the method of specimen preparation.

(*g*) From the temperature at which the discontinuity of slope in fig. 10 occurs, an estimate can be made of the density of *uncompensated* acceptor states $(N_t')_a = (N_t)_a - (N_t)_d$, since at this point the number of hole carriers in the 'compensated' acceptor states will be derived equally from the uncompensated acceptor and the compensated donor states. The *total* number of carriers at this temperature is estimated (as previously) as approximately $1{\cdot}5 \times 10^{17}\,m^{-3}$, so that

$$1{\cdot}5 \times 10^{17} \approx 2(N_t')_a \exp\{-(\epsilon' - U)/kT\}, \quad \ldots \quad (11)$$

giving $(N_t')_a \approx 2{\cdot}5 \times 10^{19}\,m^{-3}$. The compensation is thus almost complete. Note also that

$$1{\cdot}5 \times 10^{17} \approx 2(N_t)_d \exp(-\epsilon_n/2kT), \quad \ldots \quad (12)$$

Fig. 14

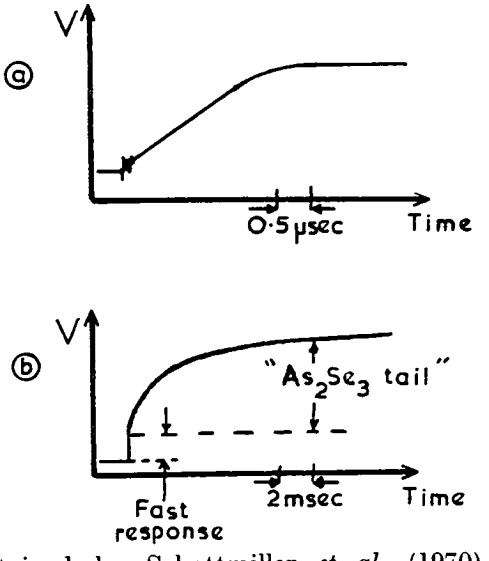

Transit pulses obtained by Schottmiller *et al.* (1970) for (*a*) selenium, (*b*) Se + 6% As.

giving $(N_t)_d \approx 8 \times 10^{24}\,m^{-3}$, a value of the same order as our previous estimate.

§ 7. The Shape of the Hole Transit Pulse

As stated previously, the transit pulses observed in this investigation were of a 'rounded' form, and also exhibited a rapidly rising initial region (fig. 4). The pulses were thus qualitatively similar to those observed by Schottmiller *et al.* (1970), in an examination of arsenic-doped selenium. In pure selenium, the hole transit pulses at room temperature are of a linear form, and show a well-defined 'transit time break point' (fig. 14*a*). Schottmiller *et al.* report that the addition of arsenic in concentrations up to 3% causes a steady reduction in the height of this pulse in a manner consistent with the production of a set of 'deep' hole trapping levels. For arsenic concentrations between 3 and 6%, the form of the transit pulse begins to change with the appearance of a slow response (termed the arsenic selenide tail) following the initial 'selenium' response. The composite pulse shape is shown in fig. 14 (*b*). Schottmiller *et al.* ascertained that the slow region was produced by the transit of carriers across the full width of the specimen, and estimated a mobility of the order of $10^{-9}\,m^2V^{-1}\,sec^{-1}$. Even higher arsenic concentrations progressively reduced the magnitude of the 'selenium' response, which became undetectable in their specimens at about 18% arsenic. The tail region retained the same effective mobility as the doping level was increased, and this mobility was the same as that measured in arsenic triselenide itself. From these results, a direct correspondence between the addition of arsenic and the production of localized levels can be deduced. The behaviour indicates that the levels reducing the selenium hole transit response lie below the Fermi level, so that the trapped carriers are eventually re-released and traverse the whole specimen thickness. It can be inferred that, between the trapping events in these localised levels, both in arsenic-doped selenium and probably in arsenic triselenide itself, the hole carriers move with a mobility of the order of that measured in pure selenium. This mobility is approximately $10^{-5}\,m^2V^{-1}sec^{-1}$ at room temperature and probably involves numerous trapping/release events in a localized tail of states above the valence band mobility edge. The addition of arsenic increases the concentration of the deeper (and, from the results of the present study, Coulombic) traps, and hence progressively reduces the carrier trapping time for these levels. However, even in arsenic triselenide itself, it is possible that for sufficiently thin specimens and high fields the hole carriers are only trapped by the Coulombic states on a few occasions during transit. This implies significant statistical variations in the transit times of individual carriers, resulting in the disappearance of any well-defined transit-time discontinuity in the response pulse. Our transit pulses in arsenic selenide, and those of Schottmiller *et al.* in arsenic-doped selenium (figs. 4 and 14 (*b*) respectively) can be interpreted in these terms. At the commencement of the transit, all the induced carriers are free, and they

will travel together as a sheet, being trapped *on average* after a time T_t. Here, we use the term 'free' to indicate that a carrier is not trapped at a particular time by one of the Coulombic localized levels, although the motion almost certainly consists of a large number of trapping/release events in the valence band tail of states (as in pure selenium). The motion in this time region gives rise to the fast response in figs. 4 and 14 (*b*). Following the first trapping event in the Coulombic centres, the charge sheet tends to spread out due to statistical variations in the time spent in the Coulombic centres and in the distance travelled between trapping events. The arrival of individual carriers at the lower specimen electrode at different times produces the rounded response curve, or 'arsenic selenide tail' region, in figs. 4 and 14 (*b*).

If μ_{free} is the carrier mobility for carriers untrapped by the Coulombic centres, then the *average* distance travelled between Coulombic trapping events is $E\mu_{free}T_t$, so that the shape of the response curve is determined by the ratio of $E\mu_{free}T_t$ to the specimen thickness, or by the average number of trapping events per transit, P. We have produced a computer simulation of the transit pulse shape for various values of P, with the results shown in fig. 15.

Fig. 15

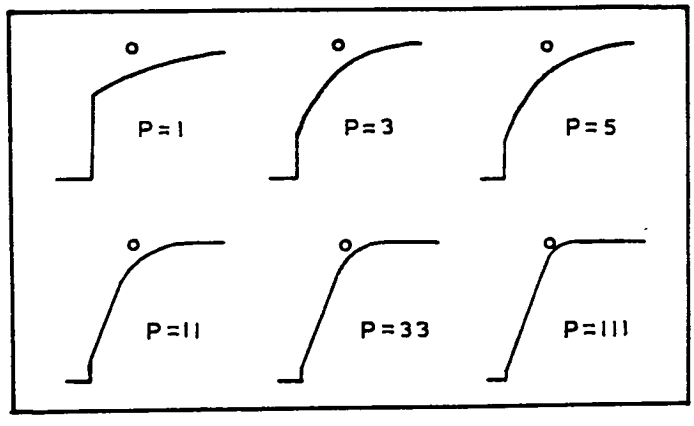

Computer simulation of transit pulses for various values of P ; the average number of trapping/release events per carrier during transit.

The ratio of the height of the fast initial response to the total pulse height gives a direct experimental measure of P,

$$(\Delta h/h) = [1 - \exp(-P)]/P$$
$$\approx (1/P) \text{ for } P > 3 . \quad . \quad . \quad . \quad . \quad . \quad . \quad . \quad (13)$$

It can be seen from fig. 15 that the slow region of the transit pulse is appreciably rounded unless $P \gtrsim 10$, and approaches a linear form only for $P \gtrsim 30$. In each of the cases shown in fig. 15, the horizontal axis has been normalized to give the same value of average transit time. The process

described in § 3 for the estimation of the transit time gives a good measure of the average value for $P \gtrsim 2$. The heights of the initial fast regions in the present experimental transit pulses are consistent with P in the region 4 to 20 depending on the specimen thickness and the applied field. This implies carrier 'mean free paths' between Coulombic trapping events of the order of 10^{-7} m. Hence, the objection to the application of the Poole–Frenkel mechanism in the case of very short carrier mean free paths is, to some extent at least, relaxed.

We note that the computer analysis provided here simulates only the statistical fluctuations in transit times due to the presence of the Coulombic localized levels, and does not consider other factors such as conventional diffusion, carrier loss by recombination, specimen inhomogeneity and non-uniform thickness, etc., which are also likely to cause rounding of the transit pulse. In fact, the simulation indicates that the 'slow' region of the pulse should become approximately linear for $P \gtrsim 30$, and that the initial 'fast' region should become negligibly small in this region. Such conditions should thus be observed in the measurements of Schottmiller *et al.* for high arsenic concentrations, and of Scharfe (1970) in arsenic selenide (aluminium electrodes). In practice, however, a 'linear' response with an identifiable transit time 'break point' is observed in neither case. This anomaly can be partially explained in terms of diffusion, recombination, etc., which would give rise to pulse rounding. However, the observations of differently shaped response pulses in As_2Se_3 specimens fitted with aluminium and gold electrodes (Scharfe) is still puzzling, particularly since essentially identical response times appear to be extracted from the continuously curved response pulses in specimens with Al electrodes (Kolomiets and Lebedev 1966, Schottmiller *et al.*, 1970, this study, etc.) and from the pulses showing transit time discontinuities in specimens with Au electrodes (Scharfe 1970). The situation here may well be worthy of further experimental investigation.

§ 8. Bistable Switching Effects

The thin film specimens used in this study exhibited a bistable (memory-type) switching action. Considerable interest has recently been expressed in this property so that, although our investigation of the phenomenon has been somewhat superficial to date, we consider the results to be worthy of mention. It is interesting to note that the effect is here observed in a material of simple composition, of relatively well-established physical properties, in contrast to the complex 'alloy' compositions in which the phenomenon has often been reported.

To observe non-destructive switching effects, it was necessary to modify the specimen mounting configuration from that shown in fig. 1. Adequate heat sinking was provided by maintaining the specimen film in thermal contact with a brass substrate by means of an intermediate layer of liquid gallium–indium alloy. A Tektronix type 575 transistor curve tracer was employed to examine the switching characteristics.

Fig. 16

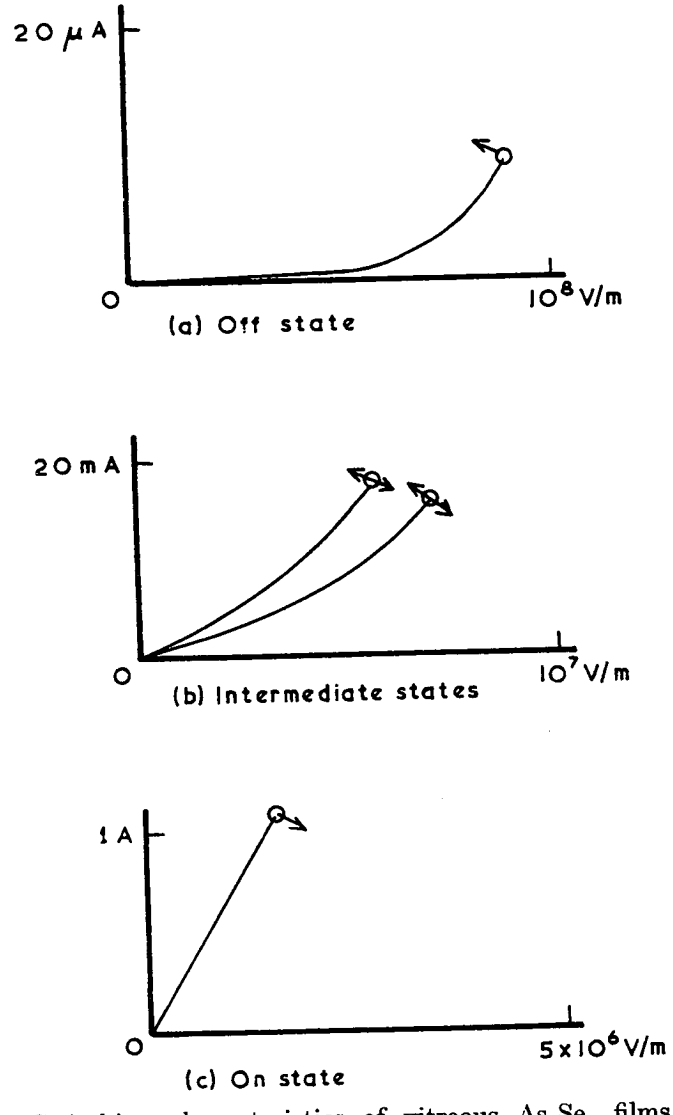

Switching characteristics of vitreous As_2Se_3 films.

The essential features of the switching action are summarized in fig. 16. Specimens in the normal 'off' state were characterized by a low-field resistivity of 10^{13} to 10^{14} ohm m. Switching occurred when the field across the specimen exceeded a value between 5×10^8 and 10^9 v/m, the critical field being constant between successive switching cycles to within 10 to 20%. On exceeding the critical field, the specimens switched to one of a set of intermediate states of resistivity of the order of 10^7 to 10^8 ohm m, depending on the resistance in series with the specimen. These states were unstable, and specimens tended to revert to the 'off' state on removal of the applied field. Increasing the field across the specimen

caused further switching into the 'on' state, in which the resistivity was of the order of 10^4 ohm m. This state was stable and was maintained on removal of the field across the specimen. Reversion to the 'off' state was accomplished by passing a large current pulse through the specimen. With the specimen dimensions adopted, 'on' resistances were in the range 1 to 10 ohms, and it was possible to pass currents in excess of 1 amp without any sign of degradation of properties.

It is interesting to note that for fields of the order of those at which switching occurred, the process could be assisted by two phenomena. Firstly, the results in § 5 indicate that the mobility activation energy would be reduced to zero and the Coulombic trapping states delocalized at a field of the order of 10^8 v/m. Secondly, the results in § 7 indicate the likelihood that a substantial fraction of the carriers would traverse the specimen thickness without being trapped by the Coulombic centres at fields of this magnitude. These processes would give rise to a rapid increase in carrier mobility as the critical field was approached, which would greatly assist any thermal switching mechanism. It is not, however, possible to account for the memory action in these terms, or to ascertain whether the 'on' state represents a true electronic transition of the material, crystallization via a molten phase, or the formation of metallic filaments of electrode material across the film. It is interesting to note in this respect that several films were found to be in the 'on' state immediately after preparation, and prior to the application of any large electric field.

§ 9. Concluding Remarks

In the present context the unusual feature of the band structure suggested in § 6 and fig. 13 is the proposition that the traps which limit the hole mobility are 'acceptor-like' states and that they are compensated by 'donor-like' states. The familiar concept of extrinsic impurity states has not previously featured in the interpretation of the properties of chalcogenide glasses. There are two reasons for this, both deduced from established experimental observations. (*a*) The electrical properties of the chalcogenide glasses are often insensitive to impurities (there are exceptions however) and (*b*) they normally appear to be intrinsic semiconductors (Owen 1970, Owen and Robertson 1970). In fact Mott (1969 a) has suggested that the disordered configuration of semiconducting glasses enables all impurities to find sites at which their normal valency is always exactly satisfied, hence precluding the possibility of 'extrinsic' behaviour. It is therefore worth recapitulating the evidence for the model of fig. 13 and discussing this briefly but critically in relation to other alternatives.

The conclusion that the localized states controlling the hole drift mobility are acceptors was deduced from the good agreement between the experimental field dependence of the mobility and the simple one-dimensional Poole–Frenkel theory. Accepting that the Poole–Frenkel

effect is responsible for the field dependence implies that the traps are *not* neutral states but are acceptors (negatively charged when empty). The compensating donor states are then necessary to explain the low conductivity and the apparent intrinsic behaviour. The moderately good agreement between the present data and those of Kolomiets and Lebedev (1966) and of Scharfe (1970) confirms the occurrence of a relatively large dependence of the drift mobility on applied field, although some difference is indicated between their evaporated and our vitreous films. The experimental verification of the Poole–Frenkel effect is, however, notoriously uncertain and it is relevant to consider other possible models.

Most of the experimental evidence given in § 6 would be satisfied by a band structure like that in fig. 13, but in which the sets of localized states within the energy gap were neutral traps. The density and depth of the trapping levels above the valence band (i.e. those controlling the hole mobility) would have the same values as those derived in § 6. The negligible electron drift mobility would be consistent with the presence of a level of traps of equal or larger density at an equivalent or greater depth from the conduction band. The difficulty would be in explaining the field dependence of the mobility, a point to which we shall return later.

Another alternative is the linear 'tail-of-localized-states' model proposed by Mott (1969 b) and illustrated, for the conduction band, in fig. 17.

Fig. 17

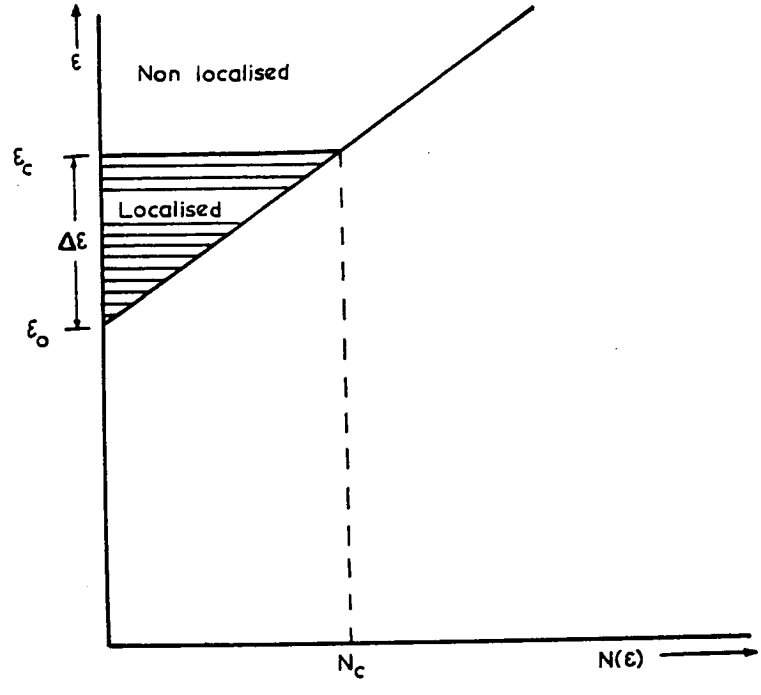

'Tail of states' model due to Mott (1969 b).

If the localized states range over an energy $\Delta\epsilon$, and the density-of-states just inside the valence band is also linear, the mobility is given (Marshall 1970) by

$$\mu = \mu_0(\Delta\epsilon/kT)\exp(-\Delta\epsilon/kT). \quad . \quad . \quad . \quad . \quad (14)$$

Analysing the data of fig. 12 in terms of this equation gives

$$\Delta\epsilon = 0{\cdot}46\,\text{ev}$$

and

$$\mu_0 \approx 2\times 10^{-4}\,\text{m}^2\text{v}^{-1}\text{sec}^{-1}.$$

This model might also be advanced as providing an explanation for the observed data (in particular, the value of μ_0 is consistent with transport in the 'diffusive states' as described by Mott (1969*a*)) were it not for the field dependence of the mobility and for the observations of Schottmiller *et al.* (1970) on the addition of arsenic to amorphous selenium.

It is possible that a field dependence of the mobility could arise from a situation of the type depicted in fig. 17, by means of the field-assisted tunnelling of carriers from the localized tail of states into the band. However, calculations by the authors indicate that such a mechanism would not be expected to give rise to a significant field effect for fields of less than $10^8\,\text{v m}^{-1}$. Likewise, the field dependence expected for thermally assisted carrier hopping (e.g. Bagley 1970) is too small to explain the observed data.

As Jonscher (1967) points out, the Poole–Frenkel effect provides, despite the uncertainties, the most plausible explanation for the dependence of the mobility (or conductivity) on the square root of applied field. Ideally, of course, we would like data over several decades of field to establish the particular functional form of the dependence. Unfortunately, this is not possible in the present experiments since the low mobility (and its rapid field dependence) make measurements impossible at fields below about $10^6\,\text{v m}^{-1}$ and switching (§ 8) sets an upper limit of about $5\times 10^7\,\text{v m}^{-1}$. Over the limited range available, the present results do fit best to a square root dependence on field (figs. 7 and 8). It is also pertinent to note that in amorphous selenium, for which the model of fig. 7 seems appropriate, the field dependence of the hole mobility is different from that observed in arsenic selenide (Marshall 1970, Tabak 1970). At temperatures above about 250°K there is no observable field effect in amorphous selenium, whilst below 250°K the hole drift mobility becomes increasingly field dependent. Even so, the dependence is not consistent with the Poole–Frenkel mechanism and a forced fit yields a Poole–Frenkel coefficient, β, which is an order of magnitude less than that observed in As_2Se_3. In other words, in a situation in which it is likely that the hole mobility is controlled by neutral traps, the field dependence is very much weaker, as would be expected.

As has been previously stated, the data of Schottmiller *et al.* (1970) on the addition of arsenic to amorphous selenium are not consistent with a

progressive increase in the 'depth' of a tail of states from about 0·2 ev (Se) to about 0·4 ev (As_2Se_3). Rather, the data indicate that an increase in the arsenic concentration produces a corresponding increase in the density of a set of localized states which are separated from and identifiably different from the 'tail of states' which control the drift mobility in pure selenium.

On the present evidence the conclusion is, therefore, that in vitreous As_2Se_3 the field dependence is best interpreted in terms of the Poole–Frenkel effect and that the localized states controlling the mobility are 'acceptor-like' states. In a compound such as As_2Se_3 the most likely origins of the donors and acceptors are anion and/or cation vacancies and interstitials. Autocompensation in large band-gap semiconductors or insulators, particularly compounds, is well known and has been described theoretically (e.g. Longini and Greene 1956), and the almost complete compensation indicated by the present data is by no means an isolated phenomenon.

References

Austin, I. G., 1971, *Phil. Mag.*, **23,** 17.

Bagley, B. G., 1970, *Solid St. Commun.*, **8,** 345.

Davis, E. A., and Mott, N. F., 1970, *Phil. Mag.*, **22,** 903.

Edmond, J. T., 1968, *J. Non-crystalline Solids*, **1,** 39.

Grant, A. J., and Yoffe, A. D., 1970, *Solid St. Commun.*, **8,** 1919.

Grunwald, H. P., and Blakney, R. M., 1968, *Phys. Rev.*, **165,** 1007.

Hartke, J. L., 1962, *Phys. Rev.*, **125,** 1177 ; 1968, *J. appl. Phys.*, **39,** 4871.

Hecht, K., 1932, *Z. Phys.*, **77,** 235.

Jonscher, A. K., 1967, *Thin Solid Films*, **1,** 213.

Kolomiets, B. T., 1964, *Phys. Stat. Sol.*, **7,** 359 and 713 ; 1968, *Proc. 9th Internat. Conf. on the Physics of Semiconductors*, Moscow, Vol. 2. *Acad. Sci.* U.S.S.R. (Leningrad : "Nauka").

Kolomiets, B. T., and Lebedev, E. A., 1966, *Soviet Phys. Solid St.*, **8,** 905 ; 1967, *Soviet Phys. Semiconduct.*, **1,** 244.

Kolomiets, B. T., and Pavlov, B. V., 1967, *Soviet Phys. Semiconduct.*, **1,** 350.

Lamb, D. R., 1967, *Electrical Conduction Mechanisms in Thin Insulating Films* (Methuen Monographs).

Longini, R. L., and Greene, R. F., 1956, *Phys. Rev.*, **102,** 992.

Marshall, J. M., 1970, Thesis, University of Edinburgh.

Mott, N. F., 1969 a, *Phil. Mag.*, **19,** 835 ; 1969 b, *Festkorperprobleme*, **9,** 22.

Owen, A. E., 1970, *Contemp. Phys.*, **11,** 227 and 257.

Owen, A. E., and Robertson, J. M., 1970, *J. Non-crystalline Solids*, **2,** 40.

Scharfe, M. E., 1970, *Phys. Rev.* B, **2,** 5025.

Schottmiller, J., Tabak, M. D., Lucovsky, G., and Ward, A., 1970, *J. Non-crystalline Solids*, **4,** 80.

Shaw, R. F., 1969, Thesis, University of Cambridge.

Spear, W. E., 1957, *Proc. phys. Soc.*, B, **70,** 669 ; 1960, *Ibid.*, **76,** 826 ; 1969, *J. Non-crystalline Solids*, **1,** 197.

Tabak, M. D., 1969, *Solid St. Commun.*, **7,** No. 11, p. viii (abstr.) ; 1970, *Phys. Rev.* B, **2,** 2104.

Tabak, M. D., and Warter, P. J., 1968, *Phys. Rev.*, **173,** 899.

Tefft, W. E., 1967, *J. appl. Phys.*, **38,** 5265.

phys. stat. sol. (a) 12, 181 (1972)

Subject classification: 14.3; 2; 22.1.3

Department of Electrical Engineering, University of Edinburgh

The Hole Drift Mobility of Vitreous Selenium

By

J. M. MARSHALL and A. E. OWEN

The drift mobility of hole carriers in vitreous selenium has been measured over a wide range of temperature and applied electric field. The results confirm an 'anomalous' temperature dependence above 250 °K. At lower temperatures, for low values of applied field, the activation energy of the mobility is (0.28 ± 0.02) eV. In addition, the mobility is found to be electric field dependent. By comparison of measurements on specimens of differing thicknesses, the field dependence is shown to be a genuine bulk property, rather than a 'time-of-flight' phenomenon. Whilst the mechanism of the field dependence has not been positively identified, the evidence suggests that field variations in the transport processes close to the 'mobility edge' may be responsible.

Es wurde die Löcherdriftbeweglichkeit von glasartigem Selen in einem weiten Temperaturbereich und in einem weiten Bereich der angelegten elektrischen Feldstärke gemessen. Die Ergebnisse bestätigen eine anomale Temperaturabhängigkeit oberhalb von 250 °K. Bei tieferen Temperaturen und kleinen Werten des angelegten Feldes beträgt die Aktivierungsenergie der Beweglichkeit (0,28 ± 0,02) eV. Es wird außerdem gefunden, daß die Beweglichkeit vom elektrischen Feld abhängig ist. Ein Vergleich der Messungen an Proben verschiedener Dicke zeigt, daß die Feldabhängigkeit eher eine echte Volumeneigenschaft als eine „Flugzeit"erscheinung ist. Obwohl der Feldabhängigkeitsmechanismus noch nicht vollständig identifiziert worden ist, weisen die Ergebnisse darauf hin, daß Feldvariationen im Transportprozeß in der Nähe der Beweglichkeitskante dafür verantwortlich sein können.

1. Introduction

Because of its status as a 'prototype' non-crystalline semiconductor, and by virtue of its commercial applications, vitreous selenium has attracted considerable attention in recent years. In particular, several examinations of the drift mobility of charge carriers have been performed. In the early studies of Spear [1] and of Hartke [2], holes were found to be the more mobile carriers, with a drift mobility of about 10^{-5} m^2 V^{-1} s^{-1} at room temperature. Both investigators reported an activation energy of 0.14 eV over the temperature range 200 to 320 °K. However, a subsequent study by Grunwald and Blakney [3] suggested an 'anomalous' reduction in the activation energy above 250 °K, and reported activation energies in the range 0.20 to 0.25 eV at lower temperatures. It was also noted that the activation energy increased with the temperature during evaporation of the amorphous specimens. The behaviour above 250 °K was associated with a saturation of the trap-controlled drift mobility, μ_d, under conditions where the trapped carrier release time, τ_r, becomes shorter than the free carrier trapping time, τ_t:

$$\mu_d = \mu_0 \frac{\tau_t}{\tau_t + \tau_r} \Rightarrow \mu_0 \quad \text{as} \quad \frac{\tau_r}{\tau_t} \Rightarrow 0 \,. \tag{1}$$

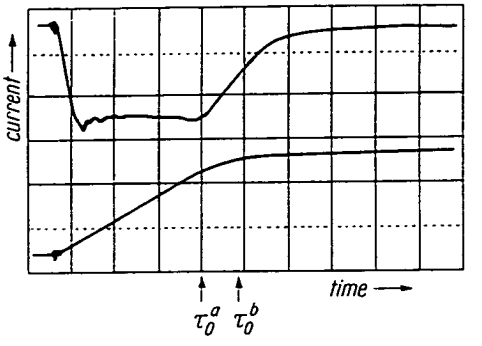

Fig. 1. Transit current pulse (top) and its integral (bottom) for a 50 μm specimen of vitreous selenium. $T = 295$ °K, $E = 2 \times 10^6$ V/m, time axis 0.5 μs per div.

too slow, but it was possible here to detect the transit pulse directly across the 10^6 Ω input resistor of a Tektronix Type L oscilloscope preamplifier, placed in series with the specimen. The combination of the high detector resistance and the specimen capacitance served to integrate the transit pulse in this mode of operation. Fig. 1 shows the current transit pulse and its integral for a specimen at room temperature, with a field of 2×10^6 V/m. The transit time of the current pulse is obtained as the point τ_0^a at which the transit current commences its rapid decline. Alternatively, a transit time τ_0^b, defined as the 'break point' of the integrated pulse, may be defined. Because of the finite dispersion of the current pulse, the former time is always somewhat shorter than the latter, and the latter corresponds to the point at which the current pulse has fallen to 50% of its steady value during transit. The dispersion of the current pulse increases with increasing transit time and with decreasing temperature as noted by Tabak [4], so that the difference between the two measured times increases. Fig. 2, also taken at room temperature but with a field of 2×10^5 V/m, illustrates the increasing relative dispersion due to a longer transit time. Fig. 3, obtained at 190 °K with a field of 8×10^6 V/m, whilst characterised by comparable values of transit time to those in Fig. 2, shows that lowering the temperature has further increased the dispersion. There has been some controversy as to whether τ_0^a or τ_0^b is the 'correct' transit time, since the former gives the mobility of the 'fastest' carriers and the latter a mobility representative of an 'average' carrier in the distribution. In the present examination, we have extensively compared τ_0^a and τ_0^b for several specimens over a wide range of temperature and applied field. We find that the ratio (τ_0^a/τ_0^b) does not vary drastically with either temperature or field; being in the range 1.1 to 1.5 at room temperature and increasing to between 2 and 3 at the lowest temperatures and fields at which measure-

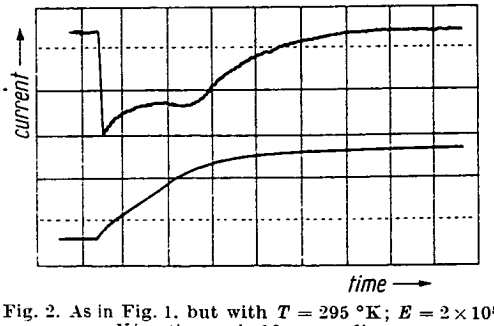

Fig. 2. As in Fig. 1, but with $T = 295$ °K; $E = 2 \times 10^5$ V/m, time axis 10 μs per div.

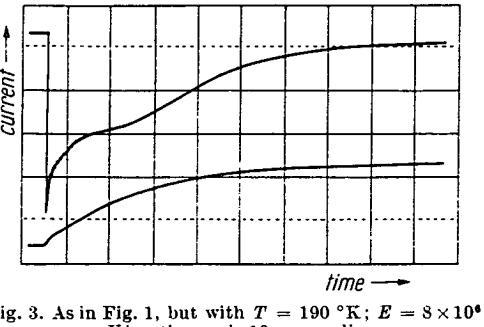

Fig. 3. As in Fig. 1, but with $T = 190$ °K; $E = 8 \times 10^6$ V/m, time axis 10 μs per div.

ments were performed. Since the mobility itself changes by more than three orders of magnitude over this range of measurement, both modes of operation should yield essentially similar values of transport parameters.

3. Experimental Results

In a preliminary examination of the hole drift mobility, the activation energy was found to decrease steadily with decreasing temperature [10]. However, it has subsequently not been possible to reproduce this effect, which we believe to have been due to the presence of an (unidentified) impurity in the starting material. Because of the irreproducibility, we do not propose to describe this data further in the present paper, although we hope to investigate the effect of impurities in a future examination. Aside from this early anomalous behaviour, our measurements on a number of specimens show good quantitative agreement, both with each other and with results published on evaporated amorphous specimens [1 to 4]. Fig. 4 and 5 show the temperature dependence of the mobility in several specimens as calculated using the current transit pulse and the integrated pulse respectively. The temperature and field dependences are found to be comparable in all cases, although the mobility is by

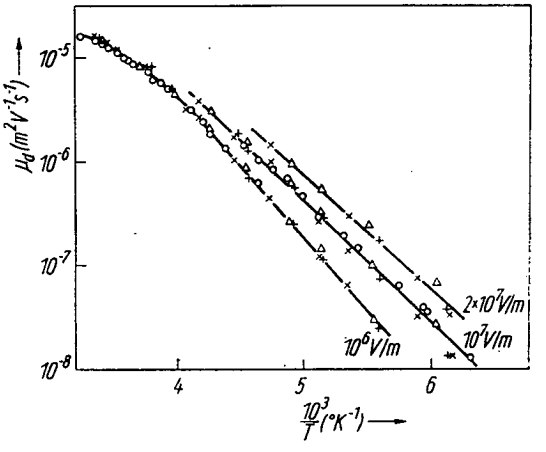

Fig. 4. Temperature dependence of the hole drift mobility, as calculated from (unintegrated) transit current pulses. ○ specimen 1, 47.5 μm, × specimen 2, 51 μm, + specimen 3, 32 μm, △ specimen 4, 22.5 μm

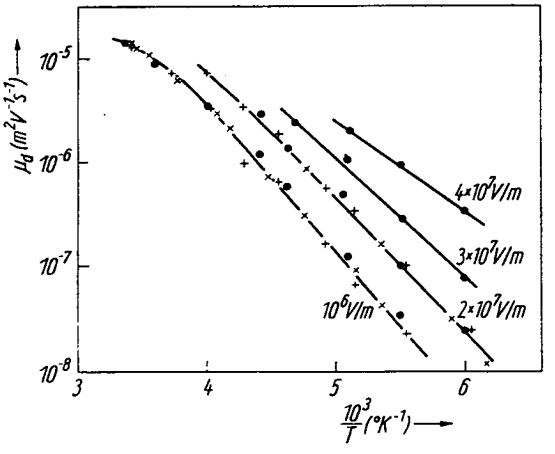

Fig. 5. Temperature dependence of the hole drift mobility, as calculated from integrated transit current pulses. × specimen 2, 51 μm, + specimen 4, 22.5 μm, ● specimen 5, 11.5 μm

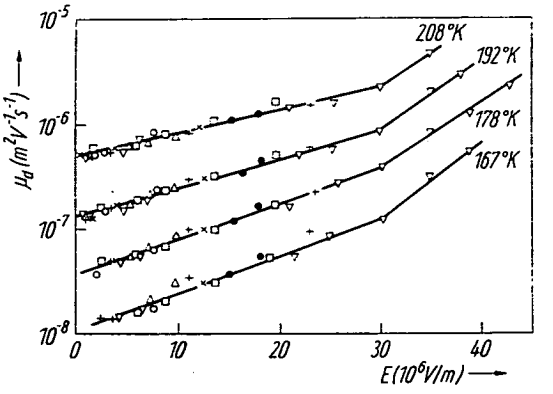

Fig. 6. Electric field dependence of the hole drift mobility, from a combination of unintegrated and integrated transit pulse measurements. Mobility multiplication factors shown in brackets below. Unintegrated measurements: △ specimen 1 (1.0); × specimen 2 (1.2); ○ specimen 3 (1.2); + specimen 4 (1.0). Integrated measurements: ■ specimen 2 (2.5); ● specimen 4 (2.0); ▽ specimen 5 (1.7)

definition somewhat lower in the latter case. Employing a suitable (small) multiplying factor for each specimen, it is possible to combine the low-temperature data obtained on various specimens from both current and integrated pulse measurements to form a single mobility versus field curve at each temperature, as shown in Fig. 6.

4. Discussion

The form of the mobility–temperature curve at low fields is similar to that obtained by previous investigators. Grunwald and Blakney [3] have associated the high-temperature region with a saturation to the μ_0 value. Whilst this suggestion cannot be positively affirmed on the basis of existing information, it appears that Grunwald and Blakney's estimate ($\mu_0 = 3.4 \times 10^{-5}$ m^2 V^{-1} s^{-1}) is more reasonable than the earlier value due to Spear (6×10^{-3} m^2 V^{-1} s^{-1}), for reasons which will become apparent. (Note that a re-assessment of μ_0 on the lines of Spear's estimate but using the higher activation energy of 0.28 eV would yield the extremely high value of 10 m^2 V^{-1} s^{-1}.) Grunwald and Blakney's estimate, although somewhat smaller than that normally envisaged as the lower limit for extended state transport [11], is probably consistent with a diffusive or percolative motion of carriers in states close to the 'mobility edge' in a non-crystalline material [12 to 14].

Below 250 °K, an activation energy of 0.28 ± 0.02 eV is observed in all specimens. The fact that this figure is slightly larger than those previously reported [3, 4] is probably due to differences between the present (bulk vitreous) and the previous (evaporated amorphous) specimens. It has been established [15] that *liquid* selenium contains substantial numbers of eight-membered atomic rings, and of chains of varying lengths. With increasing temperature, the rings are broken to form chains, the average length of which then progressively decreases. One would expect vitreous selenium, quenched from just above the melting point, to differ structurally from evaporated films in which the complex structure can only be reformed by atomic diffusion on the substrate after condensation. At the same time, the fact that neither the mobility nor its activation energy are *radically* dependent on the method of preparation suggests that the transport processes for holes are not fundamentally determined by structural considerations.

The activated form of the drift mobility can be considered in terms of motion in the extended valence band states, periodically interrupted by localisation

in a set of traps of density N_t and energy $\Delta\varepsilon$ ($= 0.28$ eV) above the valence band edge [16],

$$\mu_d = \mu_0 \frac{N_v}{N_t} \exp(-\Delta\varepsilon/kT). \quad (2)$$

Here, N_v is the effective density of states in the valence band. Taking μ_0 to be 3×10^{-5} m^2 V^{-1} s^{-1} as discussed above, then

$$N_v/N_t \approx 10^5,$$

or

$$N_t \approx 5\times10^{20} \text{ m}^{-3}.$$

Of course, higher values of μ_0 would give a proportionately higher trap density.

An alternative approach is to consider the trapping to take place in a 'tail' of localised states above the band 'mobility edge' and Mott and Davis [11] have considered such a possibility for the case of a linearly decreasing density of tail states, giving

$$\mu_d = \mu_0 \frac{\Delta\varepsilon}{kT} \exp(-\Delta\varepsilon/kT), \quad (3)$$

where $\Delta\varepsilon$ is here the depth of the tail of states. Applying equation (3) to the data gives

$$\Delta\varepsilon \approx 0.29 \text{ eV}; \quad \mu_0 \approx 3\times10^{-1} \text{ m}^2 \text{ V}^{-1} \text{ s}^{-1}.$$

The calculated figure for the microscopic mobility is much higher than the estimate of Grunwald and Blakney, and would be realistic only in the case of a very well ordered crystalline semiconductor. We thus feel that such a value is inappropriate in the present context. It is relevant to note that the value of drift mobility for holes in *crystalline* (trigonal) selenium [17] is only $2.6\times$ $\times10^{-3}$m^{2}V^{-1}s^{-1}. Also, in a photo-Hall examination of the *amorphous* material, Dresner [18] has failed to detect hole carriers with a mobility greater than 3×10^{-4} m^2 V^{-1} s^{-1}. Finally, we would expect that a high value of μ_0 would result in the observation of 'hot carrier' phenomena in the transport properties at moderate values of applied field. It therefore appears that Grunwald and Blakney's estimate represents the most reasonable value of μ_0.

We have examined the effect of varying the assumed distribution of traps in the 'tail of states' model. It is found that provided the 'tail' density decreases to zero or negligibly small values at a depth $\Delta\varepsilon$, the functional form is close to that in equation (3). If, alternatively, we postulate a slowly decreasing (e.g. exponential) tail extending past the Fermi level, it does not appear possible to derive a mobility with a small activation energy ($\Delta\varepsilon$). Also, in the latter case, one would not expect to observe a well defined drift mobility since a significant fraction of trapping events would lead to recombination rather than to subsequent release. The transient drift properties would then depend radically on the specimen thickness. Hence, it appears that the low field drift mobility is best considered in terms of periodic localisation in a set of levels at a fairly well defined energy of 0.28 eV above the valence band 'mobility edge'; and with a 'free' carrier mobility of about 3×10^{-5} m^2 V^{-1} s^{-1}.

We now turn to the electric field dependence of the mobility, as illustrated in Fig. 6. As stated previously, the thickness independence of this effect removes

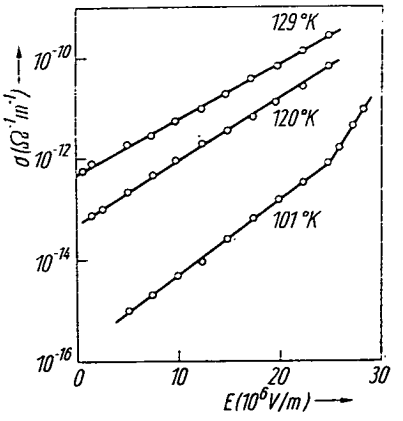

Fig. 7. Electric field dependence of the conductivity of vitreous Germanium — Tellurium eutectic (15% Ge, 85% Te)

the possibility of time of flight phenomena. Below we consider a number of possible mechanisms for field effects in the bulk material. From equation (1), it is evident that the field dependence may be a manifestation of changes in the 'free' carrier mobility, the trapping time, the release time, or in any combination of these three (the extremely high resistivity of the specimens rules out the possibility of Joule heating effects). However, before embarking on an examination of the possibilities, it is relevant to note that the field dependence observed here does not appear to be confined to the case of selenium. We have observed a closely similar functional dependence in a number of other vitreous and amorphous materials [19]. For instance, Fig. 7 shows the field dependence of the electrical conductivity in a 20 μm specimen of vitreous Ge–Te eutectic (15% Ge; 85% Te). In both cases there appears to be a linear dependence on electric field up to 2 or 3×10^7 V/m, followed by a transition to an apparently different mechanism at higher fields. It is thus necessary to consider the selenium data not in isolation, but probably as a particular instance of a fairly widespread phenomenon.

4.1 Field dependence of the release time, τ_r

The probability of 'thermal' release of a carrier localised in *any* form of potential well may be increased by field reduction of the barrier in the direction of the applied field. For the case of Coulombic centres, this behaviour is termed the Poole-Frenkel effect. In a simple one dimensional analysis [20], the field dependence is of the form

$$\mu_d(E) = \mu_d(0)\exp(\beta E^{1/2}/kT)\,, \tag{4}$$

where E is the applied field and $\beta = (e^3/\pi K \varepsilon_0)^{1/2}$. Taking Kolomiets' [21] figure for the high frequency dielectric constant of vitreous selenium ($K = 7.2$), then $\beta = 2.8\times10^{-5}$ eV/(V/m)$^{1/2}$. Generalisation of the model in three dimensions, including the possibility of thermalisation for carriers excited to within about kT of the band edge, leads to the predicted onset of a 'hyperbolic sine' dependence at low fields [22]

$$E \lesssim (kT/\beta)^2 \lesssim 2\times10^5 \text{ V/m} \quad \text{for Se at } 200\ ^\circ\text{K}\,.$$

(The estimate above was calculated by the authors using a treatment similar to that of Ieda et al. [22], but correcting for minor errors in the latter treatment. In particular, we note that it is usually inappropriate to employ a factor of $2\,kT$ in the denominator of the Poole-Frenkel equation.) We find that it is not possible to fit an $\exp(E^{1/2})$-law to the experimental data except over a limited range (3×10^6 to 2×10^7 V/m), and that even within this range the fitted value of β is only about 25% of that theoretically expected. This lower value of β would be accompanied by a transition to 'hyperbolic sine' behaviour below

5×10^6 V/m, and this behaviour is not observed experimentally. For the data on Ge–Te, it is not possible to make a satisfactory fit of the Poole-Frenkel model over *any* of the applied field range. Hence, the mechanism does not offer a satisfactory explanation of the experimental results.

When high densities of Coulombic centres exist, an appreciable overlap of the individual potential fields occurs. The maximum of the potential barrier between adjacent centres may then be fixed more or less symmetrically between the centres up to quite high values of applied field. The barrier lowering in the field direction is then $\Delta\varepsilon = -eaE$, whilst in the opposite direction the barrier is raised by an equal amount (here, $2a$ is the distance between centres). In this one dimensional analysis, the drift mobility would exhibit a dependence

$$\mu_d(E) = \mu_d(0) \cosh (eaE/kT) , \tag{5}$$

giving

$$\mu_d(E) \Rightarrow \tfrac{1}{2} \mu_d(0) \exp (eaE/kT) \text{ for } eaE \gg kT . \tag{6}$$

Application of equation (6) to the experimental data for selenium yields a value of $a \approx 10$ Å, varying somewhat with temperature. This implies a trap density of approximately 10^{27} m^{-3}; a value greatly in excess of that previously estimated, and which would imply an inordinately high value of μ_0. Furthermore, for such a value, equation (5) rather than equation (6) should be applied for fields below $E \approx kT/e\,a \approx 1.5 \times 10^7$ V/m at 200 °K. The hyperbolic cosine dependence is certainly not observed in practice over this range, so that the mechanism again does not satisfactorily explain the experimental behaviour.

Carrier localisation can, of course, occur in other types of centre than those considered above, and a degree of field dependence of the release rate is to be expected in each case. However, after considering various forms of potential well [19], an explanation of the data in these terms appears unlikely. Neutral trapping centres tend to possess a potential field of fairly short range (effective radius a few atomic spacings), and, as above, a hyperbolic rather than a simple exponential dependence is predicted over the majority of the applied field range. Screened Coulombic centres exhibit the same characteristics.

It is possible that the rate of release of trapped carriers could be enhanced by direct tunnelling from the traps into the band states. As far as carriers trapped in levels 0.28 eV from the band edge are concerned, such tunnelling should not be a significant process except at very high fields, since the tunnelling distance is too large ($\approx \Delta\varepsilon/e\,E$). The process is not therefore compatible with the experimental data, in which the same form of field dependence occurs from low fields up to 10^7 V/m or more. However, as we shall mention later, a tunnelling process could become significant when one is concerned with the motion of carriers close to the 'mobility edge' (between trapping events in the 0.28 eV levels).

4.2 Field dependence of the trapping time, τ_t

It has been suggested (e.g. Dussel and Böer [23]) that the capture rate of free carriers by Coulombic centres should be electric field dependent, since the effective radius of the potential well will decrease with increasing field as in the Poole-Frenkel effect. Dussel and Böer derive an exp $(E^{1/2})$ dependence, with a somewhat larger pre-exponential term than in the simple Poole-Frenkel case, at fields up to 5×10^6 V/m. At higher fields, the conductivity increases less rapidly than exp $(E^{1/2})$. As indicated above, the present data suggest a beha-

viour close to exp (E), and we are again unable to obtain either quantitative or qualitative agreement with the model.

For neutral and screened Coulombic centres of smaller effective dimensions, the trap radius is not expected to differ appreciably from its low field, thermal, value ($r = r^*$ such that trap depth $= kT$ at r^*) for fields in the range of interest. Hence, on a classical model, there should be no significant change in the capture cross section. A detailed analysis, taking into account any field dependence of the free carrier energy loss mechanism during the trapping process, would be of value here, but we do not think that field dependent capture cross sections are likely to be the cause of the observed behaviour.

4.3 Field dependence of the 'free' carrier mobility, μ_0

In discussing the possibility of field modification of the carrier drift processes in a *non-crystalline* semiconductor, it is necessary to consider not only the behaviour of classically free carriers, but to bear in mind that there may well be numerous interactions with very shallow localised states lying just beyond the 'mobility edge'. Thus, multiple scattering, resonant capture, and conventional trapping and release are to be expected. In the following discussion, a qualitative analysis of the possible field dependence of carrier transport close to the 'mobility edge' is attempted, as well as a consideration of the possibility of hot carrier phenomena.

A *free* carrier moving with velocity $\mu_0 E$ in the direction of an applied field E will gain energy at a rate $e\mu_0 E^2$ eV/s. Thus if energy loss processes occur at a frequency ν, the energy gained between such events is $e\mu_0 E^2 \nu^{-1}$ eV. Since the average energy loss to the lattice for each interaction is about $\frac{1}{2} kT$, one would expect the onset of hot carrier phenomena at

$$E \approx \left(\frac{kT\nu}{2e\mu_0}\right)^{1/2}. \tag{7}$$

Assuming a maximum value of scattering frequency

$$\nu \approx \nu_{\text{phonon}} \approx 10^{13}\ \text{s}^{-1},$$

then equation (7) becomes

$$E \approx 5 \times 10^7\ \text{V/m} \tag{8}$$

for a free carrier mobility of $3 \times 10^{-5}\ \text{m}^2\ \text{V}^{-1}\ \text{s}^{-1}$ and a temperature of 200 °K. It is difficult to assess the form of the field dependence which should be observed above this figure, since there are currently no satisfactory quantitative estimates of the expected variation of μ_0 and ν above the mobility edge in *non-crystalline* materials. Qualitatively, we might expect a fairly rapid increase of μ_0 and decrease of ν with energy, at least over the range just above the mobility edge, producing a sharp increase in the observed drift mobility. Avalanche processes could well occur at fields not greatly in excess of the onset of hot carrier production. In the above estimate, we have chosen a minimum value of μ_0 and a maximum value of ν, so that the estimate in equation (8) represents a lower limit for the heating of carriers at the 'mobility edge'. For higher values of μ_0, the critical field would, of course, be smaller. We note that the apparently general failure to observe hot carrier and avalanche effects below fields of 10^7 V/m is strong evidence for a low value of μ_0 in non-crystalline materials, and reinforces the probable validity of Grunwald and Blakney's estimate for amorphous selenium. The increase in field dependence observed above 3×10^7 V/m

in selenium and other materials may well be due to carrier heating, although there are a number of competing processes which might become appreciable for fields not far in excess of this value (e.g. quantum tunnelling release of carriers from the 0.28 eV levels into the valence band states).

The motion of carriers just above the mobility edge in non-crystalline materials has been regarded [12 to 14] as a percolative process with the possibility of scattering at a high density of atomic sites, whilst just below the edge Mott and Davis [11] has suggested a mechanism of quantum mechanical tunnelling (hopping) of carriers between the closely spaced sites in the localised 'tail'. In the former case, one might reasonably expect an increase in the value of applied electric field to progressively 'unblock' percolation paths through the material, so that the critical energy for extended state conduction [13, 14] should be progressively reduced. In the latter case, field enhanced tunnelling probabilities both between the shallow localised levels and between such levels and the band should occur. Mott [24] has noted the possibility of this type of 'field evacuation of traps', and indicates that the mechanism is supported by the observation [25] of enhanced conduction following a brief voltage pulse at low temperatures. Such a mechanism again effectively lowers the value of the 'mobility edge' energy. As a consequence, the effective depth of traps further into the energy gap would be reduced and one would observe a decrease in activation energy. The shift of the mobility edge could well occur continuously down to very low values of applied field, and there appears to be no reason to expect a transition to an 'ohmic' region at moderate field values as was the case for the variations of τ_t and τ_r discussed above. In addition, it is quite reasonable to expect similar behaviour in different non-crystalline materials since the phenomenon would depend primarily only on the existence of a small 'tail of states' beyond the band edge, as has been widely predicted. If, on the other hand, the field dependence involved a variation in the capture or release rates for traps well into the forbidden gap, with the type and depth of such centres differing from one material to the next, it would be more difficult to explain the observed similarity of field dependence. However, whilst we believe that a field modification of the mobility of carriers close to the 'mobility edge' presents a possible explanation of the experimental data, the theory of amorphous materials is not yet sufficiently advanced to allow a quantitative evaluation of the mechanism.

Acknowledgement

The authors wish to thank Prof. G. Miller for many valuable discussions on the subject matter of this paper.

References

[1] W. E. SPEAR, Proc. Phys. Soc. **B76**, 826 (1960).
[2] J. L. HARTKE, Phys. Rev. **125**, 1177 (1962).
[3] H. P. GRUNWALD and R. M. BLAKNEY, Phys. Rev. **165**, 1006 (1968).
[4] M. D. TABAK, Phys. Rev. B **2**, 2104 (1970).
[5] S. J. FOX and H. C. LOCKLAR, J. non-crystall. Solids, to be published.
[6] M. SILVER, K. S. DY, and I. L. HUANG, Phys. Rev. Letters **27**, 21 (1971).
[7] M. A. LAMPERT and P. MARK, Current Injection in Solids, Academic Press, 1970.
[8] J. M. MARSHALL and A. E. OWEN, Phil. Mag. **24**, 1281 (1971).
[9] W. E. SPEAR, J. non-crystall. Solids **1**, 197 (1969).
[10] J. M. MARSHALL, Thesis, University of Edinburgh, 1970.

[11] N. F. Mott and E. A. Davis, Electronic Processes in Non-Crystalline Materials, Oxford University Press, 1971.
[12] M. H. Cohen, J. non-crystal. Solids **4**, 391 (1970).
[13] J. M. Ziman, J. Phys. C (Solid State Phys.) Ser. 2, **1**, 1532 (1968).
[14] V. K. S. Shante and S. Kirkpatrick, Adv. Phys. **20**, 325 (1971).
[15] A. Eisenberg and A. V. Tobolsky, J. Polymer Sci. **46**, 19 (1960).
[16] A. Rose, RCA Rev. **12**, 362 (1951).
[17] F. K. Dolezalek and W. E. Spear, J. non-crystall. Solids **4**, 97 (1970).
[18] J. Dresner, J. Phys. Chem. Solids **25**, 505 (1964).
[19] J. M. Marshall, to be published.
[20] J. Frenkel, Phys. Rev. **54**, 647 (1938).
[21] B. T. Kolomiets, phys. stat. sol. **7**, 359 (1964): **7**, 715 (1964).
[22] M. Ieda, G. Sawa, and S. Kato, J. appl. Phys. **42**, 3737 (1971).
[23] G. A. Dussel and K. W. Böer, phys. stat. sol. **39**, 375 (1970).
[24] N. F. Mott, Phil. Mag. **24**, 911 (1971).
[25] E. A. Fagen and H. Fritzsche, J. non-crystall. Solids **2**, 170 (1970).

(Received March 17, 1972)

16. PHOTOCONDUCTIVITY AND NOISE IN CHALCOGENIDE GLASSES

C. MAIN AND A. E. OWEN

School of Engineering Science,
University of Edinburgh, Edinburgh,
Scotland.

16.1. INTRODUCTION

Several variants of the Cohen–Fritzsche–Ovshinsky (C.F.O.)[1] model of band structure—that is, a continuous distribution of localised states in the mobility gap—have been used to interpret photoconductivity data in chalcogenide glasses[2–7]. (See, for example, the discussion by Dr. Mort in Chapter 15.) The treatments differ in the distributions of states and electronic transitions involved—thus references 2–5 and 7 *assume* tails extending through the middle of the mobility gap while Mott and Davis[6] propose more limited "linear" tails. In all cases, however, the assumption at the outset of tails-of-states has been an essential feature in the interpretation and in some cases it has also been necessary to invoke a change in the nature of the localised states at some specific energy.

In the present paper the authors take a contrasting approach. Photoconductivity data on two simple amorphous chalcogenide compounds is interpreted by a band model with more or less discrete sets of localised states. *The minimum number of localised levels required to interpret the experimental data is introduced.* The data require two such levels making up, with the conduction and valence bands, a basic four-level model. The purpose of this

paper is to see how far such a model is consistent with experiment. In the following illustrations the four levels are represented in the conventional way by lines at unique energies. This is, of course, a simplification. The localised states will certainly be spread around a mean energy and the band edges will probably be "smeared out" by at least a small degree of tailing. Moreover, there may be other localised states not revealed by the present experiments.

It is relevant to note that Marshall and Owen adopted a similar approach in their paper on As_2Se_3[8]. Also, Mott and Davis[9,10] estimate that the extent of band tailing in simple chalcogenide glasses is less than 0·2 eV. while mobility measurements on some of these materials reveal much deeper states[8,11,12] presumably *not* associated with such tails.

16.2. Rate Analysis

(i) The free and trapped carrier densities under optical excitation are obtained from the rate of change of occupation in terms of the transition rates (of electrons and holes) into and out of a particular level. It is assumed that the

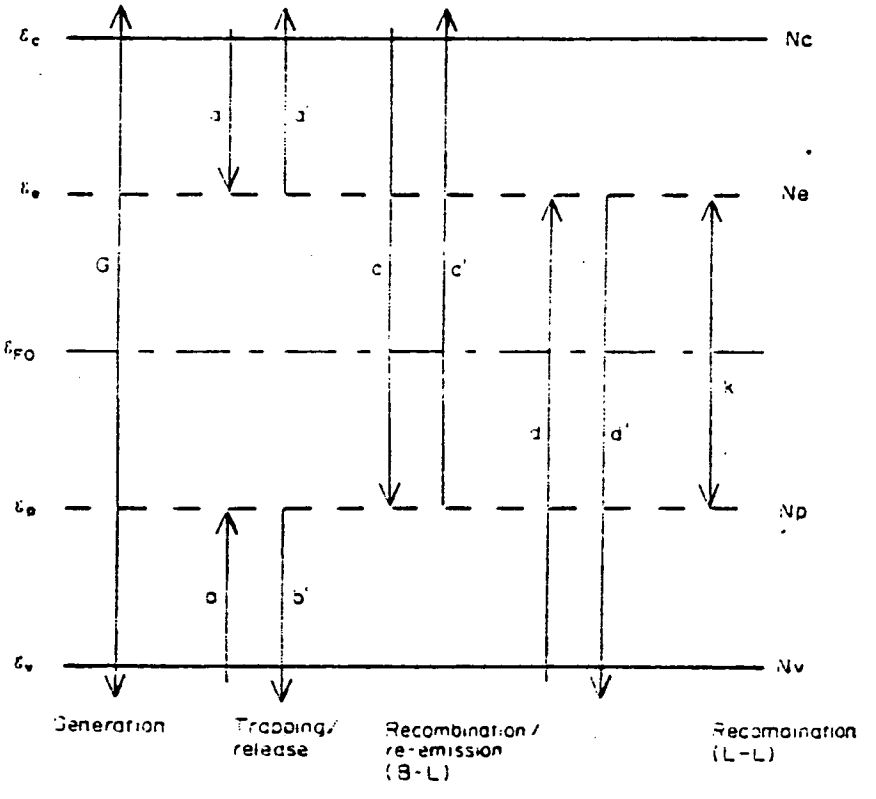

FIG. 16.1. Basic 4-level semiconductor model showing electron and hole transitions.

localised states are monovalent, and that the following discussion can be applied to centres which are charged when "occupied" (by the relevant carrier—hole or electron) or neutral, as in the C.F.O. model. It is also assumed that dc conduction is dominated by holes, as the great mass of evidence suggests.[13,14]

All the relevant parameters for the rate analysis are shown in Fig. 16.1, e.g., hole traps at energy $\mathcal{E}_p$ have density $N_p(\mathrm{cm}^{-3})$ and fractional hole occupation f_p. The capture coefficient of an unoccupied hole trap for a free hole is C_p, and C_e' is the capture coefficient of an occupied hole trap for a free electron. Thermally produced densities and occupancies are denoted by the subscript "0", while photo-produced densities and occupancies are denoted by the prefix "Δ". The figure is symmetrical so that transitions a, a', c and c' involve electrons while transitions b, b', d and d' involve holes. Similarly, f_{e_0} is the equilibrium Fermi occupation function for electron traps, while $\bar{f}_{p_0}$ is the complement of the Fermi function for hole traps. Processes a and a' are trapping and release rates for electrons, and b and b' are trapping and release rates for holes. For example, the hole trapping and release rates can be written as

$$\begin{aligned} b &= pC_pN_p(1-\bar{f}_p) = p/\tau_t\ (\mathrm{cm}^{-3}\mathrm{sec}^{-1}) \\ b' &= p_1C_pN_p\bar{f}_p = N_pf_p/\tau_{rt}\ (\mathrm{cm}^{-3}\mathrm{sec}^{-1}) \end{aligned} \tag{16.1}$$

where τ_t, τ_{rt}, are trapping and release times for holes, and p_1 obtained from detailed balance considerations is

$$p_1 = N_v \exp\left(-\frac{\mathcal{E}_p - \mathcal{E}_v}{kT}\right) \tag{16.2}$$

All the other transition rates can be expressed in a similar way.

(ii) *Recombination*

Recombination in the 4-level semiconductor of Fig. 16.1 can occur in a number of ways, one of which usually predominates. Three "paths" have been considered. The first two, paths 'd' and 'c', are two-step processes, in which rapid trapping of a free carrier in a localized state is followed by the capture of a carrier of opposite sign, usually a slower process. Thus, path 'd' involves processes 'a' and 'd', while path 'c' involves processes 'b' and 'c'. This is referred to as Band-Localised (B–L) recombination, and it is a process familiar in ordinary semiconductor physics.[15–17]

The possibility of a third recombination path involving localised–localised (L–L) transitions, when ,as in amorphous semiconductors, the densities of

localised states are high has been pointed out previously.[3,4,6,18,19] The rate for this process is $KN_p\bar{f}_pNef_e$ where K is a rate constant. Whether B–L or L–L recombination predominates in a given case is determined by the relative rates.

(iii) *Rate Equations*

The set of differential equations (D.E.) for the energy level occupancies together with the charge neutrality condition.

$$N + N_e f_e - p - N_p \bar{f}_p = 0 \quad \text{(neutral traps)} \tag{16.3}$$

give all the required information. For example, the valence band D.E. is

$$\frac{dp}{dt} = G - b + b' - d + d' = 0 \quad \text{in steady state.} \tag{16.4}$$

All terms are written as sums of thermal ('$_0$') photo-excited terms ('Δ') and solved for the latter. $G = g_0 + g$ where g is the photo-excitation rate.

A great simplification can be effected if the trapping interchange is much greater than the recombination rate. In particular, if $b'(a') \gg c(d)$, or k, then the localised levels lie well outwith the so-called demarcation levels,[20,21] and are in "quasi-thermal equilibrium" with the nearest band. Then,

$$\frac{\text{free holes}}{\text{trapped holes}} = \frac{p}{N_p f_p} = \frac{p_0}{N_p f_{p0}} = \frac{p_1}{N_p} \text{ (constant).} \tag{16.5}$$

In these circumstances, the free and trapped carrier densities are "synchronised" except for times less than the relevant *trapping* times, and the situation reduces to a "two-reservoir" problem. The overall rate equation for holes becomes

$$\frac{d(p + N_p \bar{f}_p)}{dt} = G - c - d - k \tag{16.6}$$

Finally, in the present situation, the trap densities are high, and the traps are not fully occupied under most experimental conditions, hence the following inequalities hold:

$$n, p \ll N_e f_e, N_p \bar{f}_p \ll N_e, N_p \tag{16.7}$$

Results of analysis: At low excitation levels ($\Delta p \ll p_0$ etc.) excess carriers recombine into a pool of thermally produced recombination centres (mono-

molecular kinetics), while at high excitation levels ($\Delta p \gg p_0$ etc.) the recombining species are proportional (bimolecular kinetics).

Table 16.1 shows the results of the kinetic analysis for Band–Localised, and Localised–Localised recombination.

(iv) *Band–Localised Recombination*:

The following discussion assumes path 'd' is dominant but similar answers are obtained for path 'c'. At low intensities, the rate equation is monomolecular, and the steady state solution for excess hole density Δp_m has the same features as observed experimentally i.e. a linear intensity relationship and exponential *increase* with $1/T$. The transient decay is exponential, and the decay time τ_{md} (where subscript d refers to the recombination path) has a marked temperature dependence. This is because the excess free holes actually involved in recombination constitute a small *temperature dependent* fraction of the total photoexcited hole density (free + trapped), and the recombination centre density (at $\mathcal{E}_c$) is *also* temperature dependent. As Rose pointed out, the photo decay time is much longer than the free recombination time τ_r.

i.e.

$$\tau_{md} = \tau_r \times \frac{\text{trapped holes}}{\text{free holes}} = \tau_r \times \left(\frac{N_p f_p}{p}\right) \tag{16.8}$$

where $\tau_r = (C_p' N_c f_c)^{-1}$, and both factors in eqn (16.8) are temperature dependent. At high excitation levels, the rate equation is bimolecular and the steady state solution for excess holes is of the form observed experimentally i.e. the square root intensity dependence, and an exponential *decrease* with $1/T$. Note that the "activation energy" predicted here is *half* the trap depth.

The decay is now non-exponential and has a long hyperbolic tail. In addition, the decay time τ_{bd}, defined as the time to decay to half value, is intensity dependent and much *less* temperature dependent than the monomolecular decay time. This behaviour results from the swamping of thermally produced carriers and occupied recombination centres by the photo-generated densities.

(v) *Localised–Localised Recombination*

Table 16.1 also lists the predicted photoconductivity features when L–L recombination prevails ($c, d \ll k$). Again, regions of monomolecular and bimolecular recombination are predicted, but quite different temperature dependences (for steady state and transient solutions) are obtained. For example, the steady state bimolecular solution for excess holes predicts an "activation energy" *equal* to the hole trap depth (c.f. ½ trap depth for B–L

TABLE 16.1 Recombination Models

	Rate equation	Steady state	Decay
	1 Band–Localised		
Low intensity	$\frac{d\Delta p}{dt} = g\left(\frac{p_1}{N_p}\right) - \left(\frac{1}{\tau_{md}} + \frac{1}{\tau_{mc}}\right)\Delta p$	$\Delta p_m \propto g \exp\left(\frac{\mathcal{E}_e - \mathcal{E}_{F_0}}{kT}\right)$	$\Delta p(t) = \Delta p_m \exp(-t/\tau_{md})$
	$\tau_{md} = (2C_p' f_{p_0} p_1)^{-1} : \tau_{mc} = \left(2C_e' n_1 \frac{N_p}{N_e} f_{p_0}\right)^{-1}$		$\tau_{md} \propto \exp\left(\frac{\mathcal{E}_p - \mathcal{E}_v + \mathcal{E}_e - \mathcal{E}_{F_0}}{kT}\right)$
High intensity	$\frac{d\Delta p}{dt} = g\left(\frac{p_1}{N_p}\right) - (\gamma_d + \gamma_c)\Delta p^2$	$\Delta p_b \propto g^{\frac{1}{2}} \exp\left(-\frac{\frac{1}{2}(\mathcal{E}_p - \mathcal{E}_v)}{kT}\right)$	$\Delta p(t) = \Delta p_b(1 + \Delta p_b \gamma_d t)^{-1}$
	$\gamma_d = C_p' \quad \gamma_c = C_e' \frac{n_1}{p_1} \frac{N_p}{N_e}$	(Solutions for path d)	$\tau_{bd} \propto g^{-\frac{1}{2}} \exp\left(\frac{\frac{1}{2}(\mathcal{E}_p - \mathcal{E}_v)}{kT}\right)$
	2 Localised–Localised		
Low intensity	$\frac{d\Delta p}{dt} = g\left(\frac{p_1}{N_p}\right) - \frac{1}{\tau_{mL}}\Delta p$	$\Delta p_m \propto g \exp\left(\frac{\mathcal{E}_e - \mathcal{E}_{F_0} - (\mathcal{E}_p - \mathcal{E}_v)}{kT}\right)$	$\Delta p(t) = \Delta p_m \exp(-t/\tau_m)$
	$\tau_{mL} = (2KN_p f_{p_0})^{-1}$		$\tau_{mL} \propto \exp\left(\frac{\mathcal{E}_e - \mathcal{E}_{F_0}}{kT}\right)$
High intensity	$\frac{d\Delta p}{dt} = g\left(\frac{p_1}{N_p}\right) - \gamma_L \Delta p^2$	$\Delta p_b \propto g^{\frac{1}{2}} \exp\left(-\frac{(\mathcal{E}_p - \mathcal{E}_v)}{kT}\right)$	$\Delta p(t) = \Delta p_b(1 + \Delta p_b \gamma_L t)^{-1}$
	$\gamma_L = \frac{KN_p}{p_1}$		$\tau_{bL} = (gK)^{-\frac{1}{2}}$

Note: The energy term $(\mathcal{E}_e - \mathcal{E}_{F_0})$ is an approximation, wherever it appears, to $\frac{1}{2}(\mathcal{E}_c - \mathcal{E}_{\ })$.

model), and the monomolecular decay time is much less temperature dependent as recombination does not involve a small temperature dependent fraction of the photoexcited carriers.

(vi) *Trap Limited Drift Mobility* μ_d

The trap limited hole drift mobility, given by the approximate relation

$$\mu_d \approx \mu_0 \times \frac{p}{N_p f_p} = \mu_0 \frac{p_1}{N_p} \tag{16.9}$$

(where μ_0 is the free mobility in the band) can be calculated from transient decay and growth measurements as follows.

The rate equations in Table 16.1 applied to a "step" illumination predict an initial region of linear growth of carrier density before recombination equilibrium is reached. As Ryvkin has shown,[22] there is also a region of rapid growth at very short times ($t \leqslant \tau_t$), but in the present case this cannot be resolved experimentally. The mobility is obtained from the photocurrent growth slope.

$$\left.\frac{\mathrm{d}\Delta I}{\mathrm{d}t}\right]_{t\sim 0} \propto \left.\frac{\mathrm{d}\Delta p}{\mathrm{d}t}\mu_0\right]_{t\sim 0} \propto g\left(\frac{p_1}{N_p}\mu_0\right) \propto g\mu_d. \tag{16.10}$$

Similarly, from the overall decay curve, the drift mobility can be obtained

$$\Delta I \text{ (steady state)} \propto g\frac{p_1}{N_p}\mu_0\tau \propto \tau\mu_d \tag{16.11}$$

where τ is the relevant photo decay time.

(vii) *Distributed States*

The foregoing analysis can be applied to the C.F.O. model and distributed states. Simmons,[7] Weiser [3] and Arnoldussen *et al.*,[4] for example, all assume a model with more or less featureless tails of states and introduce transition mechanisms,[3] or discontinuities in the nature of the states[4] with energy, to produce a "peaking" in the excess carrier distribution at particular energies. The results are similar to those for a model with discrete levels.

16.3. PHOTOCONDUCTIVITY IN AMORPHOUS As_2Te_3

Samples were evaporated thin films (0·5–1·5 μm) with *coplanar* gold electrodes on 7059 borosilicate substrates (typical gap 25 μm).

The results obtained in Section 16.2 apply to uniform excitation throughout a homogeneous sample. Absorption of light, surface effects, and diffusion have been neglected. It is relatively easy to include absorption effects in both steady state and transient solutions, and this has been done. Surface effects and diffusion have been shown to have little influence.

(ii) *Amorphous Arsenic Telluride*

The optical absorption constant α, necessary for interpretation of photoconductivity data, was obtained from transmission measurements. The data were fitted to the relation[23–25]

$$\alpha(\nu) = \text{const } (h\nu - \mathcal{E}_g)^2/h\nu \tag{16.12}$$

giving an optical gap of 1·0 eV at 0 K, and the temperature coefficient $-4{\cdot}7 \times 10^{-4}$ eV K^{-1}.

Dark conductivity measurements gave a conductivity activation energy of 0.42 eV, and room temperature conductivity of 10^{-4} ohm^{-1} cm^{-1}.

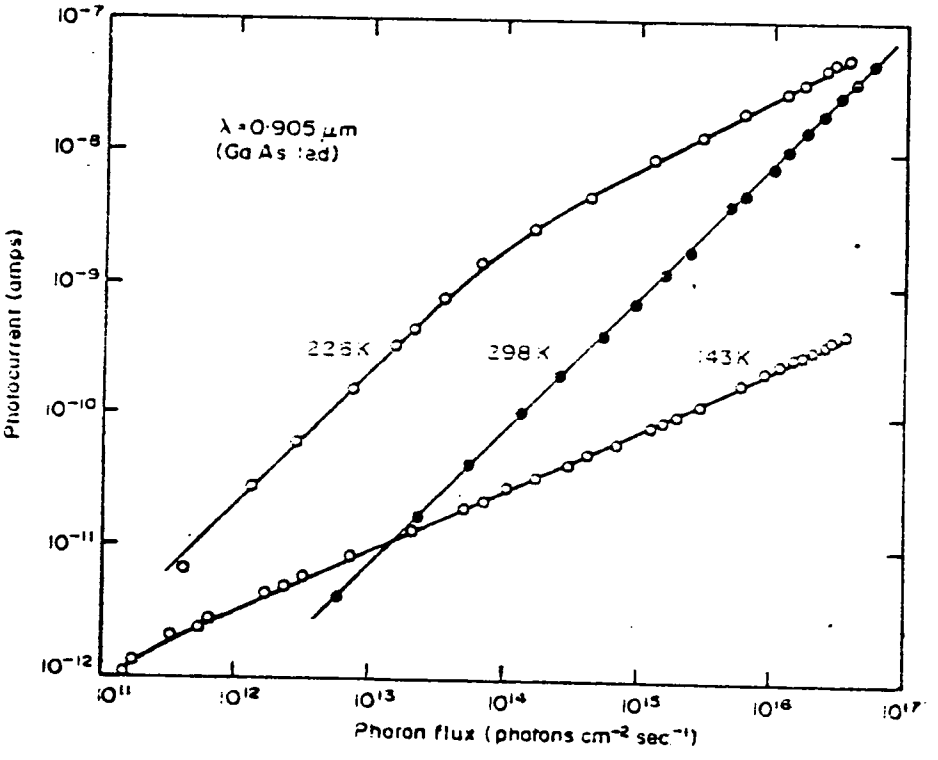

FIG. 16.2. Photocurrents versus incident photon flux for As_2Te_3.

The photocurrent versus intensity relation in Fig. 16.2 illustrates the transition from linear to square root behaviour, and the reversal of temperature dependence in the two regions. Figure 16.3 shows the temperature dependence

of the steady state photocurrent and decay time. This demonstrates the reversal of temperature dependence predicted for the steady state, and the rapid fall of the decay time with temperature in the monomolecular region (0·55 eV slope). The low temperature behaviour of τ has not been fully analysed.

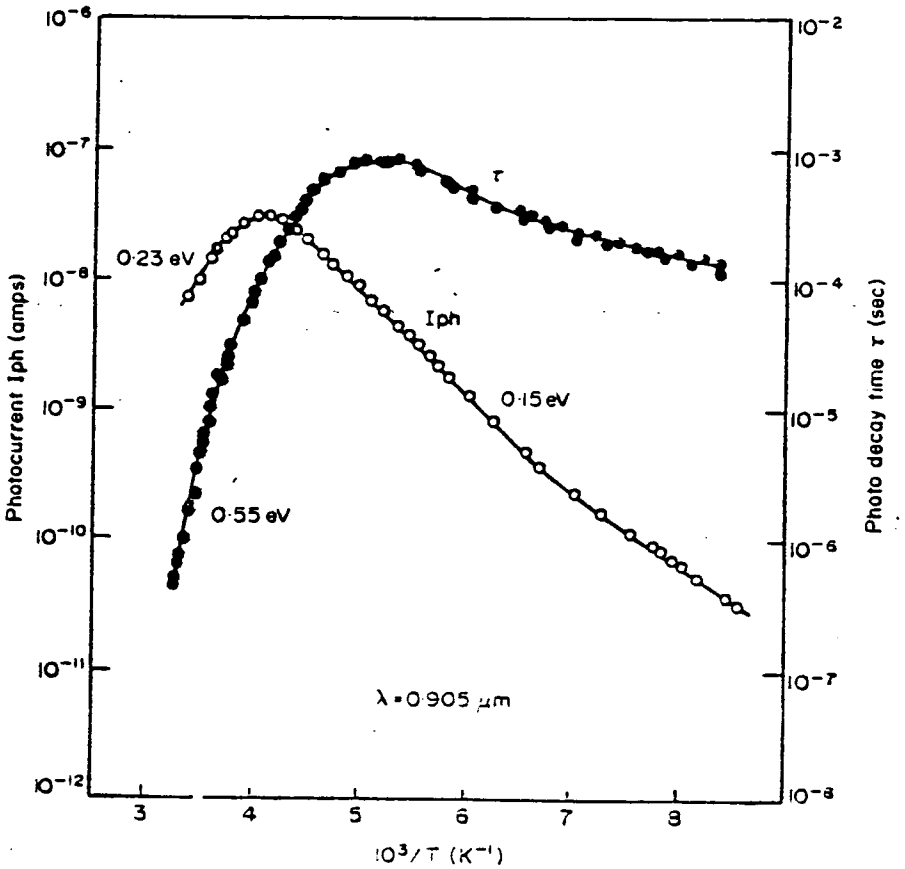

FIG 16.3 Photocurrent and decay time versus ($10^3/T$) for As_2Te_3. Photon flux = 9×10^{15} photons cm^{-2} sec^{-1}.

The hole trap limited mobility computed from eqn (16.11), and the monomolecular data, has a room temperature value of 10^{-2} cm^2 s^{-1} V^{-1}, and an activation energy of 0·33 eV, in good agreement with the data of Croitoru.[26]

Figure 16.4 illustrates schematically, the band diagram for 0 K, giving as close a fit as possible to experimental data—optical absorption, dark conductivity, and steady state photoconductivity—for B–L (path 'd') and L–L recombination. The gap is assumed to reduce uniformly with temperature. This diagram is drawn in the spirit of the simplifications mentioned in Section 16.1.

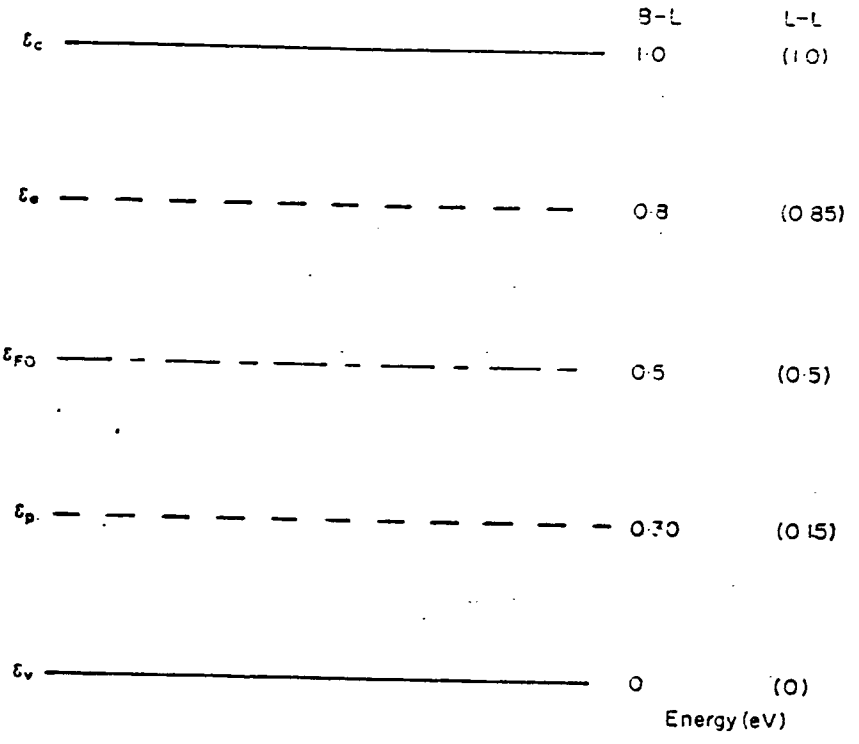

FIG. 16.4. Schematic band diagram for As_2Te_3. Energies shown for B–L and L–L recombination models.

Table 16.2 lists some of the "activation energies" predicted by the two models, and also the measured values. The quantities $\Delta\mathcal{E}_m$ and $\Delta\mathcal{E}_b$ were obtained from the slopes of the mono- and bimolecular steady state photoconductivity versus $(1/T)$, $\Delta\mathcal{E}_\mu$ is the trap-limited mobility activation energy, $\Delta\mathcal{E}_\sigma$ the dark conductivity activation energy, and $\Delta\mathcal{E}_{\tau m}$ was obtained from the slope of the monomolecular decay time τ_m versus $(1/T)$.

TABLE 16.2. Parameters for As_2Te_3 for B–L and L–L recombination

Activation energy (eV)	B–L	Measured	L–L
Monomolecular $\Delta\mathcal{E}_m$	0·20	0·23	0·20
Bimolecular $\Delta\mathcal{E}_b$	0·15	0·15	0·15
Mobility $\Delta\mathcal{E}_\mu$	0·30	0·32	0·15
Conductivity $\Delta\mathcal{E}_{F_0}$	0·5	0·42	0·5
Decay time $\Delta\mathcal{E}_{\tau m}$	0·5	0·55	0·35

Both models require $\mathcal{E}_{F0}$ to be roughly in the middle of the gap, rather higher than its measured position. (Pinning of $\mathcal{E}_{F_0}$ by localised states is being investigated.) While the B–L model gives a good fit for the parameters

(within 10%) the L–L model gives values for $\Delta\mathcal{E}_{\mu}$ and $\Delta\mathcal{E}_{\tau m}$ which are much smaller than the measured quantities.

It therefore seems probable that B–L recombination predominates. On this basis the trap density can be estimated from the mobility, conductivity, and temperature coefficient of the gap as $N_p \approx 3 \times 10^{18}\,\mathrm{cm}^{-3}$, and the product $\mu_0 N_v \approx 1 \times 10^{21}\,\mathrm{cm}^{-1}\mathrm{s}^{-1}\mathrm{V}^{-1}$. Thus if the free carrier mobility is $\mu_0 = 10\,\mathrm{cm}^2\,\mathrm{s}^{-1}\mathrm{V}^{-1}$, $N_v \approx 10^{20}\,\mathrm{cm}^{-3}$; both are reasonable figures.[25] The ratio of trapped to free holes at room temperature would be 10^3, the recombination time τ_r for a free hole about 10^{-9} sec at room temperature, and the recombination coefficient $C'_p \approx 10^{-8}\,\mathrm{cm}^3\,\mathrm{sec}^{-1}$ (rather high). Some of these results have been verified independently by noise measurements (see Section 16.4)

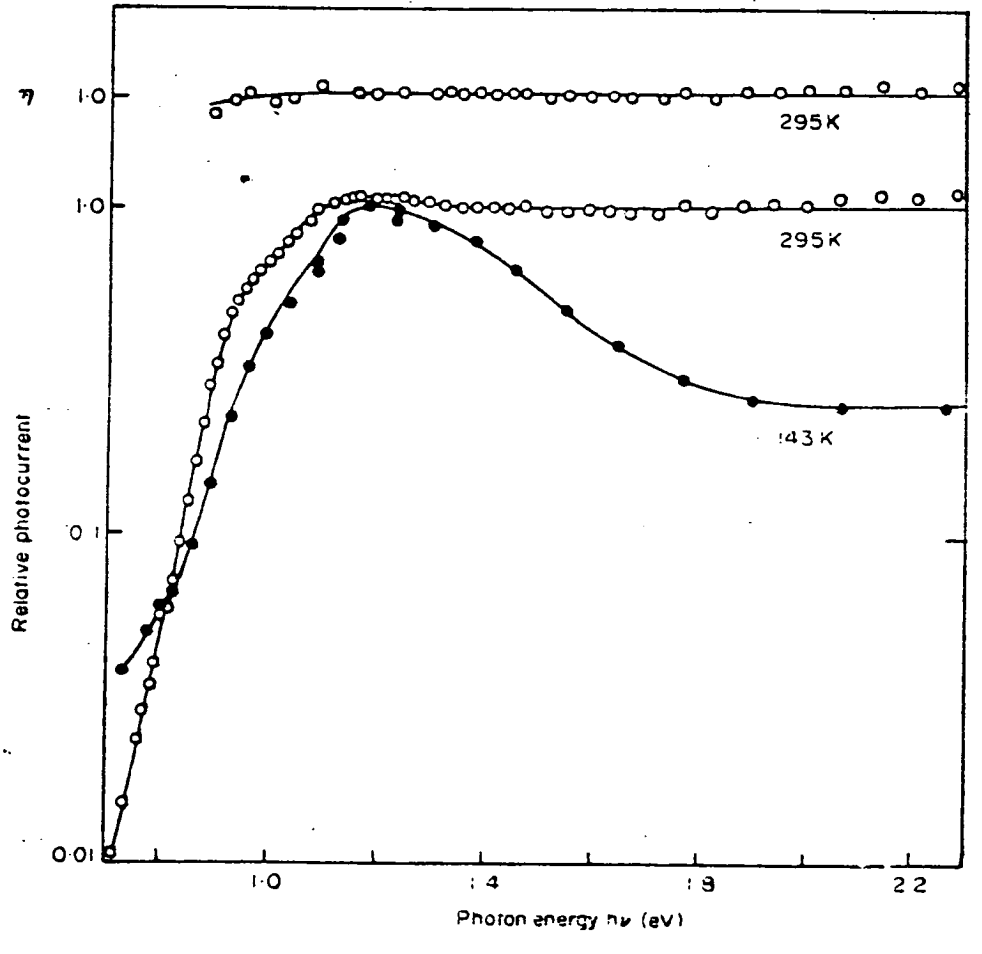

FIG. 16.5. Normalized spectral response for As_2Te_3 at 295 K and 143 K. The upper curve shows the normalized quantum efficiency η versus photon energy, at 295 K.

Spectral response and quantum efficiency

Figure 16.5 shows the normalised photocurrent per incident photon versus photon energy for amorphous As_2Te_3 at two temperatures. At 295 K, in the monomolecular region, the response rises to a constant level with photon energy, while at 143 K, in the bimolecular region, a peak occurs. The fall off at high photon energies is not due to surface effects, but results from the bimolecular bulk behaviour and the reduction of absorption depth with photon energy. Calculation of the photo-response per absorbed photon (relative quantum efficiency η) verifies this. At both temperatures this is constant for photon energies between 1·0 and 3·0 eV, implying an absolute value for η of unity.[2] At 143 K there is a slight fall in η at photon energies below 1·0 eV. In calculating the generation rate g, η was taken to be unity.

16.4. Noise in Amorphous As_2Te_3

(i) There are very few reports of noise measurements in amorphous semiconductors,[27–29] probably because of the surprisingly low level noise spectra usually obtained.

In practice, conductivity fluctuations give rise to noise in the dc current I_0, when an external source is connected to the sample, and the spectral distribution $S_i(f)$ is measured.

If the subscript "$_0$" refers to mean values and "Δ" refers to departures from the mean, the mean square noise current is

$$\overline{\Delta I^2} = I_0 \frac{\overline{\Delta p^2}}{p_0} \tag{16.13}$$

where Δp and p_0 refer to carrier *numbers* in a given sample (1 cm^3, for simplicity), and $\overline{\Delta p^2}$ is the hole number *variance*.

The main features of noise in amorphous As_2Te_3 have been investigated with the 4-level model proposed for photoconductivity. (See van Vliet and Fasset,[30] and van der Ziel[31] for the mathematical methods used).

The spectral density obtained for carrier fluctuations under conditions similar to those for low-level photoconductivity is

$$S_{\Delta p}(\omega) = \overline{4\Delta p^2}\left\{\frac{\tau_r}{1+\omega^2\tau_m^2} + \frac{\tau_t}{1+\omega^2\tau_t^2}\right\} \tag{16.14}$$

where τ_m, τ_r, τ_t, have the same values and significance as before. Equation (16.14) contains two relaxation modes; the first refers to noise due to transit-

ions from the reservoir of valence band and associated traps, to the reservoir of conduction band and associated traps(recombination component) while the second refers to noise due to trapping transitions *within* the first reservoir (trapping component).

The variance Δp^2 may be found for such a system by the generation-recombination theorem.[32,33] In this case, however, as $N_p f_p \gg p$, the individual carriers are generated independently, and poisson statistics apply.[34] The variance is then

$$\overline{\Delta p^2} = p_0 \tag{16.15}$$

and this is the highest value which can arise in thermal equilibrium. As suspected, high trap densities result in a high *total* noise level. The trapping component accounts for most of the variance, but it is spread over a wide frequency range and thus has a very low *spectral density*. Only the recombination component could be resolved experimentally and it accounts for a small fraction of the total noise—hence the reports of very low noise levels in amorphous semiconductors.

(ii) *Experimental results*

Noise measurements were made on the same thin film samples used in the photoconductivity investigations. Standard techniques were used,[35] with

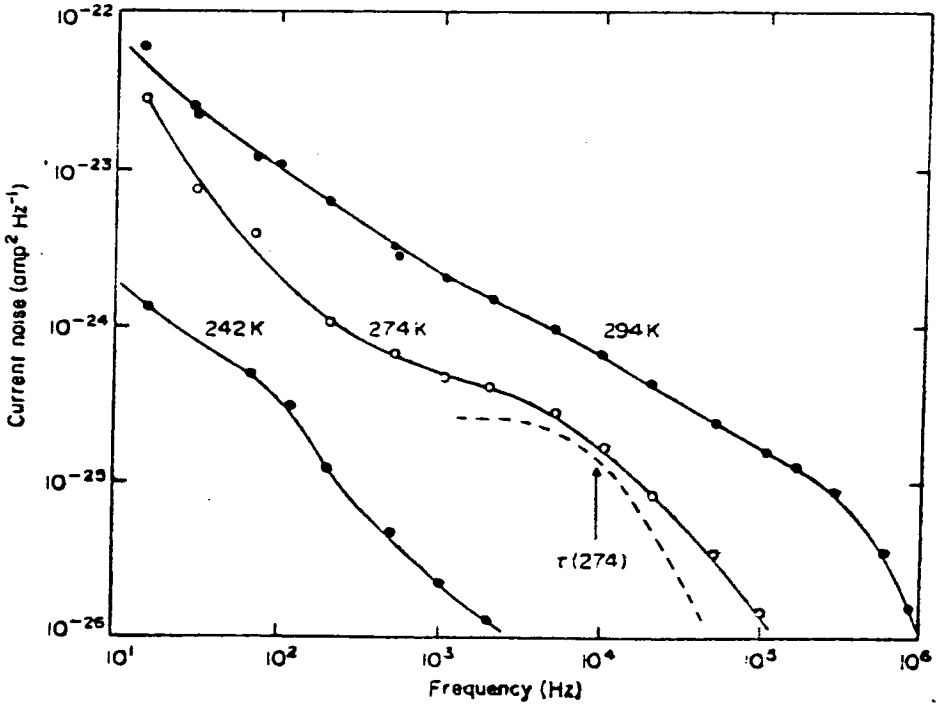

FIG. 16.6. Current noise spectra $S_i(f)$ for As_2Te_3.

low-noise wide-band and narrow-band circuitry (noise figure < 1 dB), and true r.m.s. detection.

Figure 16.6 shows the noise spectra obtained for As_2Te_3, normalised to constant applied voltage, for three temperatures. The relaxation mode (recombination component) appears as a "bump" on a featureless $1/f$ trend due probably to contacts. Good agreement was obtained between the magnitude *and* the temperature dependence of the noise "turnover" time constant, and the monomolecular photo decay time. The trapped hole *density* computed from these data (noise plateau and time constant) is, at room temperature,

$$N_p f_{p0} \approx 5{\cdot}5 \times 10^{16}\,\mathrm{cm}^{-3}$$

resulting in a trap density

$$N_p \approx 3 \times 10^{18}\,\mathrm{cm}^{-3}$$

if $(\mathcal{E}_p - \mathcal{E}_v) = 0{\cdot}3\,\mathrm{eV}$ at 0 K. This is in good agreement with the photoconductivity results and is *independent* of estimates of μ_0 and N_v.

An upper limit to the trapping time τ_t of 5×10^{-11} sec can be estimated from the fact that the trapping noise plateau must be less than $10^{-26}\,\mathrm{A^2\,Hz^{-1}}$.

The capture cross section of the traps for holes σ_p, is given by $\tau_t = (_pNv\sigma_p)^{-1}$, where v is the thermal velocity of free holes ($\approx 10^7\,\mathrm{cm\,sec^{-1}}$). Thus $\sigma_p \approx 10^{-16}\,\mathrm{cm^2}$. This is large, considering the depth of the traps (0·3 eV, but according to Lax,[36] is possible with "cascade" capture, even for *neutral* centres.

16.5 Amorphous Arsenic Selenide

(i) A similar series of experiments was carried out on thin-film As_2Se_3 samples. The results are more difficult to interpret unambiguously, however, as several trapping levels may be effective.

Optical measurements reveal a 0 K optical gap of 2·0 eV and a temperature coefficient of $-5{\cdot}7 \times 10^{-4}\,\mathrm{eV\,K^{-1}}$. The dark conductivity is $6 \times 10^{-13}\,(\Omega\,\mathrm{cm})^{-1}$ at room temperature, with activation energy 0·92 eV, in good agreement with other reports.[37]

Figure 16.7 shows the photocurrent as a function of photon flux for As_2Se_3, illustrating again the transition from linear to square-root behaviour. The reversal of temperature dependence also occurs, and is shown explicitly in Fig. 16.8, where the photocurrent at constant illumination is plotted versus $(10^3/T)$. The slopes on this plot give $-0{\cdot}37\,\mathrm{eV}$ at low temperatures, and about $+0{\cdot}37\,\mathrm{eV}$ at high temperatures but these values are sensitive to changes in the absorption constant with temperature at the photon energy used (1·9 eV). It is estimated that the value obtained from the low temperature slope could be as low as $-0{\cdot}32\,\mathrm{eV}$.

Time constant measurements show a rapid fall at high temperatures, corresponding to an activation energy of 0·8 eV, but relative insensitivity at low temperature. Note that the room temperature photo decay time, for moderate intensities (10^{15} photons cm^{-2} sec^{-1}), is about 10^{-3} sec compared with 10^{-6} sec for As_2Te_3.

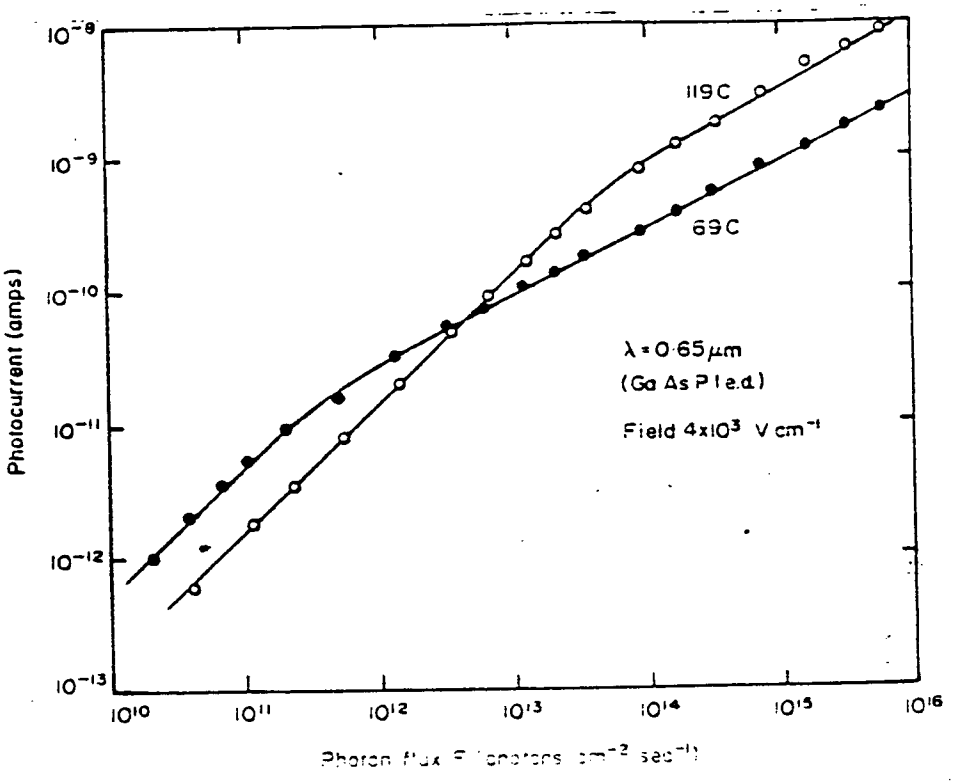

FIG. 16.7. Photocurrent versus photon flux for As_2Se_3. Excitation source: GaAsP light emitting diode (l.e.d.).

Trap limited drift mobilities, obtained from "initial slope" measurements [eqn (16.10)] give reasonable agreement with other workers[38,38] e.g. $\mu_d \approx 3 \times 10^{-5}$ cm^2 $sec^{-1}V^{-1}$ at room temperature and a field of 10^5 V cm^{-1}.

On the basis of these results, a schematic band diagram may be constructed as for As_2Te_3, but with L–L recombination predominating, as indicated by the relatively temperature independent bimolecular decay. Thus, the hole and electron traps would be 0·3 eV and 0·35 eV deep in a 2·0 eV gap. There is reason to suspect that the true picture for As_2Se_3 is not so simple, and that several trap species are present at different depths in the gap.[39]

(ii) *Spectral response*

Figure 16.9 shows the normalised photocurrent per *incident* photon for a thin-film (0·87 μm) As_2Se_3 sample, at room temperature. The peak observed

is again due to bimolecular bulk conditions, now prevailing at *room* temperature for As_2Se_3. In the same figure is the computed photocurrent per absorbed photon (η). It can be seen that η levels off well above the optical gap, and is much less (0·2) at the optical absorption edge than its saturation value. This type of behaviour has been observed in Se.[40,41]

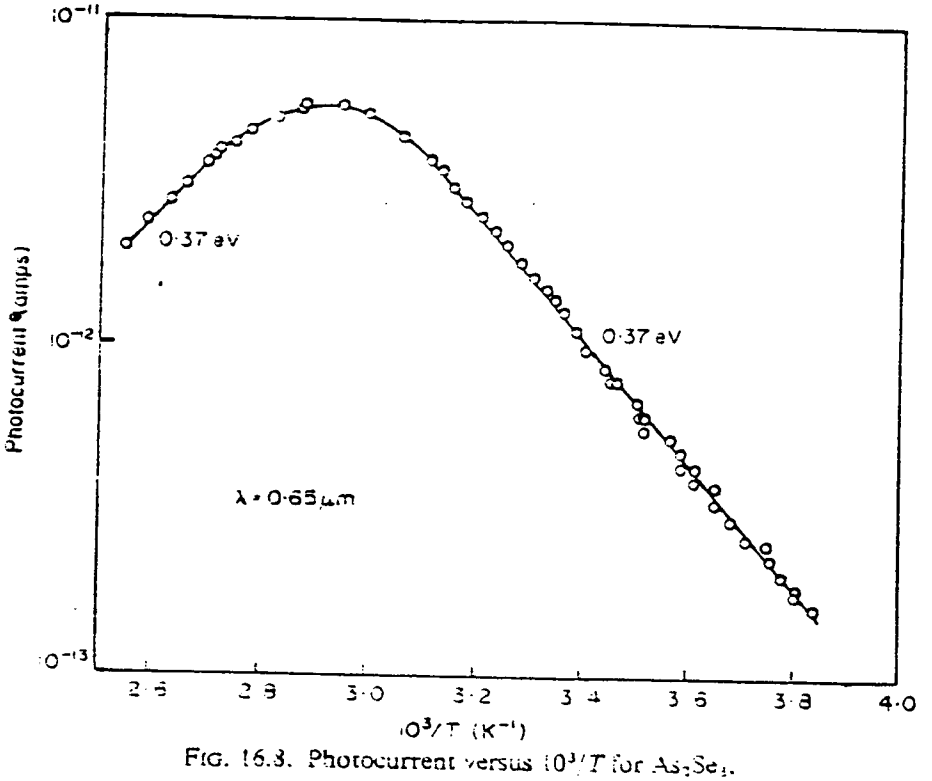

FIG. 16.8. Photocurrent versus $10^3/T$ for As_2Se_3.

Davis and Mott's interpretation involves separation of the photogenerated hole–electron pair, before geminate recombination occurs, in order that the photo-produced carriers contribute to the photocurrent. Other explanations for non-photoconducting absorption invoke the molecular nature of these materials, and excited molecular states.

(iii) *Noise in* As_2Se_3

Measurements have been made of noise in thin film sandwich samples of As_2Se_3 under optical excitation, and some of the results have already been reported.[42] Again, there is agreement between the relaxation modes in the noise spectra, and the photoconductivity time response, though detailed calculations have not yet been performed.

16.6 Conclusions and Summary

Photoconductivity data and current noise measurements in amorphous

chalcogenide compounds can be adequately interpreted through a band model with discrete levels of localised states but it is not possible to distinguish on the basis of existing data between this model and the extensive tails-of-localised states used in previous interpretations. It should be noted, however, that in contrast to the "continuous tails-of-states" school of thought, the present approach does not require the additional arbitrary assumption of a change in the nature of the states at some specific energy.[4,5] We would suggest, therefore, that a model involving more or less well defined localised states presents the best approach to the problem.

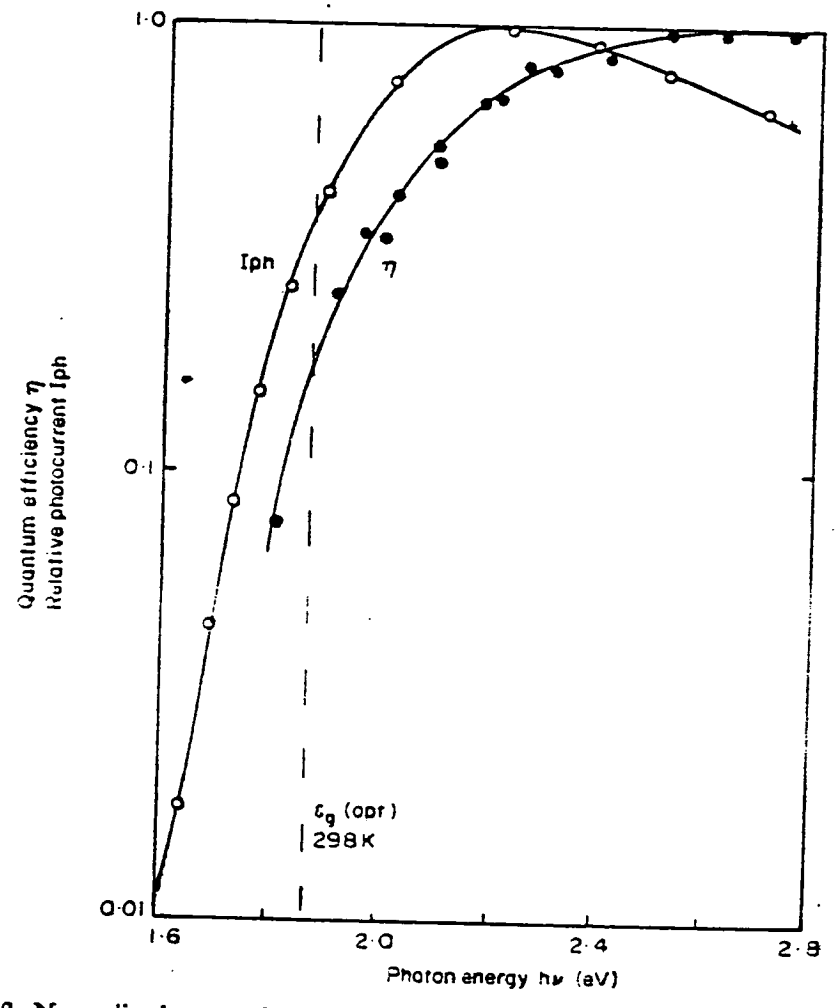

FIG. 16.9. Normalized spectral response and quantum efficiency for As_2Se_3 at room temperature.

These conclusions refer specifically to the relatively simple amorphous chalcogenide compounds such as As_2Se_3 and As_2Te_3. Structural studies have

shown that these materials have a high degree of short range order and it would not be surprising if this is reflected in their electronic band structure. In complex alloy chalcogenide glasses, where there is compositional as well as structural disorder, band tailing may well be very extensive.

Although the same basic four-level model has been used for both compounds, there are significant differences in the photoconductive behaviour of As_2Se_3 and As_2Te_3 viz.

(a) In As_2Se_3 the decay times are much slower—milliseconds, compared with microseconds in As_2Te_3.

(b) At room temperature there seems to be a region of non-photoconductive absorption in As_2Se_3 but not in As_2Te_3.

(c) In As_2Te_3 the dominant recombination transitions are band–localised while in As_2Se_3 they *may be* localised–localised.

References

1. Cohen, M. H., Fritzsche, H. and Ovshinsky, S. R., *Phys. Rev. Letters* **22**, 1065 (1969).
2. Fagen, E. A. and Fritzsche, H., *J. Non-Cryst. Solids* **2**, 180 (1970). *ibid*, **4**, 480 (1970).
3. Weiser, K., Fischer, R. and Brodsky, M. H., Proceedings of the Tenth International Conference on the Physics of Semiconductors, Cambridge, Massachusetts, 1970, U.S. Atomic Energy Commission, Oak Ridge, Tennessee, 667 (1970).
4. Arnoldussen, T. C., Bube, R. H., Fagen, E. A. and Holmberg, S., *J. Appl. Phys.* **43**, 1798 (1972).
5. Howard, W. E. and Tsu, R., *Phys. Rev.* **B1**, 4709 (1970).
6. Mott, N. F. and Davis E. A., "Electronic processes in Non-crystalline Materials." p. 229 Oxford University Press, 1971.
7. Simmons, J. G. and Taylor, G. W., *J. Non-Cryst. Solids* **8-10**, 947 (1972).
8. Marshall, J. M. and Owen, A. E., *Phil. Mag.* **34**, 1281 (1971).
9. Davis, E. A. and Mott, N. F., *Phil. Mag.* **22**, 910 (1970).
10. Mott, N. F. and Davis, E. A., "Electronic Processes in Non-crystalline Materials." p. 45 Oxford University Press, 1971.
11. Marshall, J. M. and Owen, A. E., *Phys. Stat. Sol.* (*a*) **12**, 181 (1972).
12. Grunwald, H. P. and Blakney, R. M. *Phys. Rev.* **165**, 1006 (1968).
13. Edmond, J. T., *Br. J. Appl. Phys.* **17**, 979 (1966).
14. Owen, A. E. and Robertson, J. M., *J. Non-Cryst. Solids* **2**, 40 (1970).
15. Shockley, W. and Read, W. T., *Phys. Rev.* **87**, 835 (1952).
16. Rose, A. *Phys. Rev.* **97**, 322 (1955).
17. Blakemore, J. S., "Semiconductor Statistics." Pergamon Press, Oxford, 1962.
18. Dobrego, V. P. and Ryvkin, S. M., *Sov. Phys. Solid State* **6**, 928 (1964).
19. Stern, F., *Phys. Rev.* **83**, 2636 (1971).
20. Rose, A., "Concepts in Photoconductivity and Allied Problems." p. 26, Wiley, New York, 1963.

21. Bube, R. H., "Photoconductivity of Solids." p. 64, Wiley, New York, 1960.
22. Ryvkin, S. M., "Photoelectric Effects in Semiconductors." p. 129. Consultants Bureau, New York, 1964.
23. Davis, E. A. and Mott, N. F., *Phil. Mag.* **22**, 914 (1970).
24. Tauc, J., in "Optical Properties of Solids." (ed. F. Abeles), North-Holland, 1969.
25. Weiser, K. and Brodsky, M. H., *Phys. Rev.* **B1**, 791 (1970).
26. Croitoru, N., Vescan, L., Popescu, C. and Lazarescu, M., *J. Non-Cryst. Solids* **4**, 493 (1970).
27. Kornfel'd, M. I. and Sochova, L. S., *Fiz. Tver. Tela.* **1**, 1370 (1959).
28. Main, C. and Owen, A. E., *Phys. Stat. Sol.* (*a*) **1**, 297 (1970).
29 Kolomiets, B. T., Lebedev, E. A. and Tsinman, E. A., *Sov. Phys. Semiconductors* **5**, (1971).
30. Van Vliet, K. M. and Fasset, J. R., in "Fluctuation Phenomena in Solids." (ed. R. E. Burgess), Academic Press, 1965.
31. Van der Ziel, A., "Fluctuation Phenomena in Semiconductors." Butterworths, London, 1959.
32. Burgess, R. E., *Physica* **20**, 1007 (1954).
33. Van Vliet, K. M. and Blok, J., *Physica* **22**, 231 (1956).
34. Van der Ziel, A., "Fluctuation Phenomena in Semiconductors." p. 23, Butterworths, London, 1959.
35. Brophy, J. J., *J. Appl. Phys.* **25**, (1954).
36. Lax, M., *J. Phys. Chem. Solids* **8**, 66 (1959).
37. Edmond, J. T., *Br. J. Appl. Phys.* **17**, 979 (1966).
38. Scharfe, M. E., *Phys. Rev.* **B2**, 5025 (1970).
39. Kolomiets, B. T., Proc. 9th Internat. Conf. on the Physics of Semiconductors, Moscow, Vol. 2. Acad. Sci. USSR (Leningrad: "Nauka").
40. Davis, E. A. and Knights, J., to be published.
41. Hartke, J. L. and Regensburger, P. J., *Phys. Rev.* **139**, A970 (1965).
42. Marshall, J. M., Main, C. and Owen, A. E., *J. Non-Cryst. Solids* 8-10, 760 (1972).

phys. stat. sol. (a) 25, 419 (1974)

Subject classification: 2 and 14.3; 22.1.3

Department of Electrical Engineering, University of Edinburgh

The Electron Drift Mobility in Arsenic–Selenium Glasses

By

J. M. MARSHALL, F. D. FISHER, and A. E. OWEN

The drift mobility of electron carriers in vitreous selenium and in arsenic–selenium glasses containing up to 8% As, has been measured over a range of temperature and electric field. The low-field data for selenium itself are in agreement with those in the literature, whilst at higher fields the mobility is found to increase in a manner similar to that observed for hole carriers in selenium, and for the mobility and conductivity in a number of other disordered semiconductors. The electron mobility in arsenic-containing glasses is also field-dependent, whilst the magnitude of the mobility decreases with increasing arsenic concentration. However, the effect of arsenic addition is found to be smaller than has been reported in the case of evaporated amorphous films. A model is advanced to account for the behaviour in terms of current theories of the disordered state.

Es wurde die Elektronendriftbeweglichkeit von glasartigem Selen und von Arsen–Selen-Gläsern, die bis zu 8% As enthielten, in Abhängigkeit von der Temperatur und der elektrischen Feldstärke gemessen. Bei niedrigen Feldern stimmen die Daten für Selen mit denen in der Literatur überein, während bei höheren Feldern gefunden wird, daß die Beweglichkeit steigt, wie es schon für Löcher in Selen beobachet worden ist, und für die Beweglichkeit und Leitfähigkeit in mehreren anderen gestörten Halbleitern. Die Elektronendriftbeweglichkeit von arsenhaltigen Gläsern ist ebenfalls feldabhängig, während der Beweglichkeit mit steigender Arsenkonzentration kleiner wird. Es wird gefunden, daß die Wirkung von Arsen kleiner ist als für aufgedampfte amorphe Schichten berichtet worden ist. Es wird ein Modell vorgeschlagen, um das Verhalten mit üblichen Theorien des Fehlordnungszustandes zu erklären.

1. Introduction

Arsenic–selenium glasses are particularly suitable for the study of transport properties of disordered solids. Not only are these materials of relatively simple composition, but considerable information is available on their physical properties in view of commercial applications in electrophotography and other fields. Moreover, measurements of carrier drift mobility by transit time techniques are feasible over a wide range of compositions within the binary system, and in some cases both electron and hole mobility can be determined in the same glass. In the present paper, the variation of electron drift mobility with composition is examined over the range 0 to 8% As, and the dependence of mobility on temperature and applied electric field is detailed.

The literature contains a number of reports of transport measurements in As–Se glasses. The hole mobility of amorphous selenium, first measured by Spear [1], has subsequently been re-examined by several groups [2 to 7]. It is established that the room temperature mobility is close to 2×10^{-1} cm^2 V^{-1} s^{-1}, with the value decreasing with decreasing temperature. Below 250 °K, the hole mobility possesses an activation energy of 0.25 to 0.28 eV, but at higher temperatures a saturation occurs towards a value of 3×10^{-1} cm^2 V^{-1} s^{-1} [3, 7]. The hole drift mobility increases with applied electric field according to the

relationship

$$\mu_d(\boldsymbol{E}) = \mu_d(0) \exp\left[e\, a(T) \frac{\boldsymbol{E}}{kT}\right], \quad (1)$$

where $\mu_d(\boldsymbol{E})$ and $\mu_d(0)$ are respectively the mobilities at field $\boldsymbol{E}$ and at zero field, and $a(T)$ is a temperature-dependent parameter with dimensions of length and with magnitude in the range 0 to 50 Å. A similar behaviour has been detected in mobility and conductivity measurements on a number of other disordered chalcogenides and similar materials [6 to 8].

The electron drift mobility of amorphous selenium has also been studied [2 to 5, 9], having a room temperature magnitude of 7×10^{-3} cm^2 V^{-1} s^{-1} and an activation energy of about 0.33 eV below 300 °K. At higher temperatures, the mobility again saturates, although possibly not for the same reason as in the case of hole carriers [3].

The addition of arsenic to amorphous selenium has been examined several times in an exploratory manner, with the results summarised in Table 1. Increasing concentration progressively reduces the electron mobility in magnitude, but has been suggested to leave the activation energy unchanged [4, 5]. However, measurements of the latter parameter have been confined to glasses with 2% As or less. Small concentrations of arsenic drastically reduce the hole lifetime, preventing transit time measurements of mobility for concentrations greater than 2% [5], but at lower concentrations the magnitude of the hole mobility appears insensitive to the impurity addition. The form of the hole response pulse has been examined by Schottmiller et al. [5] in alloys containing higher arsenic concentrations. A complex behaviour, apparently compounded of the individual response pulses of amorphous Se and As_2Se_3, is observed.

Table 1

Effect of arsenic concentration on the transport properties of As–Se alloys

comp. (% As)	μ_{el} (300 °K) (cm^2 V^{-1} s^{-1})	ε_{el} (eV)	electron lifetime (μs)	μ_{hole} (300 °K) (cm^2 V^{-1} s^{-1})	hole lifetime (μs)	source of data
0.00	8×10^{-3}	0.285	25	1.7×10^{-1}	0.15	[2]
0.5	2.5 to 8 $\times 10^{-3}$	0.285	—	—	—	
2.0	9×10^{-4}	0.285	—	—	—	
0.00	6.5×10^{-3}	0.28	10	1.2×10^{-1}	0.1	[4]
0.5	3×10^{-3}	0.28	10	—	—	
2	5×10^{-4}	0.28	35	—	—	
6	5×10^{-5}	—	—	—	—	
0.00	6×10^{-3}	0.33	50	1.4×10^{-1}	10 to 50	[5]
0.5	2.6×10^{-3}	0.33	40	1.4×10^{-1}	<0.3	
2	7.8×10^{-4}	0.33	200	—	<0.3	
3	2×10^{-4}	—	750	—	—	
6.6	5.4×10^{-5}	—	2000	—	—	
9	1×10^{-5}	—	3000	—	—	

2. Results and Discussion

The present examination has attempted a detailed investigation of the electron drift mobility in As–Se glasses containing less than 10% As; data being obtained over a range of temperatures and applied electric fields. Most specimens have been prepared by the quenching of molten material between mica plates under compression, thus yielding thin layers of truly vitreous material and of reliably known composition. In contrast, thermal evaporation techniques often result in compositional variations and may produce films which are structurally different from the bulk vitreous material. However, measurements have also been preformed using evaporated films of pure selenium to allow a direct comparison of transport properties with those of glassy specimens. The carrier drift mobility was determined by transit time measurements as previously outlined [7], using films from 5 to 50 μm in thickness equipped with evaporated gold electrodes.

The temperature dependence of the low-field electron drift mobility of pure selenium is shown in Fig. 1, and is in very good agreement with published data on evaporated films. Below 300 °K, the activation energy is (0.33 ± 0.02) eV. As illustrated in Fig. 2, the mobility increases with electric field in a manner consistent with (1). The mechanism causing this behaviour has not yet been established [8], but it is significant that such a field dependence has been observed in the conductivity and/or mobility of every disordered chalcogenide or related material so far investigated. Moreover, the data presented here for the electron mobility yield values of the parameter $a(T)$ which are identical within experimental error with those determined from the field dependence of the hole drift mobility in selenium [7], even though the magnitudes and activation ener-

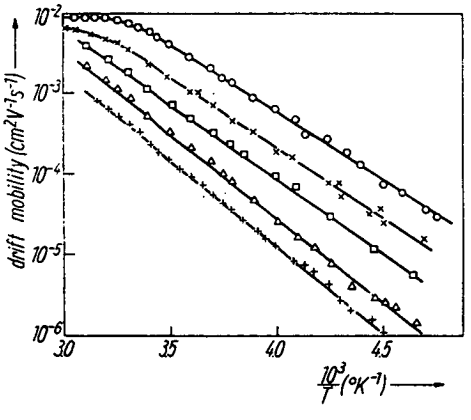

Fig. 1

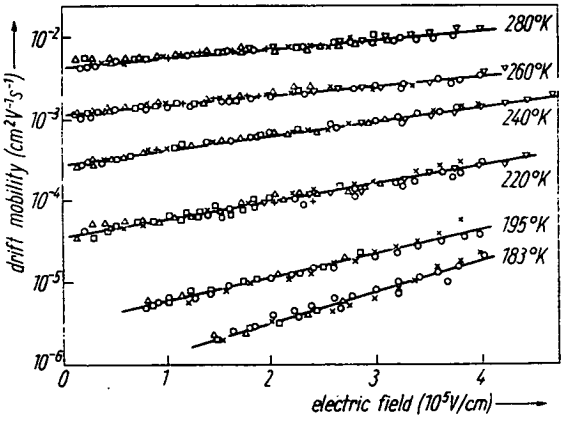

Fig. 2

Fig. 1. Temperature dependence of the electron drift mobility of vitreous selenium and arsenic–selenium alloys at low applied electric fields.
○ Se, $\varepsilon = 0.33$ eV; × As_1Se_{99}, $\varepsilon = 0.35$ eV; □ As_3Se_{97}, $\varepsilon = 0.37$ eV; △ As_5Se_{95}, $\varepsilon = 0.42$ eV, + As_8Se_{92}, $\varepsilon = 0.44$ eV

Fig. 2. Electric field dependence of the electron drift mobility of bulk vitreous selenium and of evaporated amorphous films. Vitreous: ○ 25 μm, × 25 μm, ▽ 43 μm, + 95 μm. Evaporated: △ 12 μm, □ 15 μm. (For clarity, the curves at each temperature have been normalized by the use of small ($\lesssim 2$) multiplication factors on the individual sets of mobility data)

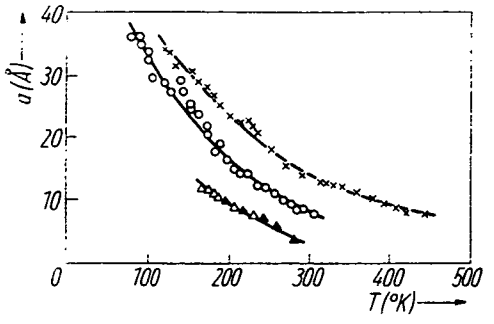

Fig. 3. Variation of the field-dependence parameter, $a(T)$, with temperature in three semiconducting glasses.
▲ electron mobility, Se; △ hole mobility, Se; ○ conductivity, $Ge_{15}Te_{85}$; × conductivity, $As_{30}Te_{48}Si_{12}Ge_{10}$

gies of the two mobilities differ appreciably. Such a correspondence of magnitude and widespread occurence of the field-dependent behaviour strongly suggest an origin associated with some general and basic feature of transport in disordered systems, rather (for example) than with field-dependent factors in the trapping and release of carriers in the particular forms of localising potential well dominating conduction in any individual case [8].

Fig. 3 shows the temperature dependence of the parameter $a(T)$ in a number of cases, illustrating both the general similarity of behaviour and the close agreement for the two carrier mobilities in selenium. Fig. 2 and 3 also contain data for evaporated selenium films, showing that the effect of changes in the degree of disorder is small in the case of pure selenium. However, differences are identifiable between the data for arsenic-doped glasses (also contained in Fig. 1) and their evaporated counterparts. Whilst the effect of arsenic addition is to reduce the mobility as previously reported, it can be seen from Table 1 that the magnitude of this reduction is somewhat larger in evaporated specimens than in the vitreous films studied here. This behaviour may in part be due to compositional changes during evaporation, but these should not be a major factor in the flash-evaporated layers of Schottmiller et al. [5]. It therefore appears that the differences must be due to structural effects resulting from varying degrees of disruption of the selenium structure by added arsenic in the two cases. One might expect the arsenic to be assimilated less destructively in a material which has passed through the liquid phase than in a film prepared by direct evaporation.

A further characteristic not previously reported is that the data in Fig. 1 show an increase in activation energy with arsenic concentration. However, it is likely that such an increase does in fact occur in evaporated films but has not been detected in the limited measurements made in materials of low (up to 2%) arsenic concentration.

There are a number of possible mechanisms which give rise to an activated carrier drift mobility, and some of the more commonly proposed of these are illustrated schematically in Fig. 4. In cases 4a and 4b, localised trapping centres occur below the extended band states, and carrier motion in the latter is periodically interrupted by trapping and subsequent re-release from the localised levels. Provided the carriers are able to attain a state of eguilibrium between the extended states and the trapping centres prior to other events such as recombination, trapping in deeper states, or carrier extraction at an electrode, then a trap-limited drift mobility can be defined. It is this mobility rather than the free carrier value which will be measured in 'time of flight' experiments such as those performed in the present study.

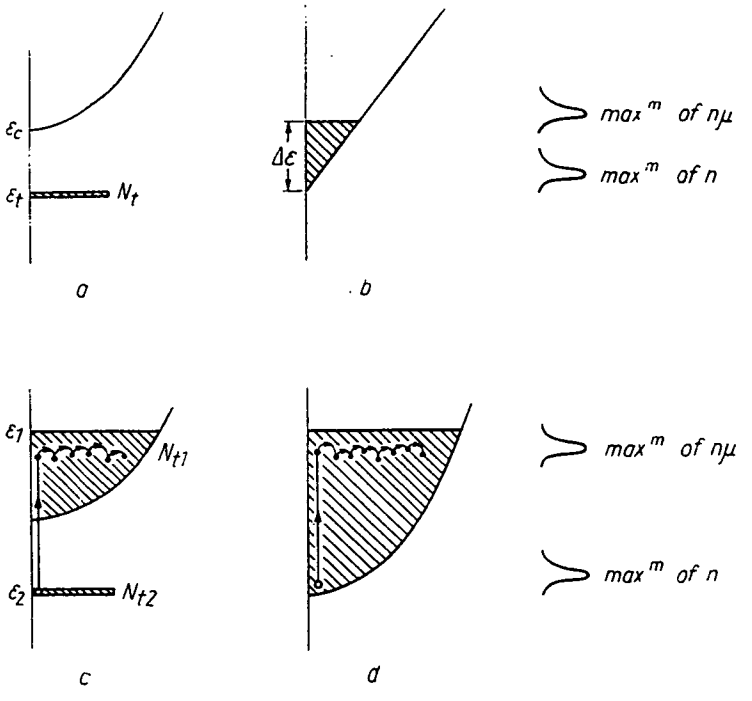

Fig. 4. Possible band structures and transport mechanisms in ordered and disordered semiconductors

For case 4a, the magnitude of the drift mobility will be [10]

$$\mu_d = \mu_0 \frac{N_c}{N_t} \exp\left[\frac{-(\varepsilon_c - \varepsilon_t)}{kT}\right], \tag{2}$$

where μ_0 is the microscopic mobility, N_c is the effective density of states in the conduction band, and N_t is the density of trapping centres.

In case 4b, a similar evaluation of the total time of flight including time spent in localised centres leads to a drift mobility of

$$\mu_d = \mu_0' \frac{\Delta\varepsilon}{kT} \exp\left(\frac{-\Delta\varepsilon}{kT}\right) \tag{3}$$

for a linear 'tail of states'. Likewise, the expression for a parabolic [i.e. $N(\varepsilon) \sim \sim \varepsilon^{1/2}$] state distribution is

$$\mu_d \approx \mu_0' \left(\frac{\Delta\varepsilon}{kT}\right)^{1/2} \exp\left(\frac{-\Delta\varepsilon}{kT}\right), \tag{4}$$

where $\Delta\varepsilon$ is the tail of states depth and μ_0' the extended state mobility at the 'mobility edge' dividing the localised and extended states. For other shapes of tail, the trap-limited mobility is still well defined provided there exists a sufficiently sharp peak in the density of *occupied* traps at some depth $\Delta\varepsilon$. Moreover, it is a widely accepted feature of the band structure of non-crystalline solids that the presence of disorder should give rise to some form of localised tail of states at a band edge [11]. It is, of course, also possible and often likely that fairly well defined sets of localised levels will occur at various energies within the band gap in addition to these tails. Provided the local order is sufficiently

similar, such sets of traps should be energetically close to the possible defect states of the corresponding crystalline phase, but would be expected to become somewhat 'smeared out' in energy due to the effects of local disorder.

Upon applying (2) to the experimental data of Fig. 1, it is found that the reduction in drift mobility due to arsenic addition is totally accounted for by the increased activation energy, whilst the pre-exponential factor is constant (within a factor of about two which is attributable to experimental error). The average value is $\approx 2\times10^{3}\ \mathrm{cm^2\,V^{-1}\,s^{-1}}$, so that taking[1] $\mu_0 \approx 1\ \mathrm{cm^2\,V^{-1}\,s^{-1}}$ and $N_c \approx \approx 5\times10^{19}\ \mathrm{cm^{-3}}$, the corresponding value of N_t is approximately $10^{16}\ \mathrm{cm^{-3}}$ which does not seem an unreasonable figure.

Whilst the pre-exponential factors of (3) and (4) are also approximately constant with composition, these models are unsatisfactory in that the required values of μ_0' are respectively 200 and $10^3\ \mathrm{cm^2\,V^{-1}\,s^{-1}}$. Such magnitudes are not expected for carriers in disordered solids and are only found in practice in a few well-ordered crystalline semiconductors. In non-crystalline materials, as the energy decreases towards that of the mobility edge, the free carrier mobility is expected to approach the lower limit for conventional extended state transport ($\approx 5\ \mathrm{cm^2\,V^{-1}\,s^{-1}}$ [11]) and subsequently to fall to still lower values (0.1 to $1\ \mathrm{cm^2\,V^{-1}\,s^{-1}}$) in a region for which carrier motion is percolative in nature [12]. Lower values of mobility are not expected within the extended states, but are possible for hopping transport below the mobility edge, as examined below. On the above grounds, the models leading to equations (3) and (4) appear unacceptable, as do similar mechanisms with differing shapes of band tail.

Carrier transport by thermally-activated hopping between localised levels in a tail of states (or elsewhere) should lead to a mobility [11]

$$\mu_{\mathrm{hop}} \approx \frac{1}{6}\nu_{\mathrm{ph}}\frac{e\,R^2}{kT}\exp\left(\frac{-W}{kT}\right), \tag{5}$$

where R is a hopping length, W the appropriate activation energy, and ν_{ph} a 'phonon' frequency determining the rate of hopping attempts. However, whilst the pre-exponential factor of (5) is expected to be of order $10^{-2}\mathrm{cm^2\,V^{-1}\,s^{-1}}$ or less [12], the experimental value is close to $10^3\ \mathrm{cm^2\,V^{-1}\,s^{-1}}$, so that this type of mechanism does not seem applicable in the above form.

The hybrid 'trap-limited hopping' models of cases 4c and 4d may overcome this objection to some degree. Here, conduction occurs predominantly at the energy for which the μn product is a maximum (where $n = N_t(\varepsilon)\,f(\varepsilon)$ is the density of *occupied* centres at a particular energy). However, most of the carriers will be located close to the lower energy for which the density n is maximised. Thus, in case 4c, the drift mobility may be obtained by combining (2) and (5) to give

$$\mu_{\mathrm{d}} \sim \frac{1}{6}\nu_{\mathrm{ph}}\frac{e\,R^2}{kT}\frac{N_{t1}}{N_{t2}}\exp\left[\frac{-(\varepsilon_1-\varepsilon_2+W)}{kT}\right] \tag{6}$$

and the pre-exponential factor may be larger than in (5) provided $N_{t1} > N_{t2}$. A corresponding expression for the mobility in case 4d could be developed by employing expressions such as (3) and (4) in place of (2).

[1]) This value of μ_0 is considered a reasonable estimate for disordered semiconductors as is explained later in the text.

Extension of such models requires a knowledge of ε_1 and ε_2 for a particular trap distribution. The latter is usually located close to the bottom of any set of traps unless $N(\varepsilon)$ is a very rapidly varying function. For example, with a localised state density varying as $(\varepsilon - \varepsilon_0)^z$ where ε_0 is the foot of the tail, it is simple to show that $\varepsilon_2 = \varepsilon_0 + zkT$. However, in evaluating ε_1, it is necessary to know the energy variation of the hopping mobility and thus of suitably averaged value of R and W. Reliable estimates of these parameters are not yet available, although it is hoped that some progress will be possible in the near future. For the present purposes, it may be sufficient to note that the measured values of electron drift mobility in selenium approach 10^{-2} cm^2 V^{-1} s^{-1}, which is close to the upper limit for hopping transport even without including the effect of deeper trapping. Thus, such conduction, if it does in fact predominate at all, must take place in centres very close to the mobility edge. Moreover, the identical field dependences suggest a strong association between the mechanisms of electron and hole transport in selenium, and measured hole mobilities exceed 10^{-1} cm^2 V^{-1} s^{-2} at room temperature. The evidence therefore strongly implies that the carrier motion occurs in the vicinity of (and probably just above) the mobility edge. In such cases, the limiting of average carrier mobility by trapping in the tails of states should lead to expressions such as (3) and (4) as previously noted.

3. Interpretation and Conclusions

Following the above arguments, any model of electron transport in Se and As–Se glasses must explain both the magnitude and activation energy of the drift mobility, and account for the progressive increase in the latter parameter with increasing arsenic concentration. A model which satisfies these requirements is shown in Fig. 5.

In the case of vitreous selenium itself, a set of traps is assumed to occur over a fairly small energy range centred 0.33 eV below the mobility edge of the conduction band. At the band edge, a further tail of localised states is present due to disorder in the material. Carrier transport occurs close to the mobility edge either by hopping in very shallow localised states or by a percolation process just inside the extended states. Depending upon the magnitude of this mobility (0.1 to 10 cm^2 V^{-1} s^{-1}) the density of the deeper lying traps is expected from (2)

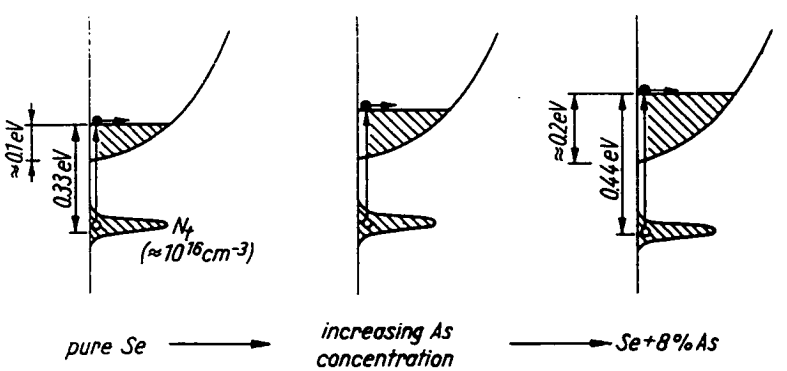

Fig. 5. Model proposed to explain the experimental variations in electron transport parameters produced by the addition of arsenic to vitreous selenium

to be in the range 10^{15} to 10^{17} cm^{-3}. These latter states are envisaged as an intrinsic feature of vitreous selenium, and are not expected to be significantly modified by addition of arsenic in the concentrations of interest here. However, by increasing the disorder in the glass, the arsenic addition serves to raise the energy of the mobility edge within the conduction band. In practice, of course, it would be expected that other modifications would also take place due to arsenic addition. For example, additional sets of localised states might emerge, and the shape of the band tail could change. Whilst the latter possibility should not significantly affect the treatment given below, it should be noted that the validity of the proposed model requires that any additional sets of traps produced by arsenic addition are created in sufficiently low densities and/or at such energies that their effect upon the electron drift mobility is small. On the other hand, it should also be noted that a similar requirement is likely to be a feature of any alternative model advanced to explain the experimental behaviour.

A further criterion of the model proposed is that the pre-exponential terms in the expression for the mobility should remain sensibly constant over the range of compositions studied. If the free carrier transport occurs above the mobility edge, then the relevant parameters are μ_0, N_c, and N_t as in (2), except that the first two of these are now the appropriate values at the mobility edge rather than at the band edge. Below, each of the three factors will be examined in turn.

N_c: In evaluating this term, it is necessary to assume both the shape of band tail and the depth of the tail in pure selenium. However, the conclusions reached do not appear to be critically sensitive to the choice of these elements. For analytical purposes here, the tail depth is taken as 0.1 eV [11] (expressed as $4kT$ below), and the density function as the conventional expression for crystalline semiconductors [13]

$$N(\varepsilon) = \frac{4\pi}{h^3}(2m_e)^{3/2}(\varepsilon - \varepsilon_0)^{1/2}\,\mathrm{d}\varepsilon\,. \tag{7}$$

To a reasonable approximation, attention may be restricted to the region within kT above the mobility edge, giving

$$N_c \sim \frac{4\pi}{h^3}(2m_e)^{3/2}\int_{4kT}^{5kT}\varepsilon^{1/2}\,\mathrm{d}\varepsilon \approx 3.25\,A\,, \tag{8}$$

where $A = (8\pi/3)\,(2m_e kT/h^2)^{3/2}$. Similarly, taking a tail depth of 0.2 eV ($\approx 8\,kT$) for the glass containing 8% arsenic, as required by the measured increase of 0.1 eV in the activation energy, then $N_c \approx 4.60A$. It therefore appears that no significant increase in N_c is to be expected over the experimental range.

N_t: The present model rests on the assumption that the density of the deeper set of trapping levels remains constant at about 10^{16} cm^{-3}, but it is necessary to examine the effect of the additional localised centres introduced at the band edge upon the mobility. From (7), this additional density should be about 10^{20} cm^{-3} for a 0.1 eV change in mobility edge energy. However, the number of electrons *actually localised* in these shallow traps compared to those contained in the deeper centres is

$$\frac{10^{20}}{10^{16}}\exp\left(\frac{-0.35}{kT}\right) \approx 10^{-2}$$

assuming an average separation of 0.35 eV between the two sets of states. Again, this is a negligible perturbation upon the trap-limited drift mobility.

μ_0: The behaviour of the free carrier mobility in disordered solids is difficult to examine quantitatively. However, current theories [11, 12] suggest that mobility values close to the mobility edge are determined by fundamental considerations of carrier motion in non-crystalline systems (as outlined above) rather than by the particular position of the mobility edge within the band. The situation is only vaguely understood, and it seems impossible at the moment to do other than assume an approximately constant mobility value at the mobility edge.

The alternative situation to the one examined above is that for which the 'free' carrier motion is by hopping just below the mobility edge. Here, μ_0 must be replaced by a hopping mobility essentially as in (6), but once more the present models of conduction suggest that this is primarily a function of energy relative to the mobility edge rather than of the position of the edge within the band. Once again, the best estimate seems to be that of a constant value in the present context. The arguments for invariant values of the trap densities N_{t1} and N_{t2} of (6) (representing the densities just below the mobility edge and in the deeper lying gap states respectively in this case) run parallel to those outlined above for N_c and N_t.

The model illustrated in Fig. 5 seems, from the analysis presented, to offer a consistent explanation of the observed transport properties, both in accounting for the behaviour of the mobility in selenium itself, and in terms of the *progressive* increase in activation energy produced by arsenic addition. Even so, corroborative evidence from as wide as possible a range of other measurements is clearly required to establish the true band structure. Some support for the above model may be provided by recent data on the optical absorption of arsenic–selenium glasses [14]. Over the range 0 to 10% As, a steady decrease is found in the parameter C in the expression

$$\alpha h\nu = C(h\nu - \varepsilon_g)^2 \tag{9}$$

which describes the parabolic region of the absorption edge. According to the interpretation proposed by Mott and Davis [11], this parameter should depend inversely upon the tail of states width $\Delta\varepsilon$, so that the experimental behaviour suggests a steady increase in this width with increasing arsenic concentration. Unfortunately, the Mott-Davis model is not the only possible interpretation of the optical data, nor can it be expected to give a quantitative expression for the width $\Delta\varepsilon$ except under ideal circumstances [14]. Even so, the absorption data seem to provide limited qualitative support for the model of Fig. 5. It is also interesting to note that recent luminescence measurements on disordered selenium appear consistent with the presence of a set of localised states situated 0.33 eV below the conduction band mobility edge [15].

The measurements by Spear [16] of the drift mobility of electrons in monoclinic crystalline selenium are also of particular relevance to the present study. The carriers are found to have a room temperature mobility of about 2 $cm^2 V^{-1} s^{-1}$ and an activation energy at lower temperatures which appears very similar to that of the disordered material. This may well suggest that the centres controlling the mobility in the latter case are closely related to those produced by defects in the monoclinic lattice. It is well established that vitreous selenium contains large numbers of the Se_8 puckered rings which are the structural units of the

monoclinic crystal, and that many properties of the two modifications are similar [5, 17]. Moreover, Schottmiller et al. [5] have suggested that the electron drift mobility in disordered selenium is directly associated with the presence of Se_8 rings, and that the effect of arsenic addition is to reduce the mobility by destroying the ring structure. However, as noted by Mort [17], such a behaviour is not consistent with a trap-limited drift mobility in that destruction of Se_8 rings and their associated trapping centres would be expected to *increase* the trap-limited drift mobility in the absence of other intervening changes. Nor does such a model appear reconcilable with the present observations of constant pre-exponential factor and steadily increasing activation energy. The alternative transport mechanism of hopping between Se_8 sites is more acceptable in principle, since a reduction of localised state density should involve a decreasing overlap integral between adjacent centres and thus a reduced rate of hopping events. However, the examination presented above indicates that neither the magnitude nor the detailed behaviour of the drift mobility are consistent with a hopping mechanism.

Whilst it is evident that both the Se_8 ring density and the electron drift mobility decrease steadily with increasing arsenic concentration [17], the experimental data do not suggest this to be a simple causal relationship. Further information upon the origin of the centres controlling the drift mobility is clearly most desirable, and it is also considered that studies on the generation of localised centres in monoclinic selenium (possibly including the effects of arsenic doping) would be of great value in clarifying the situation.

References

[1] W. E. SPEAR, Proc. Phys. Soc. B **76**, 826 (1960).
[2] J. L. HARTKE, Phys. Rev. **125**, 1177 (1962).
[3] H. P. GRUNWALD and R. M. BLAKNEY, Phys. Rev. **165**, 1006 (1968).
[4] B. T. KOLOMIETS and E. A. LEBEDEV, Soviet Phys. — Solid State **8**, 905 (1966).
[5] J. SCHOTTMILLER, M. TABAK, G. LUCOVSKY, and A. WARD, J. non-crystall. Solids **4**, 80 (1970).
[6] M. D. TABAK, Phys. Rev. B **2**, 2104 (1970).
[7] J. M. MARSHALL and A. E. OWEN, phys. stat. sol. (a) **12**, 181 (1972).
[8] J. M. MARSHALL and G. R. MILLER, Phil. Mag. **27**, 1151; (1973).
[9] W. E. SPEAR, Proc. Phys. Soc. B **70**, 669 (1957).
[10] A. ROSE, RCA Rev. **12**, 362 (1951).
[11] N. F. MOTT and E. A. DAVIS, Electronic Processes in Non-Crystalline Materials, Oxford University Press, 1971.
[12] M. H. COHEN, J. non-crystall. Solids **4**, 391 (1970).
[13] W. SHOCKLEY, Electrons and Holes in Semiconductors, Van Nostrand, 1950.
[14] J. PETURSSON, J. M. MARSHALL, and A. E. OWEN, to be published.
[15] R. A. STREET and I. G. AUSTIN, private communication.
[16] W. E. SPEAR, J. Phys. Chem. Solids **21**, 110 (1961).
[17] J. MORT, Electronic and Structural Properties of Amorphous Semiconductors, Academic Press, New York 1973.

(Received June 5, 1974)

PHILOSOPHICAL MAGAZINE, 1976, VOL. 33, NO. 3, 457–474

Field-effect measurements in disordered $As_{30}Te_{48}Si_{12}Ge_{10}$ and As_2Te_3

By J. M. MARSHALL
Department of Physics, Dundee College of Technology, Scotland

and A. E. OWEN
Department of Electrical Engineering University of Edinburgh, Scotland

[Received 22 August 1975 and in final form 22 January 1976]

ABSTRACT

Field-effect data are presented for radio-frequency sputtered films of disordered $As_{30}Te_{48}Si_{12}Ge_{10}$ and As_2Te_3. The temperature dependence of the measurements is employed in order to determine the energy of the localized states controlling the field-effect response. By this means, it is established that these centres lie approximately 0·13 eV below the bulk Fermi level, and not at the Fermi level as has been assumed in previous analyses of the field effect is disordered chalcogenides.

The experimental characteristics are discussed in terms of a variety of possible surface and bulk conditions, and it is shown that the data for both materials imply a higher density of localized states in the region within about 50 Å from the surface than that previously determined for the bulk. However, the available information does not allow a unique determination of the variation of localized-state distribution with position in the film.

The experimental data and analytical conclusions are discussed in terms of current models for carrier transport in disordered semiconductors.

§ 1. INTRODUCTION

The use of the field effect to investigate the transport properties of crystalline semiconductors is an established technique, but one which may present considerable analytical difficulties (Many, Goldstein and Grover 1965). In the case of disordered semiconductors, which are known to possess a relatively high density of localized electronic states, the problems of interpretation are as severe as, if not more severe than, those experienced with crystalline specimens. Consequently, no general analytical technique has yet been advanced to allow the density and energy distribution of localized states to be determined from field-effect measurements. In addition, the high localized-state densities present in disordered films result in much smaller modulations of field-effect conductance than are usually observed in crystalline materials. The literature contains relatively few reports of field-effect investigations of the non-crystalline state, several of which appear to be of a somewhat superficial nature.

Fritzsche and Ovshinsky (1970) reported an unsuccessful attempt to observe field-effect characteristics in multi-component chalcogenide films, and concluded that the density of localized states must exceed 6×10^{19} $cm^{-3}\,eV^{-1}$. In arriving at this estimate, the localized states concerned were

assumed to lie at the Fermi level, as envisaged in the ' C–F–O ' model of disordered semiconductors advanced by Cohen, Fritzsche and Ovshinsky (1969). No details of experimental technique were included in Fritzsche and Ovshinsky's report.

In a subsequent theoretical analysis, Barbe (1971) showed that successful field-effect measurements should be possible in semiconductors possessing the C–F–O distribution of localized states, provided that the density of surface states did not exceed $10^{14}\,cm^{-2}$. Successful measurements for disordered films of composition in the range $Te_x(Si_{0\cdot24}Ge_{0\cdot20}As_{0\cdot56})_{1-x}$ were reported by Egerton (1971) who offered two alternative interpretations of his data; either that the bulk density of states at the Fermi level was of order 10^{20} $cm^{-3}\,eV^{-1}$, or that approximately 10^{13} cm^{-2} surface states were present in addition to 10^{19} to $10^{20}\,cm^{-3}$ bulk centres. Again, it was assumed in the analysis that the localized states lay at the Fermi level, as predicted by the C–F–O model.

Spear and Le Comber (1972) advanced an analytical technique by which field-effect data could be interpreted in terms of the detailed distribution in energy of the localized states involved, and applied the system to measurements on disordered silicon films. By adopting a zero-temperature approximation to the occupation statistics, it was assumed that the field-effect response was determined by the *complete* filling of localized states which are caused to cross the Fermi level in the surface region, as opposed to the *partial* filling of states elsewhere in the energy gap. The calculated trap densities ranged from 10^{15} to $10^{18}\,cm^{-3}\,eV^{-1}$, depending upon position in the energy gap and upon details of specimen preparation.

Apart from the above investigations, application of the field-effect technique to the study of disordered semiconductors has been limited to occasional determinations of the ' Fermi-level ' density of localized states in various complex chalcogenide alloys, the data being briefly reported, usually as part of a range of measurements of various transport properties. Attempts to apply the field-effect technique to the compositionally simpler chalcogenides such as disordered Se and As_2Se_3 have so far proved unsuccessful (J. M. Marshall, unpublished, Spear 1974 a).

§ 2. Experimental techniques and data

The specimens employed in the present study were prepared by the radio frequency (r.f.) sputtering of chalcogenide source material onto a substrate of insulating glass (Corning 7059), the latter having previously been equipped with coplanar gold electrodes, photolithographically prepared, and separated by a gap of width 25 microns. Following deposition of the chalcogenide semiconductor, a thin blocking film of 7059 glass ($\sim 0\cdot1$ micron) was r.f. sputtered onto its surface, after which a layer of As_2S_3 dielectric was deposited to a thickness of order 10 microns by thermal evaporation. Finally, a gold gate electrode was thermally evaporated over the coplanar gap area, producing the completed assembly shown in fig. 1. The intermediate layer of 7059 glass was incorporated following preliminary investigations, and was found to considerably reduce electrical leakage and to minimize polarization effects caused by charge absorption in the As_2S_3 dielectric. With this specimen

configuration, electric fields of magnitude up to 10^6 V cm^{-1} could be applied across the dielectric, with leakage currents normally less than 10^{-12} Å.

In operation, the changes in specimen current induced by a change in gate voltage were found to partially relax in magnitude. The current approached its final value with a time constant of approximately 30 sec. This behaviour appear to be associated with the states in the dielectric rather than the states in the semiconductor film, and could be appreciably diminished by the use of a blocking layer as mentioned above. A standard measurement technique was adopted in which each individual gate voltage was applied for a period of 2 min prior to the recording of the current across the coplanar cell. The gate voltage was then reduced to zero for 2 min, after which the current was again noted and a new gate voltage applied. The gate voltage was cycled several times through the measurement range in suitable increments and decrements, so as to ensure the consistency of individual readings and the absence of hysteresis effects.

Fig. 1

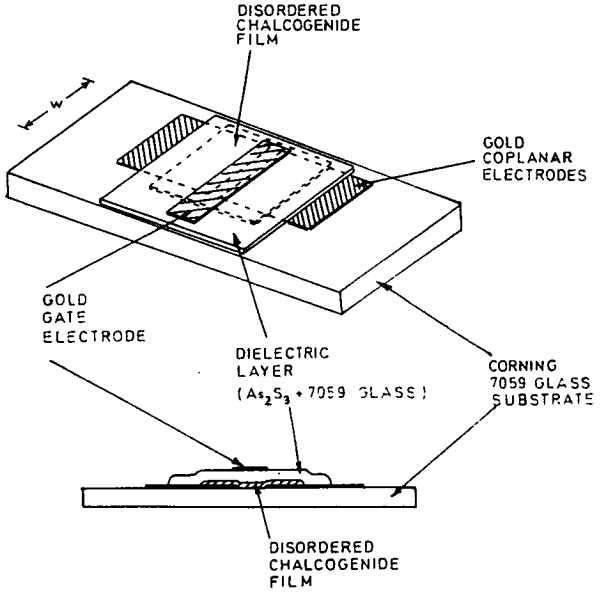

Specimen configuration for the field-effect measurements.

Figure 2 shows typical data for the change in specimen current, ΔI, in disordered $As_{30}Te_{48}Si_{12}Ge_{10}$, caused by the application of a voltage ΔV to the gate electrode. For this specimen, a 50 V change in gate voltage corresponded to an induced excess carrier density of $3{\cdot}5 \times 10^{11}$ cm^{-2} for the semiconductor film. Figure 3 presents typical corresponding data for a film of disordered As_2Te_3.

Throughout the field-effect investigations, the voltage between the coplanar electrodes was kept at 50 V or less, thereby avoiding analytical complications associated with the high-field modifications of transport properties occurring in disordered chalcogenides (Marshall and Miller 1973).

Fig. 2

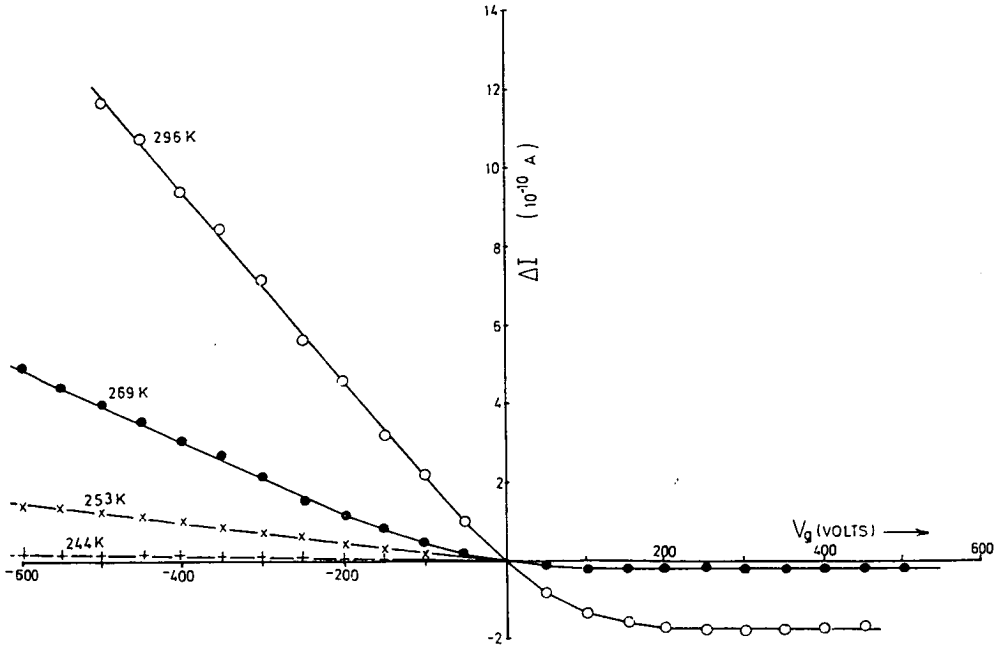

Typical field-effect response curves for a specimen of disordered $As_{30}Te_{48}Si_{12}Ge_{10}$ at various temperatures. ($E = 2 \times 10^4$ V cm^{-1}, $w = 0{\cdot}3$ cm, $\Delta Q/eV_g = 7 \times 10^9$ V^{-1}.)

Fig. 3

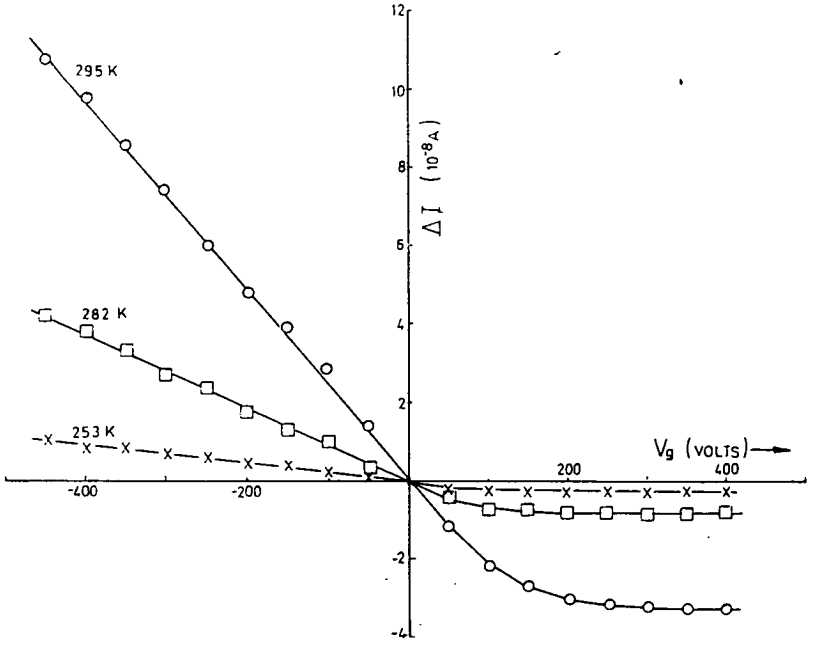

Typical field-effect response curves for a specimen of disordered As_2Te_3 at various temperatures. ($E = 4 \times 10^3$ V cm^{-1}, $w = 0{\cdot}3$ cm. $\Delta Q/eV_g = 5 \times 10^9$ V^{-1}.)

§ 3. General theoretical considerations

As mentioned above, an important limitation of previous analyses of field-effect data for disordered semiconductors lies in the assumption that the localized states controlling the behaviour are necessarily situated at the Fermi level. This postulate allows the adoption of zero-temperature occupation statistics for the localized states, thereby appreciably simplifying the

Fig. 4

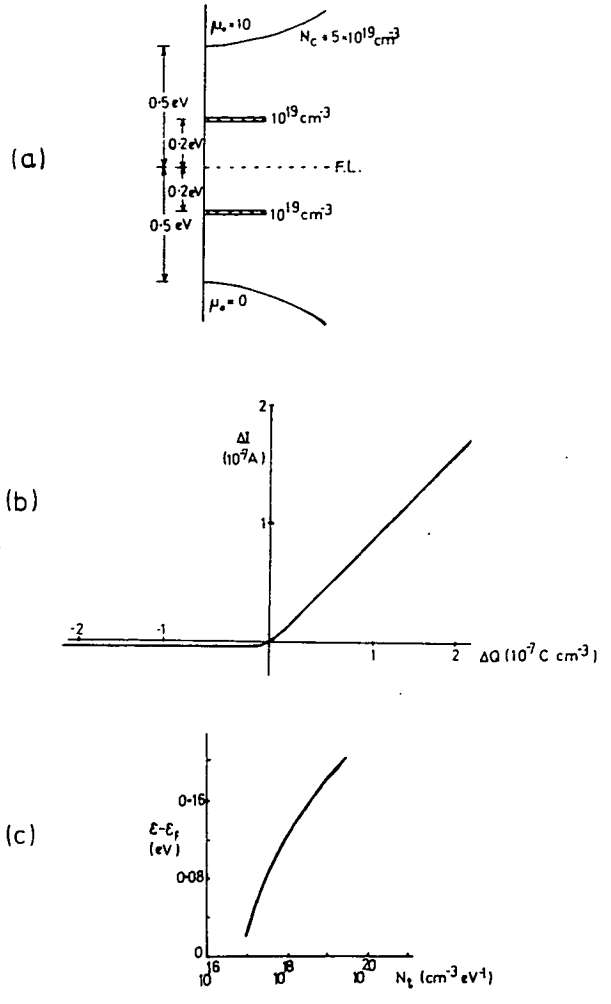

Field-effect response curve (*b*) for a simple distribution of localized states (*a*), together with the results (*c*) of an analysis of the response by the technique of Spear and Le Comber (1972). (Assumed parameters, $E = 10^4$ V cm^{-1}, $w = 1$ cm.)

analytical treatment, but can lead to rather misleading conclusions in cases where the assumption is unjustified. For example, fig. 4 (*a*) shows a simple distribution of localized states, which would result in a field effect characteristic of the type shown in fig. 4 (*b*) (Many *et al.* 1965). Analysis of this response by means of the technique evolved by Spear and Le Comber (1972)

would yield the localized state distribution shown in fig. 4 (*c*). This is clearly different from the true situation, and might be regarded as supporting the C–F–O model of localized state distribution rather than the discrete distribution chosen. It should, however, be noted that the degree of dispersion of the traps in fig. 4 (*c*) is exaggerated by the logarithmic scale of presentation. Moreover, if the analysis of the model of fig. 4 (*a*) was extended to higher voltages, degenerate surface conditions would ensue, and the response curve of fig. 4 (*b*) would then rise more steeply than in the non-degenerate regime shown. Application of the Spear–Le Comber analysis over this regime of high gate voltage would yield a falling calculated density of states, the overall effect being to produce a maximum close to the true trap energy of 0·2 eV. In disordered silicon, where the localized state densities are *relatively* low, it is feasible to achieve large surface energy displacements and to identify various peaks in localized state distribution, as in the work of Spear and his colleagues. However, in disordered chalcogenides, the localized state densities are higher, and it is not possible to attain sufficient gate voltages to displace the trap energy through the Fermi level at the surface. The response curves are similar to that of fig. 4 (*b*), and the resulting analyses of type 4 (*c*) are clearly ambiguous in their identification of trap locations and densities.

In this situation, it is most desirable to have some independent check upon the location in energy of the trapping centres which dominate the field-effect response. By taking the measurements over a range of temperature, rather than at room temperature along (as has previously been the case), such information may be obtained, as will be demonstrated below.

For data in the accumulation regime of the field-effect response, a convenient concept is that of the field-effect mobility, μ_f, for the induced excess carriers. The increase in coplanar specimen current, ΔI, produced by an induced surface charge ΔQ is given by

$$\Delta I = \Delta Q \mu_f E w, \tag{1}$$

where E is the electric field between the coplanar electrodes and w is the lateral dimension of the specimen assembly (fig. 1). Figures 5 and 6 illustrate the temperature dependence of the field-effect mobility for a number of specimens of $As_{30}Te_{48}Si_{12}Ge_{10}$ and of As_2Te_3, respectively, as calculated by interpretation of data in the accumulation regime in terms of eqn. (1).

It seems reasonable to assume, following the discussion of Marshall and Owen (1975), that transport in the materials studied in the present investigation takes place via carrier motion in the extended states beyond the ' mobility edge ', so that the field-effect mobility will be related to the free-carrier mobility, μ_0, by the ratio of free to total (free + trapped) excess induced charge ;

$$\mu_f = \mu_0 \Delta Q_{\text{free}} / \Delta Q, \tag{2 a}$$

$$\simeq \mu_0 \Delta Q_{\text{free}} / \Delta Q_{\text{trapped}}, \tag{2 b}$$

where the approximation of eqn. (2 *b*) is valid when ΔQ_{free} is much smaller than $\Delta Q_{\text{trapped}}$, as in the present case for which nearly all the induced excess carriers are localized in the trapping centres. In the case of a single discrete set of *shallow* traps of density N_t cm^{-3}, situated at an energy ϵ_t from the

extended states, the field-effect mobility will be identical to the trap-limited carrier-drift mobility, μ_d, given by Rose's (1951) expression, i.e.

$$\mu_f = \mu_d = \mu_0 \frac{N_v}{N_t} kT \exp(-\epsilon_t/kT), \tag{3}$$

where N_v is the effective density of extended states ($cm^{-3}\,eV^{-1}$). For continuous distributions of *shallow* localized states (e.g. 'tails' of states at the band edges), an essentially similar expression often applies.

Fig. 5

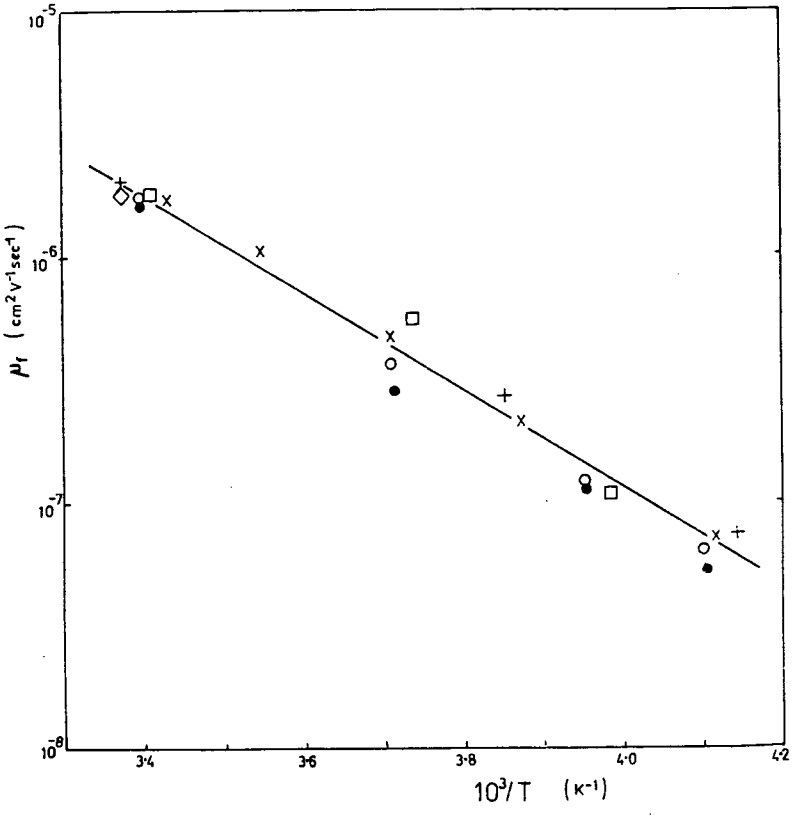

Temperature dependence of the field-effect mobility of disordered $As_{30}Te_{48}Si_{12}Ge_{10}$. The measurement sets are normalized with respect to the average room-temperature mobility value (2×10^{-6} $cm^2\,V^{-1}\,sec^{-1}$). ○—specimen 1, data at $V_g = -500$ V (×1·4); ●—specimen 1, data at $V_g = -100$ V (×1·4); □—specimen 2 (×0·4); +—specimen 3 (×0·5); ×—specimen 4 (×1·5); ◇—specimen 5 (×1·0).

Alternatively, where an appreciable density of localized states persists across the energy pseudogap as in the C–F–O model, almost all of the trapped excess charge will be localized in centres close to the Fermi level. A field-effect mobility may still be defined in terms of eqn. (1), but this will no longer truly represent the equilibrium carrier-drift mobility since a carrier which becomes localized in such deep centres has a higher probability of recombination than of subsequent re-release into the extended states. The adoption

of zero-temperature occupation statistics will be permissible for centres close to the Fermi level, and the following analysis should then provide a reasonable approximation to the behaviour.

Fig. 6

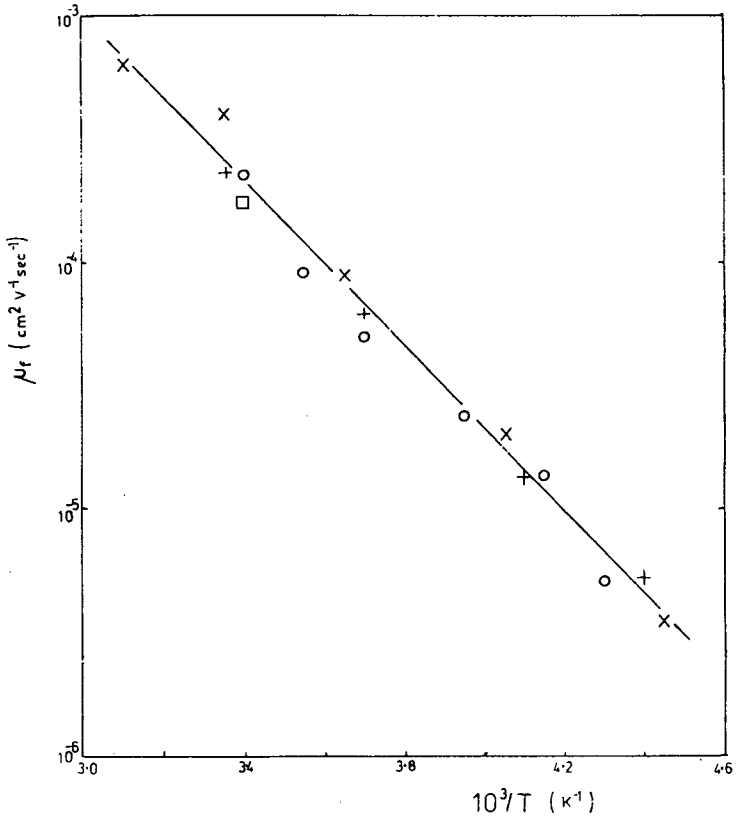

Temperature dependence of the field-effect mobility of disordered As_2Te_3. The measurement sets are normalized as noted for fig. 5. ×—specimen 1 (×1·0); ○—specimen 2 (×0·8); □—specimen 3 (×1·0); ◇—specimen 4 (×1·2).

If the induced excess charge is equivalent to the effect of a uniform movement $\Delta\epsilon$ (relative to the ' flat bands ' surface condition) of the Fermi energy, for a distance L from the surface of the semiconductor film, then the excess charge will be given by

$$\Delta Q_{\text{trapped}} = N(\epsilon_f) eL\Delta\epsilon, \tag{4}$$

where $N(\epsilon_f)$ is the density of distributed localized states at the Fermi energy (cm^{-3} eV^{-1}). The corresponding increase in the free charge density is

$$\Delta Q_{\text{free}} = N_v eLkT\,[\exp\{-(\epsilon_f - \Delta\epsilon)/kT\} - \exp(-\epsilon_f/kT)], \tag{5 a}$$

$$\simeq N_v eL\Delta\epsilon \exp(-\epsilon_f/kT), \tag{5 b}$$

where ϵ_f is the energy separation of the valence-band mobility-edge and the Fermi level in the bulk, and where the approximation of eqn. (5 *b*) is valid

for small values of $\Delta\epsilon$. Hence from eqn. (2 *b*), the field-effect mobility is given by

$$\mu_f \simeq \mu_0 \frac{N_v}{N(\epsilon_f)} \exp(-\epsilon_f/kT). \tag{6}$$

Although the above equation is approximate, it should be sufficiently correct for the present purposes. The most important approximation is the assumption of an abrupt accumulation regime, of energy displacement $\Delta\epsilon$ over a width L, as opposed to the true situation in which the energy displacement relaxes progressively between surface and bulk. However, calculations have shown that the approximation is valid both at low gate voltages (for which the surface and bulk energy distributions are so similar as to make errors negligible) and for high accumulation gate voltages (for which the induced charge is concentrated very close to the surface so that the assumption of an abrupt surface-bulk transition is reasonable).

Equations (3) and (6) therefore illustrate that the temperature dependence of the field-effect mobility (and thereby of ΔI through eqn. (1)) reflects the separation in energy of the dominant localized states from the extended states. In terms of these equations, it is possible to envisage two fundamentally different types of response-characteristic, as follows.

(i) Where a significant density of trapping centres occurs in the region of the bulk equilibrium Fermi level, then ΔI should exhibit an activation energy equal to that of the bulk conductivity at the ' flat bands ' surface condition, and should feature a progressively decreasing activation energy as the gate voltage is raised through the accumulation regime (i.e. as the energy difference between the Fermi level and the extended states is reduced in the surface region). The activation energy at a given constant gate voltage will provide a direct indication of the position of the surface Fermi level within the energy gap (thereby providing a simple check against the value calculated in analyses such as that of Spear and Le Comber).

(ii) If the localized states which dominate the field effect are shallow ($|\epsilon_t - \epsilon_f| > kT$), then ΔI should possess activation energy ϵ_t for *all* values of gate voltage in the accumulation regime, up to that at which the trapping centres approach the Fermi level in the surface region. Beyond this limit, degenerate occupation statistics will be required for the traps, and the behaviour will become less straightforward.

A complication to the above analysis arises from the possible existence of surface states in addition to the bulk trapping centres so far dealt with. While the bulk states will still determine the spatial extent of the accumulation and depletion layers (provided the surface states are truly two-dimensional in nature), much of the induced excess charge may be localized in the surface states, which will then dominate the magnitude of field-effect response. Where sufficient surface centres occur to produce such domination, changes in conductivity will depend upon the ratio of free *bulk* excess carriers to *surface-trapped* excess carriers. The excess trapped charge density will be given by

$$\Delta Q_{\text{trapped}} = eN_s \exp(-\epsilon_s/kT)\,[\exp(\Delta\epsilon/kT) - 1]\,; \tag{7 a}$$

$$\simeq eN_s \frac{\Delta\epsilon}{kT} \exp(-\epsilon_s/kT) \quad \text{for small } \Delta\epsilon \tag{7 b}$$

for a *discrete* set of shallow surface states of density N_s cm^{-2} at energy ϵ_s from the Fermi level, or by

$$\Delta Q_{\text{trapped}} = eN_s(\epsilon_f)\Delta\epsilon \tag{8}$$

for distributed surface states of density $N_s(\epsilon_f)$ at the Fermi energy. In this situation, eqns. (3) and (6) will, respectively, be replaced by

$$\mu_f = \mu_0 \frac{N_v kTL}{N_s} \exp(-\epsilon_s/kT), \tag{9}$$

and

$$\mu_f = \mu_0 \frac{N_v L}{N_s(\epsilon_f)} \exp(-\epsilon_f/kT). \tag{10}$$

This behaviour under surface-dominated conditions is similar to the bulk-controlled case in that the activation energy of the field-effect mobility identifies the position of the dominant localized states, but the parameter L now enters into the expressions. For situations in which the accumulation layer extends appreciably into the bulk of the semiconductor, the field-effect mobility will be proportionately greater than where screening occurs close to the surface. The parameter L represents a first approximation to the extent of the space-charge layer, being equivalent to the function λ_s employed by Spear and Le Comber, and similar in behaviour to the quantity L_c defined by Many *et al.* An important consequence of the dependence of effective mobility upon L is that the field-effect mobility defined by eqns. (9) and (10) will decrease with increasing gate voltage in the accumulation regime, due to the progressive reduction in L as the excess charge becomes concentrated close to the surface (see Many *et al.* 1965, figs. 4.6 and 4.7).

A further complication to the analysis of experimental field-effect data lies in the possibility that localized states above and below the Fermi level may *jointly* be involved in determining the response to changes in gate voltage. Since this situation applies to the surface as well as to the bulk localized states, and since band bending may occur in the surface region due to differing bulk and surface trap distributions, the analysis of experimental response characteristics is by no means straightforward. A unique identification of the energies and densities of the various electron and hole trapping centres in the bulk and at the surface is unlikely to be feasible in the general case, unless some of the necessary information can be derived from measurements of other transport properties. It is, however, possible to propose various models of the localized state distribution, and to compare their predicted field effect characteristics with those experimentally obtained. The problem is not so much one of obtaining agreement between model and experiment as of establishing that the model selected in the correct choice from the various possibilities yielding similar response curves.

For a particular projected model of the band structure, the field-effect response may be calculated in a fairly straightforward manner in terms of the analyses and techniques presented by Many *et al.* (1965). From given surface and bulk initial conditions, the surface potential of the model can be progressively varied, the resulting changes in free and trapped surface and bulk carrier densities being calculated at each stage. The data for free

carriers may then be interpreted in terms of induced excess current, ΔI, while the total change in trapped carrier concentration may be equated to ΔQ and thereby to the appropriate gate voltage. By this means, response characteristics of the type shown in figs. 2 and 3 may be generated and compared with experiment.

Much of the above discussion has been concerned with the field-effect response in the accumulation regime, but data for the depletion regime also provide valuable information on the localized states concerned. For instance, in an intrinsic semiconductor (i.e. equal densities of free + trapped electrons and holes) for which charge transport by one species of carrier is completely dominant, the depletion current tends asymptotically towards a limit corresponding to complete depletion of the dominant carrier over a region of depth $2L_e$,

$$\Delta I \Rightarrow -2L_e\sigma Ew, \tag{11}$$

where σ is the electrical conductivity and L_e the effective Debye length defined as

$$L_e \sqrt{\left(\frac{KK_0kT}{e^2(n_b+p_b)}\right)}. \tag{12}$$

Here, KK_0 is the dielectric constant of the semiconductor, and n_b and p_b are respectively, the trapped electron and hole concentrations in the bulk. Similarly, for extrinsic cases in which the total trapped density of the dominant carrier exceeds that of the other species, but in which the dominant carrier alone contributes to the electrical conductivity as before, then the induced current is given by

$$\Delta I = G^- L_e\sigma Ew, \tag{13}$$

where the function G^- has been defined and tabulated by Many *et al.* (1965). Since G^- is a fairly slowly increasing function of surface potential for strongly depleted conditions, it is possible to obtain a reasonable estimate for L_e and thereby for p_b and n_b in the extrinsic as well as in the intrinsic case. Where both species of carrier are significantly mobile, the depletion regime is replaced at high gate voltages by an inversion regime in which sufficiently large concentrations of the ' minority ' carrier are induced as to cause ΔI to revert to a positive value. The various characteristics have been examined in considerable detail by Many *et al.* (1965), and will not be further elaborated upon in the present discussion.

It is worth noting that the possibility exists in principle of determining the energy of the bulk trapping centres via the temperature dependence of n_b and p_b as calculated from the *depletion* data. However, since the induced depletion current modulations are small in disordered semiconductors, the accuracy of the calculations may often be too low to allow a reliable figure to be obtained in this way.

§ 4. Analysis and discussion

The response-data for the two materials studied exhibit a considerable degree of similarity, and may thus be jointly dealt with in the following

analysis. Where important differences occur, they will be noted at the appropriate places in the text.

From the information in figs. 2 and 3, and from various similar data for a range of other specimens, it is possible to draw several immediate conclusions, as itemized below.

(i) In every case studied, depletion characteristics were produced by positive gate voltages, and accumulation characteristics were produced by negative voltages. From all the available data, there is no detectable transition from depletion to inversion characteristics over the accessible range of gate voltage. These features constitute convincing evidence that the electrical transport processes in the two materials feature essentially unipolar conduction by hole carriers. Such a conclusion is supported by other data on the materials such as the thermopower (Rockstad, Flasck and Iwasa 1972, Nagels, Callaerts and Denayer 1974), and by the fact that holes have been identified as the dominant carrier in all disordered chalcogenides for which time-of-flight mobility measurements have been performed. It should be noted that the dominance of hole carriers in the transport processes does not imply that the *trapped* electron density is negligible, but only that the free electrons make little contribution to the conduction mechanisms. It is therefore possible for the trapped electron density to contribute significantly to the determination of the effective Debye length, in spite of the unipolar transport characteristics.

(ii) Figures 2 and 3 feature an almost linear variation of induced excess current with increasing negative gate voltage. In terms of eqn. (1), this indicates a fairly constant value of field-effect mobility across the accumulation regime. The slightly superlinear dependence of ΔI upon V_g (particularly apparent at low gate voltages) is consistent with the sharing of induced charge between electron and hole trapping centres. At high accumulation gate voltages, the contribution of the electron traps becomes negligible, and in this region the response is essentially linear.

(iii) The temperature dependence of the field-effect mobility determined from the accumulation data is shown in figs. 5 and 6, respectively, for $As_{30}Te_{48}Si_{12}Ge_{10}$ and As_2Te_3. The data represent average values over the accumulation regime, except in the case of specimen 1 of fig. 5, for which the influence of V_g is illustrated by the inclusion of data taken at two particular gate voltages. In these figures, the measurement sets for different specimens have been normalized with respect to their room-temperature mobility values by the use of appropriate multiplication factors as shown. This procedure was adopted for clarity of presentation in view of small differences between the various individual specimens.

It can be seen that the field-effect mobility in each material is characterized by a well defined activation energy. The appropriate energy values are $0{\cdot}40 \pm 0{\cdot}01$ eV for $As_{30}Te_{48}Si_{12}Ge_{10}$, and $0{\cdot}32 \pm 0{\cdot}01$ eV for As_2Te_3. There is no significant dependence of the activation energy upon gate voltage, for any of the specimens examined. Since the d.c. conductivity activation energies for the two materials are, respectively, 0·53 and 0·44 eV (Marshall and Owen 1975), it is evident that the trapping centres controlling the field

effect response are not situated at the energy of the bulk Fermi level, but are approximately 0·13 eV below it in each case. The insensitivity of activation energy to changes in V_g is consistent with this interpretation, as discussed in the text above.

Interpreted by means of eqn. (3), and with $\mu_0 N_c kT$ approximately 5×10^{20} cm^{-1} V^{-1} sec^{-1} (Marshall and Owen 1975), figs. 5 and 6 suggest a density of hole trapping centres of order 10^{19} to 10^{20} cm^{-3} in each of the two materials.

The above superficial analysis is consistent with transient photoresponse and other data (Marshall and Owen 1975) in that it establishes the presence of hole trapping centres approximately 0·13 eV below the Fermi level in both materials. However, significant quantitative differences emerge from a detailed comparison of the field-effect and transient photoconductive data, even though the specimens employed in the two investigations were identically prepared. Thus, the photoconductive data imply a density of only 10^{17} to 10^{18} cm^{-3} for the centres 0·13 eV from the Fermi level, as compared to the appreciably higher figure indicated by the field-effect measurements. Moreover, the photoresponse study established that these localized states dominate the transport processes only at low temperatures, while the room-temperature mobility is limited by a second set of trapping centres, of density 10^{19} to 10^{20} cm^{-3}, situated 0·22 eV from the Fermi level.

A possible explanation for these discrepancies is that the field-effect response is influenced by the presence of surface states to a much greater extent than is the photoresponse. If localized states occurred at the semiconductor/dielectric interface in sufficiently large concentrations ($\gtrsim 10^{13}$ cm^{-2}), they might well absorb a substantial proportion of the induced excess charge, thereby giving rise to a field-effect mobility which is appreciable lower than the bulk value. However, it proves difficult to fit such a model to the experimental data, if the surface states are envisaged in the conventional manner as two-dimensional entities situated precisely at the semiconductor surface. The occurrence of the parameter L in the expression for the surface-dominated mobility (eqn. (10)) leads to a progressive reduction in the mobility with increasing voltage in the accumulation regime, as previously discussed. Such a feature is not experimentally observed, in any of the present sets of data.

In the absence of a straightforward interpretation of the field-effect measurements, either in terms of a bulk density of localized states consistent with that determined by other experiments, or in terms of the influence of additional trapping centres at the semiconductor/dielectric interface, it is necessary to embark upon a more detailed analysis of the experimental data. The dominant trapping centres are still, of course, required to be 0·13 eV below the Fermi level, as established by the temperature dependence of the response. However, the density of these states and their identity as surface and/or bulk centres must be regarded as unknown. Also, the existence of various localized states above the Fermi level must be considered, together with the possibility of band-bending in the vicinity of the surface.

A procedure may be adopted whereby various reasonable models are postulated, and their field effect responses computed and compared with the experimental data to determine the optimum agreement. It is initially

necessary to assume a value for the bulk ratio of trapped holes to trapped electrons, this being equivalent in the terminology adopted by Many *et al.* (1965) to selecting a value for the bulk potential, u_b, defined by

$$p_b/n_b = \exp(2u_b). \tag{14}$$

It should be noted that the bulk potential defined in this manner is dimensionless, being expressed in units of the thermal energy kT. Next, a gate voltage corresponding to the 'flat bands' condition must be postulated, and the magnitudes of the current changes and corresponding gate voltages must be redefined relative to this datum point. It is then possible to determine the effective Debye length via eqn. (13), employing the tabulated behaviour of the function G^- as provided by Many *et al.* (1965). Thence p_b and n_b may be evaluated by the use of eqns. (12) and (14).

The model may now readily be compared in detail with the experimental data, by use of the functions G^+, G^-, g^+ and g^- which have been defined and tabulated by Many *et al.* (1965). In the accumulation regime, the induced excess current is given by

$$\Delta I = G^+ L_e \sigma E w \tag{15}$$

while the changes in the concentrations of trapped holes and electrons are given by

$$\Delta p_b = p_b L_e G^+ ; \quad \Delta n_b = p_b L_e g^-. \tag{16}$$

Similarly, in the depletion regime, ΔI is provided by eqn. (13), while the changes in trapped carrier concentration are given by

$$\Delta p_b = p_b L_e G^- ; \quad \Delta n_b = p_b L_e g^+. \tag{17}$$

It is then possible to calculate the values of gate voltage relative to the 'flat-bands' condition via the induced excess charge

$$\Delta Q_b = e(\Delta p_b - \Delta n_b). \tag{18}$$

In situations for which surface states are envisaged in addition to the bulk centres, the effect will be to increase the total induced excess charge by an amount

$$\Delta Q_s = e(\Delta p_s - \Delta n_s) \tag{19}$$

where, for shallow surface states as suggested by the activation energy data,

$$\Delta p_s = p_s \exp(v_s) ; \quad \Delta n_s = n_s \exp(-v_s). \tag{20}$$

Here, p_s and n_s are the trapped hole and electron surface concentrations at the 'flat bands' condition, and v_s is the dimensionless surface potential as defined by Many *et al.* (1965).

In this way it is possible to achieve a detailed description of the accumulation and depletion response of a particular model, and to compare the behaviour with experiment. Figure 7 shows a typical fit of such a model to the experimental data. By this means, the various measurements for the

Fig. 7

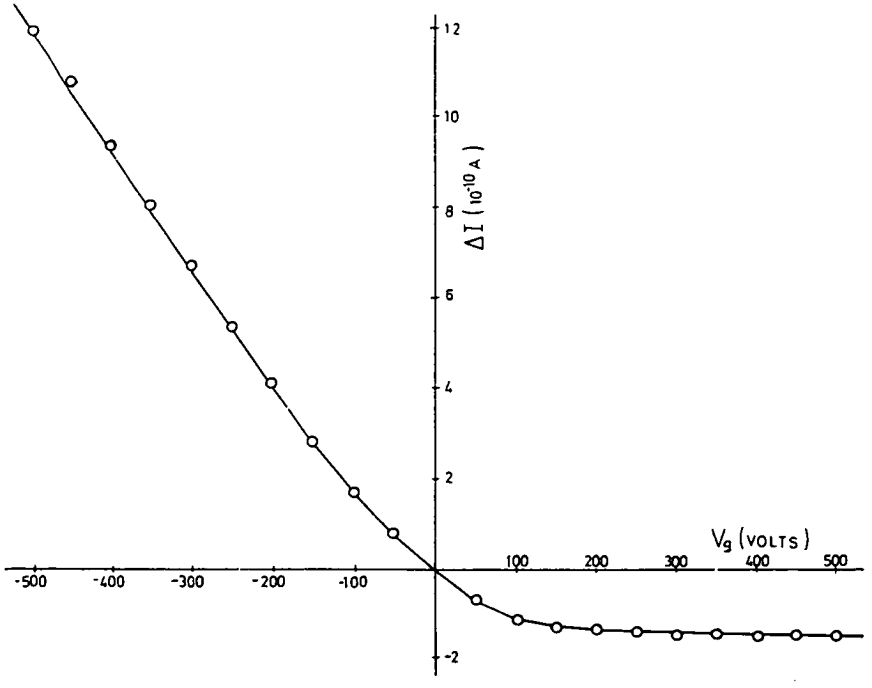

Typical illustration of the correspondence between experimental data and a fitted theoretical model of the localized state distribution (solid line). ($As_{30}Te_{48}Si_{12}Ge_{10}$, specimen 2, $T=294$ K. Fitted parameters; $u_b=0{\cdot}5$, $p_b=4{\cdot}9\times10^{17}$ cm^{-3}, bands flat at $V_g=0$, no surface states present.)

two materials studied here were found to be consistent with a localized state distribution possessing the following characteristics.

(i) *Surface states:* It was not possible to account for the experimental response in terms of states located uniquely at the semiconductor/dielectric interface. Postulation of any significant concentration of such centres leads to a sub-linear dependence of ΔI upon V_g in the accumulation regime, as previously described, whilst this type of behaviour was not a feature of any of the sets of experimental data. The invocation of a *small* density of surface states was occasionally required so as to produce a slight surface band-bending in order to achieve optimal fitting of the data to the curve. However, this was not necessary for the majority of the measurements, for which the best agreement was obtained with the ' flat bands ' condition corresponding to zero gate voltage. In the few cases where surface distortion was indicated, its magnitude was small, and in no case corresponded to values of V_g greater than 100 V.

(ii) *Bulk states:* The best agreement with the experimental data was obtained for values of bulk potential which ranged from 0 to 1 in individual cases, a large majority of the measurement sets being well fitted for $u_b=0{\cdot}5$. This suggests a slightly extrinsic nature for the bulk, with approximately twice as many trapped holes as electrons. The values of p_b calculated at room temperature for specimens of the two materials were closely similar,

being in the range 1 to 5×10^{17} cm^{-3} for various individual specimens. At lower temperatures, p_h decreased progressively in a manner consistent with the activated nature of the field-effect mobility. In both materials, the density of hole trapping centres situated 0·13 eV below the Fermi level was calculated to be in the range 10^{19} to 10^{20} cm^{-3}.

The above characteristics differ in several respects from those determined from the transient photoresponse data of Marshall and Owen (1975) which were obtained using similarly prepared specimens. The concentration of the centres 0·13 eV below the Fermi level is found to be approximately two orders of magnitude greater from the field-effect measurements than from the photoresponse. Moreover, the present study suggests that these centres are dominant at room temperature, in contrast to the transition to control by a shallower set of trapping centres (density 10^{19} to 10^{20} cm^{-3}, situated 0·22 eV below the Fermi level) detected from the photomobility data. The likely explanation for these differences is that the two experimental techniques probe different spatial regions of the semiconductor film. For the field-effect measurements, calculated effective Debye lengths were of the order of 50 Å, so that only a very shallow surface region of the specimen was being examined. In contrast, the photoresponse investigations were carried out using illumination of an energy which was not much higher than that of the optical absorption edge, so that carrier generation occurred over an appreciable fraction of the specimen thickness ($\sim$1000 Å). The experimental differences may well thus imply an increasing density of localized states in the region approaching the semiconductor surface, which might be expected to occur as a consequence of increasing positional disorder over this region and also possibly of some compositional disorder.

It is not, of course, reasonable to assume a constant density of localized states of value 10^{19} to 10^{20} cm^{-3} over the first 50 to 100 Å of the film, followed by an abrupt transition to a density of 10^{17} to 10^{18} cm^{-3} at greater distances from the surface. Any disorder-induced variation in localized state density would be expected to take place more gradually. Thus while the density determined from the field-effect studies may be regarded as a suitable average over the first 50 Å or so, the approximation is likely to be fairly crude due to the analytical assumption of a constant density of localized states in the bulk, possibly supplemented by two-dimensional surface states. However, a more precise analysis appears somewhat forbidding, and would require the assumption of a particular spatial variation of localized-state density, in addition to the various assumptions already adopted above. In the absence of such an analysis, it seems reasonable to assume that the central conclusions of the present treatment—that the field-effect response is controlled by a set of localized states with effective density 10^{19} to 10^{20} cm^{-3} close to the semiconductor surface, and of energy 0·13 eV below the Fermi level—would be reproduced by a more complete formulation.

§ 5. Conclusions and summary

From the field-effect measurements reported above, taken in combination with information provided by the transient photoresponse, it is possible to advance a model for the transport properties of disordered $As_{30}Te_{48}Si_{12}Ge_{10}$

and As_2Te_3 in which the dominant carriers are holes, which interact in the semiconductor bulk with two sets of localized states situated 0·13 and 0·22 eV from the Fermi level and with densities of 10^{17}–10^{18} and 10^{19}–10^{20} cm^{-3}, respectively. Close to the surface, the density of the deeper centres appears to increase by about two orders of magnitude, presumably as a consequence of increasing disorder in this region. At room temperature, transport in the bulk is controlled by the shallower set of traps, by virtue of their greater occupied density. However, the field-effect response is clearly dominated by the deeper-lying levels. It thus appears that the two sets of centres are not subject to the same *proportional* increase as a consequence of additional disorder in the surface region. This is not surprising since there is no theoretical reason to expect equal proportional increases in density to occur, it perhaps being more likely that equal *numerical* increments might occur so that the concentration of the shallower centres would approximately double whilst that of the deeper states increased by a factor of 100. In such circumstances, the deeper levels would become dominant as observed.

It is interesting to note that the generation of excess localized states in the surface region does not appear to result in any significant band-bending. This suggests that increases in trapped hole concentration are automatically balanced by equal increases in the density of excess trapped electrons. Following the work of Spear (1974 b) and of Anderson (1975), Mott, Davis and Street (1975) have suggested a model of localized states in disordered chalcogenides in which the energy balance conditions favour the redistribution of the ' dangling bond ' electrons so that one half of such bonds take up two electrons, leaving the remaining bonds unoccupied. The doubly-occupied centres then constitute charged hole traps, while the unoccupied bonds form electron trapping states. Such a process would be consistent with the absence of a large electron spin resonance due to singly-occupied dangling bonds, and would also be consistent with various other physical properties (Mott *et al.* 1975). Evidently, if the bulk and surface hole traps 0·13 eV below the Fermi level were identified with doubly-occupied dangling bonds in this manner, they would be associated with an equal density of unoccupied bonds states above the Fermi level, thereby pinning the surface and bulk Fermi levels and giving a bulk and surface potential of zero in the absence of other species of trapping centre. It will be recalled that analysis of the present field-effect data suggested a non-zero value of potential u_b, corresponding to a somewhat higher density of trapped holes than of trapped electrons in the bulk. However, it is not certain whether this is a genuine feature which reflects a contribution from additional localized states or whether it is simply an artefact due to the approximations involved in the analytical procedure.

Finally, it is interesting to note that the high density of localized states close to the surface, by virtue of the resulting small value of effective Debye screening length, explains the ease of formation of ohmic contacts to disordered chalcogenides. It has previously been presumed in the literature that the rarity of rectifying contact phenomena in these materials implies a very high density of localized states in the *bulk*. In contrast, lower values of bulk trap density have been indicated by investigations of such transport properties as the ' time-of-flight ' drift mobility, space-charge-limited current, transient photoconductivity, where such measurements have been made.

Similarly, it has been difficult to account for the absence of a field-effect response in materials such as disordered As_2Se_3 and Se, for which the bulk Fermi level may readily be influenced by excess carriers generated by illumination or by space-charge injection. These apparent anomalies are resolved by the invocation of an increase in localized state density close to the surface, as indicated by the analysis presented above.

ACKNOWLEDGMENTS

The authors are indebted to Professor W. E. Spear for valuable discussions, and to Mr. J. McNeil for assistance in carrying out the field effect measurements.

REFERENCES

ANDERSON, P. W., 1975, *Phys. Rev. Lett.*, **34,** 953.
BARBE, D. F., 1971, *J. Vacuum Sci. Technol*, **8,** 102.
COHEN, M. H., FRITZSCHE, H., and OVSHINSKY, S. R., 1969, *Phys. Rev. Lett.*, **22,** 1065.
EGERTON, R. F., 1971, *Appl. Phys. Lett.*, **19,** 203.
FRITZSCHE, H., and OVSHINSKY, S. R., 1970, *J. non-crystalline Solids*, **2,** 393.
MANY, A., GOLDSTEIN, Y., and GROVER, N. B., 1965, *Semiconductor Surfaces* (Amsterdam : North Holland).
MARSHALL, J. M., and MILLER, G. R., 1973, *Phil. Mag.*, **27,** 1151.
MARSHALL, J. M., and OWEN, A. E., 1975, *Phil. Mag.*, **31,** 1341.
MOTT, N. F., DAVIS, E. A., and STREET, R. A., 1975, *Phil. Mag.*, **32,** 961.
NAGELS, P., CALLAERTS, R., and DENAYER, M., 1974, *Amorphous and Liquid Semiconductors*, edited by J. Stuke and W. Brenig (London : Taylor & Francis Ltd), p. 867 ff.
ROCKSTAD, H. K., FLASCK, R., and IWASA, S., 1972, *J. non-crystalline Solids*, **8–10,** 326.
ROSE, A., 1951, *RCA Rev.*, **12,** 362.
SPEAR, W. E., 1974 a (private communication) ; 1974 b, *Amorphous and Liquid Semiconductors*, edited by J. Stuke and W. Brenig (London : Taylor & Francis Ltd), p. 1.
SPEAR, W. E., and LE COMBER, P. G., 1972, *J. non-crystalline Solids*, **8–10,** 727.

PHILOSOPHICAL MAGAZINE, 1976, VOL. 33, NO. 2, 261–275

Transport properties and electronic structure of glasses in the arsenic–selenium system

By F. D. FISHER†, J. M. MARSHALL‡ and A. E. OWEN
Department of Electrical Engineering, University of Edinburgh, Scotland

[Received 18 November 1974 and in final form 4 December 1975]

ABSTRACT

Data are presented on the transport properties of arsenic–selenium glasses containing 30–50% As. The hole carrier drift mobility and d.c. conductivity have been studied as functions of composition, temperature, and applied electric field.

The magnitude and activation energy of both the mobility and the conductivity exhibit extrema close to the stoichiometric As_2Se_3 composition. These and other data obtained are examined in terms of possible transport mechanisms for the glasses.

It is concluded that the materials possess several relatively discrete sets of trapping centres above the valance band mobility edge, and that these limit the motion of free hole carriers moving close to the mobility edge.

§ 1. INTRODUCTION

The vitreous arsenic–selenium system, with its wide range of glass formation (0–60% As) and *relatively* well characterized electrical and structural properties, is very suitable for the study of electronic transport in disordered solids. In contrast to most other amorphous semiconductors it is possible, in glasses of low arsenic content (0–2%) to measure both electron and hole carrier mobilities by transit time techniques. Moreover, at higher arsenic concentrations, the electron mobility can be measured up to 10% As and the hole mobility in the range 30–50% As. The present paper provides the first examination of mobility over the latter range, in which, except at the stoichiometric As_2Se_3 composition, transport has previously been studied by electrical conductivity and thermopower only. The dependence of the hole mobility on composition, temperature, and applied electric field has been studied, and the data are examined in conjunction with subsidiary measurements of conductivity, photoconductivity, and other related phenomena.

§ 2. EXPERIMENTAL CONSIDERATIONS

All specimens employed in the present examination were prepared by the rapid quenching of molten glass under pressure between mica plates. This technique provides platelets of thickness 10–100 μm and has the advantage

†Present address: Rank Xerox Development Laboratory, Welwyn Hall, Church Street, Welwyn, Hertfordshire, AL6 9LU, England.

‡ Present address: Department of Physics, Dundee College of Technology, Dundee, DD1 4HG, Scotland.

of producing specimens of truly vitreous material of known composition in a simple and reproducible manner. In contrast, the production of amorphous films by thermal evaporation usually yields films whose composition and structure differ from those of the starting material, and whose composition may vary through the thickness of the films themselves.

From vitreous platelets prepared in the above manner, specimens were produced with evaporated gold electrodes. These were used to determine the transit time of excess hole carriers created by bombardment of the upper specimen surface with short pulses of 8 keV electrons, as described by Spear (1968), for example. The carrier transit pulses obtained were typically of the form shown in fig. 1 (*a*), and the time of flight of a large coherent fraction

Fig. 1

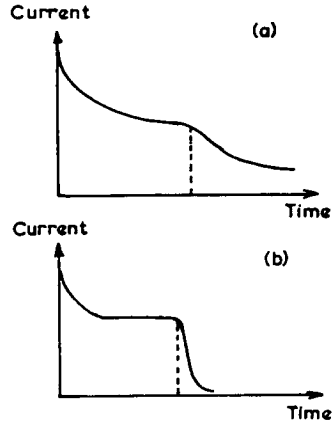

(*a*) Typical transit pulse in $As_{45}Se_{55}$. (*b*) Typical transit pulse in pure Se.

of the drifting charge was identified by the ' breakpoint ' of the trace, as illustrated. The drift times were in the range 200–500 μsec at room temperature, in contrast to times of less than 100 μsec employed in a previous study of As_2Se_3 by Marshall and Owen (1971). The significance of this difference will be discussed later in the text.

All the glasses studied in the range 30–50% As exhibited the considerable degree of charge dispersion implicit in fig. 1 (*a*), in contrast to the behaviour found for both electron and hole carriers in pure selenium (Marshall and Owen 1972, Marshall, Fisher and Owen 1974 a), for which a well-defined discontinuity of slope, and hence transit-time, is observed at room temperature (fig. 1 (*b*)). However, the hole mobilities measured in the present study were appreciably smaller than the room-temperature mobility of either carrier in selenium, and it should be noted that the degree of dispersion present in the case of transits in selenium increases progressively with decreasing temperature (and mobility) and becomes similar to that shown in fig. 1 (*a*) when the temperature is sufficiently low as to produce comparable magnitudes of mobility (Marshall and Owen 1972).

In the present examination, the degree of dispersion of the hole transit pulse increased with deviation from the As_2Se_3 stoichiometry in the ' selenium rich ' direction, until the ' breakpoint ' shown in fig. 1 (*a*) became undetectable

in glasses of composition $As_{30}Se_{70}$. In ' arsenic rich ' glasses, no detectable increase in dispersion occurred in the range investigated (up to 50% As).

It was not possible in any of the glasses studied in the *present* work to detect any pulse due to the transit of electron carriers, indicating a low carrier mobility and/or very short carrier range prior to deep trapping and recombination. As mentioned earlier, however, in glasses with less than 10% As the electron mobility can be measured, and with less than 2% As both carrier mobilities are measurable. Measurements in these compositional ranges have been reported previously by several workers (Schottmiller, Tabak, Lucovsky and Ward 1970, Marshall and Owen 1972, Marshall, Fisher and Owen 1974 a).

§ 3. Experimental data and discussion

In addition to the mobility measurements outlined above, d.c. conductivity data were obtained using the same specimens as for the transit-time studies. The low-field data obeyed the relationship.

$$\sigma = \sigma_0 \exp(-\epsilon_\sigma/kT), \tag{1}$$

with values of the pre-exponential constant in the range 300 to 500 Ω^{-1} cm^{-1} and with ϵ_σ varying between 0·91 and 0·97 eV as illustrated in the table and in

Fig. 2

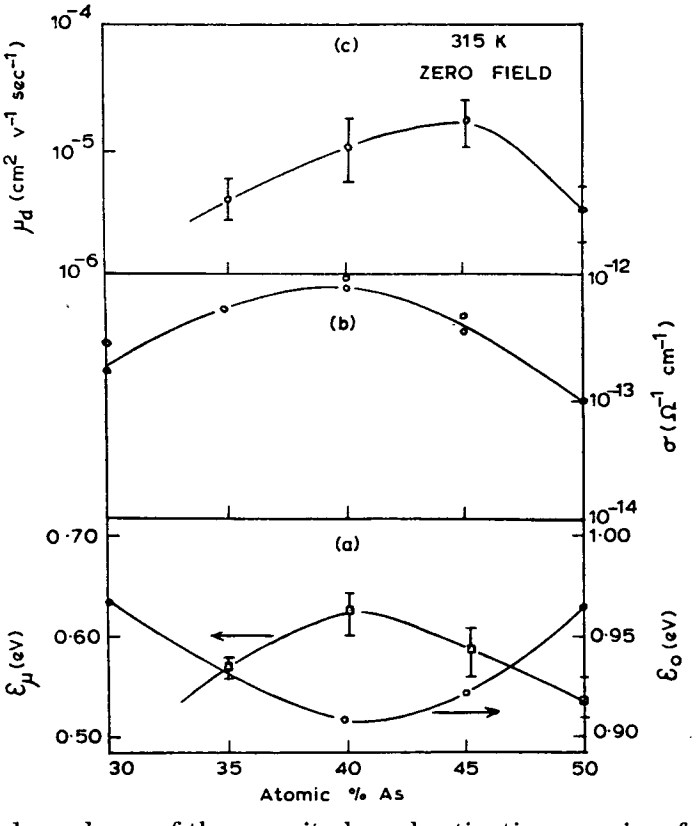

Compositional dependence of the magnitude and activation energies of the hole drift mobility and conductivity of arsenic–selenium glasses.

fig. 2 (*a*) and (*b*). These data are in good agreement with those in the literature both in magnitude and in the effect of compositional variations. The magnitude of σ_0 suggests that the carrier transport occurs within extended states rather than by a process of hopping between localized centres within the ' mobility

Fig. 3

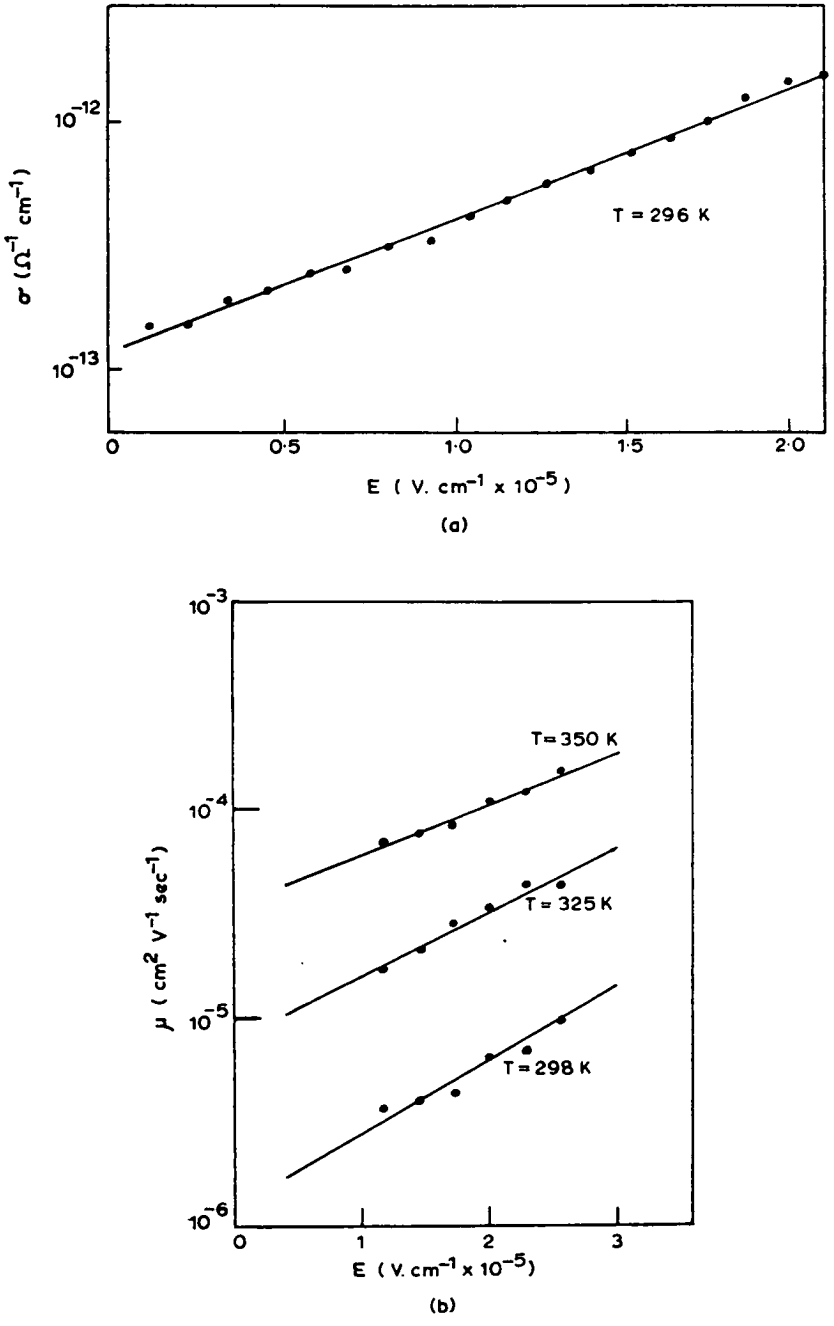

(*a*) Electric field dependence of the d.c. conductivity in $As_{35}Se_{65}$. (*b*) Electric field dependence of the hole drift mobility in $As_{35}Se_{65}$.

gap ', for which a substantially lower value of the parameter σ_0 is to be expected (Mott and Davis 1971).

Both conductivity and hole drift mobility in the range of glasses examined increase with applied electric field according to the relationships:

$$\sigma(E) = \sigma(0) \exp (e \,.\, a(T)\, E/kT), \tag{2 a}$$

$$\mu_d(E) = \mu_d(0) \exp (e \,.\, a(T)\, E/kT), \tag{2 b}$$

where $\sigma(E)$, $\sigma(0)$, $\mu_d(E)$, $\mu_d(0)$ are, respectively, the conductivity and mobility at field E and at zero field, and where $a(T)$ is a temperature-dependent parameter having the dimensions of length but not necessarily representing any physical distance. Such behaviour appears to be a universal feature of transport in disordered chalcogenides and related materials, and has been discussed by Marshall and Miller (1973). Data typical of those from the present measurements are shown in fig. 3. The compositional variation of the parameter $a(T)$ at 280 K is shown in fig. 4, which also includes data on glasses of lower arsenic content (Marshall *et al.* 1974 b) and on pure selenium (Marshall and Owen

Fig. 4

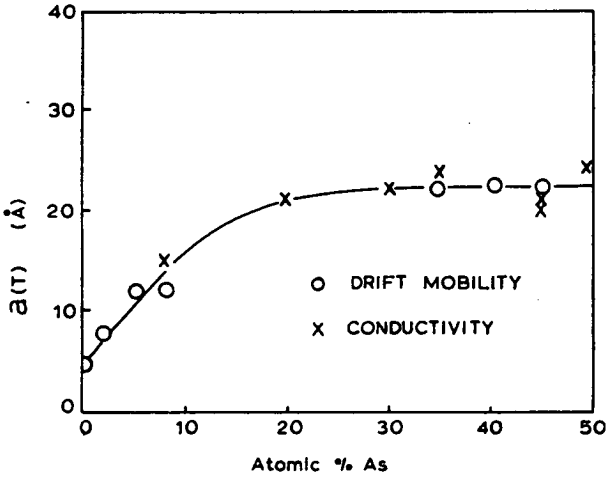

Variation of the field dependence parameter, $a(T)$, with composition at $T = 280$ K in arsenic–selenium glasses [from $\mu_d(E) = \mu_0 \exp ea(T)E/kT$].

1972, Marshall *et al.* 1974 a, b). The significant features of fig. 4 and its related measurements are:

(1) The electron and hole mobilities in selenium show the same form and magnitude of electric field dependence even though the magnitudes and activation energies of the two mobilities differ appreciably (Marshall and Owen 1972, Marshall *et al.* 1974 a, b).

(2) Over the whole range of measurements taken, there is no detectable thickness dependence of the field-dependent behaviour.

(3) Where comparisons are possible, the field dependence of the electrical conductivity is predominantly due to the field dependence of the carrier drift mobility. Any accompanying increase in the density of drifting charges ($n = \sigma/e\mu_d$) is relatively small.

(4) The parameter $a(T)$ rises rapidly over the range 0–15% As, but is much less sensitive to composition at higher concentrations. This behaviour has been associated with the progressive disruption of eight-membered Se rings which is known to be caused by the addition of arsenic in concentration up to 15% (Schottmiller *et al.* 1970, Marshall *et al.* 1974 b). At higher concentrations an extended $(As_4Se_6)_n$ matrix becomes established in the glass and is almost completely formed close to the stoichiometric As_2Se_3 composition. This feature will be discussed in more detail below.

The above characteristics, in conjunction with other available data, are considered to constitute strong evidence that the observed field-dependent behaviour arises from a field enhancement of the carrier transport processes taking place in the immediate vicinity of the mobility edge, at which energy the carriers move between periodic trapping events in localized levels at various energies within the mobility gap. The arguments leading to these conclusions have been presented in detail elsewhere (Marshall and Owen, 1972, Marshall and Miller 1973, Marshall *et al.* 1974 a, b) and will not be reproduced here. However, it should be noted that it has not yet been possible to provide a satisfactory *quantitative* description of the field-dependent processes which are expected to take place close to the mobility edge, and that even low-field transport in disordered solids is not yet adequately understood.

At low applied fields, the hole drift mobility has an activation energy which varies with composition as shown in fig. 2 (*a*). Such an activated mobility can arise either from thermally-activated hopping between localized states, or from trap-limited transport involving carrier motion in the extended states interrupted by periodic trapping/release events in localized states (Mott and Davis 1971).

The activated hopping process predicts a temperature dependence of the form

$$\mu = \frac{\nu e R^2}{6kT} \exp\left(\frac{-\Delta\epsilon}{kT}\right) \exp\left(-2\alpha R\right), \tag{3}$$

where ν is a phonon ' attempt-to-hop ' frequency for hops of length R, α is the localization parameter of the centres, and $\Delta\epsilon$ is an appropriate hopping activation energy. With reasonable values of the parameters concerned, the total pre-factor is expected to be of order 10^{-3} to 10^{-2} cm^2 V^{-1} sec^{-1} (Mott and Davis 1971).

For the As–Se glasses studied in the present investigation experimental factors of order 10^6 cm^2 V^{-1} sec^{-1} are obtained by fitting the data to eqn. (3), so that a hopping interpretation appears unacceptable. Similarly, the parameter σ_0 exceeds 10^2 Ω^{-1} cm^{-1} as opposed to the upper limit of 10 Ω^{-1} cm^{-1} expected for hopping. Hurst and Davis (1974) have shown that the conductivity

and thermopower activation energies in a range of As–Se glasses are identical within experimental error, as also have Callaerts, Nagels and Denager (1972) in As_2Se_3, although in both cases the measurements were made at temperatures well above ambient. This is not to be expected in a hopping situation, where at the most only some fraction of the mobility activation energy will normally contribute to the thermopower (Fritzsche 1971).

In the case of carrier motion at the mobility edge, periodically interrupted by localization in states within the mobility gap, a number of expressions for the mobility can be derived, depending upon the particular energy distribution of the trapping centres concerned. The simplest case, in which the localized states exist as a single, well-defined set of traps at energy ϵ_t from the mobility edge, leads to a drift mobility of the form (Rose 1951)

$$\mu_d = \mu_0 \frac{N_v}{N_t} \exp\left[(-\epsilon_t/kT)\right], \tag{4}$$

where μ_0 is the free carrier mobility, N_v the effective density of states at the valence band mobility edge, and N_t the density of trapping centres. Where this mechanism obtains, it is possible to determine the trap density from combined conductivity and mobility measurements, since $\sigma_0 = N_v\, e\, \mu_0$ if the conduction is by hole carriers only. Then, from (1) and (4)

$$N_t = \frac{\sigma}{e\mu_d} \exp\left[(\epsilon_\sigma - \epsilon_t)/kT\right]. \tag{5}$$

An alternative form of trap-controlled drift mobility which is feasible in non-crystalline semiconductors is that in which the trapping events occur in a ' tail ' of localized states at the band edge. The mobility is still expected to be activated provided the density of *occupied* traps peaks sufficiently sharply at some energy beyond the mobility edge, but the magnitude of the pre-exponential constant varies with the energy dependence of the density of states in the tail. For a linear tail (Mott and Davies 1971) of depth $\Delta\epsilon$, this constant is of magnitude $\mu_0(\Delta\epsilon/kT) \approx 10 - 10^2$ cm^2 V^{-1} sec^{-1}, while other tail shapes produce somewhat differing expressions of generally similar magnitude. In view of the experimental values of pre-factor (10^6 cm^2 V^{-1} sec^{-1}), such ' tail-of-states-limited ' models do not seem applicable in the present case, since values of μ_0 approaching 10^5 cm^2 V^{-1} sec^{-1} would be required. Values of that magnitude are only very rarely attained in crystalline solids, while μ_0 at the mobility edge in disordered semiconductors is expected to be of order 0·1–10 cm^2 V^{-1} sec^{-1} (Mott and Davis 1971). The $\mu_0 N_v$ product calculated from the data presented here is shown in the table.

Moreover, the magnitude of the mobility activation energy, ϵ_μ ($\geqslant 0{\cdot}5$ eV), does not seem consistent with the values of depth expected for tails of states in vitreous chalcogenides, such as arsenic selenide, for which a considerable degree of crystalline order is retained in the glass (Apling 1974).

Thus, it seems that an interpretation of the experimental data in terms of trap-limited band transport involving fairly discrete sets of trapping centres provides the most acceptable explanation. It should be noted, however, that eqn. (4) represents only a first-order description of the expected behaviour,

Composition (atomic % arsenic)	σ(315 K) (Ω^{-1} cm^{-1})	μ(315 K) (cm^2 V^{-1} sec^{-1})	ϵ_σ (eV)	ϵ_μ (eV)	σ_0 (Ω^{-1} cm^{-1})	N_t (cm^{-3})	N_t† (cm^{-3})	$\mu_0 N_v$ (V^{-1} sec^{-1} cm^{-1})	$\mu_0 N_v$† (V^{-1} sec^{-1} cm^{-1})
50	1×10^{-13}	3×10^{-6}	0·968	0·54	$3{\cdot}1\times10^{2}$	$1{\cdot}47\times10^{18}$	$3{\cdot}6\times10^{17}$	$1{\cdot}93\times10^{21}$	$5{\cdot}93\times10^{18}$
45	5	17	0·925	0·59	$3{\cdot}15\times10^{2}$	$4{\cdot}21\times10^{16}$	$1{\cdot}0\times10^{16}$	$1{\cdot}97\times10^{21}$	$6{\cdot}06\times10^{19}$
40	8·5	10	0·910	0·63	$3{\cdot}1\times10^{2}$	$1{\cdot}6\times10^{16}$	$4{\cdot}0\times10^{15}$	$1{\cdot}93\times10^{21}$	$5{\cdot}93\times10^{19}$
35	5	5	0·933	0·57	$4{\cdot}2\times10^{2}$	$5{\cdot}02\times10^{17}$	$1{\cdot}2\times10^{17}$	$2{\cdot}64\times10^{21}$	$8{\cdot}12\times10^{19}$
30	2	—	0·963	—	$5{\cdot}1\times10^{2}$	—	—	$3{\cdot}19\times10^{21}$	$9{\cdot}82\times10^{19}$

† These columns have been corrected to account for temperature dilation of the optical energy gap. The $\mu_0 N_v$ values have been adjusted by the factor exp ($\gamma/2k$) where $\gamma = -6\times10^{-4}$ eV K^{-1} (Main 1973) and the N_t values by an approximate factor exp ($\gamma/5k$) to allow for the traps being closer to E_F than the valence band edge. It should also be noted that the values of N_t plotted in fig. 5 are the uncorrected values.

and that a detailed analysis would involve modifications to allow for factors such as carrier scattering during motion at the mobility edge. It is not felt that the theoretical description of disordered semiconductors is sufficiently advanced at present to attempt the inclusion of such second-order terms, other than that representing the temperature dependence of the energy gap, but it should be noted that their presence may lead to errors of up to $+10$–10^2 in the magnitudes of $\mu_0 N_v$ and N_t calculated from eqn. (4).

Fig. 5

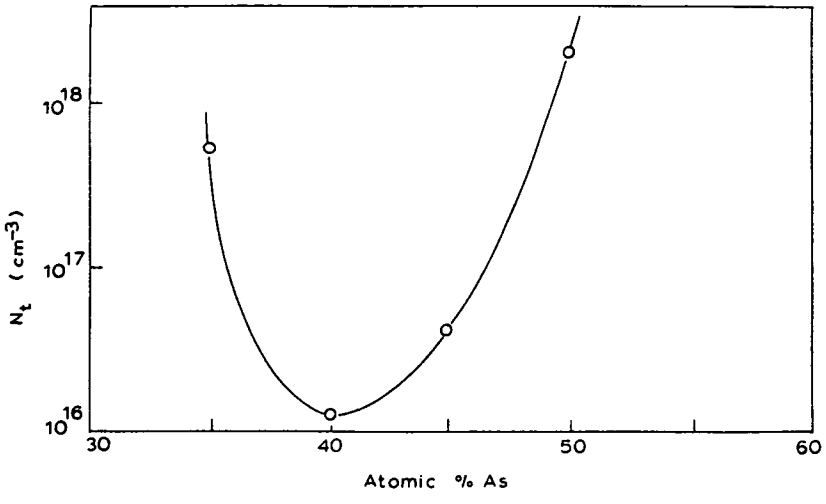

Variation of the density of traps, N_t, with composition at room temperature in arsenic–selenium glasses. (The N_t values are not corrected for dilation of the mobility gap—see the table).

Figure 5 shows the values of N_t determined by analysis of the data of fig. 2 in terms of eqn. (5). It can be seen that a fairly sharp minimum in trap density is obtained in the region of the As_2Se_3 composition, but possibly slightly on the arsenic-rich side of stoichiometry. The data of figs. 2 and 5 correlate well with an interpretation in which the localized states are derived from the compositional disorder in the As–Se glasses, this being minimized close to the As_2Se_3 composition. Such a model has been advanced previously in the literature to explain other physical properties of these glasses, and is based on the presence in the materials of an extended $(As_4Se_6)_n$ matrix. The data of Myers and Felty (1967) on glass transition temperatures and other parameters support such an interpretation, with the most ordered structural configuration occurring at a composition close to $As_{41}Se_{59}$, for which a sharp peak in T_g is obtained. A.c. and d.c. conductivity data (Edmond 1968, South and Owen 1974) have been interpreted in a similar way, but show a maximum on the selenium-rich side of stoichiometry. It is not possible to determine on which side of stoichiometry the extrema lie for the present data, in view of the experimental inaccuracy of the mobility measurements and the relatively coarse compositional measurement intervals. It may be noted however, that recent optical measurements (Petursson, Owen and Marshall 1975) on a finer compositional scale, shown in

fig. 6, do show a minimum in the optical gap at 41% As in agreement with the data of Myers and Felty. It may be, of course, that the different properties show extrema (or minima) at different compositions due to factors such as microscopic compositional variations.

Fig. 6

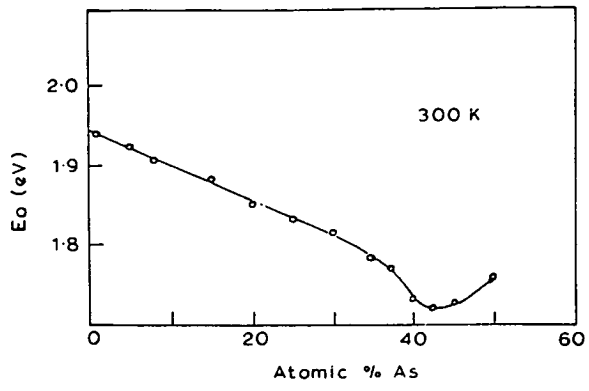

Variation of the optical gap, E_0, with composition at room temperature in arsenic–selenium glasses (after Petursson *et al.* 1975).

Recent X-ray and neutron scattering experiments (Apling 1974) have shown that As_2Se_3 is a comparatively well-ordered glass, in which structural correlations reminiscent of the crystal extend out to at least 10 Å. This conclusion is corroborated by the spectrographic work of Zallen, Drews, Emerald and Slade, (1971) and Lucovsky (1972). These results and the data obtained in the present studies indicate that the appreciable remanent short- and intermediate-range order lead to a band structure in which moderately well defined sets of localized levels—probably closely associated with defect states in the corresponding crystalline modifications—are retained, and that it is these states which control the measured trap-limited drift mobility. Such a model contrasts with the ' CFO ' model, in which extensive and effectively featureless tails of states are postulated within the mobility gap (Cohen, Fritzsche and Ovshinsky 1969).

The experimental variation of the drift mobility and its activation energy with composition implies, in terms of the above type of structural model, that the broken bonds introduced by disruption of the $(As_4Se_6)_n$ matrix result in the creation of localized centres which are energetically intermediate between the valence band mobility edge and the traps at 0·62 eV which appear to limit the mobility at the most ordered composition.

It is possible to further clarify the distribution of localized levels above the valence band, by taking the present data in conjunction with other measurements and information from the literature. Of particular relevance is the study of hole carrier drift mobility in vitreous arsenic selenide by Marshall and Owen (1971). The measurements obtained by Marshall and Owen differ from those in the present case in several important respects. Firstly, the specimens employed were appreciably thinner than those used here, being in the range 1 to 5 μm thick. Secondly, because of experimental limitations arising mainly from the high capacitance of such thin layers, it was necessary

to derive data from transit pulses which were of an integrated form compared to those in fig. 1 (*a*). Thirdly, a transit ' break point ' was not detectable in this mode of measurement, and considerations arising from an analysis of the shape and height of transit pulse led to the conclusion that measurements should be made over time intervals not exceeding 100 μsec. The analysis suggested that at longer time intervals the carriers begin to interact with deeper traps than those dominating at times below 100 μsec. Finally, the data obtained suggested the existence of a set of trapping centres at energy 0·43 eV above the valence band mobility edge.

These results are not in conflict with those of the present investigation, but rather identify two separate sets of trapping centres with which the hole carriers are in equilibrium over different time intervals. Further evidence of this and of the existence of a number of distinct sets of hole trapping centres in disordered As_2Se_3 is provided by noise and transient photoconductivity measurements (Marshall, Main and Owen 1972), which yield data of the type shown in fig. 7. It can be seen that there are (at least) three distinct time regimes

Fig. 7

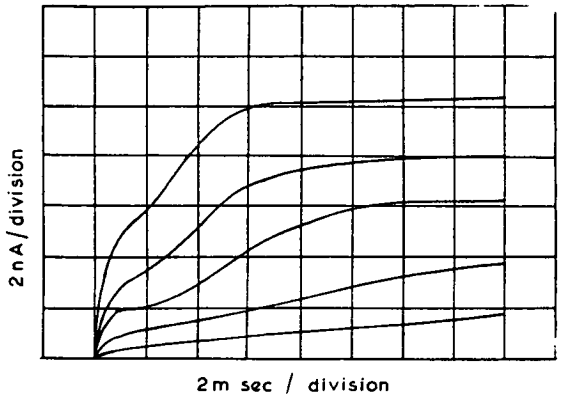

Transient rise of the photocurrent in As_2Se_3 (after Main 1973).

in this response, with time constants at room temperature of approximately 3 μsec, 125 μsec and 7 msec, although the shortest of these is not resolved in the transient photoresponse pulse shown. Main (1973) has shown that the carrier drift mobility associated with the ($3 \leqslant t \leqslant 125$ μsec) regime of the photoconductivity transient rise has an activation energy of 0·44 eV, whilst the mobility associated with the (125 μsec $\leqslant t \leqslant 7$ msec) regime possesses an activation energy of 0·65 eV, figures which compare well with the 0·43 eV activation energy measured by Marshall and Owen (1971) and the 0·62 eV activation energy measured at longer times in the present investigation. Measurements of thermally stimulated current by Street and Yoffe (1972) have identified trapping centres at a depth of 0·40 eV, whilst related depolarization experiments Kolomiets, Ljubin and Averjanov (1970) have resolved both these and centres at 0·30 eV.

The above evidence suggests therefore the existence of various distinct sets of traps, and the behaviour can be understood in terms of the achievement of quasi-equilibrium with progressively deeper-lying traps as a function of time.

It must be recognized that the achievement of quasi-equilibrium requires that the charge transit time in the drift-mobility measurement should be somewhat greater than the relevant trapping and realease time. The question arises therefore, whether it is possible to establish quasi-equilibrium, with traps of the depth suggested here, within the experiment transit times? First it may be noted that the activation energies given in fig. 2 (*a*), and the derived trap depths illustrated in fig. 8, are zero-field values. The mobility (and conductivity)

Fig. 8

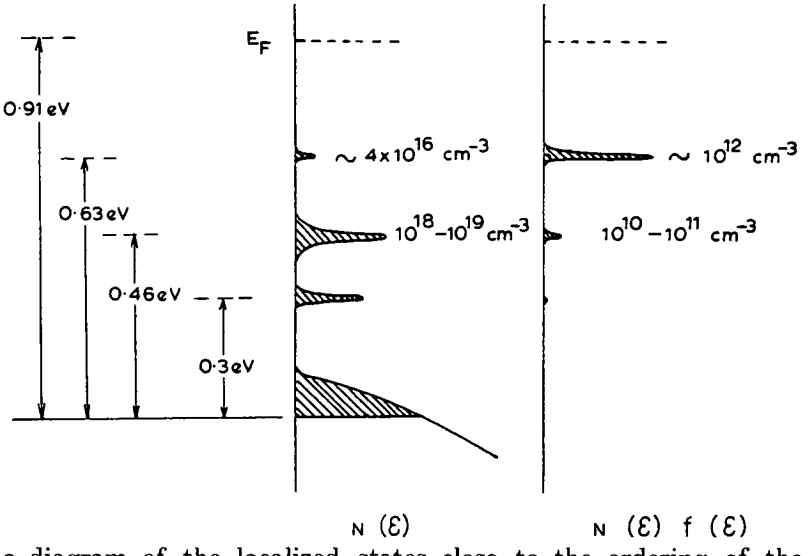

Schematic diagram of the localized states close to the ordering of the (As_4Se_6) matrix. The energies quoted are zero-field values (see the text).

is field-dependent and although the mechanism is not understood (see § 3 and, for example, Marshall and Miller 1973) the consequence is that the *effective* activation energy *decreases* with field. In the sample of fig. 3, for instance, the activation energy for mobility at the *lowest* experimental field ($\sim 10^5$ V cm^{-1}) is 0·54 eV compared with the zero-field value of 0·58 eV (as plotted in fig. 2 (*a*)). At the highest field used in the present measurements ($\sim 3 \times 10^5$ V cm^{-1}) the activation energy has decreased to 0·45 eV. In considering the trap release rate, for example, it is the effective activation energy at the field in question which is relevant. The experimental transit times at the lowest practical fields ($\sim 10^5$ V cm^{-1}) were approximately 0·5 msec and according to the computer simulation of hole transit pulses reported by Marshall and Owen (1971) a relatively well-defined average transit time is apparent after as few as three to four trapping and release events. Use of the higher figure implies that the trap release time $\tau_r \leqslant 0{\cdot}1$ msec. An independent indication that the release time is indeed of this magnitude is found by combining the present data with Main's (1973) analysis of the transient photoconductive response. According to the latter, the trapping time τ_t for excess holes in amorphous As_2Se_3 is approximately 4×10^{-10} sec and hence, as

$$(\mu_d/\mu_0) \approx (\tau_t/\tau_r),$$

a measured μ_d of 10^{-5}–10^{-4} cm^2 V^{-1} sec^{-1} with μ_0 in the range 1–10 cm^2 V^{-1}

sec^{-1}, implies that the release time τ_r is of the order 0·1 msec or less. Writing, in simplest terms, $\tau_r = \nu^{-1} \exp(\epsilon_t/kT)$ and taking the sample of fig. 3 for which at 10^5 V cm^{-1} (the lowest field used) $\epsilon_t = 0{\cdot}54$ eV requires, with $T \sim 300$ K, that the ' attempt-to-escape frequency ' $\nu \sim 10^{13}$ sec^{-1}. The Raman spectra of glassy As_2Se_3 reported by Ward (1972) shows that the maximum in the phonon spectrum occurs at 8×10^{12} sec^{-1}, corresponding to a phonon energy of 0·031 eV. Hence $\nu \sim 10^{13}$ sec^{-1} is reasonable, but looked at in this way the trapping and release transitions are clearly multiphonon processes, involving 10–20 phonons. A more rigorous discussion of the problem is not possible at the present time as their is no theory available for multiphonon release processes in amorphous materials. The theoretical work of Englman and Jortner (1970) on radiationless transitions in large molecules has been invoked (e.g. see Mott, Davis and Street 1975) and it is possible to estimate a release rate of the right order of magnitude from their theoretical formulae. It is not profitable, for several reasons, however, to pursue this approach at the moment. The most favourable assumptions have to be made, crude estimates of important variables must be accepted and, in any case, it seems unlikely that the Englman–Jortner theory is strictly applicable. In the first place, it deals with direct transitions whereas in the present case indirect transitions via intermediate states are almost certainly involved. Secondly, and perhaps more important, the Englman–Jortner theory considers transitions between two discrete energy levels, in contrast to the situation of interest here where one of the ' levels ' is a continuum (the valence band). Thus, it is not possible to make a realistic estimate of the multiphonon trap release rate appropriate to the present situation. In concluding these remarks, however, it is relevant to note that using the concept of a capture cross-section (σ) and applying ' detailed balance ' (e.g. see Lampert and Mark 1970), the attempt-to-escape-frequency of 10^{13} sec^{-1} implies, with $N_v \sim 10^{20}$–10^{21} cm^{-3} (see the table), a capture cross-section in the range 10^{-14}–10^{-15} cm^2. This is a large value but, as Lax (1960) points out, is reasonable for deep (attractive) centres where, as in the present case, the transition is likely to occur via intermediate levels. Moreover, from his transient photoconductivity data on amorphous As_2Se_3, Main (1973) obtains $\sigma \sim 2 \times 10^{-15}$ cm^2 for traps at about the same energy as those under discussion. Once again, therefore, there is order-of-magnitude agreement with an independent experiment, but the mechanism of release from the traps remains an unresolved problem.

It is also clear from the data presented that extreme caution is necessary in performing transit time measurements in this type of material. For instance, a comparison of measurements in specimens of sufficiently different thicknesses at the same value of applied field might well be taken to imply a thickness-dependent mobility, whereas this effect would in fact be an artefact caused by a transition to a longer time regime in the thicker films. Such an effect may account for the behaviour reported by Pai and Scharfe (1972) in amorphous As_2Se_3. It should be noted that Scher (1974) assumes that transport occurs by a hopping process and he invokes a statistical distribution of transit times to account for both the field-and apparent thickness-dependence of the drift mobility (the latter as observed by Pai and Scharfe (1972)). Scher's approach, however, does not appear to predict the widely reported field dependence of conductivity which often parallels that of the mobility (for further references see Marshall

and Miller (1973)). Pai and Scharfe's (1972) results are, rather surprisingly, exceptional in this respect in *not* showing a field-dependent conductivity.

Following the above arguments, it is proposed that the transport of holes in glasses close to the most ' well-ordered ' composition is controlled by the localized states shown in fig. 8. The present evidence is inconclusive as to whether the most well-ordered composition is exactly at stoichiometry or not. It must also be stressed that the centres shown represent only those identified by the transport measurements discussed above, and that other localized levels almost certainly exist both close to the mobility edge (as in the tail of states included in the diagram) and closer to the Fermi level (particularly since field-effect measurements suggest that very little movement of the Fermi energy can be achieved). In addition, it is to be expected that localized levels also occur above the Fermi level and control the transport of electron carriers. The effect on the hole drift mobility of increasing compositional disorder, illustrated in figs. 2 and 5, may then be qualitatively envisaged in terms of the broadening of the fairly discrete distributions of fig. 8. Due to the much greater density of the shallow (0·45 eV) states, these will quickly mask the 0·63 eV level. The maximum in the density of occupied traps will move closer to the valence band, accompanied by a progressive increase of the calculated trap density, as observed. There may, of course, also be an increase in the total density of traps due to disruption of the $(As_4Se_6)_n$ matrix.

Finally, some further comment may be appropriate on the possible origins of the centres present in glasses close to As_2Se_3 stoichiometry. The results discussed above have identified centres at energies 0·3, 0·45 and 0·63 eV (approximately) above the valence band mobility edge. It is relevant to note that measurements on *crystalline* As_2Se_3 by Kolomiets (1968) have indicated sets of traps at energies 0·49, 0·58 and 0·72 eV above the valence band edge. These traps correspond roughly with those in the glass provided allowance is made, proportionally, for the difference in optical energy gap of the crystal and glass (2·1 and 1·9 eV respectively). This suggests that the localized states in the vitreous material may be closely related to defect states in the crystal, as might be expected from the ' extended matrix ' model outlined above. If this is so, it should be possible to identify the origins of states in the glass by careful examination of suitably doped crystals, and investigations on these lines have recently been initiated.

Acknowledgment

The authors are grateful to Mr. J. McNeil for technical assistance with the experimental work described in this paper.

References

Apling, A. J., 1974, *Electronic and Structural Properties of Amorphous Semiconductors*, edited by P. G. Le Comber and J. Mort (Academic Press), p. 243.
Callaerts, R., Nagels, P., and Denayer, M., 1972, *Physics Lett.*, **38**A, 15.
Cohen, M. H., Fritzsche, H., and Ovshinsky, S. R., 1969, *Phys. Rev. Lett.*, **22**, 1065.
Edmond, J. T., 1968, *J. Non-crystalline Solids*, **1**, 39.
Englman, R., and Jortner, J., 1970, *Molec. Phys.*, **18**, 145.
Fritzsche, H., 1971, *Solid State Communs.*, **9**, 1813.

HURST, C. H., and DAVIS, E. A., 1974, *Amorphous and Liquid Semiconductors*, Vol. 1, edited by J. Stuke and W. Brenig (London: Taylor & Francis Ltd), p. 349.

KOLOMIETS, B. T., 1968, *Proc. 9th Int. Conf. on the Physics of Semiconductors*, Vol. 2 (Leningrad: Acad. Sci. U.S.S.R.—" Nauka "), p. 1259.

KOLOMIETS, B. T., LJUBIN, V. M., and AVERJANOV, V. L., 1970, *Mater. Res. Bull.*, **5**, 655.

LAMPERT, M. A., and MARK, P., 1970, *Current Injection in Solids* (Academic Press), p. 146 *et seq.*

LAX, M., 1960, *Phys. Rev.*, **119**, 1502.

LUCOVSKY, G., 1972, *Phys. Rev.*, **136**, 1480.

MAIN, C., 1973, Ph.D. Thesis, University of Edinburgh.

MARSHALL, J. M., FISHER, F. D., and OWEN, A. E., 1974 a, *Phys. Stat. Sol.* (a), **25**, 419; 1974 b, *Amorphous and Liquid Semiconductors*, Vol. 2, edited by J. Stuke and W. Brenig (London: Taylor & Francis Ltd), p. 1305.

MARSHALL, J. M., MAIN, C., and OWEN, A. E., 1972, *J. Non-crystalline Solids*, **8–10**, 760.

MARSHALL, J. M., and MILLER, G. R., *Phil. Mag.*, **27**, 1151.

MARSHALL, J. M., and OWEN, A. E., 1971, *Phil. Mag.*, **24**, 1281; 1972, *Phys. Stat. Sol.* (a), **12**, 181.

MOTT, N. F., and DAVIS, E. A., 1971, *Electronic Processes in Non-crystalline Materials* (Clarendon Press).

MOTT, N. F., DAVIES, E. A., and STREET, R. A., 1975, *Phil. Mag.*, **32**, 961.

MYERS, M. B., and FELTY, E. J., 1967, *Mater. Res. Bull.*, **2**, 535.

PAI, D. M., and SCHARFE, M. E., 1972, *J. Non-crystalline Solids*, **8–10**, 752.

PETURSSON, J., OWEN, A. E., and MARSHALL, J. M., 1975 (private communication).

ROSE, A., 1951, *R.C.A. Rev.*, **12**, 362.

SCHER, H., 1974, *Amorphous and Liquid Semiconductors*, Vol. 1, edited by J. Stuke and W. Brenig (London: Taylor & Francis Ltd), p. 135.

SCHOTTMILLER, J., TABAK, M., LUCOVSKY, G., and WARD, A., 1970, *J. Non-crystalline Solids*, **4**, 80.

SOUTH, R. B., and OWEN, A. E., 1974, *Amorphous and Liquid Semiconductors*, Vol. 1, edited by J. Stuke and W. Brenig (London: Taylor & Francis Ltd), p. 305.

SPEAR, W. E., 1968, *J. Non-crystalline Solids*, **1**, 197.

STREET, R. A., and YOFFE, A. D., 1972, *Thin Solid Films*, **11**, 161.

WARD, A. T., 1972, *Adv. Chem.*, No. 110, 163.

ZALLEN, R., DREWS, R. E., EMERALD, R. L., and SLADE, M. L., 1971, *Phys. Rev. Letts.*, **26**, 1564.

Electronic properties and localised states in amorphous semiconductors

A. E. Owen

Department of Electrical Engineering, University of Edinburgh

W. E. Spear

Carnegie Laboratory of Physics, University of Dundee

Recent experiments which probe the localised state distribution of amorphous semiconductors are reviewed using as examples two types of material, chalcogenide glasses in the Se–As system and amorphous silicon. The experimental evidence is drawn mainly from studies of carrier mobilities, photoconductivity, luminescence spectra, and the field effect. For both types the data are consistent with the presence of relatively well defined features in the localised state distribution which are probably largely determined by specific defect structures rather than by the lack of long range order. It seems very likely that this conclusion is generally true of amorphous semiconductors.

In this article we review a particular aspect of amorphous semiconductors (a-semiconductors) in which significant progress has been made in recent years, namely the close and often critical dependence of the electronic properties of these materials on the distribution of localised states. Although the connection between these two basic aspects had long been realised, it is only in the last few years that sufficient quantitative information on the density of state distribution has emerged and made it possible to explore the subject in greater detail. The most extensive data have come from field effect measurements, particularly in a-Si where the distribution of localised states has now been determined throughout most of the mobility gap. For many other materials relevant information has been obtained from the interpretation of drift mobility, photoconductivity, and luminescence results.

Most of the research on amorphous solids has been carried out on two main groups, the chalcogenide glasses and the tetrahedrally bonded semiconductors. We shall therefore confine the following to a discussion of typical examples from each group, the Se–As system representing the first and a-Si the second, preceded by a general introduction to electronic transport, localisation, and the density of state distribution in amorphous solids. Finally, some recent ideas on the nature of the defect states in both groups will briefly be discussed.

Electronic transport in amorphous solids

Two conduction mechanisms are generally observed in amorphous materials. For the purpose of discussion, consider the schematic density of state distribution shown in Figure 1(a) in which $N(E)$ denotes the number of states per unit volume in unit energy interval and is plotted here against the electron energy, E. The energy spectrum can be divided according to the electronic character of the states into extended states, *ES*, band tail states, *T*, and gap states, *G*. The last two, shown shaded in Figure 1(a), are localised states, and this important concept will be discussed later.

First consider the conduction in the extended states, that is for electrons at energies just above E_c and

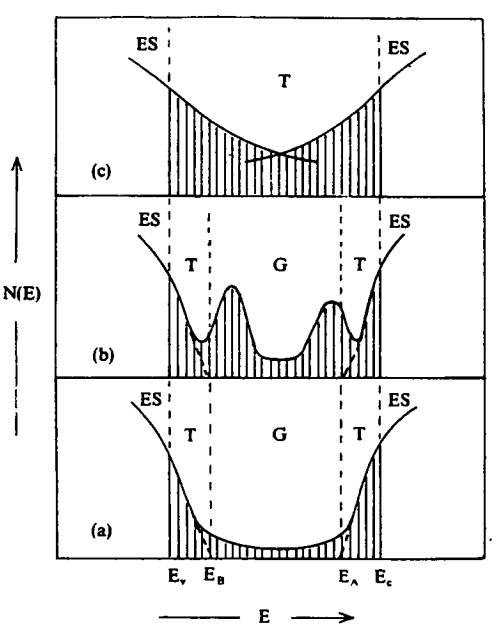

Figure 1. *Schematic density of states diagrams for a semiconducting glass*
(a) an "ideal" glass
(b) a glass with defect states
(c) the Cohen–Fritzsche–Ovshinsky model[5]

for holes just below E_v. In these regions the effects of random potentials and of fluctuations in the interatomic distances begin to dominate the transport. In the case of electrons, the mean free path just above E_c and the coherence length of the electrons wave functions approach the interatomic separation, so that one can no longer regard transport just above E_c as band motion with occasional scattering. Cohen[1] pointed out that in this borderline region conduction is essentially a diffusive process, quite similar to Brownian Motion. The electron can be envisaged as jumping from site to site with an atomic frequency ν_{el}, but without any thermal activation. Adopting this classical picture one obtains the relation

$$\mu \approx (1/6)[ea^2/kT]\nu_{el} \quad (1)$$

where a is the average interatomic distance and ν_{el} is an electronic frequency of the order of $10^{15}\,s^{-1}$. The estimated drift mobility is about $10\,cm^2\,V^{-1}\,s^{-1}$. A more exact analysis of the transport just above E_c is based on the so-called random phase model[2] in which the extended wave functions are represented as a linear combination of atomic wave functions which have no phase relation from one site to the next. This leads to

$$\mu = [\pi e a^2 z J^2 N_c(E)]/hkT \quad (2)$$

where J is an electronic transfer integral between nearest neighbours, z is the coordination number, and $N_c(E)$ is the effective density of states just above E_c. Evaluation with $a=3$ Å, $z=4$, $J=1$ eV, $T=300$ K, and $N_c(E)=10^{21}\,eV^{-1}\,cm^{-3}$ gives a mobility of $7\,cm^2\,V^{-1}\,s^{-1}$ but this is to be regarded as the maximum plausible value for conduction in extended states by the diffusive process. It will be considerably lower if, for example, the density of states is lower than the assumed value. Cohen[1] regards $10^{-2}\,cm^2\,V^{-1}\,s^{-1}$ as a lower limit for the diffusive mobility in extended states.

Below the energy E_c localisation sets in. This fairly sudden transition is of fundamental importance in the theory of the noncrystalline state. Mott[3] in his extensive work on this problem regards the Anderson localisation theorem as the key to our understanding of electronic behaviour in amorphous solids. Anderson[4] originally considered a three dimensional, crystalline array of potential wells, each associated with a single bound s-state. In accordance with the tight-binding approximation used in the calculation, the width of the band, B, formed by the interaction of nearest neighbour states is proportional to the overlap integral. The essential point of the model is that the site energies are distributed in a random way over a range U_0. Anderson showed that with increasing U_0 the ratio U_0/B approaches a critical value at which an electron placed on a given well at $T=0$ will no longer diffuse away and thus become localised. It is assumed that this critical condition is reached at the energy E_c. The band tail states below E_c are then localised in the sense that the average over these states of a relevant physical quantity, such as the electrical conductivity, vanishes in a rigid lattice. The importance of the Anderson theorem lies in the fact that it provides a physical basis for localisation in the presence of an appreciable wave function overlap.

The second transport mechanism is hopping conduction through the localised state distribution consisting of tail and gap states, which can take place only with phonon assistance. The mobility, $\mu(E)$, for this thermally activated hopping transport at an energy E is normally written in the form

$$\mu(E) \simeq [eR^2(E)/kT]\nu_{ph} \exp(-2\alpha R) \exp(-W/kT) \quad (3)$$

where R is the average hopping distance, which depends on the density of state distribution and is thus a function of energy, the term $\exp(-2\alpha R)$ describes the overlap of the wave functions on neighbouring hopping sites, with the parameter α representing the spatial decay of a localised wave function, and $\nu_{ph}\exp(-W/kT)$ represents the probability per second that the localised electron hops to a new site, at an energy W above the original one. Equation (3) predicts hopping mobilities at room temperature of $10^{-2}\,cm^2\,V^{-1}\,s^{-1}$ or less, which means that near E_c and E_v the mobility drops by something like three orders of magnitude. This defines the so called mobility gap which has become an important concept in the field of noncrystalline solids. Evidently, in addition to extended state conduction, there are many current paths through the localised states all of which can contribute to the observed electric properties. It is likely that one of these will predominate at a given temperature and we shall see that this helps considerably in the interpretation of the electrical measurements. A particular case is the so called variable range hopping mechanism which sets in at very low temperatures where it can become energetically more favourable for a carrier to hop beyond the nearest neighbour sites in order to find a final site close in energy ($\cong kT$) to its initial sites. Thus conduction occurs near the Fermi energy, E_F, and Mott[3b,d] has shown that for three dimensional hopping with a density of states, $N(E_F)$, the conductivity is given by

$$\sigma = \sigma_0 \exp(-T_0/T)^{\frac{1}{4}} \quad (4)$$

with $T_0 \approx 18[\alpha/kN(E_F)]$.

Localised states in amorphous solids

Figure 1(a) illustrates a somewhat "idealised" distribution of localised states which is not necessarily representative of real amorphous solids. In the elemental and compound materials it has been estimated[3c] that the extent of the tail states (E_c–E_A or E_B–E_v) is about 0·1–0·2 eV, approximately equal to the magnitude of the disorder potential. In the case of a-Si this is supported by the directly measured distribution shown in Figure 11. On the other hand, the deeper lying gap states in the above materials are determined not by the disorder but by structural defects in the random network, such as broken or dangling bonds, vacancies, nonbridging atoms, or chain ends. It is likely that such defects are reasonably

well defined within the range of the existing short range order; one would therefore expect that the energy levels associated with defect centres should lead to recognisable features in $N(E)$.

Figure 1(b) shows a more realistic gap state distribution. It is applicable to a-Si (Figure 11) and could in general outline represent $N(E)$ in other elemental and also compound amorphous materials. The main point is that the gap state spectrum now shows a broadened "structure" associated with the defects in the random network. The charge distribution in the defect states largely determines the position of the Fermi level, so that the defect structure has an important bearing on the electronic properties of the material.

A basically different model, shown in Figure 1(c), has been proposed by Cohen, Fritzsche and Ovshinsky[5] (C-F-O). Here it is assumed that the valence and conduction band tails extend throughout the mobility gap in a featureless distribution. Overlap of these states occurs near the centre of the gap, pinning the Fermi level. For some years the C-F-O model was often regarded as characteristic of amorphous semiconductors although its authors did point out[5] that their model was specifically proposed for the complex alloys of four or five components often used in switching devies (e.g. the so called STAG glass, $As_{30}Te_{48}Si_{12}Ge_{10}$). In complex materials of this sort there is compositional as well as structural disorder and the connectivity of the covalent network may change randomly at each site depending on the (varying) valence of the atom occupying the site; intuitively one would expect both factors to broaden and deepen the tails of states from both bands, perhaps to the extent that they spread right across the gap and overlap.

It will be evident from the following sections that a distribution such as that shown in Figure 1(b), with a reasonably well defined defect structure, is the most likely both in elemental and compound amorphous semiconductors. There is also some evidence that such a model may be applicable to simple two component amorphous alloys and possibly also to more complex systems.

Chalcogenide glasses in the Se–As system

Glasses in the Se–As system may readily be prepared by quenching techniques with from 0 to nearly 60 at % As, a range which embraces the compound As_2Se_3. These materials have important applications in electrophotography, and the electrical and optical properties of many compositions in the glass-forming range have been investigated in detail. Of particular relevance so far as the problem of localised states is concerned are measurements of carrier mobilities by time-of-flight techniques, steady state and transient photoconductivity studies, and luminescence spectra. In the following, we will first of all consider selenium and glasses in the Se–As system with up to about 10 at % As, utilising mainly the results of carrier mobility by direct transit time measurements. Discussion of the compound As_2Se_3, largely on the basis of photoconductivity studies, will follow and the section will conclude with a brief consideration of luminescence in chalcogenide glasses.

Carrier mobility measurements and localised states

In contrast to most other systems, it is possible in glasses of low As content (0–2%), to measure both the electron and hole mobilities by transit time techniques. At higher As concentrations the electron mobility can be measured up to 10% As and hole transport in the range 30–50% As (which includes the compound As_2Se_3).

Before considering the results it is necessary to describe, briefly, the basic principle of the experimental technique used to measure the relatively low mobilities often observed in materials of high resistivity. The sample is in the form of a film or platelet with metal electrodes on opposite surfaces. One surface is exposed to an appropriate source of excitation, such as a pulse of highly absorbed light ($h\nu >$ optical gap) or a pulse of energetic electrons (several keV). Excess electrons and holes are created and it is assumed that they are formed in a surface layer of thickness, δ, which is much less than the sample thickness, d. Depending on the polarity of the applied field, either electrons or holes drift through the sample, and the resulting charge displacement is usually displayed directly on an oscilloscope. If the circuit time constant is greater than the transit time, $CR \gg \tau_t$, then an integrated pulse representing the charge displaced around the circuit is observed. On the other hand, if $CR \ll \tau_t$, a current pulse, I, is displayed. Once the transit time has been measured the drift mobility is obtained from $\mu = d/F\tau_t$ where d is the sample thickness and F is the applied field. In some cases the carriers drift through the sample without significant deep trapping and a well defined transit time can be observed. Appreciable trapping will reduce the number of drifting carriers during the transit and may also cause significant broadening or "dispersion" of the transit pulse. It is then much more difficult to identify a transit time unambiguously and in some of the materials of interest the analysis of the pulse shape, or the degree of "dispersion", is an important factor in the interpretation. The basic technique of carrier transit time measurements was first applied to an amorphous solid in 1957 and since then has been used and developed considerably.[6]

It is convenient to consider the experimental results by progressing from pure selenium to As–Se glasses with up to ~10% As and, finally, to the stoichiometric compound As_2Se_3 which is representative of glasses in the composition range 30–50% As.

Pure selenium

Both the electron and hole drift mobilities can be measured in amorphous selenium by the technique outlined above, and at temperatures above about 200 K, at any rate, a well defined transit time is observed.

At least nine different groups have investigated the

carrier mobilities in amorphous Se:[6–14] their data are summarised in Table 1 (entries 1–9) and typical results are shown in Figure 2. Below about 270 K an activated mobility is observed in all cases, i.e.

$$\mu = \mu_0' \exp(-E/kT) \qquad (5)$$

where μ, μ_0', and E refer to electrons or holes as the case may be. At temperatures in the region of 200 K and above, the slopes decrease and both electron and hole mobilities tend to a limiting value. Note, however, the good agreement between the various results, particularly for the electron mobility, μ_e, and its activation energy, E_e. There is some variation in the activation energy for hole mobility, E_h, with the results tending to fall into two groups, either ~0·14–0·16 eV or ~0·23–0·30 eV. There is no doubt that the discrepancy is due to the different ranges of temperature measurement. The smaller values were obtained from earlier experiments limited to temperatures above ~230 K, and in this region the slope is decreasing with $1/T$ because of the approach of μ_h to its saturation value (Figure 2). More recent measurements[9–14] down to temperatures of 200 K or less seem to agree on a higher value for E_h in the range 0·26 – 0·30 eV. Note also, in Figure 2 the field dependence of both electron and hole mobilities which becomes increasingly apparent as the temperature is reduced. This is a manifestation of the general field dependence of mobility and conductivity observed in chalcogenide glasses.[14] It means that the activation energies are slightly field dependent and the values quoted in entry 9 of Table 1 correspond to extrapolated "zero field" figures. There is therefore general agreement about the experimental data.

There are two possible interpretations of these results. Firstly, they could be described by Equation (3) for thermally activated hopping transport. It should be noted, however, that small polaron theory also leads formally to a similar expression for the conduction of a self-trapped electron so that it would be difficult to distinguish between these two types of hopping transport on the basis of mobility measurements alone. Secondly, the results could be interpreted in terms of a trap-limited mobility in which the observed activation energy corresponds to the energy difference between a predominant level of shallow localised states (traps) and the appropriate mobility edge.

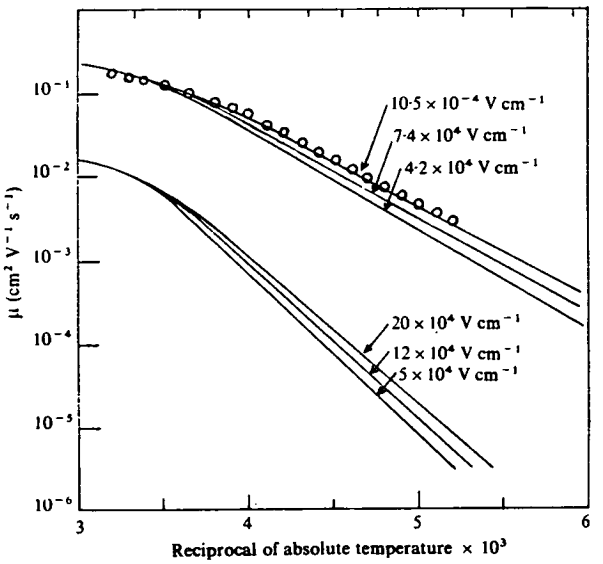

Figure 2. *The electron and hole drift mobilities in amorphous Se as functions of temperature with electric field as a parameter. The upper curves show the hole mobility μ_h (O O O References 6 and 13, —Reference 14a) and the lower curves the electron mobility*[14b]

Table 1. *Electron and hole mobilities in amorphous selenium and As–Se alloys with up to ~10 at% As.*

	Arsenic (%)	μ_e(300 K) ($cm^2 V^{-1} s^{-1}$)	E_e (eV)	Electron lifetime (μs)	μ_h(300 K) ($cm^2 V^{-1} s^{-1}$)	E_h (eV)	Hole lifetime (μs)	Notes
1	0	$5{\cdot}2 \times 10^{-3}$	0·285		$1{\cdot}35 \times 10^{-1}$	0·14		Spear[6]
2	0	6×10^{-3}	0·285	25	$1{\cdot}5 \times 10^{-1}$	0·14	0·15	Hartke[7]
3	0	$6{\cdot}5 \times 10^{-3}$	0·29	10	$1{\cdot}2 \times 10^{-1}$	0·13	0·13	Kolomiets & Lebedev[8a]
4	0	$4{\cdot}5 \times 10^{-3}$	0·287		$1{\cdot}1 \times 10^{-1}$	0·20		Grunwald & Blakney.[9a] Several evaporated Se films measured, prepared on substrates at varying temperatures (25–58°C); figures quoted correspond to limiting values
	↓	↓	↓		↓	↓		
	0	$5{\cdot}8 \times 10^{-3}$	0·332		$1{\cdot}2 \times 10^{-1}$	0·247		
5	0	—	—		$1{\cdot}9 \times 10^{-1}$	0·30		Juska *et al.*[10]
6	0	3×10^{-3}	0·32		$1{\cdot}6 \times 10^{-1}$	0·26		Dolezalek & Spear.[11] Pressure dependence looked for but not observed
7	0	$6. \times 10^{-3}$	0·33	50	$1{\cdot}4 \times 10^{-1}$	0·16	10→50	Schottmiller *et al.*[12]
8	0	—	—		$1{\cdot}6 \times 10^{-1}$	0·23		Tabak[13]
9	0	6×10^{-3}	0·33		$1{\cdot}1 \times 10^{-1}$	0·28		Marshall *et al.*[14] Measurements on glassy Se. Quoted activation energies correspond to low temperatures (< 250 K) and "zero" field
10	0·5	2×10^{-3}	0·28	—	$1{\cdot}2 \times 10^{-1}$	0·14		Hartke[7]
11	0·5	3×10^{-3}	0·28	10	—	—	—	Kolomiets & Lebedev[8a]
12	0·5	$2{\cdot}6 \times 10^{-3}$	0·33	40	$1{\cdot}4 \times 10^{-1}$	—	<0·3	Schottmiller *et al.*[12]
13	1	$1{\cdot}5 \times 10^{-3}$	0·35	—	—	—	—	Marshall *et al.*[14b]
14	2	6×10^{-4}	0·28	—	$1{\cdot}1 \times 10^{-1}$	0·15	—	Hartke[7]
15	2	5×10^{-4}	0·28	35	—	—	—	Kolomiets & Lebedev[8a]
16	2	$7{\cdot}8 \times 10^{-4}$	0·33	200	—	—	<0·3	Schottmiller *et al.*[12]
17	3	2×10^{-4}	—	750	—	—	—	Schottmiller *et al.*[12]
18	3	$6{\cdot}5 \times 10^{-4}$	0·37	—	—	—	—	Marshall *et al.*[14b]
19	5	3×10^{-4}	0·42	—	—	—	—	Marshall *et al.*[14b]
20	6	5×10^{-5}	—	—	—	—	—	Kolomiets & Lebedev[8a]
21	6·6	$5{\cdot}4 \times 10^{-5}$	—	2000	—	—	—	Schottmiller *et al.*[12]
22	8	$1{\cdot}3 \times 10^{-4}$	0·44	—	—	—	—	Marshall *et al.*[14b]
23	9	1×10^{-5}	—	—	—	—	—	Schottmiller *et al.*[12]

The first alternative does not seem likely, particularly for hole transport. The constant μ_0' of Equation (5) can be estimated from Equation (3) and using typical values of ν, R, and α the result is $\mu_0' \sim 10^{-3}$–10^{-2} cm^2 V^{-1} s^{-1}. With these values, the predicted mobility in the temperature range covered in Figure 2 would be orders of magnitude lower than actually observed. Or, put in another way, the μ_0' values for both electrons and holes in selenium, obtained by extrapolation of the experimental results (Figure 2), are 10^{+3} cm^2 V^{-1} s^{-1}. Pfister,[15] however, has recently presented brief and qualitative arguments to suggest that hopping transport might be expected to show a tendency to saturate towards a limiting value, as in Figure 2. On the other hand, the absence of pressure dependence, observed by Dolezalek & Spear[11] (entry 6 of Table 1) for both electron and hole mobilities, is a significant argument against hopping since transport by hopping mechanisms is expected to be sensitive to pressure, as has been shown in the case of orthorhombic sulphur for instance.[11]

In the case of trap-controlled transport, the other possible interpretation, the current is carried by excess electrons (or holes) in the extended states with a mobility μ_0. During their transit they interact through trapping and thermal release with shallow localised states and we shall assume for the moment that interaction takes place predominantly with a fairly well defined range of states lying, in the case of electrons, at an energy E_t below E_c. Because the measured values of τ_t include the total time an electron spends in traps during transit, the calculated drift mobility, μ, will generally be appreciably smaller than the mobility μ_0 in the extended states. If the electron distribution remains in quasi-thermal equilibrium during transit, it is easy to relate μ and μ_0. The result[6c] is

$$\mu = \mu_0[1 + (N_t/N_c)\exp(E_t/kT)]^{-1} \qquad (6)$$

where N_t is the density of localised states (traps) at E_t and N_c is the effective density of states at E_c. A similar equation can be written for hole transport. Assuming that μ_0 is determined by lattice scattering, and hence is proportional to $T^{-3/2}$, Grunwald & Blakney[9a] and Juska *et al.*[10] find good agreement between their results for hole mobility and Equation (6) over the whole temperature range covered, including the region where μ is tending to saturate, with μ_0 for holes between 0·3 and 0·4 cm^2 V^{-1} s^{-1} at room temperature. This mobility is, however, too low to be consistent with lattice scattering. On the other hand, Equation (2) for diffusive transport in extended states (with μ_0 varying approximately as T^{-1}), in conjunction with Equation (6), would not substantially affect the agreement with the experimental results.

Thus, the weight of the present evidence is that hole transport in amorphous selenium occurs by the trap-limited drifting of carriers in extended states. For electrons the situation is less certain. The experimental results of Figure 2 show that an expression like Equation (6) is still appropriate but they imply a μ_0 value of about 5×10^{-2} cm^2 V^{-1} s^{-1}. This is perhaps more indicative of hopping, either by thermally assisted tunnelling or polaron hopping, although Cohen[1] has suggested that values down to 10^{-2} cm^2 V^{-1} s^{-1} are consistent with the diffusive transport in extended states. The situation is a borderline one and it appears from the magnitude of the mobility that electron transport in amorphous selenium could occur by diffusive motion in extended states just above the mobility edge, or by hopping in states immediately below the edge, or by polaron hopping. The lack of any pressure dependence of either is, however, evidence against any form of hopping transport[11] and for the present, therefore, it is concluded that electron transport also takes place in extended states by the diffusive process.

In a disordered material like amorphous selenium there will certainly be a "tail" of localised states (traps) extending from both the conduction and valence bands. For a tail of localised states with a density decreasing linearly with energy and extending over a range of energy, ΔE, it is easy to show that the trap-limited mobility is given by (see p. 209 of Reference 16)

$$\mu = \mu_0\left(\frac{\Delta E}{kT}\right)\exp -(\Delta E/kT). \qquad (7)$$

Comparison of Equation (7) with the experimental data leads, however, to unacceptably high values for μ_0 (e.g. 3×10^3 cm^2 V^{-1} s^{-1} for holes and 200 cm^2 V^{-1} s^{-1} for electrons) and similar results are also obtained if other forms of dependence on energy are assumed for the concentration of localised states in the tail. Alternatively, the traps may be situated at relatively discrete energies below the conducting states. In that case, Equation (6) with $[(N_t/N_c)\exp(E_t/kT)] \gg 1$ gives

$$\mu = \mu_0\frac{N_c}{N_t}\exp -(E_t/kT) \qquad (8)$$

where N_c is the density of states for electrons. A similar expression applies for excess holes. Assuming that conduction takes place in extended states just above a mobility edge, then $N_c \sim 5 \times 10^{19}$ cm^{-3}.[16] Taking as an upper estimate, $\mu_{0(e)} \sim 10^{-1}$ cm^2 V^{-1} s^{-1} and $\mu_{0(h)} \sim 3 \times 10^{-1}$ cm^2 V^{-1} s^{-1} (from Grunwald & Blakney[9a]) comparison of Equation (8) with the experimental results gives $N_t = 5 \times 10^{15}$ cm^{-3} for electron traps and 5×10^{14} cm^{-3} for hole traps.

These figures seem reasonable and, therefore, trap-limited conduction involving traps at relatively well defined energy levels (in contrast to a broad "tail" of traps) offers the more consistent interpretation of the data. It is relevant to note, in this context, that Spear[17] has reported that in monoclinic crystalline selenium the electron and hole mobilities have activation energies of 0·25 and 0·3 eV, respectively; these figures are close to the values found in amorphous selenium (0·33 and 0·28 eV). Moreover, Spear[17] estimates the density of electron traps in monoclinic selenium as 10^{14} cm^{-3} suggesting that the traps have the same origin in both crystalline and amorphous forms but with a rather greater density in the latter, as would be intuitively expected. This apparent similarity between

carrier transport in the two forms would be difficult to account for on the basis of a model involving "tails" of localised states since in the amorphous form the "tail" would presumably be of much greater extent. Likewise, the observations of Grunwald & Blakney[9a] and Juska *et al.*[10] on the influence of substrate temperature on the carrier mobilities in amorphous selenium are not consistent with transport dominated by "tails" of states. In both cases they find that as the substrate temperature, and hence the degree of polymerisation, increases the trap densities decrease and the activation energies increase slightly. This is the opposite to what would be expected if the traps controlling the mobility were associated with tails of localised states induced by the presence of structural and/or compositional disorder.

The conclusion is, therefore, that electron and hole transport in amorphous selenium is determined by trapping in states at relatively discrete energies and the experimental data allow estimates to be made of the trap densities and their energies (measured from the conducting states). The picture which emerges for the electronic band structure of amorphous selenium is illustrated in Figure 3. The mobility gap has been taken as equal to the optical gap for amorphous selenium ($\sim$2·1 eV[16]) and it is assumed that carrier transport does in fact occur in extended states just beyond the mobility edges which are arbitrarily fixed at 0 eV (for holes) and 2·1 eV (for electrons). This certainly seems reasonable for holes as the hole mobility tends towards a limiting value (Figure 2) which is characteristic of diffusive motion in extended states just beyond a mobility edge.[1] For electrons the situation is perhaps less clear as the electron mobility is tending to saturate at about 10^{-2}–10^{-1} cm^2 V^{-1} s^{-1} (Figure 2), a value which is borderline between hopping and diffusion in extended states.[1] The conclusion that the electron mobility is trap-limited is probably valid but it is possible, in view of the borderline μ_0 value, that transport occurs by hopping in states very close to the mobility edge.

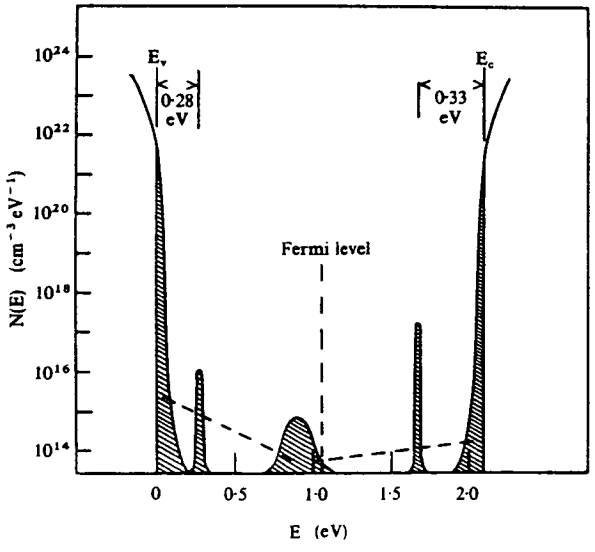

Figure 3. *The density of states distribution for amorphous Se*

Note in Figure 3 that the density axis is plotted in number per unit energy (cm^3 eV^{-1}). The two relatively sharp levels at 0·28 eV above the valence band mobility edge and 0·33 eV below the conduction band edge are obtained directly from the mobility data already discussed. Some "tailing" of states is to be expected in any amorphous material, of course, and tails of localised states of about 0·1 eV in extent have been drawn more or less arbitrarily, below the conduction band and above the valence band. It is worth noting, however, that Mott & Davis[16] (p. 47) have estimated that in elemental or simple compound amorphous materials the band tailing is less than 0·2 eV. The small peaked concentration of localised states around the Fermi level and the position of the Fermi level itself were obtained from the space charge limited current data of Hartke.[7] The dashed lines in Figure 3 indicate in a general way the possible background density of localised states extending right across the mobility gap and are taken from the analysis of photoconductivity data by Carles *et al.*[18]

As–Se glasses with up to 10 *at% As*

The effects of adding As to amorphous selenium are quite different for electron and hole transport.

Electron transport. The magnitude of the electron pulse in the transit time experiment decreases fairly smoothly with As concentration. The electron mobility, μ_e, decreases but remains measurable at least up to $\sim$10 at% As. In fact, as can be seen from entries 10–23 in Table 1, μ_e decreases approximately exponentially with As concentration while the activation energy, E_e, changes slowly at first and then increases approximately linearly.

Using the same arguments as before and applying Equation (8), it has been shown[14b] that the decrease in electron mobility with increasing As can be entirely accounted for by an increase in E_t (i.e. E_e) with N_t remaining constant at approximately 10^{15}–10^{16} cm^{-3}. Thus the effect of As can be interpreted as causing either

1. an increase in the energy separation of the conduction band, and hence of the electron mobility edge, relative to the electron traps, or vice versa, or
2. an increase in the extent of the tail of localised states and hence a shift of the electron mobility edge away from the electron traps.

The data cannot distinguish between these two possibilities but it is intuitively reasonable to suppose that as a second component (As) is added to amorphous selenium the "disorder" will increase (because there is then the possibility of compositional as well as structural disorder) with a concomitant increase in the tailing of localised states at the conduction band edge. Thus, for the present purposes, it is suggested that the effect of adding As is as depicted in Figure 4. Experiment shows that the density of electron traps remains essentially unchanged and it is postulated that their position (relative to the Fermi level) also remains unchanged. With increasing As, however, the extent of

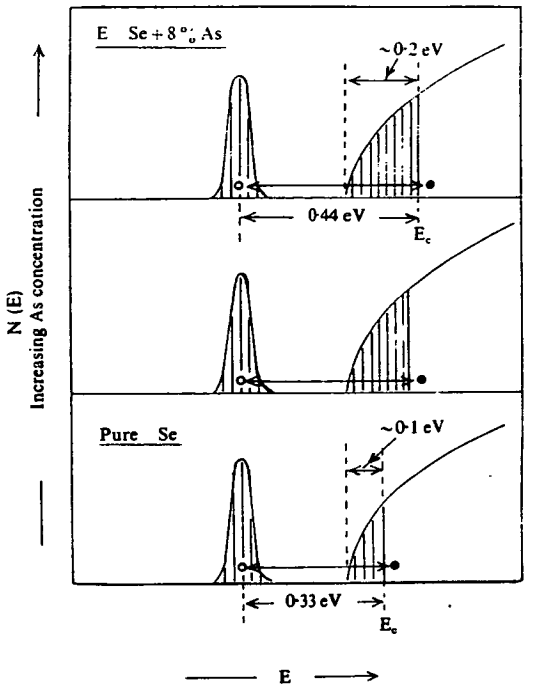

Figure 4. *A partial band model for the possible influence of As on the density of states diagram for Se. This model is deduced from electron mobility measurements and hence refers to the conduction band and states above the Fermi energy*

the tail of localised states increases and the mobility edge moves further into the conduction band. At the composition Se–8 at % As, for example, the trap depth relative to the electron mobility edge is 0·44 eV and it is postulated that the depth of the tail of localised states has increased to approximately 0·2 eV (Figure 4).

Hole transport. It is important to realise that the effect of As additions on the hole transport is qualitatively quite different. At arsenic concentrations of less than about 1 at % the hole transit pulses in the drift mobility experiment are well defined and the mobility remains essentially the same as in pure Se. The addition of 1–2 % As, however, causes the hole lifetime to decrease by as much as two orders of magnitude (see Table 1) and the hole response in the transit time experiment also decreases. In the region from 2 to approximately 6 % As, hole transit pulses are not observed at all but with more than about 6 % As a different behaviour is observed. After an initial fast response, still reminiscent of pure Se, and corresponding to the intial trapping of holes, there is a slowly varying signal with an effective transit time approximately 10^5 times longer than in pure Se at equivalent thicknesses and fields. The situation is summarised in Figure 5 for the composition range 0–22 % As, taken from Schottmiller *et al.*[12] The slowly varying response is typical of the signal observed in hole drift experiments in amorphous As_2Se_3 and is sometimes referred to, therefore, as the "As_2Se_3 tail" (see inset of Figure 5). This slowly varying response is an extreme example of the less well defined transit pulses mentioned in above. Note also, that there is no parallel growth of a slowly varying electron signal at higher As concentrations. According to all reported observations, the electron transit remains undetectable at concentrations greater than about 10 % As.

Unlike the electron case, therefore, the effect of As on hole transport cannot be explained by a gradual change in the depth of traps relative to conducting states. There is little doubt that the addition of As causes the formation of new hole traps at an energy deeper than those responsible for modulating the transport in pure Se. Arsenic enters the selenium network in threefold coordination forming ($AsSe_{3/2}$) groups. Schottmiller *et al.*[12] associated the fast hole response (inset of Figure 5) with the remaining Se network and the slow response with the ($AsSe_{3/2}$) groups. At low concentrations (0–~8 % As) they suggested that the latter are structurally isolated and act as deep traps, reducing the hole lifetime. At higher concentrations, however, a more or less continuous $(AsSe_{3/2})_n$ network begins to develop and the "As_2Se_3-type" transport is observed.

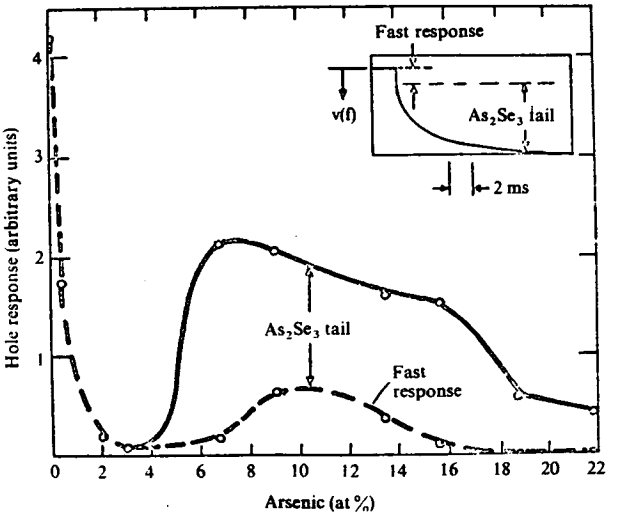

Figure 5. *The hole response in transit time measurements on Se–As glasses. The inset illustrates a typical pulse shape in integrated form*[12]

Arsenic selenide (As_2Se_3) glass

It is convenient to consider first the photoconductivity of vitreous As_2Se_3, and Figure 6 shows the results reported by Main & Owen[19] for the steady state photocurrent, ΔI_{ph}, as a function of reciprocal temperature at two different light intensities. Also shown for comparison is the dark current, I_d. The photoconductivity of several chalcogenide glasses has now been studied in some detail and the data of Figure 6 are typical.[20–23] There are two distinct regions in the results shown in Figure 6:

1. a region where the photocurrent increases with $1/T$, is much less than the dark current, and is proportional to the light intensity; i.e. it follows monomolecular kinetics

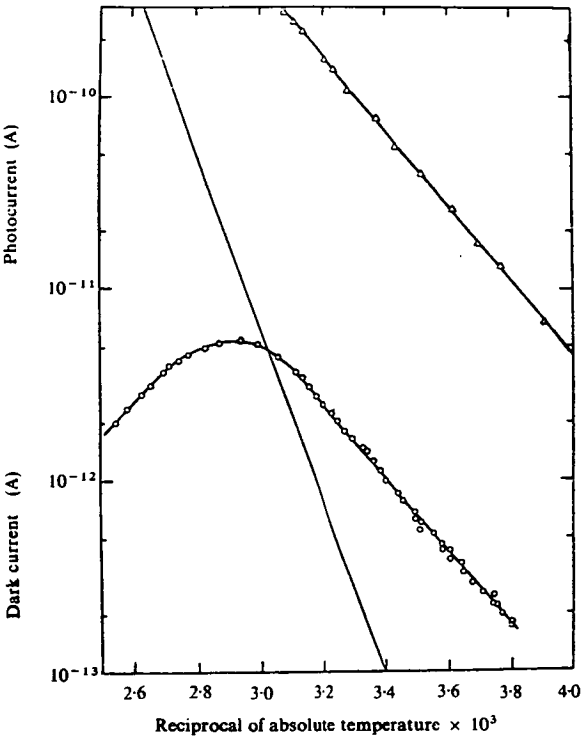

Figure 6. *The steady state photocurrent, ΔI_{ph}, as a function of temperature in amorphous As_2Se_3 at two different light intensities*

○ 5×10^{11} photons $cm^2\ s^{-1}$
Δ 10^{15} photons $cm^{-2}\ s^{-1}$
— dark current, I_d, shown for comparison

2. a region where the photocurrent decreases with $1/T$ and eventually becomes greater than the dark current. In this region ΔI_{ph} varies linearly with intensity at low intensities, but becomes proportional to (light intensity)$^{\frac{1}{2}}$ at high fluxes; i.e. it follows bimolecular kinetics.

In some cases a third region is observed, viz:

3. at low temperatures, where the photocurrent is much larger than the dark current and approaches a constant value; this region was not observed in the experiments leading to Figure 6 but it has been reported in As_2Se_3 by Bube *et al.*[22] although they do not show the actual data.

The interpretation of photoconductivity results depends on the model used to describe the processes of recombination of excess carriers. Main & Owen[19] have used a simple four-level model in which the states are situated at more or less discrete energies; this is illustrated in Figure 7, where E_c and E_v represent the mobility edges and $E_{t(e)}$ and $E_{t(h)}$ electron and hole traps respectively. Simmons & Taylor[24] have proposed an identical model with similar results. It is, of course, an approximation to use states at discrete energies as, in an amorphous material, one would expect all states to be spread over a range of energies. It is also quite likely that there are more states than those shown in Figure 7, but a four-level model seems to be the minimum required to account for the steady state photoconductivity.

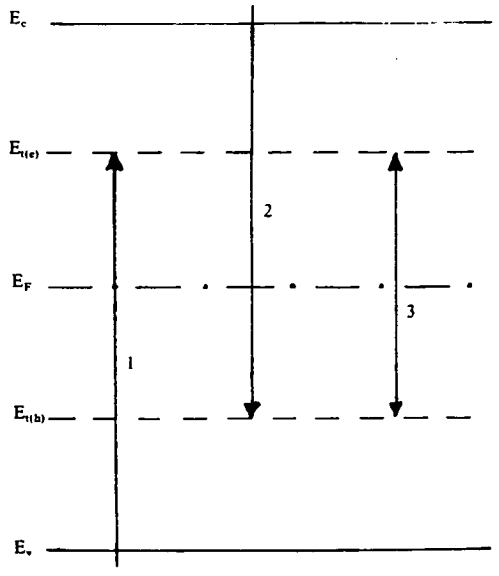

Figure 7. *The basic four level model used to interpret photoconductivity results in chalcogenide glasses*[19]

In the four-level model, recombination of excess carriers may occur via band–localised (B–L) transitions, such as paths 1 and 2 in Figure 7, or directly by localised–localised (L–L) transitions as in path 3. Initially, Main & Owen[19] tentatively suggested that recombination in As_2Se_3 proceeded by L–L transitions, unlike the situation in As_2Te_3, but a more detailed analysis has shown that B–L transitions predominate.[25] In this case, for the low intensity monomolecular region,

$$\Delta I_{ph} \alpha \Delta p \alpha g \exp\left[(E_{t(e)} - E_F)/kT\right] \tag{9}$$

and, for the high intensity bimolecular region,

$$\Delta I_{ph} \alpha \Delta p \alpha g^{\frac{1}{2}} \exp\left[-(E_{t(h)} - E_v)/2kT\right] \tag{10}$$

where g is the generation rate and Δp is the density of excess holes.[19,25] It is assumed here, of course, that, as in the dark, the photoconductivity is determined mainly by the more mobile holes. In Figure 6 the slopes of both regions correspond to energies of 0·37 eV. (n.b. Bube *et al.*[22] quote values of 0·35 eV for the monomolecular region and 0·39 eV for the bimolecular region). These measurements were, however, made with a light emitting diode radiating at 0·655 μm; thus the excitation line was close to the optical gap (1.86 eV at room temperature) and the temperature dependence of the optical gap has an appreciable effect on the slope of $\ln\Delta I_{ph}$ against $(1/T)$ in the lower temperature bimolecular region. When corrected for this the slope in that region corresponds to an energy of 0·33 eV. Thus, the energies in Equations (9) and (10) are $E_{t(e)} - E_F = 0{\cdot}37$ eV and $E_{t(h)} - E_v = 0{\cdot}66$ eV.

The transient photoconductivity can also provide valuable information on localised states and in particular Main[25] has shown that from the transient rise in photocurrent a drift mobility may be derived.

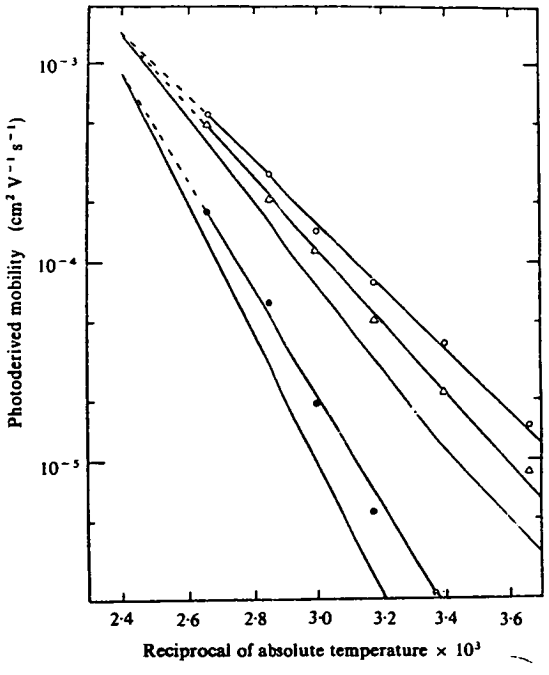

Figure 8. *Trap limited mobilities derived from transient photoconductivity measurements on amorphous As_2Se_3 with electric field as the parameter. The upper three lines correspond to the initial transient and the lower two lines to a second transient rise*

○ $1{\cdot}2 \times 10^6$ V cm^{-1}
Δ 6×10^2 V cm^{-1}
—— zero field extrapolation
● $1{\cdot}2 \times 10^6$ V cm^{-1}
—— zero field extrapolation

Typical results are shown in Figure 8. The mobility at two different fields from the initial transient is given in the upper curves; when adjusted for the field dependence, the zero field mobility has an activation energy of 0·44 eV. In some cases a second transient rise is also observed,[25] as is also shown in Figure 8, and this has an activation energy of 0·65 eV which corresponds closely to the value of 0·66 eV for $(E_{t(e)} - E_v)$ mentioned above. Unlike the time-of-flight technique, however, the derivation of a mobility from the transient photoconductivity does not determine the sign of the carriers. It is assumed that they refer to the trap-limited drift mobility of holes and this seems reasonable in view of the correspondence with the energies at ~0·65–0·66 eV noted above and the consistency with other experiments mentioned below.

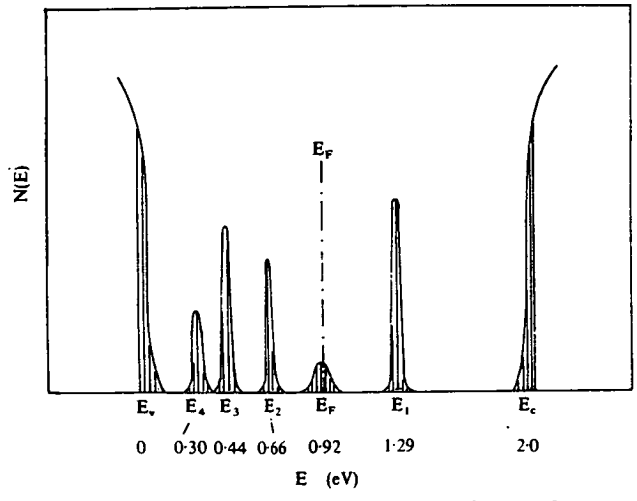

Figure 9. *Suggested qualitative density of states diagram for amorphous As_2Se_3*

At this stage we can construct the schematic band diagram for the density of states in vitreous As_2Se_3 illustrated in Figure 9, where E_c and E_v are the mobility edges and all energies are measured from E_v. The activation energy for the dark conductivity has been used to fix the position of the Fermi level, E_F, with respect to E_v and the optical gap extrapolated to 0 K has been taken as equivalent to the mobility gap, $E_c - E_v$. There is some variation in both these parameters between different workers but the values used in Figure 9 are representative.[16] The other features have been put into Figure 9 in the spirit of the rest of this article, namely that the electronic properties of amorphous semiconductors may often be determined by localised states at relatively discrete energies. The states E_1 and E_2 are indicated by the steady state photoconductivity results and correspond to $E_{t(e)} - E_F$ and $E_{t(h)} - E_v$ in Equations (9) and (10). Evidence for the states at E_3 comes from the mobilities derived from the transient photoresponse and there is also additional evidence from the same type of measurement for E_2. The states at E_4 are suggested by the measurements of thermally stimulated depolarisation reported by Kolomiets *et al.*[26] They are included because it seems possible that they correspond to the hole trapping states at 0·33 eV which seem to be an established feature of pure Se (see Figure 3). If, as proposed earlier, the effect of adding As to Se is to introduce new, deeper hole traps, it is possible that the states at 0·33 eV are retained, albeit at a reduced density, but with the deeper states having an overriding influence on transport. It is also likely that there are some states at E_F.[16]

Transport studies by the direct time-of-flight measurements are not easy in amorphous As_2Se_3. As mentioned earlier in connection with glasses in the composition range 2–10% As, electron transits have not been observed at all and hole transits are complicated by the long tail, or "dispersion", illustrated in the inset of Figure 5. Nevertheless, several measurements of trap-limited hole drift mobilities have been reported.[8b, 27–29] In particular, Marshall & Owen[30] and Fisher *et al.*[31] have shown that measurements with transit times < 100 μs give hole mobilities with an activation energy of 0·43 eV but with transit times in the region 200–500 μs the activation energy is 0·63 eV. These energies, and the actual values of mobility, are in good agreement with those derived from the photoconductivity studies, and Fisher *et al.* interpret these results to mean that as the transit time increases the drifting carriers (holes) come into pseudo-equilibrium with deeper sets of states. Thus the drift mobility measurements are consistent with the picture drawn in Figure 9. Instrumental factors would make it difficult, if not impossible, to observe the shallowest states at 0·3 eV.

In the discussion on amorphous Se an important piece of evidence in favour of trap-limited transport in extended states was the absence of any pressure dependence of both electron and hole mobilities.[11] It is pertinent to note, therefore, that Pfister[32] reports that by contrast the hole drift velocity in amorphous As_2Se_3 increases exponentially with pressure but that the magnitude of the effect is much too great to be explained by the pressure dependence of the overlap integral between hopping sites. In fact, the pressure dependence of the hole velocity is very close to that of the forbidden (optical) gap in amorphous As_2Se_3. Thus, the evidence from pressure effects is inconclusive in this case, although it does seem to indicate that the traps controlling the hole transport in As_2Se_3 are of a kind different from those in amorphous Se, and not just at a different depth (energy).

In concluding this section we must recognise that there are other ways of interpreting the photoconductivity and time-of-flight experiments in chalcogenide glasses such as As_2Se_3. Weiser *et al.*,[20] for example, analyse their photoconductivity and luminescense experiments in terms of the C-F-O model with a continuous distribution of states across the mobility gap. It was necessary, however, for Weiser *et al.* to assume that the carrier thermalisation probability, P_{th}, decreases more rapidly with energy into the gap than the recombination probability, P_r, so that a "recombination edge" could be defined where $P_{th}=P_r$. Arnoldussen *et al.*[21] also use the C-F-O model but again it was necessary to introduce an effective discontinuity in the density of recombination centres in the mobility gap by assuming a rapid change either in the variation with energy of the density of localised states or in the recombination rates. By contrast, the discrete level model does not require such assumptions and, moreover, there is now growing experimental and theoretical evidence which will be discussed below that relatively well defined defect states do indeed exist in amorphous materials.[33–35]

A note of qualification is also required on the derivation of a mobility from the transit time experiment on materials such as amorphous As_2Se_3. Scher[36] and Scher & Montroll,[37] for example, interpret the "dispersive" type of transit pulse, which is so characteristic of As_2Se_3 and other As–Se glasses, in terms of a stochastic process involving transport by hopping through localised states and leading to a distribution of transit times. This contrasts with the analysis of Marshall *et al.*[14b, 30, 31] which is based on the conclusion that transport occurs in extended states, probably by the diffusive mechanism. Scher's theories account for the observed field dependence of mobility but they do not, however, appear to predict the widely reported field dependence of conductivity which often parallels that of mobility (see, for example, Marshall & Miller[38]). Moreover, as Marshall & Owen [14a] and Pfister[15] show in the case of amorphous Se, there is a gradual change from transit pulses with well defined transit times to, at lower temperatures, the "dispersive" type of pulse, *but the slope of the logarithm of the hole velocity versus reciprocal temperature does not change*[14a, 15]. This implies that the activation energy of the transport process, whatever it is, does not change and hence that the basic transport mechanism also remains unchanged. Pfister[15] in fact conjectures that in amorphous Se the mechanism involved over the whole temperature range covering well defined transit pulses at high temperatures to dispersive pulses at lower temperatures ($\lesssim 180$ K) is hopping, and infers that the same is true in other chalcogenides, like As_2Se_3, where normally only dispersive pulses are observed. On the other hand, as argued earlier, the weight of the present evidence suggests that hole, and probably also electron, transport in amorphous Se occurs by trap-limited band transport and since there is no change in activation energy this must also apply at low temperatures (<180 K) where the time-of-flight experiment results in dispersive transit pulses. Thus, at the present moment at any rate, there seems to be no reason, *a priori*, to associate dispersion in the transit pulse with hopping transport.

One other experimental observation often adduced as evidence for hopping transport in chalcogenide glasses is that the activation energy for thermopower, E_s, is usually less than that for conduction E_σ.[39, 40] Unipolar conduction is assumed (by holes since the thermpower is invariably positive) and the difference, $E_\sigma - E_s$, is equated with the activation energy for hopping mobility. In relatively conducting chalcogenide glasses, of which As_2Te_3 is typical, $E_\sigma - E_s$ is often found to be about 0·15 eV. The thermopower is much more difficult to measure in more resistive glasses such as As_2Se_3 but Seager & Quinn[39] have reported a value of 0·31 eV for $E_\sigma - E_s$ in that material. One possible interpretation is hopping in the tail of localised states[40, 41] but, as Seager & Quinn point out, the pre-exponential constant for conductivity is too large for that type of process and they favour polaron hopping. Alternatively, however, the common observation that $E_s < E_\sigma$ could be explained by ambipolar band conduction with a hole mobility rather greater than the electron mobility and this possibility does not seem to have been properly explored. It should also be noted that if transport does indeed take place by hopping just below the conduction band mobility edge in the case of electrons, or just above the valence band mobility edge for holes, this would not substantially affect the earlier discussions and the conclusion expressed in Figures 3, 4, and 9.

Luminescence in chalcogenide glasses

In recent years studies of luminescence have provided an important additional source of information on localised states in chalcogenide glasses.[42–47] Typical luminescence, L, excitation, E, and absorption, α, spectra for amorphous Se[46a] and As_2Se_3[46b] observed in the region 4–10 K, are shown in Figure 10. The luminescence spectrum is excited by the absorption of light of energy close to the band gap energy. After excitation the excess electrons and holes thermalise rapidly until captured into localised band tail

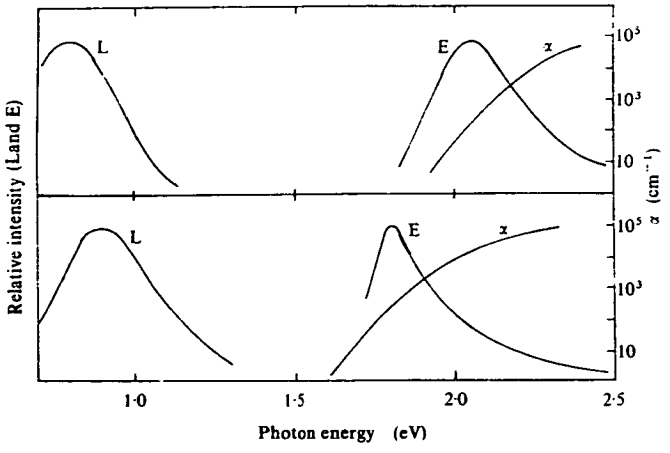

Figure 10. *The luminescence spectrum,* L, *excitation spectrum,* E, *and optical absorption,* α, *at 10 K for amorphous Se (upper diagram*[46b]*) and amorphous* As_2Se_3 *(lower diagram*[46c]*)*

states or deep centres. Some recombine radiatively to give luminescence but others recombine through non-radiative centres. The luminescence spectrum gives information about the distribution and properties of the radiative centres while the excitation spectrum represents the dependence of the luminescence intensity on excitation energy. The luminescence intensity decreases with increasing temperature, probably because a carrier captured by a radiative centre can be thermally re-excited and transferred to a non-radiative centre; hence luminescence measurements are usually made at low temperatures (< 50 K).

The main feature in the luminescence spectra of chalcogenide glasses is a broad band centred at about half the band gap energy (Figure 10). The luminescence bands are symmetrical and show no fine structure at a resolution of 0·01 eV. Generally speaking, both the peak position and the line width increase with band gap energy, E_g, but Se is an exception in this respect because although it has a larger value of E_g the peak position is 0·1 eV lower than in As_2Se_3 (Figure 10). In Se the luminescence intensity is also 10–100 times weaker than in the arsenic chalcogenides[46a] but Street *et al.*[46c] find that in the Se–As system there is a linear relationship between luminescence intensity and arsenic concentration between 0·3 and 40 at % As. On the other hand, there is no observable change in the peak position through the Se–As system so the shift of about 0·1 eV to the peak position of amorphous Se must occur at very low As concentrations. It is also pertinent to note that where measurements have been made there is a marked similarity between the spectra of glasses and crystals.[46b] Most significant, however, is the observed separation between the luminescence and the corresponding absorption, providing evidence for strong electron–phonon coupling with a Stoke's shift, U, approximately equal to half the energy difference between the luminescence and excitation peaks.

The similarity between spectra for glasses and crystals indicates very clearly that the mechanism of luminescence cannot depend substantially on disorder. On the other hand the fact that there is a small activation energy for the thermal quenching of luminescence and that the excitation spectrum is found to be near the fundamental absorption edge (Figure 10), both suggest that localised band tail states are involved in the radiative transition.[47] Hence, the energy of the deep radiative centre relative to the bands can be determined and this energy, E^*, is generally found to be only about 0·1–0·2 eV less than the band gap energy, E_g.[47] (n.b. E_g is defined by Street[47] as the energy at which the optical absorption coefficient equals 10^3 cm^{-1} and is slightly less than the mobility gap). The undistorted radiative centre is, therefore, close to the band edge.

For thermal activation, however, the deep centre will require an excitation energy different from that involved in optical processes as the Franck–Condon principle will no longer apply. According to Street[47] the trap depth, E_t, for thermal excitation is given by $E_t = E_g - \Delta - E^* + U$, where Δ is the total width of the two band tails. With typical experimental values this gives, for As_2Se_3, $E_t \approx 0{\cdot}45$ eV.[47] This compares well with the hole trap depth of 0·43–0·44 eV determined from transient photoconductivity[25] and transit time measurements[30,31] and it may also be relevant to note in this connection that Street & Yoffe[48] detected traps at 0·4 eV in As_2Se_3 from an analysis of thermally stimulated current. The agreement is reasonable and the comparison with the transport measurements suggests that the deep radiative centres are hole rather than electron traps. Moreover, this interpretation of the luminescence spectra is generally consistent with the basic idea presented earlier, namely that the electronic properties of the chalcogenide glasses are determined largely by traps located at relatively well defined energy levels and which are not associated with band tails.

Amorphous silicon

One of the most striking features of the group of tetrahedrally coordinated amorphous solids is the critical dependence of their electronic properties on the method of preparation and on the detailed experimental conditions during specimen deposition. This does not seem to apply to other groups of amorphous solids such as the chalcogenides or the more complicated alloy glasses, where there is generally good agreement in the electrical and optical data obtained in different laboratories and on specimens prepared by different techniques. The apparent lack of consistency found in most of the earlier work on a-Ge and a-Si is now known to have been caused by differences in the defect structure in the gap states. This aspect will be discussed below.

The most widely used methods of specimen preparation have been evaporation in a vacuum of about 10^{-6} torr or less and sputtering from a single crystal cathode. A promising approach has been the preparation of semiconductor films from the gas phase by

decomposing the hydride in a radio frequency glow discharge. For instance, a-Si specimens are formed in this way from silane gas, a-Ge from germane, and a-C from acetylene. It has been found that the electronic properties of specimens prepared by this technique are determined to a much lesser extent by the defect structure in the gap states so that experimental results are more representative of the intrinsic properties of the amorphous phase. In this respect the study of glow discharge a-Si has made important contributions to our basic understanding of the subject and most of the following sections will be concerned with the discussion of these results.

Density of state distribution

It has already been shown that the distribution of the localised states in the mobility gap of an amorphous semiconductor has a determining influence on the electronic properties of the material. The independent measurement of the distribution function $N(E)$ is therefore an important first step towards the detailed understanding of these properties. Unfortunately this presents major experimental and computational problems and, so far, glow discharge deposited Si is the only amorphous material for which $N(E)$ is known with reasonable certainty throughout most of the mobility gap. The results shown in Figure 11 were obtained by the field effect technique.[49–51] In this experiment, the localised states are moved in energy with respect to the Fermi level by applying an external electric field normal to the free surface of the film. This is done in a step-by-step process and the energy range moving past E_F in each step can be calculated from the change in the specimen conductivity. From a computerised analysis of the spatial and energetic distribution of the induced charge, $N(E)$ can be obtained.

Curves 1 and 2 in Figure 11 are typical distribution curves for glow discharge deposited Si;[51,52] $N(E)$ is plotted against the energy measured from E_c. Curve 1 has been obtained from specimens deposited at a substrate temperature, T_d, between 500 and 550 K. The electron band tail states, mainly associated with the structural disorder, lie between E_c and E_A in a range of about 0·2 eV. The gap states, formed by structural defects, show a deep minimum in $N(E)$ located approximately in the centre of the mobility gap. There are two peaks at E_x and E_y in the spectrum of the defect states which will be referred to again. The most important feature of curve 1 is the remarkably low overall density of gap states that can be achieved by this technique at high T_d. At the Fermi level position, indicated by the arrow, $N(E_F)$ can be as low as 2×10^{17} cm^{-3} eV^{-1}.

Curve 2, from a specimen deposited at 350 K, illustrates the effect of lowering T_d. The overall density of states has been appreciably increased and E_F has moved to the left of the minimum. Curve 3, representative of an evaporated Si specimen, shows the comparatively high level of gap states that is generally obtained by this preparation method. Under these conditions, only a small energy range close to E_F can be investigated by the field effect technique. However, other workers[53] have also found values of $N(E_F) \sim 10^{20}$ cm^{-3} eV^{-1} in evaporated Si annealed at 400°C.

Electronic transport

The results of conductivity, drift mobility,[54,55] thermoelectric power,[56] and field effect measurements on glow discharge deposited Si have led to a reasonably consistent picture of the electronic transport in this material. The predominant conduction mechanism depends of course on the temperature, but is also determined by T_d, the substrate temperature during specimen deposition, illustrating the close relation between the density of state distribution and transport.

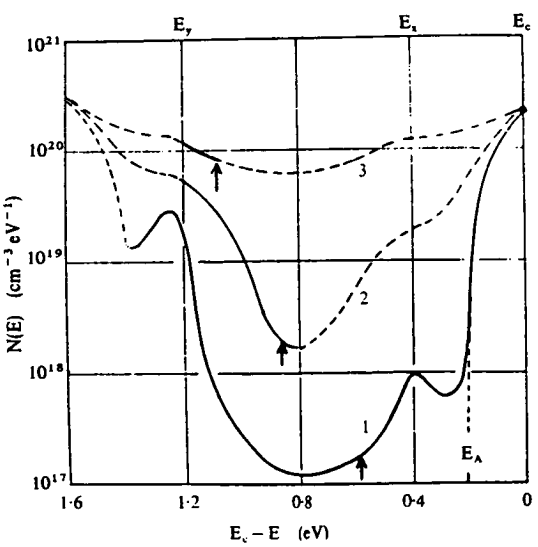

Figure 11. *Density of state distributions for a-Si specimens. Curve 1, glow discharge specimen, $T_d \sim 520$ K; curve 2, glow discharge specimen, $T_d \sim 350$ K; curve 3, evaporated specimen. The full lines indicate results obtained from field effect experiments and the arrow on each shows the position of* E_F[51,52]

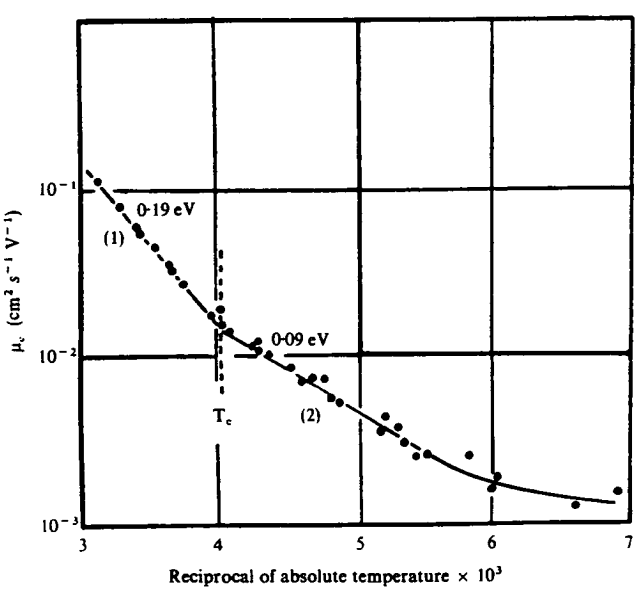

Figure 12. *Temperature dependence of the electron drift mobility in an amorphous silicon film, 1·3 μm thick*[54]

Figure 12 is a typical electron drift mobility–temperature curve for a high T_d glow discharge deposited specimen. The striking feature is the change in activation energy at $T_c \simeq 250$ K, which can also be seen in most cases on the corresponding conductivity graphs. The interpretation of the results is summarised in Figure 13(a). Above 250 K multi-trapping transport occurs, as already discussed for the Se–As glasses. The injected pulse of excess electrons drifts in the extended states just above E_c and during transit interacts through trapping and thermal release with a fairly well defined region of the localised states spectrum. The activation energy of 0·19 eV for $T > T_c$ indicates that these states lie close to E_A in the rapidly decreasing edge of the tail states. The latter will be in quasi-thermal equilibrium with the extended electron states during the transit, so that the occupation of these states is proportional to $N(E)\exp[-(E-E'_F)/kT]$, where E'_F denotes the position of the quasi-Fermi level. The occupation function calculated from the distribution in Figure 11 goes through a reasonably well defined maximum just above E_A[49] and it is therefore understandable that the multi-trapping transport is dominated by a single activation energy.

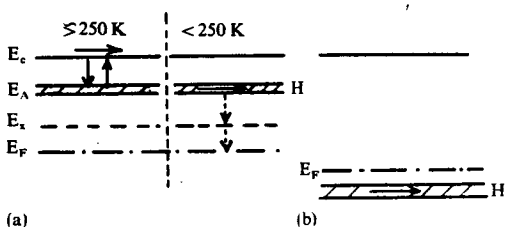

Figure 13. *Conduction paths in glow discharge a-Si*
(a) high T_d specimen
(b) low T_d specimen: H denotes phonon assisted hopping conduction

With the information from the drift mobility and field effect experiments it is possible to estimate the electron mobility in the extended states. Values between 3 and 16 $cm^2 V^{-1} s^{-1}$ have been found[55] which support the theroetical predictions for transport in the extended states near E_c as given earlier in the paper.

With decreasing temperature, the probability of thermal release from states near E_A becomes rapidly smaller and at $T_c \lesssim 250$ K hopping through states around this energy becomes the predominant transport mechanism; Figure 13(a). As shown by Equation (3), the gradient of the curve now gives directly the hopping energy, W, which is about 0·09 eV. This interpretation is supported by conductivity–temperature graphs on the same specimens which show a change in activation energy from $|E_c - E_F|$ above T_c to $|E_A - E_F + W|$ below T_c. With further reduction in temperature, the occupation probability at E_A decreases and the predominant conduction path will sink to perhaps E_x and eventually to within a few kT of the Fermi level.

The observation of extended state conduction above 250 K is an exceptional property of high T_d glow discharge deposited specimens and is a direct consequence of the low density of gap states shown in Figure 11 (curve 1). Once the overall density of states is allowed to increase as in curve 2, by deposition at a lower T_d, the electronic properties of the glow discharge deposited specimens change drastically. The modified defect distribution causes the Fermi level to shift to about 1 eV below E_c and the predominant transport, even at room temperature, is now by phonon assisted hopping of holes,[55] as illustrated in Figure 13(b). The results suggest that the most likely current path lies near the energy, E_y, (Figure 11) at which the density of holes is high.

The transport behaviour of a low T_d glow discharge deposited specimen tends towards that of evaporated or sputtered specimens.[50] There is little doubt that the high density of gap states in these materials (Figure 11, curve 3) will lead to phonon assisted hopping except perhaps at very high temperatures.[56] However, the transport path need not necessarily lie around E_y as in the low T_d glow discharge deposited specimens. It will be largely determined by the position of the Fermi level, which in turn depends critically on the preparation conditions.

The temperature dependence of the thermoelectric power, S, can yield useful additional information on the transport properties of amorphous materials. It is a far more sensitive experimental approach than the measurement of conductivity, indicating directly the position of the predominant conduction path with respect to the Fermi energy in a form which is independent of the transport mechanism. The results for high T_d glow discharge deposited Si specimens confirm the occurrence of extended state conduction;[57] but they also show another component in the thermoelectric power which has been ascribed to the effect of phonon drag. If this is correct, it provides an interesting new aspect on transport in the random phase region above E_c. In high T_d Ge specimens phonon drag is smaller than in Si, and the results clearly show the thermoelectric power expected for extended state conduction, going over to tail state hopping at lower temperature.[58]

The temperature dependence of the thermoelectric power in evaporated and sputtered a-Si and Ge presents a very different picture to the one described above.[59] At room temperature and below, S is small (about 50 $\mu V K^{-1}$) and largely temperature independent. This behaviour, normally associated with metallic transport, is caused by the predominant hopping conduction at the Fermi level and is a direct consequence of the high value of $N(E_F)$ shown in Figure 11, curve 3. In the same temperature range the conductivity follows the $T^{-1/4}$ relation for variable range hopping near the Fermi level mentioned in Equation (4).

Photoconductivity and luminescence

Glow discharge deposited Si specimens, particularly those prepared at high T_d, are very photoconductive[60–62] and also show photoluminescence at lower

temperatures.[63–65] This does not apply to evaporated or sputtered Si films,[66] mainly because of the short lifetime of photo-generated carriers, as the high density of gap states leads to numerous nonradiative electron–hole recombination paths.

In Figure 14 the room temperature photoconductivity, σ_p, is plotted against the dark Fermi level position $E_c - E_{Fo}$ for a number of high T_d a-Si specimens which include undoped and also n- and p-type films. All data were taken with an incident flux of 2×10^{13} photons s^{-1} and at a photon energy of 2 eV. It can be seen that a good undoped specimen approaches the unit quantum efficiency line which as been calculated for a typical applied field of 3×10^3 V cm^{-1}. Slight phosphorus doping increases σ_p well above unit quantum efficiency and maximum response is attained in specimens in which the dark Fermi level lies about 0·4 eV below E_c.

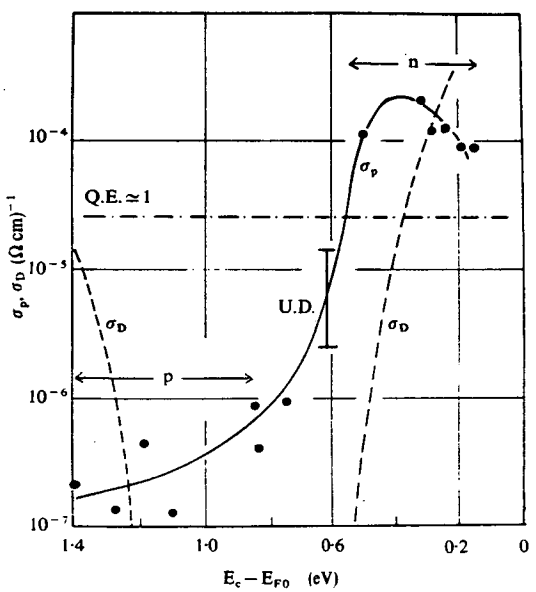

Figure 14. *Room temperature photoconductivity (full line) and dark conductivity (broken lines) plotted against the position of the dark Fermi level*[62]

The spectral dependences of the photoconductivity and of the absorption coefficient are shown in Figure 15 for a series of undoped specimens prepared at different T_d.[60] The ordinate represents the number of photo-generated carriers at room temperature flowing round the circuit for each photon entering the specimen. It has been established[61] that in high T_d specimens the transport of the photogenerated carriers proceeds along the same current paths as shown in Figure 13(a) for the dark current. The observed onset of photoconductivity at photon energies between 0·6 and 0·7 eV is practically identical to the activation energy $E_c - E_F$ obtained from the dark conductivity and therefore involves transitions of electrons from just below E_F to E_c. The shoulder between 1·1 and 1·3 eV in most curves may well reflect transitions to E_c from the density-of-state maximum at E_y. The optical gap deduced from both photoconductivity and absorption measurement lies between 1·5 and 1·6 eV.

One of the most interesting aspects of photoconductive studies is the information they can give on the recombination process[67] and its relation to the density-of-state distribution. Recent work on the temperature and intensity dependence of photoconductivity in glow discharge deposited Si specimens has shown that at room temperature and up to moderate light intensities, the recombination in an undoped specimen is a monomolecular process and involves the transition of an electron from E_A to E_{Fo}. With decreasing temperature and/or higher intensity, a bimolecular recombination path develops. One now has to consider the distribution of the excess positive and negative charge in the system and the movement of these distributions with temperature and intensity. In this connection Rose's concept of the "demarcation level",[68] separating kinetically and thermally controlled occupation of states, is particularly useful. It is found that predominantly bimolecular recombination sets in when the electron demarcation level has reached the energy E_x (Figure 11). Most of the excess negative charge will then be concentrated in the maximum. Little is known about the positive counter charge, but the region near E_y seems the most likely location. It is therefore suggested that, with decreasing temperature, bimolecular recombination occurs mainly between states at E_x and E_y.

With doped specimens[62] it becomes possible to move the electron demarcation level above E_x; states at E_x are now kinetically controlled and their occupation decreases. Under these conditions, σ_p reaches its maximum (Figure 14).

At temperatures below 80 K, high T_d specimens show pronounced photoluminescence. This aspect has been investigated by Engemann & Fischer[63,64]

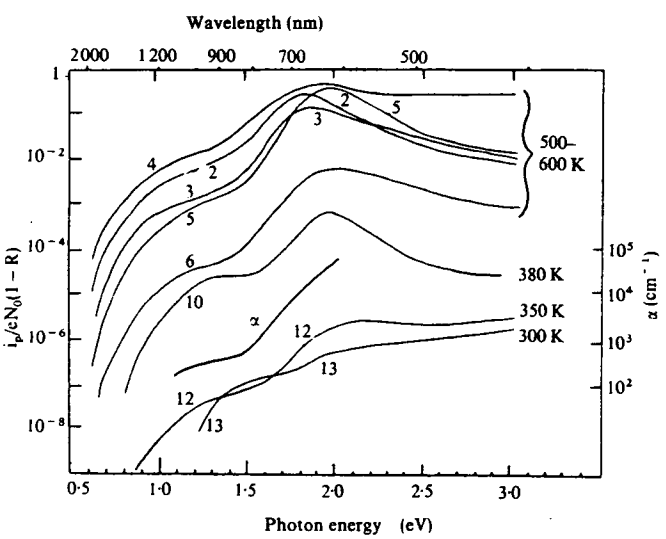

Figure 15. *Spectral dependence of photoconductivity in glow discharge Si specimens prepared at the deposition temperatures indicated. The ordinate represents the number of charge carriers flowing around the circuit per photon entering the specimen. The line marked α shows the absorption coefficient for a 500 K specimen*[60]

with interesting results. Figure 16 shows the luminescence spectrum at 25 K excited by a Kr laser. The main features labelled 1, 2, and 3 appear to be reasonably consistent with the density-of-states distribution of Figure 11, curve 1. Peak 1 is almost certainly a radiative transition between the localised tail states of the conduction and valence bands (e.g. from E_A to the corresponding level above E_v). Peaks 2 and 3 can be associated with transitions from one of the band tails to deeper lying localised states near the opposite band, such as E_y or E_x. For instance, if the Stokes shift in the luminescence is fairly small ($\lesssim$0·1 eV), then peak 3 could be interpreted as a transition from E_A to E_y.

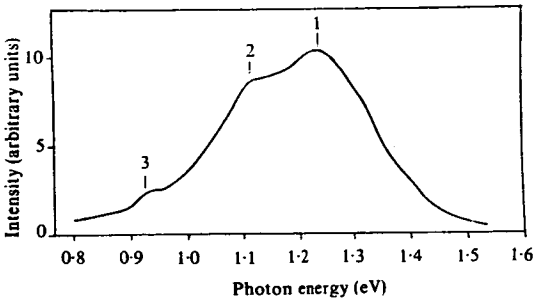

Figure 16. *Photoluminescence spectrum at 52 K for a high* T_d *a-Si specimen*[63]

At temperatures above 120 K, the luminescence begins to decrease rapidly with an activation energy of 0·13 eV. An exciton model[65] has recently been proposed in which the radiative recombination probability decreases at the higher temperature because of the competing thermal dissociation of the exciton. Like the photoresponse, the efficiency of the luminescence depends critically on preparation conditions. It drops rapidly when T_d is decreased or when the specimen is ion bombarded, and it can no longer be observed in evaporated Si specimens. The higher density of gap states thus quenches the luminescence and effectively reduces the photoconductivity.

Doped amorphous semiconductors

Finally, a new development in the field of amorphous semiconductors will be discussed. Last year, the Dundee group showed[52,69] that substitutional doping of a-Si and a-Ge is possible in the gas phase and can lead to a systematic control of the electronic properties over a remarkably wide range. For the preparation of n-type films, small but accurately determined amounts of phosphine are added to the silane used in the specimen preparation. Similarly, traces of diborane will produce p-type a-Si.

Figure 17 shows the room temperature conductivity, σ_{RT}, for a series of n- and p-type a-Si specimens plotted against the gaseous impurity ratio. On the right, N_{PH_3}/N_{SiH_4} denotes the number of phosphine to silane molecules in the gas mixture, whereas on the left the corresponding diborane to silane ratio is

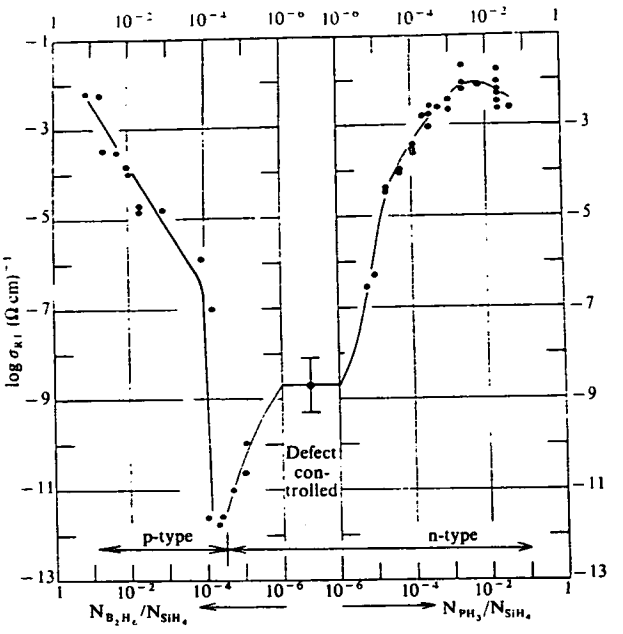

Figure 17. *Room temperature conductivity of n- and p-type a-Si specimens plotted against the gaseous impurity ratio. The centre refers to undoped specimens*[52]

shown. The centre of the graph represents typical conductivity values for undoped specimens. It can be seen that even a minute quantity of phosphine, 10^{-5} parts per volume (ppv), increases σ_{RT} by over two orders of magnitude. Such a conductivity change requires a movement of E_F towards E_c of 0·13 eV, which means that the excess electrons introduced by the donors must fill the gap states within this range. The high sensitivity to substitutional doping is therefore a direct consequence of the low density of gap states achievable in high T_d glow discharge deposited specimens. At an impurity ratio of about 2×10^{-3}, σ_{RT} begins to saturate near 10^{-2} $(\Omega\,\text{cm})^{-1}$; E_F then lies approximately at E_A. With light boron doping, σ_{RT} decreases at first until compensation of defect states has moved E_F to the centre of the minimum in $N(E)$; hole conduction then begins to predominate. Figure 17 leaves little doubt that systematic control of the electronic properties of glow discharge Si by phosphorus or boron doping is a very real possibility. The Fermi level position can be moved through a range of about 1·2 eV, essentially between the onset of the electron and hole tail states.

Recent Hall effect measurements on doped a-Si specimens[70] have led to interesting results. For lightly doped n-type specimens transport takes place predominantly in the random phase region as described previously; the Hall mobility, μ_H, is constant between 400 and 250 K and equal to about 0·1 $\text{cm}^2\,\text{V}^{-1}\,\text{s}^{-1}$, approximately 1/30 of the room temperature drift mobility. Both these observations are in agreement with Friedman's theory.[71] With increasing doping a second, lower mobility conduction path becomes important. Analysis of the results suggests that a

donor band has formed in which thermally activated hopping between donor states takes place. In heavily doped specimens ($\gtrsim 2 \times 10^{-3}$ ppv) donor band conduction begins to predominate, even at room temperature. The band is centred at about 0·13 eV below E_c and could extend through most of the tail states. Although the magnitude and temperature dependence of μ_H in a-Si can be interpreted in a fairly consistent manner, the sign of the Hall coefficient is completely anomalous: in phosphorus doped specimens, where there is no doubt about electron conduction from thermoelectric and field effect data, the Hall coefficient corresponds to that for positive carriers, in boron doped films it has the sign expected for free electrons. This curious double reversal cannot be explained at present.

It is appropriate to end this section on a hopeful note concerning the future of amorphous semiconductors. The fact that sensitive doping can now be carried out in a systematic way has opened up promising device possibilities. A first step in this direction has been the preparation of the first amorphous thin film p-n junction.[72] It is therefore possible that during the coming years amorphous semiconductors, most likely glow discharge deposited Si, may find application in large area devices such as display panels, solar cells[73] or photoconductive junctions.

The nature of the defect states in amorphous semiconductors

When the subject of "amorphous semiconductors" first came into prominence in the latter half of the 1960s there was some uncertainty, particularly among theoreticians, about whether or not it was possible to have such a material. As Ziman[74] put it, the assumption that there are "band gaps" in amorphous semiconductors which are analogous to those of the corresponding crystal is qualitatively justified in chemical terms "by appealing to the concept of saturated chemical bonds", but rigorous quantitative calculations on systems without long range order "do not preserve the band gaps". Nevertheless, the existence of some kind of energy gap, or band gap in disordered materials is experimentally well established. Apart from the solid amorphous materials with typical semiconducting properties which have been the subject of so much recent interest, it has been known for many years that some crystalline semiconductors retain their semiconducting properties in the molten state.[75,76] The optical transparency of the common silicate glasses is also evidence of a band gap of sorts in a disordered material.

The dichotomy is more apparent than real, however, when it is recognised that the general features of electronic band structure are determined largely by the local atomic configuration, or short range order.[77] All glasses, amorphous solids, and liquids retain a high degree of short range order which is often identical with that in the corresponding crystalline material: the disorder is in the long range structure and is mainly topological.[78] It is not surprising, therefore, that there are such things as "amorphous semiconductors" and it follows that the "chemical bond" approach should provide at least a good approximation to the band structure. Moreover, as a high degree of short range order is retained, it also follows that specific structural defect centres may exist and, just as in the crystal, could lead to the formation of localised electronic states in the band gap at relatively discrete energy levels. The evidence reviewed in earlier sections of this paper shows that for two different types of amorphous semiconductor this does indeed appear to be the case. Contrary to earlier views[5] it seems that the intrinsic disorder of an amorphous material does not necessarily introduce a sufficiently large density of states in the gap to dominate effects due to specific "defect states". The important question, of course, is what is the origin and nature of these defect states?

Defect states in chalcogenide glasses

The arguments outlined above suggest that the localised defect states in a glass may be closely related to similar states in the corresponding crystal and there is, in fact, supporting evidence for this point of view in the literature from several years ago. For example, in 1970, Kolomiets *et al.*[42a,79] reported that the band structure of arsenic sulphide (As_2S_3). in the energy range of interband transitions, does not change appreciably on going from the crystalline to the glassy state and that the electronic properties of the glass are determined by localised states in the gap of a kind which probably also occur in the crystal. Unfortunately, there have been no systematic studies of the electronic properties of good quality single crystals of the chalcogenide compounds. Kolomiets[80] has described measurements on what are probably polycrystalline specimens of As_2Se_3, however, and he reports the presence of several trapping levels which, as Fisher *et al.*[31] point out, correspond roughly in energy to those observed in the glass. The marked similarity between the luminescence spectra of chalcogenide glasses and crystals[42–47] is further evidence of a close correlation in their electronic band structures. Thus, the evidence for specific structurally related electronic defect states in chalcogenide glasses is strong and the first explicit proposals of band models like those of Figures 3, 4, and 9 were probably made by the Edinburgh group.[14,19,30,31,81]

It remains, however, to identify the origins of the various defect states which may exist in a chalcogenide glass. For a material like As_2Se_3 it is easy to speculate that missing As or Se atoms, leaving "dangling" (i.e. unsatisfied) bonds (on Se or As atoms), could be a sources of localised defect states. More complex centres such as divacancies or clusters are also possible. Kolomiets *et al.*[82] have attempted to relate the existence of localised states in vitreous As_2Se_3 with the polymeric structure of the material and they suggest that the ends of "macromolecules", or the joins between macromolecules, could form electronic defect states. More specifically, from the observed increase

in luminescence intensity with As concentration in the As–Se system. Street *et al.*[46,47] concluded that the defect states responsible for radiative recombination are dangling bonds located on As atoms. Recent measurements on the electron spin resonance (ESR) stimulated by illumination at low temperatures suggest, however, that the situation is more complicated and in As_2S_3 and As_2Se_3 there is evidence for ESR signals corresponding to both arsenic and chalcogen.[83] From these experiments Bishop *et al.*[83] conclude that in the chalcogenide compounds both types of dangling bond are present with an electron centre localised on the As atoms and a hole centre localised on the chalcogen. The differences in the luminescence spectra between pure Se and As_2Se_3 and the different pressure dependence of transport properties, both described earlier in the paper, provide additional evidence that defect states associated with Se and As have different properties.

It is not difficult therefore to identify the origins of localised defect states in chalcogenide glasses in general terms based on the idea of dangling bonds. It is much more difficult to provide a theoretical framework for such states. The first theoretical model was proposed by Mott, Davis & Street;[33] it assumes that a dangling bond, which when neutral contains an unpaired electron, may be occupied by zero, one, or two electrons. The three states are labelled D^+, D^0, and D^- respectively (the superscripts indicating the total charge on the centre) and, following the ideas of Anderson,[84] it is further assumed that the lattice distortion is strong enough for the reaction $2D^0 \rightarrow D^+ + D^-$ to be strongly exothermic. In the ground state of the system all the states are therefore either positively or negatively charged and the neutral D^0 state occurs only by excitation. The electronic levels of the dangling bond are largely determined by the lattice distortion and the level applicable to a particular experiment depends on whether a thermal or an optical process is involved. The model accounts for the absence of ESR or paramagnetism[16] under normal equilibrium conditions (e.g. no illumination) because all of the centres are either D^+ or D^-. The absence of optical absorption at energies below the band gap energy also follows. Moreover, the model predicts that the Fermi level is pinned near the middle of the gap, as widely observed,[16] and it is also generally consistent with photoconductivity and transport measurements described earlier in the paper. The lattice distortion (electron–phonon coupling) is the essential feature required to explain the Stokes shift observed in the luminescence spectra described earlier.

Kastner, Adler & Fritzsche[35] have recently proposed an alternative model. They point out that a simple dangling bond is energetically unfavourable and propose instead the concept of valence alternation pairs (VAP) which result, for example, when a pair of normally twofold coordinated chalcogen atoms combine to form one threefold coordinated atom and one singly coordinated atom. It is suggested that these states are unstable towards charge transfer and that the former would normally be positively charged and the latter negatively charged. The formation of a VAP depends on the particular bonding configurations which arise from the presence of nonbonding (or lone pair) orbitals associated with the chalcogen atoms[85] and it follows therefore that valence alternation pairs are impossible in the tetrahedrally coordinated materials like amorphous Si.

It should be noted, however, that neither the Mott–Davis–Street nor the Kastner–Adler–Fritzsche model is specific to amorphous materials except perhaps in the latter case when an estimate is made of the concentration of defects. The models should therefore be equally applicable to crystalline chalcogenides and this is not surprising in view of the arguments presented earlier in this section. Thus, a more detailed experimental comparison of crystals and glasses, especially as a function of stoichiometry, should provide more quantitative information on the defect states. An important theoretical and experimental question which remains unanswered is whether the configurational entropy, which is a characteristic property of a glass, makes possible the formation of specific defect centres of a kind different from those which might reasonably be expected in a crystal, as well as presumably being the basic cause of the tailing of states from the valence and conduction bands.

Defect states in amorphous silicon

The study of the defect structure and its dependence on the preparation conditions is an interesting though difficult problem. The recent work of the Marburg and Harvard groups on evaporated and sputtered a-Si and Ge has made important contributions to this field. The general conclusion, similar to that for the chalcogenides, is that the electronic properties of the amorphous semiconductors Ge and Si are largely determined by the defect structure in the gap states and not by the lack of long range order. Brodsky & Title[86] originally suggested, on the basis of ESR measurements, that most of the defects are associated with vacancies. Unsaturated bonds on internal surfaces of multi-vacancies (or voids) introduce states which interact both with the electrons in the system and also with impurities, mainly hydrogen and oxygen. The vacancies contain some electron states with unpaired spins so that ESR measurements and the analysis of line shape and line width can provide useful additional information. In their recent work Connell & Pawlik[87] estimate that in a-Ge sputtered on to a substrate at 25° C voids are typically 5 Å across, and contain 10–20 dangling bonds. Spin densities of the order of 10^{19} cm^{-3} are found, although the density of unsaturated bonds appears to be much higher in this material.

Stuke and his collaborators[88,89] have used ion implantation techniques to study the defect structure created by rare gas ion bombardment and also the effect of H^+ and O^+ implantation. The defects so introduced can be removed almost completely by progressive annealing so that conductivity, thermoelectric power, and spin density may be studied as a function of defect density.

In particular, the implantation experiments have provided interesting information on the effect of hydrogen and oxygen in evaporated films. It has been established that during preparation in a vacuum of about 10^{-6} torr the residual hydrogen and oxygen in the system tends to saturate dangling bonds on void surfaces. As expected, the interaction is more pronounced at small deposition rates. Under these preparation conditions, the effect of the residual gases becomes the main factor in determining the electronic properties. It is found that saturation of dangling bonds moves the Fermi level through the density of states minimum (Figure 11, curve 3) into the upper half of the mobility gap. If, on the other hand, films are prepared by relatively fast evaporation in an ultra-high vacuum,[90] then there is little saturation of bonds and the introduced defect states control the electronic properties. In this case, E_F tends to move towards E_v. Under most evaporation and annealing conditions the Fermi level position is likely to be determined by a combination of the above two effects and this provides a general explanation for the frequently complex behaviour of evaporated and sputtered specimens.

How do glow discharge specimens fit into this picture? High T_d specimens generally do not give a detectable ESR signal, and an upper limit of about 10^{16} spins cm^{-3} has been quoted which is some three orders of magnitude less than in specimens prepared by other methods. This result is consistent with the low density of defect states derived from the field effect. It seems, however, most unlikely that the unique properties of high T_d glow discharge specimens are caused simply by the presence of nascent hydrogen during decomposition of SiH_4. This, for example, is clearly shown by heavily hydrogenated sputtered Ge specimens[91] which still give the thermoelectric power curves typical of evaporated or sputtered films described in an earlier section. We believe that the explanation lies in the different preparation technique whereby Si atoms are deposited, possibly singly, from the gas phase. At higher T_d such atoms will have appreciable surface mobility and the majority of bonds in the random network will be satisfied, although some of the remaining defects may of course form Si–H bonds.

Another significant difference may be the smaller average void size produced in glow discharge decomposition.[89] It has been suggested[50, 51] that the divacancy, a stable and much studied defect centre in irradiated crystalline Si, may describe to first approximation the electronic states associated with the voids in glow discharge Si. Reasonable agreement exists between the energy levels of the divacancy and the peaks at E_x and E_y in Figure 11. However, the unequal size of the peaks indicates that only some of the defect states at E_y can be described in this way. In the Mott–Davis–Street model the E_x and E_y states are associated with pairs of dangling bonds acting as acceptors and donors respectively. Unlike the situation in the chalcogenide glasses, however, it is unlikely that lattice distortion (Stokes shift) effects are very large in a-Si.

References

1. Cohen, M. H. (1970). *J. Non-cryst. solids* **4**, 391.
2a. Hindley, N. K. (1970). *J. Non-cryst. solids* **5**, 17.
b. Friedman, L. (1971). *J. Non-cryst. solids* **6**, 329.
3a. Mott, N. F. (1968). *Phil. Mag.* **17**, 1259.
b. Mott, N. F. (1969). *Phil. Mag.* **19**, 835.
c. Mott, N. F. (1970). *Phil. Mag.* **22**, 7.
d. Mott, N. F. (1972). *J. Non-cryst. solids* **8–10**, 1.
4. Anderson, P. W. (1958). *Phys. Rev.* **109**, 1492.
5. Cohen, M. H., Fritzsche, H. and Ovshinsky, S. R. (1969). *Phys. Rev. Lett.* **22**, 1065.
6a. Spear, W. E. (1957). *Proc. Phys. Soc.* **B70**, 1139.
b. Spear, W. E. (1960. *Proc. Phys. Soc.* **76**, 826.
c. Spear, W. E. (1969). *J. Non-cryst. solids* **1**, 197
7. Hartke, J. L. (1962). *Phys. Rev.* **125**, 1177.
8a. Kolomiets, B. T. & Lebedev, E. A. (1966). *Soviet Phys. Solid St.* **8**, 905.
b. Kolomiets, B. T. & Lebedev, E. A. (1967). *Soviet Phys. Semicond.* **1**, 244.
c. Kolomiets, B. T. & Lebedev, E. A. (1973). *Soviet Phys. Semicond.* **7**, 134.
9a. Grunwald, H. P. & Blakney, R. M. (1968). *Phys. Rev.* **165**, 1006.
b. Blakney, R. M. & Grunwald, H. P. (1967). *Phys. Rev.* **159**, 664.
10. Juska, G., Matulionis, A. & Viscakas, J. (1969). *J. Phys. Stat Solidi* **33**, 533.
11. Dolezalek, F. K. & Spear, W. E. (1970). *J. Non-Cryst. solids* **4**, 97.
12. Schottmiller, J., Tabak, M., Lucovsky, G. & Ward, A. (1970). *J. Non-Cryst. solids* **4**, 80.
13. Tabak, M. D. (1970). *Phys. Rev. B*, **2**, 2104.
14a. Marshall, J. M. & Owen, A. E. (1972). *Phys. Stat. Solidi A.* **12**, 181.
b. Marshall, J. M., Fisher, F. D. & Owen, A. E. (1974). *Phys. Stat. solidi A.* **25**, 419.
15. Pfister, G. (1976). *Phys. Rev. Lett.* **36**, 271.
16. Mott, N. F. & Davis, E. A. (1971). *Electronic processes in non-crystalline materials.* O.U.P.
17. Spear, W. E. (1961). *J. Phys. Chem. Solids* **21**, 110.
18. Carles, D., Vautier, C. & Viger, C. (1973). *Thin solid films* **17**, 67.
19. Main, C. & Owen, A. E. (1973). *Electronic and structural properties of amorphous semiconductors.* Ed. P. G. Le Comber & J. Mort. p. 527. Academic Press.
20. Weiser, K., Fisher, R. & Brodsky, M. H. (1970). *Proc. Tenth Int. Conf. Physics Semiconductors*, Cambridge, Mass., p. 767.
21. Arnoldussen, T. C., Bube, R. H., Fagen, E. A. & Holmerg, S. (1972). *J. appl. Phys.* **43**, 1798.
22. Bube, R. H., Mahan, J. E., Shiah, R.T-S. & Vander Plas, H. A. (1974). *Appl. Phys. Lett.* **25**, 419.
23. Arnoldussen, T. C., Menezes, C. A., Nakagawa, Y. & Bube, R. H. (1974). *Phys. Rev. B*, **9**, 3377.
24a. Simmons, J. G. & Taylor, G. W. (1974). *J. Phys. C*, **7**, 3051.
b. Taylor, G. W. & Simmons, J. G. (1974). *J. Phys. C*, **7**, 3067.
25. Main, C. (1973). *Photoconductivity, noise and related phenomena in some amorphous chalcogenide semiconductors.* Thesis. Edinburgh University.
26. Kolomiets, B. T., Ljubin, V. M. & Averjanov, V. L. (1970). *Mater. Res. Bull.* **5**, 655.
27. Scharfe, M. E. (1970). *Phys. Rev. B*, **2**, 5025.
28. Tabak, M. D. (1971). *Proc. Third Int. Conf. Photoconductivity*, Ed. E. M. Pell, p. 87. Pergamon.
29. Pai, D. M. & Scharfe, M. E. (1972). *J. Non-Cryst. Solids* **8–10**, 752
30. Marshall, J. M. & Owen A. E. (1971). *Phil. Mag.* **24**, 1281.
31. Fisher, F. D., Marshall, J. M. & Owen, A. E. (1976). *Phil. Mag.* **33**, 261.
32. Pfister, G. (1974). *Phys. Rev. Lett.* **33**, 1474.
33a. Mott, N. F., Davis, E. A. & Street, R. A. (1975) *Phil. Mag.* **32**, 961.
b. Street, R. A. & Mott, N. F. (1975). *Phys. Rev. Lett.* **35**, 1293.
34. Street, R. A. (1976). *Proc. Sixth Int. Conf. Amorphous and Liquid Semiconductors: Electronic phenomena in noncrystalline semiconductors.* Ed. B. T. Kolomiets. p. 116. Leningrad.
35. Kastner, M., Adler, D. & Fritzsche, H. To be published.
36. Scher, H. (1974). *Amorphous and liquid semiconductors.* Vol. 1. Ed. J. Stuke & W. Brenig, p. 135. Taylor & Francis Ltd.
37. Scher, H. & Montroll, E. W. (1975). *Phys. Rev. B*, **12**, 2455.
38. Marshall, J. M. & Miller, G. R. (1973). *Phil. Mag.* **27**, 1151.
39. Seager, C. H. & Quinn, R. K. (1975). *J. Non-Cryst. Solids* **17**, 386.
40a. Grant, A. J., Moustakas, T. D., Penney, T. & Weiser, K. (1974). *Amorphous and liquid semiconductors.* Vol. 1. Ed. J. Stuke and W. Brenig, p. 325. Taylor and Francis Ltd.
b Weiser, K., Grant, A. J. & Moustakas, T. D. (1974) *Amorphous and liquid semiconductors*, Vol 1. Ed. J. Stuke & W. Brenig, p. 335. Taylor & Francis Ltd.
41. Grant, A. J. & Davis, E. A. (1974). *Solid St. Commun.* **15**, 563.
42a. Kolomiets, B. T., Mamontova, T. N. & Babaev, A. A. (1970). *J. Non-Cryst. Solids* **4**, 289.
b. Kolomiets, B. T., Mamontova, T. N. & Babaev, A. A. (1972). *J. Non-Cryst. Solids* **8–10**, 1004.
43. Fischer, R., Heim, U., Stern, F. & Weiser, K. (1971). *Phys. Rev. Lett.* **26**, 1182.
44a. Bishop, S. G. (1973). *Phys. Lett.* **44A**, 107.
b. Bishop, S. G. & Mitchell, D. L. (1973). *Phys. Rev. B*, **8**, 5696.

45a. Cernogora, J., Mollot, F. & Benoit a la Guillaume, C. (1973). *Phys. Stat. Solidi A.* **15**, 401.
b. Mollot, F., Cernogora, J. & Bernoit a la Guillaume, C. (1974). *Phys. Stat. Solidi A.* **21**, 181.
46a. Street, R. A., Searle, T. M. & Austin, I. G. (1974). *Phil Mag.* **29**, 1157.
b. Street, R. A., Austin, I. G., Searle, T. M. & Smith, B. A. (1974). *J. Phys. C.* **8**, 1293.
c. Street, R. A., Searle, T. M. & Austin, I. G. (1974). *Phil. Mag.* **30**, 1181.
47. Street, R. A. *Adv. Physics.* To be published.
48. Street, R. A. & Yoffe, A. D. (1972). *Thin solid films* **11**, 161.
49. Spear, W. E. & Le Comber, P. G. (1972). *J. Non-cryst Solids* **8–10**, 727.
50. Spear, W. E. (1974). *Amorphous and liquid semiconductors.* Ed. J. Stuke and W. Brenig, p. 1. London: Taylor & Francis Ltd.
51. Madan, A., Le Comber, P. G. & Spear, W. E. (1976). *J. Non-Cryst. Solids* **20**, 239.
52. Spear, W. E. & Le Comber, P. G. (1976). *Phil. Mag.* **33**, 935.
53. Neudeck, G. W. & Malhotra, A. K. (1975). *J. appl. Phys.* **46**, 239.
54. Le Comber, P. G. & Spear, W. E. (1970). *Phys. Rev. Lett.* **25**, 509.
55. Le Comber, P. G., Madan A. & Spear, W. E. (1972). *J. Non-Cryst. Solids* **11**, 219.
56. Lewis, A. J. (1972). *Phys. Rev. Lett.* **29**, 1555.
57. Jones, D. I., Spear, W. E. & Le Comber, P. G. (1976). *Comm. Phys.* **1**, 39.
58. Jones, D. I., Spear, W. E. & Le Comber, P. G. (1976). *J. Non-Cryst. Solids* **20**, 259.
59. Beyer, W. & Stuke, J. (1975). *Phys. Stat. Solidi A.* **30**, 511.
60. Loveland, R. J., Spear, W. E. & Al-Sharbaty, A. (1973/74). *J. Non-Cryst. Solids* **13**, 55.
61. Spear, W. E., Loveland, R. J. & Al-Sharbaty, A. (1974). *J. Non-Cryst. Solids* **15**, 410.
62. Anderson, D. A. & Spear, W. E. To be published.
63. Engemann, D. & Fischer, R. (1974). *Amorphous and liquid semiconductors.* Vol. 2. Ed. J. Stuke and W. Brenig, p. 947. London Taylor & Francis Ltd.
64. Engemann, D. & Fischer, R. (1974). *Proc. 12th Int. Conf. Physics of Semiconductors,* Stuttgart, p. 1042. Teubner.
65. Engemann, D. & Fischer, R. To be published.
66. Fischer, J. E. & Donovan, T. M. (1972). *Non-Cryst. Solids* **8–10**, 202.
67. Mott, N. F., Davis, E. A. & Street, R. A. (1975). *Phil. Mag.* **32**, 961.
68. Rose, A. (1963). *Concepts in photoconductivity.* Interscience, New York.
69. Spear, W. E. & Le Comber, P. G. (1975). *Solid St. Comm.* **17**, 1193.
70. Le Comber, P. G., Jones, D. I. & Spear, W. E. To be published.
71. Friedman, L. (1971). *J. Non-Cryst. Solids* **6**, 329.
72. Spear, W. E., Le Comber, P. G. Kinmond, S. & Brodsky, M. H. (1976). *Appl. Phys. Lett.* **28**, 105.
73. Carlson, D. E. & Wronski, C. R. (1976). *Appl. Phys. Lett.* **28**, 671.
74. Ziman, J. M. (1970). *J. Non-Cryst. Solids* **4**, 426.
75. Blyum, A. I. & Regel, A. R. (1951). *Zh. Tekh. Fiz.*, **21**, 316.
76. Ioffe, A. F. & Regel, A. R. (1960). *Prog. Semiconductors*, **4**, 237.
77. Keller, J. & Ziman, J. M. (1972). *J. Non-Cryst. Solids*, **8–10**, 111.
78. Wright, A. W. & Leadbetter, A. J. (1976). *Physics Chem. Glasses* **17**, 122.
79. Kolomiets, B. T., Mazets, T. F., Efendiev, Sh. M. & Andreish, A. M. (1970). *J. Non-Cryst. Solids* **4**, 45.
80. Kolomiets, B. T. (1968). *Proch Ninth Int. Conf. Physics of Semiconductors*, Leningrad, Vol. 2, p. 1259. USSR, Academy of Science.
81. Marshall, J. M., Main, C. & Owen, A. E. (1972). *J. Non-Cryst. solids* **8–10**, 760.
82. Kolomiets, B. T., Ljubin, V. M., Shilo, V. P. & Averjanov, V. L. (1972). *J. Non-Cryst. Solids* **8–10**, 1017.
83a. Bishop, S. G., Strom, U. & Taylor, P. C. (1975). *Phys. Rev. Lett.* **34**, 1346.
b Bishop, S. G., Strom, U. & Taylor, P. C. (1976). *Phys. Rev. Lett.* **36**, 543.
c. Bishop, S. G., Strom, U. & Taylor, P. C. (1976). *Solid St. Commun.* **18**, 573.
84. Anderson, P. A. (1975). *Phys. Rev. Lett.* **34**, 953.
85. Kastner, M. (1972). *Phys. Rev. Lett.* **28**, 355.
86. Brodsky, M. H. & Title, R. S. (1969). *Phys. Rev. Lett.* **23**, 581.
87. Connell, G. A. N. & Pawlik, J. R. (1969). *Phys. Rev.* B, **13**, 787.
88. Beyer, W., Stuke, J. & Wagner, H. (1975). *Phys. Stat. Solidi* (a) **30**, 231.
89. Stuke, J. (1976). *Proc. Sixth Int. Conf. Amorphous and Liquid Semiconductors: Electronic phenomena in noncrystalline semiconductors.* Ed. B. T. Kolomiets, p. 193. USSR. Leningrad Academy of Science.
90. Beyer, W. & Stuke, J. (1975). *Phys. Stat. Sclidi A.* **30**, K155.
91. Lewis, A. J., Connell, G. A. N., Paul, W., Pawlik, J. R. & Temkin, R. J. (1974). *Tetrahedrally bonded amorphous semiconductors.* Ed. M. H. Brodsky, S. Kirkpatrick & D. Weaire, p. 27. A.I.P., New York.

The Raman spectra and structure of glasses in the As–S and As–Se systems

P. J. S. Ewen, M. J. Sik & A. E. Owen*

Department of Electrical Engineering, University of Edinburgh

The room-temperature Raman spectra of bulk glasses in the range $As_{35}S/Se_{65}$ to $As_{55}S/Se_{45}$ have been recorded. The spectra of the glasses on the S/Se-rich side of stoichiometry have been analysed in terms of the Lucovsky-Martin molecular model and indicate the replacement of the As–S/Se–As links between the AsS/Se_3 pyramid units by As–S/Se–S/Se–As links as the S/Se content is increased. There is no indication of Se_8 rings in the selenides, but the presence of S_8 rings is increasingly apparent in the compositions more S-rich than $As_{37}S_{63}$. In the case of the As-rich sulphides sharp spectral features characteristic of c-As_4S_4 appear near stoichiometry and increase smoothly as the As content is increased. The presence of c-As_4S_3, c-As_4S_5 and As–As bonds in the glassy matrix is also indicated. The spectra of the As-rich selenides show no crystalline features and indicate only the increasing presence of As–As bonds with increasing As content.

1. Introduction

This paper is a detailed study of the Raman spectra of glasses within ± 5 atomic % of the stoichiometric composition $As_{40}X_{60}$ (where X = S or Se). Measurements have been made on eleven near-stoichiometric glasses extending in each system from 35 to 45 atomic % As in one atomic % steps, augmenting Ward's[1,2] broader investigation of these systems. Some crystalline and amorphous compositions outside this range have also been examined.

Kobliska & Solin[3] have emphasized the importance of polarization measurements in Raman scattering investigations of amorphous solid structure and have defined a new type of spectrum called the depolarization spectrum. Accordingly, the polarization spectra for each glass have been measured, in addition to the unanalysed spectra, and from these have been derived the depolarization spectra.

2. Experimental

All the amorphous samples were annealed bulk glasses. Chemical analysis showed no significant difference from the expected compositions and no measurable inhomogeneity throughout the samples. The near-stoichiometric sulphide glasses were red and transparent, apart from the two most As-rich compositions which were pink, opaque and granular in appearance. All the selenides were black and opaque.

The c-As_4S_3 used was prepared by slowly cooling a melt of this composition and the c-As_4S_5 was obtained using the method outlined by Whitfield[4]. Crystalline samples of As_2Se_3, As_2S_3 and As_4S_4 were obtained from external sources.

The sulphide spectra were excited with red light of either 6328 Å from a He–Ne laser or 6471 Å from a Kr-ion laser. The sulphides are very strong scatterers at these wavelengths and peak signals of ≈ 5000 counts/sec were typical. Because of the high absorption coefficients of the selenides at red wavelengths, the selenide spectra were obtained using the 7993 Å IR line of the Kr laser.

A Spex 1400 monochromator with a cooled RCA-C31034A photomultiplier operating in the photon-counting mode was used for detection. The spectra were all recorded at room temperature using right angle transmission geometry for the transparent samples and back reflection for the opaque glasses. A spectral slit width of $\approx 3\ cm^{-1}$ was used.

To avoid the damaging effect of focused radiation[3] the selenide samples were spun in the focused beam, while an unfocused 3 mm diameter beam was used for the sulphides. The beam powers used were approximately 50 mW (6328 Å), 60 mW (7993 Å) and 240 mW (6471 Å). Although no gross physical damage occurred in the sulphides when unfocused radiation was used, a gradual loss of signal, $\approx 3\%$ per hour, was observed. A non-annealed sample of $As_{36}S_{64}$ gave three times this rate of count loss. The decrease in signal could not be attributed to changes in beam power. When an irradiated sample was examined under a polarizing microscope, the cylindrical path of the laser beam through the sample was clearly visible, indicating that laser-induced changes are taking place inside the glass. All the spectra presented here have been corrected for this intensity decrease, which is approximately linear with time over the first few hours of exposure. The effect is consistent with an increase in the optical absorption coefficient of these materials with exposure.[5,6]

Several experiments were performed to show that this count loss was not accompanied by any spectral changes which might be attributed to structural changes in the glasses. The selenide spectra, recorded from the spinning samples, did not exhibit any signal loss.

*Present address: Department of Clinical Physics and Bio-Engineering, 11 West Graham St, Glasgow G4 9LF.

Some features in Ward's spectrum of a-As_2S_3[1] have been attributed to plasma lines[7] and particular care was taken to exclude such spurious features. Spectra obtained with the He-Ne laser were identical with corresponding spectra excited with the Kr laser so that the spectral features presented in this study cannot be attributed to plasma lines.

3. Results and discussion

A. The Stoichiometric Glasses

With the IR Kr laser line as excitation the low energy region of the a-As_2Se_3 Raman spectrum was recorded, as well as the main band, and the spectra indicate vibrations at 106, 136, 223 and 275 cm^{-1} plus a thermal peak at 23 cm^{-1}. The polarization spectra, the unanalysed spectrum (see Figure 3) and the depolarization spectrum (see Figure 2) were all taken into account in deriving these frequencies. In the case of the sulphide the results indicate vibrations at 160, 185, 208, 231, 315, 338, 395 and 490 cm^{-1} plus the thermal peak at 29 cm^{-1}. The 160 cm^{-1} frequency is obtained from the depolarization spectrum[5,8] (see Figure 2), though there is a broad weak feature around this frequency in the Raman spectra. The vibration at 315 cm^{-1} appears as a shoulder in the unanalysed spectrum (see Figure 1) but is present as a sharp peak in the VH polarization spectrum. The knee at 395 cm^{-1} has not been reported in previous Raman studies and corresponds to the minimum in the depolarization spectrum. A similar knee and minimum are found at 275 cm^{-1} in the corresponding selenide spectra.

In the molecular model[9,10] the glasses are considered to be made up of pyramidal AsX_3 units loosely coupled via bent As–X–As chains. c-As_2S_3 and c-As_2Se_3 are also made up of pyramidal units bridged by S or Se atoms so it is not surprising that the two amorphous vibrational spectra scale by a factor of 0·71, as in the crystal spectra[11,12]. The corresponding pairs of frequencies are 106/160, 136/185, 223/315, 246[13]/338 and 275/395; the three exceptions, the features at 208, 231 and 490 cm^{-1} in a-As_2S_3, are discussed below. As in the crystal spectra the most intense Raman peak in each of the unanalysed glass spectra does not correspond to the same vibration. In Figure 2 the depolarization spectrum of a-As_2S_3 has been compressed along the frequency axis by the scaling factor 0·71.

The sulphide features at 208, 231 and 490 cm^{-1} probably arise from structural features not present in perfect c-As_2S_3, *viz.*, As–As and S–S bonds. 230 cm^{-1} is the dominant frequency in the IR spectrum of a-As[14] while the Raman spectrum of a-As contains a broad, flat-topped band extending from $\approx$190 to $\approx$250 cm^{-1}. The feature at 231 cm^{-1} in a-As_2S_3 becomes more pronounced as the As content of the glass is increased (see Section C) and resonance Raman studies of this material[15,16] show that the region around 230 cm^{-1} behaves differently from the rest of the spectrum and resonates about the "optical gap" energy, $\approx$2·32 eV at 300 °K. The

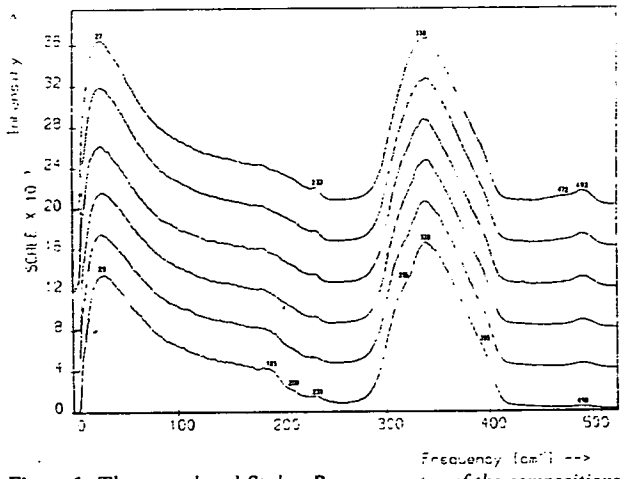

Figure 1. *The unanalyzed Stokes Raman spectra of the compositions $As_{40}S_{60}$–$As_{35}S_{65}$. The spectra are normalized to the height of the 338 cm^{-1} band and are displaced above one another, starting with the a–$As_{40}S_{60}$ spectrum at the bottom and going up in order of increasing S content to the $As_{35}S_{65}$ spectrum at the top.*

features at 208 and 490 cm^{-1} are discussed in Section B. Similar features may be present in the spectrum of a-As_2Se_3 but probably coincide with the main band and are not so easily detected. The other frequencies can all be accounted for by the molecular model.

B. The Chalcogen-rich Glasses: $As_{40}X_{60}$–$As_{35}X_{65}$

The molecular model can be extended to the chalcogen-rich glasses if the extra chalcogen atoms are incorporated in the chains linking the pyramidal molecules. In the case of the S-rich glasses it was found that the changes in the spectra with respect to the a-$As_{40}S_{60}$ spectrum arise from two sources: the appearance of S_8 rings and the above-mentioned replacement of As–S–As links with the As–S–S–As chains. Figure 1 shows the unanalysed S-rich spectra and three regions of change can be seen. As the sulphur content is increased a new band grows steadily at $\approx$492 cm^{-1}, the shoulder at 315 cm^{-1} disappears gradually and a change in profile occurs around 180–240 cm^{-1}, with a small peak appearing at 233 cm^{-1}. The shoulder on the 492 cm^{-1} band appears at $\approx$63 atomic % sulphur and is resolved into

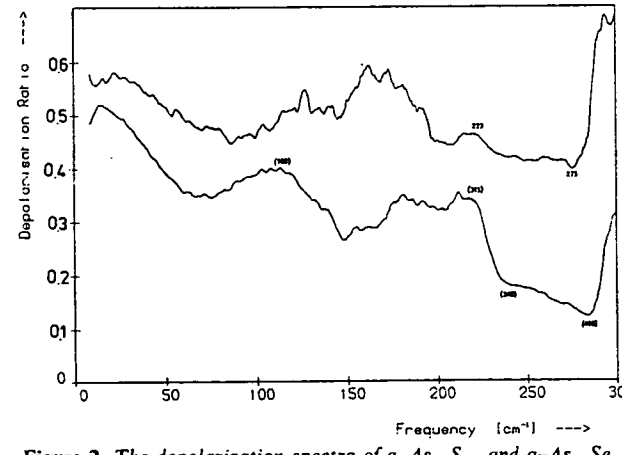

Figure 2. *The depolarization spectra of a–$As_{40}S_{60}$ and a–$As_{40}Se_{60}$. The frequency scale applies only to the a–$As_{40}Se_{60}$ since the a–$As_{40}Se_{60}$ spectrum has been compressed by a factor of 0·71 along the frequency axis. The bracketed frequencies are those actually measured for a–$As_{40}S_{60}$.*

a peak at 472 cm^{-1} in the VV spectra. The knee at 395 cm^{-1} and the maximum at 160 cm^{-1} in the depolarization spectrum are present for all five S-rich glasses and there is no shift in the positions of the main peak frequencies. These observations are not surprising as it is expected that the pyramids and As–S–As chains are retained in the structure.

A more exact set of values for the new frequencies is provided by the difference spectra obtained by subtracting the a-$As_{40}S_{60}$ spectrum from each of the others. They are 176, 208, 233, 325, 472 and 492 cm^{-1}, with the possibility of another frequency on the high energy side of the asymmetric main band. Ward's work[1,2] on the very S-rich glasses shows two new features appearing on the main band at 337 and 354 cm^{-1}, which may correspond to the frequencies in this region suggested by the difference spectra.

The features at 233 and 472 cm^{-1}, which first appear at the composition $As_{37}S_{63}$, are associated with the presence of S_8 rings. In the spectra of the glasses more S-rich than $As_{35}S_{65}$, also reported by Ward[1,2], these lines are accompanied by others of the S_8 spectrum and grow very rapidly with increasing S-content, soon overtaking the other emerging features.

Standard valence force field calculations show that the non-S_8 frequencies can be attributed to a bent As–S–S–As chain but not to a linear chain. The A_2B_2 molecule of C_2 symmetry has six normal modes of vibration, all Raman active[17]. It is found that the torsional frequency for the A_2S_2 "molecule" is very low and would be difficult to detect in the glass spectra. The other five frequencies, however, are in reasonable agreement with the five experimental values. The 492 cm^{-1} vibration corresponds to the symmetric stretch of the S–S bond and is responsible for the weak feature at $\approx$490 cm^{-1} in the a-As_2S_3 spectrum.

In the case of the selenides the analysis is complicated by the fact that many of the observed frequencies for the various forms of pure selenium and the predicted frequencies for the pyramid and chains are close to one another. Figure 3 shows the unanalysed, reduced Se-rich spectra normalized by area and superimposed. There are no changes in the low frequency region, the only change in the spectrum being the growth of a feature on the high energy side of the main band. Difference spectra in this region show a peak growing at $\approx$265 cm^{-1}. The most intense line in the Raman spectra of Se_8 and a-Se occurs at 250 cm^{-1}. Although there is nothing in the difference spectra to suggest the presence of these forms in the glasses Ward's work on the Se-rich compositions beyond $As_{35}Se_{65}$ show a feature steadily growing at this frequency.

There is, however, no feature in the pure selenium spectra at 265 cm^{-1}. The valence force field calculation for the As–Se–Se–As chain yields a value of 268 cm^{-1} for the symmetric stretch frequency of the Se–Se bond. The ratio of the frequencies designated symmetric stretch for the sulphur and selenium rich glasses is 1·86, which agrees with the frequency scale

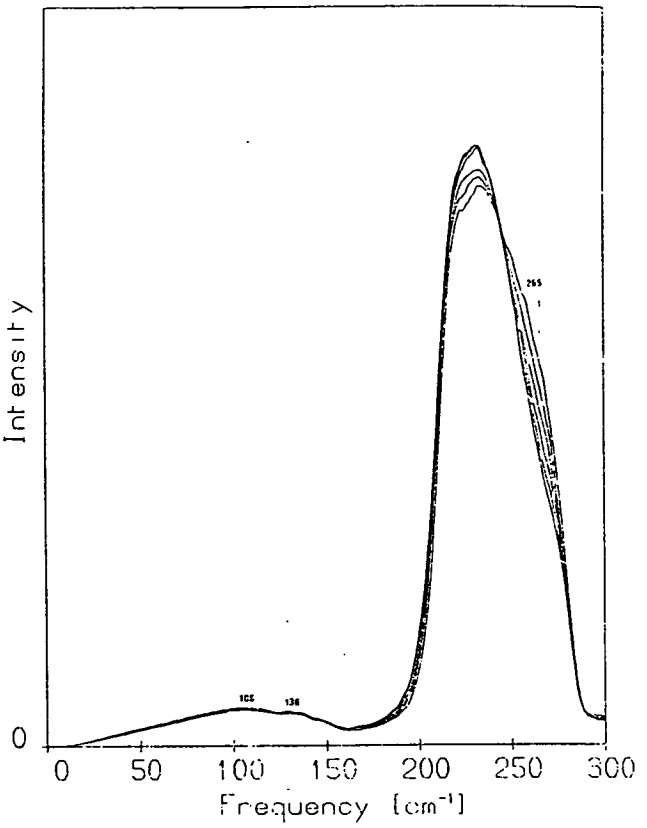

Figure 3. *The unanalyzed Stokes Raman spectra of the compositions $As_{40}Se_{60}$–$As_{35}Se_{65}$. The spectra have been reduced by the Shuker–Gammon method and are normalized by area. The changes occurring at the peak frequency are due to the normalization.*

factor relating S_8 to Se_8 observed by Lucovsky *et al.*[18]

Although structure has been observed in the difference spectra near other frequencies predicted by the chain calculation, it cannot be definitely attributed to the As–Se–Se–As "molecule" for the reason mentioned earlier. There is no sign of the low frequency bending modes of the As–Se–Se–As chain in the region $< 160\ cm^{-1}$, which does not change at all, but this might be expected since the bending modes of the pyramids and As–Se–As links yield very weak features in the spectrum of a-As_2Se_3.

C. *The As-rich Glasses: $As_{40}X_{60}$–$As_{45}X_{55}$*

In the As-rich sulphide glasses sharp features start to appear in the spectra for even small amounts of excess arsenic, as also observed by Ward[1,2]. The lines are mostly characteristic of the crystal β-As_4S_4[19], but some frequencies – 133,231 and 270 cm^{-1} – cannot be ascribed to α- or β-As_4S_4. These results indicate the presence of small amounts of c-As_4S_3 and possibly c-As_4S_5, but no c-As_2S_3, in the glasses, although in the scanning electron microscope the material still appeared to be a homogeneous glass up to 43% As. The feature at 231 cm^{-1} probably arises from As–As bonds in the glassy matrix, which is also responsible for the continuous background in the spectra.

The change from transparent to opaque occurs abruptly at some composition between $As_{43}S_{57}$ and $As_{44}S_{56}$. Electron micrographs of the As-rich sulphides show no features in the transparent glasses but

for the opaque samples reveal pockets of material embedded in a matrix. These abrupt changes are not apparent in the Raman spectra, where the "crystalline" lines grow steadily as the As content is increased beyond 40 atomic %.

In the case of the As-rich selenides phase-separation does not occur, although c-As_4Se_4 also exists. The spectral features (see Figure 4) remain broad and can be associated with the appearance of As–As bonds in the glasses. The new bands growing at 230 and $\approx 155\ cm^{-1}$ both appear in the vibrational spectra of a-As.

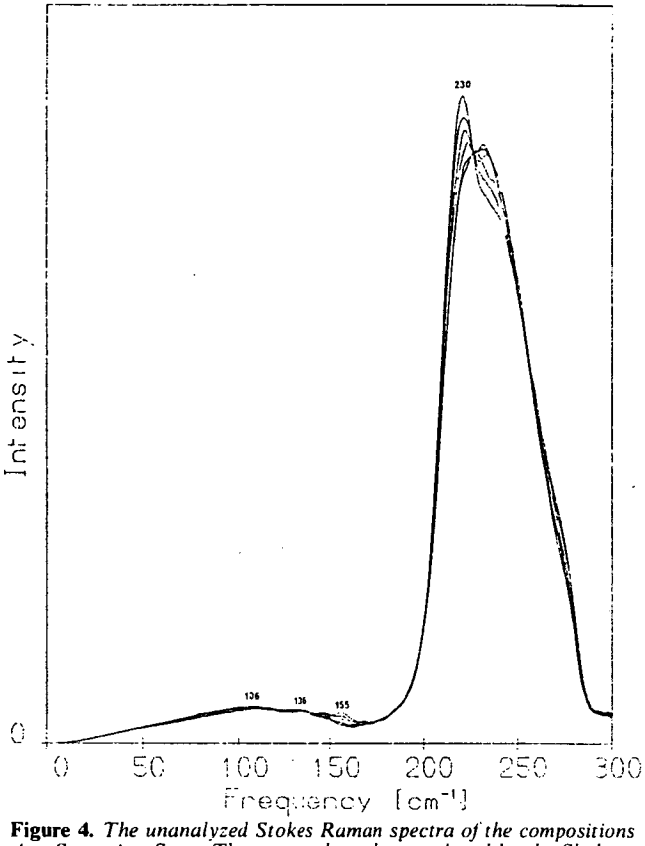

Figure 4. *The unanalyzed Stokes Raman spectra of the compositions $As_{40}Se_{60}$–$As_{45}Se_{55}$. The spectra have been reduced by the Shuker–Gammon method and are normalized by area. The changes occurring on the high energy side of the main peak are due to the normalization.*

Similar conclusions on the structure of the chalcogen- and arsenic-rich glasses have been reached by Lucovsky *et al.*[20]

Acknowledgements

The cooperation of Professor W. Cochran, Dr W. Taylor and their colleagues in the Light Scattering Group of the Physics Department, University of Edinburgh in providing the excellent Raman facilities is gratefully acknowledged.

P. J. S. Ewen would like to thank the Science Research Council for their support.

References

1. Ward, A. T. (1968). *J. Phys. Chem.* **72,** 4133.
2. Ward, A. T. (1972). *Adv. in Chemistry* **110,** 163.
3. Kobliska, R. J. & Solin, S. A. (1973). *Phys. Rev.* **B 8,** 756.
4. Whitfield, H. J. (1973). *JCS Dalton* 1740.
5. Tanaka, K. & Kikuchi, M. (1972). *Solid State Commun.* **11,** 1311.
6. de Neufville, J. P., Moss, S. C. & Ovshinsky, S. R. (1974). *J. Non-Cryst. Solids* **13,** 191.
7. Kobliska, R. J. & Solin, S. A. (1972). *J. Non-Cryst. Solids* **8,** 191.
8. Finkman, E., De Fonzo, A. P. & Tauc, J. (1973). *Proc. 5th Int. Conf. on Amorphous and Liquid Semiconductors*, Garmisch-Partenkirchen, Taylor & Francis Ltd, p. 1275.
9. Austin, I. G. & Garbett, E. S. (1971). *Phil. Mag.* **23,** 17.
10. Lucovsky, G. & Martin, R. M. (1972). *J. Non-Cryst. Solids* **8–10,** 185.
11. Zallen, R., Slade, M. L. & Ward, A. T. (1971). *Phys. Rev.* **B 3,** 4257.
12. Zallen, R. & Slade, M. L. (1974). *Phys. Rev.* **B 9,** 1627.
13. Lucovsky, G. (1972). *Phys. Rev.* **B 6,** 1480.
14. Lucovsky, G. & Knights, J. C. (1974). *Phys. Rev.* **B 10,** 4324.
15. Razzetti, C. & Fontana, M. P. (1975). *Phys. Stat. Sol.* **(B) 70,** 173.
16. Howard, R. E., Macedo, P. B. & Moynihan, C. T. (1975). *Solid State Commun.* **17,** 1475.
17. Herzberg, G. (1945). *Infrared and Raman Spectra of Polyatomic Molecules*, Van Nostrand, New York.
18. Lucovsky, G., Mooradian, A., Taylor, W., Wright, G. B. & Keezer, R. C. (1967). *Solid State Commun.* **5,** 113.
19. Porter, E. J. & Sheldrick, G. M. (1972). *JCS Dalton*, 1347.
20. Lucovsky, G., Galeener, F. L., Geils, R. H. & Keezer, R. C. Paper presented at this symposium.

PHILOSOPHICAL MAGAZINE B, 1978, VOL. 38, NO. 1, 57–70

Electrical contact properties of semiconducting chalcogenide glasses

By A. M. WALLACE†, A. E. OWEN and J. M. ROBERTSON
Department of Electrical Engineering, University of Edinburgh, Scotland

[Received 1 August 1977 and accepted 13 May 1978]

ABSTRACT

Measurements of the d.c. conductivity of radio-frequency sputtered thin films of a Ge–As–Te chalcogenide glass, sandwiched between a variety of metallic electrodes, indicate the absence of any blocking barrier associated with the metal-amorphous semiconductor contact, except when an oxidizing electrode such as Al is used. These results are confirmed by measurements of the capacitance and a.c. conductance as a function of frequency and are analysed in terms of a model of the metal-amorphous semiconductor contact in which transport occurs by a parallel combination of thermionic field emission, band-to-band recombination/generation via localized gap states, and tunnelling at the Fermi level followed by thermal excitation into the conduction band. Calculations show that recombination/generation is the dominant mechanism of transport across the contact.

§ 1. INTRODUCTION

A general experimental feature of most amorphous semiconductors is that, in contrast to crystalline semiconductors, it is apparently easy to form non-blocking contacts. It is probable, however, that space charge regions are present at contacts or surfaces on amorphous semiconductors, just as they are in crystalline materials, although perhaps different in form and magnitude; their existence is confirmed by the detection of bipolar contact photovoltages in sandwich-type devices similar to those under discussion here (Wey and Fritzsche 1972, Wallace 1975). Experimentally, this paper is concerned with the electrical contact properties of thin films prepared from a chalcogenide glass of composition $Ge_{10}As_{40}Te_{50}$ and with various combinations of metal electrodes (§ 2). The experimental data (§§ 3 and 4) again demonstrate the absence of any effective electrode barriers and possible reasons for this are discussed, in mechanistic terms, in § 5.

The interface between a metal and an amorphous semiconductor is compared to a typical rectifying contact between a metal and an n-type crystalline semiconductor in fig. 1, taken from a review article by Fritzsche (1974). A large density of localized states exists within the space charge layer of the amorphous material, but they are distributed throughout the forbidden gap. The Fermi level is normally pinned near the centre of the gap, unlike an extrinsic crystalline semiconductor where it is closer to the band edge. Calculations for the screening length, λ, in materials containing a high density of states at the

† Present address: Ferranti Ltd, Robertson Avenue, Edinburgh, Scotland.

Fig. 1

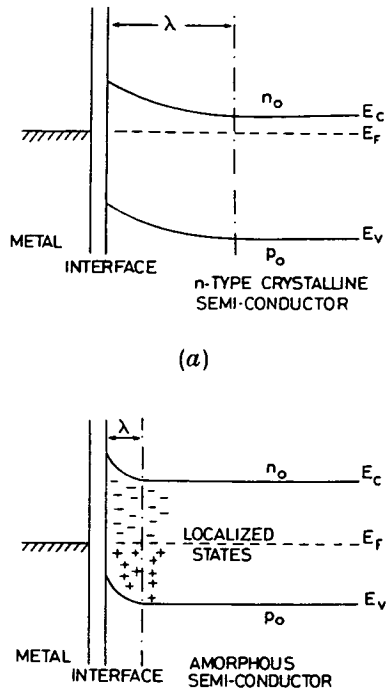

Potential distribution at the metal-semiconductor contact. (*a*) *n*-type crystalline semiconductor; (*b*) amorphous semiconductor.

Fermi level have been reported by several authors, for example Mott (1971) and Barbe (1971). Using the standard expression,

$$\lambda = (\epsilon_r \epsilon_0 / q^2 N_F)^{1/2}, \tag{1}$$

where N_F is the density of localized states at the Fermi level, ϵ_r is the dielectric constant, ϵ_0 is the permittivity of free space and q is the electronic charge, values for λ of less than 10 nm are deduced for reported values of N_F (i.e. 10^{24}–$10^{25}\,m^{-3}\,eV^{-1}$) in chalcogenide alloys (Spear 1973). Thus, the screening length in amorphous semiconductors is much shorter than that usually associated with crystalline semiconductors. This fact has been cited, in a qualitative way, as the reason for the absence of blocking contacts, the suggestion being that carriers can readily tunnel through such short barriers. The calculations described in § 5 indicate, however, that this is not the case but that current continuity across the contact is maintained by band-to-band recombination and generation via localized gap states.

§ 2. Sample preparation

A sandwich-type electrode configuration was used for all measurements. This consisted of a lower metal electrode deposited on an insulating (Corning 7059) glass substrate, followed by a film prepared by radiofrequency sputtering from a source of powdered bulk chalcogenide glass, $Ge_{10}As_{40}Te_{50}$, giving films of thickness in the range 0·2–5·0 μm. Finally, a top metal electrode was deposited

at right angles to the lower electrode. Thus the sample area (0·25 mm^2) was defined by the crossover of the top and bottom electrodes. Subsequent analysis of selected glass films by spectrophotometric techniques showed a consistent increase in the Ge and Te concentration, and a decrease in the As concentration relative to the parent glass. Deviations in glass composition do not substantially effect the behaviour of the contacts however, nor do they basically alter the analysis presented at a later stage.

The electrical contact behaviour of 11 metals was investigated, viz. Au, Mo, Sb, Ag, Cu, Al, Sn, Pb, In, Ni and Fe. Each series of sputtered glass samples was produced with four electrode combinations: Au–Au, Au–X, X–Au and X–X, where the first quoted is the bottom electrode, the second the top electrode, and X refers to a metal from the above list. Thus, by considering experimental data on all four electrode combinations, variations associated with batch preparation were eliminated.

§ 3. D.C. CONDUCTIVITY DATA

Prior to investigation of the properties of the contacts, the d.c. conductivity of thin films of the chalcogenide glass was determined as a function of temperature and applied field, using sandwich-type devices with either Au or Mo electrodes. The data obtained are reported by Wallace (1975), and are similar to those observed in a variety of amorphous materials, by for example, Fagen and Fritzsche (1970), De Wit and Crevecoeur (1972) and Marshall and Miller (1973). In each case the conductivity, σ, can be expressed in the form

$$\sigma = \sigma_0 \exp(-\Delta E/kT) \exp(F/F_0), \tag{2}$$

where σ_0 is a constant, ΔE is the activation energy, k is Boltzmann's constant, T is the absolute temperature, F is the applied field and F_0 is a field constant. The value of the low-field d.c. conductivity at 294 K is approximately 3×10^{-4} ohm^{-1} m^{-1}, and E is calculated to be between 0·47 and 0·48 eV, in good agreement with the values quoted by Tanaka (1971) for a similar composition.

§ 4. METAL-AMORPHOUS SEMICONDUCTOR CONTACT DATA

A standard technique for the detection of blocking layers associated with barrier regions requires the measurement of the resistance of sandwich samples of various thicknesses. Any series resistance associated with the contact should be evident as a non-zero intercept, R_0, of the extrapolated resistance-thickness curve. Thus the expression for device resistance would be:

$$R = R_0 + \rho_B . t/A, \tag{3}$$

where ρ_B is the bulk resistivity, and t and A are the sample thickness and area, respectively. Figure 2 illustrates the variation of low-field sample resistance with thickness for a series of samples with molybdenum electrodes. The bars indicate the range of values obtained for the ten devices fabricated on each substrate. Within the limits imposed by variations in composition from batch to batch, fig. 2 demonstrates the absence of any large series contact resistance.

Typical room temperature, current–voltage characteristics of thin film sandwich devices with various electrode combinations are illustrated in fig. 3. The characteristics are completely symmetrical at low fields ($< 10^6$ V m^{-1}), but

Fig. 2

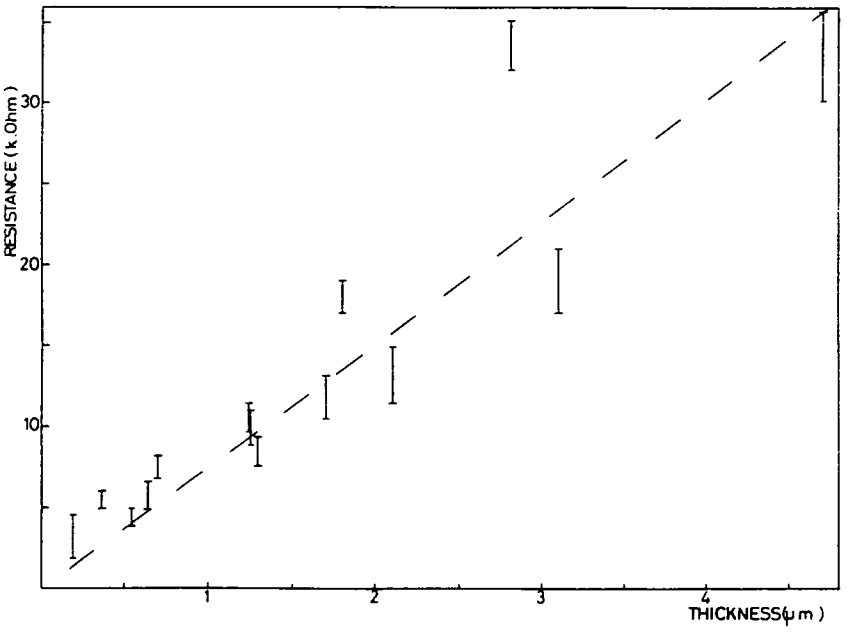

Variation of resistance of Ge–As–Te sandwich devices with specimen thickness (temperature = 294 K).

Fig. 3

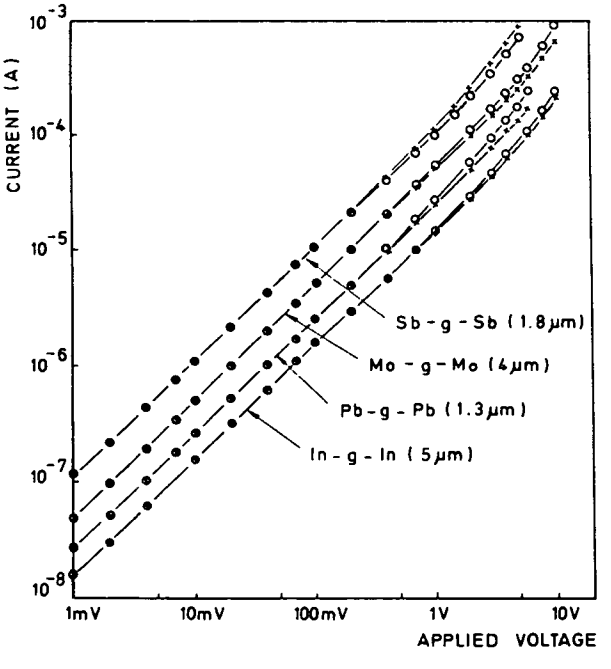

Current–voltage characteristics of Ge–As–Te sandwich devices with various electrodes (temperature = 294 K). + = Top electrode positive. ○ = Bottom electrode positive.

at high fields slight rectification is evident. The degree of rectification was observed to be a function of the particular batch rather than the electrode permutation, varying from batch to batch in both magnitude and sense, and the essential symmetry of the characteristic (and the small high-field asymmetry) was maintained throughout the exper mental temperature range, 120–300 K. Similarly, computed values of the glass resistivity varied according to the particular batch rather than the electrode combination, and were generally within a factor of two of the measured bulk resistivity. Thus, the conduction process in sandwich devices of this type appears to be bulk-limited, and independent of the electronic and physical characteristics of the metal electrodes used.

An exception to this rule is observed when an easily oxidized metal is used as the lower electrode. In that case a thin insulating layer is formed between the metal and the chalcogenide glass film. This is evident from the data on batches prepared with Au and Al electrodes, as illustrated in fig. 4; where Al forms the lower electrode. Breaking the vacuum before deposition of the chalogenide film results in a thin layer of Al_2O_3 over the lower electrode. At low bias values, the current–voltage characteristics are limited by the high series resistance of the oxide layer, resulting in a low-field device resistance which is approximately two orders higher than that of the corresponding Au–chalcogenide–Au device. At high bias values, the limiting factor is again the bulk series resistance of the chalcogenide film.

Fig. 4

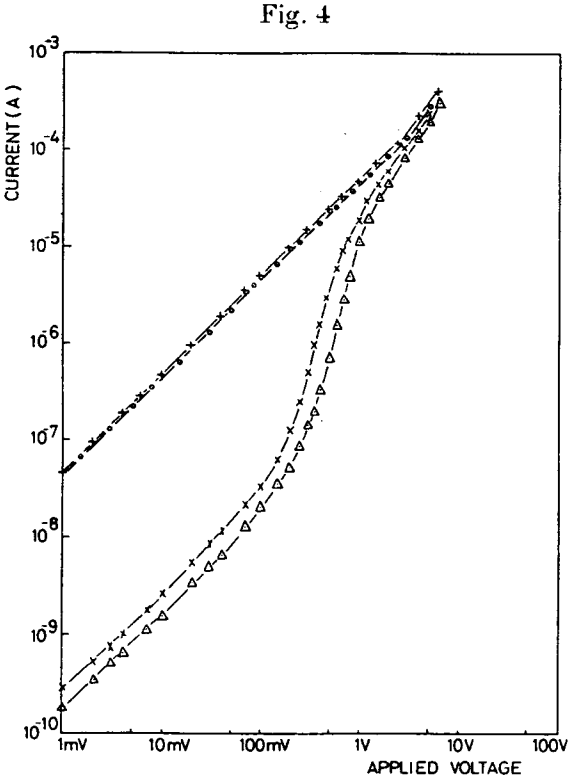

Current–voltage characteristics of Ge–As–Te sandwich devices (temperature = 294 K). + Au = chalcogenide–Al; ● Au = chalcogenide–Al; × Al = chalcogenide–Au; Δ Al = chalcogenide–Al.

It is necessary to emphasize that the data of fig. 4 are in all cases symmetrical. When Al forms the top electrode no oxide barrier is formed, and the characteristics are similar to those devices where non-oxidizing metals are used. When Al forms the lower electrode, a metal-oxide–semiconductor-metal (M.O.S.M.) structure is formed, and a symmetrical, monotonic increase in conductance with applied bias is obtained similar to that reported in the literature for other Al–Al_2O_3-amorphous semiconductor systems (e.g. Osmun 1975, Sauvage, Mogab and Adler 1972). It is probable that recent measurements by Dove and Irani (1976) on Al–$Ge_4Te_{15}As$–Al devices can also be interpreted in this way, rather than in terms of a Schottky barrier formed between the aluminium and the semiconductor.

Confirmation of these results has been obtained from measurements of the capacitance and a.c. conductance of these devices as a function of frequency in the range 20–10^5 Hz, as illustrated in fig. 5. Typical characteristics of non-oxidizing metal electrode devices are frequency-independent, but for the Al-chalcogenide–Al device there is a rise in capacitance and fall in a.c. conductance at low frequencies. The behaviour of the latter device can, therefore, be represented by a simple parallel combination of the resistance and capacitance corresponding to a thin Al_2O_3 layer of the order of 10 nm in series with a further parallel combination of the bulk resistance and capacitance. Good agreement with the data of fig. 5 can be obtained by inserting values for the low-field d.c. resistance of the oxide layer and the glass film obtained from fig. 4, and calculating values for the oxide capacitance and the glass film capacitance from the standard formula,

$$C = \epsilon_r \epsilon_0 A/d, \tag{4}$$

where A and d are the relevant dimensions and ϵ_r the relevant dielectric constant.

Fig. 5

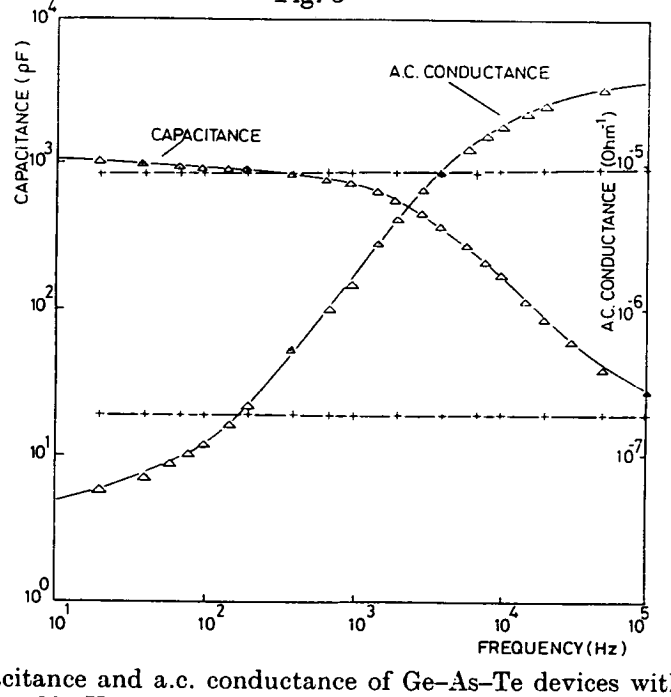

Variation of capacitance and a.c. conductance of Ge–As–Te devices with frequency (temperature = 294 K). + Au = chalcogenide–Au; Δ Al = chalcogenide–Al.

Returning to the data for the Au–chalcogenide–Au sample, it is instructive to compare these with data recently published by Wey (1976) for $Ge_{16}As_{35}Te_{28}S_{21}$ samples with Au and Sb electrodes. Similar frequency-independent behaviour was found with freshly prepared samples, but Wey observed a gradual increase in low-frequency capacitance over a period of 6 months when Au was used as an electrode. This behaviour was attributed to slow alloying of Au with the amorphous semiconductor to form a thin, 'high-sensitivity' contact barrier, and it is relevant to note that no corresponding effect was observed here over a period of 6 months.

§ 5. Analysis and discussion

The apparent differences between the electrical characteristics of metal-amorphous and metal-crystalline semiconductor structures indicates important differences in the dominant transport mechanisms across the contacts and the lack of any noticeable barrier resistance in amorphous devices can be explained in terms of the model of fig. 6. For the purposes of the model, electron transport (as opposed to hole transport) is considered as the dominant conduction mechanism, and space charge regions are assumed to be parabolic rather than

Fig. 6

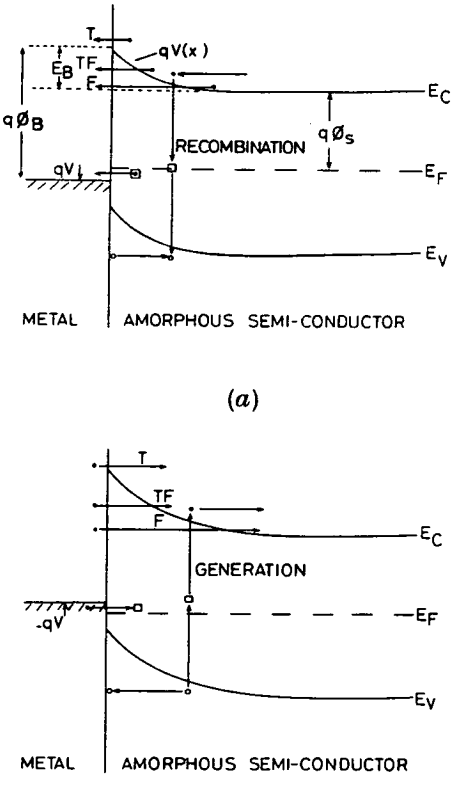

Transport processes in the metal-amorphous semiconductor contact. (*a*) Forward bias; (*b*) reverse bias.

exponential in form, as this facilitates adaptation of existing theories to the amorphous case. However, these assumptions do not significantly affect the conclusions drawn from the following calculations.

In fig. 6 charge continuity at the interface can be considered as a combination of three parallel components;

(i) Electron transport across the barrier, which can be further subdivided into a parallel combination of thermionic (T), thermionic field (TF) and field emission (F).

(ii) Recombination/generation processes via localized states in the semiconductor depletion region.

(iii) Tunnelling to and from localized states at the Fermi level, coupled with thermal excitation to and from the conduction band.

An expression for the current density, J, of component (i) can be derived from the expression of Crowell and Rideout (1969), i.e.

$$J/J_m = (J_{ma}/J_m)\exp(-q(\phi_B-\phi_s)/E_0)\cdot\exp(qV/E_0)\cdot(1-\exp(-qV/kT)), \quad (5)$$

where E_B is the amount of band bending at the interface, and is given by

$$E_B = q(\phi_B-\phi_s-V)$$

as illustrated in fig. 6(*a*), and V is the applied bias, q is the electronic charge, k is Boltzmann's constant and T is the absolute temperature. E_0 is expressed by

$$E_0 = E_{00}\coth\left[\frac{E_{00}}{kT}\right],$$

where E_{00} is a material constant associated with the transmission of the barrier for carriers of energy $E=0$, first introduced by Padovani and Stratton (1966), expressed by

$$E_{00} = 18\cdot10^{-12}\left[\frac{N_F}{m_r\cdot\epsilon_r}\right]\text{eV},$$

where N_F is the impurity concentration in units of cm^{-3}, ϵ_r the relative dielectric constant, and m_r the tunnelling effective mass measured in units of the free electron mass. J_{ma} is the apparent normalized flat band current density, where

$$J_m = A^{**}T^2\exp[-q\phi_s/kT],$$

and is the flat band current density incident on the depletion layer associated with the Maxwell distribution of carriers. Computerized solutions for J_{ma}/J_m are obtained from Cromwell and Rideout (1969) as a function of E_B/kT and kT/E_{00}. The use of expression (5) is valid in the relatively high carrier concentration, low-temperature range ($E_{00}\geqslant kT$), and thus covers the range of experimental data presented here since $E_{00}=kT$ at 482 K for the stated parameters. This temperature is above the glass transition point for the alloy used in this work.

In order to obtain a quantitative estimate of this component, a parabolic barrier of width 7·4 nm and equilibrium height approximately 0·5 eV is assumed. This is obtained from eqn. (1) by substituting a value of $N_F = 10^{25}\,m^{-3}\,eV^{-1}$ obtained from field-effect measurements (Wallace 1975) and typical of the multicomponent chalcogenide glasses (Spear 1973). The impurity concentration

is assumed independent of temperature and the contribution of free electrons is assumed small compared to that of charge trapped in localized states. Image-force lowering and quantum mechanical reflection of carrier near the top of the barrier are neglected; the effect of their inclusion would be to substantially increase the current density when the maximum in the energy spectrum of transmitted current occurs near the top of the barrier (Padovani 1971), but when, as in this case, transport occurs via a combination of TF and F emission, the error is small. The relative effective electron mass, m_r, is assumed independent of energy and equal to 0·2, taken from calculations by Stratton (1962) for triangular and parabolic barriers. The use of non-degenerate statistics is considered valid, since, in the case of semiconducting chalcogenide glasses, the presence of a high density of localized states within the gap leads to the formation of thin barrier layers, while the Fermi level remains pinned at the gap centre. Finally, a value of $\epsilon_r = 10$ is used, appropriate to materials of this type (Cohen, Fritzsche and Ovshinsky 1969, Owen and Robertson 1970), and in agreement with values calculated from the data of fig. 5.

Charge continuity at the interface may also be maintained by recombination and generation processes via localized states within the barrier region and a high density of such states is present in chalcogenide glasses, as is evident from field-effect data. In addition the Fermi level is centrally located within the semiconductor energy gap, resulting in approximately equivalent densities of free holes and free electrons, in contrast to the normal crystalline case. Hence the hole conductance in the barrier region is equivalent to the electron conductance in the bulk, except for the difference in the electron and hole mobilities and as the barrier thickness is small relative to the electrode separation the effect of any conductance difference should be negligible. The accumulation of holes in the barrier region, and enhanced mobility due to the barrier field will also increase the hole conductance in the barrier region.

An estimate of the magnitude of the recombination/generation component can be obtained from the expression (Yu and Snow 1968, Rhoderick 1974).

$$J = \frac{q n_i \lambda}{\tau_e} (\exp(qV/kT) - 1), \tag{6}$$

where n_i is the intrinsic carrier density,

$$n_i = N_{c,v} \exp\left(\frac{-Eg}{2kT}\right),$$

and τ_e is the effective lifetime for carriers

$$\tau_e = 2/\sigma_{p,n} \nu_{ph} N_t$$

Eg is the energy band gap, $N_{c,v}$ refers to the density of conduction band states and valence band states respectively, ν_{ph} is the carrier thermal velocity, N_t is the trap density and $\sigma_{p,n}$ refers to the capture cross sections of holes and electrons respectively, assumed equal. In order to quantify eqn. (6), an identical set of parameters to that used in the TF emission case is assumed, with a density of traps $N_t = 10^{25}\,\mathrm{m^{-3}\,eV^{-1}}$ at the Fermi level where communication between the conduction band and valence bands tends to be greatest. An estimate of τ_e is obtained from measurements by Main (1973) on the free carrier recombination lifetime in amorphous As_2Te_3, a justifiable approach in view of the many

Fig. 7

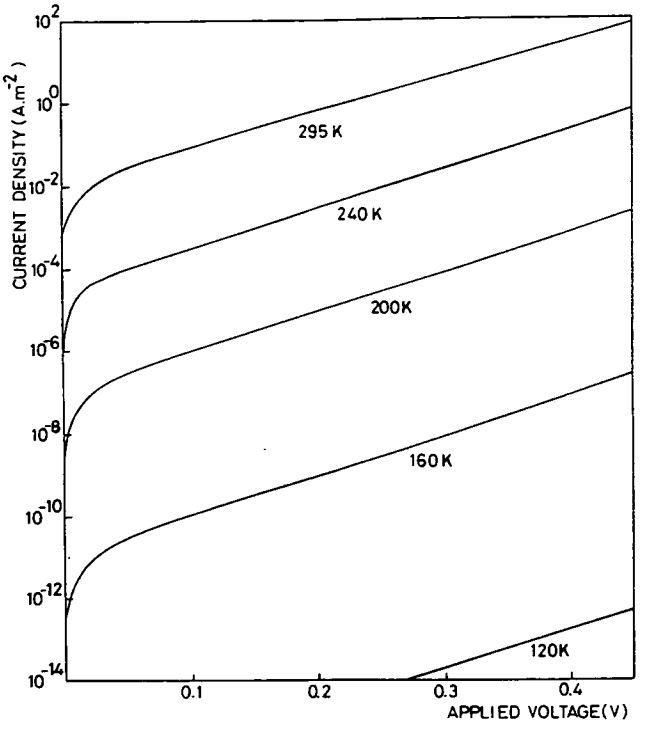

(*a*)

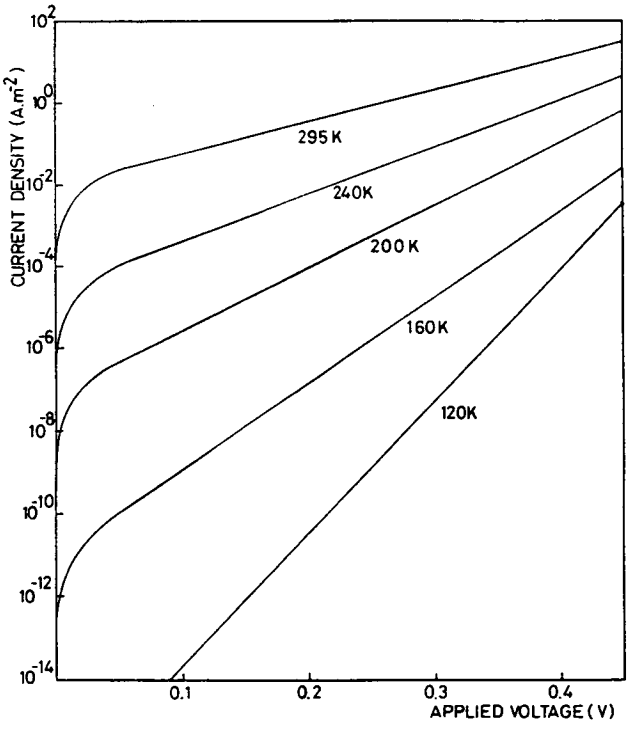

(*b*)

TF emission characteristics for the metal-amorphous semiconductor contact. (*a*) Forward bias; (*b*) reverse bias.

Fig. 8

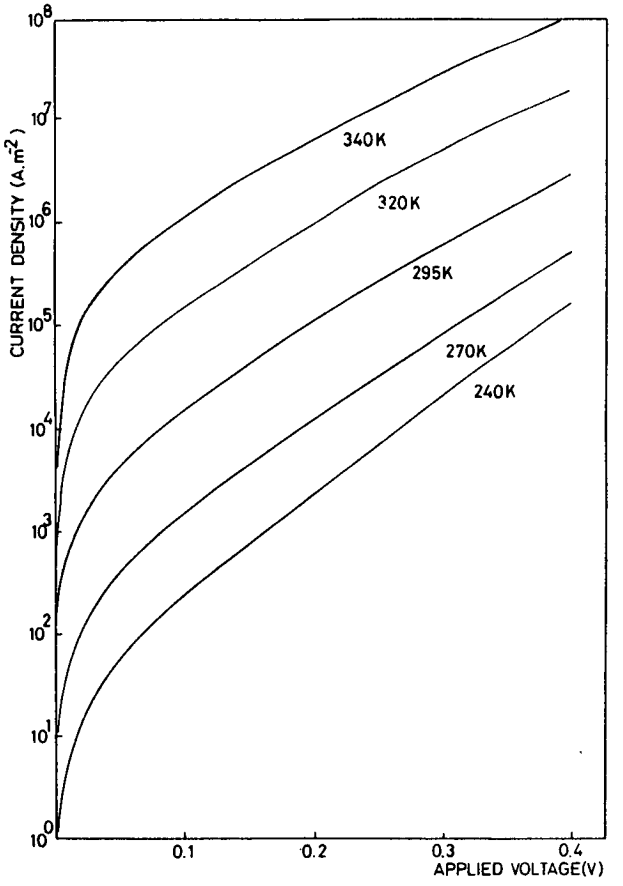

(*a*)

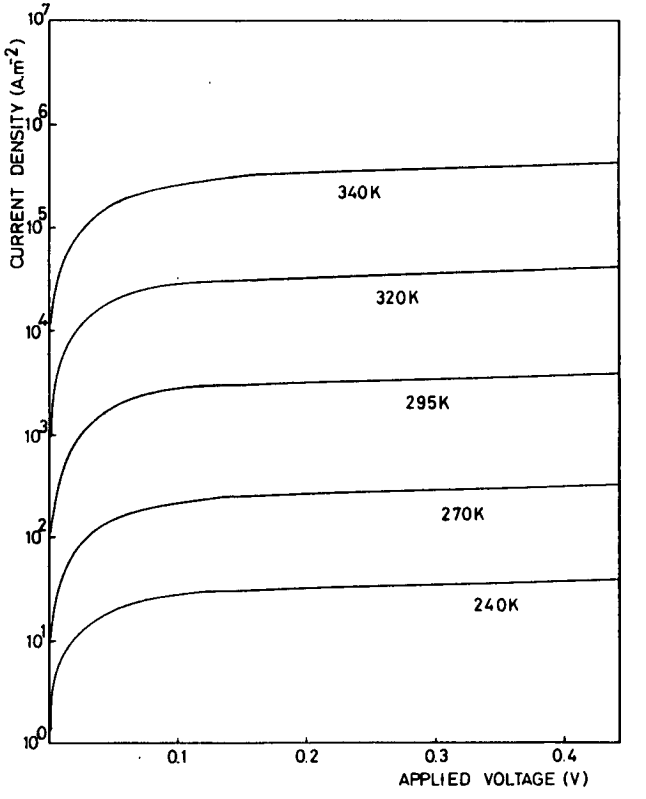

(*b*)

Recombination/generation characteristics for the metal-amorphous semiconductor contact. (*a*) Forward bias; (*b*) reverse bias.

Fig. 9

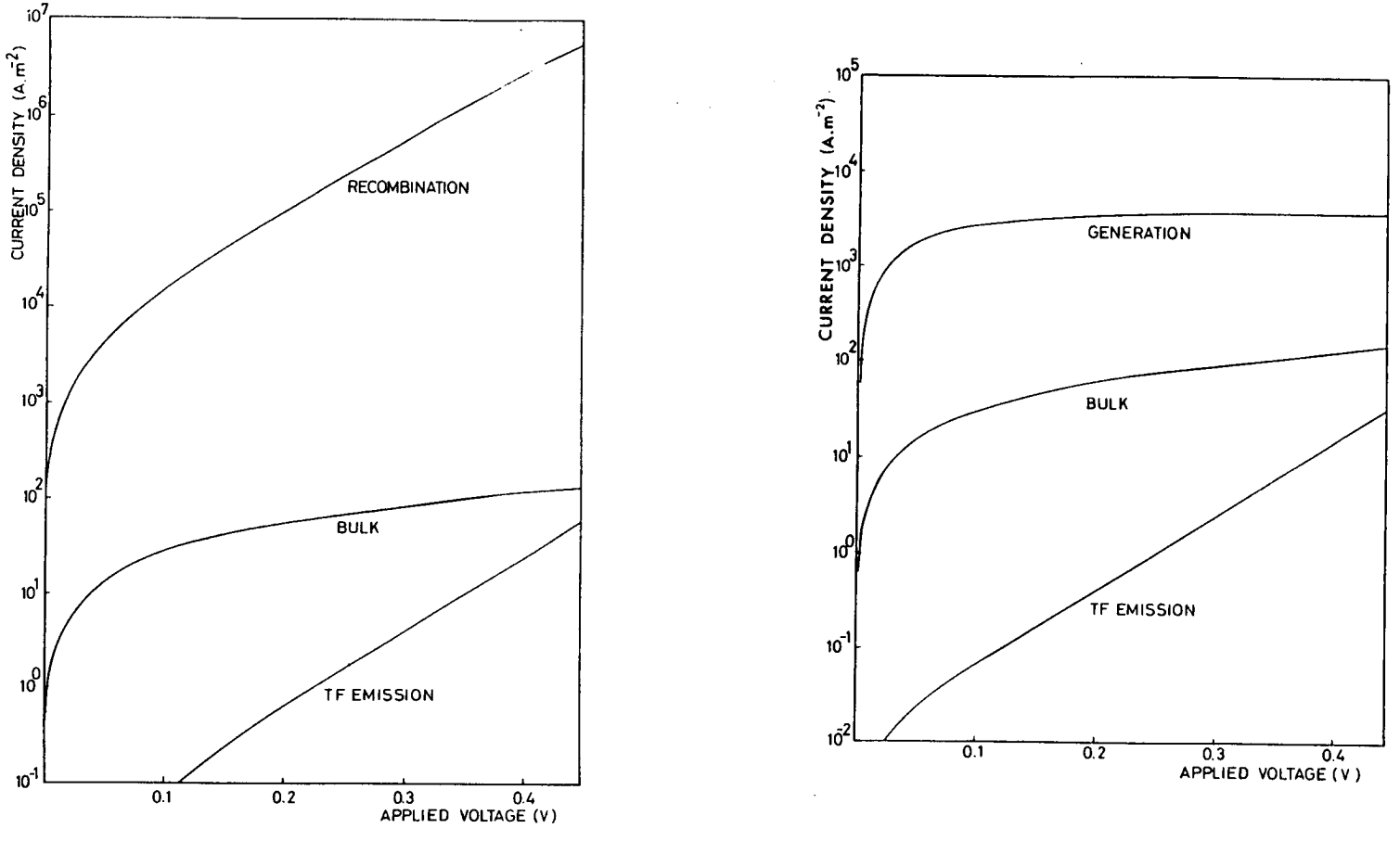

(*a*) (*b*)

Comparison of the various current density components through the metal–chalcogenide–metal sandwich device at 295 K. (*a*) Forward bias; (*b*) reverse bias.

similarities in electronic behaviour with the Ge–As–Te glass used in the present work. The computed TF emission characteristics for the metal-chalcogenide glass contact are presented in fig. 7(*a*) and (*b*) for forward and reverse bias, respectively, while the equivalent characteristics for the recombination/generation process are presented in fig. 8(*a*) and (*b*). The current path through the complete device can be considered as a series combination of transport in the bulk and depletion regions, the latter being a parallel combination of the mechanisms illustrated in fig. 6(*a*). Considering a typical device of thickness $1\,\mu m$ and bulk resistivity $3 \times 10^{-4}\,\text{ohm}^{-1}\,\text{m}^{-1}$ at a representative temperature of 295 K, fig. 9(*a*) and (*b*) indicate that current transport is necessarily a bulk limited process for both forward and reverse bias, and that the tunnelling mechanism in itself cannot be responsible for the negligible contact resistance observed, but rather charge continuity at the interface is provided by a generation/recombination mechanism.

No numerical estimate has been made of the third possible component in which a charge carrier may first tunnel from the metal into a vacant trap and then be thermally excited into the conduction band for transport through the bulk. Recent calculations by Gupta and Van Overstraeten (1975) on a similar process in M.N.O.S. systems suggest, however that this process may also contribute to charge continuity at the interface, providing an additional mechanism working against the formation of blocking barriers.

In conclusion, therefore, it seems unlikely that blocking contacts can be formed between metals and semiconducting chalcogenide glasses except where oxide barriers are present, as in the case of aluminium contacts. This has long been recognized as an experimental fact but the calculations presented here, based on conventional semiconductor physics, indicate that steady-state transport through thin-film, sandwich-type devices is generally bulk limited with continuity at the contacts maintained by a relatively large recombination/generation current, rather than by a TF tunnelling process. The present experiments and results are based on results for a Ge–As–Te glass but unpublished measurements by the authors on As_2Te_3 and $Si_{12}Te_{48}As_{30}Ge_{10}$, and evidence elsewhere in the literature, suggest that this behaviour is typical of most of the relatively conducting chalcogenide glasses.

Acknowledgments

One of the authors (A.M.W.) is grateful to the Science Research Council for the provision of a Research Studentship. This paper is based on a thesis presented for the degree of a Ph.D. at Edinburgh University (Wallace 1975).

References

Barbe, D. F., 1971, *J. vac. Sci. Tech.*, **8**, 102.

Cohen, M. H., Fritzsche, H., and Ovshinsky, S. R., 1969, *Phys. Rev. Lett.*, **22**, 1065.

Crowell, C. R., and Rideout, V. L., 1969, *Solid St. Electron.*, **12**, 89.

De Witt, H. J., and Crevecoeur, C., 1972, *J. non-crystalline Solids*, **8–10**, 787.

Dove, D. B., and Irani, R. F., 1976, *Thin Solid Films*, **34**, 77.

Fagen, A. E., and Fritzsche, H., 1970, *J. non-crystalline Solids*, **2**, 170.

Fritzsche, H., 1974, *Amorphous and Liquid Semiconductors*, Chap. 5 (New York: Plenum Press).

GUPTA, H. M., and VAN OVERSTRAETEN, R. J., 1975, *J. appl. Phys.*, **46**, 2675.
MARSHALL, J. M., and MILLER, G. R., 1973, *Phil. Mag.*, **27**, 1151.
MOTT, N. F., 1971, *Phil. Mag.*, **24**, 911.
OSMUN, J. W., 1975, *Phys. Rev.* B, **11**, 5008.
OWEN, A. E., and ROBERTSON, J. M., 1970, *J. non-crystalline Solids*, **2**, 40.
PADOVANI, F. A., 1971, *Semiconductors and Semi-metals*, Chap. 2 (New York: Academic Press).
PADOVANI, F. A., and STRATTON, R., 1966, *Solid St. Electron.*, **9**, 695.
RHODERICK, E. M., 1974, *Proceedings of the Conference on Metal-semiconductor Contacts* (UMIST), p. 3.
SAUVAGE, J. A., MOGAB, C. J., and ADLER, D., 1972, *Phil. Mag.*, **25**, 1305.
SPEAR, W. E., 1973, *Proceedings of the 5th Conference on Amorphous and Liquid Semiconductors* (Garmisch-Partenkirchen), p. 1.
STRATTON, R., 1962, *J. Phys. Chem. Solids*, **23**, 1177.
TANAKA, K., *et al.*, 1971, *Jap. J. appl. Phys.*, **40**, 73.
WALLACE, A. M., 1975, Ph.D. Thesis, University of Edinburgh.
YU, A. Y. C., and SNOW, E. M., 1968, *J. appl. Phys.*, **39**, 3008.
WEY, H. Y., 1976, *Phys. Rev.* B, **13**, 3495.
WEY, H. Y., and FRITZSCHE, H., 1972, *J. non-crystalline Solids*, **8–10**, 336.

Journal of Non-Crystalline Solids 35 & 36 (1980) 1191-1196

RESONANCE RAMAN SCATTERING IN As-S GLASSES

P.J.S. Ewen and A.E. Owen
Dept. of Electrical Engineering,
University of Edinburgh,
Edinburgh,
U.K.

The Raman spectra of glasses with compositions in the range $As_{35}S_{65}$ to $As_{43}S_{57}$ have been recorded using near band-gap excitation (λ_i = 5145 Å) and also weakly absorbed excitation (λ_i = 6328 Å). With 5145 Å excitation there is a significant enhancement at ~231 cm^{-1} for the glasses with ⩾ 40 at. % As. This band is attributed to the presence of As-As bonds in the As-S network. Both As-As and S-S bonds are believed to occur in the stoichiometric glass, a-$As_{40}S_{60}$, though in small numbers. The enhancement of the 231 cm^{-1} band for 5145 Å excitation is shown to be primarily a resonance effect, suggesting that As-As bonds constitute electronic "defect" states within the mobility gap.

INTRODUCTION

A fundamental question in the study of amorphous solids is the relation between their structure and their electronic properties. In the case of the arsenic chalcogenides various models have been proposed relating their electronic properties to defects such as wrong bonds (1) and, in particular, valence alternation pairs (2) and dangling bonds (3). Resonance Raman scattering (RRS) seems an appropriate experimental technique for elucidating the relation between structure and electronic properties because it yields simultaneously information on both electronic and vibrational energy levels. Although RRS in crystalline materials has been extensively studied the technique has only recently been applied to non-crystalline solids. The first observation of RRS in an amorphous solid was reported by Kobliska and Solin (4) using the prototype chalcogenide glass a-$As_{40}S_{60}$. Razzetti and co-workers (5,6) have since used RRS to probe the nature of the electronic states near the band edge in a-$As_{40}S_{60}$ and are currently studying the effect in the related material a-$As_{40}Se_{60}$. Howard et al. (7) have used RRS to study the second-order Raman spectrum of a-$As_{40}S_{60}$ and the effect has recently been observed in a-Si (8). In the present paper we report RRS in a number of As-S glasses with compositions close to the stoichiometric composition $As_{40}S_{60}$.

EXPERIMENTAL

All the samples examined were annealed bulk glasses. Resonance spectra were excited with 5145 Å (2.41 eV) radiation from an Ar-ion laser. (The room temperature band-gap energy, E_g, for a-$As_{40}S_{60}$ is 2.32 eV (9).) For the purpose of comparison, non-resonance spectra were also recorded, using 6328 Å (1.96 eV) radiation form a He-Ne laser. The back-reflection geometry was used in all the experiments. A double grating monochromator and photon-counting system was used for detection. All spectra were recorded at room temperature.

RESULTS AND DISCUSSION

In their study of RRS in the bulk glass a-$As_{40}S_{60}$ Razzetti and Fontana (5) showed that although the scattering efficiency is enhanced as the incident photon energy approaches E_g, the resonance for most the the spectrum is not band-like, that is, the scattering efficiency continues to increase when the incident energy is increased above E_g. The absence of band-like resonance over most of the spectrum is possibly due to the fact that the highest valence band in a-$As_{40}S_{60}$ is composed of non-bonding lone-pair electrons. Razzetti and Fontana show, however, that one feature of the vitreous $As_{40}S_{60}$ spectrum - a weak band near 231 cm^{-1} - does exhibit band-like resonance. Fig. 1, which is based on results obtained in the present study, compares the non-resonance spectrum of the glass excited by 6328 Å light with the resonance spectrum excited with near band-gap radiation.

In the resonance spectrum the 231 cm^{-1} feature is clearly considerably enhanced relative to other spectral features. The poorer signal-to-noise ratio of the resonance spectrum and the divergence in intensities as one approaches the origin is due to the increasing absorption of the sample at 5145 Å compared with 6328 Å.

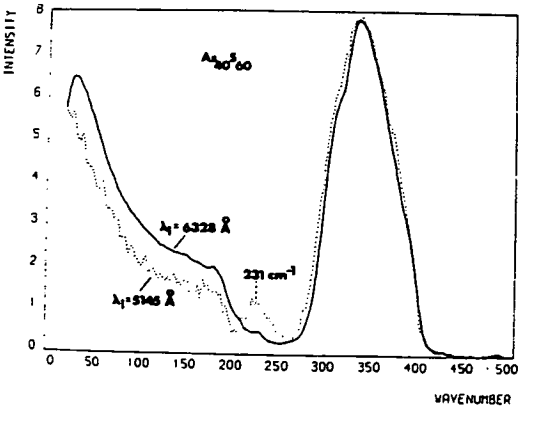

FIG. 1 The Raman spectrum of vitreous $As_{40}S_{60}$ excited by 5145 Å and 6328 Å radiation. The spectra are normalised to the height of the ~338 cm^{-1} band.

Razzetti and Fontana (5) speculate that the 231 cm^{-1} feature of the Raman spectrum is due to the presence of sulphur complexes in the glass. Since the spectra of the glasses with S content greater than 60 at. % also exhibit a weak feature near 231 cm^{-1} which can be associated with the S_8 ring (10-12) this suggestion seems reasonable. However, although there is no significant change in the Raman spectrum near 231 cm^{-1} as the S content increases above 60 at. % the polarisation properties of this feature change considerably. Fig. 2 shows the depolarisation spectra for a number of S-rich glasses with compositions close to stoichiometry. The largest change in the depolarisation spectra occurs around 230 cm^{-1} and consists of the transformation of a dip in the $As_{40}S_{60}$ spectrum to a peak. This suggests that the 231 cm^{-1} feature of the $As_{40}S_{60}$ Raman spectrum does not arise from the same structural element as the 231 cm^{-1} peaks in the S-rich spectra. Furthermore, if the 231 cm^{-1} features in the spectra of Fig. 2 did arise from the same structural element the resonance spectra of the S-rich glasses would also be expected to exhibit an enhanced band at this frequency. Our results indicate that this is not the case. The resonance and non-resonance spectra of $As_{35}S_{65}$ glass, which certainly contains S_8 rings (10-12), are similar.

We have also observed no sign of resonance enhancement at 231 cm^{-1} for the composition $As_{39}S_{61}$. The absence of resonance in the S-rich glasses cannot be attributed to the compositional shift in E_g (9).

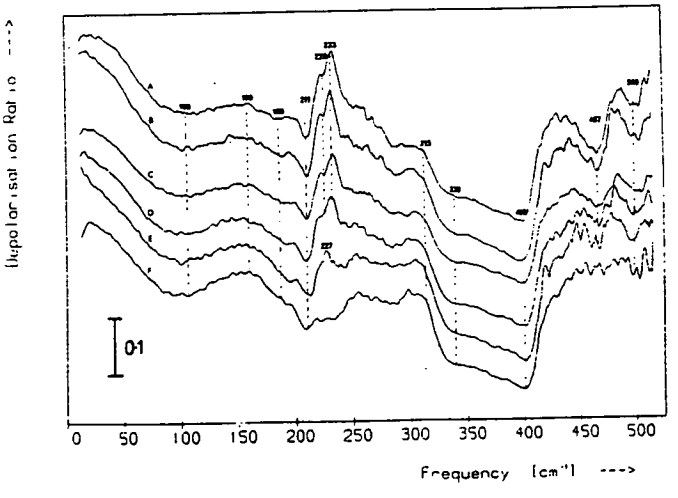

FIG. 2 Depolarization spectra for the glasses with the compositions $As_{35}S_{65}$ (A), $As_{36}S_{64}$ (B), $As_{37}S_{63}$ (C), $As_{38}S_{62}$ (D), $As_{39}S_{61}$ (E) and $As_{40}S_{60}$ (F).

In an earlier study of the non-resonance spectra of As-S glasses (12) we concluded that the 231 cm^{-1} feature of the $As_{40}S_{60}$ spectrum is in fact due to the presence of As-As bonds in the network; the RRS results support this assignment. The evidence for this assignment is as follows. The temperature dependence of the 231 cm^{-1} band differs from that of the rest of the spectrum (13) and there is no feature near this frequency in the vibrational spectra of crystalline $As_{40}S_{60}$ (which ideally contains no As-As bonds), so the band is unlikely to be associated with the AsS_3 and As_2S "molecules" that are the basic structural units of these materials. In the vibrational spectra of the various forms of elemental As the bands due to the stretching of As-As bonds all occur in the region of 230 cm^{-1}, and our results for the non-resonance spectra of the As-rich sulphide glasses show that the 231 cm^{-1} feature grows as the As content increases above 40 at. %. (This band cannot be attributed to the As_4S_4 molecules that are present in these As-rich glasses.) The fact that no resonance is observed at 231 cm^{-1} for the composition with an excess of only 1 at. % S ($As_{39}S_{61}$) suggests that the structural element responsible for the resonance feature disappears rapidly as the S content is increased above 60 at. %) which is consistent with this feature being attributed to As-As bonds, since such bonds are not expected to occur in the S-rich glasses (14). Finally, if As-As bonds are a genuine feature of the vitreous $As_{40}S_{60}$ structure then S-S bonds should also be present in the network; our results on the S-rich glasses indicate that such bonds are indeed present in the network and are responsible for the weak feature at 490 cm^{-1} in the $As_{40}S_{60}$ spectrum. The weakness of the bands at 231 and 490 cm^{-1} suggests that the number of like-atom bonds is small, about 1% for each type.

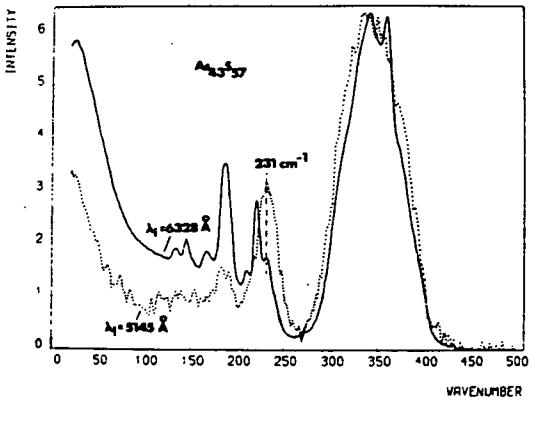

FIG. 3 The Raman spectrum of vitreous $As_{43}S_{57}$ excited by 5145 Å and 6328 Å radiation. The spectra are normalised to the height of the ~338 cm^{-1} band.

If the 231 cm^{-1} feature of the a-$As_{40}S_{60}$ spectrum is associated with the same structural element as the 231 cm^{-1} peaks of the As-rich glasses then these peaks should also be enhanced when near-band-gap radiation is used to excite the spectra. This is in fact the case, as is shown in Fig. 3 which compares the resonance and non-resonance spectra of the glass $As_{43}S_{57}$, the limiting composition of the glass-forming region. The 231 cm^{-1} peak of the resonance spectrum is considerably larger than the corresponding peak in the non-resonance spectrum. In molecules the fundamental displaying resonance is usually bond-stretching in nature (15), which suggests that As-S and S-S bonds cannot be responsible for the 231 cm^{-1} feature since the characteristic bond-stretching frequencies for these bonds are ~340 and 470 cm^{-1} respectively.

The absence of many of the sharp bands in the resonance spectrum of Fig. 3 is probably due to the light-induced polymerisation of As_4S_4 molecules. Porter and Sheldrick (16) have shown that in c-As_4S_4 the Raman bands of the discrete molecules disappear after prolonged irradiation with red light. This effect has also been observed in the non-resonance spectra of the As-rich alloys (17). In addition, it is found that for both c-As_4S_4 and the As-rich alloys a band grows near 231 cm^{-1} during irradiation, which confirms that the 231 cm^{-1} band in the glasses does not arise from the As_4S_4 molecules. Porter and Sheldrick interpret the light-induced spectral changes in c-As_4S_4 as evidence of polymerisation; As-As bonds will certainly be present in the network resulting from the polymerisation of these molecules so the growth of the 231 cm^{-1} band is likely to be due to the formation of such bonds in the network. Although these light-induced effects may be contributing to the intensity of the 231 cm^{-1} band in the spectra excited with 5145 Å light, our results, and those of Fontana at al. (5) suggest that the enhancement of this band is primarily a resonance effect.

We believe that As-As and S-S bonds are a genuine feature of the vitreous $As_{40}S_{60}$ structure and that our results are not due to deviations in the stoichiometries of the samples used. The 231 and 490 cm^{-1} features are present in the spectra of the commercial samples of a-$As_{40}S_{60}$ we have examined (supplied by the American Optical Company) as well as in the spectra of samples made in our laboratories. Also, the weak features at 231 and 490 cm^{-1} in the a-$As_{40}S_{60}$ spectrum have been observed by other workers (7,13,17,18). The fact that features attributable to As-As and S-S bonds appear in the spectra obtained for a-$As_{40}S_{60}$ indicates that the composition is correct since As-As (S-S) bonds are not expected to occur in the S(As)-rich glasses (14). Furthermore, these "like-atom" bonds are incorporated into the network rather than existing in discrete units such as As_4S_4 molecules or S complexes.

REFERENCES

(1) Halpern, V., Phil. Mag. 34 (1976) 331.

(2) Kastner, M., Adler, D. and Fritzsche, H., Phys. Rev. Lett. 37 (1976) 1504.

(3) Mott, N.F., Davis, E.A. and Street, R.A., Phil. Mag. 32 (1975) 961.

(4) Kobliska, R.J. and Solin, S.A., Solid State Commun. 10 (1972) 231.

(5) Razzetti, C. and Fontana, M.P., Phys. Stat. Sol. (B) 70 (1975) 173.

(6) Razzetti, C. and Lottici, P.P., Phys. Stat. Sol. (B) 87 (1978) 479.

(7) Howard, R.E., Macedo, P.B. and Moyninan, C.T., Solid State Commun. 17 (1975) 1475.

(8) Bermejo, C., Cardona, M. and Brodsky, M.H., Proc. 7th Int. Conf. on Amorphous and Liquid Semiconductors, Edinburgh (Spear, E.W., editor) C.I.C.L., Edinburgh, 1977, p.343.

(9) Kosek, F. and Tauc, J., Czech. J. Phys. B20 (1970) 94.

(10) Ward, A.T., Adv. in Chemistry, 110 (1972) 163.

(11) Ward, A.T., J. Phys. Chem. 72 (1968) 4133.

(12) Ewen. P.J.S., Sik, M.J. and Owen, A.E. in "The structure of Non-Crystalline Materials" (Gaskell, P.H., editor), Taylor and Francis, London 1977 p.231.

Ewen, P.J.S., Ph.D. Thesis, University of Edinburgh, October 1978.

(13) Finkman, E., DeFonzo, A.P. and Tauc, J., Proc. 5th Int. Conf. on Amorphous and Liquid Semiconductors, Garmisch-Partenkirchen, Germany (Stuke, J. and Brenis, W., editors), Taylor and Francis, London 1974, p.1275.

(14) Lucovsky, G., Galeener, F.L., Geils. R.H. and Keezer, R.C. in "The Structure Non-Crystalline Materials (Gaskell, P.H., editor), Taylor and Francis, London 1977, p.127.

(15) Clark, R.J.H. in "Advances in Infrared and Raman Spectroscopy" Vol.1, (Clarke, R.J.H. and Hester, R.E., editors), Heyden, London 1975, p. 143.

(16) Porter, E.J. and Sheldrick, G.M., J.C.S. Dalton (1972) 1357.

(17) Bertoluzza, A., Fagnano, C., Monti, P, and Semerano, G., J. Non-Crystalline Solids 29 (1978), 49.

(18) Tauc, J., Proc. 3rd Int. Conf. on Light Scattering in Solids, Campinas, Brazil, Flammarion, Paris 1976, p.621.

STRUCTURAL CHANGES IN AMORPHOUS ARSENIC SULPHIDE FILMS ON PHOTODOPING WITH SILVER STUDIED BY RAMAN SPECTROSCOPY

A.P. Firth, P.S. Ewen* and A.E. Owen

Department of Electrical Engineering, University of Edinburgh, King's Buildings, Edinburgh EH9 3JL, UK

**Department of Physics, University of Edinburgh, James Clerk Maxwell Building, Edinburgh EH9 3JL, UK*

ABSTRACT

Raman spectroscopy has been used to study the structural changes occurring in films of As-S glasses of compositions $As_{41}S_{59}$, $As_{38}S_{62}$, $As_{30}S_{70}$ and $As_{20}S_{80}$, after photodoping with Ag. Only the photodoped film of composition $As_{30}S_{70}$ produced a single-phase homogenous material. In the other photodoped compositions there is evidence of phase separation. An explanation of these observations is given.

1. INTRODUCTION

The phenomenon known as metal photodoping is one of a variety of photostructural effects which are known to occur in chalcogenide glasses, and although widely studied there is no complete physical model for the photodoping mechanism. In recent years interest in metal photodoping has increased considerably because of its potentially important applications in submicron photolithography (Janai 1981). This paper reports on an investigation, based on Raman spectroscopy, of the photodoping of films of As-S glasses with silver.

2. EXPERIMENTAL

Films of As-S glasses, of thickness up to 5 μm and with stoichiometries ranging from As_2S_3 to As_2S_8, were prepared by vacuum evaporation. The compositions of the deposited films were determined by electron probe microanalysis, and the compositions quoted are accurate to within ±0·5 atom per cent.

The photodoping experiments were carried out as follows. Half the area of a glass slide was first coated with a layer of Al. The whole area was then coated with an evaporated layer of Ag, 0·5–1·0 μm thick, followed by the As-S glass layer, 5–8 μm thick. The purpose of the Al film was to provide a reflective layer with low Raman scattering. Samples were then exposed to a 500 W projector lamp which was cooled by a fan to prevent heat reaching the sample. As the slide was only half covered with Al it was possible to see when all the Ag had dissolved into the chalcogenide film. When the photodoping was complete the film was etched in alkaline solution to remove the undoped As-S layer. The final thickness of the (Ag-doped) As-S film was in the range 1·5–3·5 μm. Conventional back-reflection scattering was used to obtain the Raman spectra with the 6764 Å line from a Kr ion laser (Firth *et al.* 1981).

3. RESULTS

In Figure 1, curves A and B are the spectra of As-S film of composition $As_{41}S_{59}$ and $As_{38}S_{62}$, respectively. The sharp features of these spectra are attributed to molecular units of As_4S_4, and the feature at 491 cm^{-1} to the symmetric stretching mode of S-S bonds (Nemanich *et al.* 1978). Spectra C and D in Figure 1 are of the Ag photodoped films corresponding again to the original compositions $As_{41}S_{59}$ and $As_{38}S_{62}$, respectively (i.e., as in curves A and B). These two spectra are similar, each having two broad Raman bands in the regions 150–300 cm^{-1} and 300–400 cm^{-1}. Curve E in Figure 1 is the Raman spectrum of amorphous As, and this closely matches the band in the 150–300 cm^{-1} region in spectra C and D. The other band, in the region 300–400 cm^{-1} in curves C and D, is probably due to amorphous Ag-As-S phases, as it

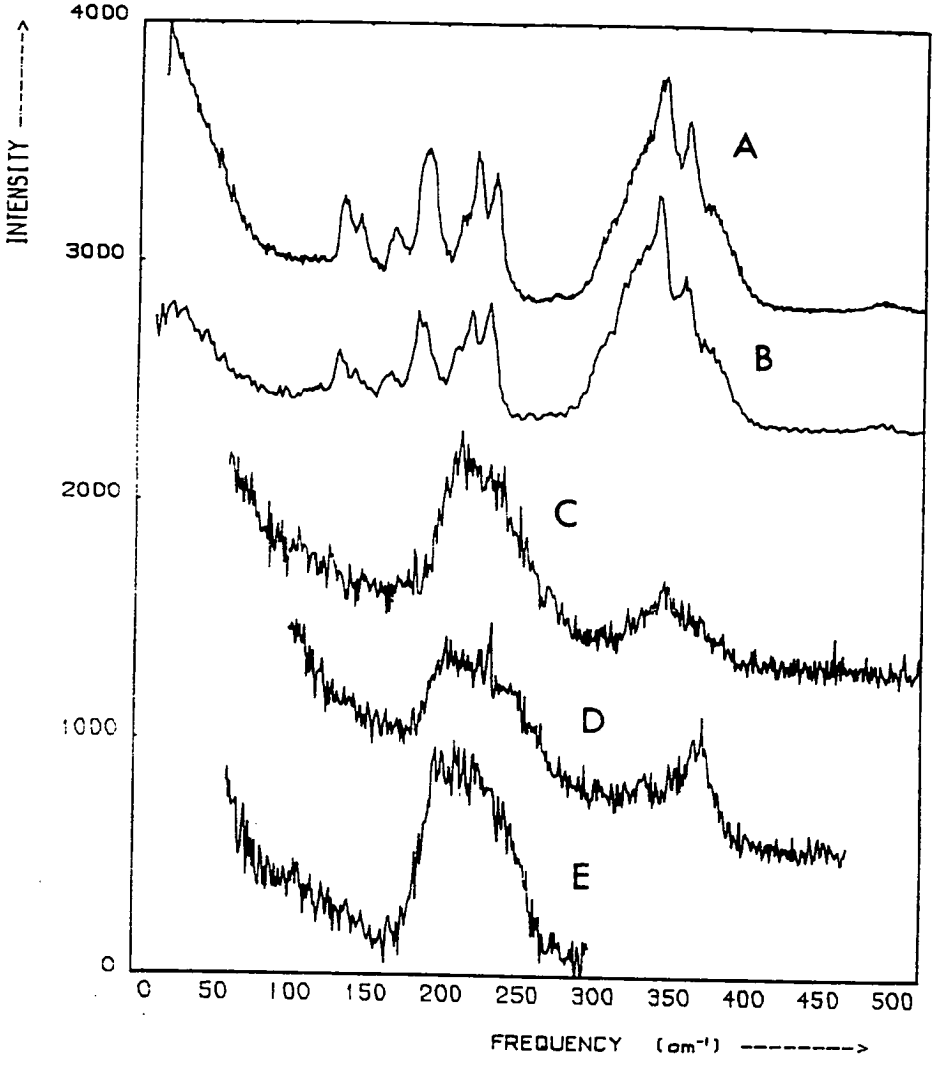

Figure 1. Raman spectra of films of composition $As_{41}S_{59}$ (curve A) and $As_{38}S_{62}$ (curve B). Curves C and D are the spectra for Ag photodoped $As_{41}S_{59}$ and $As_{38}S_{62}$, respectively. Curve E is the Raman spectrum of amorphous As.

is known that bulk glasses in the Ag-As-S system have strong Raman bands in the same spectral region (Firth *et al.* 1981).

Curve A in Figure 2 is the Raman spectrum for a film of composition $As_{30}S_{70}$, which agrees well with that of a bulk glass of the same composition (Ewen 1978). The features in the region 425-525 cm^{-1} are attributed to S in S_8 rings and S-S bonds in linear As-S_n-As linkages. Curve B is the Raman spectra of the Ag photodoped material.

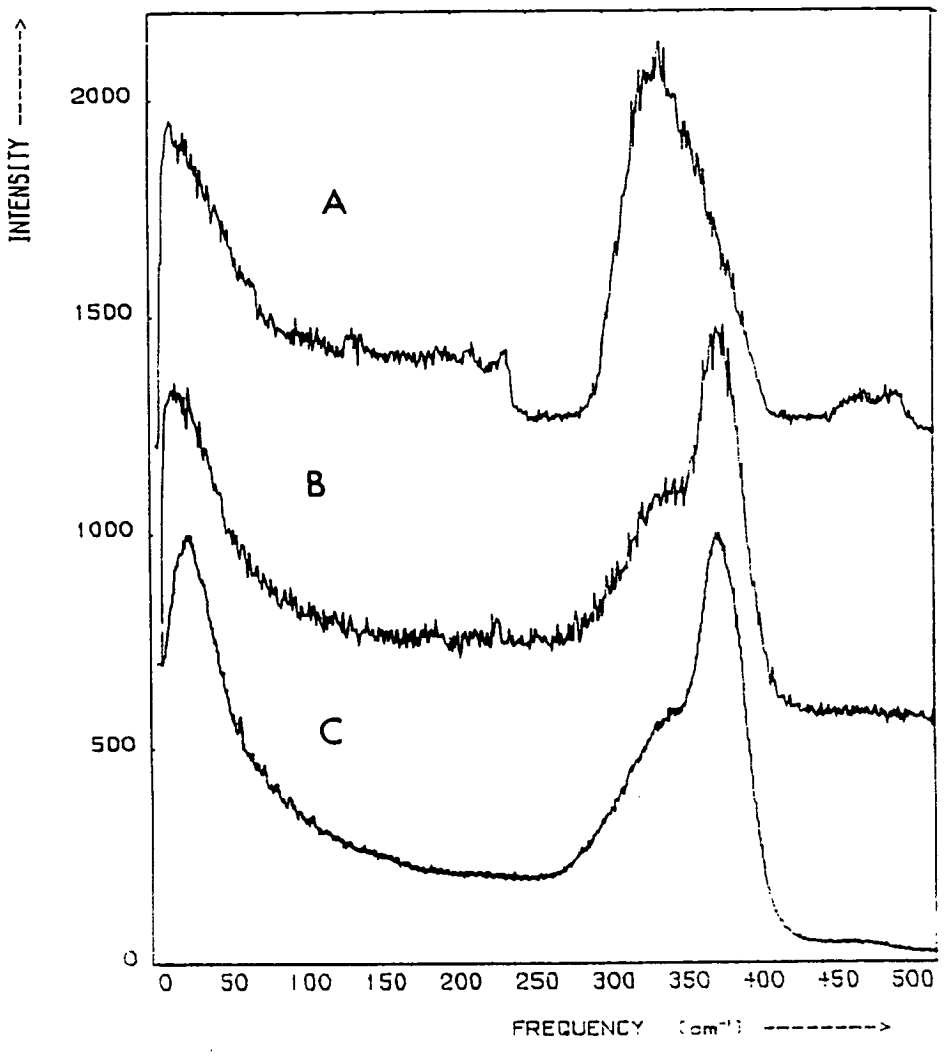

Figure 2. Raman spectra of films of composition $As_{30}S_{70}$ (Curve A). Curve B is the spectrum of Ag photodoped $As_{30}S_{70}$. Curve C is the spectrum of a bulk Ag-As-S glass of composition $Ag_{30}As_{22}S_{48}$.

It has a broad spectrum and comparison with the spectrum of a bulk glass of composition $Ag_{30}As_{22}S_{48}$, shown in curve C, suggests that the photodoped film has the same structure.

In Figure 3, curve A is the Raman spectrum of a film of composition $As_{20}S_{80}$, and again this is very similar to the spectrum of a bulk glass of the same composition (Ewen 1978). The sharp features are due to the vibrations of distorted S_8 rings. The Raman spectrum of the Ag photodoped film (curve B) has a very broad band in the region

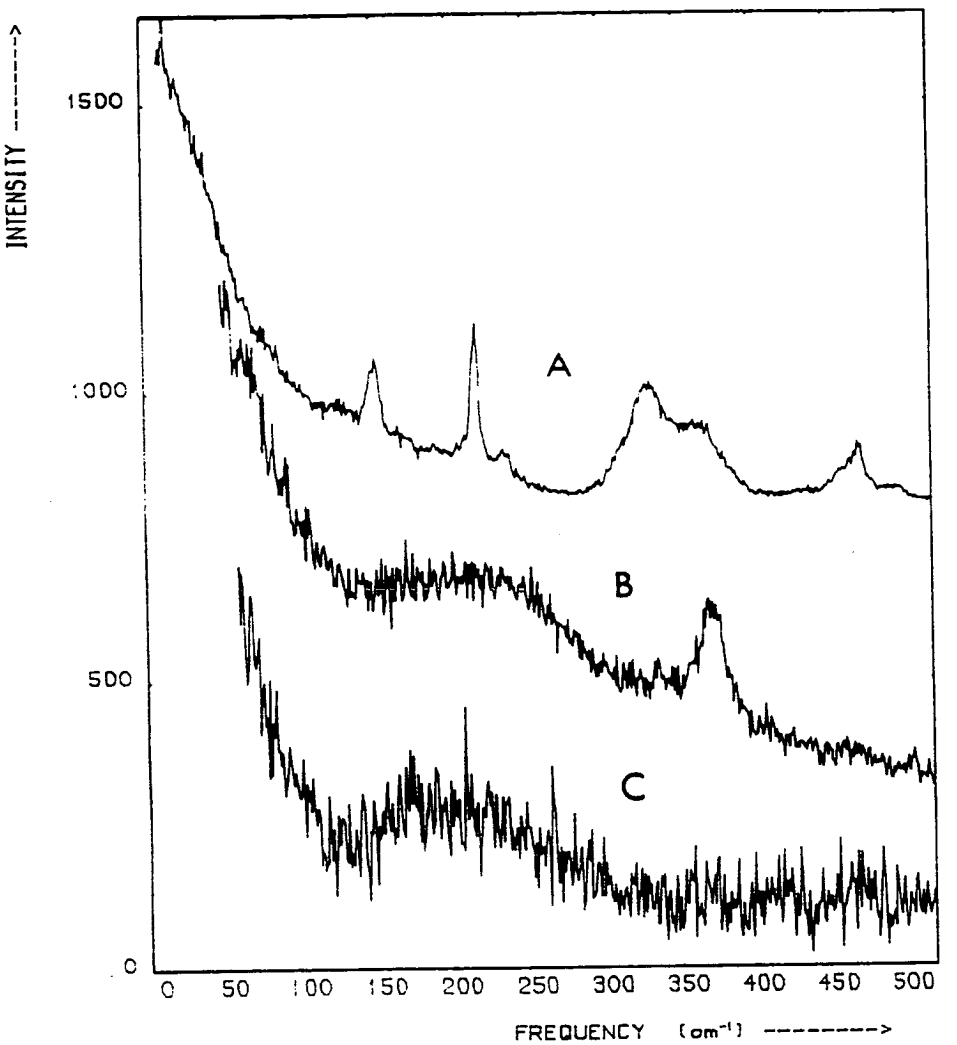

Figure 3. Raman spectra of films of composition $As_{20}S_{80}$ (curve A). Curve B is the spectrum for Ag photodoped $As_{20}S_{80}$. Curve C is the spectrum of a Ag_2S film formed by reacting S vapour with a Ag film.

100-300 cm^{-1} and a relatively sharp feature at 350-400 cm^{-1}. The other spectrum (curve C) was obtained from a film of Ag_2S formed by reacting S vapour with a Ag film which was about 0·5 μm thick. A comparison of spectra B and C suggests that Ag_2S is present in the photodoped As-S film, which was originally $As_{20}S_{80}$. The band between

350-400 cm^{-1}, formed during the course of the experiment, probably arises from the formation of a Ag-As-S glassy phase.

4. DISCUSSION

Figure 4 illustrates the phase diagram for the Ag-As-S system and it shows the principal crystalline compounds as well as the glass-forming regions determined by Kawamoto *et al.* (1974). Also drawn

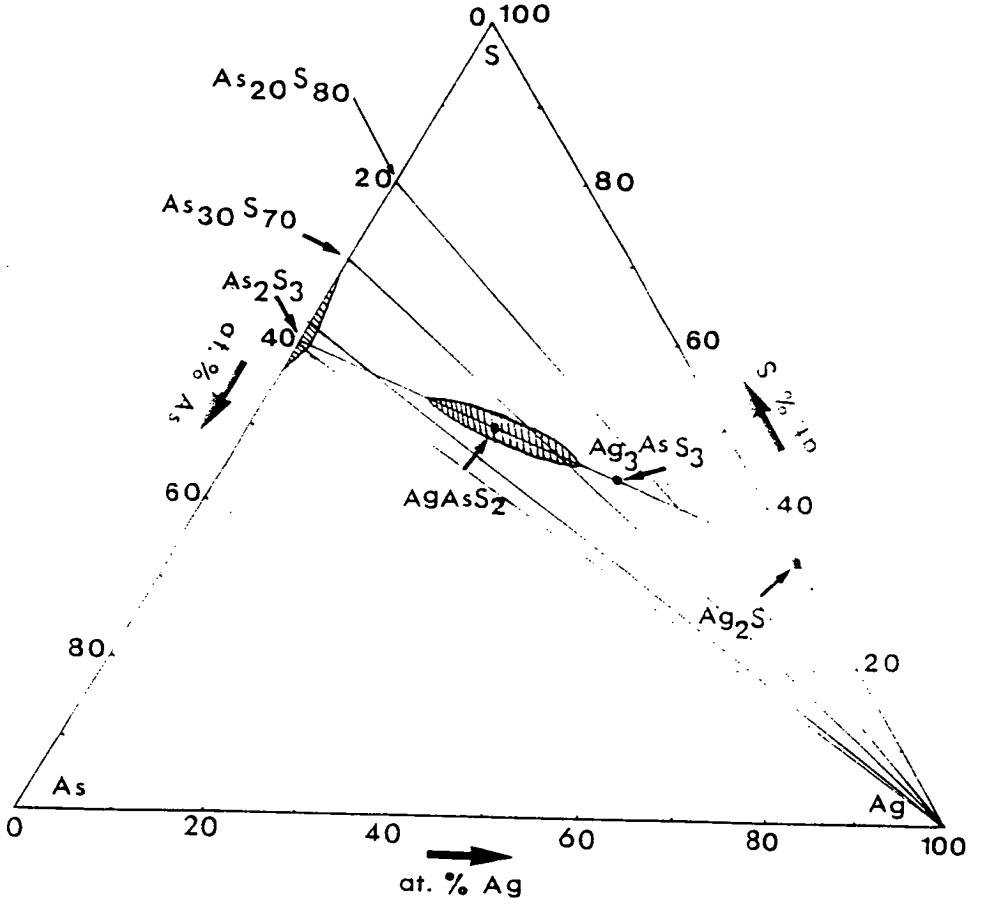

Figure 4. Phase diagram of the Ag-As-S system showing the compositions investigated in this paper and some of the knonw ternary compounds. Cross-hatching indicates glass-forming regions.

on the diagram are tie lines joining elemental Ag with four As-S compositions studied in this work (the composition $As_{41}S_{59}$ is taken to be approximately As_2S_3). As the photodoping proceeds the resulting overall composition must move along these tie lines. Of those four lines, only the one joining Ag with $As_{30}S_{70}$ intersects the central glass-forming region. This is in accord with Raman results which show that Ag photodoped $As_{30}S_{70}$ has a structure very similar to that of a bulk glass within the central region of glass formation and close, in composition, to the Ag-$As_{30}S_{70}$ tie line (Firth *et al.* 1981). It is possible therefore that in this case the Ag photodoped film remains a homogeneous, uniform phase.

The tie lines joining Ag with $As_{41}S_{59}$ (As_2S_3) and $As_{38}S_{62}$ are on the As-rich side of the central glass-forming region but they do not intersect it. The Raman results indicate that amorphous As and an amorphous Ag-As-S phase, corresponding in structure to a composition within the glass-forming region, are present in the photodoped material. This implies that when the overall photodoped composition lies outside the glass-forming region, the photodoping also involves a process of phase separation. The evidence is that the Ag-As-S component which is formed is actually within the glass-forming region and that excess As is precipitated, probably in an amorphous form.

For the system Ag-$As_{20}S_{80}$ the tie line also does not intersect the central glass-forming region. In this case, the Raman results suggest that initially, Ag_2S is formed (although it is by no means certain that it is stoichiometric Ag_2S), and only after prolonged exposure is there a further photoinduced effect towards the formation of a glassy Ag-As-S phase.

It is premature to extrapolate the latter observation (i.e., Ag_2S formation) to the whole system, but in general the results of this work do suggest that the photodoping process is a two-stage solid-state reaction. The initial reaction may be between Ag and S in As-S films and it should be noted here that even in stoichiometric glassy As_2S_3, -S-S- bonds are present (Ewen 1978). It is imagined that these homopolar -S-S- bonds are involved in the initial reaction. The second reaction is between Ag_2S and the remaining As-S matrix.

This reaction will proceed only if the reaction products are more stable than the reactants. It is likely that this will be so if the reaction products are within, or close to, the central glass-forming region. The structure of Ag-As-S glasses is based on AsS_3 pyramids joined by -S-Ag-S- linkages (Kawamote *et al.* 1974; Firth *et al.* 1981), so that very little structural rearrangement is required in the second reaction.

ACKNOWLEDGMENTS

The authors gratefully acknowledge the help of research grants from the Science and Engineering Research Council, and the co-operation of Dr. W. Taylor of the Physics Department of Edinburgh University in making available the experimental facilities for Raman spectroscopy.

REFERENCES

EWEN, P.J.S., 1978, *The Raman Spectra and Structure of Glasses in the Arsenic-Sulphur and Arsenic-Selenium Systems* (Ph.D. Thesis, University of Edinburgh), pp. 143-175.

FIRTH, A.P., OWEN, A.E. & EWEN, P.J.S., 1981, *Journal de Physique*, 42, Colloque C4, Suppl. No. 10, 903-906.

JANAI, M., 1981, *Journal de Physique*, 42, Colloque C4, Suppl. No.10, 1105-1113.

KAWAMOTO, Y., AGATA, M. & TSUCHIHASHI, S., 1974, *Journal of the Ceramics Association of Japan*, 82, 502-507.

NEMANICH, R.J., CONNELL, G.A.N., HAYES, T.M. & STREET, R.A., 1978, *Physical Review B*, 18, 6900-6918.

ELECTRON TRANSPORT IN CHALCOGENIDE GLASSES

A. E. Owen

Department of Electrical Engineering
University of Edinburgh
King's Buildings
Edinburgh EH9 3JL
Scotland

A brief general account of the band structure and transport mechanisms of amorphous semiconductors is first presented. Special features of the electronic band structure of chalcogenide glasses are reviewed, with particular emphasis on chemical bonding considerations and the formation of defect states associated with abnormal configurations. Experimental data on d.c. conductivity, thermopower, Hall mobility and drift mobility are described, with measurements on Se, As_2Se_3 and related compositions as examples. The data are interpreted in terms of band models in which relatively discrete defect levels within the mobility gap control the transport processes.

I. BACKGROUND

A. INTRODUCTION

There are sound arguments for the proposition that the one-dimensional one-electron density-of-states distribution in an ideal amorphous

semiconductor is as shown schematically in Figure 1(a).[1,2] An ideal amorphous structure is a fully connected three-dimensional disordered network of atoms of finite size, i.e. a degree of short-range order is imposed but there are no unsaturated bonds. The label ES in Figure 1(a) means Bloch-type extended states above an energy E_C in the conduction band and below an energy E_V in the valence band. The label T indicates localized tail states which are split-off from the Bloch-type states of the valence and conduction bands but which retain the characteristics of their parentage; G indicates gap states of indefinite origin which are assumed present in low but uniform density across the energy gap (e.g. $\sim 10^{14}$ cm^{-3}). The tail and gap states are localized in the sense that electrons in these states have wave functions ψ_{loc} which decay exponentially in space, i.e. in one-dimension (x), -

$$\psi_{loc} \sim \exp - (\alpha x)$$

where α is a decay factor and is typically ~ 0.1 A^{-1}.

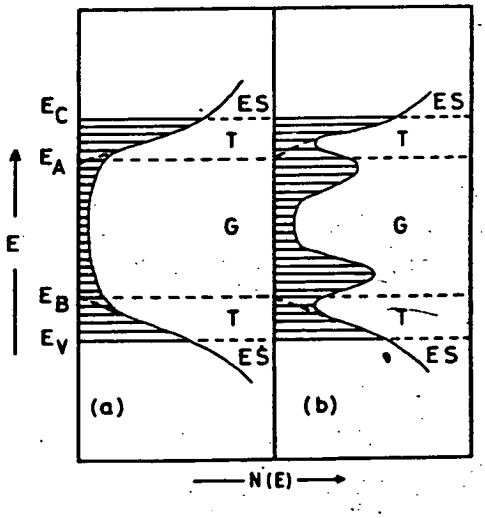

Fig. 1. Schematic one-electron one-dimensional density-of-states diagrams, (a) for an ideal amorphous semiconductor, and (b) for a real amorphous semiconductor.

A real amorphous semiconductor is thought to have a one-dimensional density-of-states more like that depicted schematically in Figure 1(b). There are still extended, tail and gap states but in addition there is evidence for energetically rather well-defined maxima in the gap state distribution and these features are attributed to specific structurally-related defects such as dangling (broken) bonds, deviations from stoichometry and/or wrong bonds in the case of compounds, and even perhaps to impurities.

B. THE MOBILITY GAP MODEL

Leaving aside the difficult question of the transition from extended Bloch states to localized tail states (is it gradual or is there a true discontinuity at some critical energy?), Figures 1(a) and 1(b) lead to the mobility-gap notion which has been the accepted basis for interpreting electronic transport in amorphous semiconductors since the early days of the subject. The mobility-gap idea is shown diagrammatically in Figure 2. In extended states just above E_C, or just below E_V, carrier transport is essentially a diffusive Brownian-type motion and hence the carrier mobility μ is approximately,[2]

$$\mu \approx \frac{1}{6} \frac{ea^2}{kT} \nu_{el} \tag{1}$$

where a is the average interatomic distance and ν_{el} is an electronic frequency of the order of $10^{15}\ s^{-1}$. The estimated drift mobility in extended states just above E_C or just below E_V is therefore about $1\ cm^2\ v^{-1}\ s^{-1}$ at room temperature. In localized states (T or G) transport can only occur by phonon-assisted hopping and the mobility is given by

$$\mu(E) \approx \frac{eR^2(E)}{kT} \nu_{ph} \exp(-2\alpha R) \exp(-W/kT) \tag{2}$$

where R is the average hopping distance which depends on the density-of-states distribution and is a function of energy (N.B. R may be greater than a), ν_{ph} is a phonon frequency ($\sim 10^{13}\ s^{-1}$) and W (the activation energy) is the energy difference between the initial and final localized states involved in the hopping motion. Close to E_C and E_V, $R \rightarrow a$ and $W \rightarrow 0$, hence $\mu \sim 10^{-2}\ cm^2\ V^{-1}\ s^{-1}$ at room temperature. Thus, near E_C and E_V the carrier mobility changes by three orders of magnitude or more and this defines the mobility gap, illustrated schematically in Figure 2(b) where μ is plotted as a function of energy.

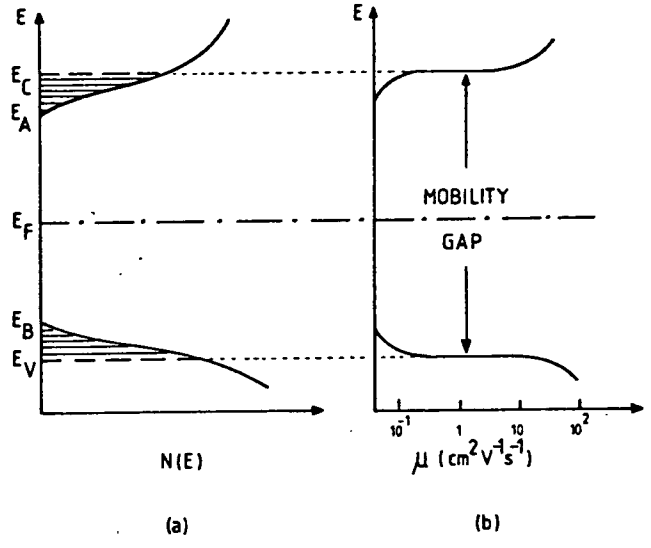

Fig. 2. Illustrating the mobility gap model for an amorphous semiconductor. (a) The one-electron density-of-states (the hatched regions indicate the tails of localized states in which the carrier mobility is low). (b) The mobility as a function of energy, corresponding to (a).

C. GENERAL CONDUCTION MECHANISMS - TEMPERATURE DEPENDENCE

Accepting the mobility gap idea, four mechanisms of conduction may be expected and each will dominate the d.c. conductivity in an appropriate range of temperature.[3] Starting at high temperatures, the four processes are as follows:

(a) Conduction by carriers excited into extended states just above E_C or just below E_V. In the case of hole transport, for instance, the conductivity will be given by

$$\sigma = C_o \exp[-(E_F - E_V)/kT] \tag{3}$$

Optical measurements usually show that the band gap of amorphous semiconductors decreases approximately linearly with temperature, i.e.

$$(E_F - E_V) = E(0) - \gamma T \tag{4}$$

where $E(0)$ is the value of $(E_F - E_V)$ at $T = 0$ K and γ is its

temperature coefficient. Thus,

$$C_o = \sigma_o \exp(\gamma/k)$$

In chalcogenide glasses, the temperature coefficient of t fundamental optical absorption edge, which is *approximately* equ (see Section 3) to the mobility gap, is usually found experimental to be in the region of 4×10^{-4} to 8×10^{-4} eV deg^{-1}. Moreov the Fermi level E_F is invariably situated near the middle of the g and hence values of γ roughly half that magnitude are to expected; the magnitude of $\exp(\gamma/k)$ is therefore likely to be in t range 10-100. The constant σ_o is generally equated with σ_{min} t so-called minimum metallic conductivity. Mott defined σ_{min} as t smallest non-zero value the conductivity can have at absolute zer i.e. the lowest value of the conductivity contributed by carriers ju at E_C (in the case of electrons) before the start of activate processes. Mott derived the simple relationship

$$\sigma_{min} = \text{Constant } (e^2/ha)$$

where a is the interatomic distance. The constant depend somewhat on structure and is in the region 0.03 to 0.1 so that σ_m is 200-800 ohm^{-1} cm^{-1}, if a = 3 Å. For conduction in extende states therefore the pre-exponential constant C_o (Eqs. (3) and (5) should be roughly 10^3-10^4 ohm^{-1} cm^{-1}.

(b) Transport by carriers excited into the tail of localized states a energies close to E_A or E_B (see Figure 2) and migrating by hopping mechanism. Assuming conduction by electrons again,

$$\sigma = C_1 \exp[-(E_F - E_B + W_1)/kT)]$$

where W_1 is the activation energy for hopping. It is not easy t make an estimate of C_1 but the lower mobility and the lowe density-of-states near E_A compared with E_C, will make it severa decades smaller than C_o. The energy difference $(E_F - E_B)$ is also expected to depend upon temperature but that is again difficult t determine.

(c) At low temperatures a significant number of carriers is not excited but if the density-of-states at the Fermi level is finite there will be a contribution from carriers with energies near E_F hopping between localized states. In this case,

$$\sigma = C_2 \exp(-W_2/kT) \tag{8}$$

where W_2 is the appropriate hopping energy and $C_2 < C_1$.

(d) At still lower temperatures it is probable that carriers will tend to hop beyond their spatially nearest neighbour states to states which are closer energetically. This is the so-called variable range hopping mechanism and Mott showed that if the density-of-states at E_F is $N(E_F)$, -

$$\sigma = C_3 \exp[-(T_o/T)^{1/4}] \tag{9}$$

with $T_o \simeq [18\ \alpha^3/kN(E_F)]$

D. POLARON TRANSPORT

If a charge carrier remains in the vicinity of a particular site long enough its field will tend to displace or polarize the surrounding atoms and in its bound state the carrier cannot move unless the polarization cloud also moves with it.[4,5] The trapped carrier and the surrounding polarized region can be treated as an entity known as a polaron; if the polarization cloud extends over only a few interatomic distances the particle is called a small polaron. The polaron has a lower energy than a free electron but a larger effective mass since it must carry the induced deformation when it moves from site to site; the decrease in energy relative to that of the electron in an undistorted lattice is called the polaron binding energy W_p.

In a crystal, the small polaron states may overlap sufficiently to form a polaron band in an analogous way to electron energy band formation in the undistorted lattice.[6] The small polaron band is usually narrow and its width decreases exponentially with temperature. In general therefore a small polaron can move by two different mechanisms. At low temperatures band conduction without phonon interaction is possible; at higher temperatures the small polaron can migrate only by hopping between equivalent sites. The deformation of the lattice to form equivalent adjacent sites requires energy from phonons and the hopping motion can therefore be regarded as phonon assisted tunnelling between sites.

Thus, polaron hopping depends on the occurrence of occasional structural fluctuations causing adjacent occupied and unoccupied sites to have momentarily coincident deformations. At each coincident event the carrier will have a certain jump probability, P, which can be written as the product of two terms:[6]

$$P = P_1 P_2 \tag{10}$$

with P_1 the probability of occurrence of a coincidence event, and P_2 the probability of charge transfer during that event.

The probability of a coincident configuration can be written as

$$P_1 = (\omega_o/2\pi) \exp(-W_H/kT) \tag{11}$$

where $(\omega_o/2\pi)$ is a phonon frequency and W_H, the polaron hopping energy, is the minimum energy necessary to bring two adjacent sites into equivalence. The hopping energy is related to the polaron binding energy by $W_H = (W_p/2)$. Two particular cases are distinguished:

1. The adiabatic regime in which the carrier jumps between the coincident sites several times during the period that the two sites are equivalent in energy.
2. The non-adiabatic regime in which the carrier cannot follow the lattice vibrations and the time required for the carrier to hop is long compared with the duration of a coincidence event.

In the adiabatic regime the hopping probability is high, i.e. $P_2 \simeq 1$. In the non-adiabatic regime $P_2 \ll 1$.

According to Holstein, in the non-adiabatic regime,

$$P_2 = \frac{2\pi}{h\omega_o} \left(\frac{\pi}{W_H kT}\right)^{1/2} J^2 \tag{12}$$

where J is the electronic overlap integral between sites. Hence, writing for the conductivity mobility μ,

$$\mu = (ea^2/kT)P \tag{13}$$

using Eqs. (10), (11) and (12) gives

$$\mu = \frac{ea^2}{kT} \frac{1}{h} \left(\frac{\pi}{WkT}\right)^{1/2} J^2 \exp\left(-\frac{W_H}{kT}\right) \tag{14}^*$$

* Note: Eq. (2) could also be used as an approximate expression for the polaron mobility, with $W = W_H$ and $R = a$. Eq. (14) is a more explicit relationship for the polaron case.

The polaron hopping mobility is therefore thermally activated at high temperatures but when $kT < W_H$, the pre-exponential term varying as $T^{-3/2}$ is predominant. The polaron hopping mobility is usually much less than 1 $cm^2\ V^{-1}\ s^{-1}$ at or near room temperature.

The possibility of small polaron formation in amorphous semiconductors and insulators has been propounded particularly by Emin. The theory developed for crystals still applies except that the site-to-site disorder energy W_D, characteristic of an amorphous solid, also contributes and the total hopping energy W' is given by

$$W' = W_H + \tfrac{1}{2} W_D \qquad (15)$$

It must be recognized that the localized tail states and other gap states, which are the characteristic features of the band model of amorphous semiconductors described in the preceding sections, would be redundant features insofar as transport is concerned if polaronic mechanisms are applicable and it follows that the mobility gap model would have no basis.

Small-polaron energy levels typically lie within the optical energy gap of insulators or semiconductors, and the likely relationship between the optical gap and small-polaron levels for electrons and holes (E_C^{sp} and E_V^{sp} respectively) is illustrated schematically in Figure 3.[7] In crystals the polaron levels would be at discrete energies but, as noted above, in an amorphous solid they are distributed over a range of energy equal to the disorder energy W_D. The Franck-Condon principle implies that optical absorption associated with interband transitions is determined by the density-of-states in Figure 3(b) and the levels E_C and E_V. In Figure 3 small polaron states are shown for both electrons and holes but situations may occur in which only one species of carrier is self-trapped while the other moves in quasi-free Bloch states.

An important parameter in polaron mechanisms is the Hall mobility, μ_H. The calculation of the Hall mobility is difficult and it depends on the local geometry of sites. For a triangular lattice, Friedman and Holstein have derived for the non-adiabatic case,[8]

$$\mu_H = \frac{ea^2}{\pi} \left(\frac{\pi}{12kTW}\right)^{1/2} J. \exp\left(-\frac{W}{3kT}\right) \qquad (16)$$

The theory also predicts a sign anomaly. If conduction is due to the hopping of small polaron *holes*, for example, the sign of the Hall effect is *negative* while the sign of the thermopower is positive (as expected from the polarity of the carrier).

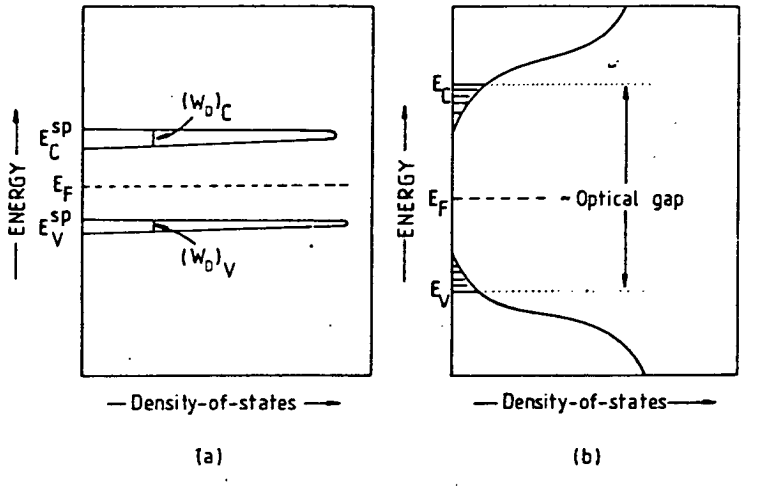

Fig. 3. (a) Proposed density-of-states diagram for small polarons in an amorphous semiconductor. The energy levels E_C^{sp} and E_V^{sp} are for electron and hole polarons, respectively, broadened by the small disorder energies $(W_D)_C$ and $(W_D)_V$. (b) Typical electron density-of-states diagram illustrating the likely relationship of the optical gap, to the polaron levels in (a) (See Ref. 7.)

II. THE ELECTRONIC BAND STRUCTURE OF CHALCOGENIDE GLASSES

A. INTRODUCTION

In all chalcogenide compounds the chalcogen atoms (S, Se or Te) are normally in two-fold coordination. The compounds of most interest are those formed with pnictide elements, such as arsenic, which normally bond in three-fold co-ordination but chalcogens and pnictides can vary their valency and atoms in abnormal coordination configurations are important, electronically, in the formation of defects.

The band structure of chalcogenide glasses is best approached in terms of normal chemical bonding however and this will be considered in the next Section, taking Se and As_2Se_3 as examples. Defect states are discussed in Section 2.3 and Section 2.4 is concerned with the effects of impurities.

B. BONDS AND BANDS

The outer electronic configuration of atomic As is $(4s)^2\ (4p)^3$ and of Se $(4s)^2\ (4p)^4$. The essential features of the band structure of solid Se and

As_2Se_3 in crystalline or glassy forms can be seen from simple molecular orbital considerations with slightly different results depending on whether or not hybridization of the atomic s- and p-states is assumed.

(a) Se

Figures 4(a) and 4(b) illustrate, in simplest terms, two possible molecular orbital configurations for Se. In Figure 4(a) it is assumed that the s- and p-states are first hybridized to form an sp^3-state. In bonding the atomic sp^3-state is split into a lower σ bonding state (b), an upper σ^* anti-bonding state (a) and the two doubly occupied sp^3-states form an intermediate lone-pair (LP) non-bonding (n) level in the molecular orbital scheme.

In Figure 4(b), there is no hybridization and the molecular orbitals are formed from pure s- and p-states. In bonding, the p-states again split into a σ lower bonding state (b), an upper σ^* anti-bonding state (a) and an intermediate non-bonding (n) lone-pair (LP) level. The atomic s-state forms a molecular level well below the bonding p-states. Note that in this case

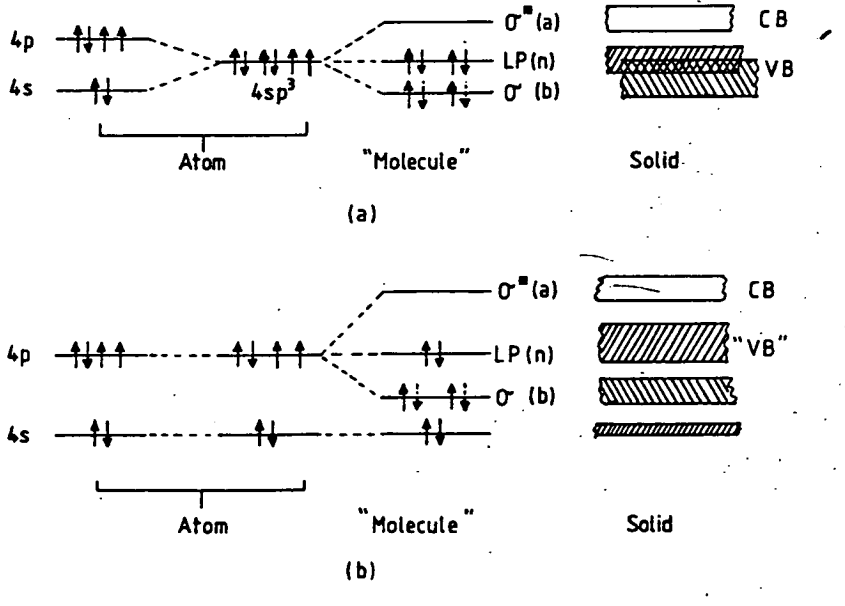

Fig. 4. Molecular orbital schemes for electronic conffgurations in Se. (a) Assuming sp^3 hybridization of atomic states. (b) Without hybridization. (see Refs. 9-12.)

however the LP level has half as many states (and electrons) as in the hybridized scheme.

Tutihasi and Chen,[9] and Chen[10] have proposed detailed molecular orbital models for the band structure of trigonal and monoclinic Se, and for amorphous Se containing rings (monoclinic) and chains (trigonal). An important feature of their calculations is that in solid Se (crystalline or amorphous) there is considerable overlap and mixing of the σ (b) and LP (n) molecular levels and hence both bonding and non-bonding states contribute to the uppermost *filled* band, i.e. to the valence band. This is also illustrated schematically in Figure 4(a).

Kastner,[11] following Mooser and Pearson,[12] proposed a band model for chalcogenide semiconductors based on the scheme of Figure 4(b), i.e. no hybridization. The important feature of this picture is that in the solid state, the lone pair levels remain well separated from the σ bonding states, and hence the uppermost filled band, conventionally called the valence band in semiconductor terminology, is made up entirely of non-bonding electrons. Strictly speaking the term "valence band" is a misnomer.

(b) As_2Se_3

The corresponding schemes for As_2Se_3, with and without sp^3 hybridization, are illustrated in Figure 5(a) and 5(b) respectively.[13] The numbers in parentheses correspond to the number of electrons in a "molecule" of As_2Se_3. Once again, calculations by Chen indicate strong mixing of bonding and nonbonding orbits,[10] and hence also in the uppermost filled (valence) band of solid As_2Se_3. By contrast, the picture based on pure s- and p-states leaves the lone pair (non-bonding) band separated from and above the σ-bonding band.

It is not all clear which of the two molecular orbital schemes - sp^3-hybridization (Figure 4(a) and 5(a)), or pure s- and p-state orbitals (Figures 4(b) and 5(b)) - is correct. Evidence from optical spectra favours pure p-state bonding (Figures 4(b) and 5(b)),[13] and this has certainly become the accepted basis for models of defect states associated with *chalcogen* elements in amorphous chalcogenide semiconductors, although sp^3-hybridization is invoked to explain corresponding defect states associated with pnictide atoms (Section 2.3). As Chen[10] points out however there is also evidence that light of band-gap energy can cause bond breaking in chalcogenide glasses, resulting for example in photo-dissociation and photo-induced crystallization. This seems more consistent with the mixing of bonding and non-bonding orbitals, from both the chalcogen and pnictide element, to form the valence band.

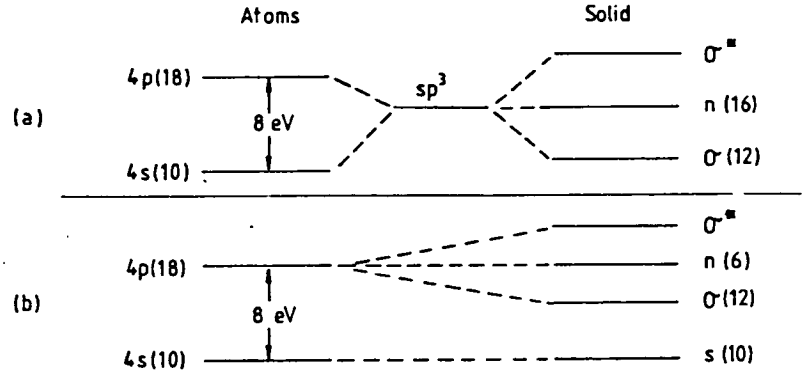

Fig. 5. Molecular orbital schemes for electronic conffgurations in As_2Se_3. (a) Assuming sp^3 hybridization of atomic states. (b) Without hybridization. (see Ref. 13.)

C. DEFECT STATES IN THE BAND GAP OF CHALCOGENIDE ELEMENTS AND COMPOUNDS

Chalcogenide glasses are diamagnetic and show no e.s.r. response, i.e. there appear to be no dangling bonds in the gap. On the other hand the Fermi-level appears to be pinned, suggesting a finite density of gap states. It was largely to resolve this contradiction that models of defect states were first proposed.

The earliest model was suggested by Mott, Davis, and Street (the so-called MDS model)[14,15,16] and it has proved successful in explaining a wide variety of phenomena in chalcogenides, such as the constant activation energy of the DC conductivity (i.e. the pinning of the Fermi-level), magnetism, luminescence, drift mobility and a.c. conductivity. In this model, bonding defects can have three charged states denoted D^+, D^- and D^0, associated with different local atomic configurations. The neutral dangling bond (D^0), say a singly-coordinated chain-end Se atom, would normally possess spin but it is unstable. Consider two such chain-end defects as in Figure 6. Provided the temperature is high enough so that some atomic movement is possible, one of the end atoms moves closer to and cross-links with the LP p-electrons of a Se atom in a neighbouring chain. The three coordinated Se atom now gives up an electron to the remaining dangling bond. The former becomes D^+, the latter D^-, and both are now diamagnetic. The reaction

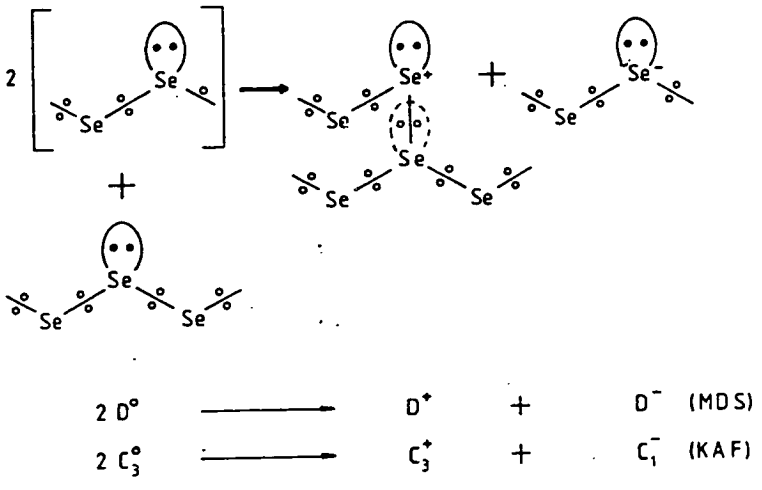

Fig. 6. An illustration of the formation of characteristic chalcogenide electronic defect states in elemental amorphous Se, corresponding to D°, D^+ and D^- in the Mott, Davis and Street (MDS) scheme (Refs. 14-16) or C_3°, C_3^+ and C_1^- in the Kastner, Adler and Fritzsche (KAF) model (Refs. 18-22).

$$2D^\circ \rightarrow D^+ + D^- \qquad (17)$$

is exothermic because of a negative correlation (or Hubbard) energy, the potential energy decrease resulting from spin-sharing more than compensating the Coulomb-repulsive energy increase. The decrease in energy can also be regarded as the result of converting a non-bonding lone pair of electrons into a lower lying σ bonding state by dative bonding. The D^+ and D^- centres lie in the gap and determine the position of the Fermi-level, rather like donors and acceptors in a compensated semiconductor.

In the model of Kastner, Adler and Fritzsche (KAF) the chalcogen atom is denoted by C and its coordination by a subscript.[17–22] The dangling bond C_1° is considered to cross-link with the nearest neighbour on an adjoining chain, so that its bonds are satisfied. It therefore becomes a normal C_2°, and the neighbour must use one of its LP electrons to become the three-fold coordinated neutral C_3°.

If atomic movement is possible while the glass is formed, this rearrangement is spontaneous. The reason is that C_1° and its neighbour C_2° are involved in only three bonds between them, but C_2° and C_3° form five bonds, a gain of two bond energies. In contrast with the MDS model, therefore, the common neutral defect in the glass is C_3°. The unsatisfied

fourth p-electron of C_3^o renders it paramagnetic however and still relatively unstable. For the same reasons as in the MDS model the exothermic reaction

$$2C_3^o \rightarrow C_3^+ + C_1^- \qquad (18)$$

then leads to a "valence alternation pair" (VAP). Its members are identical to the D^+ and D^- centres of Eq. (17) and have the same properties.

Group V elements (pnictides) can also undergo valence alternation. The situation is more complicated than that of the chalcogens, because non-bonding s electrons become available for over-coordination only after hybridization. The bonding configuration of normally and defectively coordinated chalcogen and pnictide elements are compared in Figure 7. In a pnictide element, the lowest energy neutral defect, corresponding to C_3^o, is considered to be P_4^o formed by hybridizing the s and p states to create three equivalent sp^3 orbitals containing the 5 valence electrons, two of which remain in a non-bonding lone pair. In close analogy with the chalcogens, the lowest energy defects are charged VAPs, not neutral P_4^o. The negative

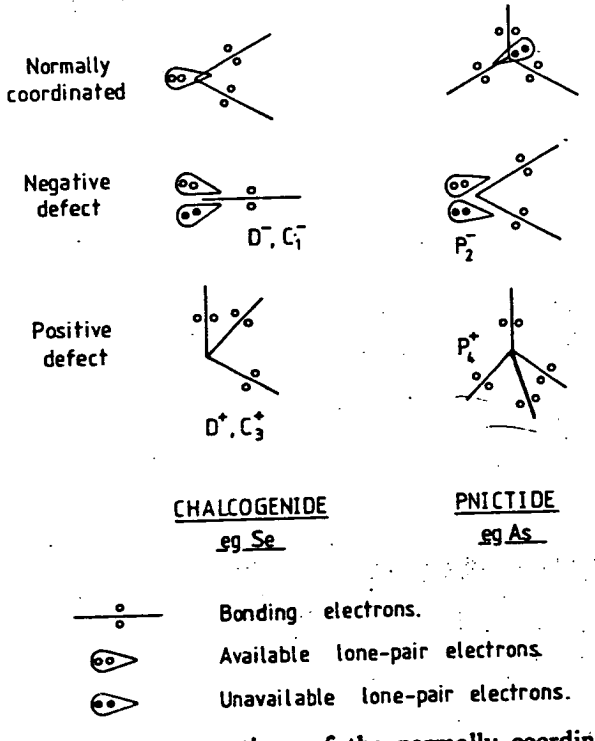

Fig. 7. Schematic representations of the normally coordinated atoms, negative defects and positive defects in chalcogenide and pnictide elements (Ref. 18).

correlation energy gained by transferring charge is larger in pnictides than in chalcogens, so that although the initial creation energy for P_4^o is greater than for C_3^o, the net energy gained in forming VAPs is comparable for the two group of elements. As a first step, P_4^+ and P_4^- defect states are created by transferring an electron from one P_4^o to another and this involves a positive correlation energy, but P_4^- is unstable and the following exothermic reaction takes place:

$$P_3^o + P_4^- \rightarrow P_2^- + P_3^o \tag{19}$$

This involves breaking a bond to one of the four neighbouring P_3^os, placing the two anti-bonding electrons into lone-pair (p-like) orbitals, and dehybridizing the P_4^o to make it a normal P_3^o. The complete exothermic reaction becomes

$$2P_4^o \rightarrow P_4^+ + P_2^- \tag{20}$$

the VAP P_4^+, P_2^- being the equivalent of D^+ and D^- in this case.

When both chalcogen and pnictide elements are combined in a glass such as As_2Se_3, all the stable defects, viz. P_4^+, C_3^+, P_2^-, C_1^-, will be present though in different concentrations. The following reactions will be simultaneously in equilibrium at a high temperature ($>T_g$ the glass transition temperature), assuming only chalcogen and pnictide bonds are present:

$$2C_2^o \rightarrow C_3^+ + C_1^-$$

$$2P_3^o \rightarrow P_4^+ + P_2^-$$

$$P_3^o + C_2^o \rightarrow P_4^+ + C_1^-$$

$$C_2^o + P_3^o \rightarrow C_3^+ + P_2^-$$

In alloys with non-stoichiometric composition the situation is even more complicated because three types of bond may exist (P–C and P–P or C–C) each with a different energy. To determine which reaction dominates, and which defects have the highest density, requires a knowledge of the relative magnitudes of the individual reaction energies. Kastner and Fritzsche[18] believe that C_1^- is always the dominant negative defect, but that either C_3^+ or P_4^+ could be the dominant positive partner depending on a number of considerations. They also argue that under preparation conditions where the defects are allowed to come into thermal equilibrium, P_4^+ and C_1^- will be the

predominant VAPs although C_3^+ and P_2^- centres may also be present in lesser concentrations. Street and Lucovsky[23] have claimed that the predominance of P_4^+ and C_1^- is not proved.

Mott and Street have suggested the possible clustering of D^+, D^- centres due to their Coulomb attraction.[16] Such an overlapping D^+D^- pair has been called an "intimate" valence alternation pair (IVAP) and an IVAP is a neutral (actually a dipole) centre. IVAPs can annihilate each other even at temperatures well below T_g. Since separated VAPs represent charged centres, transport properties are more sensitive to VAPs than IVAPs. Even in a glass in which the ratio of VAP to IVAP density is small, the density of VAPs may be sufficiently high to pin the Fermi-level. Unlike VAPs, IVAPs are not likely to act as traps and therefore are not expected to play a large part in trap controlled transport or conductivity. Approximate calculations by Adler and Yoffa[24] suggest that the density of VAPs is of the order of 10^{18} cm^{-3} and of IVAPs, 10^{19} cm^{-3}.

Joannopoulos has calculated the energy levels of a variety of defect configurations in As_2Se_3 with the results shown schematically in Figure 8.[25]

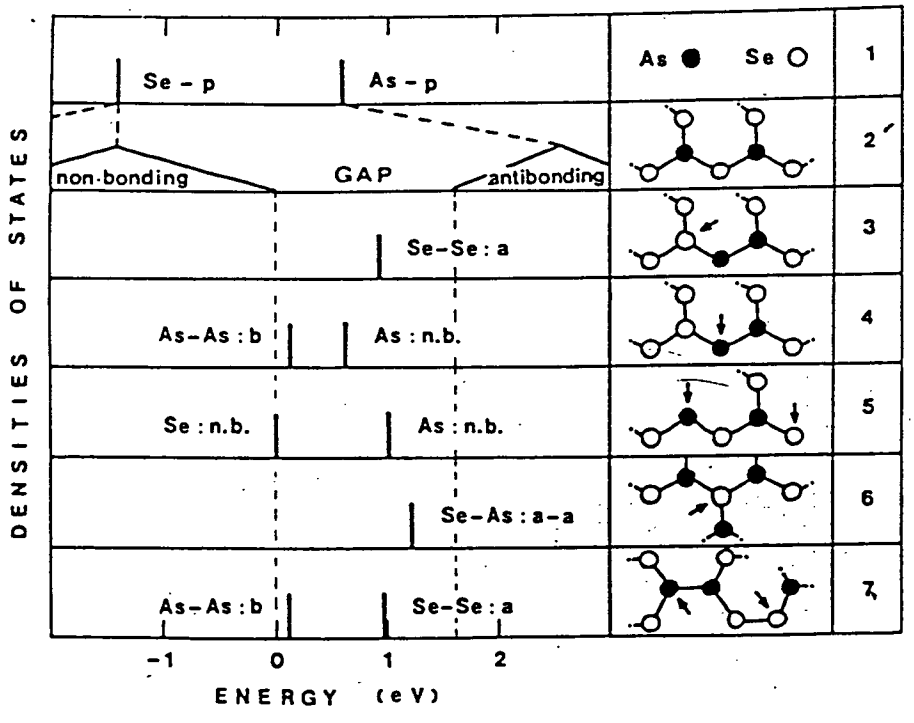

Fig. 8. Results of theoretical calculations of the electronic energy levels of several configurational defects in As_2Se_3 (Ref. 25).

The arrows in rows 3 to 7 indicate the atoms whose local density-of-states is shown in the left-hand part of the diagram. Rows 1 and 2 show the transition from atomic states to bonding states and bands in As_2Se_3. Rows 3 and 4 relate to a defect caused by an exchange of neighbouring As and Se atoms. The states in row 5 result from an As dangling bond (a p-orbital) which interacts strongly with a Se non-bonding orbital. Row 6 describes a three-fold Se defect which is very similar to the three-fold Se defect in elemental Se (Figure 6). In row 7 the defect configurations arise from like-atom bonds where the normal bonding coordination of each atom is reatined. Note that even in the last case the defect states occur at energies within the band gap.

D. THE INFLUENCE OF IMPURITIES

Mott has suggested that certain impurities either destroy bond centres of one sign, or form charged centres (D-centres) which are compensated by defect centres of the opposite sign.[26] In the case of metallic additives such as Mn, there will be very few defects of the same sign as the impurity atoms, by the law of mass action ($[D^+][D^-] = \text{const}$). The Fermi-level will become unpinned and the conductivity activation energy should decrease to 2/3 of its original value.

Kastner[27] and Fritzsche and Kastner[28] also consider the addition of foreign elements to the melt or annealing the adulterated chacogenide glass at T_g. Most of the foreign atoms would seek their lowest energy bonding configuration and remain neutral but some may be incorporated in the host material in a charged state. Thus both neutral and ionized impurities may be present simultaneously. Ionized impurities affect the density of VAP centres. In general, additives with electronegativity near that of the host atoms are less likely to ionize, whereas those which form ionic bonds, i.e. additives from the extreme ends of the periodic table (halogens, alkali metals), are expected to influence the VAP centre concentration strongly.

Kastner and Fritzsche[28] consider two separate cases which arise from different preparation conditions, viz. (a) when the charged impurity is allowed to equilibrate with VAPs in the melt or during annealing at T_g, and (b) when the charged impurity is not allowed to come to equilibrium with the VAPs, as for example in co-evaporation from separate sources onto a substrate below T_g.

In case (a) the charged impurity alters the total VAP density $\left(\left[C_3^+\right] + \left[C_1^-\right]\right)$ as a result of charge compensation. It is predicted that the

conductivity activation energy remains essentially unchanged, although the magnitude of the conductivity may increase. For example, as the concentration of a positively charged impurity is increased, the concentration of negative VAPs rises, reducing the influence of impurities on conductivity in two ways. Firstly, they tend to prevent the occurrence of charged impurities. Therefore, the VAPs remain the source of the charge carriers. Unlike Mott,[26] Kastner and Fritzsche[28] do not predict a decrease of conductivity activation energy, except possibly at high temperatures and under exceptionally strong doping. Instead, under normal conditions and in equilibrium, the conductivity activation energy should remain constant.

In case (b), the charged impurities do not interact chemically with VAPs and therefore the VAP concentration remains unaltered. As long as the concentration of charged impurities is less than that of VAPs, the situation is not much different from case (a) but when it exceeds the VAP concentration, the conductivity activation energy decreases, and a much greater increase in conductivity is expected than in case (a). The Fermi-level becomes unpinned and determined by the impurities, moving towards one of the band edges. At sufficiently high doping level the chalcogenide behaves like an ordinary partially compensated and nearly degenerate semiconductor, with the charged impurities acting either as shallow acceptors or donors.

The traps which control the hole mobility in amorphous chalcogenides are thought to be the negatively charged centres C_1^-. In the case (a) of the KAF model, the addition of positively charged impurities, say A^+, would result in an increase in the C_1^- by the same amount, so that the mobility should vary as $(A^+)^{-1}$. The mobility activation energy is expected to remain constant however, except at very high concentrations when broadening of the impurity level may occur and provide a new transport level. Kastner and Fritzsche do not explicitly consider the effect on the hole mobility of A^+ impurities not equilibriated with the VAPs. Under these conditions, one would expect no change in C_1^- concentrations, nor therefore in mobility or its activation energy.

III. D.C. CONDUCTIVITY, THERMOPOWER AND HALL EFFECT

A.

Over a wide temperature range, the d.c. conductivity of most chalcogenide glasses obeys an equation of the form,

$$\sigma = C \exp(-E_\sigma/kT) \tag{21}$$

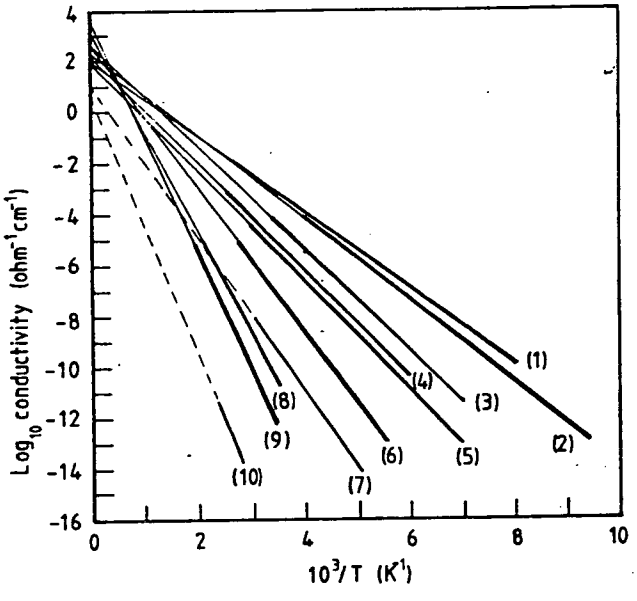

Fig. 9. Typical plots of the logarithm of conductivity vs. reciprocal temperature for a number of chalcogenide glasses, illustrating the characteristic straight line behaviour over a substantial range of temperature. (1) GeTe; (2) $As_2Te_3{\cdot}Tl_2Se$; (3) As_2Te_3; (4) $4As_2Te_3{\cdot}As_2Se_3$; (5) $Ge_{15}Te_{81}S_2Sb_3$; (6) $As_2Se_3{\cdot}Tl_2Se$; (7) $As_{30}Te_{48}Si_{12}Ge_{10}$ (the so-called STAG glass); (8) $3As_2Se_3{\cdot}2Sb_2Se_3$; (9) As_2Se_3; (10) As_2S_3.

in which E_σ denotes the activation energy for conduction.[29,30,31] Several examples of typical results are shown in Figure 9, plotted in the usual log σ vs. (1/T) form and extrapolated to (1/T) = 0 (i.e. to give the pre-exponential constant C). Depending on composition, the activation energy E_σ is in the range of a few tenths of an eV to 1 eV or more, and almost invariably values of $2E_\sigma$ are close to the photon energy E_{opt} corresponding to the onset of strong optical absorption.[29–32*] With few exceptions C is 10^2 ohm^{-1} cm^{-1} or greater, and for many typical chalcogenide glasses such as Se and As_2Se_3 it is in the range $10^3 - 10^4$ ohm^{-1} cm^{-1}. Notable exceptions are As_2S_3 and the so-called STAG glass.

Also with few exceptions (some examples will be mentioned later), reasonably linear plots are normally obtained over the whole experimental temperature range. In particular variable-range hopping conduction, behaving even approximately according to Eq. (9), is not generally observed.

* Optical phenomena are considered in the article by P. C. Taylor, in this volume (ref. 32).

Nor, usually, is there any evidence of a lower activation energy at low temperatures although it must be recognized that the relatively low conductivities and large activation energies of the majority of chalcogenide glasses makes it difficult to extend measurements to very low temperatures.

The thermoelectric power has been measured for many chalcogenide glasses and it is always found to be *positive*.[29,30,31] It has a magnitude typical of semiconductors (mV K^{-1}), and it decreases with temperature according to the simple equation established for semiconductors, i.e.

$$S = -\frac{k}{e}\left(\frac{E_S}{kT} + A\right) \tag{22}$$

where E_S is the activation energy for thermopower and A is a constant (often $\sim$1).

It was noted in Section I.C that values of the pre-exponential constant in the range $10^3 - 10^4$ ohm^{-1} cm^{-1} are consistent with conduction in extended states at the mobility edge. Thus, C and E_σ in Eq. (21) are to be equated with C_o and $(E_F - E_V)$ in Eq. (3); the evidence is therefore that in most chalcogenide glasses, the main transport mechanism involves holes at or close to the mobility edge and that the Fermi-level is close to the centre of the mobility gap. The smaller value of C for As_2S_3 and the STAG glass (Figure 9) presumably indicates conduction by hopping in localized states well away from E_V (or E_C).

A critical question is whether the activation energy for conduction, E_σ, is the same as that for thermopower, E_S. For As_2Se_3 the answer is inconclusive. The results of thermopower measurements on As_2Se_3 by Hurst and Davis,[33] Seager and Quinn,[34] and Chiu[35] are shown in Figure 10, and although there is some difference in the magnitude of S, Hurst and Davis and Chiu agree that $E_S = 0.90$ eV, which is essentially the same as E_σ, while Seager and Quinn find a substantially lower value of $E_S = 0.60$ eV. On the other hand there is well documented evidence for differences $(E_\sigma - E_S)$ of about 0.15 eV for glassy "alloys" in the $As_2Te_3Si_x$ and $As_2Te_{(2-x)}Se_x$ systems.[31,36,37]

The low conductivities and mobilities of chalcogenide glasses make Hall effect measurements extremely difficult but there are nevertheless several reports of the Hall-effect mobility μ_H. The Hall coefficient of these p-type materials is normally *negative* and this anomaly can be understood either in terms of the random-phase diffusive type transport of carriers in a 3-site motion through extended states at a mobility edge, or in terms of polaron hopping. Despite general agreement on the sign anomaly however, quantitatively the experimental situation for As_2Se_3 is again not clear.

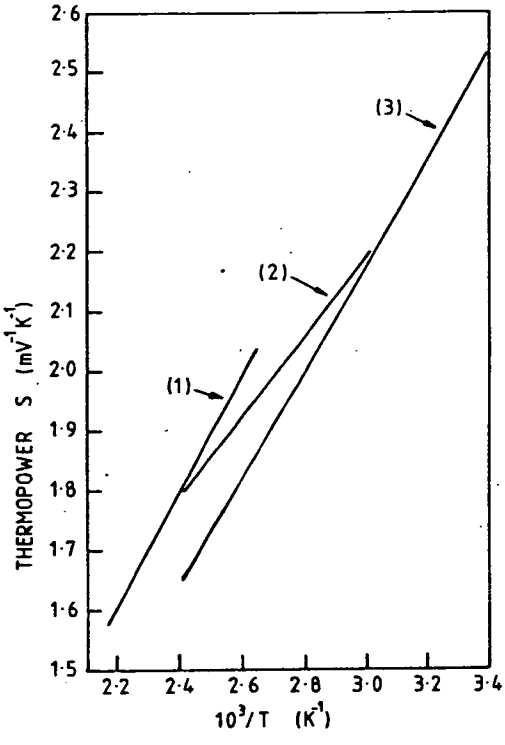

Fig. 10. Thermopower (S) vs. reciprocal temperature for vitreous As_2Se_3. Data from - (1) Hurst and Davis (Ref. 33), (2) Seager and Quinn (Ref. 34) and (3) Chui (Ref. 35).

According to Mytilineou and Roilos,[36] and Nagels et al,[31,37] μ_H in vitreous As_2Se_3 is small ($\sim 10^{-1}$ cm^2 v^{-1} S^{-1}) and unactivated, while Klaffke and Wood[38] report a small activation energy. For the $As_2Te_3Si_x$ and $As_2Te_{(3-x)}Se_x$ systems however there is general agreement that the Hall mobility is activated, i.e.

$$\mu_H = \mu_{Ho} \exp(-E_H/kT)$$

with E_H in the range of 0.03 - 0.05 eV. It is notable that these are the same materials for which consistent values of $(E_V - E_S) \sim 0.15$ eV are also reported.

At the present time therefore the weight of the evidence seems to be that in the case of As_2Se_3 Eq. (3) is applicable, that conduction occurs by hole transport in extended states close to the valence band mobility edge E_V, and that

$$E_\sigma = (E_F - E_V) = E_S = 2E_{opt},$$

implying that the Fermi-level is close to the centre of the mobility gap.

However, in at least a number of chalcogenide glasses, of which the alloys $As_2Te_3Si_x$ and $As_2Te_{(2-x)}Si_x$ are typical, there is clear evidence that:

[i] The thermopower has a smaller temperature dependence than the d.c. conductivity with $(E_\sigma - E_S) \sim 0.15$ eV.

[ii] The Hall mobility is activated with an activation energy in the range 0.03 - 0.05 eV.

Two possible interpretations of these observations are currently considered to be likely explanations.

Nagels et al have proposed a two-path conduction process in which transport may occur almost simultaneously by holes in extended states *just* below E_V and by holes hopping in localized states *just* above E_V.[31,37] Using the subscript 1 to indicate extended state conduction and 2 for hopping conduction then

$$\sigma_1 = C_{01} \exp [-(E_F - E_V)/kT] \tag{23}$$

and

$$\sigma_2 = C_{02} \exp [-(E_F - E_B + W)/kT] \tag{24}$$

with the total conductivity σ,

$$\sigma = \sigma_1 + \sigma_2 . \tag{25}$$

Provided the rate constants of σ_1 and σ_2 do not differ greatly, a log σ vs. (1/T) plot will change its slope only gradually, and over at least a limited range of temperature it will not differ appreciably from a straight line. The thermopower is the weighted sum,

$$S = \frac{(S_1\sigma_1 + S_2\sigma_2)}{\sigma} \tag{26}$$

with

$$S_1 = \frac{k}{e}\left[\frac{(E_F - E_V)}{kT} + A_1\right] \tag{27}$$

and

$$S_2 = \frac{k}{e}\left[\frac{(E_F - E_B)}{kT} + A_2\right] \tag{28}$$

The expected form of log σ vs. (1/T) and S vs. (1/T) is shown schematically in Figure 11. Because the two thermopowers are similar for (1/T) = 0, the form of S in the transition region depends sensitively on the sharpness of the transition in σ and the slope of S vs. (1/T) has little significance in the transition region. The Hall mobility is also given by the weighted sum,

$$\mu_H = \frac{\mu_1\sigma_1 + \mu_2\sigma_2}{\sigma} . \tag{29}$$

Nagels et al assume that $\mu_2 = 0$, so that

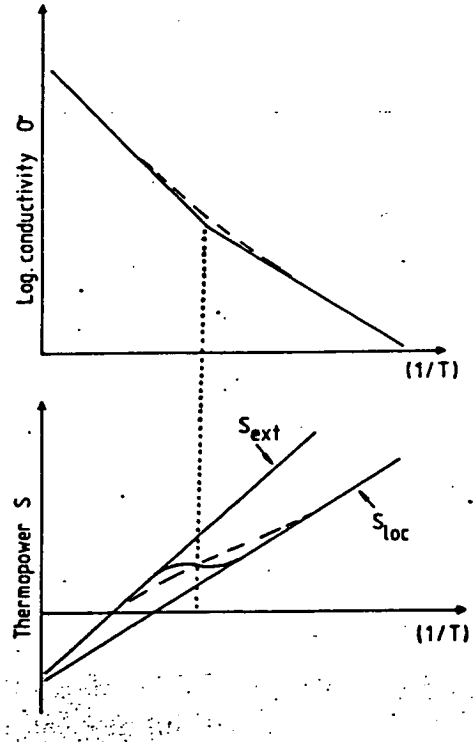

Fig. 11. Schematic plots of the logarithm of conductivity and thermopower vs. reciprocal temperature in the range of two-path conduction where transport changes from conduction in extended states above the mobility edge to hopping in localized states below the edge. The line S_{ext} is the thermopower for transport in extended states and S_{loc} for transport in localized states. (See Refs. 31 and 37.)

$$\mu_H = \frac{\mu_1 \sigma_1}{\sigma} . \tag{30}$$

When conduction occurs *mainly* in extended states μ_H is equal to μ_1, but when hopping also contributes the Hall voltage is generated by the few carriers remaining at the mobility edge E_V and from Eqs. (23), (24) and (30)

$$\mu_H = \mu_1 \left[1 + \frac{C_{02}}{C_{01}} \exp\left(E_B - E_V - W\right)/kT\right]^{-1} \tag{31}$$

The alternative interpretation, first proposed by Emin and coworkers,[5,39] and favoured by Seager and Quinn,[34] is that transport is by small polarons (see Section I.C). In that case the difference $(E_\sigma - E_S)$ gives the hopping energy W directly, and the activation energy for the Hall mobility is (W/3) (see Eq. (16)). From the available experimental data it seems as though the Hall mobility activation energy is approximately $[(E_\sigma - E_S)/3]$ and Emin[7] points out that C_0 values of $\sim 10^3$ ohm^{-1} cm^{-1} are also compatible with small-polaron hopping transport.

Thus trap-modulated hopping of holes at or near the mobility edge E_V, OR polaron hopping, are equally valid interpretations of transport measurements on a number of the more complex chalcogenide glasses and a definitive experiment is lacking at the present time. Mott[40] suggests that indirect evidence *against* the polaron model is provided by the ON-state of threshold switching devices based on complex chalcogenide glasses. The high ON-state conductance implies mobilities of ~ 10 cm^2 V^{-1} S^{-1} and although it is not known which species (electrons or holes) is the major current carrier, it is clear that either electrons or holes, at least, are moving in quasi-free Bloch states.

The conclusions reached from measurements of d.c. conductivity, thermopower, Hall mobility and the optical absorption edge are summarized diagrammatically in Figure 12.* These experiments reveal nothing, directly, about states well within the mobility gap, such as the defect centres discussed in Section II.C, and the influence of gap states is considered in the next section.

* If carrier transport involves polaronic mechanisms however a band model like that of Figure 3(a) would be appropriate.

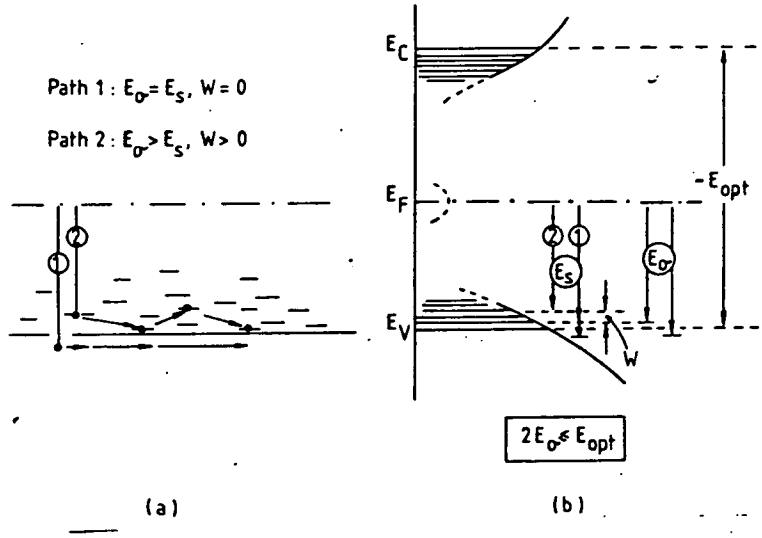

Fig. 12. A diagrammatic summary of the information derived on transport (a) and band structure (b) from measurements of d.c. conductivity, thermopower, Hall mobility and optical absorption (see text, Section III). E_σ is the activation energy for d.c. conduction (Eq. (21)), E_S is the activation energy for thermopower (Eq. (22)), W is a hopping energy (Eq. (7)), and the optical gap E_{opt} is obtained from the fundamental optical absorption edge.

IV. THE INFLUENCE OF STATES IN THE GAP

A. INTRODUCTION

Localized states in the mobility gap influence the electronic transport properties of chalcogenide glasses in a variety of ways, e.g.:[41]

1. Pinning of the Fermi level E_F at or close to the middle of the mobility gap. Fritzsche[42] has pointed out that the characteristic straight line plots of log σ vs. (1/T) over a wide range of temperature (see Figure 9) is evidence that E_F is fixed (pinned) by a large density of localized states, rather than of intrinsic conductions. Marshall and Owen[43,44] have proposed specific models for As_2Se_3, As_2Te_3 and the STAG glass (as in Figure 9), in which E_F is pinned midway between donor- and acceptor-like states.

2. The creation of a high concentration of space-charge density at interfaces and metal contacts. As a result the field effect conductance in

chalcogenide glasses is very small, and again this can be interpreted in terms of E_F positioned midway between large densities of localized states at relatively discrete energies.[44,45] A concomitant effect associated with a large density of gap states is a very short screening length (e.g. ~100 Å) and this explains the apparent ohmic behaviour of most metal-chalcogenide contacts.[46]

3. Localized gap states provide several possibilities for enhanced carrier hopping between neighbouring sites, i.e. for dipolar activity which contributes to the a.c. conductivity and dielectric behaviour.[47,48,49†]

4. The carrier drift mobility in chalcogenide glasses is determined by interactions with localized states and in some circumstances mobility measurements can give information on the energies and distributions of gap states which can be correlated with the models of defect states described in Section 2.3. Mobility data for amorphous Se and As_2Se_3 are discussed in Section 4.3 but first a brief account of the experimental technique is given.

B. TIME-OF-FLIGHT MEASUREMENTS OF DRIFT MOBILITY[50]

The chalcogenide glass sample is prepared in the form of a thin film (e.g. 0.1 - 10 μm thick) with metallic contacts on the opposite surfaces. The top contact is usually semitransparent and it is illuminated with an electron beam pulse or a pulse of strongly absorbed light to generate a thin sheet of excess carriers (electrons and holes) close to the contact. A bias is applied and, depending on its polarity, a unipolar current I(t) of electrons OR holes flows through the sample to be collected at the other electrode. In an ideal case the injected carriers drift through the sample as a coherent unbroadened sheet of charge which reaches the back electrode after a definite time transit time t_τ and a drift mobility μ can be derived from

$$\mu = \frac{\ell}{t_\tau E_{app}} \qquad (32)$$

where ℓ is the sample thickness and E_{app} is the applied field. The I(t) vs. time plot for this ideal situation is illustrated in Figure 13(a). Normally the drift velocities of the individual carriers have a Gaussian distribution and the charge sheet, which propagates with a constant *mean*

† The a.c. conductivity of amorphous semiconductors is considered in detail in the article by E. A. Davis, in this volume (Ref. 49).

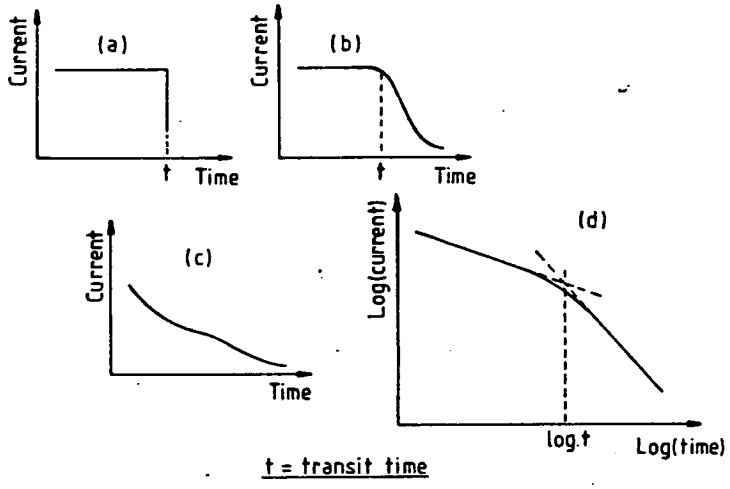

Fig. 13. Illustrations of typical transit current pulses observed in carrier mobility experiments by time-of-flight techniques. (a) An ideal pulse obtained if the sheet of carriers drift without broadening. (b) Broadening due to a Gaussian distribution of mobilities. (d) Strong dispersive broadening. Note: In (a), (b) and (c) current (I) and time (t) are plotted linearly. (d) The current pulse (c) plotted in the form log (I) vs. log (t).

drift velocity, is broadened slightly. As a result the I(t) vs. t curves is rounded-off slightly, as shown in Figure 13(b), but a well-defined transit time can still be distinguished.

In some experiments on amorphous materials a *linear* I(t) vs. t plot has the rather featureless form shown in Figure 13(c). There is, at the most, a slight "knee" in the curve and there is not a well-defined transit time. Very often, however, a *logarithmic* plot [log I(t) vs. log (t)] yields two straight lines of different slopes - see Figure 13(d) - and the intersection of these lines is used to define a transit time. The mobility derived from this transit time often depends on the field strength and the sample thickness.

The fundamental cause of the logarithmic I(t) vs. t curves is that as the sheet of charge moves through the sample the mean velocity of the carriers decreases with time and the charge sheet becomes dispersed rather than drifting as a coherent packet. Various models have been proposed for this "dispersive" transport and a common feature is the presence of some stochastic variable which is responsible for the dispersion in the transit times. Possible mechanisms are as follows:

(1) HOPPING BETWEEN LOCALIZED STATES[51-54]

The temperature-independent hopping distance R, in Eq. (2), is assumed to vary stochastically. As R appears as an exponent in the tunnelling factor [exp $(-2\alpha R)$] a small change in R may cause an amplified change of the hopping probability from site to site, i.e. of the release time after a carrier is trapped. An injected carrier moves towards the collecting electrode with a constant hopping energy W (Eq. (21)) but occasionally it will be trapped at a site in which it remains for a long time. Therefore, only a small fraction of the injected carriers, i.e. the fastest ones, will reach the collecting electrode without passing a "difficult" hopping site, while most of the carriers are delayed by a different number of such hops. Scher and Montroll[52] showed that the probability for a carrier to jump to its next site at time t after having arrived at $t = 0$ is a slowly decaying function which can be approximated by

$$f(t) \propto t^{-(1-\alpha)} \tag{33}$$

where $0 < \alpha < 1$, and hence that the transient current decays algebraically as

$$I(t) \propto \begin{cases} t^{-(1-\alpha)} & \text{for } t < t_\tau \\ t^{-(1+\alpha)} & \text{for } t > t_\tau \end{cases} \tag{34}$$

On logarithmic scales, therefore, the current trace should appear as two straight lines intersecting at $t \simeq t_\tau$ with initial slope $-(1-\alpha)$ and final slope $-(1+\alpha)$, as in Figure 13 (d). A consequence of the algebraic distribution in Eq. (33) is that the mean displacement of the carrier sheet depends on time as t^α and hence that

$$t_\tau \propto \ell^{(1/\alpha)} \tag{35}$$

The drift of the carriers is spatially biased by the applied field and assuming that this asymmetry increases linearly with field strength, Scher and Montroll also derive

$$t_\tau \propto E_{app}^{-(1/\alpha)} \tag{36}$$

Thus, t_τ scales with sample thickness and applied field as

$$t_\tau \propto \left[\frac{\ell}{E}\right]^{1/\alpha} \tag{37}$$

and to derive a mobility from Eq. (32) would lead to a field and thickness dependent mobility such that

$$\mu \propto \left[\frac{E}{\ell}\right]^{(1-\alpha)/\alpha} \tag{38}$$

It is to be noted that as R is independent of temperature, hopping between localized states implies a temperature independent dispersion. If the hopping energy W (Eq. (2)) is included as a stochastic variable however, then the dispersion will be temperature dependent.

(2) TRAP-LIMITED BAND TRANSPORT[55-60]

In this case, carriers move in extended states (electrons just above E_C or holes just below E_V) but are occasionally trapped in localized states and a distribution of the energies of the trapping levels accounts for the dispersive nature of the transient current pulses. The dispersion is temperature dependent, i.e. the shape of the I(t) vs. t curve changes with temperature, otherwise the features described above apply. In particular, it has been demonstrated several times that the integration of individual trap release probabilities of the form

$$g(t) \propto \exp(-t/\tau)$$

over a distribution of traps decreasing exponentially with depth leads to results closely matching those of the Scher and Montroll theory.[58–60]

(3) TRAP-CONTROLLED HOPPING[54,61]

Charge transport occurs by hopping through localized states, as in (1), but with occasional trapping in deeper localized states. Generally, the deeper trapping states will be present in much lower density than the shallower transport states and hence one may expect temperature activated transport processes but a temperature independent dispersion.

C. AMORPHOUS Se AND As_2Se_3: A "DEFECT-STATE" APPROACH

Of the many chalcogenide glasses, transit-time drift mobility measurements have been applied most thoroughly to amorphous Se and As_2Se_3. Comprehensive reviews of the experimental data and their interpretation have been published (see Enck and Pfister,[62] and Owen and Spear[63]) and it is not necessary to repeat the details here but a brief account

will be presented of a particular view which interprets the influence of gap states on transport phenomena in terms of specific electronic defect states of the kind discussed in Section II.C.

Amorphous Se is unusual amongst the chalcogenide glasses in that although holes are the more mobile carrier (i.e. Se is p-type, like most of the chalcogenides), the electron drift mobility is also easily measurable over a wide range of temperature. At least nine different groups have reported data on the electron or hole mobility and in general the agreement is surprisingly good.[62,63] Above about 200 K a well-defined transit time is observed (i.e. a transient current pulse as shown schematically in Figure 13(b)), but below 200 K the pulse shape becomes progressively more dispersive (as in Figure 13(c) and 13(d)). At about 300 K or a little higher, the hole mobility in amorphous Se tends to a constant (temperature independent) value, μ_o, in the region of 0.3 to 0.4 $cm^2\ V^{-1}\ S^{-1}$ while for electrons μ_o is about 0.05 $cm^2\ V^{-1}\ S^{-1}$. Below about 270 K the mobility for both electrons and holes is activated, i.e.

$$\mu = \mu_o \exp(-E/kT) \tag{39}$$

with E in the region of 0.28 - 0.30 eV for holes and approximately 0.33 eV for electrons.[62,63] It is important to note that plots of $\log \mu$ vs. (1/T), or log (inverse transit time) vs. (1/T) are continuous, with the same values of activation energy, from relatively high temperatures (>270 K) where the transit pulses are Gaussian, to low temperatures (<270 K) where dispersive pulses are observed.

The μ_o value for holes is consistent with diffusive transport in extended states (see Section I.B), and while the value for electrons is lower it is still above the lower limit for diffusive mobility estimated by Cohen.[2] Thus, the evidence is that electron and hole motion in amorphous Se occurs by a process of trap-limited transport in extended states just beyond or very close to their respective mobility edges. The traps responsible for limiting the mobility could occur over relatively discrete range of energies (as in Figure 1(b)) or they could be part of a broad distribution of traps, decreasing in density with increasing depth. Marshall and Owen,[64] and Owen and Spear[63] have argued for the former possibility and this implies that at low temperatures (<270 K) a distribution of trap depth over a small range of energies is responsible for the dispersion of the transient current pulses. Combining the drift mobility experiments with d.c. conductivity, optical absorption and space-charge-limited current data, Owen and Spear have proposed the electronic density-of-states distribution shown in Figure 14(a). The mobility gap ($E_C - E_V$) = 2.1 eV is equated with the fundamental optical

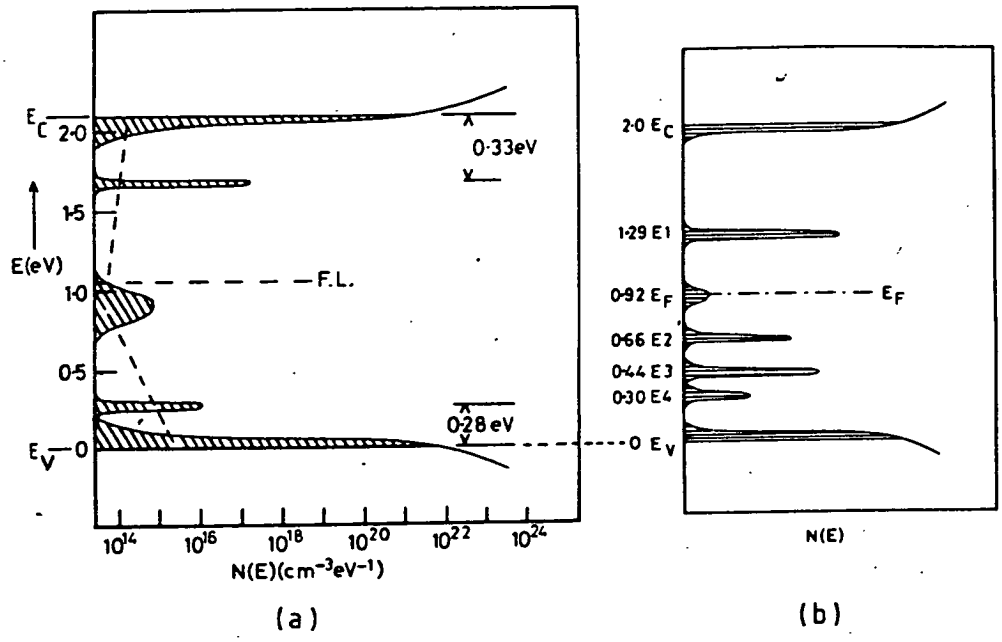

Fig. 14. Electronic density-of-states diagrams constructed from a variety of transport and optical measurements interpreted in the spirit of defect states. (a) Amorphous Se. (b) Amorphous As_2Se_3. (See Ref. 63.)

absorption edge E_{opt}, and the position of the Fermi level is determined by the activation energy for d.c. conductivity.

It is interesting to note that by the following argument Mott has tentatively correlated the electron and hole trapping states in Figure 14(a) with the defect states discussed in Section II.C (using the Kastner, Adler and Fritzsche notation): If valence alternation pairs (VAPs) act as traps, the capture of an electron or a hole produces the *same* centre, C_o. The trap depth for electrons, ϵ_1, is determined by the reaction

$$C_3^o \rightarrow C_3^+ + \text{electron}$$

and the trap depth for holes, ϵ_2, by

$$C_3^o \rightarrow C_1^- + \text{hole}$$

Thus an electron falling into a trap yields an energy ϵ_1 and a hole yields an

energy ϵ_2, with the formation of two C_o centres. To return the system to normal, an energy E is gained through the reaction

$$2C_3^o \rightarrow C_1^- + C_2^+ \tag{40}$$

and

$$E + \epsilon_1 + \epsilon_2 = E_g \tag{41}$$

where E_g is the band gap. Note that the reaction in Eq. (40) is the same as that depicted in Figure 6. Mott equates the energy E with the chain scission energy of Se, less the energy to form the VAP. From NMR data, the Se chain scission energy is 1.4 eV at room temperature, or ~2 eV at 0 K; the atomic fraction of VAPs at 300 K is about 10^{-5} and hence $\exp(-W/2\,kT) \simeq 10^{-5}$, giving W = 0.5 eV for the energy of VAP formation. Thus E is 1.5 eV. Adding the trapping energies ϵ_1 and ϵ_2 (see Figure 14(a)) gives

$$E_{opt} = 1.5 + 0.33 + 0.28 = 2.1 \text{ eV}$$

in good agreement with the experimental value (see also Figure 14(a)).

Drift mobility data for As_2Se_3 are more difficult to interpret, on two counts. First, only hole transits are observable, and electron mobilities are not therefore determinable, and secondly even at the highest temperature at which measurements have been made (~370 K) the hole transit times are two to four orders of magnitude longer than in Se. Nevertheless, hole transport in amorphous As_2Se_3 is clearly an activated process and Marshall et al[55,65] have observed that the activation energy depends on the time scale of the measurement. For transit times <100 μs they report an activation energy of 0.43 eV, while for transit times >200 μs it is 0.63 eV. These trapping energies are in good agreement with the more detailed studies of steady-state and transient photoconductivity which it is possible to make on amorphous As_2Se_3, which also provide evidence for electron traps at about 0.71 eV from the conduction band mobility edge, E_C.[66]

The conclusion from Section III was that amorphous As_2Se_3 is a p-type semiconductor and that hole transport occurs in states at or very close to the valence band mobility edge E_V. Thus, the hole transport phenomena observed in drift mobility and photoconductivity experiments are trap-limited processes. Owen and Spear[63] have collected together the data from measurements of d.c. conductivity, optical absorption, drift mobility, photoconductivity and space-charge-limited current, and interpreted it in terms of the electronic density-of-states model shown in Figure 14(b). It is

relevant to note here that transport experiments on amorphous Se with progressive additions of As indicate that some "Se-like" features are retained in the As–Se compositions, while very effective hole traps are also introduced by the addition of As.[63,67] There is, in addition, evidence that the electron traps at 0.33 eV in amorphous Se move farther away from the conduction band mobility edge E_C as As is added in concentrations of up to 8 atomic %.[68]

It is clear from Section II.C that there is a variety of likely electronic defect states in a chalcogenide compound such as As_2Se_3 and, as Joannopoulos's calculations suggest[25] (Figure 8), several of them are likely to be located within the band gap. At the present however it is not possible to attempt even the tentative correlation between the proposed band model and specific defect states as was described above for amorphous Se.

As mentioned at the beginning of this section, the interpretation presented here is a particular view derived from the notion that amorphous semiconductors may have structurally-related electronic defect states located at relatively discrete energies within the mobility gap. Density-of-states diagrams like those shown in Figure 14 were first proposed purely on the basis of a consistent analysis of experimental results on the assumption that such states exist.[43,66] The subsequent development of specific models for structurally-related defect states in amorphous semiconductors (Section 2.3) provided *post-facto* theoretical justification.[14–25] It should be noted that other data, such as that obtained from field-effect measurements, have been interpreted in a similar way.[44,45] Drift mobility experiments on pure and metal-doped amorphous As_2S_3 are also consistent with trap-limited transport involving defects of the same kind.[69–71]

It must be recognized however that other interpretations are possible. For example, Tiedje and Rose[60] have shown that the dispersive current transient pulses which seem to be so characteristic of transit-time mobility measurements on many, but *not all*, amorphous semiconductors can be explained by trap-limited transport in an exponential distribution of traps. This mechanism is obviously not applicable to amorphous Se however as the transient pulses in that material are only Gaussian-broadened at high temperatures (>200K). Moreover, the low temperature region, where dispersive pulses are observed in amorphous Se, seems to be continuous with the higher temperature range, i.e. there is no evidence of a change in the transport mechanism as the form of the current transient pulses change from Gaussian to dispersive.

Taylor and Ngai[72] have proposed that the dispersive hole transport observed in As_2Se_3 and Se (at low temperatures) can be explained by

polaronic mechanisms. The balance of the evidence from d.c. conduction, optical absorption and thermopower however is that hole transport in amorphous As_2Se_3 occurs at or very close to the valence band mobility edge (see Section III and Figure 12).

V. CONCLUSIONS

Charge transport in the relatively simple amorphous chalcogenide semiconductors such as Se and As_2Se_3 most likely involves trap-limited processes. Carriers migrate via extended states or via states at or close to the mobility edges, E_C and E_V. The evidence from a variety of experiments is consistent with the view that the traps which limit carrier mobilities are located at relatively well-defined energies within the mobility gap, and that these traps originate from structurally-related electronic defects characteristic of various bonding abnormalities associated with the chemistry of chalcogenide elements and compounds.

The situation in more complex multi-component and/or non-stoichiometric chalcogenide glasses is more problematical. The additional compositional disorder associated with the chemical complexity will certainly affect transport mechanisms, perhaps encouraging multi-path conduction processes, polaron formation and probably also smoothing out the density-of-states distribution.

REFERENCES

1. N. F. Mott and E. A. Davis, "Electronic Processes in Non-Crystalline Materials" 2nd Edition, Chap. 1, pp. 39-52 and Chap. 6, pp 209-215 (Oxford University Press) (1979).
2. M. H. Cohen, J. Non-Cryst. Sol. 4, 391 (1970).
3. Ref. 1. Chap. 6, pp. 219-222 (1979).
4. D. Emin, Adv. in Phys. 22, 57 (1973).
5. D. Emin, in "Electrical and Structural Properties of Amorphous Semiconductors" Ed: P.G. Le Comber and J. Mort, pp. 261-328 (Academic Press) (1973).
6. T. Holstein, Ann. Phys. (NY) 8, 343 (1959).
7. D. Emin, to be published in Comments in Solid-State Physics.
8. L. Friedman and T. Holstein, Ann. Phys. (NY) 21, 494 (1963).
9. S. Tutihasi and I. Chen, Phys. Rev. 158, 623 (1967).
10. I. Chen. Phys. Rev. B8, 1440 (1973).
11. M. Kastner. Phys. Rev. Lett. 28, 355 (1972).
12. E. Mooser and W. B. Pearson, in "Progress in Semiconductors" Vol. 5, p. 104. (Heywood and Co., London) (1960).
13. G. Weiser, in "The Physics of Selenium and Tellurium" Ed: E. Gerlach and P. Grosse, p. 230, No. 13 of Springer Series in Solid-State Science (Springer-Verlag) (1979).
14. R. A. Street and N. F. Mott. Phys. Rev. Lett. 35, 1293 (1975).
15. N. F. Mott, E. A. Davis and R. A. Street, Phil. Mag. 32, 961 (1975).
16. N. F. Mott and R. A. Street, Phil. Mag. 36, 33 (1977).
17. M. Kastner, D. Adler and H. Fritzsche, Phys. Rev. Lett. 37, 1504 (1976).

18. M. Kastner and H. Fritzsche, Phil. Mag. B37, 199 (1978).
19. H. Fritzsche, "Proc. 7th Int. Conf. Amorphous and Liquid Semiconductors", p. 3. Ed: W. E. Spear (CICL, Edinburgh, U.K.) (1977).
20. H. Fritzsche, J. Phys. Soc. Japan 49, Suppl. A, 39 (1980).
21. M. Kastner, J. Non-Cryst. Sol. 31, 223 (1978).
22. M. Kastner, J. Non-Cryst. Sol 35-36, 807 (1980).
23. R. A. Street and G. Lucovsky, Sol. State. Commun. 31, 285 (1979).
24. D. Adler and E. J. Yoffa, Can. J. Chem. 55, 1920, (1977).
25. J. D. Joannopoulos, J. Non-Cryst. Sol. 35-36, 781 (1980).
26. N. F. Mott, Phil. Mag. 34, 1101 (1976).
27. M. Kastner, Phil. Mag. 37, 127 (1978).
28. H. Fritzsche and M. Kastner, Phil. Mag. 37, 285 (1978).
29. A. E. Owen, Contemp Phys. 11, 227 and 257 (1970).
30. See for example: Ref. 1 Chap 9, pp. 452-460.
31. P. Nagels, in "Amorphous Semiconductors," Ed. M. H. Brodsky, pp. 113-159 Vol. 36 of "Topics in Applied Physics" (Springer-Verlag) (1979).
32. P. C. Taylor - see this Volume.
33. C. H. Hurst and E. A. Davis, J. Non-Cryst. Sol. 16, 343 (1974).
34. C. H. Seager and R. K. Quinn, J. Non-Cryst. Sol. 17, 386 (1975).
35. D. M. Chui. "Photo- and Thermal Effects in Arsenic Chalcogenides" M.Sc. thesis (University of Edinburgh) (1976).
36. E. Mytilineou and M. Roilos, Phil. Mag. B37, 387 (1978).
37. P. Nagels, R. Callaerts and M. Denayer, in "Proc. 11th Int. Conf. Phys. of Semicond." Ed: M. Miasek, p. 549 (Polish Scientific Publishers, Warsaw) (1972).
38. G. R. Klaffke and C. Wood in "Proc. 4th Int. Conf. on Physics of Non-Crystalline Solids" Ed: G. H. Frischat, p. 236 (Trans. Tech. Publ.) (1977).
39. D. Emin, C. H. Seager and R. K. Quinn, Phys. Rev. Lett. 28, 813 (1972).
40. N. F. Mott, J. Phys. C13, 5433 (1980).
41. See for example: Ref. 1, pp. 460-490.
42. H. Fritzsche, pp. 55-125 of Ref. 5.
43. J. M. Marshall and A. E. Owen, Phil. Mag. 24, 1281 (1971).
44. J. M. Marshall and A. E. Owen, Phil. Mag. 33, 457 (1976).
45. R. C. Frye and D. Adler, Phys. Rev. Lett. 46, 1027 (1981).
46. A. Wallace, A. E. Owen and J. M. Robertson, Phil. Mag. 38, 57 (1978).
47. Ref. 1. Chap. 6, pp. 223-235.
48. A. E. Owen, J. Non-Cryst. Sol. 25, 370 (1977).
49. E. A. Davis - see this Volume.
50. F. K. Dolezalek, in "Photoconductivity and Related Phenomena" Ed: J. Mort and D. M. Pai Chap. 2, pp. 27-70 (Elsevier) (1976).
51. H. Scher and M. Lax, Phys. Rev. B7, 4491 and 4502 (1973).
52. H. Scher and E. W. Montroll, Phys. Rev. B12, 2455 (1975)
53. H. Scher, ref. 50, Chap. 3, pp. 71-116 (1976).
54. G. Pfister and H. Scher, Adv. in Phys. 27, 747 (1978).
55. J. M. Marshall and A. E. Owen, Phil. Mag. 24, 1281 (1971).
56. J. M. Marshall and A. C. Sharp, J. Non-Cryst. Sol. 35 and 36, 99 (1980).
57. A. C. Sharp, J. M. Marshall and H. S. Fortuna, J. de Physique, Colloque C4, Suppl. No. 10, 42, 159 (1981).
58. M. Silver and L. Cohen. Phys. Rev. B15, 3267 (1977).
59. F. Schmidlin, Phys. Rev. B16, 2362 (1977).
60. T. Tiedje and A. Rose, Sol. St. Comm. 37, 49 (1980).
61. G. Pfister and H. Scher, Phys. Rev. B15, 2062 (1971).
62. R. C. Enck and G. Pfister, Ref. 50, Chap. 7, pp. 297-302 (1976).
63. A. E. Owen and W. E. Spear, Phys. Chem. Glasses 17, 174 (1976).
64. J. M. Marshall and A. E. Owen, Phys. Stat. Sol. (a) 12, 181 (1972).
65. F. D. Fisher, J. M. Marshall and A. E. Owen, Phil. Mag. 33, 261 (1976).

66. C. Main and A. E. Owen. Ref. 5, pp. 527-545 (1973).
67. J. Schottmiller, M. Tabak, G. Lucovsky and A. Ward, J. Non-Cryst. Sol. 4, 80 (1970).
68. J. M. Marshall, F. D. Fisher and A. E. Owen, Phys. Stat. Sol. (a) 25, 419 (1974).
69. M. Burman and J. Hirsch, J. Non-Cryst. Sol. 35-36, 987 (1980).
70. M. Burman, J. Hirsch and T. Ramdean, J. Phys. C. 14, 117 (1981).
71. M. Burman "Hole Mobility in Doped and Undoped As_2Se_3 Layers" Ph.D. Thesis (University of London) (1982).
72. P. C. Taylor and K. L. Ngai, Sol. State Commun. 40, 525 (1981).

PHILOSOPHICAL MAGAZINE B, 1984, VOL. 50, NO. 4, 463–475

Reversible photodarkening and structural changes in As_2S_3 thin films

By M. FRUMAR†, A. P. FIRTH and A. E. OWEN
Department of Electrical Engineering, University of Edinburgh, King's Buildings, Edinburgh EH9 3JL, Scotland

[Received 29 July 1983 and accepted 1 May 1984]

ABSTRACT

The photodarkening effect in evaporated As_2S_3 films has been studied. Optical transmissivity was measured and its dependence on intensity, wavelength, temperature and previous thermal history was found. A structural investigation was also made using Raman spectroscopy. A feature at 231 cm^{-1} in the Raman spectra, which is associated with homopolar As–As bonds, is enhanced after photodarkening. A model based on the redistribution of chemical bonds under illumination is used to explain the results.

§ 1. INTRODUCTION

The strong illumination of many amorphous chalcogenides by light whose energy is near that of the optical gap may cause changes in optical transmissivity, refractive index, microhardness, density and other physical and chemical properties (see, for example, Tanaka and Ohtsuka 1978, Grigorovici and Vancu 1981, Averjanov, Kolobov, Kolomiets and Lyibin 1980). These so-called photostructural effects have a variety of potential applications in optical and optoelectronic devices, and in recent years they have been the subject of considerable research.

Many materials have been investigated, among them thin films in the amorphous As–S system and in particular the composition As_2S_3. The compound As_2S_3 is favoured because of its relative structural simplicity; it is easily prepared and amorphous thin films are stable with a low tendency to crystallize. During evaporation the vapour phase of As_2S_3 dissociates into molecular-like particles such as As_2S_2, As_3S_4, As_4 and S_n, and these molecular units can be found in the as-evaporated films condensed onto cold substrates (Nemanich, Connell, Hayes and Street 1978, Solin and Papatheodorou 1977, Keneman, Bordogna and Zemel 1978 a). The films can be 'polymerized', either by annealing near the glass transformation temperature T_g or by strong illumination with photons of energy close to that of the optical gap, E_g. The 'polymerization' is accompanied by an irreversible change in structure and other physical properties of the films. The final structure of well-annealed thin films is similar to that of bulk glasses of As_2S_3 (Solin and Papatheodorou 1977, Nemanich *et al.* 1978). The illumination of well-annealed

† Present address: University of Chemical Technology, 53210 Pardubice, Czechoslovakia.

samples by light with an energy near that of the band gap produces further changes in optical transmissivity, and other properties, which are reversible. The original state can be fully restored by annealing near T_g, or partly restored by illumination with light of energy lower than E_g.

Several models have been suggested to explain the reversible photostructural changes. Unfortunately they are mostly speculative, without directly supporting evidence, and cannot explain all the experimental observations. Berkes, Ing and Hillegas (1971), Keneman *et al.* (1978 a, b) and Tanaka and Kikuchi (1972) have all proposed that illumination of the films changes the distribution of chemical bonds in the material, and that products of photolysis such as sulphur and arsenic are formed. It is suggested that arsenic oxide is also formed when illumination is carried out in air (Berkes *et al.* 1971).

Another model of photo-induced reversible changes in chalcogenide layers assumes that there occurs photo-induced polymerization of the layers (see, for example, Grigorovici and Vancu 1981). As already mentioned, however, annealing of samples at temperatures near T_g ' erases ' the photo-induced changes ; if this model were correct the annealing process would be connected with depolymerization, but there is no experimental evidence to support this. Moreover, the polymerization model predicts densification and a consequent decrease in the thickness (volume) of the sample after illumination, in contradiction to the experimental results for As_2S_3 (Tanaka 1976, Hamaka, Tanaka and Iizima 1977).

A third approach to the explanation of reversible photostructural changes in chalcogenide films is essentially phenomenological (see, for example, Tanaka 1980, Krasnov and Remesnik 1980, Averjanov *et al.* 1980). It is proposed that at least two metastable states connected with a rearrangement of chemical bonds and atomic positions occur in amorphous chalcogenide films. Bandgap illumination is supposed to change the electron densities, and consequently the positions of some of the atoms are also changed. This stabilizes the new state and the previous optical properties are changed.

In this paper we report results on the optical transmissivity and its temperature and spectral dependence, as well as new results of a Raman study of photostructural changes in As_2S_3 films. Both annealed and photodarkened states have been studied, as well as the behaviour of amorphous As_2S_3 during illumination at different wavelengths and light intensities. The aim of the work is to provide new data on the reversible part of the photostructural changes in thin films of amorphous As_2S_3.

§ 2.. Experimental

Thin films of amorphous As_2S_3 were deposited by vacuum evaporation onto microscope slides or slides of Corning 7059 glass, using as the source material small fragments of bulk As_2S_3 glass of 99·999% purity. The vacuum was less than 10^{-5} Torr, and the substrate was at room temperature. For some of the Raman experiments the substrate was first covered with a thin evaporated layer of Al. During deposition the thickness of the amorphous As_2S_3 films was measured with a quartz thickness monitor. Films of total thickness ranging from 1 to 5 μm were prepared, at a deposition rate of

2–5 nm s^{-1}. The As_2S_3 layers were annealed at 200–210°C for at least 1 hours; the heating and cooling took between 2 and 4 hours. To avoid oxidation of the As_2S_3, the samples were subsequently both annealed and illuminated in an atmosphere of dry N_2.

Raman spectra were measured using conventional back-reflection scattering. The samples were excited mainly with red light of wavelengths 676·4 and 647·1 nm from a Kr-ion laser. Green lines at 568·2 and 530·9 nm and the blue line at 488·0 nm were also used. A Coderg computer-controlled T800 triple spectrometer with a cooled RCA-C3 1034A photomultiplier operating in the photo-counting mode were used for detection. All spectra were measured at room temperature with a spectral slit width of ~ 3 cm^{-1}. The laser was only slightly focused, and the power was kept below 50 mW. Plasma lines were removed by a prism filter.

Samples were photodarkned with a 500 W tungsten lamp at a distance of 20 cm. A solution of 1M $CuSO_4 . 5H_2O$, 2 cm thick, was used as an infrared filter. Samples were also illuminated by an Ar-ion laser fitted with a spatial filter and a beam-expanding system. Intensities up to 200 mW cm^{-2} at wavelengths of 488·0 and 514·5 nm were used. In some cases samples were actually photodarkned during the recording of the Raman spectra using the exciting wavelengths of 568·2, 530·9 and 488·0 nm. The optical transmissivity of the films was also measured during the recording of the Raman spectra.

§ 3. Results

The optical transmissivity of thin films of As_2S_3 is influenced strongly by the intensity and wavelength of illumination, the ambient temperature and

Fig. 1

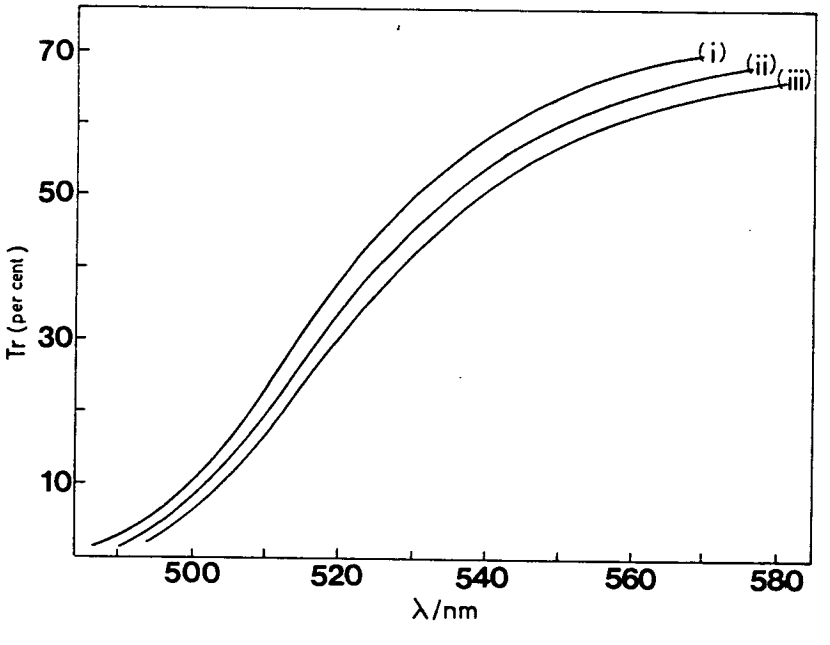

(*a*)

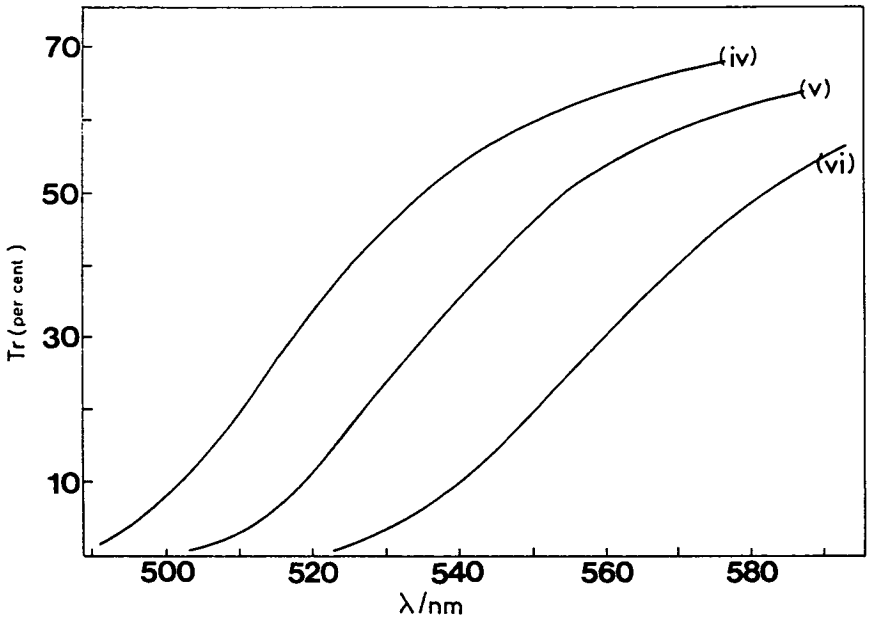

(*b*)

The spectral dependence of the transmissivity of As_2S_3 thin films. (*a*) Curve (i) as-evaporated film, curve (ii) annealed film, curve (iii) annealed film exposed to tungsten lamp for 1 hour. (*b*) Annealed film measured at (i) 300 K, (ii) 405 K, (iii) 501 K.

the thermal history of the film. Typical results are shown in figs. 1 to 4. Curve (i) in fig. 1 (*a*) shows the transmissivity as a function of wavelength for an as-deposited, vacuum-evaporated thin film of As_2S_3 ; curve (ii) is for an annealed film (200°C, 1 hour) and curve (iii) for a film after illumination (tungsten lamp, 1 hour) ; all curves were measured at room temperature. The sequence of measurements could be (i)→(ii)→(iii)→(ii)→(iii) and so on, or (i)→(iii)→(ii)→(iii) and so on. In fig. 1 (*b*) the curves (iv), (v) and (vi) are for an annealed film measured at 300, 405 and 501 K, respectively ; these results simply correspond, of course, to the decrease in optical energy gap with increasing temperature and illumination.

Figure 2 illustrates in more detail the effect of temperature (and heat treatment) on transmissivity at four different wavelengths. Again, these results could be obtained in a variety of ways. For example, curve (*c*) ($\lambda =$ 510 nm) could be traced out by starting at point 1, corresponding to an annealed film at about room temperature. Illumination would cause the transmissivity to decrease down a vertical line to point (2). On raising the temperature the transmissivity decreases still further (as in fig. 1 (*b*)), and at a high enough temperature (in this case about 160°C) the sample is at least partially ' annealed '. In the particular experiment illustrated the temperature was then decreased continuously to about −170°C and the upper curve, corresponding to an annealed sample, was traced out. At −170°C the film was illuminated and the transmissivity decreased down the vertical line. On reheating the transmissivity decreased further, along the lower line, and the

Fig. 2

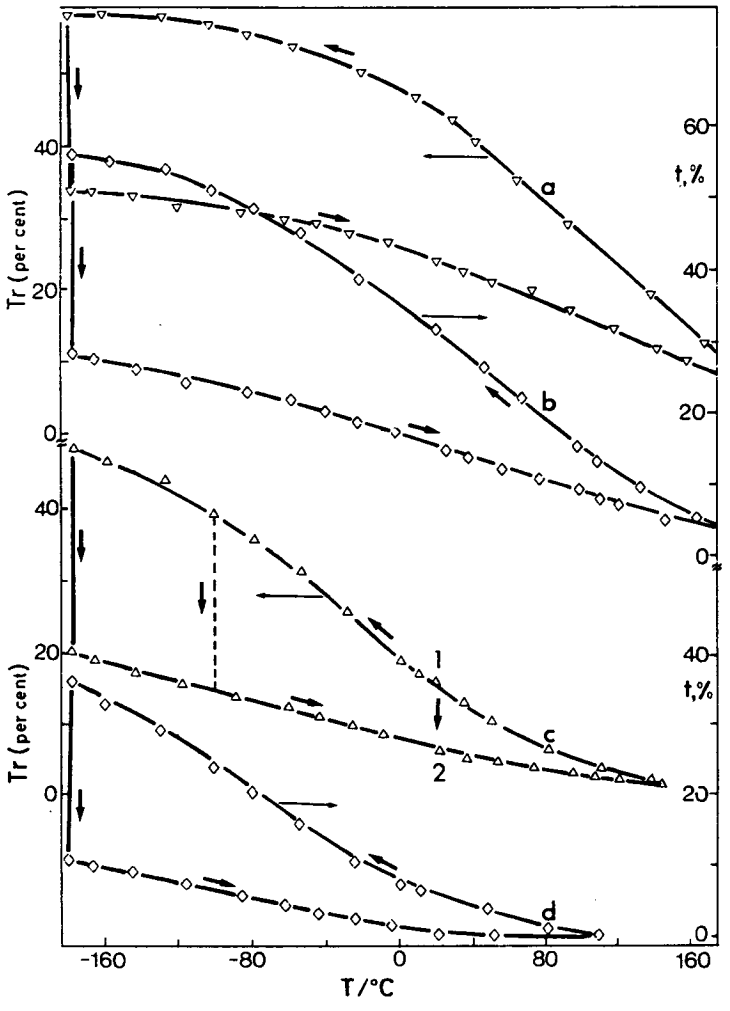

The temperature dependence of the transmissivity of As_2S_3 thin films measured at (*a*) $\lambda = 530$ nm, (*b*) $\lambda = 520$ nm, (*c*) $\lambda = 510$ nm and (*d*) $\lambda = 500$ nm. The vertical lines correspond to the change in transmissivity produced by illumination by a tungsten lamp for 1 hour.

loop could be retraced. It would also be possible, of course, to stop at any intermediate temperature to carry out the photodarkening process, for example, as indicated by the dashed vertical line at about -100°C. Note, however, that the temperature cycling of the upper part of the loop could be followed in either direction, but the vertical transitions (photodarknening) can occur only in the downward direction.

Figure 3 illustrates the development of the photodarkening effect at room temperature as a function of time, but with the illumination turned off and on at arbitrary intervals ; during the on-periods the intensity of illumination remained constant. A similar experiment is recorded in fig. 4, but here the illumination was subjected to several arbitrary decreases or increases in

Fig. 3

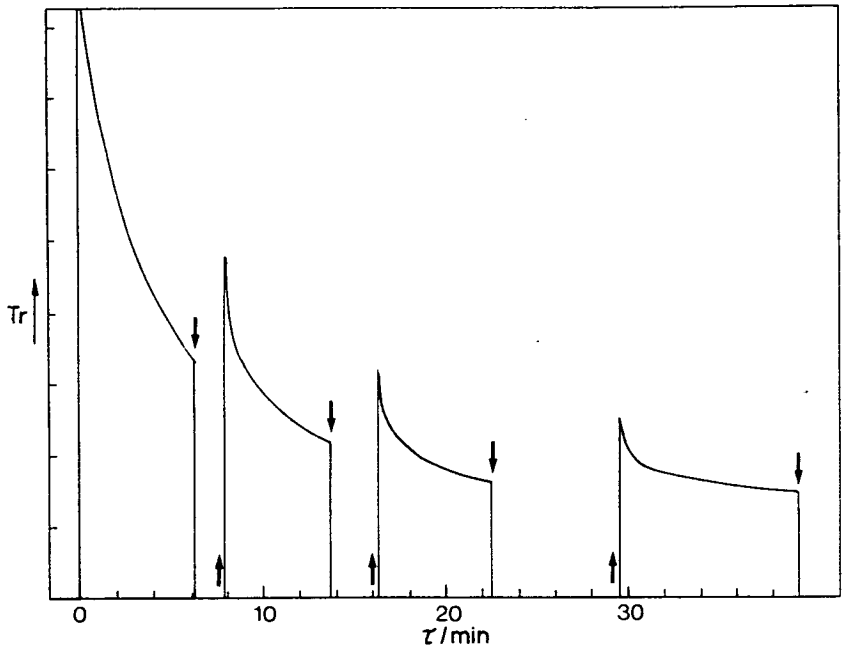

The change in the transmissivity of annealed As_2S_3 thin films during illumination at a constant intensity by 514·5 nm laser light. The vertical arrows correspond to the closing (↓) and opening (↑) of a shutter. The measurements were made at room temperature.

intensity at different times. The following points should be noted from figs. 3 and 4.

(1) A small annealing effect is observed, even at room temperature.
(2) On illumination there is an initial rapid decrease in optical transmissivity (photodarkening), but on interrupting the illumination the transmissivity increases (annealing) and then decreases again on further illumination (fig. 3).
(3) On decreasing the intensity of illumination, photobleaching is observed (fig. 4), whereas on increasing the intensity further photo-darkening occurs.
(4) The rates of photodarkening and bleaching are not the same (fig. 4). This asymmetry implies that the changes in transmissivity cannot be caused by thermal effects (that is, by the small changes in sample temperature during and after illumination).
(5) After prolonged exposure at a particular intensity the optical transmissivity decreased to a saturation value. In the saturated state the photodarkening is determined, at a given temperature, by the wavelength and intensity of illumination. This implies, that for a given intensity, the cycles of changes traced out in fig. 2 are unique provided the photodarkening (that is, the lower part of the cycle) has reached its saturation value.

Fig. 4

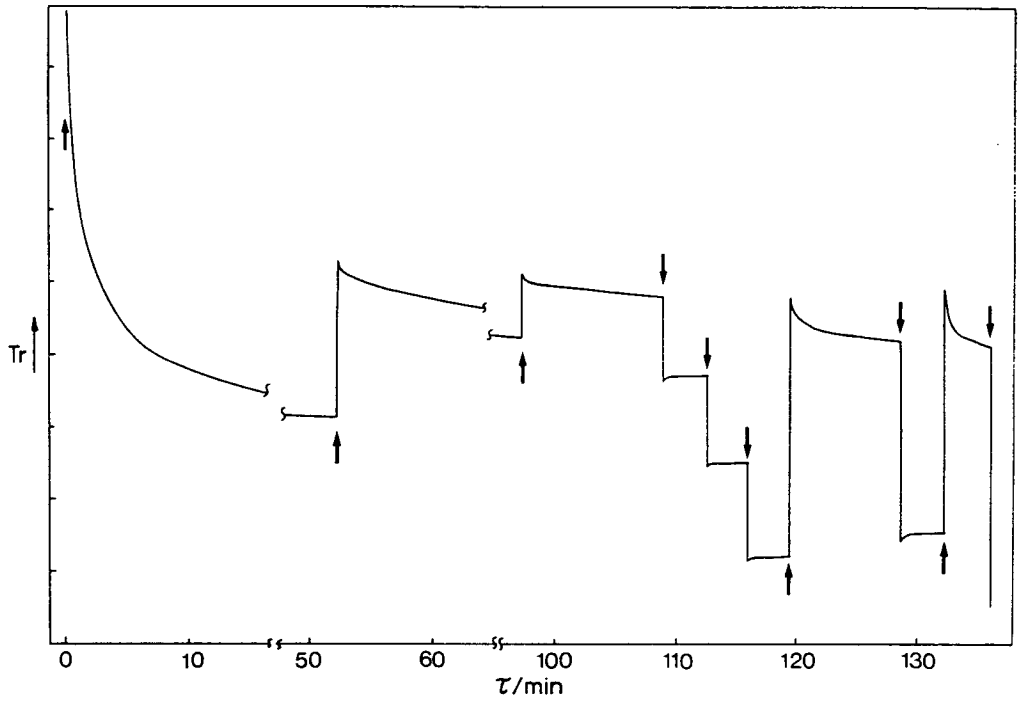

The change in the transmissivity of As_2S_3 thin films when illuminated by 514·5 nm laser light. The vertical arrows correspond to increasing (↑) and decreasing (↓) incident laser intensity. The curves were measured at room temperature.

The total change in transmissivity for the reversible part of the photostructural change was greater than 90% of its initial value at a wavelength of 514·5 nm. The upper level of the intensity of illumination which can be applied is limited by irreversible processes which would lead to melting and disintegration of the sample.

The Raman spectra of evaporated As_2S_3 films are shown in fig. 5. Curve (*a*) shows the as-deposited film. The characteristic sharp features in the region 100–250 cm^{-1} have been assigned to molecular units such as As_4S_4, S_n and As_4 (Ewen 1978, Nemanich *et al.* 1978, Solin and Papatheodorou 1977). After annealing the film curve (*b*) was obtained. The sharp features are considerably reduced, but relatively broad features with maxima at 187 and 231 cm^{-1} remain. Similar results were observed by Nemanich *et al.* (1978) and were taken as evidence that some ' wrong ' bonds of the type As–As and S–S exist even in well-annealed As_2S_3 films.

Figure 6 shows the effect of illumination on the Raman spectra of As_2S_3 layers. It can be seen that the bands with maxima at 187 and 231 cm^{-1} are clearly affected by the illumination. The intensity of the band at 231 cm^{-1} is increased, while the intensity of the band at 187 cm^{-1} is decreased. Similar results were obtained by Ewen (1978) on bulk As_2S_3 glasses. Ewen observed a general decrease in the intensity of the Raman spectrum during illumination, but the relative intensity of the band at 231 cm^{-1} increased. The results are

Fig. 5

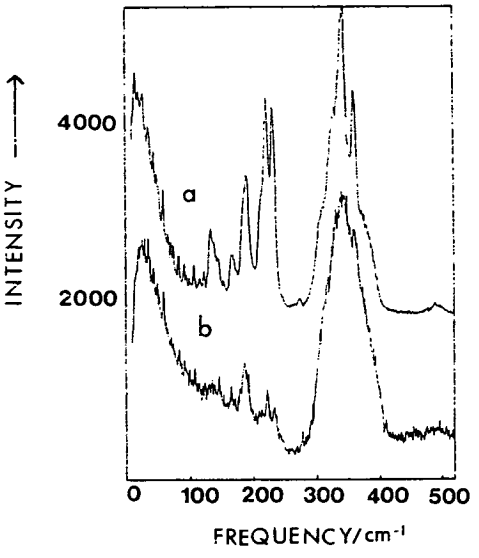

Raman spectra of (*a*) an as-evaporated and (*b*) an annealed As_2S_3 thin film.

Fig. 6

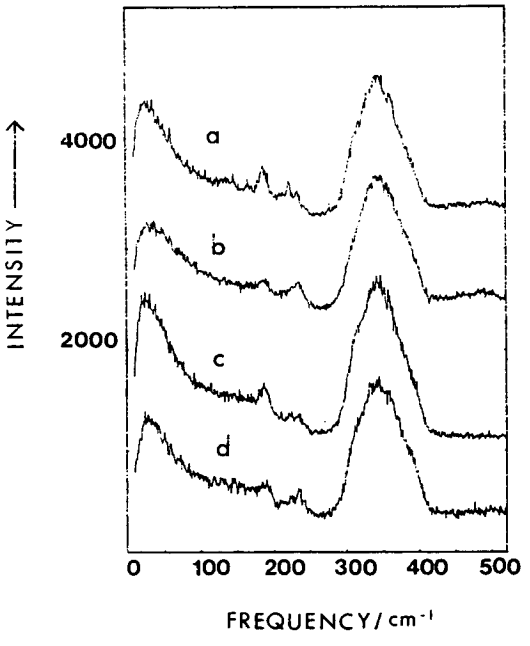

The Raman spectra of a typical As_2S_3 film illustrating reversible photodarkening. (*a*) The first annealed state, (*b*) the photodarkened state produced by Ar-ion laser illumination, (*c*) the second annealed state and (*d*) the second photodarkened state produced by Ar-ion laser illumination. All the spectra were recorded using the 647·1 mm wavelength, and were normalized to the height of the 340 cm^{-1} Raman band.

also in agreement with those of Bertoluzza, Fagnano and Monti (1979) who found that illumination of As_2S_x glasses with $x \leqslant 3$ changed the Raman spectra. The Raman band near 231 cm^{-1} was enhanced, and the intensity of the band at 187 cm^{-1} reduced.

Curve (*c*) in fig. 6 was obtained after annealing the film a second time. It is clearly similar to curve (*a*), showing that the observed reversible photodarkening is connected with reversible changes in structure. Curve (*d*) was obtained after the sample was illuminated again. The enhanced 231 cm^{-1} band and the reduced 187 cm^{-1} Raman band are again seen. The cycling between the well-annealed and photodarkened state was repeated many times with reproducible results.

Figure 7 shows the Raman spectra of As_2S_3 films which were photodarkened using the exciting wavelength. The Raman spectra were recorded after the photodarkening had saturated. Curve (*b*), (*c*) and (*d*) were recorded using wavelengths of 568·2, 530·9 and 488·0 nm, respectively, and they reveal a further enhancement of the 231 cm^{-1} Raman band compared with the photodarkening state shown in fig. 6. Curve (*a*) shows the Raman spectrum of a well-annealed film for comparison ($\lambda_{exc} = 647{\cdot}1$ nm). Changes in the Raman spectra (fig. 7) and transmissivity were reversible, and after annealing the original state (fig. 7, curve (*a*)) was restored. The reversibility was demonstrated several times.

Since the results are similar over a broad range of wavelengths (568·2–488·0 nm) this indicates that the observed enhancement of the 231 cm^{-1} band does not result from a resonance effect.

Fig. 7

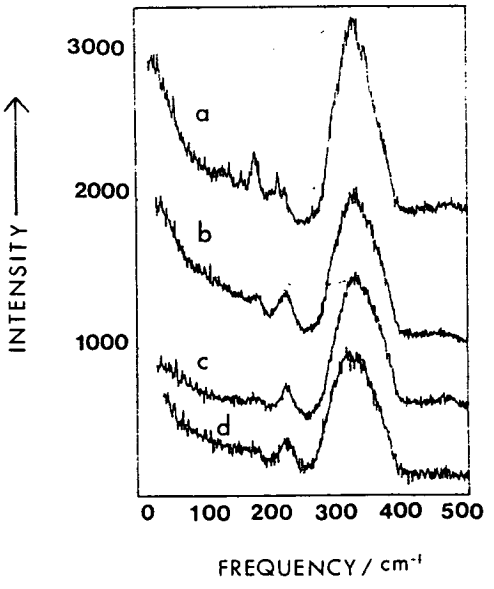

Raman spectra of As_2S_3 thin films. (*a*) An annealed film ($\lambda_{exc} = 647{\cdot}1$ nm). (*b*, *c*, *d*) The spectra of films that were photodarkened and excited using the wavelengths 568·2, 530·9 and 488·0 nm, respectively.

The sharp Raman band at 231 cm^{-1} in the Raman spectra of As_2S_x glasses has been assigned to the vibrations of As–As bonds, as reported by Ewen (1978), Nemanich *et al.* (1978), and Kosek, Cimpl, Matyas and Pisarcik (1982). In these papers the increase in the intensity of the Raman band at 231 cm^{-1} was correlated with an increase in the As content of the glass, and was thus related to an increase in the As–As bond density. Moreover, the Raman spectrum of amorphous arsenic has a broad band between 170 and 310 cm^{-1}, the centre being at ~ 225 cm^{-1} (Lannin 1977, Davis 1981). Lucovsky and Knights (1974) studied the infrared absorption spectra of amorphous As and found a strong absorption band centred at 230 cm^{-1} which they connected with the vibrations of As_4 pyramids.

§ 4. Discussion

From these results we deduce that the enhanced 231 cm^{-1} band in the Raman spectra of As_2S_3 thin films is caused by an increase in the density of As–As bonds in photodarkened layers. The band is not as broad as the band at 231 cm^{-1} found in amorphous As (Lannin 1977, Davis 1981), which may be a result of the more molecular nature and the weaker coupling of As–As atoms into the amorphous network in photodarknened films. Since we have found that the intensity of the Raman band at 231 cm^{-1} is increased with photodarkening and decreased with annealing, this suggests that the reversible part of the photodarkening effect is associated with a redistribution of chemical bonds in As_2S_3 layers which involves an increase in the density of As–As bonds under illumination.

In well-annealed films of As_2S_3, the hetero-type bonds of As–S are preferred, and the reversible structural change connected with photodarkening can be described by

$$2|\text{As–S}| \rightarrow |\text{As–As}| + |\text{S–S}|. \tag{1}$$

Equation (1) shows that the bond statistics of As_2S_3 films are shifted by strong illumination from a state which is close to the chemical ordered model towards a state described by the random network model. The randomness of the chemical bond distribution is therefore increased.

In a chemical approach the photodarkening process can be described as a photolytic reaction,

$$As_2S_3 \underset{A(T),\, h\nu_2,\, I_2}{\overset{h\nu_1,\, I_1}{\rightleftharpoons}} As_2S_{3-x} + xS, \tag{2}$$

where I_i is the incident light intensity ($I_1 > I_2$), $h\nu_i$ is the incident light energy ($h\nu_2 \geqslant h\nu_1$; $h\nu_1 = E_g$ of the glass). $A(T)$ indicates thermal annealing at a temperature T. Similar suggestions have already been made by several authors, but mostly without the support of direct evidence.

The formation of homo-type bonds (As–As and S–S) from hetero-type bonds in As–S layers is possible without large structural rearrangement ; a proposed mechanism is illustrated in fig. 8. The final products of this reaction are probably As_n ($n \geqslant 2$) clusters.

The formation of relatively stable homo-type bonds in compound chalcogenides (for example, As–As bonds in As_2S_3), which corresponds to a decrease in the formal valence state of ' metallic ' atoms, is possibly the factor which

Fig. 8

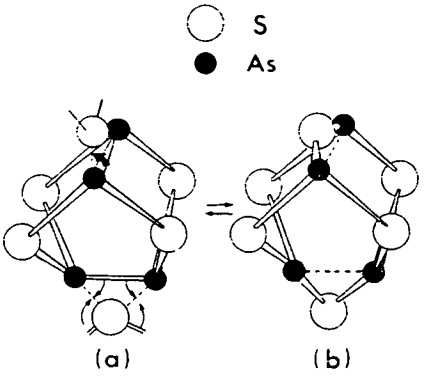

A simplified model illustrating the structural units in (*a*) photodarkened and (*b*) annealed As_2S_3 films. The formation of As_n clusters with $n \geqslant 2$ will be a further stage in the process.

enables the formation of two metastable states in these compounds. Photostructural effects have been found in chalcogenide systems containing As, Sb and Ge, and each of these elements can form lower-valence chalcogenides and relatively strong homo-type bonds.

The chemical reactions described by eqns. (1) and (2) are thermodynamically unfavourable (ΔG is positive). The As–As bonds or As clusters formed by photodarkening can be spontaneously ' dissolved ' and converted back to As–S bonds. The rate of this process is slower at low temperature, and only in the vicinity of T_g, where the atoms are relatively mobile, can thermal bleaching ' dissolve ' all types of As_n clusters ($n \geqslant 2$) and completely reverse the photodarkening process. At lower temperatures, where only partial photobleaching occurs, the smaller As_n clusters ($n = 2$) represented by single As–As bonds can probably be dissolved, and larger As clusters—for example, As_4 pyramids—may be relatively stable and form the steady-state part of the photodarkening effect. As the formation of As clusters involves the absorption of several photons, the density of As–As bonds at a given temperature and wavelength depends on the intensity of illumination. Changes in the density of As clusters, or of As–As bonds, which are directly related to changes in optical density, will be influenced by changing the intensity of the incident light or by the temperature of the layer (see figs. 2–4).

The photodarkening effect is thus a dynamic process, and some photobleaching of films can be observed even at room temperature (see figs. 3 and 4). The observed intensity of the 231 cm^{-1} Raman band is lower in samples measured several hours after photodarkening (fig. 6) than in samples photodarkened to saturation by the exciting wavelength used to record the Raman spectra.

The amorphous state contains many defects of local structure, and the energy of individual bonds has no sharp value. Thus, as we have found, even illumination of As_2S_3 layers with $h\nu < E_g$ can produce the photodarkening effect, but the change in transmissivity is lower than the change produced by

bandgap illumination. This result is also in accordance with the data obtained by Tanaka (1980).

In crystalline As_4S_n ($n=3, 4$), and probably in the amorphous As–S systems, As–As bonds are longer than As–S bonds (for example, in As_4S_4 As–As = 2·59 Å and As–S = 2·24 Å, and in As_4S_3 As–As = 2·45 Å and As–S = 2·21 Å; Porter and Sheldrick 1972). In our model the photodarkening is connected with the breaking of some As–S bonds. Instead of shorter As–S bonds, longer As–As bonds are formed. The reported increase in the thickness of As_2S_3 layers after illumination (Tanaka 1976, Hamaka *et al.* 1977), which was confirmed in this work, can be accounted for if it is assumed that a small fraction of the As–S bonds contribute to the change in thickness. Only changes in bond length perpendicular to the substrate plane contribute to the thickness change ΔX;

$$\Delta X = \Delta b \sin \psi, \tag{3}$$

where the change in bond length per bond, Δb, is given by

$$\Delta b = \tfrac{1}{2}(b_{\mathrm{As-As}} + b_{\mathrm{S-S}}) - b_{\mathrm{As-S}}, \tag{4}$$

and ψ is the angle between a given bond direction and the substrate plane. Thus, the mean value of ΔX is

$$\overline{\Delta X} = (\Delta b/\pi) \int_0^{\pi} \sin \psi \, d\psi = 2\Delta b/\pi. \tag{5}$$

A similar expression can be obtained for the average layer thickness $\overline{X_0}$ of the original As–S bonds;

$$\overline{X_0} = 2b_{\mathrm{As-S}}/\pi$$

and hence

$$\overline{\Delta X}/X_0 = \Delta b/b_{\mathrm{As-S}}. \tag{6}$$

For the bond lengths quoted above, and with $b_{\mathrm{S-S}} = 2{\cdot}2$ Å, these equations give $\overline{\Delta X}/X_0 = 0{\cdot}068$.

According to Hamaka *et al.* (1977), the relative change in thickness determind experimentally is 0·004, and hence the fraction of As–S bonds involved in the photostructural change is 0·004/0·068 = 0·059, approximately 6% of the total.

§ 5. Conclusions

We have found that the reversible part of the photodarkening effect observed in As_2S_3 films is accompanied by an increase in the Raman band with its maximum at 231 cm^{-1}. This was interpreted as an increase in the As–As bond density as a result of illumination. This experimental evidence supports previous speculative suggestions about bond redistribution or a photolytic chemical reaction connected with photo-darkening. The actual redistribution of chemical bond depends on the intensity and wavelength of the illumination, and also on the temperature of the film. Photodarkening is a dynamic equilibrium which can be shifted by changes in temperature and in the conditions of illumination. Our interpretation gives a structural meaning to the double-well model, and also predicts the increase in volume of illuminated films.

ACKNOWLEDGMENTS

The authors gratefully acknowledge the receipt of research grants from the Science and Engineering Research Council, and the cooperation of Dr. W. Taylor of the Physics Department of Edinburgh University in making available the experimental facilities for Raman spectroscopy.

REFERENCES

AVERJANOV, V. L., KOLOBOV, A. V., KOLOMIETS, B. T., and LYUBIN, V. M., 1980. *Phys. Stat. Sol.* (a), **57,** 81.

BERKES, J. S., ING, S. W., and HILLEGAS, W. J., 1971, *J. appl Phys.*, **42,** 4908.

BERTOLUZZA, A., FAGNANO, C., and MONTI, P., 1979, *Molecular Spectroscopy of Dense Phases*, edited by M. Grosman *et al.* (New York : Elsevier), p. 405.

DAVIS, E. A., 1981, *J. Phys., Paris*, **42,** C4, Suppl. No. 10, 855.

EWEN, P., 1978, Ph.D. Thesis, Edinburgh University.

GRIGOROVICI, R., and VANCU, A., 1981, *J. Phys., Paris*, **42,** C4, Suppl. No. 10, 391.

HAMAKA, H., TANAKA, K., and IIZIMA, S., 1977, *Solid St. Commun.*, **23,** 63.

KENEMAN, S. A., BORDOGNA, J., and ZEMEL, J. N., 1978 a, *J. opt. Soc. Am.*, **68,** 32 ; 1978 b, *J. appl. Phys.*, **49,** 663.

KOSEK, F., CIMPL, Z., MATYAS, M., and PISARCIK, M., 1982, *Czech. J. Phys.* B, **32,** 719.

KRASNOV, V. F., and REMESNIK, V. G., 1980, *Avtometroya*, **6,** 101.

LANNIN, J. S., 1977, *Phys. Rev.* B, **15,** 3836.

LUCOVSKY, G., and KNIGHTS, J. S., 1974, *Phys. Rev.* B, **10,** 4324.

NEMANICH, R. J., CONNELL, A. N., HAYES, T. M., and STREET, R. A., 1978, *Phys. Rev.* B. **18,** 6900.

PORTER, E. J., and SHELDRICK, G. M., 1972, *J. chem. Soc., Dalton Trans.*, p. 1347.

SOLIN, S. A., and PAPATHEODOROU, G. N., 1977, *Phys. Rev.* B, **15,** 2084.

TANAKA, K., 1976, *Structure and Excitation of Amorphous Solids*, edited by G. Lucovsky and F. L. Galeener, A.I.P. Conf. Proc. No. 31 (New York : American Institute of Physics), p. 148 ; 1980. *Solid St. Commun.*, **34,** 201.

TANAKA, K., and KIKUCHI, M., 1972, *Solid St. Commun.*, **11,** 1311.

TANAKA, K. and OHTSUKA, Y., 1978, *Thin Solid Films*, **48,** 17.

PHILOSOPHICAL MAGAZINE B, 1985, VOL. 52, NO. 3, 347–362

Photo-induced structural and physico-chemical changes in amorphous chalcogenide semiconductors

By A. E. OWEN, A. P. FIRTH and P. J. S. EWEN

Department of Electrical Engineering, University of Edinburgh, Edinburgh EH9 3JL, Scotland

[*Received 21 January 1985 and accepted 4 March 1985*]

ABSTRACT

The various photo-induced phenomena that occur in chalcogenide glasses are classified and described, with particular emphasis on the photo-dissolution effect. The detailed mechanisms responsible for many of these processes are still unknown, although in the case of photo-darkening in annealed a-As_2S_3 films, Raman experiments indicate that a light-induced change in the bond distribution from that for a chemically-ordered network towards one characteristic of a random network may be the principal cause. New results on the photo-dissolution of silver into As–S films are presented which indicate that the actinic radiation initiating the effect is absorbed in the photo-doped layer, close to the interface with the undoped region of the chalcogenide film. The basic mechanism responsible for the effect, however, is still not known.

§ 1. INTRODUCTION

A wide variety of light-induced changes has been observed in amorphous chalcogenide semiconductors, ranging from relatively subtle effects involving minor atomic rearrangements and manifested mainly by shifts in the optical absorption edge (i.e. photo-darkening and photo-bleaching), to more substantial atomic and molecular reconfigurations which cause a variety of physical and chemical changes (e.g. photo-polymerization, photo-crystallization, photo-enhanced dissolution of metals etc.). These effects are of interest because of the information they yield on defects and metastable structural states in amorphous solids, and because they are mostly unique to the amorphous state. Reviews of photo-induced phenomena in amorphous chalcogenides have been presented by Tanaka (1981a,b) who concluded that the mechanisms responsible for these changes are not yet fully understood.

Photo-induced effects in chalcogenide glasses are of considerable technological importance, having applications in optical-imaging, hologram recording and optical mass memories (Shimizu, Kokado and Inoue 1975, Shirakawa, Shimizu, Kokado and Inoue 1975, Asahara and Izumitani 1975, Bordogna and Keneman 1977). Photo-sensitive chalcogenide systems also have potential as photo-resists for micro-lithography in the fabrication of integrated circuits (Tai, Ong and Vadimsky 1982), and as some of the effects can be stimulated by X-rays and electron beams, as well as by light, very high resolution can be achieved.

In this paper we describe and classify the various types of photo-induced effects which occur in amorphous chalcogenides, with particular emphasis on the As–S system, and present some new results on the photo-dissolution of metals.

§2. Classification of photo-induced effects

At least seven distinct photo-induced structural or physico-chemical changes have been observed in amorphous chalcogenides, when samples in a suitable form are exposed to light or other irradiation, viz. photo-crystallization, photo-polymerization, photo-decomposition (in compounds), photo-induced morphological changes, photo-vaporization, photo-dissolution (of certain metals); and light-induced changes in local atomic configuration. In general these changes are accompanied by changes in the optical constants of the material and particularly shifts in the absorption edge, i.e. photo-darkening or photo-bleaching. Other characteristics of the material, such as the elastic constants, may also be affected (Tanaka, Kawakami and Odajima 1981). These photo-induced phenomena may be classified according to whether they are primarily structural or physico-chemical in nature and whether they are reversible or irreversible, in the sense that the system may partly revert to its initial state after some annealing treatment at a temperature higher than that at which illumination took place, or will recover completely on annealing at the glass transition temperature, T_g.

The reversible effects are generally observed most readily in well-annealed vapour-deposited films, or in melt-quenched glasses, which are also comparatively well annealed as a natural consequence of their method of preparation. By contrast, those irreversible changes which are primarily structural are found mainly in poorly-annealed vapour-deposited films, while the irreversible physico-chemical phenomena occur whatever the state of annealing of the amorphous sample. The inter-relationships between the reversible or irreversible, and structural or physico-chemical effects are illustrated schematically in fig. 1.

§3. Reversible photo-induced effects

3.1. *Photo-induced changes in local atomic structure*

Photo-induced reversible changes in local atomic structure are subtle effects which are induced by light of photon energy close to that of the optical band-gap, E_g, of the chalcogenide glass. They are manifested mainly by small red-shifts in the optical absorption edge (photo-darkening) which are accompanied by small changes in the radial distribution function, determined by diffraction experiments, or in vibrational spectra and also, normally, by barely discernible changes in volume (contraction or expansion). Amorphous As_2S_3 is the best known example of a chalcogenide glass in which these structural changes are suggested to occur (Tanaka 1981a,b) but it is important to note that photo-darkening does not occur in crystalline As_2S_3, indicating that this particular photo-induced effect is unique to the amorphous state (Tanaka 1981a,b). It has been proposed that reversible photo-induced changes in local atomic structure also occur in the related material a-As_2Se_3, a-GeS_2, amorphous Ge-Se compounds (particularly a-$GeSe_2$) and in a-As_4Se_5Ge (Tanaka 1980). Since photo-darkening is sensitive to pressure (Tanaka 1984, Tsutsu, Tamura and Endo 1984) van der Waals bonding may have a role in the process (Tanaka 1983).

These effects are reversible in that annealing restores the initial structure and properties, and in some cases the initial state can also be recovered by exposure to light whose photon energy is less than that used to photo-darken the sample (Hamanaka, Tanaka, Tsuji and Minomura 1981). A photo-induced blue-shift in the absorption edge is termed 'photo-bleaching'.

It has been suggested that the structural change induced by light consists of minor bond rearrangements involving the chalcogen atoms relaxing between the minima of

Fig. 1

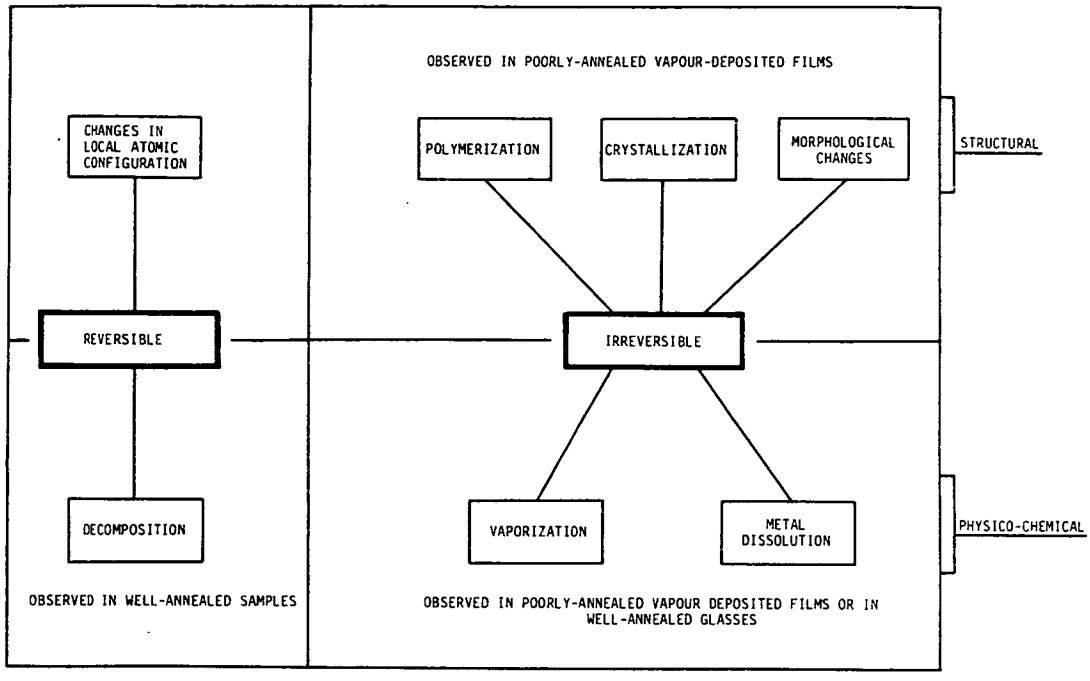

Classification of photo-induced structural and physico-chemical phenomena in amorphous chalcogenide semiconductors.

double-well potentials (Tanaka 1980, Averianov, Kolobov, Kolomiets and Lyubin 1980). Figure 2 shows a schematic model of conjectured bistable local bonding geometries in a-As_2S_3 and the associated double-well potential: illumination induces a transition from arrangement A to arrangement A', possibly as a result of the strong electron–phonon coupling involved in the recombination of a photo-excited valence electron (Murayama, Suzuki and Ninomiya 1980). The details of the mechanism, particularly the actual structural change that occurs, are not known.

If such photo-induced changes in atomic structure do not occur in *crystalline* chalcogenides then in the context of possible mechanisms it is significant to note that basically the same model of atomic relaxation between the minima of double-well potentials is generally accepted to be the explanation for the anomalously high low-temperature specific heat and for the extremely broad dielectric relaxation spectra which are also regarded as unique characteristics of amorphous solids (Mott and Davis 1979).

Another type of photo-induced change in local atomic structure which may also occur in chalcogenides is that produced by the 'self-trapped exciton' (Biegelsen and Street 1980). This involves the breaking of bonds—for example, in the case of a-As_2Se_3, an optically excited electron–hole pair would cause an As–Se bond to break and a Se–Se bond to form, resulting in a pair of metastable defects Se_3^+ and As_2^-, possibly accompanied by deformation of the local structure. Further work is necessary to confirm the existence of these photo-induced changes.

A third type of local structural change has been proposed to account for the appearance of optical anisotropy in certain chalcogenides when illuminated with plane-polarized light (Zhdanov and Malinovskii 1977, Hajto and Ewen 1979, Zhdanov, Kolomiets, Lyubin and Malinovskii 1979, Hajto, Janossy and Forgacs 1982,

Fig. 2

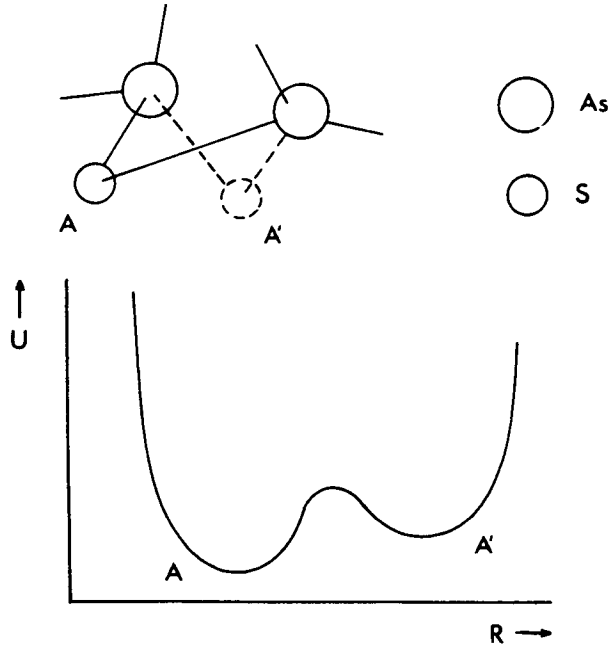

A schematic model of bistable local bonding geometries in a-As_2S_3 and the corresponding double-well potential. *A* and *A'* represent atomic configurations before and after illumination. *R* is some configurational coordinate and *U* the potential.

Grigorovici, Vancu and Ghita 1983). This phenomenon, which has been termed the 'vectorial effect', is believed to involve the re-orientation of small anisotropic structural units already present in the amorphous material. The principal axes of these units are initially randomly oriented but under illumination with plane-polarized light the units are forced to re-orient themselves in such a way that the axes become aligned with some preferred direction defined by the plane of polarization. In the case of $GeSe_2$, it has been suggested that the anisotropic units are the 'outrigger rafts' identified by Phillips (1981). The induced anisotropy can be erased by unpolarized or circularly polarized light (Hajto *et al.* 1982).

3.2. *Photo-decomposition*

As the name implies, photo-decomposition is the light-induced dissociation of a compound into its constituents. It has been studied most frequently in amorphous As–S and As–Se compositions and illumination of photon energy greater than E_g is necessary (Berkes, Ing and Hillegas 1971, Asahara and Izumitani 1975, Hamanaka, Tanaka, Matsuda and Iizima 1976, Keneman, Bordogna and Zemel 1978, Tanaka 1981a,b). Absorption of a photon of energy greater than E_g causes a dissociation of the arsenic–chalcogen bond, and this is followed by thermal diffusion of the arsenic to form arsenic clusters, which are highly absorbing. Photo-decomposition causes small but detectable changes in X-ray diffraction and vibrational spectra, but is manifested mainly by a red-shift in the optical absorption edge, i.e. photo-darkening. Provided the energy and intensity of illumination are not too great the photo-decomposition is reversible on annealing at T_g. Clearly, the proportion of dissociated bonds must be small.

Small clusters of arsenic atoms can, in fact, be formed without significant diffusion of the arsenic: a local bond reorganisation such as that illustrated for a-As_2S_3 in fig. 3

Fig. 3

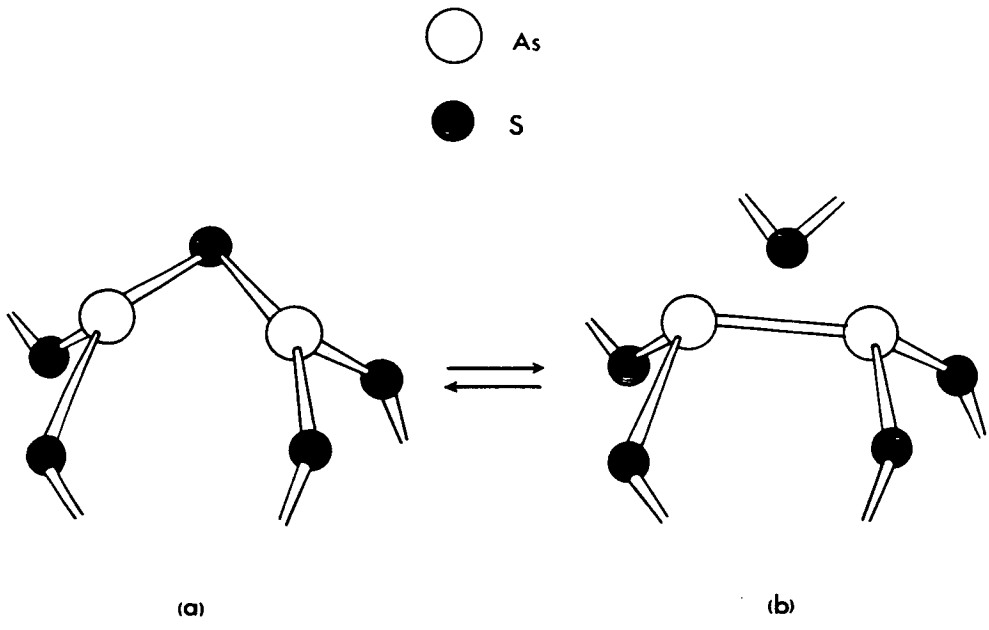

A schematic model of local bond reorganisations in a-As_2S_3 leading to the formation of an As–As bond. The transition between the initial structure (*a*) and the reorganised structure (*b*) is reversible.

will give rise to As_2 units (i.e. As–As bonds) and several such reorganisations occurring in the same locality will produce clusters of three or four arsenic atoms. In well-annealed films or bulk samples of a-As_2S_3 heteropolar As–S bonds are favoured, although a small percentage (about 1%) of homopolar As–As and S–S bonds may be present (Ewen and Owen 1980). It is possible that above-band-gap illumination alters the bond statistics from a distribution close to that for the chemically-ordered-network model towards one characteristic of a random-network model, that is the randomness of the bond distribution is increased.

Isolated As–As bonds are energetically unfavourable and when produced by the process illustrated in fig. 3 will soon revert to the initial state (fig. 3 (*a*)). Larger clusters, in contrast, are expected to be relatively stable and hence can give rise to the photo-darkening. At T_g, however, the atoms are more mobile, and annealing at this temperature causes even larger clusters to 'dissolve', so that the effect is reversible. Exposure to below-band-gap illumination also reverses the photo-darkening.

Direct evidence for the formation of As–As bonds in well-annealed a-As_2S_3 after exposure to above-band-gap light has been obtained in Raman studies (Frumar, Firth and Owen 1984). Spectra (*a*) and (*b*) of fig. 4 were recorded from an annealed a-As_2S_3 film under identical conditions before and after exposure to 488 nm (2·54 eV) light from an Ar-ion laser (E_g for a-As_2S_3 is about 2·4 eV). The increase after exposure in the relative intensity of the band at 231 cm^{-1}, which from earlier studies (Ewen, Sik and Owen 1977) is known to arise from As–As bonds, suggests an increase in the concentration of these bonds. Spectrum (*c*) was obtained after annealing the film a second time and its similarity to the original spectrum, (*a*), is evidence of the reversibility of the effect. Spectrum (*d*) was recorded after the sample was illuminated again with 488 nm light and is similar to the spectrum after the initial exposure, (*b*).

Fig. 4

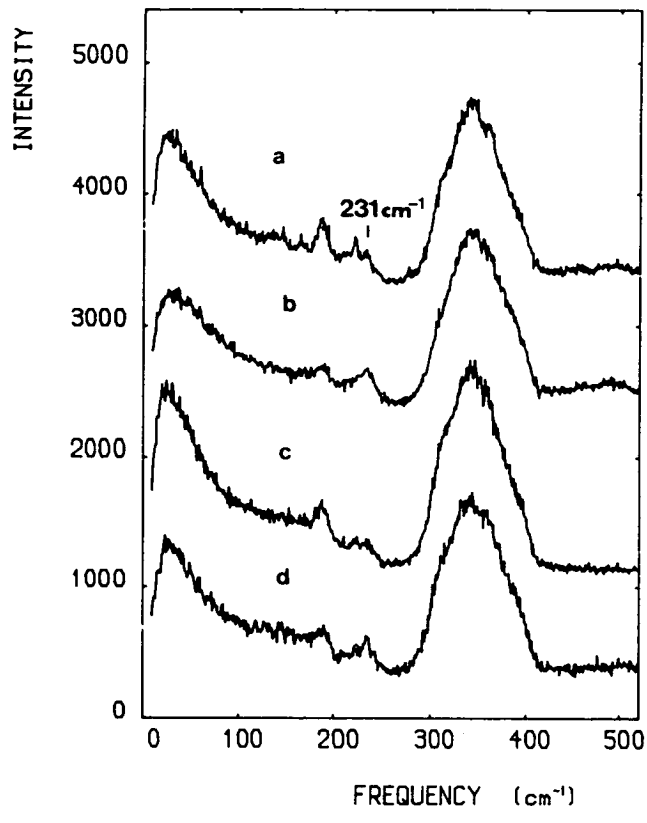

Raman spectra of an annealed evaporated film of a-As_2S_3. (*a*) The first annealed state, (*b*) the photo-darkened state, (*c*) the second annealed state and (*d*) the second photo-darkened state. All spectra were recorded using 647·1 nm excitation and are normalized to the height of the 340 cm^{-1} band. Photo-darkening was produced by Ar-ion laser illumination. (Frumar *et al.* 1984).

Cycling between the annealed and photo-darkened states can be carried out many times with reproducible results.

The increase in film thickness that accompanies this photo-darkening in a-As_2S_3 is accounted for by the increase in the average bond length resulting from the replacement of As–S bonds by the longer As–As bonds. Measurements of the fractional change in film thickness can thus be used to estimate the percentage of As–S bonds converted to As–As bonds under illumination, and a value of 6% has been derived by Frumar *et al.* (1984).

It is interesting to note that if isolated As–As bonds *were* stable, the two structures depicted in fig. 3 could be described as bistable bonding arrangements, by analogy with the two bistable bonding geometries shown in fig. 2. It is thus possible that *stable* homopolar bond formation in chalcogenides is one origin of metastable states.

§4. Irreversible photo-induced effects

4.1. *Photo-crystallization*

The photo-crystallization of amorphous solids is well-known and was first observed over a decade ago in a-Se (Dresner and Stringfellow 1968, de Neufville 1974). Photo-induced crystallization and 're-amorphization' has been studied in thin films of

As–Te–Ge compositions, using Kr–ion and dye lasers (von Gutfeld and Chaudhari 1972, Weiser, Gambino and Reinhold 1973). Thus, in a sense the process is reversible, but 're-amorphization' requires that the temperature of the film first be raised to the *melting point* of the crystals, and this can be achieved with a laser pulse. Strictly, therefore, this is an irreversible process.

4.2. *Photo-polymerization*

When chalcogenide compounds are deposited as thin films by evaporation the as-deposited material often contains some of the molecular species of which the vapour is composed, for example As_4S_4 molecules have been identified in As_2S_3 vapour (Solin and Papatheodorou 1977) and in as-deposited a-As_2S_3 films (Nemanich, Connell, Hayes and Street 1978). In the case of a-As_2S_3 these molecular species are embedded in an amorphous As–S network and illumination causes them to polymerize and combine with the network (Treacy, Strom, Klein, Taylor and Martin 1980). Polymerization causes densification and in general, on prolonged exposure, the density and structure of the thin film becomes virtually identical with that of melt-quenched glasses and well-annealed films (Chang and Hou 1978, Chang and Chen 1978, Kolwicz and Chang 1980).

Photo-polymerization has been proposed as an explanation of *reversible* photo-darkening in well-annealed amorphous As–Se films (Grigorovici and Vancu 1981). For such a model to be applicable molecular species must exist in the film prior to exposure and annealing must cause de-polymerization. It is not clear how photo-polymerization can result in the film expansion that often accompanies reversible photo-darkening.

Photo-polymerization of As_4S_4 molecules has been reported in crystals α- and β-As_4S_4 (Porter and Sheldrick 1972) so that this particular photo-induced effect is not unique to the amorphous state.

4.3. *Photo-induced morphological changes*

'Photo-induced morphological changes' is a term we propose should be used to denote effects usually described in the literature as 'photo-volumetric changes' or 'photo-contraction', since the phenomenon has its origin in changes in the macroscopic structure of chalcogenide thin-films, that is in their morphology. Changes in morphology have been observed mainly in thin films of Ge–Se compositions which, during vapour-phase deposition, grow on the supporting substrate in a columnar structure (Singh, Rajagopolan, Bhat, Pandya and Chopra 1979, 1980; Singh, Rajagopolan and Chopra 1980). On illumination, particularly with u.v. light, the films contract in volume. The magnitude of the change depends to some extent on composition but mainly on the angle of incidence at which the vapour-deposited film is grown. Contractions in volume of up to 12% can occur. The effect is thought to be due to a collapse of the columnar morphology of the films, precipitated by a photo-electronic excitation of the electronic defect states which are characteristic of amorphous chalcogenides (Singh, Rajagopolan and Chopra 1980).

4.4. *Photo-dissolution of metals*

The usual sample configuration used in observing the photo-dissolution/photo-doping effect consists of a 0·1–1 μm thick amorphous chalcogenide film on (or beneath) which has been deposited a thin metallic layer, typically 0·01–0·05 μm in thickness. Illumination from either the chalcogenide or metallic side with light above *or below* E_g for the chalcogenide causes the metal to dissolve rapidly into the amorphous film and

migrate through it. A review of photo-dissolution studies has been presented by Janai (1982).

Most of the reported work on photo-dissolution has been concerned with a-As_2S_3 and glasses in the Ge–Se system, particularly those close to the compositions $GeSe_3$ and $GeSe_2$. It is probable, however, that the effect occurs in most amorphous chalcogenides, whether in the form of poorly-annealed vapour-deposited films of well-annealed melt-quenched glasses. Silver and copper are used most frequently as the dissolving metal, but gold is also effective and it is likely that other metals such as indium and thallium would be susceptible to photo-dissolution. The metallic source is not necessarily a vacuum-evaporated film of an elemental metal but can be a suitable compound deposited as a thin coating by some other technique. In the case of silver, for example, silver halides, silver nitrate, silver selenide and potassium silver selenide have been used successfully. It is often sufficient simply to dip the chalcogenide into a solution of a silver compound to produce the coating. Photo-dissolution also occurs in chalcogenides deposited on bulk substrates, for example Ag_2S (Ewen, Taylor, Firth and Owen 1983).

High concentrations of metal may be driven considerable depths by the dissolution process. In a-As_2S_3, for example, silver concentrations of 10–40 at.% are reached at depths of 20 μm or more on exposure for about one minute to u.v. light of intensity 10–100 mW cm^{-2} (Inoue, Kokado and Shimizu 1974, Kokado, Shimizu and Inoue 1976). A very important characteristic of photo-dissolution is that for vertical illumination the metal migrates vertically with negligible lateral movement in most cases. Also, in the case of silver dissolution it is generally reported that the concentration profile for the dissolved atoms is step-like, which implies that the phenomenon is not a straightforward diffusive process (Inoue *et al.* 1974, Yamamoto and Itoh 1976, Goldschmidt, Bernstein and Rudman 1977).

The metal photo-dissolution effect is currently under intensive study in several laboratories because of its potential technological importance as the basis of a high-resolution (well below 1 μm) photo-resist in the micro-lithography of integrated circuits. Recent work on the photo-enhanced dissolution of silver in the amorphous As–S system is described in more detail in § 5.

4.5. *Photo-vaporization*

Photo-vaporization has been studied mainly in amorphous As_2S_3 thin-films. It is strictly a photo-oxidation reaction followed by thermal evaporation of the volatile oxidation products (Janai and Rudman 1974, Janai 1981a).

§ 5. The photo-dissolution of silver in As-S glasses

One of the main questions concerning the photo-dissolution process is how the dissolved metal atoms (or ions) are incorporated into the chalcogenide, and in particular what, if any, new compounds are formed in the film? In the case of silver photo-dissolution into a-As_2S_3, Ag_2S has been assumed to form (Malinowski and Buroff 1978) but is not generally observed in structural studies except in films which are heavily doped with silver (Inoue *et al.* 1974). X-ray diffraction measurements indicate that the *thermal* dissolution of silver in a-As_2S_3 at 200°C for silver concentrations below 20 at.% yield As_4S_4, $AgAsS_2$ and Ag_3AsS_3 crystallites, but photo-dissolution to produce a silver concentration of up to 20 at.% does not yield any new compounds (Janai 1982). Which compounds might form depends on the composition of the

Fig. 5

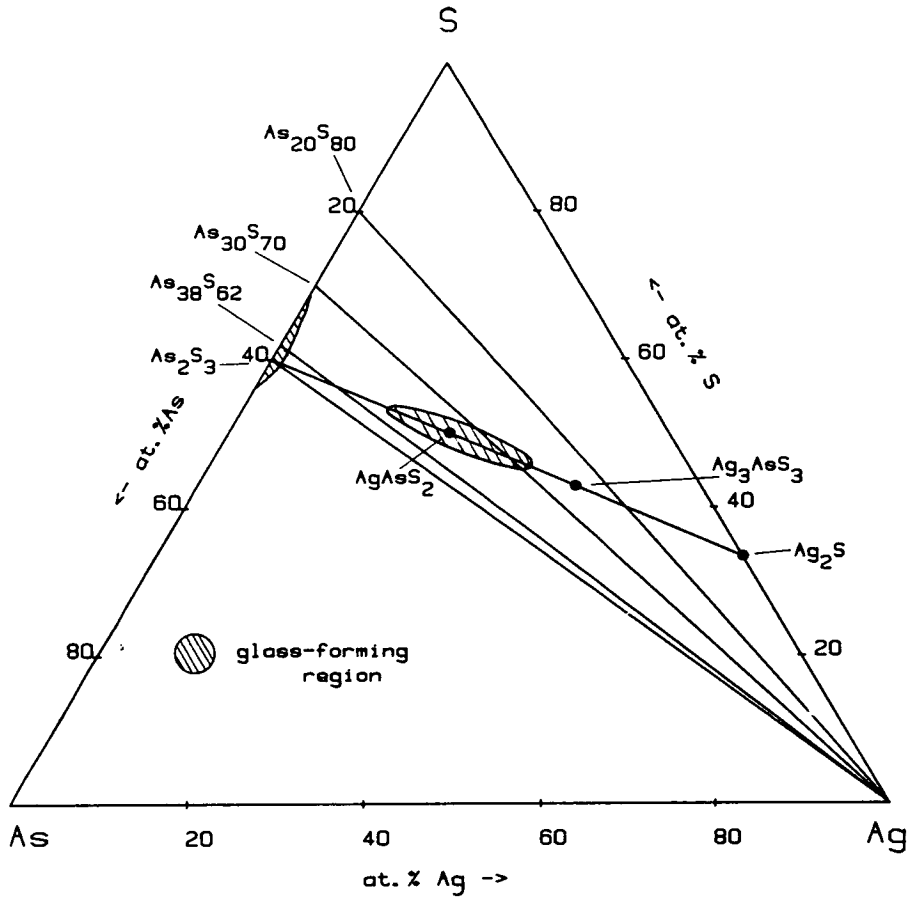

Phase diagram of the Ag–As–S system showing the principal ternary compounds and the glass-forming regions (cross-hatched areas). The tie-lines are discussed in the text. (Firth, Ewen and Owen 1983).

chalcogenide film, and also on the composition of the source layer. The principal compounds of the As–S–Ag system together with the glass-forming regions are shown in the phase diagram of fig. 5 (Kawamoto, Agata and Tsuchihashi 1974, Blachnik and Wickel 1980). Also drawn are five tie-lines: four linking the compositions As_2S_3, $As_{38}S_{62}$, $As_{30}S_{70}$ and $As_{20}S_{80}$ with silver and one between As_2S_3 and Ag_2S, which can also be used as a source of photo-dissolved silver. When a pure silver source is used with one of the four As–S compositions, the resulting *overall* composition during photo-dissolution must move along the appropriate tie-line terminating at the silver vertex. None of these four tie-lines passes through any of the known ternary compounds and only the tie-line for $As_{30}S_{70}$ passes through the central glass-forming region. Thus of the four As–S compositions only $As_{30}S_{70}$ can yield a *homogeneous* photo-doped film, the others must give rise to phase-separated structures. Raman results suggest that photo-doped as-evaporated films of As_2S_3, $As_{38}S_{62}$ and $As_{20}S_{80}$ are indeed phase separated whereas photo-doped $As_{30}S_{70}$ films have a structure similar to that of a bulk glass within the central region of glass formation and close to the Ag–$As_{30}S_{70}$ tie-line (Firth, Ewen and Owen 1983). The Raman spectra A and B of fig. 6 are for an evaporated $As_{30}S_{70}$ film before and after photo-doping respectively. Spectrum C is that

Fig. 6

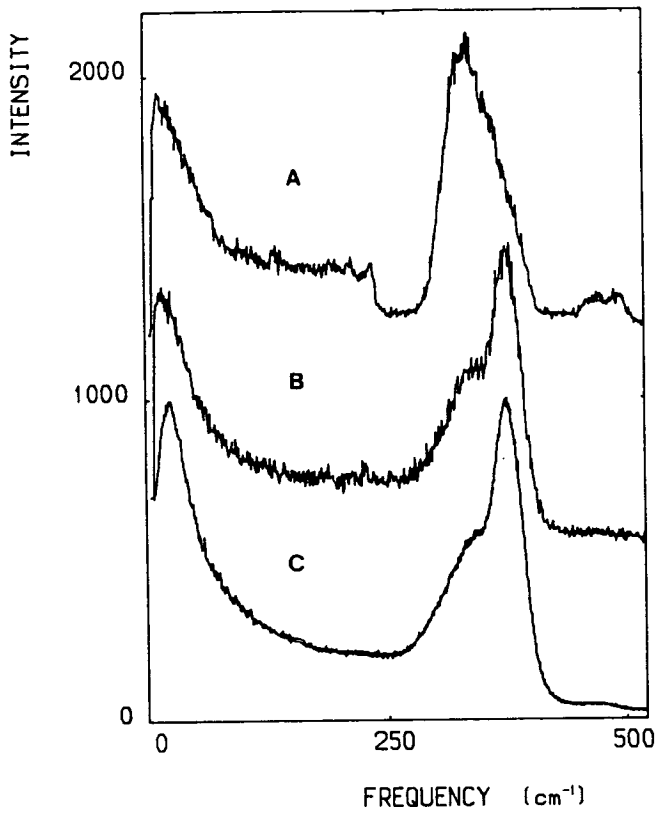

Raman spectra of films of composition $As_{30}S_{70}$. Spectrum A is prior to photo-doping with Ag and spectrum B that of the photo-doped film. Spectrum C is for a bulk glass of composition $Ag_{30}As_{22}S_{48}$. (Firth *et al.* 1983).

of a bulk glass of composition $Ag_{30}As_{22}S_{48}$ (Firth, Owen and Ewen 1981) and is clearly similar to the photo-doped spectrum B.

The tie-lines passing through the glass-forming region to silver correspond to compositions in the approximate range $As_{36}S_{64}$ to $As_{28}S_{72}$. Interestingly, it has recently been shown (Petrova, Simidchieva and Buroff 1984) that the amount of silver which can be taken up by an evaporated As–S film on dipping in $AgNO_3$ solution is at its lowest over this range of compositions, reaching a minimum at $As_{33}S_{67}$. This result might be due to the fact that additional silver can be incorporated at the boundaries between phase-separated regions, so that minimum silver uptake occurs for those As–S compositions yielding homogeneous films.

If a-As_2S_3 is photo-doped from an Ag_2S source then, assuming the Ag_2S participates as a whole in the process, the overall composition during photo-dissolution will again move along the tie-line between As_2S_3 and Ag_2S, which passes through the glass-forming region and the ternary compounds $AgAsS_2$ and Ag_3AsS_3. Raman experiments are consistent with this picture and show that Ag_3AsS_3 is the photo-dissolution product (Ewen *et al.* 1983). Figure 7 shows four spectra recorded at successive stages during the photo-doping of as-evaporated a-As_2S_3 on bulk Ag_2S substrates. Spectra A and B were recorded during the induction period which usually preceded photo-dissolution: changes in the sharp structure of spectrum B relative to that in spectrum A are associated with the irreversible structural changes which occur in the a-As_2S_3 film

Fig. 7

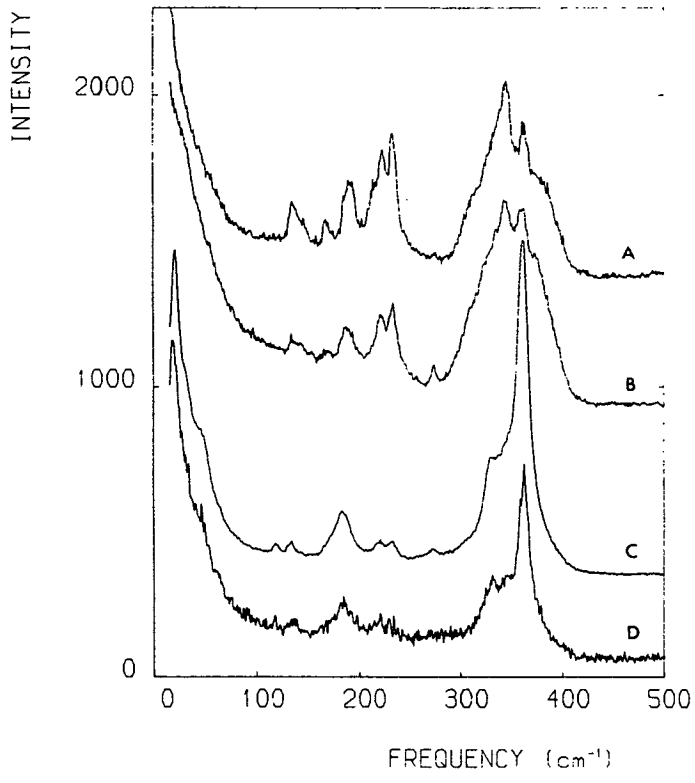

Raman spectra recorded at various stages A–D (described in text) during the photo-doping of as-evaporated a-As_2S_3 with silver from a bulk Ag_2S substrate. The spectra are normalized by maximum intensity. (Ewen *et al.* 1983).

itself under illumination. Spectrum C was recorded shortly after the onset of photo-dissolution and is characteristic of crystalline Ag_3AsS_3 (Ewen, Taylor and Paul 1983). Spectrum D was recorded after the film had been completely photo-doped and is similar to C but considerably weaker in intensity (note that the four spectra are normalized by maximum intensity). This reduction in intensity is probably due to the formation of a second, highly absorbing compound in the film, for example Ag_2S. The compound Ag_2S itself has an extremely weak Raman spectrum and is difficult to detect directly in Raman experiments.

Another important question concerning the photo-dissolution process is where is the actinic radiation, which initiates the process, absorbed? The spectral dependence of the photo-dissolution rate follows the absorptance profile of the chalcogenide (Janai 1982), which suggests that the basic optical excitation occurs in the amorphous film. However, photo-dissolution can still be stimulated effectively by below-band-gap illumination, which has led some investigators (Goldschmidt and Rudman 1976, Kokado, Shimizu, Tatsuno and Inoue 1976, Lavine, Lis, Goldberg and Masters 1982) to conclude that the actinic photons are absorbed in the metallic film or substrate. On the basis of a computer study of the absorptance of Ag/As_2S_3 multilayer structures in the vicinity of the Ag–As_2S_3 interface, Janai (1982) has suggested that the actinic radiation is absorbed in the layer of reaction products, that is in the photo-doped region between the silver and the undoped a-As_2S_3. Recent experiments in these laboratories confirm this suggestion and show, furthermore, that the actinic radiation is absorbed primarily near the interface between the doped and undoped regions.

Fig. 8

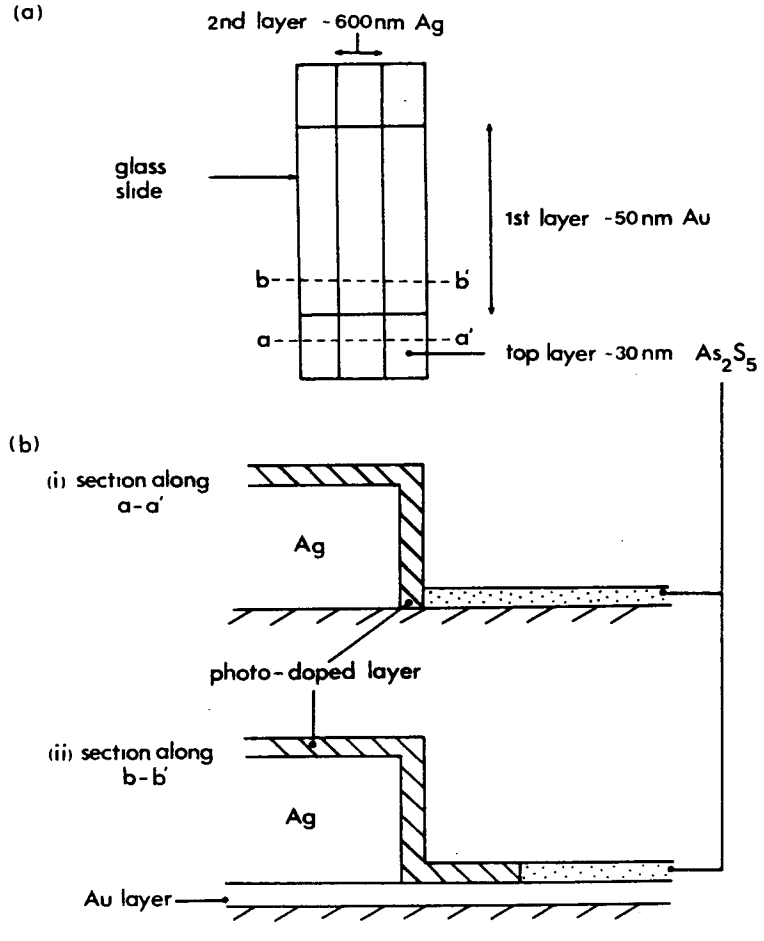

The sample geometry used in the lateral photo-dissolution experiments: (*a*) plan view, (*b*) cross-sections at indicated regions.

Figure 8 shows schematically the sample geometry used in these experiments, which were designed to investigate the lateral migration which can occur when photo-dissolution is carried out on a conducting substrate (Matsuda and Kikuchi 1973). A film of gold (which does not significantly photo-dissolve into amorphous arsenic sulphides (Fitzgerald 1982)) was first deposited on a section of the surface of a glass slide and then a silver band 5 mm wide and 600 nm thick was evaporated on top. Finally an As_2S_5 film 30 nm thick was evaporated over the whole surface. The large difference between the thicknesses of the silver strip and As–S film, which is apparent in the cross-section of fig. 8(*b*), is necessary to provide a reservoir of silver for lateral photo-dissolution over the surface of the substrate.

By focussing the light source through a microscope objective it was possible to illuminate small areas of the As–S film. When a region of the As–S film in contact with the silver was illuminated photo-dissolution occurred in the normal way and the thin As–S layer was quickly converted to the dark-red photo-doped state. Illumination of the As–S film above the gold had no effect. However, if a photo-doped region and a neighbouring undoped region above the gold were illuminated simultaneously then silver migrated into the undoped region. By tracking the illuminated spot across the film surface it was possible to draw out a photo-doped strip. Figure 9 shows a

Fig. 9

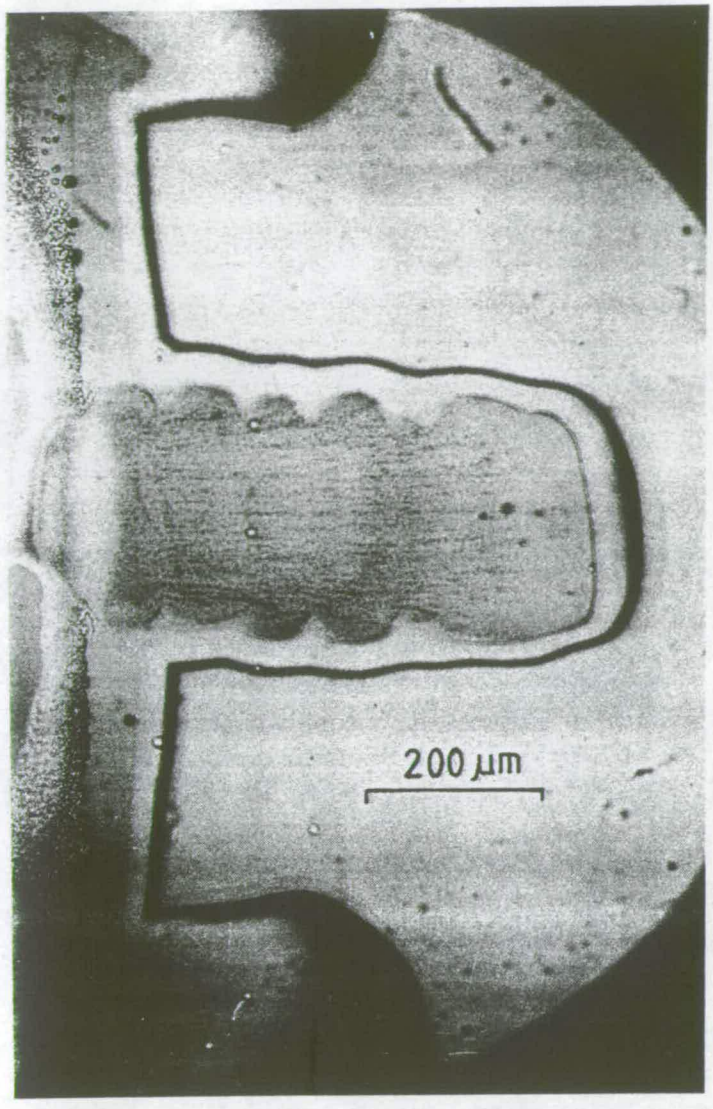

Photomicrograph of photo-doped strip drawn out in an As–S film above a gold layer. The silver source is on the left.

photomicrograph of such a strip. To produce the strip only a segment of the interface between the photo-doped and undoped regions had to be in the illuminated spot; it was not necessary to illuminate the photo-doped region between this interface and the silver band or the silver band itself. This indicates that the actinic radiation is being absorbed in the photo-doped region close to the interface with the undoped region.

The photo-doped strip could be drawn out indefinitely provided the source of silver was not consumed. Figure 10 shows, as a function of time, the distance advanced by the segment of the interface in the illuminated spot (i.e. the tip of the photo-doped strip) as the spot was tracked stepwise across the As–S film over the gold. The plot is linear, indicating a constant speed of dissolution, and its slope gives the rate of advance as approximately 1 μm min^{-1}.

These experiments also yield some insight into the role of electrons in the process. The fact that this lateral photo-dissolution occurred only over the conducting gold-

Fig. 10

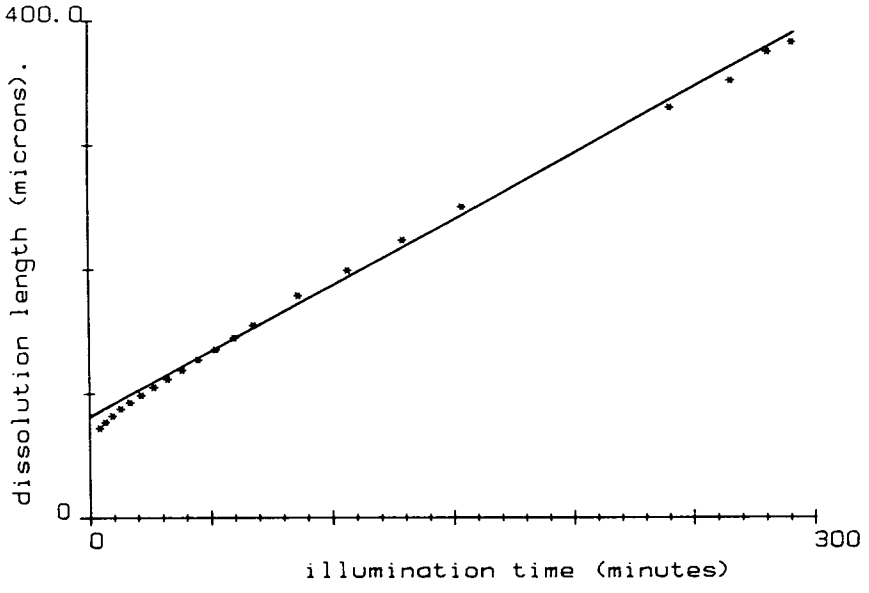

Distance travelled by the photo-dissolution front (dissolution length) against time. The straight line is a linear fit to the data points and has a gradient of about 1 μm min^{-1}.

coated part of the substrate suggests that a supply of electrons is necessary for photo-dissolution to proceed, which is expected from electro-chemical considerations (Stone 1955). Ordinarily, the electrons are supplied by the silver source and must diffuse through the reaction products to reach the interface, but for the situation of lateral photo-dissolution described above, electrons can be supplied by the gold and never have to diffuse further than the thickness of the As–S layer.

A final question concerning the photo-dissolution effect is whether it occurs in crystals. Although it has been stated in the past (Janai 1981b) that the phenomenon is unique to the amorphous state, it has recently been shown (Imura, Kubota, Hiraki and Tanaka 1983) that mineral samples of crystalline As_2S_3 can be photo-doped with silver, although the process is considerably slower than for amorphous As_2S_3. That the effect should occur in crystals is possibly not surprising, since photo-induced migration of silver is known to occur in crystalline Ag_3AsS_3 (Smolenskii, Sinii, Prokhorova, Kuz'minov and Godovikov 1982).

§6. Conclusions

Photo-induced phenomena in amorphous chalcogenide semiconductors have been classified according to whether they are primarily structural or physico-chemical in nature and whether they are reversible or irreversible. Seven effects have been described, with particular emphasis on the photo-dissolution effect and it is concluded that the detailed mechanisms responsible for many of these processes are still unknown. In particular direct evidence is required to establish the existence of some of the more subtle photo-induced structural changes. Raman experiments suggest that photo-darkening in a-As_2S_3 arises from a change in the bond distribution, from that for a chemically-ordered network towards one characteristic of a random network, but it is possible that other effects, such as switching between bistable bonding geometries, are occurring in parallel.

Another phenomenon that requires further investigation is the photo-dissolution effect. New results on the photo-dissolution of silver into As–S films have been presented aimed at resolving one of the main questions concerning this effect, namely where the absorption of the actinic radiation that initiates the process is taking place. These results, which are concerned with the lateral migration of silver atoms which occurs when photo-dissolution is carried out on a conducting substrate, indicate that the actinic radiation is absorbed in the photo-doped layer, close to the interface between the doped and undoped regions. However, the basic mechanism responsible for the photo-dissolution process is still not established.

References

ASAHARA, Y., and IZUMITANI, T., 1975, *Phys. Chem. Glasses*, **16**, 29.

AVERIANOV, V. L., KOLOBOV, A. V., KOLOMIETS, B. T., and LYUBIN, V. M., 1980, *Phys. Stat. Sol.* (a), **57**, 81.

BERKES, J. S., ING, S. W., and HILLEGAS, W. J., 1971, *J. appl. Phys.*, **42**, 4908.

BIEGELSEN, D. K., and STREET, R. A., 1980, *Phys. Rev. Lett.*, **44**, 803.

BLACHNIK, R., and WICKEL, V., 1980, *Z. Naturf.* b, **35**, 1268.

BORDOGNA, J., and KENEMAN, S. A., 1977, *Holographic Recording Media*, edited by H. M. Smith (Berlin: Springer-Verlag), p. 229.

CHANG, M. S., and CHEN, J. T., 1978, *Appl. Phys. Lett.*, **33**, 892.

CHANG, M. S., and HOU, T. W., 1978, *Thin Solid Films*, **55**, 463.

DE NEUFVILLE, J. P., 1974, *Amorphous and Liquid Semiconductors*, edited by J. Stuke and W. Brenig (London: Taylor and Francis), p. 1351.

DRESNER, J., and STRINGFELLOW, G. B., 1968, *J. Phys. Chem. Solids*, **29**, 303.

EWEN, P. J. S. and OWEN, A. E., 1980, *J. non-crystalline Solids*, **35–36**, 1191.

EWEN, P. J. S., SIK, M. J. and OWEN, A. E., 1977, *The Structure of Non-Crystalline Materials*, edited by P. H. Gaskell (London: Taylor and Francis), p. 231.

EWEN, P. J. S., TAYLOR, W. T., FIRTH, A. P., and OWEN, A. E., 1983, *Phil. Mag.* B, **48**, L15.

EWEN, P. J. S., TAYLOR, W. T., and PAUL, G. L., 1983, *J. Phys.* C, **16**, 6475.

FIRTH, A. P., EWEN, P. J. S., and OWEN, A. E., 1983, *The Structure of Non-Crystalline Materials, 1982*, edited by P. H. Gaskell, J. M. Parker and E. A. Davis (London: Taylor and Francis), p. 286.

FIRTH, A. P., OWEN, A. E., and EWEN, P. J. S., 1981, *J. Phys., Paris*, **42**, 903.

FITZGERALD, A. G., 1982, *Thin Solid Films*, **98**, 101.

FRUMAR, M., FIRTH, A. P., and OWEN, A. E., 1984, *Phil. Mag.* B, **50**, 463.

GOLDSCHMIDT, D., BERNSTEIN, T., and RUDMAN, P. S., 1977, *Phys. Stat. Sol.* (a), **41**, 283.

GOLDSCHMIDT, D., and RUDMAN, P. S., 1976, *J. non-crystalline Solids*, **22**, 229.

GRIGOROVICI, R., and VANCU, A., 1981, *J. Phys., Paris*, **42**, 391.

GRIGOROVICI, R., VANCU, A., and GHITA, L., 1983, *J. non-crystalline Solids*, **59–60**, 909.

HAJTO, J., and EWEN, P. J. S., 1979, *Phys. Stat. Sol.* (a), **54**, 385.

HAJTO, J., JANOSSY, I., and FORGACS, G., 1982, *J. Phys.* C, **15**, 6293.

HAMANAKA, H., TANAKA, K., MATSUDA, A., and IIZIMA, S., 1976, *Solid St. Commun.*, **19**, 499.

HAMANAKA, H., TANAKA, K., TSUJI, K., and MINOMURA, S., 1981, *J. Phys., Paris*, **42**, 399.

IMURA, T., KOBUTA, K., HIRAKI, A., and TANAKA, K., 1983, *J. phys. Soc. Japan*, **52**, 2459.

INOUE, E., KOKADO, H., and SHIMIZU, I., 1974, *Jap. J. appl. Phys.*, **43**, Suppl. p. 101.

JANAI, M., 1981a, *J. Phys., Paris*, **42**, 1105; 1981b, *Phys. Rev. Lett.*, **47**, 726; 1982, *Proc. Electrochem. Soc.*, **82–89**, 239.

JANAI, M., and RUDMAN, P. S., 1974, *Amorphous and Liquid Semiconductors*, edited by J. Stuke and W. Brenig (London: Taylor and Francis), p. 425.

KAWAMOTO, Y., AGATA, M., and TSUCHIHASHI, S., 1974, *J. Ceram. Assoc. Jpn*, **82**, 502.

KENEMAN, S. A., BORDOGNA, J., and ZEMEL, J. N., 1978, *J. appl. Phys.*, **49**, 4663.

KOKADO, H., SHIMIZU, I., and INOUE, E., 1976, *J. non-crystalline Solids*, **20**, 131.

KOKADO, H., SHIMIZU, I., TATSUNO, T., and INOUE, E., 1976, *J. non-crystalline Solids*, **21**, 225.

KOLWICZ, M. D., and CHANG, M. S., 1980, *J. electrochem. Soc.*, **127**, 135.

LAVINE, J. M., LIS, S. A., GOLDBERG, G. M., and MASTERS, J. I., 1982, *Proc. electrochem. Soc.*, **82–89**, 265.

MALINOWSKI, J., and BUROFF, A., 1978, *Contemp. Phys.*, **19**, 99.

MATSUDA, A., and KIKUCHI, M., 1973, *Jap. J. appl. Phys.*, **42**, Suppl. p. 239.

MOTT, N. F., and DAVIS, E. A., 1979, *Electronic Processes in Non-Crystalline Materials*, second edition (Oxford: Clarendon Press), Chap. 6.

MURAYAMA, K., SUZUKI, H., and NINOMIYA, T., 1980, *J. non-crystalline Solids*, **35–36**, 915.

NEMANICH, R. J., CONNELL, G. A. N., HAYES, T. M., and STREET, R. A., 1978, *Phys. Rev.* B, **18**, 6900.

PETROVA, S., SIMIDCHIEVA, P., and BUROFF, A., 1984, *Proceedings of the Conference 'Amorphous Semiconductors – 84'*, edited by E. Fahri-Vateva and A. Buroff (Sofia: Bulgarian Academy of Sciences), p. 256.

PHILLIPS, J. C., 1981, *J. non-crystalline Solids*, **43**, 37.

PORTER, E. J., and SHELDRICK, G. M., 1972, *J. Chem. Soc. Dalton*, p. 1347.

SHIMIZU, I., KOKADO, H., and INOUE, E., 1975, *Photogr. Sci. Engng*, **19**, 136.

SHIRAKAWA, T., SHIMIZU, I., KOKADO, H., and INOUE, E., 1975, *Photogr. Sci. Engng*, **19**, 139.

SINGH, B., RAJAGOPOLAN, S., BHAT, P. K., PANDYA, D. K., and CHOPRA, K. L., 1979, *Solid St. Commun.*, **29**, 167; 1980, *J. non-crystalline Solids*, **35–36**, 1053.

SINGH, B., RAJAGOPOLAN, S., and CHOPRA, K. L., 1980, *J. appl. Phys.*, **51**, 1768.

SMOLENSKII, G. A., SINII, I. G., PROKHOROVA, S. D., KUZ'MINOV, E. G., and GODOVIKOV, A. A., 1982, *Sov. Phys. Crystallogr.*, **27**, 82.

SOLIN, S. A., and PAPATHEODOROU, G. N., 1977, *Phys. Rev.* B, **15**, 2084.

STONE, F. S., 1955, *Chemistry of the Solid State*, edited by W. E. Garner (London: Butterworth Scientific Publications), Chap. 2.

TAI, K. L., ONG, E., and VADIMSKY, R. G., 1982, *Proc. Electrochem. Soc.*, **82–89**, 9.

TANAKA, K., 1980, *J. non-crystalline Solids*, **35–36**, 1023; 1981a, *Fundamental Physics of Amorphous Semiconductors*, edited by F. Yonezawa (Berlin: Springer-Verlag), p. 104; 1981b, *Amorphous Semiconductor Technologies and Devices 1982*, edited by Y. Hamakawa (Tokyo: Ohmsha), p. 227; 1983, *J. non-crystalline Solids*, **59–60**, 925; 1984, *Phys. Rev.* B, **30**, 4549.

TANAKA, K., KAWAKAMI, N., and ODAJIMA, A., 1981, *Jap. J. appl. Phys.*, **20**, L874.

TREACY, D. J., STROM, U., KLEIN, P. B., TAYLOR, P. C., and MARTIN, T. P., 1980, *J. non-crystalline Solids*, **35–36**, 1035.

TSUTSU, H., TAMURA, K., and ENDO, H., 1984, *Solid St. Commun.*, **52**, 877.

VON GUTFELD, R. J., and CHAUDHARI, P., 1972, *J. appl. Phys.*, **43**, 4688.

WEISER, K., GAMBINO, R. J., and REINHOLD, J. A., 1973, *Appl. Phys. Lett.*, **22**, 48.

YAMAMOTO, Y., and ITOH, T., 1976, *J. appl. Phys.*, **47**, 3603.

ZHDANOV, V. G., KOLOMIETS, B. T., LYUBIN, V. M., and MALINOVSKII, V. K., 1979, *Phys. Stat. Sol.* (a), **52**, 621.

ZHDANOV, V. G., and MALINOVSKII, V. K., 1977, *Sov. tech. Phys. Lett.*, **3**, 387.

Journal of Non-Crystalline Solids 107 (1989) 155–162
North-Holland, Amsterdam

PHOTODISSOLUTION OF SILVER IN ARSENIC SULPHIDE FILMS – AN EXAFS STUDY

A.T. STEEL [a]*, G.N. GREAVES [b], A.P. FIRTH [c] and A.E. OWEN [c]

[a] Chemistry Department, University of Manchester, Manchester M13 9PL, UK
[b] SERC Daresbury Laboratory, Daresbury, Warrington, Cheshire WA4 4AD, UK
[c] Department of Electrical Engineering, University of Edinburgh, King's Buildings, Edinburgh EH9 3JL, UK

Received 15 July 1988
Revised manuscript received 5 October 1988

Silver K-edge EXAFS measurements have shown that the photodissolved silver site in arsenic sulphide films is very similar to that in the bulk ternary glasses of the general composition $Ag_x(As_2S_3)_{(1-x)}$. Neither the films nor the glasses show a marked resemblance to any of the simple crystalline sulphides. In particular silver is 3-fold coordinated to sulphur without any pronounced Ag–Ag or Ag–As correlations. In those cases where a surfeit of silver has been added the EXAFS of the photodoped films exhibit a second neighbour peak which is interpreted as an incomplete dissolution of silver.

1. Introduction

The photodoping of silver (and copper) into chalcogenide glasses is of interest in sub-micron lithographic applications because photodissolution is almost perfectly normal to the surface with very little lateral diffusion [1,2].

Raman spectroscopy of photodoped films based on arsenic sulphide compositions $As_xS_{(1-x)}$ ($x = 20$, 30, 40) has indicated that when $x = 30$ the structure is very similar to the bulk glass and the photodoped material is a homogeneous, uniform phase [3]. The arsenic–sulphur–silver phase diagram is shown in fig. 1 with a tie line joining silver to $As_{30}S_{70}$ which intersects the central glass-forming region. A phase-separated glassy material containing amorphous arsenic and an amorphous Ag–As–S phase has been proposed [3,4] in the $x = 40$ composition. Formation of a silver sulphide phase is proposed in the $x = 20$ composition.

Early X-ray diffraction work on silver photodissolution in As_2S_3 films indicated no obvious change in the average structure [13]. It was concluded that silver did not bond with the glass matrix but penetrated into spaces within the glass structure. The glass was assumed to comprise As_4S_6 molecules following an earlier model of de Neufville et al. [15], in contrast to the layered structure of crystalline As_2S_3 (orpiment).

We have made EXAFS measurements at the silver K-edge, in view of the uncertainty in the

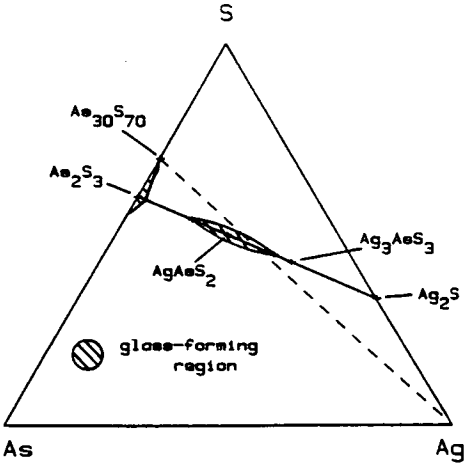

Fig. 1. Phase diagram of the Ag–As–S system showing the glass-forming region (shaded) after Kawamoto [14].

* Current address: Unilever Research, Port Sunlight Lab., Quarry Rd. East, Bebington, Wirral, Merseyside, L63 3JW, UK.

environment of photodissolved silver in arsenic sulphide films. We have been able to determine the environment of photodoped silver in the films and the presence of metallic silver in overdoped specimens. Results from photodoped films are compared with bulk ternary glasses and crystalline model systems.

2. Sample preparation

Films were prepared by evaporating a layer of Ag and then a layer of the desired As–S composition on mylar (10 μm thick), with no break in the vacuum (2×10^{-5} bar) between evaporations. The As–S evaporation sources were powdered melt quenched glasses of either As_2S_3 or As_2S_4. Electron microprobe analysis indicated that the stated film compositions are correct to ± 0.5 at.%. The thickness of the Ag layer was kept constant at 1000 Å and the As–S film thickness was varied between 4000–6000 Å to produce different Ag/As film thickness ratios. The various film thicknesses were measured in situ using a quartz crystal thickness monitor.

A 200 W Hg lamp with the spectral range 350–550 nm, with an IR filter, was used to photodissolve the Ag into the As–S film. The exposure time chosen was sufficient to photodissolve the Ag into the whole volume of the As–S film. Under these circumstances, which are the basis of the lithographic application, the sample cannot be etched with dilute alkaline solution. The overall and relative thickness of the metal and arsenic sulphide layers was important. The photodoped films were completely clear with the above prescription; however, if only 4000 Å of arsenic sulphide was used with 1000 Å of silver the reacted film showed a slight milkiness, indicative of inhomogeneity. A similar effect was observed when attempts were made to photodope greater than one micron of silver into approximately 4.5 microns of arsenic sulphide.

Ag containing glasses were prepared by reacting the elemental components in a vacuum sealed quartz tube, which was heated to 900 °C in a furnace, agitated for 2 days and then rapidly cooled by plunging into iced water. A structural study of these glasses using Raman spectroscopy has previously been reported [4]. The mineral smithite, $AgAsS_2$, is a rare crystal and was prepared according to the method outlined by Holmqvist and Pask [19]. Confirmation that the material produced was smithite was obtained from Raman spectroscopy by comparing the spectrum obtained with that given in the literature [20]. The minerals acanthite, Ag_2S, and proustite, Ag_3AsS_3, were 5N pure and obtained from BDH Co.

3. EXAFS – results and analysis

EXAFS spectra at the silver K-edge (25.521 keV) were recorded on the wiggler EXAFS station, 9.2, at the SERC's Synchrotron Radiation Source (SRS) Daresbury Laboratory. The SRS ran at an energy of 2.0 GeV and an average current of 200 mA. The data were collected at room temperature in the transmission mode. Films were self-supporting on mylar and approximately eighty thicknesses were required to achieve an absorbance of ~ 2. Samples of the bulk glasses and the crystalline "model" compounds were finely ground and supported on adhesive tape. Absorption data was background-subtracted, to obtain the step-height normalised function, $\chi(k)$, using standard techniques [5].

Fitting procedures were performed in reciprocal space with $\chi(k)$ weighted by k^3, where k is the photoelectron wave vector, on raw (i.e. unfiltered) data. The EXAFS analysis code EXCURVE was used, which is based on the curved-wave theory [6] and requires calculated photoelectron scattering factors (in this case for silver, arsenic and sulphur). Initial values for these phase-shifts were taken from the Daresbury EXAFS databank [7]. EXAFS data from silver foil was fitted to the first four interatomic radii. Slight differences from crystallographic values [8] were corrected by refinement of the silver phase-shifts. Excellent agreement was achieved, as can be seen from fig. 2. Proustite, Ag_3AsS_3, is a useful model compound for checking the sulphur phase-shifts, in that the two principal coordinated sulphur atoms occupy a single well-defined subshell at 2.44 Å. The remaining sulphur atoms occur at 2.89

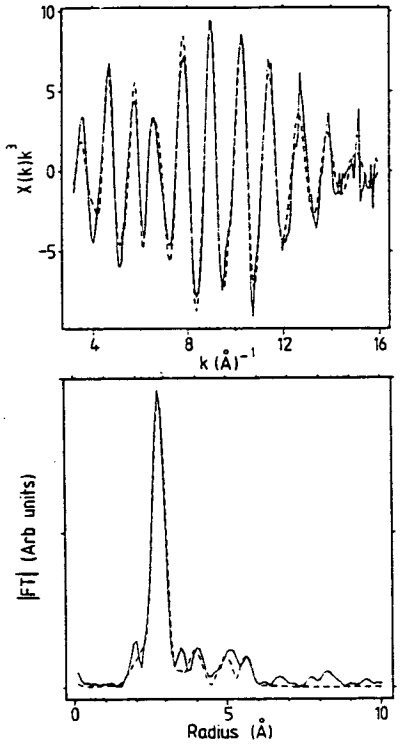

Fig. 2. k^3-weighted EXAFS and Fourier-transform for silver metal (solid line experimental; dotted line theoretical fit).

Å and 3.18 Å [9]. Accordingly the EXAFS data was fitted with a three-component sulphur shell using the refined silver central atom phase-shifts. Final values agreed well with the crystallographically determined distances; thus no refinement of the databank sulphur phase-shifts was required.

Two additional model systems smithite, $AgAsS_2$, and acanthite, Ag_2S, were investigated. These are more strongly disordered than proustite and served as further tests of the silver and sulphur phase-shifts and as comparisons for the films and bulk glasses. Smithite was modelled for analysis using several sulphur subshells, replicating the large spread of interatomic distances [10]. There is good agreement between the pair distribution functions derived from k^3 EXAFS analysis and from X-ray diffraction. Fig. 8 shows Gaussian-broadened histograms for the model compounds investigated, obtained from the interatomic radii, as derived from the EXAFS fits or from crystallographic values. The Debye-Waller term was used as the Gaussian broadening factor and the weighting of each shell or subshell was equal to the coordination number. Like smithite, acanthite has a wide spread of silver-sulphur distances and has a distinct second shell contribution [11], clearly visible in its Fourier-transform (fig. 3). The second shell contribution arises from backscattering from non-bonded silver atoms located between 3.0 and 3.2 Å. Multi-shell refinement clearly gives a good fit to the data (fig. 3) and to the crystallographic pair-distribution function (PDF) (fig. 8).

A number of Ag–As–S glasses of composition $Ag_x(As_2S_3)_{(1-x)}$ has been examined. The EXAFS spectra are all practically identical as is apparent upon inspection of the raw data in fig. 4a. All spectra are dominated by one major shell at approximately 2.50 Å with no evidence for

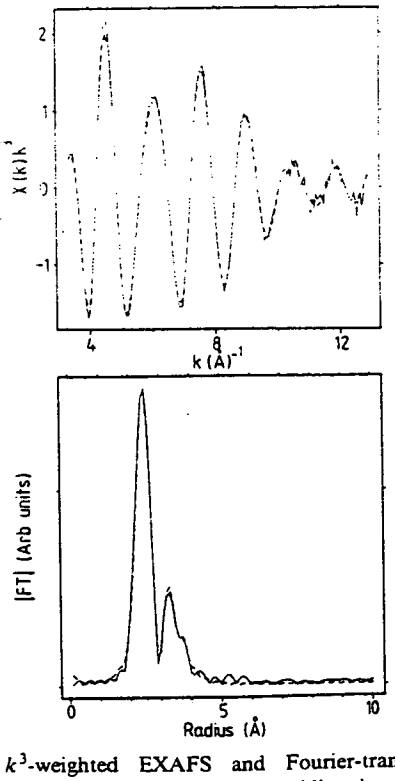

Fig. 3. k^3-weighted EXAFS and Fourier-transform for acanthite (solid line experimental; dotted line theoretical fit).

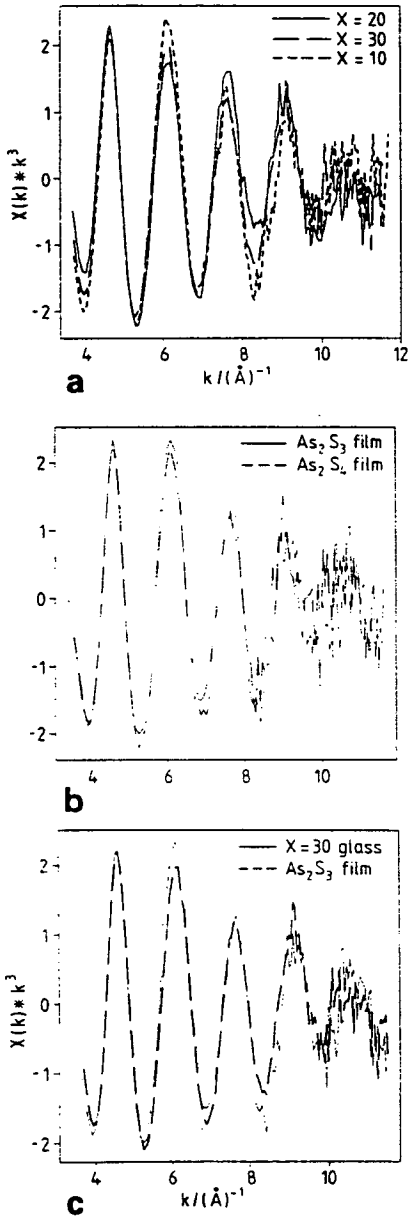

Fig. 4. Comparisons of k^3-weighted EXAFS for Ag–As–S glasses and photo-diffused films. (a) $Ag_x(As_2S_3)_{(1-x)}$ glasses with $x = 30, 20, 10$; (b) films prepared from As_2S_3 and As_4S_4 bulk arsenic sulphide composition; (c) comparison of film 1, prepared from As_2S_3, and bulk ternary glass with $x = 30$.

silver–silver or silver–arsenic correlations. Fig. 5 shows the k^3 weighted EXAFS and Fourier transform together with the corresponding fit for $Ag_{20}(As_2S_3)_{80}$ glass. Clearly silver is well coordinated by sulphur atoms in these bulk glasses. The same subshell fitting procedure was employed for the glasses, in view of the disorder present in the first shell of crystalline sulphides. Separate radii coalesced on refinement thus indicating no measurable static disorder in the silver–sulphur distances. Direct coordination of silver to arsenic in addition to silver–sulphur bonds, whilst not being a feature of the crystalline compounds, may, in principle, be possible in glassy systems. Attempts to place arsenic in the first coordination shell at approximately 2.7 Å (sum of covalent radii of silver and arsenic) resulted in a much worse fit and an unrealistically high Debye–Waller factor.

Arsenic K-edge EXAFS spectra, recorded for several of the glasses, showed no signs of a second shell and displayed only a single shell comprising three sulphur atoms. The absence of any well-de-

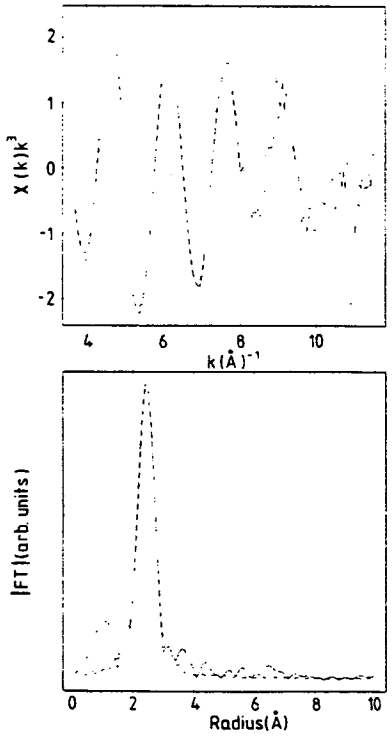

Fig. 5. k^3-weighted EXAFS and Fourier-transform for $Ag_{20}(As_2S_3)_{80}$ glass (solid line experimental; dotted line theoretical fit for single three sulphur atom shell).

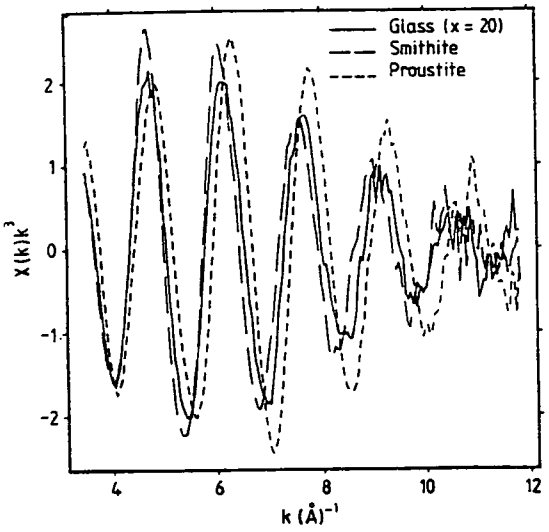

Fig. 6. Comparison of experimental k^3-weighted EXAFS for proustite, smithite and a ternary glass ($x = 20$).

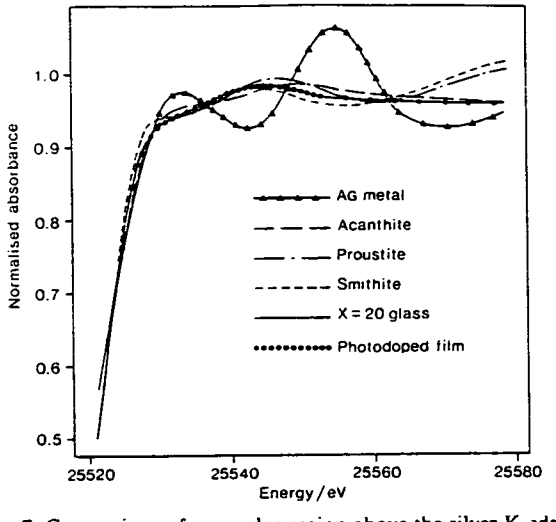

Fig. 7. Comparison of near-edge region above the silver K-edge for the model compounds, glasses and films.

fined cation–cation correlations from both Ag and As EXAFS points to considerable bond angle distortion at sulphur sites in these glasses. The As–As correlations are comparatively weak [17], even in As_2S_3 glass. The addition of silver would appear to add slightly more bond angle disorder.

The undistorted silver–sulphur environment observed in these glasses is not like that of proustite, principally because of a higher first shell radius and the lack of any longer silver–sulphur distances as can be observed by a comparison of their EXAFS (fig. 6). Differences between the glasses and smithite can also be observed in the EXAFS although these are more subtle. A comparison of the PDFs derived from the values obtained in detailed fitting of the EXAFS shows marked differences in the coordination environment (fig. 8). The glass has a far more symmetrical arrangement of coordinating sulphur atoms and the average bond length is shorter. The principle silver–sulphur distance (R_{max}) in acanthite is close to that in the glass (table 1), but the long-range environment is different from that of the glass which does not exhibit a second (silver) shell. The overall silver–sulphur environment in acanthite is much broader than in the glasses (table 1).

The EXAFS of a range of films prepared from various bulk arsenic sulphide compositions were measured. They are compared in fig. 4b. The EXAFS of the films are almost identical and show a symmetrical silver–sulphur environment. Moreover they are also very similar to the annealed glasses with a coordination number of three, at a mean radius of 2.50 Å and $2\sigma^2$ of 0.025 Å^2. A glass and a film are directly compared in fig. 4c. Fig. 4 demonstrates the striking resemblance of the silver environment in the melt-quenched glasses and the photodiffused films. For films and glasses there is no close resemblance to the crystalline model compounds. Silver dissolves in amorphous arsenic sulphide under the action of band gap

Table 1

Parameters derived from PDFs (fig. 6).

Compound	R_{mean} (Å)	R_{max} (Å)	FWHM (Å)	Coord. number
acanthite	2.77	2.51	0.95	3.5
smithite	2.64	2.60	0.55	4
proustite	2.74	2.48	1.11	4
silver	2.89	2.89	0.24	12
glass	2.50	2.50	0.26	3
film	2.50	2.50	0.26	3

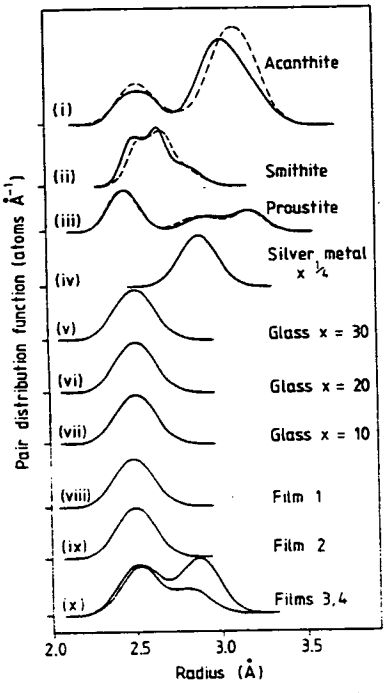

Fig. 8. Ag–S and Ag–Ag pair distribution function for the various model compounds, glasses and films (solid lines relate to EXAFS-derived values and the dotted lines relate to crystallographically-derived values). (i) acanthite, (ii) proustite, (iii) smithite, (iv) silver metal $x = 1/4$, $Ag_x(As_2S_3)_{(100-x)}$ bulk glasses, (v) $x = 30$, (vi) $x = 20$, (vii) $x = 10$, (viii) film 1, prepared from As_2S_4 bulk glass, (ix) film 2, prepared from As_2S_3 bulk glass, (x) film 3 (higher second shell amplitude) inhomogeneous thick film, film 4, inhomogeneous thin milky film.

light and adopts a silver–sulphur environment similar to that in bulk Ag–As–S glasses. Further confirmation of this can be found by comparing the near-edge regions (fig. 7). The differences between the glass and film are small but both differ significantly from those of the crystalline model systems. The EXAFS measurements demonstrate conclusively that photodissolved silver bonds to sulphur in a well-defined fashion.

Films photodoped from too great a reservoir of silver metal showed signs of devitrification. For instance attempts to photodope a one-micron film of silver into a thick arsenic sulphide layer (4.5 microns) resulted in the Fourier transform of the silver K-edge EXAFS displaying a second peak at around 2.8 Å. This peak can be readily seen in fig. 8 and in fig. 9, which shows the EXAFS and corresponding Fourier-transform, together with the overlaid fit. Inhomogeneities in the photodoped films have been observed in SEM studies where surface features as large as 2 microns have been detected. The second shell is almost certainly due to silver backscattering as it occurs at a distance which corresponds to the Ag–Ag contact in silver metal (fig. 8). The amplitude of this shell gives a coordination number of 3 (with the same Debye-Waller factor as that found for the first shell in silver metal). Given that the coordination number of f.c.c. silver is 12 this result would indicate that after photodoping approximately one-quarter of the silver has remained undissolved as silver metal. The first shell of this thick film which is due to silver–sulphur correlations has a slightly higher radius that that found in the clear

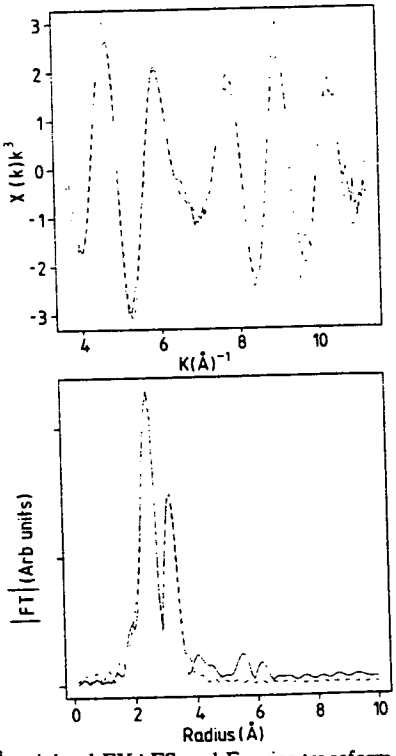

Fig. 9. k^3-weighted EXAFS and Fourier transform for the bad film prepared from very thick layers of silver and arsenic sulphide. The dotted line represents the theoretical fit to three coordinating sulphur atoms and three silver atoms at approx. 2.8 Å.

films and glasses, which may indicate precipitation of a crystalline ternary phase. The thin milky film prepared from 4000 Å of arsenic sulphide and 1000 Å of silver also exhibited a second shell (fig. 8) of lower amplitude, suggesting only 10% undissolved silver. The sulphur shell for this film is much more like those of the clear films in that it has the same radius and Debye–Waller factor. In both cases where surplus silver metal has been used EXAFS is clearly a useful diagnostic tool for detailing (micro) phase separation. A similar approach was useful in identifying devitrification of small quantities of iron included in arsenic sulphide glass [12].

4. Conclusions

The present work demonstrates that the silver–sulphur environment in As–S films photodoped with Ag is very similar to that of the bulk As–Ag–S glasses. The structure of the films and glasses does not resemble any of the crystalline model compounds thus suggesting homogeneous dissolution of silver. There is no evidence that silver occupies non-bonded sites in the glass matrix as proposed earlier by Salik and Nadiv [13]. Silver–arsenic atom contacts have not been detected from the silver EXAFS which gives clues as to the likely diffusion routes in the glass structure. Unlike the molecular model of the Neufville et al. [15], the arsenic sulphide glass is envisaged as a continuous, random network based on AsS_3 pyramidal units. The glass structure in the short range can be pictured as layer-like with layers being connected via arsenic and sulphur lone pair orbitals in back-bonding configurations, following Leadbetter and Apling [16]. It is reasonable to envisage silver diffusing between layers, bonding to the more electronegative sulphur atoms and forming AgS_3 units.

The occurrence of As_4S_4 units – the molecular species in the vapour phase – is possible in the films and in the arsenic-rich glasses. EXAFS work at the arsenic K-edge on photostructural and annealing changes in As_2S_3 films and glasses indicated the possibility of some As_4S_4-like groups [17,18]. The action of light or heat causes some re-ordering in the medium range and there is evidence from the arsenic environment that such As_4S_4 units polymerize into layer-like units, which make up the rest of the structure. The occurrence of photoexpansion is also consistent with changes in the short and medium range order. If these structural modifications take place in the presence of silver, diffusion is likely to be aided by an "opening-up" of the interlayer routes.

Excess photodoping of Ag results in silver precipitation. The present work has shown that devitrification can be readily identified in the silver EXAFS by the presence of a second near-neighbour shell of atoms at 2.8–3.0 Å.

The Director and Staff of the SERC's Daresbury Laboratory are thanked for provision of synchrotron radiation and computing facilities.

References

[1] M. Janai, 9th Int. Conf. on Amorphous and Liquid Semconductors, Grenoble, France, July 1981.
[2] T. Shirakawa, I. Shimizu, H. Kokado and E. Inoue, Phot. Sci. Eng. 19 (2) (1975) 139.
[3] A.P. Firth, P.S. Ewen and A.E. Owen, in: Structure of Non-Crystalline Materials, P.H. Gaskell, ed. (Taylor and Francis, London, 1982).
[4] A.P. Firth, A.E. Owen and P.S. Ewen, J. Phys. (Paris), Coll., C4 42 (1981) 903.
[5] See, e.g., data reduction described in: S.K. Harbron, S.J. Higgins, W. Levason, M.C. Feiters and A.T. Steel, Inorg. Chem. 25 (1986) 1789.
[6] S.J. Gurman, I. Ross and N. Binsted, J. Phys. C 17 (1984) 143;
P.A. Lee and J.B. Pendry, Phys. Rev. B 1 (1975) 2975.
[7] E. Pantos and D. Firth, EXAFS and Near Edge Structure, Proc. Int. Conf., Frascati, Italy, Sept. 13–17, 1982, A. Bianconi, L. Inoccia and S. Stipchich, eds. (Springer, Berlin, 1983).
[8] M.E. Straumanis and S.M. Riad, Trans. Met. Soc. AIME 233 (1965) 964.
[9] P. Engel and W. Nowacki, Neues Jb. Miner. Mh. 6 (1966) 181.
[10] E. Hellner and H. Burzlaff, Naturwissenschaft 51 (1964) 35.
[11] R. Sadanaga and S. Sueno, Miner. J. 5 (2) (1967) 124.
[12] G.N. Greaves, X.L. Xiang, S.R. Elliott and T. Fowler, in: Physics of Disordered Materials, D. Adler, H. Fritzsche and S.R. Ovshinsky, eds. (Plenum, New York, 1985), p. 189.
[13] J. Salik and S. Nadiv, Phys. Stat. Sol. (a) 38 (1976) 177.

[14] Y. Kawamoto, M. Agata and S. Tsuchihashi, J. Ceram., Assoc. Japan, 82 (1974) 502.
[15] J.P. de Neufville, S.C. Moss and S.R. Ovshinsky, J. Non-Cryst. Solids 13 (1873) 91.
[16] A.J. Leadbetter and A.J. Apling, J. Non-Cryst. Solids 15 (1974) 250.
[17] A.J. Lowe, S.R. Elliott and G.N. Greaves, Phil. Mag. B 54 (1986) 483.
[18] R.J. Nemanich, G.A.N. Connell, T.M. Hayes and R.A. Street, Phys. Rev. B 18 (1978) 6900.
[19] G.A. Holmqvist and J.A. Pask, J. Amer. Ceram. Soc. 62 (1979) 183.
[20] V.Yu. Silvka, Yu.M. Vysochanskii, V.A. Stefanovich, V.S. Gerasimenko and D.V. Chepur, Sov. Phys. Solid State 24 (3) (1982) 392.

Exploratory observations of random telegraphic signals and noise in homogeneous hydrogenated amorphous silicon

W. K. Choi and A. E. Owen
Department of Electrical Engineering, University of Edinburgh, Edinburgh EH9 3JL, Scotland

P. G. LeComber and M. J. Rose
Department of Applied Physics and Electronic & Manufacturing Engineering, University of Dundee, Dundee DD1 4HN, Scotland

(Received 4 December 1989; accepted for publication 27 February 1990)

Noise measurements on unhydrogenated and hydrogenated rf sputtered intrinsic amorphous silicon reported by D'Amico, Fortunato, and Van Vliet [Solid-State Electron. 28, 837 (1985)] have $1/f$ and Lorentzian spectra, respectively. Similar noise measurements on glow-discharge deposited hydrogenated amorphous intrinsic silicon reported by Bathaei and Anderson [Philos. Mag. B 55, 87 (1987)] gave a $1/f^m$ spectrum with $0.7 < m < 1$. Even more recently Ley and Arce [Proc. MRS Symposium, San Diego (1989)] have reported random telegraph signals in a-Si:H/a-Si$_{1-x}$N$_x$:H double barrier structures. The associated noise was a Lorentzian noise spectrum. In this paper the first observation of random telegraph signals in notionally homogeneous heavily doped (p^+) glow-discharged-deposited amorphous silicon is reported. It was found that the current passing through the sample fluctuates between two easily identifiable levels with the periods of fluctuations separated by a quiescent period. The occurrence of these fluctuations is unpredictable but the current noise spectrum obtained during quiescent periods is Lorentzian, probably indicative of a generation-recombination process. Noise measurements are not possible at higher biases ($> 10^5$ V/cm) as the current fluctuates chaotically and this is also the prebreakdown regime of the sample.

I. INTRODUCTION

There are two previous reports on electrical noise in notionally homogeneous amorphous silicon thin films.[1,2] D'Amico and co-workers[1] studied rf sputtered unhydrogenated intrinsic amorphous silicon (a-Si) and obtained a $1/f$ noise spectrum which they attributed to mobility fluctuations involving phonon-assisted hopping. They also presented data on rf sputtered hydrogenated intrinsic amorphous silicon (a-Si:H) and in this case a Lorentzian spectrum was obtained. D'Amico and co-workers[1] suggested that this could be due to discrete traps, below the Fermi level, temporarily immobilizing carriers that participate in conduction. Bathaei and Anderson[2] studied intrinsic glow-discharge deposited a-Si:H. The intrinsic layer (i) was sandwiched between two heavily n-doped layers (i.e., a n^+-i-n^+ structure). The noise had a $1/f^m$ dependence with $0.7 < m < 1.1$, the exact value of m depending on temperature. The occurrence of the $1/f^m$ dependence in this case was explained in terms of a model involving fluctuations in carrier density.

Related to noise is the phenomenon of random telegraph (RTS) which has recently been observed in a number of small area devices ($1-100 \times 10^{-6}$ mm^2) such as tunnel diodes,[3-6] and metal-oxide-semiconductor field effect transistors.[7-10] RTS are usually attributed to statistical fluctuations in the capture and emission (trapping and detrapping) processes in devices having only a small number of electrons—hence the need for devices of small area. Very recently, Arce and Ley[11,12] reported observation of RTS in a-Si:H/a-Si$_{1-x}$N$_x$:H double barrier structures. The area of their devices was 0.25 mm^2, i.e., three to five orders of magnitude larger than the area of the devices in which RTS were previously observed.[4,5,10] In order to explain this Arce and Ley assumed that the current passing through their structures was confined to microchannels of cross-sectional area $< 1 \times 10^{-6}$ mm^2. Such microchannels were not observed experimentally, however, and to support their assumption Arce and Ley refer to a report by the present authors of filament formation in a-Si:H memory devices.[13] The RTS were then explained by the random charging and discharging of individual traps in the vicinity of the current channels and the noise power spectra were fitted by a superposition of several Lorentzians.

In this paper we report some preliminary noise measurements and, notably, the first observations of RTS in notionally homogeneous a-Si:H sandwich structures with contact areas $\sim 10^{-4}$ mm^2.

II. EXPERIMENT

Heavily p-doped (p^+) amorphous silicon was prepared by the rf glow-discharge decomposition of SiH_4 containing 10^4 vppm of B_2H_6. Samples were fabricated in a sandwich structure with chromium forming the top and bottom contact, i.e., a Cr-p^+-Cr structure, and with an active contact area of $\sim 10^{-4}$ mm^2. The p^+ a-Si:H thickness was of the order of several thousand angstroms. A typical current versus voltage (I-V) characteristic for these samples is shown in Fig. 1. It can be seen that the characteristic is symmetrical with an ohmic region at low bias ($0.01 < V < 0.1$ V) followed by a nonohmic region ($V > 0.1$ V).

The samples were loaded into a cryostat (Oxford Instrument D10200) with a temperature controller that set the ambient temperature. A battery power supply was used to

 0021-8979/90/130120-04$03.00

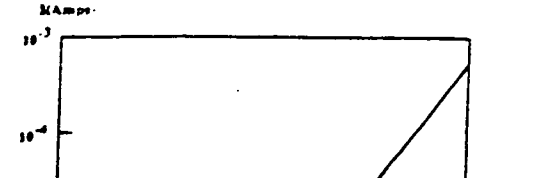

FIG. 1. Typical current vs voltage (I-V) characteristic for a-Si:H Cr-p^+-Cr sample (ASi645) with p^+ layer 1200 Å and contact area $\sim 10^{-4}$ mm^2. Note both positive and negative characteristics are identical.

provide a constant voltage for the experiment. A series resistor of approximately one half the sample resistance was used to detect the fluctuations in sample current. The signal was then amplified and fed to a Hewlett-Packard spectrum analyzer (HP3538A). The noise produced by the measurement system was determined by replacing the sample with a simple resistance (at $V = 0.2$ V) of equivalent value. This background noise was found to be less than 0.1% of the noise generated by the sample in the frequency range investigated here.

III. RESULTS

Figure 2 shows the room-temperature result of a series of noise measurements on sample ASi645 taken over a period of 10–25 h; each point represents the average of five individual observations each of which requires 2–5 min. Apart from a general trend towards a decrease ($\sim 1/f$) in $S_I(f)$ with increasing frequency there was no discernable pattern; it was also noticed that during the experiment there were occasional bursts of excessive noise. To eliminate the possibility that this "disturbance" originated from other sources some current versus time (I-t) measurements were carried out. Figures 3(a) and 3(b) show the I-t charts for the same sample at $V = 0.2$ V, with $T = 300$ and 373 K, respectively; at $T = 373$ K the fluctuations are much more pronounced than at $T = 300$ K. At $T = 373$ K, the current fluctuates between two levels for the first 4–5 h, (i.e., region I) and then settles down to a constant value (region II). It should be noted, however, that the behavior typical of region I can reoccur at any time after a period of quiescence, as shown schematically in Fig. 3(b), but its occurrence is unpredictable. Figure 3(c) depicts in more detail the I-t graph at $T = 373$ K in region I obtained on another specimen from the same deposition run. The current jumps between two identifiable states, i.e., a more conducting (A) state and a less conducting (B) state with $\Delta I/I$ varying from 1 to 10%. The current fluctuates more pronouncedly in the A state than in B state. With higher bias, the I-t characteristics exhibit a much more complex pattern of fluctuations, as depicted in Figs. 4(a) and 4(b) for $T = 300$ and 373 K, respectively. It is not possible to easily identify distinct levels of current with the complex pattern of fluctuations illustrated in Fig. 4. This chaotic pattern of fluctuations in current is often observed at higher bias ($> 10^5$ V/cm) and it also leads to eventual breakdown of the samples. This behavior is similar to that reported by Farmer, and co-workers[4] and Neri, and co-workers[10] in thin silicon dioxide films.

Bearing in mind these observations, the results shown in Fig. 2 were reexamined and points corresponding to quiescent periods [i.e., region II in Fig. 3(b), or the base level B in Fig. 3(c)] were selected and the rest disregarded. The result

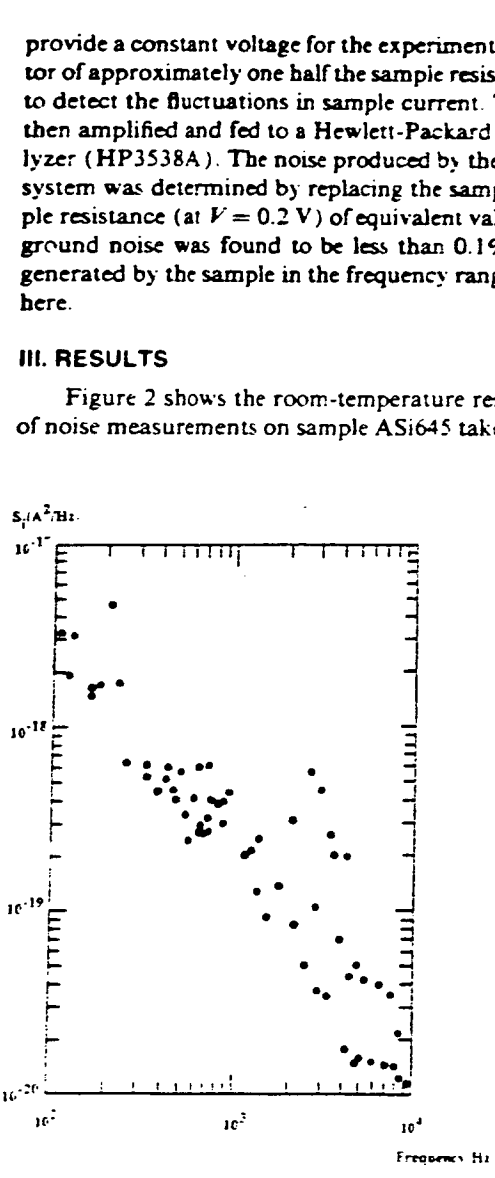

FIG. 2. The noise current spectral density $S_I(f)$ vs frequency for ASi645 at $V = 0.2$ V and $T = 300$ K.

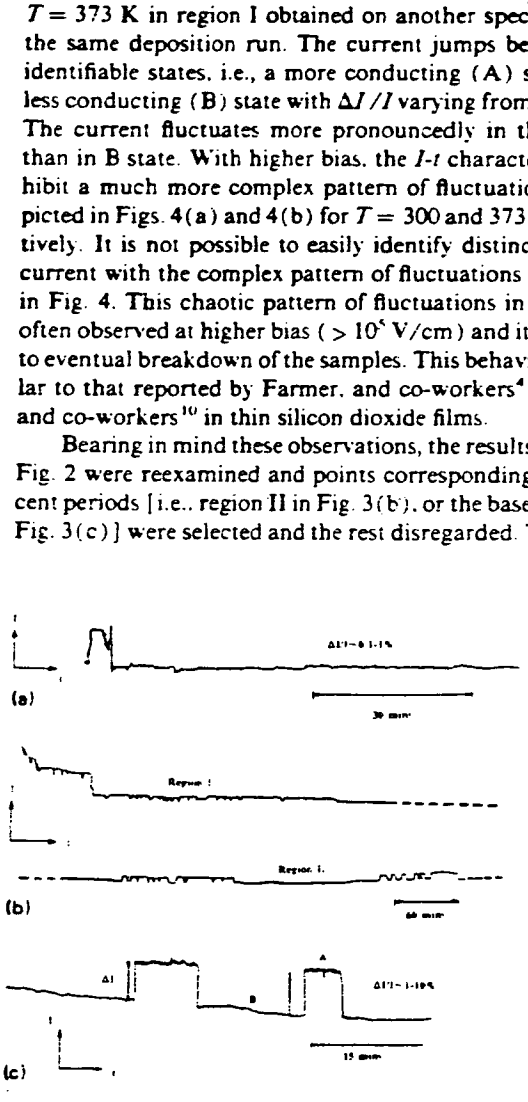

FIG. 3. The current vs time (I-t) characteristics for ASi645 with $V = 0.2$ V at (a) $T = 300$ K and (b) $T = 373$ K. Figure 3(c) shows in more detail the I-t characteristic of another ASi645 sample at $T = 373$ K.

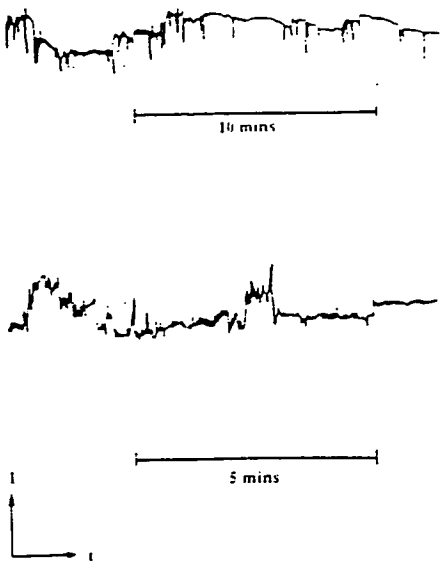

FIG. 4. The current vs time (I-t) characteristics for ASi645 with higher bias ($V = 1.5$ V) at (a) $T = 300$ K and (b) $T = 373$ K.

is shown in Fig. 5(a) in which it can be seen there is a plateau in $S_I(f)$ in the frequency range $f \sim 200$–1000 Hz. In Fig. 5(b) there are three noise spectra obtained from three more Cr-p^--Cr samples, also taken during quiescent period, and they all show the plateau in the same frequency range.

IV. DISCUSSION

We believe that this is the first observation of RTS in homogeneous amorphous silicon. The results agree in certain respects with those reported by Arce and Ley[11,12] in heterogeneous a-Si:H/a-$Si_{1-x}N_x$:H junctions. Arce and Ley found three plateaus located at approximately $f = 10^{-1}$–5 Hz, $f = 10$–800 Hz, and $f = 800$–10^4 Hz. In the present case we observed only one plateau with $f = 200$–1000 Hz but the frequency range is more limited than that used by Arce and Ley.

In the I-t graph (Fig. 3) only two levels of current are observed at reasonable biases, rather than the multilevels reported by Arce and Ley. The multilevel RTS, as shown in Fig. 4, is observed only at higher voltage. A single Lorentzian spectrum is obtained when the current is quiescent, in contrast ot Arce and Ley's results where three plateaux were identified with RTS present. An important point to note is that the current level in the noise measurements of D'Amico and co-workers[1] and the present authors is $> 10^{-6}$ A, whereas Arce and Ley carried out their experiments at currents less than 10^{-9} A. It is interesting to note that D'Amico and co-workers reported a recombination-generation noise ($f = 10$–600 Hz) in their intrinsic a-Si:H samples with no mention of RTS.

The devices used in the RTS studies in metal-oxide-semiconductor tunnel diodes[3,4] and field effect. capacitors[10] usualy have very small active areas (1–100×10^{-6} mm^2) and thin oxide layers (~ 50 Å). As already noted, the contact area in Arce and Ley's devices was much larger (0.25

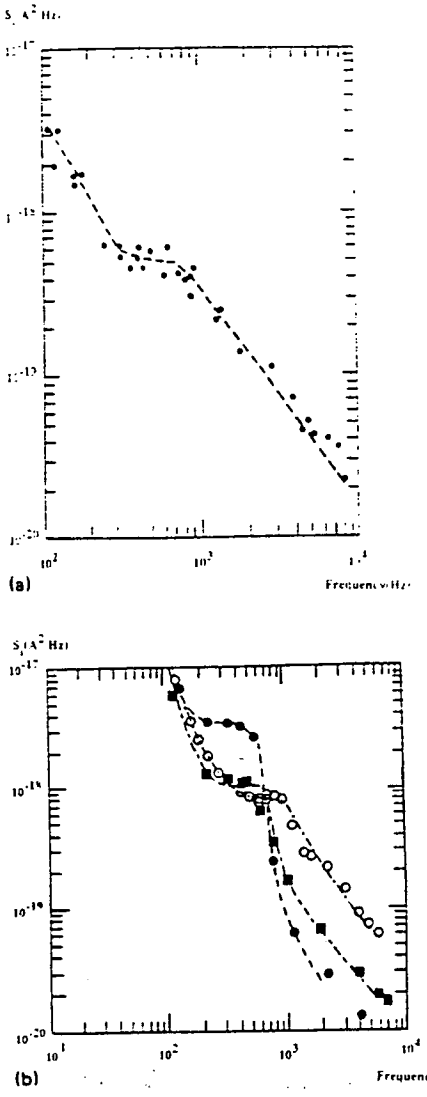

FIG. 5. (a) The noise current spectral density $S_I(f)$ vs frequency (f) for ASi645 at $V = 0.2$ V and $T = 300$ K. Note that the noise data are taken when the current is in its quiescent period. (b) The $S_I(f)$ vs f for three more samples of ASi645 at $V = 0.2$ V and $T = 300$ K taken at the quiescent period.

mm^2). They reconciled this by suggesting that the RTS would either require the correlated emptying and filling of 10^5 traps equally distributed over the whole area, or a current path that is confined to a filament of cross-sectional area of $\leq 1 \times 10^{-6}$ mm^2. Arce and Levy reckoned the filamentary explanation to be the more likely since current filaments of comparable size ($\leq 2.5 \times 10^{-7}$ mm^2) have been reported in a-Si:H p^+-n-i memory devices.[13] In the present Cr-p^--Cr samples, the devices have an active area of $\sim 10^{-4}$ mm^2, comparable to areas of the devices studied by Farmer, and co-workers,[4] Judd *et al.*,[6] and Neri and co-workers,[10] and the alternative suggestions offered by D'Amico and co-workers[1] and Neri and co-workers[10] may provide possible explanations in our case. Neri and co-workers report a $1/f$ noise in metal-oxide-silicon field effect transistors with very

thin (< 10 nm) oxide layers and they suggested that the noise is probably caused by the filling (emptying) of localized electron states (traps) in the tunneling barrier. When a trap in a strategic position give rise to a detectable modulation of the total current, the noise is no longer flickerlike, but becomes a RTS. Similar to our observation, Neri and co-workers also concluded that noise measurements were not possible in this regime. D'Amico and co-workers postulated that in *a*-Si:H, there are discrete traps below the Fermi level that temporarily immobilize the carriers participating in the conduction process. In our samples there may well exist a dominant trap level that controls the noise process so that a single Lorentzian is observed. It is not possible to identify the dominant trap level at present due to the absence of a comprehensive set of noise measurements as a function of temperature. On the other hand, we have recently reported memory results[14] on *a*-Si:H Cr-p^+-Cr and Cr-p^+-V structures and have concluded that the top metal contact (i.e., Cr or V) influences the subsequent analog memory switching behavior. If the transport mechanism is contact limited, it is still possible to obtain a Lorentzian because a contact generated noise would have the same I^2 dependence.

Two models[10] related to breakdown in thin thermal oxide films have been used to provide an explanation of RTS in this material. The first model involves breakdown caused by resonances in oxide tunneling characteristics which occur as a result of a suitable trap center located near the injecting interface. This can cause a fluctuation of the electrical potential by filling (emptying) another trap at a sufficiently short distance from the critical center, thus producing a detectable modulation of the total current. In the other model, breakdown in thin thermal oxide films is caused by weak spots with higher conductivity compared to the remainder of the device. A considerable amount of the total current is localized in this region and the filling (emptying) process of a trap near enough to the weak spot, can, by modulating the barrier height, produce notably abrupt variations of the total current, and this model is adopted by Arce and Ley. We have observed filament formation in Cr-p^+-Cr memory devices after forming[15] and it is possible that the above explanation may also apply to our observations.

V. CONCLUSIONS

We believe that this is the first observation of random telegraph signals associated with noise in notionally homogeneous hydrogenated amorphous silicon. At or above room temperature, the current versus time characteristics exhibit a distinctive behavior with the current fluctuating between two easily identifiable levels with the periods of fluctuations separated by a quiescent periods. The difference in current between the two states (ΔI) is more pronounced ($\Delta I / I \sim 1\%-10\%$) at $T = 373$ K than at room temperature ($\Delta I / I \sim 0.1\%-1\%$). The occurrence of the fluctuations is, however, unpredictable. The current noise spectrum obtained during the quiescent period is Lorentzian, indicative of a recombination-generation process. With higher biases, the *I-t* characteristics exhibit a chaotic pattern of fluctuations and no easily identifiable current levels can be located. It is not possible to carry out noise measurements in this regime and the high applied fields ($> 10^5$ V/cm) also lead to eventual breakdown of the sample.

ACKNOWLEDGMENTS

The authors would like to thank S. Kimmond and A. Carrie for their technical assistance, and BP Research International for the financial support of this work. We would also like to express our sincere gratitude to Professor L. Ley of Universitat Erlangen for discussion of RTS in double barrier structures and providing reprints prior to publication.

[1] A. D'Amico, G. Fortunato, and C. M. Van Vliet, Solid-State Electron. **28**, 837 (1985).
[2] F. Z. Bathaei and J. C. Anderson, Philos. Mag. B **55**, 87 (1987).
[3] K. R. Farmer, C. T. Rogers, and R. A. Buhrman, Phys. Rev. Lett. **59**, 2255 (1987).
[4] K. R. Farmer, R. Saletti, and R. A. Buhrman, Appl. Phys. Lett. **52**, 1749 (1988).
[5] R. T. Wakai and D. J. Van Harlingen, Appl. Phys. Lett. **49**, 593 (1986).
[6] T. Judd, N. R. Couch, P. H. Beton, M. J. Kelly, T. M. Kerr, and M. Pepper, Appl. Phys. Lett. **49**, 1652 (1986).
[7] K. S. Ralls, W. J. Skocpol, L. D. Jackel, R. E. Howard, L. A. Fetter, R. W. Epworth, and D. M. Tennent, Phys. Rev. Lett. **52**, 228 (1984).
[8] M. J. Uren, D. J. Day, and M. J. Kirton, Appl. Phys. Lett. **47**, 1195 (1985).
[9] M. J. Kirton and M. J. Uren, Appl. Phys. Lett. **48**, 1270 (1986).
[10] B. Neri, P. Olivo, and B. Ricco, Appl. Phys. Lett. **51**, 2167 (1987).
[11] R. Arce and L. Ley, MRS Symp. Proc. **118**, 329 (1988).
[12] R. Arce and L. Ley, in *Proceedings of the Thirteenth International Conference on Amorphous and Liquid Semiconductors*, Asheville, edited by M. Paesler, S. C. Agarwal, and R. Zallen (North-Holland, Amsterdam, 1989).
[13] P. G. LeComber, A. E. Owen, W. E. Spear, J. Hajto, A. J. Snell, W. K. Choi, M. J. Rose and S. Reynolds, J. Non-Cryst. Solids **77&78**, 1373 (1985).
[14] M. J. Rose, J. Hajto, P. G. LeComber, S. M. Gage, W. K. Choi, A. J. Snell, and A. E. Owen, in *Proceedings of the First International Conference on Amorphous Semiconductors Technology*, Asheville, edited by M. J. Thompson and D. E. Carlson (North-Holland, Amsterdam, 1989).
[15] S. M. Gage, Ph.D. thesis, University of Edinburgh, 1989 (unpublished).

PHILOSOPHICAL MAGAZINE B, 1991, VOL. 63, NO. 5, 1169–1179

On the kinetics of Ag photodissolution in As_2S_3 chalcogenide glass films: oscillatory behaviour of the reaction rate

By E. MARQUEZ†, R. JIMENEZ-GARAY†, A. ZAKERY, P. J. S. EWEN and A. E. OWEN

Department of Electrical Engineering, University of Edinburgh, Edinburgh EH9 3JL, Scotland

[*Received 28 March 1990 and accepted 14 June 1990*]

ABSTRACT

The kinetics of Ag photodissolution into As_2S_3 glass films have been investigated by monitoring the electrical resistance of the Ag layer during the process. The thickness dependence of the Ag electrical resistivity predicted by the thick-film approximation of Sondheimer's theory has been used (reasonable agreement was found), in order to obtain the curve of Ag thickness against illumination time. The thickness ranges of Ag and As_2S_3 layers studied were around 1000–1500 Å and 3000–5000 Å respectively. The main feature found is the appearance of an oscillatory behaviour of the reaction rate, with the illumination from the As_2S_3 side and wavelengths lower than a threshold value, which increased when the thicknesses of the layers were increased. In contrast, when the samples were irradiated on the Ag side, the sigmoidal kinetic curve very often reported was observed. These data could support the idea that the actinic light absorption occurs in the vicinity of the doped–undoped chalcogenide interface.

§1. INTRODUCTION

The photostimulated reaction between films of Ag and chalcogenide glasses, known variously as 'photodissolution' or 'photodoping', has been the object of many investigations (for example Kostyshin, Mikhailovskaya and Romanenko (1966), Janai (1981), Kluge (1987), Ewen, Zakery, Firth and Owen (1988), Kolobov, Elliott and Taguirdzhanov (1990)). Some researchers have shown the possibility of technical applications of this phenomenon, especially for preparation of inorganic photoresists for ultra-high-resolution lithography (Chen and Tai 1980, Yoshikawa, Ochi and Mizushima 1980, Firth, Ewen and Owen 1985a, Firth, Ewen, Owen and Huntley 1985b) and infrared grating fabrication (Zakery, Slinger, Ewen, Firth and Owen 1988). However, the actual mechanism of photodissolution still remains unclear. In particular, there is uncertainty concerning where the actinic radiation is absorbed and what is the photodissolution rate-limiting step. In this paper, some new experimental data for clarifying the kinetics of the photodoping process of Ag into amorphous As_2S_3 (*a*-As_2S_3) are reported. From these results it is possible to address the above-mentioned fundamental questions. Specifically, the photodissolution rate of the metal has been monitored by the electrical resistance measurement technique described elsewhere (Goldschmidt and Rudman 1976) and, principally, samples with thick Ag layers have

† Permanent address: Departamento de Estructura y Propiedades de los Materiales, Facultad de Ciencias, Universidad de Cadiz, ap. 40 11510 Puerto Real, Cadiz, Spain.

been investigated. The main kinetic characteristic that will be reported is the appearance of an oscillatory behaviour of the reaction rate (OBRR), when the Ag/As_2S_3 system was illuminated from the chalcogenide side of the sample.

§2. Experimental details

Films of $a–As_2S_3$ were prepared by thermal evaporation, in a vacuum of about 10^{-5} Torr; Ag metal was pre- or post-deposited also by evaporation (Ewen *et al.* 1988). The As_2S_3 evaporation source was powdered melt-quenched glass and the metal source was fragments of Ag wire. The sample configuration is illustrated in fig. 1. The substrate was a glass microscope slide, each slide containing ten silver strips. The dimensions of the silver strips and the chalcogenide glass film were approximately 1 mm × 2 cm and 1·3 cm × 6·5 cm respectively. In order to generate this pattern, two masks were used during the evaporation. The deposited thicknesses were determined by means of a quartz oscillator thickness monitor which had been calibrated against a Sloan Dektak IIA surface profiler. The As_2S_3 and Ag layer thicknesses ranged mostly between around 3000 and 5000 Å and around 1000 and 1500 Å respectively. The ratio of the thicknesses of Ag to As_2S_3 layers selected was slightly lower than 1 to 3, in order to make sure that the silver strip was completely exhausted (Firth *et al.* 1985a). The electrical contacts with the silver strip were made with tungsten probes with springs and an x–y–z micromanipulator attached (fig. 1). With this arrangement a gentle contact pressure and, consequently, a stable electrical resistance, essential in this experiment, was achieved. The two-terminal resistance measurements were made using a Keithley 195 programmable digital multimeter (DMM), microcomputer controlled via an IEEE-488 interface, so that the data could be logged and processed

Fig. 1

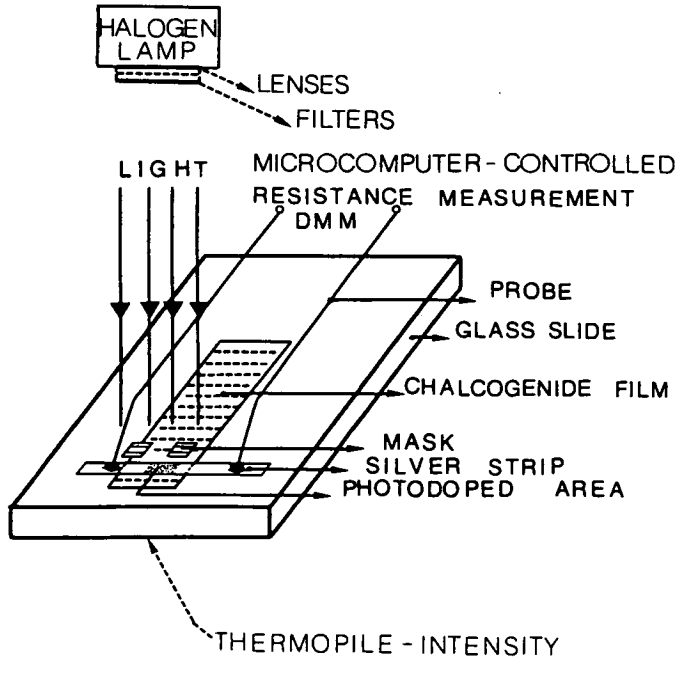

The experimental set-up for measuring the electrical resistance of the silver layer as a function of irradiation time, during the Ag photodissolution effect.

automatically. To check that Joule self-heating or electromigration effects did not occur significantly, some results were also obtained using a 1 μA constant current method for measuring the resistance. The results were similar in both cases and the DMM has the advantage of offering a higher signal-to-noise ratio (this instrument has a $10^{-4}\,\Omega$ sensitivity). The light irradiation of the sample was by means of a 150 W W–halogen lamp with light guide and heat filter. The wavelength of the radiation was controlled by suitable optical filters, and the light intensity (which was measured with a thermopile) was modified by varying the distance between the sample and the outlet of the light guide. Care was taken with the uniformity of the light beam over the illuminated area of the sample. All measurements reported here were performed at room temperature.

§ 3. Relationship between Ag thickness and resistance increase

The measurement of the Ag layer resistance continuously during illumination has enabled the change in Ag layer thickness to be determined also continuously, based on the equation

$$\Delta R(d) = (l/w)[\rho(d)/d - \rho(d_0)/d_0], \tag{1}$$

where l is the length (in the direction of the current) of the zone of the silver strip to be illuminated and d its thickness (during the reaction), and w and d_0 are the width and initial thickness of the silver strip; ΔR is the increase in the resistance and ρ is the electrical resistivity of Ag. The expression for the electrical resistance in the present configuration, $R = R_c + \rho l'/wd_0$, l' being the interprobe distance, has two terms corresponding to the contact resistance and the resistance of the Ag layer. Using the latter equation and measuring the resistance for several widths and interprobe distances, the resistivity of Ag was calculated (a good fit to a linear relationship between the resistance and aspect ratio l'/w was generally found).

Furthermore, the thickness dependence of resistivity predicted by the thick-film approximation of Sondheimer's theory (for example, Sondheimer (1952), Berry, Hall and Harris (1968), Larson (1971)), for the most realistic case of inelastic scattering at the film boundaries is

$$\rho(d) = (mv_F/ne^2)(1/\lambda_\infty + 3/8d) = \rho_\infty(1 + 3\lambda_\infty/8d), \tag{2}$$

where m, v_F, n and e are the electron mass, the Fermi speed, the density of electrons and the electron charge; ρ_∞ and λ_∞ are the resistivity and mean free path of the electrons corresponding to infinite film thickness (λ_∞ includes each of the effects that limit the mean free path of the electrons, such as phonons, impurities, defects and grain boundaries). Good agreement between this theory and the experimental results, using Ag evaporated films, in the thickness range from about 100 to 2000 Å, has been obtained (Reynolds and Stilwell 1952). The significant feature of the sample preparation procedure used in that investigation was the high evaporation rate employed (about 500 Å s^{-1} or higher). The value of the mean free path found was 520 Å and the Ag bulk resistivity value used was 1·62 $\mu\Omega$ cm. In the present study, slightly higher values of the resistivity have been obtained because of the lower deposition rate achieved, around 100 Å s^{-1}. The value of the electrical resistivity clearly depends on the deposition rate as a consequence of the strong influence of the evaporation rate on the final structure of the film (table 1 shows some typical results). In addition, it is assumed that the photodissolution process is also influenced by the structural characteristics of the Ag film and, for this reason, the Ag resistivity provides useful preliminary

Table 1. Electrical resistivity of Ag films 1300 Å thick prepared with different deposition rates and the ratio of these experimental values to the resistivity predicted by eqn. (2) (with $\rho_\infty = 1{\cdot}62\,\mu\Omega\,\text{cm}$ and $\lambda_\infty = 520\,\text{Å}$), $1{\cdot}86\,\mu\Omega\,\text{cm}$.

Deposition rate (Å s^{-1})	$\rho_{\text{experimental}}$ ($\mu\Omega\,\text{cm}$)	Resistivity ratio
10	5·40	2·90
50	2·57	1·38
100	2·05	1·10

information. On the other hand, as a result of the difference between the values of resistivity reported by Reynolds and Stilwell and those obtained in this investigation, it was necessary to recalculate the parameters ρ_∞ and λ_∞ from the silver resistivity found. In the case of $d_0 = 1300\,\text{Å}$ with $\rho = 2{\cdot}05\,\mu\Omega\,\text{cm}$, $\lambda_\infty = 466\,\text{Å}$ and $\rho_\infty = 1{\cdot}81\,\mu\Omega\,\text{cm}$ (the effective mean free paths were similar for the majority of the Ag film thicknesses analysed). It should be taken into account that $\lambda_\infty^{-1} = \lambda_{\text{ph}}^{-1} + \lambda_{\text{imp}}^{-1} + \lambda_{\text{def}}^{-1} + \lambda_{\text{bdy}}^{-1} + \ldots$, that is each of the effects that limit the mean free path may be considered to act independently of the others (only the supposedly main contributions have been indicated explicitly here). Thus it is assumed that eqn. (2), with the readjusted parameters, accounts for the Ag resistivity increase as a consequence of the Ag thickness reduction during the photodoping process with reasonable accuracy. (If, as suggested in § 4, the Ag reacts preferentially at grain boundaries to produce an uneven interface, then the Ag thickness d will be an average value.) Finally, combining eqns. (1) and (2), the Ag thickness as a function of the resistance increase is deduced:

$$d(\Delta R) = [d_0/\alpha(\Delta R)]\{1 - [1 + 4\alpha(\Delta R)\beta]^{1/2}\}, \tag{3}$$

where the dimensionless magnitudes α and β are given by

$$\alpha(\Delta R) = 1 + \beta + \Delta R w d_0/\rho_\infty l, \quad \beta = 3\lambda_\infty/8d_0.$$

§ 4. Results and discussion

Some significant experimental results concerning photodissolution in the Ag/As_2S_3 system will now be presented. Firstly, the electrical resistance as a function of illumination time, for two values of the exciting light intensity, 1·10 and 4·30 mW cm^{-2}, is shown in fig. 2. These results correspond to samples whose initial Ag and chalcogenide glass thicknesses are approximately 1300 and 4700 Å respectively. Unfiltered light was used in this particular case and the illumination took place from the chalcogenide side of the sample. The intensity range studied in this work, when 'white' light was employed, was about 1–10 mW cm^{-2}. The outstanding feature of these typical curves plotted in fig. 2 is that there are several changes in the sign of the quantity d^2R/dt^2 during the photodissolution process; in the case of the lower intensity there are three inflection points and with the higher intensity there are only two. Secondly, in fig. 3, the electrical resistance data converted by means of eqn. (3) to Ag thickness, as a function of exposure time, are shown. Both time dependences show that the reaction speeds initially increase and then decrease, repeating this oscillatory behaviour once more during the process. In addition, the corresponding photodoping rate derived by the Gregory–Newton numerical differentiation method against the normalized quantity, fraction of Ag reacted, for both light intensities is plotted in the same figure. Two peaks are observed in these curves and a characteristic of them is that the

Fig. 2

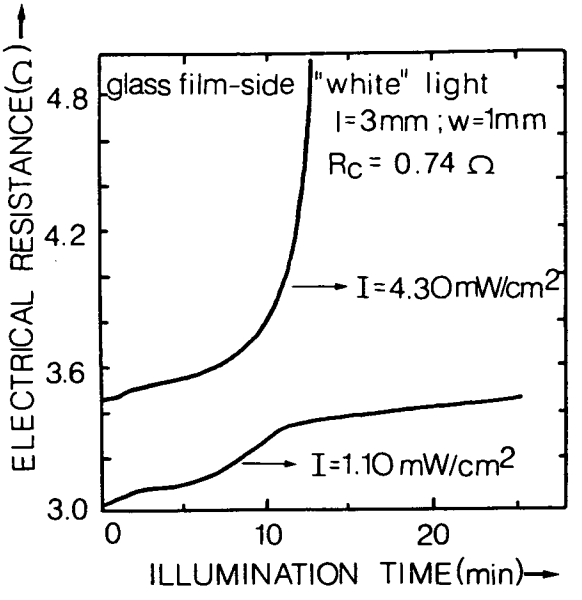

The Ag electrical resistance against exposure time curve corresponding to two light intensities (unfiltered light was used). The dimensions l and w of the illuminated area of the sample and the average contact resistance in the present measurements are indicated in the figure.

difference between the reaction rates at the first maximum is considerably less than at the second maximum; moreover, the difference between the positions of the first maxima is also insignificant in comparison with that existing between the positions of the second maxima (table 2). Furthermore, the plots of Ag thickness against exposure dose (light intensity multiplied by exposure time) for the different power densities studied do not follow a common curve, so that the OBRR does not obey the reciprocity law, that is the interchangeability of light intensity and irradiation time. To illustrate this characteristic, for an exposure dose of $1\,J\,cm^{-2}$, light intensities of 1·1, 4·3 and $8{\cdot}5\,mW\,cm^{-2}$ yield Ag thicknesses of 540, 970 and 1010 Å respectively. On the other hand, when this particular type of sample was irradiated from the chalcogenide side using filtered light with different wavelengths, whose values were 400, 525, 570 and 650 nm respectively, the kinetic characteristics observed with unfiltered light continued to appear in the case of the first three wavelengths; however, for the longest wavelength of 650 nm no oscillation in the reaction rate was observed. The latter experimental finding is of fundamental importance in order to discover the origin of the phenomenon. Other experimental results belonging to samples with different initial Ag and As_2S_3 thicknesses, $d_0(Ag) \approx 1200$ Å and $d_0(As_2S_3) \approx 4100$ Å, with the illumination from the chalcogenide side, are plotted in fig. 4. These curves of electrical resistance against illumination time have been obtained using 525 nm green light (fig. 4 (*a*)) and unfiltered light (fig. 4 (*b*)); the inflection points of these curves, which give rise to OBRR, may be seen more clearly in this figure (these are marked in the plots with arrows).

In contrast, when the samples investigated were illuminated on the Ag side their behaviour was different; a three-stage kinetic curve was obtained, similar to that very often reported in the literature (for example Goldschmidt and Rudman (1976), Yaji and

Fig. 3

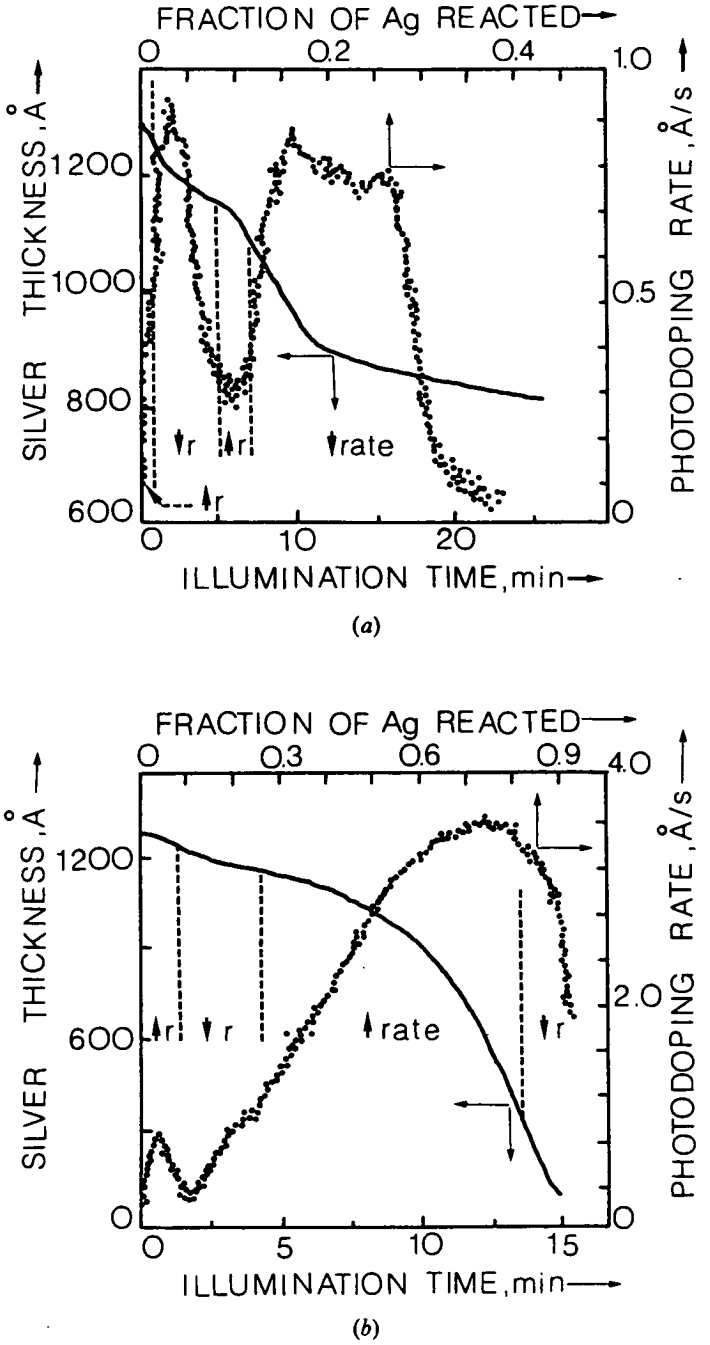

Variation in Ag thickness as a function of illumination time and variation in the photodissolution rate as a function of fraction of Ag reacted, as derived from the Ag resistance against exposure time curves plotted in fig. 2: (*a*) 1·10 mW cm^{-2}; (*b*) 4·30 mW cm^{-2}. In this figure are also shown the distinct stages of the process in which $dr/dt > 0$ or $dr/dt < 0$. The inflection points of these kinetic curves, with $dr/dt = 0$, have been deduced from the associated photodoping rate against normalized Ag thickness plots.

Table 2. Values of the photodissolution rate and the percentage of Ag layer photodoped, at the first and second maximum of the curves showing the variation in the rate during the process plotted in fig. 3.

Unfiltered light power density ($mW\,cm^{-2}$)	First-maximum photodoping rate ($Å\,s^{-1}$)	Second-maximum photodoping rate ($Å\,s^{-1}$)	First-maximum position (%)	Second-maximum position (%)
1·10	0·93	0·87	2·5	16
4·30	0·81	3·59	3·0	73

Fig. 4

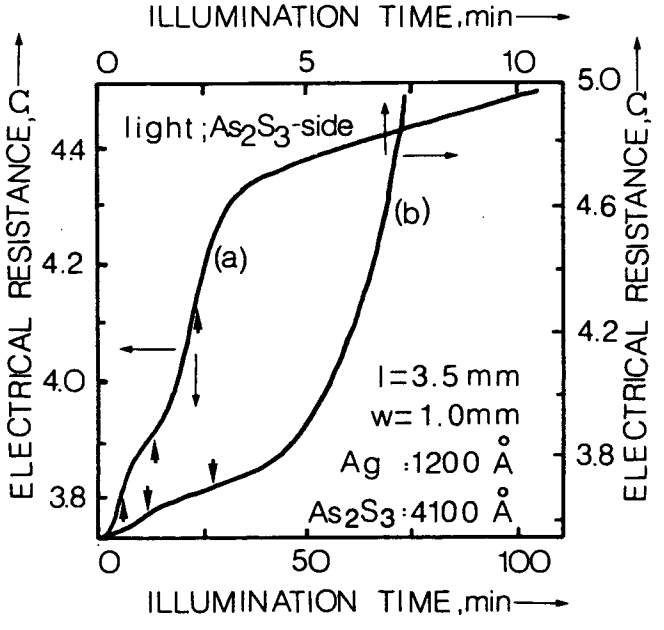

Time dependence of Ag resistance for (*a*) 525 nm green light, with $I = 1{\cdot}50\,mW\,cm^{-2}$, and (*b*) unfiltered light, with $I = 8{\cdot}10\,mW\,cm^{-2}$. The thicknesses of the two layers and the length and the width of the irradiated region are also indicated in the figure.

Kurita (1983), Konan, Galibert and Calas (1988)), with a sigmoidal form, that is with an acceleratory period (the so-called induction period), a linear stage and, finally, a deceleratory step. The linear stage is usually interpreted as a chemical-reaction-limited process and part of the deceleratory period may be presumably due to a diffusion process (the movement of the interface between the photodoped and the Ag layers being limited by the motion of Ag^+ ions through the photodoped layer), since a square root time dependence has been seen after the linear stage. Finally, the violation of the parabolic law observed at the end of the photodoping process could be caused by the reduction in the amount of light reaching the reaction interface, due to absorption in the highly absorbing photodoped layer (see § 5); this would produce an additional decrease in the reaction rate. As a typical result (fig. 5), an induction period of 23·5 min and a photodoping rate corresponding to the linear stage of $0{\cdot}15\,Å\,s^{-1}$ was found for a

sample with an initial Ag thickness of approximately 1000 Å and an initial As_2S_3 thickness of approximately 3100 Å, using 400 nm ultraviolet light and a photon flux density of $1{\cdot}13 \times 10^{15}$ photons $cm^{-2}\,s^{-1}$. Moreover, the part of the deceleratory period in which the thickness of the reacted Ag layer is proportional to $t^{1/2}$ is displayed in fig. 5 (the parabolic rate constant derived from this interval was $1{\cdot}5 \times 10^{-7}$ cm $s^{-1/2}$). When this type of sample was illuminated from the As_2S_3 side employing filtered light with the above-mentioned distinct wavelengths, the OBRR shown in fig. 3 disappeared for

Fig. 5

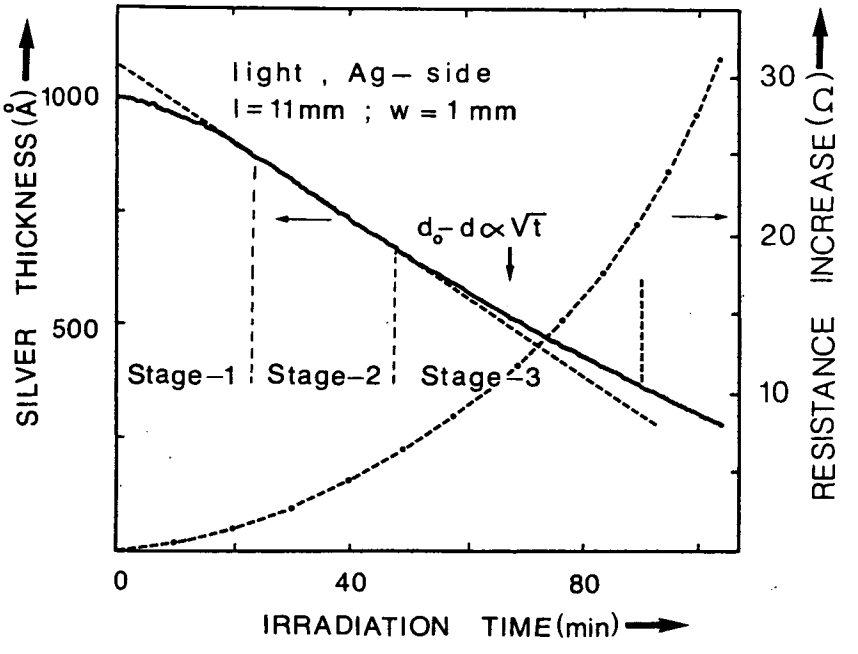

Decrease in Ag thickness during irradiation, with 400 nm ultraviolet light incident on the Ag side of the sample, the initial As_2S_3 layer thickness being around 3100 Å ($I = 0{\cdot}56$ mW cm^{-2}). The curve of Ag resistance increase against illumination time is also plotted. The dimensions of the illuminated zone are also indicated in the figure.

Table 3. Spectral dependence of the linear stage photodoping rate ($I = 1{\cdot}4$ mW cm^{-2}). The oscillations observed with $\lambda = 400$ nm appeared after the initial linear step, and therefore it was possible to derive the photodoping rate associated with this period. Other results (Zakery 1990) relating to a–As_2S_3, obtained by optical reflectivity measurements (this technique is described by Ewen *et al.* (1988)) are consistent with those found by electrical resistance measurements. From the former data, it has been determined that the photodissolution rate decreases very sharply for $\lambda \gtrsim 500$ nm.

Light wavelength (nm)	Photon energy (eV)	Linear stage photodoping rate (Å s^{-1})	Photodoping rate normalized to r(525 nm)
400	3·11	1·14	0·49
525	2·37	2·34	1·00
570	2·18	1·06	0·45
650	1·91	0·25	0·11

all wavelengths except in the shortest wavelength of 400 nm; the kinetic curve when the oscillations disappeared, with the light incident on the As_2S_3 side, was analogous to that displayed in fig. 5, except that there was no induction period or it was too short to be measured, such as has been seen in the OBRR plots (some values of the linear stage photodoping rate are shown in table 3). The non-appearance of OBRR when the light is incident on the Ag side of the sample has also been observed in very thin films. As a representative example, in a sample with $d_0(\text{Ag}) \approx 200$ Å and $d_0(\text{As}_2\text{S}_3) \approx 700$ Å, the S-shaped kinetic curve was again found, and the induction period and linear stage photodoping rate were 46 s and 0·40 Å s^{-1}. These results were obtained with $\lambda = 570$ nm and $I = 1{\cdot}45$ mW cm^{-2}. The exposure time in order to photodissolve completely the illuminated zone of the silver strip was 13 min. This exposure time is determined from the electrical resistance against irradiation time curve; when the Ag layer is exhausted, the measured resistance is commonly about several megohms ($R = 2{\cdot}5$ MΩ in the example under consideration) and this value corresponds to the doped layer resistance (the ratio of the resistance of the undoped area to that of the Ag-doped area was 7×10^4 in this particular case). Note that the doped-layer resistance is around six orders of magnitude higher than the initial Ag resistance, justifying the correctness of the basic assumption of the electrical method used for monitoring the kinetics of the phenomenon, namely $\rho_{\text{Ag}} \ll \rho_{\text{As}_2\text{S}_3}$ and $\rho_{\text{Ag/As}_2\text{S}_3}$.

In summary, from the experimental data of the present study the following features regarding the kinetics of the effect may be deduced.

(1) The structure of the kinetic curve showing OBRR depends clearly on the exciting power density (reciprocity behaviour was not observed).
(2) The existence of OBRR depends on whether the light passes through the Ag polycrystalline layer first, or whether the light passes through the chalcogenide glass layer first.
(3) The role of the light wavelength for finding the OBRR was crucial, since in the cases investigated when the wavelength was increased this disappeared, depending on the initial thicknesses of the two layers (note that most of the initial Ag thicknesses used have been higher than those employed in the majority of the kinetic studies by electrical resistance measurement and other techniques, which used films of thicknesses 1000 Å or less).

Analogous results for the Ag photodoping of a–As_2S_3 with the irradiation on the chalcogenide side have been reported (Arai *et al.* 1989), using annealed and photodarkened samples in this study. It has been argued that the time dependence of the reaction shows a clear two-stage behaviour. During the initial stage of the irradiation, the Ag–doped-chalcogenide interface shift exceeds the decrease in Ag thickness, while in the second stage the process is inverted. The spectral dependence of the phenomenon was also studied and suggested that only photons with energy higher than the As_2S_3 optical bandgap, $E_g = 2{\cdot}33$ eV, are able to give rise to the second stage of the process. From these results and Rutherford backscattering data, it was concluded that the mechanism responsible for the first stage is different from that for the second stage.

A corresponding investigation in a–$GeSe_2$ has also reported similar behaviour (Rennie 1986, Rennie and Elliott 1987). Small oscillations superimposed on the Ag thickness against illumination time curves, again when the light exposure was from the chalcogenide side of the sample, were also observed. Such oscillations, together with those found in the photodoping rate as a function of the initial Ag thickness, were

interpreted as an optical interference process occurring in this multilayer optical system; their presence allows the possibility of determining where in the sample the absorbed light leads to reaction. From calculations of the light intensity at various points of the multilayer structure, it was concluded that the light stimulating metal photodoping is absorbed at the photodoped–undoped chalcogenide interface. Another conclusion to be drawn from this analysis in relation to the interpretation of the present results is that the number of oscillations in the photodissolution rate during the process decreases considerably when the light wavelength is increased, as would be expected if this were an interference effect.

Considering only the shape of the plots of photoreaction rate against the fraction of Ag reacted shown in fig. 3, it would be plausible to argue that the phenomenon consists of two stages with distinct mechanisms, such as has been suggested for annealed and photodarkened a–As_2S_3, the second step being much more sensitive to the value of the incident power density. However, since the oscillations disappeared when the radiation wavelength was increased (when d_0(Ag) and $d_0(As_2S_3)$ were increased, the threshold wavelength at which the OBRR disappeared was also increased), it seems reasonable to think that, on the contrary, these observations for a $-As_2S_3$ may be a consequence of an optical interference effect, which would give rise to oscillatory variations of the actinic light intensity. Furthermore, although the above-mentioned calculations of intensity also predict the OBRR with illumination from the Ag side, the polycrystalline nature of the as-deposited Ag film may give rise to a preferential reaction at the grain boundaries (due presumably to increased stress and defect concentration generally found in these regions), producing an uneven Ag–photodoped chalcogenide interface (S. R. Elliott 1989, private communication) and therefore a strong reduction in the interference effect. It could explain the non-appearance of OBRR when the light passes through the Ag layer first. On the other hand, the OBRR observed with white light (broad-band illumination) could occur because of the spectral dependence of the photodoping rate (table 3) and the spectral irradiance distribution of the W–halogen lamp used. This relative spectral energy increases monotonically from around 300 nm, being 12% at 400 nm, 36% at 500 nm and 60% at 600 nm. From the combination of these two spectral dependences may result a dominant contribution of a reasonably narrow wavelength range, which would justify the existence of OBRR even with unfiltered light. Moreover, the peak positions of the OBRR curves could be affected by the value of the incident light intensity (the corresponding interference pattern would not depend on the power density), because the photodissolution process is supposedly controlled, not only by the chemical reaction at the doped–undoped interface, but also by the diffusion of Ag^+ ions through the doped layer.

§ 5. Concluding remarks

A comprehensive study of the optical constants (refractive index and absorption coefficient) of undoped and Ag-doped As–S glasses is currently being carried out in this laboratory (Zakery *et al.* 1988, Zakery, Zekak, Ewen, Slinger and Owen 1989) which will enable a computer simulation of this effect to be carried out. The calculations required for the light amplitudes at the two interfaces of the sample will be carried out by a matrix method using the Fresnel coefficients described by Heavens (1955), which is a more convenient technique. The Fresnel coefficients depend on the quantities Δn and $\Delta\alpha$, the difference between the refractive indices and absorption coefficients of the doped and undoped material. As a representative instance of results found in the above study of the optical constants, for the composition $As_{30}S_{70}$ and the most heavily doped

sample ($d_0(As_{30}S_{70}) \approx 5000$ Å and $d_0(Ag) \approx 1500$ Å), which contained approximately 27 at.% Ag, $\Delta n > 0{\cdot}5$ over the wavelength range 500–2000 nm and the values of α of undoped and doped films at, for example, 514 nm are $4{\cdot}5 \times 10^2$ and $6{\cdot}9 \times 10^4$ cm^{-1} respectively, the ratio of these two values of α in the visible spectrum being approximately 10^2. The results of modelling the kinetics of the process by the procedure proposed could strongly support the explanation of OBRR in a–As_2S_3 based on the variations in the intensity at the doped–undoped chalcogenide interface. In other words, the actinic light absorption would take place in that region of the multilayer system (it should be noted that according to the absorption coefficients the photodoped zone is significantly more absorbing), as has also been deduced from the experiments of the lateral migration of Ag in As–S films in contact with a conducting substrate (Owen, Firth and Ewen 1985) and other recent experiments (Kolobov *et al.* 1990).

ACKNOWLEDGMENTS

The authors are grateful to Mr J. Wilson and Mr A. Zekak for their helpful cooperation during this investigation and would like to thank Dr S. R. Elliott for valuable discussions relating to this work. One of us (E.M.) is also grateful to the Spanish Ministry of Education and Science for the concession of a research grant.

REFERENCES

ARAI, T., WAKAYAMA, Y., KUDO, H., KISHIMOTO, T., LEE, J., OGAWA, T., ONARI, S., 1989, *J. non-crystalline Solids*, **114**, 40.

BERRY, R. W., HALL, P. M., and HARRIS, M. T., 1968, *Thin Film Technology* (Princeton, New Jersey: Van Nostrand).

CHEN, C. H., and TAI, K. L., 1980, *Appl. Phys. Lett.*, **37**, 605.

EWEN, P. J. S., ZAKERY, A., FIRTH, A. P., and OWEN, A. E., 1988, *Phil. Mag.* B, **57**, 1.

FIRTH, A. P., EWEN, P. J. S., and OWEN, A. E., 1985a, *J. non-crystalline Solids*, **77–78**, 1153.

FIRTH, A. P., EWEN, P. J. S., OWEN, A. E., and HUNTLEY, C. M., 1985b, *Advances in Resist Technology and Processing II*, Proc. SPIE, Vol. 539, edited by L. F. Thompson (Bellingham, Washington: SPIE), p. 160.

GOLDSCHMIDT, D., and RUDMAN, P. S., 1976, *J. non-crystalline Solids*, **22**, 229.

HEAVENS, O. S., 1955, *Optical Properties of Thin Solid Films* (London: Butterworth).

JANAI, M., 1981, *Phys. Rev. Lett.*, **47**, 726.

KLUGE, G., 1987, *Phys. Stat. sol.*, **101**, 105.

KOLOBOV, A. V., ELLIOTT, S. R., and TAGUIRDZHANOV, M. A., 1990, *Phil. Mag.* B, **61**, 857.

KONAN, K., GALIBERT, G., and CALAS, J., 1988, *Phys. Stat.* sol., **107**, 273.

KOSTYSHIN, M. T., MIKHAILOVSKAYA, E. V., ROMANENKO, P. F., 1966, *Fizika tverd. Tela*, **9**, 571.

LARSON, D. C., 1971, *Physics of Thin Films*, edited by G. Hass and R. E. Thun (London: Academic Press), p. 81.

OWEN, A. E., FIRTH, A. P., and EWEN, P. J. S., 1985, *Phil. Mag.* B, **52**, 347.

RENNIE, J. H. S., 1986, Ph.D. Thesis, Jesus College, Cambridge.

RENNIE, J. H. S., and ELLIOTT, S. R., 1987, *J. non-crystalline Solids*, **97–98**, 1239.

REYNOLDS, F. W., and STILWELL, G. R., 1952, *Phys. Rev.*, **88**, 418.

SONDHEIMER, E. H., 1952, *Adv. Phys.*, **1**, 1.

YAJI, T., and KURITA, S., 1983, *J. appl. Phys.*, **54**, 647.

YOSHIKAWA, A., OCHI, O., and MIZUSHIMA, Y., 1980, *Appl. Phys. Lett.*, **36**, 107.

ZAKERY, A., 1990 (private communication).

ZAKERY, A., SLINGER, C. W., EWEN, P. J. S., FIRTH, A. P., and OWEN, A. E., 1988, *J. Phys.* D, **21**, S78.

ZAKERY, A., ZEKAK, A., EWEN, P. J. S., SLINGER, C. W., and OWEN, A. E., 1989, *J. non-crystalline Solids*, **114**, 109.

PHILOSOPHICAL MAGAZINE B, 1991, VOL. 63, NO. 1, 15–31

Optical absorption in As–Se glasses

By JÓN PÉTURSSON†, J. M. MARSHALL‡ and A. E. OWEN§

† Science Institute, University of Iceland, Dunhaga 3, IS-107 Reykjavík, Iceland
‡ Department of Materials Engineering, University College of Swansea, Singleton Park, Swansea SA2 8PP, Wales
§ Department of Electrical Engineering, University of Edinburgh, Kings Buildings, Edinburgh EH9 3JL, Scotland

[*Received 12 June 1990 and accepted 15 June 1990*]

ABSTRACT

The optical absorption above the fundamental edge has been measured as a function of temperature for 15 compositions from Se to AsSe. The samples were thin films made by blowing bubbles from the melt. The optical gap has a minimum near $As_{43}Se_{57}$. Tauc plots for absorption at different temperatures but the same composition appear to converge to a single point. An unexpected linear relation is observed between composition and the inverse square of the slopes of the Tauc plots. An inverse correlation is observed between optical gap and the glass-transition temperature.

§ 1. INTRODUCTION

Considerable work has been published on the Urbach edge in As–Se glasses (Hurst and Davis 1974, Andreev, Kolomiets, Mazets, Manukyan and Pavlov 1976, Sussmann, Austin and Searle 1975, Ihm 1985a, b). The behaviour of the Urbach tail slope with temperature and composition in As–Se and Ge–Se glasses is unusual (Oheda 1979). This has been interpreted in terms of microscopic structure and disorder, invoking 'buckling' that causes increasing disorder with decreasing temperature (Ihm 1985a, b).

It is generally accepted that the almost universal occurrence of an Urbach edge in amorphous solids is caused by structural and thermal disorder. Numerical calculations indicate that random electric fields (Dow and Redfield 1972) or a Gaussian site energy distribution in a coherent-potential approximation lead to the right kind of exponential dependence of absorption on photon energy (Abe and Toyozawa 1981, Schreiber and Toyozawa 1982). This work has been extended theoretically in a number of papers (Cohen, Chou, Economou, John and Soukoulis 1988, and references cited therein, Grein and John 1989) and applied to hydrogenated amorphous silicon (a-Si : H) for which detailed experimental results are available (Cody, Tiedje, Abeles, Brooks and Goldstein 1981, Cody 1984).

The absorption region above the Urbach tail has received less attention although the empirical Tauc (1974) law is nearly as universal in amorphous materials. The effects of increasing Gaussian site disorder and of varying band correlation on the Tauc plot slope and intercept were discussed in some of the work already mentioned (Abe and Toyozawa 1981). Cody *et al.* (1981) found a linear relation between the Tauc gap and the inverse slope of the Urbach tail in a-Si : H when the temperature and hydrogen content change.

The slope of the Tauc plot has been mostly ignored in the literature, although effects of temperature in amorphous As_2Se_3 (a-As_2Se_3) (Street, Searle, Austin and Sussman

0141-8637/91 $3·00

1974) and of composition in amorphous silicon–carbon (a-Si_xC_{1-x}) (Sussmann and Ogden 1981) and amorphous silicon–nitrogen (a-Si_xN_{1-x}) alloys (Han and Feldman 1988) have been reported.

Unfortunately it is all too common to find reports on the Tauc gap or the slope of the Urbach edge with the Tauc slope or Urbach pre-exponential omitted. This is to be regretted since, apart from possible interest of these parameters in their own right, they are needed to evaluate the absolute value of the optical absorption at different energies.

In this paper we report a detailed study of the Tauc region as a function of composition in As_xSe_{1-x} glasses for $0 < x < 0{\cdot}5$. The results are compared with previous work on the Urbach tail in the same system and available theoretical work.

§2. Sample preparation

Large batches of As_2Se_3 were prepared from high-purity (99·9999%) elemental As and Se from Koch Light Ltd. by melting in an evacuated quartz tube and reacting in a rocking furnace at 800–1000°C for 24 h followed by quenching in water. The non-stoichiometric compositions were then prepared in similar manner from As_2Se_3 and As or Se in suitable proportions.

Thin films were produced in a glove box, by blowing bubbles from melts in a nitrogen atmosphere. In this way, compositional changes during preparation were avoided. After overnight storage to get rid of static charge, good pieces from the bubbles were selected by visual inspection. The pieces were glued to an Al sample holder with small amounts of silicone grease.

§3. Experimental details

Optical transmission was measured with a Zeiss MM 12 double-prism single-beam monochromator. For each composition at least one transmission spectrum was taken with the Zeiss sample holder, which could be operated only at room temperature. The sample was then transferred to a home-built cryostat with facilities for evacuation and temperature control to $\pm 0{\cdot}5$°C. This was mounted on a platform of adjustable height and with two stop screws to set sample and reference positions corresponding to two identical sample and reference holes (2 mm in diameter). Both positions were readjusted for each temperature to compensate for variation in sample holder length caused by thermal expansion and were also checked occasionally during runs. The monochromator bandwidth was kept below 0·010 eV, which is considered adequate for amorphous materials with less sharp edges than the corresponding crystals.

Transmission spectra for each sample were measured from a wavelength corresponding to 0·001% transmission out to 2·5 μm. The interference fringes in the long-wavelength part of each spectrum were used to determine the optical path length through the sample. The absolute order of the fringes was determined only for the thinnest samples. However, according to the equation $2n_i d = m\lambda$, a plot of the change in fringe order m against inverse wavelength has a slope of $2n_i d$. Actually, since the long-wavelength refractive index n_i increases slightly with decreasing wavelength, this method gave about 10% lower values for the $n_i d$ product than a direct application of the interference equation in cases where the absolute order was known.

After a sample had been used for transmission measurements, its thickness was measured mechanically by placing a Talysurf stylus on it and observing the step as the stylus left the sample. These measurements were rather difficult for small pieces of unmounted films. To normalize data to unit thickness it was found preferable to divide by the $n_i d$ values as determined from the slope of the fringe plots. The mechanically

determined thicknesses were then used to find an average $n_i = 2{\cdot}8$ (a plot of n_i against As content gives values from 2·5 to 3·1, but this does not imply dependence on As content).

The transmission range below 15% was used to determine the optical absorption by inverting the equation

$$T = \frac{(1-R)^2 \exp(-\alpha d)}{1 - R^2 \exp(-2\alpha d)}, \tag{1}$$

where T is the transmission, R the reflectance, α the absorption coefficient and d the sample thickness. The value of R was taken to be 0·27 (corresponding to refractive index $n = 3{\cdot}2$). It is estimated that the error involved in using $n = 3{\cdot}2$ is less than $\pm 0{\cdot}2$ for the compositions and photon energies covered in the present work. Calculation shows that the resulting error in absorption is negligible except for the lowest values measured where it can approach 6%. The transmission range 0·010–15% corresponds to $1 < \alpha d < 8$. By combining results from samples of different thicknesses, the corresponding range in absorption coefficients was extended several times. The range of absorption coefficients obtained was typically from below 6×10^3 to $9 \times 10^4\ \mathrm{cm}^{-1}$ and in no case covered less than one decade.

Most of our data were found to be in agreement with the widely observed Tauc law, that is

$$\alpha h\nu = C(h\nu - E_T)^2, \tag{2}$$

where $h\nu$ is photon energy, E_T the Tauc gap and C is a constant indicating how steeply the absorption rises with energy.

In the initial analysis it was found convenient to plot $(\alpha d h\nu)^{1/2}$ against $h\nu$. This does not affect the extrapolated gap E_T, but gives a slope $(Cd)^{1/2}$. These could then be normalized by the method described above, that is by calculating $C = Cd\,2{\cdot}8/n_i d$.

Se is a well known exception from Tauc's law (Davis 1970) and in the range 2·1–3·1 eV, follows a linear law

$$\alpha h\nu = C_1(h\nu - E_1). \tag{3}$$

Here C_1 is a constant and E_1 an extrapolated optical gap. The measurements for pure Se and Se with 0·1 and 1% As were plotted according to both eqn. (2) and eqn. (3) to investigate the transition from linear to square law with increase in As content.

§4. Results

4.1. *Interband absorption and power laws*

The room-temperature results on amorphous Se (a-Se) and amorphous $As_{40}As_{60}$ (a-$As_{40}Se_{60}$) are shown in figs. 1 and 2. Included for comparison are results on thermally evaporated Se and r.f. sputtered $As_{40}Se_{60}$ obtained in the present study, as well as results from the literature.

The present results on sputtered and evaporated films agree closely with the corresponding results of Knights and Davis (1974) and Felty and Myers (1971). For films prepared from bubbles a slight shift is observed to higher photon energies for absorption in Se and to lower energies in $As_{40}Se_{60}$. A larger shift to lower energies was observed on going from a thermally evaporated film of composition $As_{43}Se_{57}$ to a bubble film $As_{42{\cdot}5}Se_{57{\cdot}5}$. It is well established that the absorption edge of virgin evaporated tetrahedral or a-Se films lies at lower photon energies than in corresponding annealed or bulk films (Fritzsche 1973, De Neufville 1976), and that in

Fig. 1

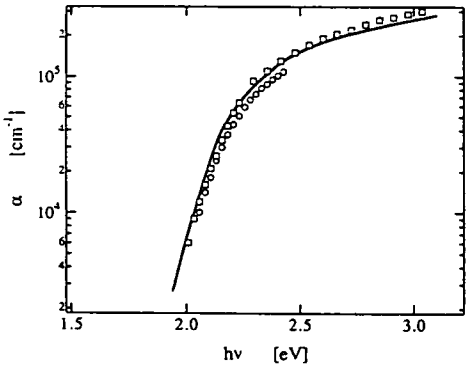

Optical absorption in a-Se as a function of photon energy: (——), Knights and Davis (1974); (○), bubbles, 296 K, present work; (□), evaporated, 290 K, present work.

Fig. 2

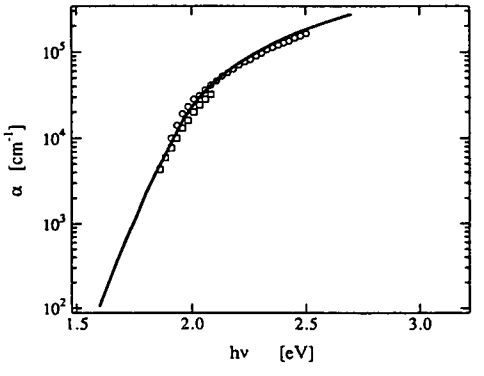

Optical absorption in a-$As_{40}Se_{60}$ as a function of photon energy: (——), Felty and Myers (1971); (○), bubbles, 290 K, present work; (□), r.f. sputtered films, 300 K, present work.

$As_{40}Se_{60}$ and $As_{40}S_{60}$ the opposite effect is observed. According to Fritzsche (1973), annealing of evaporated or sputtered films in all cases shifts the edge towards that of the bulk material. Thus it appears that the films prepared from bubbles and used in the present study are close to bulk vitreous material in their optical properties. This is consistent with the preparation method since it is estimated that during the bubble-blowing process the material cools from a temperature near its liquidus temperature to well below T_g in 10–100 ms.

It was found that eqn. (2) applies to all blown films of compositions As_1Se_{99} to $As_{50}Se_{50}$. Typical results are plotted in fig. 3, from which it is apparent that both the gap E_T and the slope of the Tauc plot decrease with increasing As content. This is indeed a general trend over most of the composition range. Thick samples of most compositions showed deviation from eqn. (2) at photon energies slightly above E_T, indicating a transition to an exponential form of absorption. For most compositions, there was no deviation from the square law at the highest absorption values measured in this study, exceptions being $As_{25}Se_{75}$ and films with 1% As or less.

Fig. 3

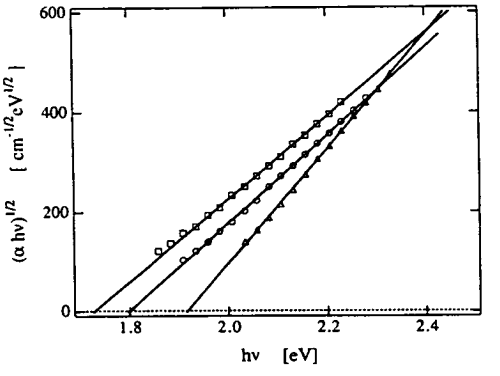

Tauc plots for three As–Se compositions: (△), As_5Se_{95}; (○), $As_{30}Se_{70}$; (□), $As_{45}Se_{55}$. The straight lines intersect at high energies, but not at a single point.

Fig. 4

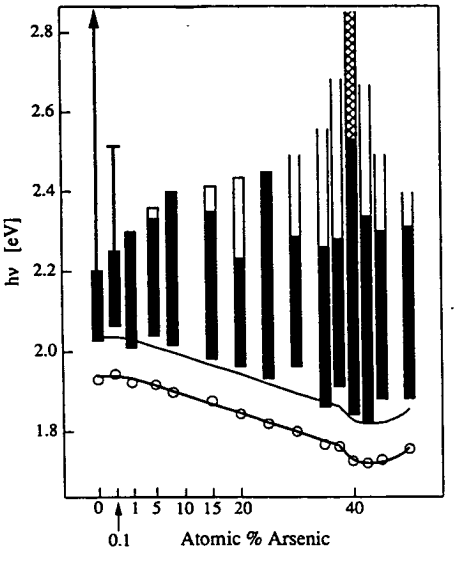

Histogram indicating the observed room-temperature ranges of Tauc's law in this work (measured on bubble samples) (■) and by Weiser (1970) (▨): □, expected wider ranges of Tauc's law; (⊖), E_T(300 K); (——), E_T(300 K) + 0·1 eV; I linear range, observed only for pure Se and $As_{0\cdot1}Se_{99\cdot9}$. For clarity the scale of the horizontal axis is different for compositions below 1% As.

Figure 4 is a histogram indicating the range of photon energies for which Tauc's law was shown to hold in this work, for the 15 compositions. Open columns indicate that no deviation was observed at the highest energies measured and thus Tauc's law is expected to continue to apply. Weiser (1970) found no deviation from eqn. (2) for photon energies as high as 3·5 eV in evaporated $As_{40}Se_{60}$. This is indicated in fig. 4 by a cross-hatched column. Clearly the upper limit increases with increasing As content. The upper solid line indicates approximately the energy at which the transition to the exponential region starts. It is clear that this occurs about 0·1 eV above the Tauc gap which is also included in fig. 4.

Fig. 5

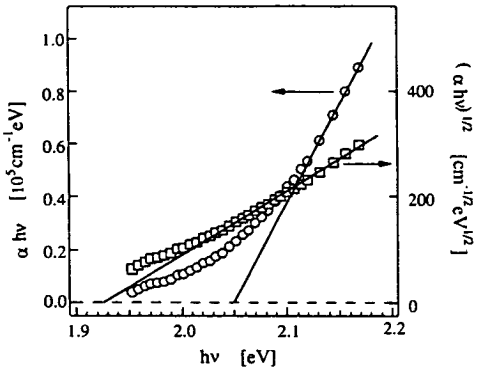

Comparison of linear law plot (○, left-hand vertical axis) and Tauc (square root) plot (□, right-hand vertical axis) of data on a sample of evaporated Se. The square root plot gives a better fit in the 2·0–2·2 eV range. The linear law holds at higher energies (not shown) up to 3·1 eV as observed by Davis (1970).

Bubble films of pure Se obey eqn. (3), the linear law, from slightly above the extrapolated gap E_1 to the highest energy at which absorption could be measured (2·4 eV). For evaporated Se the absorption curve follows eqn. (3) up to 2·9 eV and becomes slightly superlinear at higher energies. Davis (1970) found similar behaviour with superlinearity starting at 3·2 eV. Bubbles of $As_{0.1}Se_{99.9}$ also obey the linear eqn. (3) but over a more limited energy range (2·2–2·45 eV). The addition of less than 1% As to pure Se is enough to cause a complete transition from the anomalous linear behaviour of eqn. (3) to Tauc's law. The extent of the linear fit is indicated in fig. 4 by solid vertical lines.

Data for Se and $As_{0.1}Se_{99.9}$ can be fitted to eqn. (2) over a narrow range between the linear and exponential regimes. There would be little point in such an exercise were it not for the fact that the values of E_T and C obtained from such plots agree very closely with those extrapolated from glasses with higher As concentrations. Figure 5 gives a comparison of the same data for evaporated Se plotted according to both eqn. (2) and eqn. (3).

The extrapolated gaps (averaged over several samples) occur at $E_T = 1{\cdot}94$ eV and $E_1 = 2{\cdot}08$ eV respectively in bubbles and at 0·02 eV lower energies in evaporated Se; a difference in agreement with the comment at the beginning of this paragraph. It is interesting that these energies correpond closely to the energies at which Sussmann *et al.* (1975) observed a kink and a maximum respectively in the electroabsorption spectrum for a-Se, indicating two superimposed peaks. Possibly there is a link between these results. If that is the case, then the maximum in room-temperature electroabsorption at 2·05 eV might be associated with E_1 and should disappear with the addition of 1% As, leaving only the lower maximum at 1·95 eV corresponding to E_T.

4.2. *Variation in the gap with composition*

Figure 6 shows the Tauc gap against As content at room temperature, and extrapolated to absolute zero. The gap E_T decreases linearly with increasing As content up to nearly 40% As and has a minimum at about 43% As. Each circle in fig. 6 represents an average over three to five samples (bubbles) and each square an average over two to four bubbles. The different values of E_T for sputtered and evaporated films are also

Fig. 6

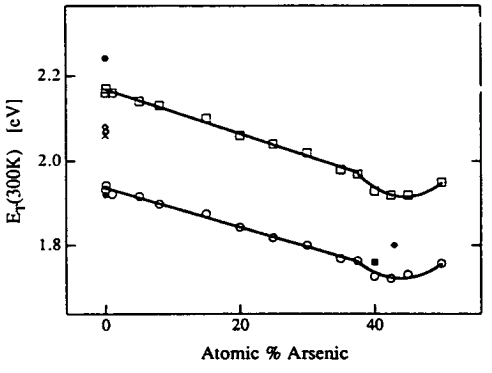

Optical (Tauc) gaps (○, □, ◆, ■) and linear gaps (◇, ●, ×) of As–Se films as a function of As content: (○, ◇), bubble specimen at 300 K; □, ●, bubble specimen gaps extrapolated to 0 K; ◆, ×, evaporated specimens at 300 K; ■, sputtered specimens at 300 K. Lines are drawn to aid the eye.

Fig. 7

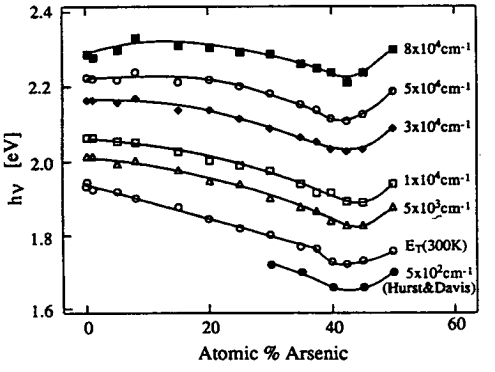

Room-temperature isoabsorption curves (■, ○, ◆, □, △) and the Tauc gap (○) for As–Se bubbles. The figure also includes data on bulk As–Se (●) from Hurst and Davis (1974).

included in fig. 6 as well as E_1 for pure and slightly doped (0·1% As) Se. The room-temperature results are plotted again in fig. 7 together with several 'isoabsorption lines'. Clearly the Tauc gap follows very closely in shape the constant absorption lines for $\alpha < 10^4\ \mathrm{cm}^{-1}$. The higher-absorption lines level off towards the Se end of the diagram, reflecting the steeper slope of the Tauc plot for those compositions.

Figure 7 includes some results on 'hot-pressed' samples obtained by Hurst and Davis (1974) which are in excellent agreement with the present results. This gives further support to our contention that the bubbles are close to the bulk material in their optical properties.

It is interesting to consider the above results in relation to other arsenic chalcogenides. According to Asahara and Izumitani (1974) evaporated $As_{70}Se_{30}$ has $E_T = 1{\cdot}7\,\mathrm{eV}$ and Greaves, Knights and Davis (1974) give $E_T = 1{\cdot}2\,\mathrm{eV}$ for a-As. Comparison with the present results demands that there be a maximum in E_T

somewhere in the composition range 50–70% As, perhaps at 57% As concentration where a minimum in density has been reported (Kunugi, Ota, Yamagishi and Fukutani 1969).

A similar form is likely for the As–S system, which has extrema in several properties near the stoichiometric composition, as does the As–Se system (Myers and Felty 1967). There is no indication of extrema in E_T in the a-As_xTe_{1-x} system (Cornet and Rossier 1973) nor in the electrical gaps, glass transition or structural properties of that system.

4.3. *Variation in the gap with temperature*

Figure 8 shows typical results for a bubble sample at four different temperatures. As usual, both the gap and the slope of the Tauc plot decrease with increasing temperature. This invites the question of a possible common focal point to which plots for different temperatures converge when extrapolated to higher energies. This will be discussed later. The energy gap E_T varies approximately linearly with temperature above 150 K but is generally observed to vary more slowly at lower temperatures. This can be seen in fig. 9 for the case of $As_{15}Se_{85}$ bubble films. Unfortunately, facilities were not available for measurements below 100 K. This means that our data are not sufficient to allow fitting to the equation expected to describe the variation in the gap with temperature;

$$E_T(T) = E_T(0) - \frac{K}{\exp(\Theta_E/T) - 1}, \tag{4}$$

where K is a constant and Θ_E the Einstein temperature. This function, which was discussed by Cody (1984), is almost constant below $\Theta_E/4$ but changes approximately linearly with temperature above $\Theta_E/2$. The slope tends to $-K/\Theta_E$ in the higher-temperature range. Measurements in both temperature ranges of the E_T against T curve are needed to determine uniquely all parameters in eqn. (4).

The normalized temperature coefficient in the high-temperature region is given in fig. 10. A least-squares fit gives a line independent of composition, suggesting that, for the glasses investigated,

$$E_T(T) = E(0)(1 - \phi T), \tag{5}$$

with $\langle\phi\rangle = (3{\cdot}5 \pm 0{\cdot}2) \times 10^{-4}\,K^{-1}$, independent of composition. The parameter $E(0)$ in eqn. (5) corresponds to the 0 K extrapolation from the nearly linear part of the E_T

Fig. 8

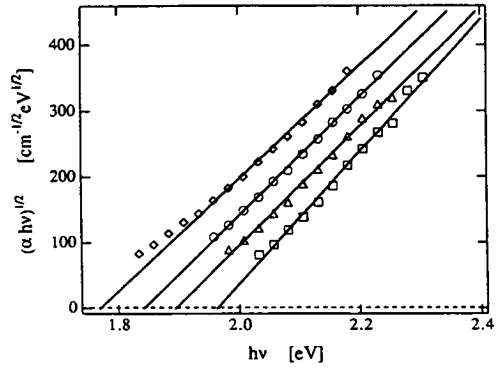

Tauc plots for $As_{20}Se_{80}$ at four different temperatures: (○), 290 K; (◇), 387 K; (△), 200 K; (□), 112 K. The straight-line fits converge if extrapolated to higher photon energies.

Fig. 9

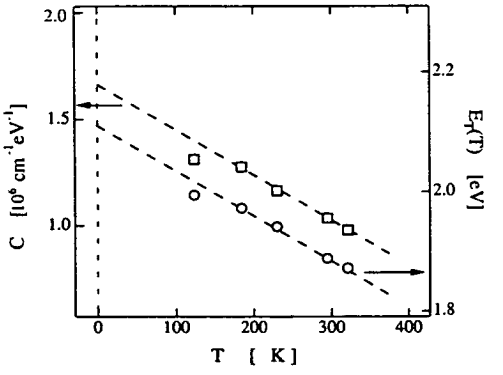

Temperature dependence of the two parameters that are obtained from Tauc plots for $As_{15}Se_{85}$: the Tauc gap and the square of the slope. Linear extrapolation to 0 K of E_T data above 150 K overestimates the zero-temperature gap.

Fig. 10

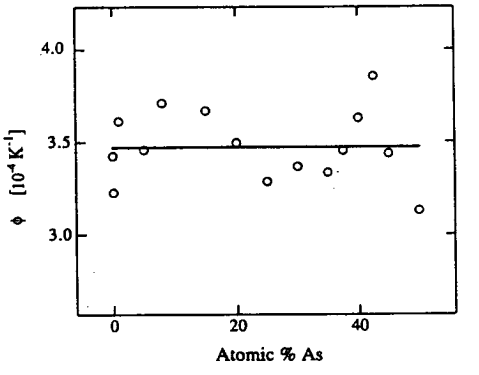

Dependence of the normalized temperature coefficient of the Tauc gap on As content in As–Se bubbles. A straight-line fit is independent of composition.

against T curves. Note that $E(0)$, whose variation with As content is shown in fig. 6, is larger than the actual gap $E_T(0)$. As expected from the different definition of the optical gap, the values of $\gamma = dE_T/dT$ in the present study are numerically slightly lower than those obtained by Hurst (1973) who found γ values from $-8{\cdot}1 \times 10^{-4}$ to $-9{\cdot}5 \times 10^{-4}$ eV K^{-1} for the $As_{30}Se_{70}$ to $As_{50}Se_{50}$ systems at $\alpha = 500\,cm^{-1}$. For pure Se the present value is $\gamma = -7{\cdot}4 \times 10^{-4}$ eV K^{-1} or $\langle\gamma\rangle = -7{\cdot}6 \times 10^{-4}$ eV K^{-1} (from $\langle\phi\rangle$). It is interesting to note that the temperature coefficient of E_1 is smaller, that is $dE_1/dT = -5{\cdot}6 \times 10^{-4}$ eV K^{-1}, which may indicate (since $E_1 > E_T$) that the electron–phonon interaction decreases away from the bandgap. This is consistent with a Tauc edge slope C that decreases with increasing temperature.

4.4. *The Tauc edge slope*

The parameter C in eqn. (2) is plotted as a function of As content in fig. 11 for room temperature and 120 K, and in fig. 12 the inverse of C is plotted. Each point represents an average over two to five samples. The most remarkable result of the present work is

the good fit of both sets of data in fig. 12 to straight lines over the whole composition range:

$$C^{-1} = ax + b, \tag{6}$$

where x is the atomic fraction of As, $a = (2{\cdot}0 \pm 0{\cdot}1) \times 10^{-6}$ eV cm and is almost independent of temperature, $b = 6{\cdot}7 \times 10^{-7}$ eV cm at room temperature and $3{\cdot}9 \times 10^{-7}$ eV cm at 120 K. The extrema observed in almost all other properties near the stoichiometric composition $As_{40}Se_{60}$ do not show up in the variation in the steepness of absorption above the Tauc gap.

§ 5. Discussion

5.1. *Correlation with glass transition temperature and density*

The form of the E_T against As content curve in fig. 6 suggests an inverse correlation with the well known results of Myers and Felty (1967) for glass transition temperature against As content. This is indeed the case as is borne out by the excellent fit to a

Fig. 11

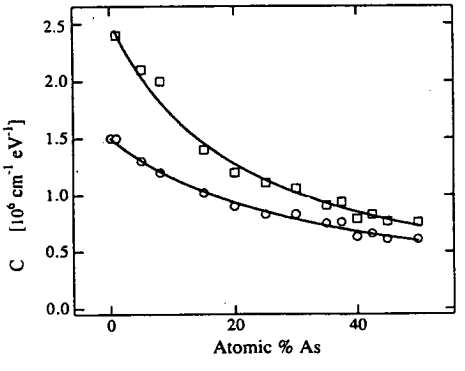

Dependence of the parameter C (square of the slope in Tauc plots) on As content at two temperatures: (□), 120 K; (○), 300 K; (——), an aid to the eye.

Fig. 12

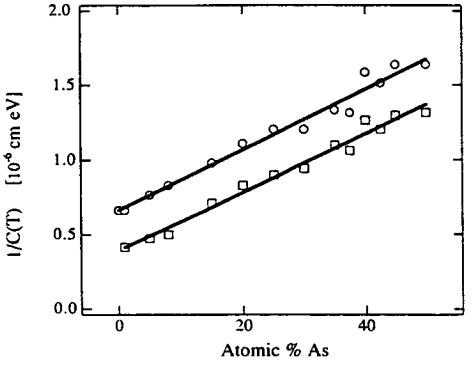

Same data as in fig. 11 plotted as the inverse of C against As content: (□), 120 K; best fit is $0{\cdot}67 \times 10^{-6} + 2{\cdot}01 \times 10^{-6}x$; (○), 300 K, best fit is $0{\cdot}39 \times 10^{-6} + 1{\cdot}95 \times 10^{-6}x$; (——), best line fits, whose slopes are almost identical.

Fig. 13

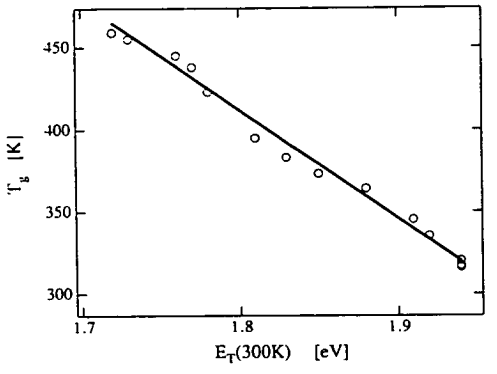

Glass-transition temperature (○) plotted as a function of the Tauc gap in As–Se at 300 K showing excellent linear correlation between the glass-transition temperature data of Myers and Felty (1967) and the Tauc gap data of the present work: (——), $T_g = 1600 - 660E_T$.

straight line in fig. 13, which is a plot of $T_g(x)$ (taken from Myers and Felty (1967)) against $E_T(x, 300\,\mathrm{K})$ for the corresponding composition as determined in the present study. The line in fig. 13 may be expressed as

$$T_g(x) = 320\,\mathrm{K} + 660\,\mathrm{K\,eV^{-1}}(\Delta E_T(x)), \tag{7}$$

where $\Delta E_T(x) = E_T(\mathrm{Se}) - E_T(\mathrm{As}_x\mathrm{Se}_{1-x})$. An even better fit to a straight line is obtained for a plot of T_g against $E_T(x, T_g)$, the Tauc gap extrapolated to T_g for each composition. Correlations between T_g and other parameters have been observed for other amorphous semiconductors. Nunoshita and Arai (1972) found that $\ln(T_g) \propto E_\sigma$ in Si–As–Te glasses. Koos and Kósa Somogyi (1985) report that

$$T_g = [\exp(3{\cdot}43m - 3) + 273]\,\mathrm{K},$$

in $\mathrm{Ge}_x\mathrm{Se}_{1-x}$ glasses as well as $\mathrm{As_2Se_3}$ and $\mathrm{GeS_2}$. Here m is a mean coordination or average number of bonds per atom. This relation also fits the T_g results of Myers and Felty in the range from pure Se to $\mathrm{As_{40}Se_{60}}$ but not for higher concentration of As.

In fig. 14 we have plotted E_T at room temperature as a function of density, using two sets of density data from the literature, that is those of Chernov, Dembovskii and Chistov (1968) and Kunugi *et al.* (1969). The curve using the latter results is much closer to a straight line. In both cases, however, the deviations from a straight line are less than the differences between the two sets of density results. A fit to the data gives the relation

$$E_T = (4{\cdot}60 - 0{\cdot}62\rho)\,\mathrm{eV}, \tag{8}$$

where ρ is the density in grams per cubic centimetre. The errors that arise when comparing results from differently prepared samples in different laboratories make it difficult to conclude whether or not density and optical gap really are linearly related in the As–Se system. It seems likely, however, bearing in mind Kastner's (1973) analysis of $(\mathrm{d}E_g/\mathrm{d}P)_T$ and $(\mathrm{d}n/\mathrm{d}P)_T$ in amorphous semiconductors, and the observation by Arai, Hattori, Namikawa and Saito (1973a) and Arai *et al.* (1973b) of a relation of a similar kind for conductivity.

Fig. 14

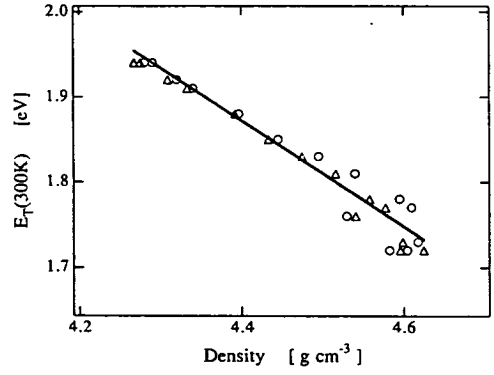

Tauc gap plotted against density of As–Se glasses, showing a comparison of the present Tauc gap results with density data from the work of Kunugi *et al.* (1969) (△) and Chernov *et al.* (1968) (○): (——), 4·60 − 0·62 × density.

5.2. *The Tauc gap and d.c. conductivity*

In fig. 15 we compare the conductivity activation energy E_σ as measured by Fisher, Marshall and Owen (1976), and the linear extrapolation to 0 K of the optical gap $E(0)$ as defined in eqn. (5). The zero energy is taken at the Fermi level. The quantity $E(0)$ is the difference between the top and bottom curves. Further comparison is given in the table, demonstrating that $2E_\sigma/E(0)$ is within 6% of unity in the composition range where conductivity data are available. Thus the Fermi level is pinned almost exactly in the middle of the gap.

5.3. *The Tauc gap and the Urbach edge*

Several workers have reported measurements of the Urbach edge as a function of composition or temperature in As–Se glasses (Sussman, Austin and Searle 1975, Hurst and Davis 1974, Andreev, Kolomiets, Mazets, Manukyan and Pavlov 1976, Kolomiets and Raspopova 1977). There is some scatter in the results, expecially for $As_{50}Se_{50}$, where the reported inverse slope at room temperature ranges from 49 to 60 meV. Ihm (1985a, b) has discussed the Urbach tails in As–Se and Ge–Se glasses in some detail. He

Fig. 15

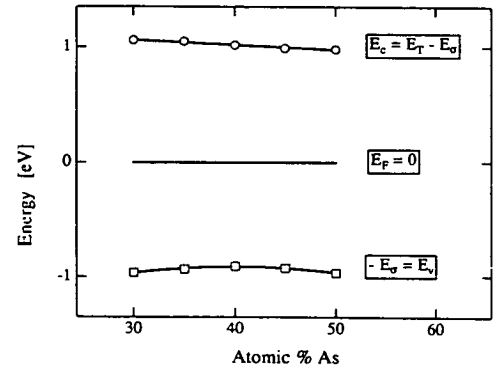

Dependence of the band edges on As content. Calculated from the dark-conductivity activation energy as measured by Fisher *et al.* (1976) and the 0 K extrapolated Tauc gap (present work).

Table 1. Comparison of compositional dependence of the Tauc gap (present work) and the conductivity activation energy (Fisher *et al.* 1976).

Composition	E_σ (eV)	$E(0)$ (eV)	$E_\sigma/E(0)$
$As_{30}Se_{70}$	0·963	2·019	0·48
$As_{35}Se_{65}$	0·933	1·980	0·47
$As_{40}Se_{60}$	0·910	1·925	0·47
$As_{45}Se_{55}$	0·925	1·916	0·48
$As_{50}Se_{50}$	0·968	1·950	0·50

suggested that the temperature independence of the slope below room temperature requires a structural change (at these temperatures) which has the opposite effect to that of temperature-induced disorder:

$$E_0 = Ak(T^* + \Theta_s). \tag{9}$$

Here A is a constant of order unity measuring the coupling strength between lattice vibrations and electrons, holes or excitons, k is the Boltzmann constant, T^* the effective temperature and Θ_s is a structural term. Ihm argues that T^* continues to vary at lower temperatures than does E_0; therefore Θ_s must include a term that varies in the opposite way. He proposed a 'buckling model' in which As–Se and Ge–Se glasses retain some of the short- and medium-range order of the related crystals, including their layered structure. At low temperatures, electrons can be localized by buckling of the layers, thus resulting in increase in disorder. As temperature increases, the activation barrier of the buckling is overcome and the layers 'straighten out'. According to Ihm the compositional variation in E_0, that is a minimum near $As_{40}Se_{60}$, is due to a temperature-independent part of Θ_s that measures the degree of structural disorder. Buckling is not expected to have much effect above the edges, but that does not mean that the Tauc region is unaffected by disorder.

It is natural to look to the most thoroughly investigated amorphous material for methods to analyse the present results. Cody *et al.* (1981) have found an empirical relation between E_T and E_0 in a-Si:H, which includes both temperature-induced disorder and structural disorder. This was analysed (Cody 1984) in the context of the model of Abe and Toyozawa (1981). They assumed a 'virtual crystal' and then introduced a Gaussian distribution of the site energies and a correlation parameter that relates disorder in the valence and the conduction bands. Numerical calculations indicate the following main features.

(1) Exponential edges exist over several decades in absorption.
(2) An increase in disorder reduces the slope of the edge.
(3) The graphs corresponding to different degrees of disorder (thermal or structural) in the same material extrapolate to a common point at the zero disorder energy gap.
(4) At higher energies, Tauc's law emerges as shown by straight lines on a square root plot.
(5) Tauc's plots corresponding to different degrees of disorder extrapolate to the same focal point as the exponential plots.
(6) Change from a positive to a negative correlation between potential fluctuations in conduction and valence band shifts the exponential edge lower in energy without a change in slope, and at the same time reduces the Tauc plot slope.

According to Cody (1984) the focal point for a-Si:H is at $\alpha = 1{\cdot}5 \times 10^6\,\mathrm{cm}^{-1}$ and $h\nu = 2{\cdot}2\,\mathrm{eV}$ for the exponential plots. However, Tauc plots for a-Si:H, sputtered a-Si and a-Si prepared by chemical vapour deposition (CVD), all extrapolate to identical absorption at $E_{FT} = 3{\cdot}6\,\mathrm{eV}$, the same energy as the direct transition of c-Si. The difference between the positions of the Urbach and Tauc foci contradicts the prediction of the numerical calculations discussed above (feature (5) in the above list). This is to be expected in a real solid as explained by Cody (1984). The Urbach parameter E_0 depends only on thermal and structural disorder, whereas changes in E_T can also be caused by chemical and coordination effects on the bands or, in the model of Abe and Toyozawa (1981), by changes in correlation of site energy disorder between the conduction and valence bands. As discussed by Cody, changes in E_T and E_0 should still be related when they are exclusively due to changing disorder, for example variation with temperature. The relation between the Tauc gap and inverse exponential slope in a-Si:H is according to Cody

$$E_T = (-6{\cdot}2E_0 + 2{\cdot}0)\,\mathrm{eV}, \tag{10}$$

indicating a focus at 2·0 eV since zero disorder corresponds to $E_0 = 0$. Thus the 'virtual crystal' that corresponds to a-Si:H is ascribed a direct gap of $2{\cdot}0\,\mathrm{eV} < E_{FU} < 2{\cdot}2\,\mathrm{eV}$, about 1·5 eV lower than E_{FT}. Sputtered a-Si and CVD-prepared a-Si do not fit eqn. (10).

To apply a similar analysis to the As–Se system, we look for focal points in the available experimental results. The results of Siemsen and Fenton (1967) for a-Se are well known. They found a focal point at $(\alpha_F, E_{FU}) = (10^7\,\mathrm{cm}^{-1}, 2{\cdot}4\,\mathrm{eV})$ for their measurements of the exponential slope between −200 and +400°C. This range extends nearly 200°C above the melting point of a-Se.

Andreev *et al.* (1976) reported measurements of the Urbach edge in $As_{40}Se_{60}$ and $As_{50}Se_{50}$ in the amorphous and liquid states. We have replotted their results in a way that minimizes the danger of a forced fit in the extrapolation. Firstly two points were read off the $\log(\alpha)$ against energy graph for every measurement temperature, these being the photon energies corresponding to absorption coefficients of 1000 and $100\,\mathrm{cm}^{-1}$. These were used to calculate the pre-exponential factor α_0 and the slope $1/E_0$ where

$$\alpha = \alpha_0 \exp(h\nu/E_0).$$

The existence of a focal point at (α_F, E_{FU}) implies that

$$\alpha_0 = \alpha_F \exp(-E_{FU}/E_0), \tag{11}$$

where α_F is independent of temperature. Therefore a plot of $\ln(\alpha_0)$ against $1/E_0$ will give a straight line with slope $-E_{FU}$ if there is a focus.

Figure 16 shows the results extracted from the data of Andreev *et al.* (1976) plotted in this way. The data fit very well to straight lines with the exception of a single point at 77 K for the $As_{40}Se_{60}$ composition, which represents the only measurement below room temperature. The focal energy parameter $E_{FU} = 2{\cdot}1\,\mathrm{eV}$ for both compositions and α_F is $0{\cdot}5 \times 10^6\,\mathrm{cm}^{-1}$ for $As_{50}Se_{50}$ and $3{\cdot}0 \times 10^6\,\mathrm{cm}^{-1}$ for $As_{40}Se_{60}$. The fact that the only low-temperature point is significantly out is in agreement with Ihm's discussion, and with the anomalous low-temperature behaviour of E_0 in $As_{40}Se_{60}$. The E_T against T curve does not begin to level off until below 150 K. Thus a relation similar to eqn. (10) will not hold for $As_{40}Se_{60}$ below room temperature.

The nearly constant E_0 below room temperature corresponds to a parallel shift of the $\log(\alpha)$ against $h\nu$ curve without a change in slope. This suggests an explanation

Fig. 16

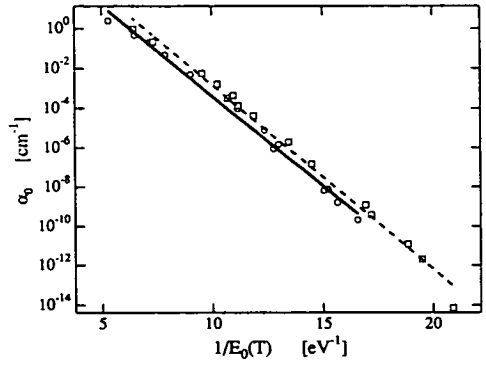

Replotted data from the literature (Andreev *et al.* 1976) showing a linear relationship between the slope $1/E_0$ of plots of logarithmic absorption against energy and the pre-exponentials α_0: (○), $As_{50}Se_{50}$; (□), $As_{40}Se_{60}$. The data are for temperatures from 77 to 816 K corresponding to glassy and liquid states.

Fig. 17

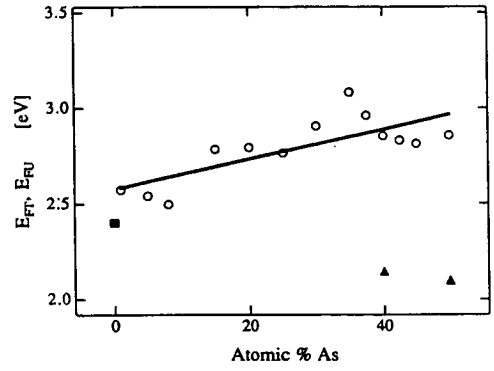

Focal point energy as a function of As content: (○), E_{FT}, determined by the application of eqn. (14) to the results of Tauc plots corresponding to data measured at different temperatures; (——), $2{\cdot}57+0{\cdot}78x$; (▲), E_{FU} (Andreev *et al.* 1976); (■), E_{FU} (Siemsen and Fenton 1967).

within the framework of the Abe–Toyozawa model, namely that the interband correlation of the site disorder may be changing.

The existence of a focal point for Tauc plots at different temperatures requires that

$$\alpha_F E_{FT} = \text{constant} = C(E_{FT} - E_T)^2. \tag{12}$$

The only variables in this equation are C and E_T; so they must be related. It then follows from eqn. (12) that

$$E_{FT} = E_T(T) + 2C(T)\frac{dE_T}{dT}\Big/\frac{dC}{dT}, \tag{13}$$

$$E_{FT} = \frac{E_{T2}C_2^{1/2} - E_{T1}C_1^{1/2}}{C_2^{1/2} - C_1^{1/2}}, \tag{14}$$

where the subscripts 1 and 2 refer to temperatures T_1 and T_2.

Fig. 18

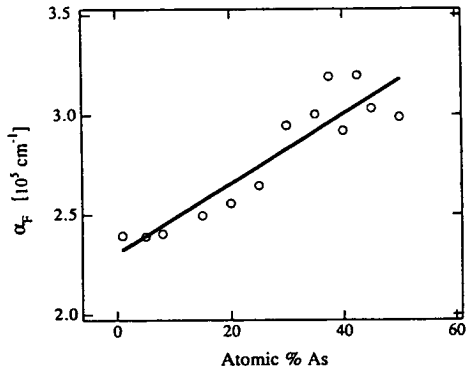

The focal point absorption parameter α_F (○) as determined from the data in fig. 17 and eqn. (12): (——), 231 000 + 175 000x.

We have applied eqn. (14) to our results for bubble films. Figure 17 is a plot of E_{FT} against As content for the 1–50% As range. The values of E_{FT} are scattered between 2·50 and 3·05 eV because any errors in C or E_T are amplified by the extrapolation. A best line fit to the data in fig. 17 gives

$$\langle E_{FT} \rangle = (2{\cdot}57 + 0{\cdot}74x)\,\text{eV}. \tag{15}$$

Also included in fig. 17 are Urbach edge focal energy E_{FU} from Siemsen and Fenton (1967) and also the values from fig. 16 derived from Adreev *et al.* (1976).

The focal parameter α_F against As content, calculated from eqns. (15) and (12), is given in fig. 18.

The present results certainly show that Tauc plots for two different temperatures for any composition in the 1–50% As range will intersect. However, the number of samples where results were obtained at more than two temperatures are limited. The data that we have indicate that the focal point is fuzzy. Either this may be due to experimental inaccuracy, or it may be that eqn. (12) is not exact. Further experiments over a wider range of temperatures are required to assert the validity of eqns. (12)–(14). The best material for such work is one with a large value of dC/dT, for example As_5Se_{95}.

§6. Conclusions

A wide range of thin As–Se films with bulk-like properties has been studied optically. Because the films were not on a substrate, the results are unaffected by differential strains due to changes in measurement temperature. Absorption above the fundamental edge follows the familiar Tauc law. The Tauc gap has a minimum slightly on the As-rich side of the stoichiometric composition, that is near $As_{43}Se_{57}$ which is the composition with the highest glass-transition temperature. A curve of the Tauc gap against As content is a negative replica of the well known glass transition against As content curve of Myers and Felty (1967). The normalized temperature coefficient of the Tauc gap is $-3{\cdot}5 \times 10^{-4}\,K^{-1}$, independent of composition. The previously observed linear absorption relation for a-Se disappears with the addition of 1% As. The temperature and compositional dependence of the slope of the Tauc plots have been investigated systematically.

The inverse square of the Tauc slope varies linearly with As content. The Tauc plots for differing temperatures in any individual composition seem to converge to a common point for that composition. Further measurements over a wide range of

temperatures are needed to determine how exact the convergence is. The ideal composition for such an experiment is As_5Se_{95}, with large dC/dT and Tauc's law valid over a substantial range in absorption.

The focal points for the Urbach edge and for the Tauc plots are nearly at the same energy for Se-rich compositions but diverge with increasing As content so that $E_{FT} - E_{FU} = 1$ eV for $As_{50}Se_{50}$. The results have been compared with the model of Abe and Toyozawa, and Cody's results on absorption in a-Si:H.

References

ABE, S., and TOYOZAWA, Y., 1981, *J. phys. Soc. Japan*, **50**, 2185.

ANDREEV, A. A., KOLOMIETS, B. T., MAZETS, T. F., MANUKYAN, A. L., and PAVLOV, S. K., 1976, *Soviet Phys. Solid St.*, **18**, 29.

ARAI, K., HATTORI, Y., NAMIKAWA, H., and SAITO, S., 1973a, *Jap. J. appl. Phys.*, **12**, 1717.

ARAI, K., KUMATA, K., KADOTA, K., YAMAMOTO, K., NAMIKAWA, H., and SAITO, S., 1973b, *J. non-crystalline Solids*, **13**, 131.

ASAHARA, Y., and IZUMITANI, T., 1974, *J. non-crystalline Solids*, **15**, 343.

CHERNOV, A. P., DEMBOVSKII, S. A., and CHISTOV, S. F., 1968, *Inorg. Mater. U.S.S.R.*, **4**, 1658.

CODY, G. D., 1984, *Semicond. Semimetals* B, **21**, 11.

CODY, G. D., TIEDJE, T., ABELES, B., BROOKS, B., and GOLDSTEIN, Y., 1981, *Phys. Rev. Lett.*, **47**, 1480.

COHEN, M. H., CHOU, M. Y., ECONOMOU, E. N., JOHN, S., and SOUKOULIS, C. M., 1988, *IBM J. Res. Dev.*, **32**, 82.

CORNET, J., and ROSSIER, D., 1973, *Phil. Mag.*, **27**, 1335.

DAVIS, E. A., 1970, *J. non-crystalline Solids*, **4**, 107.

DE NEUFVILLE, J. P., 1976, *Optical Properties of Solids: New Developments*, edited by B. O. Seraphin (Amsterdam: North-Holland), pp. 437–472.

DOW, J. D., and REDFIELD, D., 1972, *Phys. Rev.* B, **5**, 594.

FELTY, E. J., and MYERS, M. B., 1971, cited in *Electronic Processes in Non-Crystalline Materials*, by N. F. Mott and E. A. Davis (Oxford: Clarendon), p. 250.

FISHER, F. D., MARSHALL, J. M., and OWEN, A. E., 1976, *Phil. Mag.*, **33**, 162.

FRITZSCHE, H., 1973, *Electronic and Structural Properties of Amorphous Semiconductors*, edited by P. G. Le Comber and J. Mort (London: Academic), pp. 575–588.

GREAVES, G. N., KNIGHTS, J. C., and DAVIS, E. A., 1974, *Proceedings of the Fifth International Conference on Amorphous and Liquid Semiconductors*, edited by W. Brenig and J. Stuke (London: Taylor & Francis), p. 369.

GREIN, C. H., and JOHN, S., 1989, *Sold St. Commun.*, **70**, 87.

HAN, HE-XIANG, and FELDMAN, B. J., 1988, *Solid St. Commun.*, **65**, 921.

HURST, C. H., 1973, Ph.D thesis, University of Cambridge.

HURST, C. H., and DAVIS, E. A., 1974, *J. non-crystalline Solids*, **16**, 343.

IHM, J., 1985a, *Solid St. Commun.*, **53**, 293; 1985b, *J. Phys.* C, **18**, 4741.

KASTNER, M., 1973, *Phys. Rev.* B, **7**, 5237.

KNIGHTS, J. C., and DAVIS, E. A., 1974, *J. Phys. Chem. Solids*, **35**, 543.

KOLOMIETS, B. T., and RASPOPOVA, E. M., 1977, *Proceedings of the International Conference on Amorphous Semiconductors*, Balatonfüred, 20–25 September 1976, edited by I. Kósa Somogyi (Budapest: Académiai Kiadó), pp. 183–187.

KOOS, M., and KÓSA SOMOGYI, I., 1985, *J. non-crystalline Solids*, **77 & 78**, 1145.

KUNUGI, M., OTA, R., YAMAGISHI, T., and FUKUTANI, S., 1969, *Zairyo*, **18**, 807.

MYERS, M. B., and FELTY, E. J., 1967, *Mater. Res. Bull.*, **2**, 535.

NUNOSHITA, M., and ARAI, H., 1972, *Solid St. Commun.*, **11**, 213.

OHEDA, H., 1979, *Jap. J. appl. Phys.*, **18**, 1973.

SCHREIBER, M., and TOYOZAWA, Y., 1982, *J. phys. Soc. Japan*, **51**, 1544.

SIEMSEN, K. J., and FENTON, E. W., 1967, *Phys. Rev.*, **161**, 623.

STREET, R. A., SEARLE, T. M., AUSTIN, I. G., and SUSSMANN, R. S., 1974, *J. Phys.* C, **7**, 1582.

SUSSMANN, R. S., AUSTIN, I. G., and SEARLE, T. M., 1975, *J. Phys.* C, **8**, L182.

SUSSMANN, R. S., and OGDEN, R., 1981, *Phil. Mag.* B, **44**, 137.

TAUC, J. (editor), 1974, *Amorphous and Liquid Semiconductors* (New York: Plenum), pp. 159–220.

WEISER, K., 1970, cited by Owen, A. E., *Contemp. Phys.*, **11**, 257.

VOLUME 66, NUMBER 14 PHYSICAL REVIEW LETTERS 8 APRIL 1991

Quantized Electron Transport in Amorphous-Silicon Memory Structures

J. Hajto, A. E. Owen, S. M. Gage, and A. J. Snell
Department of Electrical Engineering, University of Edinburgh, Edinburgh EH9 3JL, Scotland

P. G. LeComber and M. J. Rose
Department of Applied Physics and Electronic and Manufacturing Engineering, University of Dundee, Dundee DD1 4HN, Scotland
(Received 26 March 1990)

Conduction in the ON state of amorphous-silicon memory devices is constrained to a narrow conducting filament. We present experimental evidence to show that the memory ON state is associated with quantized electron transport which is presumably related to quantum confinement effects in the small conducting filament. Current-voltage characteristics of typical ON states exhibit discrete steps which correspond to quantized resistance states and the steps split appropriately in a magnetic field. An especially notable feature is that the quantization can be observed at relatively high temperatures (up to ~ 190 K).

PACS numbers: 73.40.Sx, 72.80.Ng

We have previously shown that amorphous-silicon metal-p^+-n-i-metal and metal-p^+-metal junctions exhibit nonvolatile, polarity-dependent digital and analog memory-switching phenomena after initial conditioning by means of a moderately high applied potential ("forming").[1-4] An essential feature of this forming process is the creation of a filamentary region of highly conducting material. In the ON state the current is carried primarily through this region, which is much less than 1 μm in diameter. Experimental evidence for filamentation comes from studies of the ON-state resistance, which show R_{ON} to be independent of area, by thermal imaging with liquid crystals, and by direct observation with a scanning electron microscope combined with microanalysis. The latter technique indicated that the formation of the current filament is associated with local diffusion of the top metal contact into the amorphous silicon, resulting in a region of mixed or "alloyed" metal and silicon. More recent experimental work has resulted in a new metal-p^+-metal amorphous-silicon device which, rather than exhibiting two-state digital operation, has a continuum of stable conductance states which are nonvolatile and fully programmable by single 10-ns voltage pulses.[4] These new analog memory devices have applications as nonvolatile, reprogrammable memory elements in analog neural networks. In this paper we present new results showing that the current-voltage characteristics of such structures at low temperatures exhibit steplike features associated with quantized transport.

The samples used for this work were amorphous-silicon Cr-p^+-V sandwich structures configured as shown in Fig. 1. The 1000-Å-thick p^+ amorphous-silicon layer was prepared by rf-glow-discharge decomposition of SiH_4 containing 10^4 ppm by volume of B_2H_6, with the contact area defined by a 10-μm-diam pore in an insulating layer. The top and bottom metal electrodes were prepared by vacuum evaporation. By applying 300-ns voltage pulses of progressively increasing magnitude, the resistance of the as-prepared device can be gradually lowered from 10^9 Ω to $\sim 10^3$-10^4 Ω. After this initial forming step, all subsequent memory-switching operations can be performed with 10-100-ns pulses, 1.5-5 V in magnitude. Under these conditions the devices exhibit fast analog switching;[4] i.e., they show a continuum of nonvolatile states with resistances ranging from $R_{ON} = 10^3$ Ω to $R_{OFF} = 10^6$ Ω. In the present work we have studied the low-temperature conductivity behavior of the devices in a range of such analog memory states.

Typical current-voltage characteristics of a formed memory ON state measured at 4.2 K are shown in Fig. 2. In the voltage region from 0 to 0.37 V, the current in-

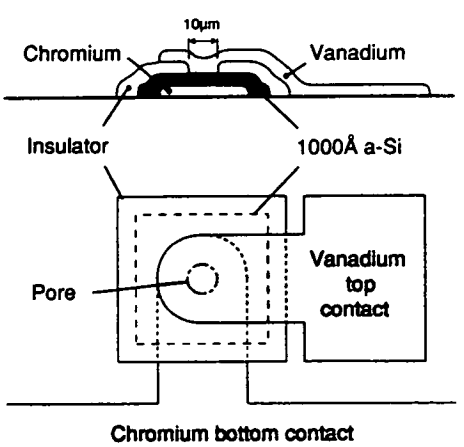

FIG. 1. Structure of the amorphous-silicon device.

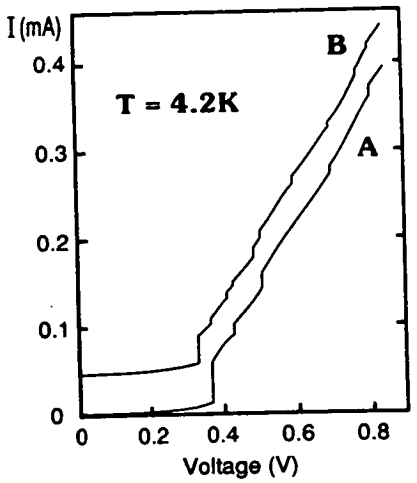

FIG. 2. *I-V* curves at 4.2 K with and without magnetic field. Curve *B* has been offset by 50 μA on the current scale for clarity.

creases continuously in a non-Ohmic manner. At a critical voltage V_{cr}, in this instance at 0.37 V, there is a distinct change in the behavior of the sample. A sudden current jump occurs at this point and the resistance of the sample is lowered to the order of a few kΩ. After the first current jump at 0.37 V, further current steps can be observed at 0.43, 0.51, 0.70, and 0.81 V (curve *A* in Fig. 2). The current-voltage characteristics are symmetrical about the origin.

Curve *B* in Fig. 2 depicts the current-voltage characteristics of the same sample under the influence of a 0.2-T magnetic field. The curve has been displaced by 50 μA on the current scale for clarity. The direction of the magnetic field is 30° with respect to the filament. Further steps can now be observed at 0.33, 0.41, 0.49, 0.60, and 0.78 V in addition to those observed in the zero-magnetic-field case (curve *A*). The effect of the magnetic field is completely reversible. Similar *I-V* characteristics have been obtained for a range of samples with varying initial resistance states. The critical voltage V_{cr} at which the first current jump occurs and the amplitude of this first current jump are dependent on the resistance of the memory ON state investigated. After the first jump, however, the characteristics for each sample investigated lie on a similar curve, suggesting a similar conduction mechanism at voltages above V_{cr}.

Figure 3 shows the effect of temperature on the current-voltage characteristics of a different sample from the one shown in Fig. 2. The curves have been shifted along the current axis for clarity. The magnitude of the current steps gradually decreases with increasing temperature until the effect is no longer observable at ~190 K. Figure 4 shows the data for curve *A* in Fig. 2 replotted to show resistance as a function of applied voltage. The steps in the current are clearly seen to be associated

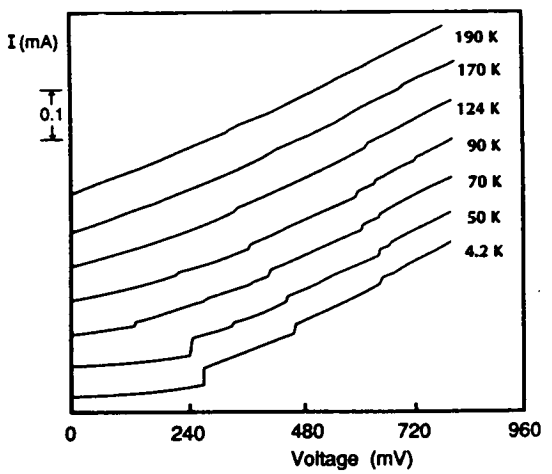

FIG. 3. *I-V* curves as a function of temperature. The curves have been offset on the current scale for clarity.

with a quantized resistance $R = h/2ie^2$, where i is an integer. In the voltage range from 0.3 to 0.8 V, there are five steps in the current in curve *A*, Fig. 2, corresponding to values for i of 2, 3, 4, 5, and 6. Higher voltages have not been applied to the sample because these could change the resistance of the particular memory state. With a magnetic field applied to the same sample further quantization of resistance is observed at values $R = h/2(i + \frac{1}{2})e^2$. Theoretical considerations predict that the steps should be flat, as shown by the dashed lines in Fig. 4. That they are not flat in the present results is thought to be due to the presence of a parallel conduction path through the bulk of the amorphous silicon around the filament. Figure 5 shows that a sample in a given resistance state exhibits reproducible behavior at low temperatures even after thermal cycling. Curves *a* and *b* show

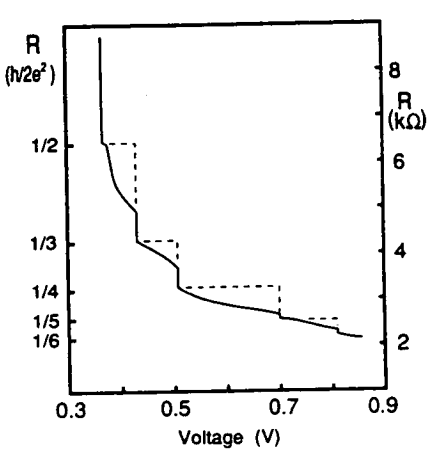

FIG. 4. Resistance vs voltage at 4.2 K with no magnetic field. The dashed line indicates the behavior predicted by theory.

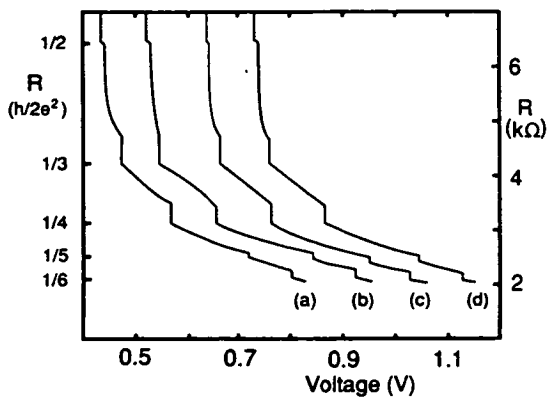

FIG. 5. Reproducibility of resistance characteristics before and after thermal cycling. Curves are offset by 0.1 V on the voltage scale for clarity.

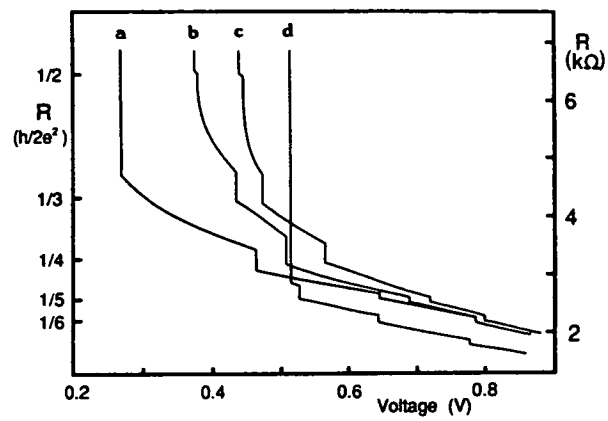

FIG. 6. Reproducibility of the resistance-voltage characteristics obtained on different samples.

the electrical characteristics of a sample at 4.2 K with a delay of several hours between measurements. Curves *c* and *d* show measurements on the same sample after temperature cycling between room temperature and 4.2 K.

Figure 6 shows the reproducibility of the observed quantized resistance jumps for four different samples (denoted by *a*, *b*, *c*, and *d*). (Curve *a* was obtained by replotting the current-voltage characteristics in Fig. 3 at 4.2 K.) These curves represent the largest deviation among the samples measured—the resistance-voltage curves of all of the other samples measured lay within these values. It is important to note that in this case there is no offset between the curves; i.e., they are directly replotted from the measured current-voltage characteristics. The critical voltage V_{cr} and the voltage values at which the quantized resistance jumps occur are different for the different samples but the quantized jumps are always very close to the values of the quantized resistance $R = h/2ie^2$. The typical deviations are $\pm 2\%$ at $i=2$, $\pm 2.5\%$ at $i=3$, $\pm 6\%$ at $i=4$, $\pm 4\%$ at $i=5$, and $\pm 4\%$ at $i=6$. The first jump, however, occurs from $R = 15\,200\ \Omega$ to $4820\ \Omega$ in curve *a*, which is apparently a 12% deviation from the quantized resistance value of $R = 4291\ \Omega$ (at $i=3$). Also, in the case of curve *d*, the resistance jumps first to $R = 4820\ \Omega$ at $V_{cr} = 0.51$ V followed by another closely spaced jump (at $V = 0.525$ V) to $R = 2550\ \Omega$, which is very close to the quantized value of $R = 2575\ \Omega$ (at $i=5$). These relatively large discrepancies are always associated with the *first* current jump in the *I-V* characteristics at V_{cr}, and hence with a change in the conduction mechanism. This first transition at V_{cr} might not be expected to occur therefore at a voltage corresponding to a change in quantized resistance value.

The experimental data presented above show that we have observed discrete steps in the *I-V* characteristics for the ON state of amorphous-silicon Cr-p^+-V structures which are associated with a quantized resistance. The current-voltage characteristics (see Fig. 2) indicate that the filament has a relatively large resistance around zero bias. Such an anomalously high zero-bias resistance in metal/amorphous-silicon/metal structures was recently shown to be consistent with the assumption that electron transport in the filament at low bias is dominated by tunneling between small metallic particles embedded in a dielectric medium (presumably amorphous silicon).[3] We assume that the conducting filament is composed of two parts—small-scale inclusions of permanently changed material connected by conducting channels which are formed, broken, dimensionally changed, reformed, etc., during switching. The evidence is that the overall diameter of the filament at the top contact is $\ll 0.5\ \mu m^2$. The length of the channels must be consistent with tunneling. With increasing applied voltage, the tunneling current increases exponentially. This implies that at the critical voltage V_{cr}, the tunneling barrier effectively "breaks down" and a much larger current flow occurs. This is not a destructive effect as the process is completely reversible and no material changes ensue. Assuming that the metallic inclusion has a curved shape, the current flow would be restricted to a *very localized area*. The observation of quantized resistance suggests that the channel can be considered to be an electron waveguide with confinement being brought about by the combination of the applied field and the geometry and constitution of the conducting filament.

There is a wide range of experimental and theoretical work on electrical transport through quantum point contacts.[5] These are short and narrow constrictions in a two-dimensional electron gas, with a width of the order of the Fermi wavelength λ_F. Because of the high mobility, elastic impurity scattering and inelastic scattering are negligible and therefore the mean free path of the electrons is longer than the length of the conduction channel. In this case ballistic transport takes place and the resistance of such quantum point contacts is quantized in

units of $h/2e^2$. The notion of a very small conducting filament in the amorphous silicon devices being made up of metallic inclusions has similarities to the idea of quantum point contacts and it is possible, therefore, that the quantized resistance states described here are a result of the same sort of mechanism. The crucial question is whether ballistic transport is possible in the amorphous-silicon device. Carrier mobilities in amorphous silicon are normally trap limited and are orders of magnitude lower than expected for ballistic behavior (e.g., $\sim 10^{-2}$ $cm^2\ V^{-1}sec^{-1}$). It is worth noting, however, that we have previously estimated a carrier mobility as high as 100 $cm^2V^{-1}sec^{-1}$ from magnetoresistance measurements on devices similar to those used in the present experiments and that mobility is certainly related to the conducting filament rather than the "bulk" amorphous silicon.[4] On the other hand, it is entirely unexpected that quantized resistance states associated with ballistic transport should be observed when, as in the present case, the applied voltage is greater than kT (or greater than the spacing between subbands).[6,7] At the moment, therefore, the issue is unresolved and it is not realistic to speculate further about mechanisms except to note that the observed quantized transport effects suggest the importance of the dimensions of the conducting channel rather than material parameters. The significance of using amorphous-silicon devices lies in the forming process which promotes the formation of very small features which then dominate conduction.

[1]A. E. Owen, P. G. LeComber, G. Sarrabayrouse, and W. E. Spear, IEE Proc. Part I: Solid State Electron Devices **129**, 51–54 (1982).

[2]M. J. Rose, J. Hajto, P. G. LeComber, S. M. Gage, W. K. Choi, A. J. Snell, and A. E. Owen, J. Non-Cryst. Solids **115**, 168 (1989).

[3]S. M. Gage, J. Hajto, S. Reynolds, W. K. Choi, M. J. Rose, P. G. LeComber, A. J. Snell, and A. E. Owen, J. Non-Cryst. Solids **115**, 171 (1989).

[4]P. G. LeComber, A. E. Owen, W. E. Spear, J. Hajto, A. J. Snell, W. K. Choi, M. J. Rose, and S. Reynolds, J. Non-Cryst. Solids **77/78**, 1373 (1985).

[5]H. van Houten, C. W. J. Beenakker, and B. J. van Wees (to be published); in *Semiconductors and Semimetals*, edited by M. A. Reed (Academic, New York, 1990).

[6]B. J. van Wees, H. van Houten, C. W. J. Beenakker, J. G. Williamson, L. P. Kouwenhoven, D. van der Marel, and C. T. Foxon, Phys. Rev. Lett. **60**, 848 (1988).

[7]D. A. Wharam, M. Pepper, H. Ahmed, J. E. F. Frost, D. G. Hasko, D. C. Peacock, D. A. Ritchie, and G. A. C. Jones, J. Phys. C **21**, L887 (1988).